

Microfluidic biosensor systems for real-time *in vivo* clinical bioanalysis

Sally A. N. Gowers

Department of Bioengineering
Imperial College London

A thesis submitted for the degree of

Philosophiæ Doctor (PhD)

March, 2015

Imperial College
London

The publications arising from this thesis are:

- M. L. Rogers, P. A. Brennan, C. L. Leong, S., A., N. Gowers, T. Aldridge, T. K. Mellor and M. G. Boutelle. Online rapid sampling microdialysis (rsMD) using enzyme-based electroanalysis for dynamic detection of ischaemia during free flap reconstructive surgery, *Analytical and Bioanalytical Chemistry*, 2013 (405) 3881-3888, DOI: 10.1007/s00216-013-6770-z

- S. A. N. Gowers*, V. F. Curto*, C. A. Seneci, C. Wang, S. Anastasova, P. Vadgama, G. Z. Yang and M. G. Boutelle. A 3D printed microfluidic device with integrated biosensors for online analysis of subcutaneous human microdialysate, *Analytical Chemistry*. *In press (2015)*

- K. Hamaoui*, S. A. N. Gowers*, S. Damji, N. Bullock, M. L. Rogers, C. L. Leong, G. Hanna, A. Darzi, M. G. Boutelle and V. Papalois. Rapid sampling microdialysis as a novel tool for parenchyma assessment during static cold storage and hypothermic machine perfusion in a translational porcine kidney model, *Journal of Surgical Research*. *Submitted (2015)*

I thank the co-authors for all their support and declare that the work presented in this thesis is of my own work except where it is otherwise acknowledged.

SALLY GOWERS

The copyright of this thesis rests with the author and is made available under a Creative Commons Attribution Non-Commercial No Derivatives licence. Researchers are free to copy, distribute or transmit the thesis on the condition that they attribute it, that they do not use it for commercial purposes and that they do not alter, transform or build upon it. For any reuse or redistribution, researchers must make clear to others the licence terms of this work.

Abstract

The aim of this thesis was to develop online biosensing systems for dialysate tissue metabolite detection in real time, to provide an insight into the health of tissue in various *in vivo* applications.

An autocalibration system was developed using LabSmith programmable components to improve the accuracy of results obtained over long monitoring times. A method of collecting dialysate into storage tubes for online analysis while retaining temporal resolution was developed and validated.

Microfluidic biosensor systems were developed for online measurement of glucose and lactate. One approach employed the use of biosensors, using a combined needle electrode with enzyme encapsulated in a hydrogel layer. The dynamic range of the biosensors was extended by adding an outer polyurethane layer. An alternative approach used automated syringe pumps and valves to develop a microfluidic system for in-flow enzyme addition to the dialysate stream.

The existing rsMD system was applied for detection of tissue ischaemia during and after free flap surgery, by measuring dialysate glucose and lactate levels in real time. The system was able to detect flap failure, both during surgery and afterwards in the intensive therapy unit (ITU), much earlier than traditional methods.

The rsMD system was adapted to enable monitoring of lactate levels in two dialysate streams and was applied for monitoring isolated porcine kidneys during two methods of cold preservation and subsequent re-warming. Significant differences in the lactate concentrations were observed between the two techniques. The system was extended for use with human transplant kidneys and with both porcine and human pancreases.

A novel 3D printed wearable biosensor system was developed for direct integration with a clinical microdialysis probe. The system considerably improved the lag time and dispersional smearing compared with the existing rsMD system. The device was used in a proof-of-concept study with wireless potentiostats to monitor cyclists during exercise.

Acknowledgements

I would like to thank my supervisor, Martyn, for giving me the opportunity to work on this project. I am extremely grateful for his endless encouragement, advice and guidance throughout, and for being so generous with his time. I would also like to express my gratitude to all the lab members for their advice and support, and for making my time in the lab so enjoyable. I have been very fortunate to work on many collaborative projects and I would like to thank everyone who has been involved in this work for sharing their knowledge and experience.

I am immensely thankful to my family for their unfailing support and encouragement, particularly to my mum, dad and sister Kate. I am also very grateful to all my friends for their support and for always taking an interest in my work.

I am grateful for funding from the NIHR Biomedical Research Centre of Imperial College London and from the EPSRC ESPRIT programme led by Prof. Guang-Zhong Yang, without which this work would not have been possible.

Contents

List of Figures	15
List of Tables	21
1 Introduction	23
1.1 The extracellular space	23
1.2 Measurement requirements	26
1.3 Cellular metabolism	27
1.4 Methods of <i>in vivo</i> monitoring	28
1.4.1 Implantable sensors	30
1.4.2 Tissue sampling	31
1.5 Microdialysis	32
1.5.1 Recovery	33
1.5.2 Tissue damage	35
1.5.3 Offline analysis	36
1.5.4 Online analysis	36
1.6 Thesis outline	38
2 Methods & materials	41
2.1 Electroanalytical techniques	41
2.1.1 Cyclic voltammetry	41
2.1.2 Amperometry	42
2.2 Microdialysis	44
2.2.1 Microdialysis probes	44
2.2.2 T1 perfusion solution	44
2.3 Rapid sampling microdialysis (rsMD)	45
2.3.1 Injection valve	45
2.3.1.1 One dialysate stream, two analytes	46
2.3.1.2 Two dialysate streams, one analyte	47
2.3.2 Enzyme reactors	47

CONTENTS

2.3.3	Radial flow cell	49
2.3.4	The clinical trolley	49
2.3.5	Calibrating the rsMD system	49
2.3.6	Data acquisition and analysis	50
2.3.7	Storage tubing	51
2.4	Microfluidic polydimethylsiloxane (PDMS) chip fabrication	51
2.5	Microelectrode biosensors	52
2.5.1	Needle electrode fabrication	52
2.5.2	Electrode characterisation	54
2.5.3	Biosensor fabrication	55
2.5.3.1	Poly(phenol) glucose biosensors	55
2.5.3.2	Hydrogel biosensors	56
2.5.4	Calibrating biosensors	58
2.5.5	Wireless potentiostats	59
2.6	Common solutions and standards	59
2.6.1	Ferrocene monocarboxylic acid (Fc) buffer solution	60
2.6.2	Phosphate buffered saline	60
2.6.3	Substrate standards	60
3	Clinical analysis system for dialysate metabolites	61
3.1	Introduction	61
3.1.1	Biosensors	61
3.1.2	Enzymes	62
3.1.3	Enzyme kinetics	66
3.2	Autocalibration	67
3.2.1	Autocalibration board	68
3.2.2	RsMD autocalibration	70
3.2.3	On-chip biosensor autocalibration	72
3.3	Hydrogel biosensors	75
3.4	Extending the biosensor dynamic range	78
3.4.1	Preliminary investigations	79
3.4.2	Effect of multiple layers of polyurethane	82
3.4.3	Reproducibility	83
3.4.4	Protocol optimisation	85
3.4.5	Polyurethane-coated biosensor characteristics	86
3.4.6	Summary	87
3.5	In-flow enzyme addition	87
3.5.1	Experimental setup	87

3.5.2	Calibration	88
3.5.3	Stability	90
3.5.4	Script optimisation	91
3.5.5	In-flow enzyme addition - donor kidney analysis board	95
3.5.6	ATP detection	97
3.5.7	Pyruvate detection	100
3.5.8	Conclusion	103
3.6	Dialysate collection in storage tubing	103
3.6.1	Validation	103
3.6.2	Stability	104
3.6.3	Summary	109
3.7	Conclusion	109
4	Transplant organ viability assessment: Part I	111
4.1	Introduction	111
4.1.1	The kidney	111
4.1.2	Kidney transplantation	112
4.1.3	Renal ischaemia	114
4.1.4	Clinical preservation methods	114
4.1.5	Viability assessment	116
4.1.6	Lactate and the kidney	117
4.1.7	Aims	118
4.2	Methodology for kidney studies	118
4.2.1	Organ retrieval	118
4.2.2	Microdialysis probe insertion	118
4.2.3	Online rsMD analysis system	119
4.2.4	Delayed analysis using storage tubing	120
4.2.5	Data analysis and statistical analysis	121
4.3	Methodology for comparing renal preservation methods	125
4.3.1	Experimental protocol	125
4.3.1.1	Static cold storage	127
4.3.1.2	Hypothermic machine perfusion	127
4.4	Results: during preservation	130
4.4.1	SCS cortex and medulla	130
4.4.2	HMP cortex and medulla	134
4.5	Results: during passive warming	135
4.5.1	SCS warming	135
4.5.2	HMP warming	137

CONTENTS

4.6	Comparison of preservation methods	140
4.6.1	During preservation	140
4.6.2	During warming	141
4.7	Cortex versus medulla	148
4.8	Discussion	149
4.8.1	Our results in the context of other microdialysis studies of renal metabolism	152
4.8.2	Limitations and future work	153
5	Transplant organ viability assessment: Part II	155
5.1	Monitoring kidneys immediately after retrieval	155
5.2	Varying cold ischaemia time	157
5.2.1	Experimental protocol	157
5.2.2	Results	159
5.2.3	Discussion	161
5.3	Measuring multiple metabolites	162
5.4	Online analysis of discarded human kidneys	165
5.4.1	Case study 1	165
5.4.2	Case study 2	170
5.5	Treatment with protective proteins	175
5.5.1	Results	175
5.5.2	Discussion	177
5.6	Online analysis of transplant pancreases	177
5.6.1	Introduction	178
5.6.2	Methodology for pancreas studies	180
5.6.3	Porcine pancreases	181
5.6.4	Online analysis of human pancreases	185
5.6.5	Discussion	188
5.7	Miniaturised analysis system	189
5.8	Conclusion	193
6	Online monitoring during free flap surgery	195
6.1	Introduction	195
6.2	Methodology	196
6.2.1	Surgical procedure and microdialysis probe insertion	196
6.2.2	Online analysis system	197
6.2.3	Delayed analysis using storage tubing	198
6.2.4	Data and statistical analysis	199
6.2.5	Sterility considerations	200

6.3	Results	200
6.3.1	Case study 1	201
6.3.2	Case study 2	203
6.3.3	Case study 3	206
6.3.4	Case study 4	207
6.3.5	Case study 5	210
6.3.6	Case study 6	212
6.3.7	Case study 7	215
6.4	Discussion	216
7	Athlete monitoring: the bioanalytical problem	219
7.1	Introduction	219
7.2	Sample collection in storage tubing for delayed analysis	221
7.2.1	Microdialysis procedure	222
7.2.2	Sample collection and analysis	222
7.2.3	Experimental protocol	223
7.2.4	Microdialysis resolution enhancement	224
7.2.5	Offline results at 5 μ l/min	225
7.2.6	Offline results at 1 μ l/min	228
7.2.7	Preliminary conclusions	231
7.3	Online analysis of dialysate	232
7.3.1	Configuring the online system	232
7.3.2	Improved experimental protocol	236
7.3.3	Results: rsMD	236
7.3.3.1	Cyclist 1	237
7.3.3.2	Cyclist 2	240
7.3.3.3	Cyclist 3	241
7.3.3.4	Summary	243
7.3.4	Results: online biosensors	245
7.3.5	Conclusion	247
8	Athlete monitoring: a wireless microfluidic device	249
8.1	Introduction	249
8.1.1	Wearable microfluidic device	249
8.1.2	Device requirements	251
8.2	Design and fabrication of microfluidic device	252
8.3	Microfluidic device: design 1	253
8.4	Microfluidic device: design 2	257
8.5	Microfluidic device: design 3	261

CONTENTS

8.6	Effect of channel size on biosensor response	263
8.7	Microfluidic device: design 4	265
8.8	Cycling trials with wearable device	270
8.8.1	Microdialysis procedure	270
8.8.2	Online analysis using wearable device	270
8.8.3	Monitoring protocol	271
8.8.4	Results	272
8.9	Conclusion	278
9	Conclusions and future work	279
9.1	Overview	279
9.2	Future work	282
	Bibliography	285

List of Figures

1.1	Geometry of the extracellular space.	24
1.2	Schematic representation of sources and sinks in the ECF.	25
1.3	Summary of tissues monitored in this thesis.	26
1.4	Summary of aerobic metabolism.	27
1.5	Summary of aerobic and anaerobic pathways.	27
1.6	Scanning electron micrography images of the tips of glucose sensors.	31
1.7	Microdialysis probe.	33
1.8	Recovery of a microdialysis probe <i>in vitro</i> and <i>in vivo</i>	34
1.9	Effect of microdialysis probe on glial cells.	36
1.10	Schematic of response caused by 1 m of connection tubing.	37
1.11	Taylor dispersion.	38
2.1	Cyclic voltammetry.	42
2.2	Electropolymerisation.	43
2.3	RsMD Cheminert flow injection valve.	45
2.4	RsMD setup for measurement of glucose and lactate in one dialysate stream.	46
2.5	RsMD setup for measurement of lactate in two dialysate streams.	47
2.6	Reaction sequence occurring within the immobilised enzyme bed.	48
2.7	The clinical trolley.	50
2.8	Combined needle electrode.	52
2.9	Examples of poor electrode characteristics.	54
2.10	CVs indicating the reference electrode has shifted.	55
2.11	CV of a bare electrode and after coating with poly(phenol).	56
2.12	CV of a bare electrode and after coating with mPD.	57
2.13	Dip-coating needle electrode in enzyme solution using micro-manipulator.	58
2.14	Wireless potentiostat system.	59
3.1	Structure of glucose oxidase.	63
3.2	Structure of lactate oxidase.	64
3.3	Structure of horseradish peroxidase.	65

LIST OF FIGURES

3.4	Summary of HRP mechanism.	65
3.5	LabSmith components.	68
3.6	Schematic of autocalibration board.	69
3.7	Schematic of experimental setup for rsMD autocalibration.	71
3.8	Results of rsMD lactate autocalibration.	72
3.9	Photograph of experimental setup for on-chip biosensor autocalibration.	73
3.10	Raw data for on-chip glucose and lactate autocalibration.	74
3.11	Calibration curves for on-chip autocalibration.	75
3.12	SEM images of GOx hydrogel.	76
3.13	Typical hydrogel biosensor calibration curves.	77
3.14	Schematic cross-section of needle biosensor tip.	78
3.15	Effect of polyurethane outer layer on lactate biosensor response.	79
3.16	Lactate biosensor calibration before and after coating with polyurethane.	81
3.17	SEM images of GOx hydrogel after coating with polyurethane in THF.	82
3.18	Effect of multiple layers and coating time on lactate biosensor response.	83
3.19	Microscope images of polyurethane-coated lactate biosensors.	84
3.20	Response time of polyurethane-coated lactate biosensors.	85
3.21	Typical polyurethane biosensor calibration curves.	86
3.22	Experimental setup for dosing in enzyme for in-flow sensing.	88
3.23	Glucose and lactate calibrations using in-flow sensing system.	89
3.24	Repeated glucose calibrations with and without poly(phenol) film on electrode.	91
3.25	Effect of script on glucose and lactate response.	92
3.26	Automated board for enzyme optimisation.	93
3.27	Results of LOx optimisation.	94
3.28	Schematic of analysis system to monitor two analytes in two donor kidneys.	95
3.29	Measurement of glucose and lactate in two sample streams.	96
3.30	Calibration of microfluidic analysis board.	97
3.31	Schematic of analysis system to measure dialysate ATP.	98
3.32	ATP detection using in-flow enzyme addition.	100
3.33	Schematic of analysis system for pyruvate detection.	101
3.34	Pyruvate detection and optimisation.	102
3.35	Validation of collection in storage tubing for delayed analysis.	104
3.36	Dialysate collected from one microdialysis probe in multiple storage tubes.	105
3.37	Variability in dialysate collected from one microdialysis probe in multiple storage tubes.	106
3.38	Experimental setup used to fill lengths of storage tubing.	107
3.39	Sample storage tubes kept at -80°C.	108

LIST OF FIGURES

4.1	Structure of the kidney.	112
4.2	Photograph of porcine kidney with two microdialysis (MD) probes inserted.	119
4.3	Extract of raw data current peaks for alternating kidneys.	120
4.4	Schematic comparison between the online and stored analysis methods.	121
4.5	Deripling algorithm.	122
4.6	Data analysis protocol.	123
4.7	Calibration drift over an experiment.	124
4.8	Experimental protocol for the two preservation groups.	126
4.9	Experimental setup for SCS preservation.	127
4.10	Experimental setup for preservation by HMP.	128
4.11	Effect of additional cooling during HMP.	129
4.12	Dialysate cortical lactate profiles during SCS.	131
4.13	Concentration artefact caused by microdialysis probe movement.	133
4.14	Dialysate medullary lactate profiles during SCS.	133
4.15	Dialysate cortical lactate profiles during HMP.	134
4.16	Dialysate medullary lactate profiles during HMP.	135
4.17	Dialysate cortical lactate profiles during passive warming after SCS.	136
4.18	Dialysate medullary lactate levels during passive warming after SCS.	137
4.19	Dialysate cortical lactate profiles during passive warming after HMP.	138
4.20	Dialysate cortical lactate profile during warm perfusion after HMP.	139
4.21	Dialysate medullary lactate levels for HMP kidneys during passive warming.	140
4.22	Dialysate cortical lactate levels for kidneys undergoing SCS and HMP.	141
4.23	Dialysate medullary lactate levels for kidneys undergoing SCS and HMP.	141
4.24	Dialysate cortical lactate levels during passive warming after SCS or HMP.	143
4.25	Dialysate medullary lactate levels during passive warming after SCS or HMP.	144
4.26	Area-under-the-curve analysis of kidney lactate profiles during warming.	145
4.27	Cortical lactate profiles during warming, with and without movement.	146
4.28	Cortical lactate profiles during warming, after varying lengths of SCS.	147
4.29	Analysis of renal effluent metabolite concentrations during HMP.	150
5.1	Experimental setup for portable collection of dialysate in storage tubing.	156
5.2	Dialysate cortical lactate profile immediately after organ retrieval.	157
5.3	Experimental protocol for varying the length of CIT.	158
5.4	Dialysate cortical lactate profiles for two pairs of kidneys undergoing HMP after varying amounts of CIT.	160
5.5	Dialysate cortical lactate and glucose profile immediately after organ retrieval.	163
5.6	Experimental setup for glucose biosensor in microfluidic chip.	164

LIST OF FIGURES

5.7	Dialysate cortical metabolite levels for kidneys undergoing HMP after varying CIT length.	165
5.8	Dialysate cortical metabolite levels in a human kidney during HMP.	167
5.9	Dialysate cortical metabolite levels in a human kidney during reperfusion.	168
5.10	Dialysate medullary metabolite levels in a human kidney during HMP and reperfusion.	169
5.11	Experimental protocol for investigating the effect of protein treatment.	171
5.12	Experimental setup for perfusion of human kidney.	172
5.13	Dialysate cortical lactate profiles during haemoperfusion in human kidneys with and without protein pretreatment.	173
5.14	Dialysate medullary lactate profiles during haemoperfusion in human kidneys with and without protein pretreatment.	174
5.15	Dialysate cortical lactate profiles of kidneys undergoing haemoperfusion with and without protein pretreatment.	176
5.16	Experimental protocol for transplant pancreases.	180
5.17	Experimental setup for perfusion of porcine pancreas.	181
5.18	Dialysate metabolite levels for porcine pancreases.	183
5.19	Experimental setup for perfusion of a discarded human pancreas.	186
5.20	Dialysate metabolite levels in human pancreas 1 during HMP and reperfusion.	187
5.21	Dialysate lactate levels in human pancreas 2 during reperfusion.	188
5.22	Experimental setup for glucose and lactate measurement in two dialysate streams.	189
5.23	Raw data showing metabolite levels alternating between two dialysates.	190
5.24	Dialysate metabolite levels for porcine and human pancreases.	191
5.25	Average dialysate metabolite levels for porcine and human pancreases.	192
6.1	Microdialysis probe inserted into a radial forearm flap.	197
6.2	Clinical trolley for online monitoring.	198
6.3	Raw data from dialysate collected into storage tubing during surgery.	199
6.4	Photograph of non-sterile equipment inside camera drape.	200
6.5	Dialysate metabolite levels during free flap surgery for patient 1.	201
6.6	Dialysate metabolite levels in the ITU after free flap surgery for patient 1.	203
6.7	Dialysate metabolite levels during free flap surgery for patient 2.	204
6.8	Dialysate metabolite levels in the ITU after free flap surgery for patient 2.	205
6.9	Dialysate metabolite levels during free flap surgery and in the ITU for patient 3.	207
6.10	Dialysate metabolite levels during free flap surgery and in the ITU for patient 4.	208

LIST OF FIGURES

6.11	Histograms showing dialysate metabolite levels at key time points.	209
6.12	Dialysate metabolite levels during free flap surgery for patient 5.	211
6.13	Dialysate metabolite levels in the ITU after free flap surgery for patient 5.	212
6.14	Dialysate metabolite levels during free flap surgery for patient 6.	213
6.15	Dialysate metabolite levels in the ITU after free flap surgery for patient 6.	214
6.16	Dialysate metabolite baseline levels and levels in the ITU for patient 7.	215
6.17	Dialysate metabolite levels at key time points for cases 1 and 6.	217
7.1	Online sample collection in storage tube.	223
7.2	Schematic diagram showing the experimental protocol.	223
7.3	Experimental setup.	224
7.4	Schematic comparison of temporal resolution at different flow rates.	225
7.5	Results at 5 $\mu\text{l}/\text{min}$: dialysate metabolite levels during the cycling protocol.	226
7.6	Choice of microdialysis flow rate.	227
7.7	Example 1 at 1 $\mu\text{l}/\text{min}$: dialysate metabolite levels during the cycling protocol.	229
7.8	Example 2 at 1 $\mu\text{l}/\text{min}$: dialysate metabolite levels during the cycling protocol.	230
7.9	Dynamic range of lactate biosensors.	233
7.10	Online analysis experimental setup.	234
7.11	A 5-point calibration of the two online analysis systems.	235
7.12	The clinical trolley for online analysis.	236
7.13	Dialysate metabolite levels and recorded exercise parameters for cyclist 1.	238
7.14	Dialysate metabolite levels during the cycling protocol for cyclist 2.	240
7.15	Dialysate metabolite levels during the cycling protocol for cyclist 3.	242
7.16	Dialysate levels during key points in cycling protocol.	244
7.17	Dialysate metabolite levels for cyclist 1 obtained by rsMD and online biosensors.	246
7.18	Dialysate metabolite levels for cyclist 3 obtained by rsMD and online biosensors.	247
8.1	Schematic of wearable microfluidic device.	252
8.2	Conventional setup of commercial microdialysis probe.	253
8.3	Schematic diagram of design 1 of microfluidic chip.	254
8.4	Needle electrode placed inside LabSmith one-piece fitting.	255
8.5	Design 1 of the microfluidic device with electrode holders.	256
8.6	Schematic diagram of design 2 of microfluidic chip.	258
8.7	Detailed schematic of needle holder.	259
8.8	Design 2 of the microfluidic chip with electrode holders.	260

LIST OF FIGURES

8.9	Cross-sectional cut-out of the microfluidic chip.	261
8.10	Schematic diagram of design 3 of microfluidic chip.	262
8.11	Comparison of concentration step change in different sized channels.	264
8.12	Schematic drawings of design 4 of microfluidic chip.	265
8.13	Schematic representation of modular microfluidic device.	266
8.14	Typical biosensor calibration curves in the microfluidic device.	267
8.15	Response of rsMD compared with microfluidic device.	269
8.16	Wearable microfluidic device with wireless potentiostats during cycling protocol.	271
8.17	Dialysate metabolite levels during the cycling protocol for cyclist 1.	272
8.18	Dialysate metabolite levels during the cycling protocol for cyclist 2.	274
8.19	Dialysate and blood metabolite levels at key points in cycling protocol.	277

List of Tables

2.1	Summary of microdialysis probes used for each application.	44
2.2	Composition of T1 perfusion solution	45
2.3	RsMD membrane enzyme concentration	49
2.4	Composition of enzyme hydrogel solution	57
2.5	Composition of ferrocene monocarboxylic acid (Fc) buffer solution	60
2.6	Composition of 0.1 M PBS solution	60
3.1	Glucose and lactate hydrogel biosensor responses.	77
3.2	Effect of polyurethane coating time on lactate biosensor response.	80
3.3	Variability in lactate biosensor responses.	84
3.4	Glucose and lactate polyurethane biosensor responses.	86
4.1	Maastricht categories of DCD donors	113
4.2	Summary of median cortical and medullary values during SCS and HMP.	148
5.1	Porcine pancreas WIT and CIT.	182
7.1	Subcutaneous dialysate metabolite levels for cyclist 1.	239
7.2	Subcutaneous dialysate metabolite levels for cyclist 2.	241
7.3	Subcutaneous dialysate metabolite levels for cyclist 3.	242
8.1	Effect of electrode position on biosensor response time	263
8.2	Effect of channel dimensions on T_{90} response.	264
8.3	Biosensors characteristics at 1 $\mu\text{l}/\text{min}$ inside microfluidic channel (n=6).	267

LIST OF TABLES

Chapter 1

Introduction

This chapter introduces the extracellular space (ECS) and methods of *in vivo* monitoring. More detailed reviews specific to the tissues studied in this thesis are discussed in the relevant chapters.

1.1 The extracellular space

The ECS is a complex environment and is the passage through which substances, such as metabolites and drugs, move between cells and the bloodstream. As a result, information regarding the function of cells in the vicinity can be obtained by probing the ECS.

In free solution, in the absence of convection, molecules move by diffusion, governed by Fick's first law, shown in equation 1.1.

$$J = -D\left(\frac{dC}{dx}\right) \quad (1.1)$$

Where J is the flux and is proportional to the solute diffusion coefficient (D) and the change in concentration (C) per unit distance (x).

This governs both the flux to a cell or to a measurement device, which attempts to impose a local concentration gradient. Devices include implantable sensors or a sampling device, such as a microdialysis probe. It is important to consider how this changes when the measurement or sampling device is placed in tissue.

The ECS contains the extracellular fluid (ECF) and molecular transport occurs through diffusion. Many studies have described the intricate and tortuous nature of the ECS (1), as shown in figure 1.1. The ECS has several functions in the body. Apart from providing a path for substances to move between cells and blood vessels, it also provides a reservoir of ions to maintain resting and action potentials, and mediates active chemical signalling (1).

1. INTRODUCTION

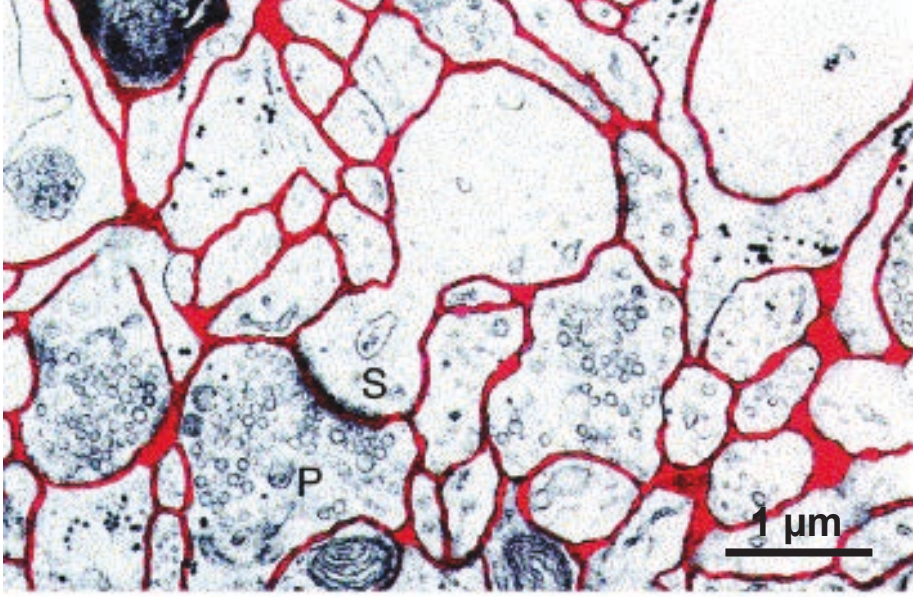


Figure 1.1: Geometry of the extracellular space. Image taken from (2). Electronmicrograph of a small region of a rat cortex, showing a dendritic spine (S) and a presynaptic (P) terminal. The ECS is outlined in red.

The effective diffusion coefficient in the ECS (D_{ECS}) is defined by equation 1.2.

$$D_{ECS} = \frac{D_{aq}}{\lambda^2} \quad (1.2)$$

Where D_{aq} represents the aqueous diffusion coefficient and λ represents the tissue tortuosity.

In the brain ECS, λ has been found to be 1.5-1.6 (2), but it is likely to vary for different regions. Moreover, λ may be affected by different pathological conditions. In addition, tissue damage caused by device implantation is likely to affect mass transport parameters as well as local uptake or release. Equation 1.2 is sometimes seen with an additional term ϕ , representing the excluded volume (typically 0.2 in the brain). However, it has recently been argued that this should only be included if tissue concentration is measured in homogenised tissue (1). The relationship between the concentration measured in homogenised tissue (C_H) and the concentration measured in the ECF (C_{ECF}) is given by equation 1.3. All concentrations in this thesis refer to ECF levels and therefore it is not necessary to correct for this.

$$C_H = \phi C_{ECF} \quad (1.3)$$

Interpretation of chemical measurements in the ECS also requires consideration of analyte generation and removal processes, as well as the pathological processes that would alter mass transport. The ECS contains many different analytes, all of which have specific

sources (sites of chemical release) and sinks (uptake sites). During *in vivo* measurements, the analyte must diffuse away from its release site, through the ECS, to the measurement device to be detected. However, during diffusion, analytes can be removed from the ECS by metabolism or uptake before reaching the device. Therefore, the concentration of an analyte in the ECS represents a balance between molecules released into and those removed from this space, including by the measurement device. A simplified schematic representation of these sources and sinks is given in figure 1.2.

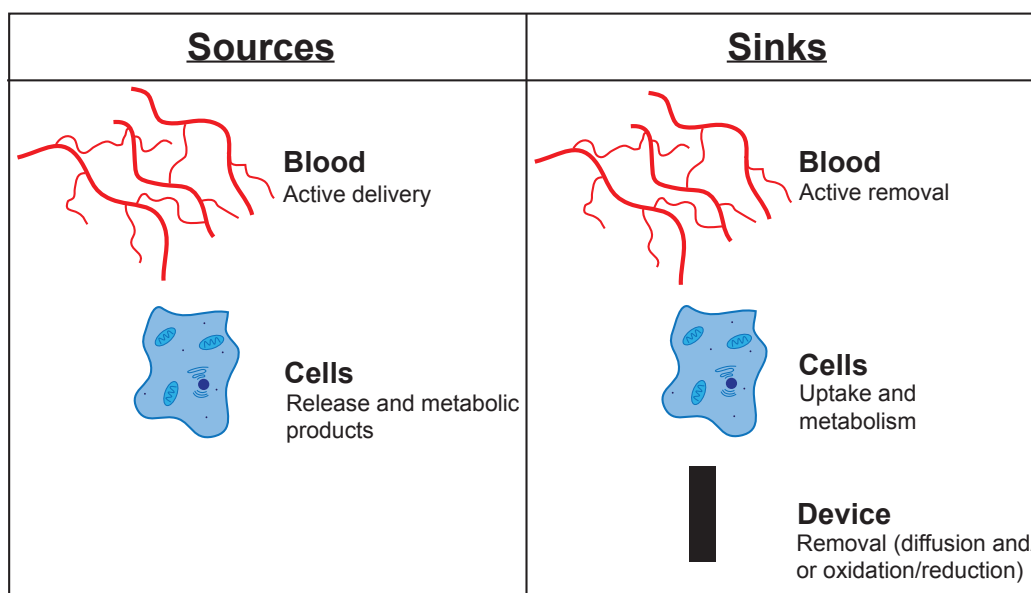


Figure 1.2: Schematic representation of sources and sinks in the ECF. Adapted from (3).

The change in concentration as a result of diffusion per unit time is governed by Fick's second law, which defines the change in flux per unit distance, shown in equation 1.4.

$$\frac{\delta C}{\delta t} = -\frac{\delta J}{\delta x} = D \frac{\delta^2 C}{\delta x^2} \quad (1.4)$$

However, the analyte concentration is also affected by chemical reactions that occur, including both removal (R_{tissue}) and generation (G_{tissue}) processes. Equation 1.4 can therefore be amended to include terms to account for these chemical reactions, described in equation 1.5.

$$\frac{\delta C}{\delta t} = D \frac{\delta^2 C}{\delta x^2} - R_{tissue} + G_{tissue} \quad (1.5)$$

In addition, the analytical measurement or sampling device can act as a sink, removing analyte. Therefore, equation 1.5 can be rewritten to incorporate a term that accounts for removal of analyte by the measurement device (R_{device}), described in equation 1.6.

1. INTRODUCTION

$$\frac{\delta C}{\delta t} = D \frac{\delta^2 C}{\delta x^2} - R_{tissue} + G_{tissue} - R_{device} \quad (1.6)$$

Equation 1.6 shows that concentration changes observed in the tissue are a result of diffusional processes, analyte generation, analyte removal or sink processes in the tissue and removal by the analytical measurement device. If the release and removal processes are balanced, then the measured concentration would remain constant.

The above analysis assumes there is no ECF convection, which would act as both a source and a sink for analytes. However, in normal tissue there is a flow of ECF from the arteries. Most of this flow is reabsorbed by the veins, but some is taken into the lymphatic system. This was most recently observed in the brain (4).

1.2 Measurement requirements

In this thesis, *in vivo* measurement of several different tissues will be discussed. These are shown in figure 1.3.

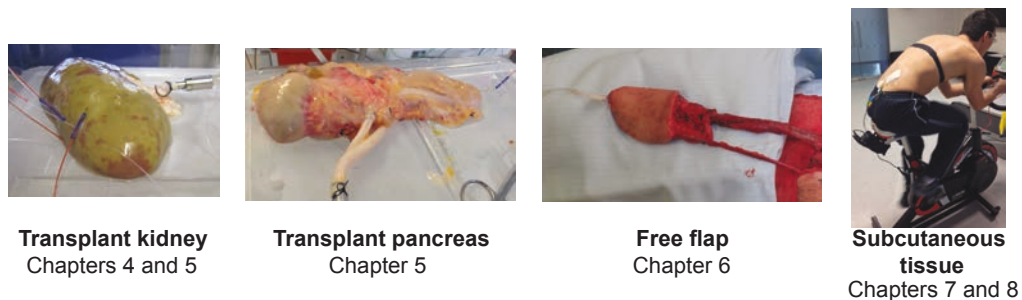


Figure 1.3: Summary of tissues monitored in this thesis. Monitoring of transplant kidneys is discussed in chapters 4 and 5. Monitoring of transplant pancreases is described in chapter 5. Chapter 6 describes monitoring of free flaps during and after surgery. Monitoring of subcutaneous tissue in cyclists during exercise is discussed in chapters 7 and 8.

Although on the face of it these are very different situations, they all share the common factor of hypoxia (low tissue oxygen levels) or ischaemia (failure of blood flow and hence delivery of oxygen and glucose). As a result, analyte sources are compromised. In addition to compromised sources, the utilisation by local sinks is often greatly upregulated. Therefore, in all cases, analysis of tissue metabolism, by measurement of the intermediate concentrations in the ECF, can provide important information about the state of the tissue.

1.3 Cellular metabolism

Under normal physiological conditions, glucose and oxygen are delivered to the tissue by the bloodstream and are removed by cellular metabolism, as shown in figure 1.4.

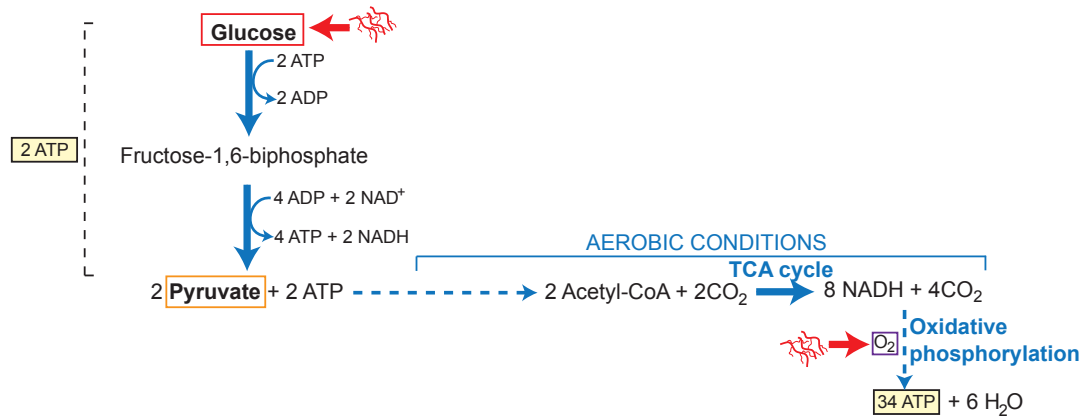


Figure 1.4: Summary of aerobic metabolism. Normal physiological metabolism, when oxygen levels are sufficient for aerobic metabolism to occur.

Ischaemia is a loss of blood supply to the tissue, such as occurs during vessel occlusion, for example, during harvest of a transplant organ. This results in a disruption in the supply of oxygen and glucose to the tissue. The metabolic pathway in the absence of oxygen is added to the schematic diagram of the aerobic pathway in figure 1.5.

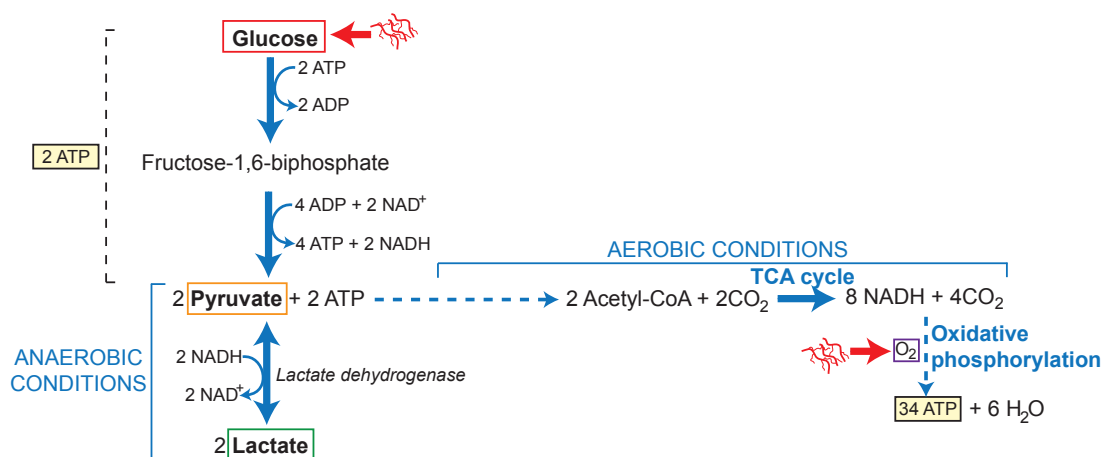


Figure 1.5: Summary of aerobic and anaerobic pathways. Anaerobic metabolism generates a net product of 2 ATP molecules, whereas aerobic metabolism generates a net product of 36 ATP molecules.

Failure of oxygen supply, such as during ischaemia or hypoxia, means that metabolism cannot follow the aerobic pathway summarised in figure 1.5. Production of pyruvate from

1. INTRODUCTION

glucose generates 2 ATP molecules and does not require oxygen, but it does require NAD^+ and therefore eventually the process would stop if NAD^+ is not regenerated. Instead, cells switch to anaerobic metabolism, converting pyruvate to lactate, which regenerates NAD^+ , allowing the pathway to run continuously. However, over time, accumulation of lactate in the cells results in a decrease in pH, which eventually inhibits glycolysis. As shown in figure 1.5, the net result of anaerobic metabolism is the production of lactate and 2 molecules of ATP compared with the 36 molecules that would have been produced by the aerobic pathway.

During ischaemia, glucose supply decreases as a result of the lack of blood supply, but its consumption by metabolism increases as anaerobic processes are less efficient than aerobic processes. Similarly, oxygen supply decreases during ischaemia. In ischaemic tissue, removal of pyruvate by the tricarboxylic acid (TCA) cycle is no longer possible because of the lack of oxygen. Pyruvate is instead removed by conversion to lactate by lactate dehydrogenase, causing an increase in lactate, removal of which decreases because of the lack of oxygen.

Critically, ischaemia is characterised by a decrease in glucose and an increase in lactate in the ECS. Measurement of these metabolites *in vivo* allows us to ‘listen’ to the cells work in real time.

1.4 Methods of *in vivo* monitoring

In this thesis I am considering new methods for monitoring transplant organs, free flap surgery and exercising athletes. The suitability of a particular *in vivo* chemical measurement method for these applications depends on a number of factors. Tissue ECS consists of a variety of chemicals, spanning a range of concentrations. Therefore, *in vivo* chemical analysis methods are required to meet strict demands in terms of selectivity, sensitivity and dynamic range (5). As a result of the heterogeneity of tissue, spatial resolution is important. Moreover, temporal resolution is critical for measurement of dynamic changes. In addition, for clinical monitoring, the method has to meet strict sterility considerations. A variety of non-invasive and invasive techniques exist for *in vivo* monitoring, an overview of which will be discussed in this section.

Non-invasive *in vivo* monitoring methods include near-infrared spectroscopy (NIRS), which can be used for greater depths than can typically be employed with conventional imaging techniques, as tissue absorption is lower at these wavelengths of light. NIRS measures oxygen levels via oxyhaemoglobin and de-oxyhaemoglobin levels (6) and therefore cannot be used to measure levels of other metabolites. Functional magnetic resonance imaging (fMRI) is another example of a non-invasive monitoring technique. However, this method has poor spatial resolution and the temporal resolution is not good enough for the

applications covered in this thesis. Moreover, practical considerations make this method particularly unsuitable for continuous monitoring of cyclists during exercise, or during free flap surgery, because of the large equipment that is necessary. One study has gone beyond conventional magnetic resonance imaging (MRI) techniques, employing nanoswitches for continuous monitoring of analytes including glucose (7). These nanoswitches maintain an equilibrium between dispersed nanoparticles (low- T_2) and a microaggregate state (high- T_2) that is mediated by binding proteins. The position of the equilibrium is dependent on analyte concentration. When in the MRI machine, the sensor emits a radio frequency signal that reflects its chemical environment. An advantage of MRI is that the magnetic field and emitted radio frequency radiation penetrates tissue well. However, this monitoring method still requires a large MRI machine, which is impractical for continuous monitoring. In addition, concerns regarding potential toxicity of injected nanoparticles means that this method is unsuitable for clinical applications.

Optical imaging techniques can provide a versatile and non-invasive method of *in vivo* monitoring in clinical practice. Optical coherence tomography (OCT), in which the skin is irradiated with coherent light and the back-scattered radiation is recorded, has been used to measure subcutaneous glucose levels (8). However, in this study it was found that changes in glucose concentration detected by OCT were maximal in the dermis and that changes were not detected in the epidermis and the upper dermis layers. In addition, OCT is sensitive to the pressure applied to the probe (9). Fluorescence sensing can provide a non-invasive/minimally invasive method of analyte detection (10, 11). In particular, near-infrared fluorescence imaging can achieve greater penetration depths (mm to cm) than conventional fluorescence techniques (12). Subcutaneously injected fluorescent nanosensors for detection of glucose and ions have been developed and tested in mice (13, 14). Nanosized photonic explorers for bioanalysis with biologically localised embedding (PEBBLES) encapsulate an analyte-specific dye and a reference dye within an inert matrix (15, 16) and provide information regarding intracellular analyte concentrations. The sensors are encapsulated inside a matrix and are therefore protected from interferences. As a result of their small size, they do not disrupt the cell environment a great deal and they offer versatility in accommodating different sensing needs. Studies have demonstrated their use for sensing glucose (17), oxygen (18, 19), potassium (20), pH and calcium (21). However, these sensors have several drawbacks, as the cytotoxicity of the dyes may interfere with cellular processes. Moreover, photons can only penetrate tissue to a finite depth (typically 500 μm), limiting the applicability of these sensors for *in vivo* use (22). Imaging agent toxicity is a major concern for these techniques and prohibits their use clinically.

Implanted methods are still most commonly used for *in vivo* monitoring. These include implantable sensors and tissue sampling methods, which will be discussed in more detail

1. INTRODUCTION

in the following sections.

1.4.1 Implantable sensors

Implantable sensors have been widely used to measure metabolism in animal models (23, 24, 25, 26, 27), and subcutaneous needle-type glucose biosensors have been reported for continuous monitoring of diabetic patients (28, 29, 30, 31, 32).

Implantable biosensors are particularly attractive for *in vivo* chemical measurements as they have high temporal (10 ms) and spatial (tens of μm^3) resolution, although this varies depending on the particular sensor and can be considerably lower (33). Their small size means that tissue damage caused by their insertion is minimal (34, 35). Implantable sensors have been used to detect a wide range of analytes, including oxygen (25, 36), lactate (37, 38, 39, 40), glucose (23, 26, 29, 40, 41), pyruvate (40), glutamate (42) and adenosine (43).

Although guidelines exist for validation of *in vivo* chemical sensors (44), there are many challenges associated with implantable sensors (45, 46, 47, 48), such as issues with selectivity, *in vivo* calibration, biofouling and sterility. These will be discussed in more detail below.

Biosensors are used for the detection of non-electroactive chemicals and consist of a biorecognition element, such as an enzyme, and a transduction component, such as an electrode (45). Biosensors typically require application of a high potential for amperometric detection of the enzyme reaction product. However, oxidation of other electroactive chemicals, such as ascorbic acid, can contribute to the overall signal and can compromise the accuracy of the measurement. As a result, considerable research has been dedicated to strategies to minimise electroactive interference (46). Approaches to improve selectivity include coating the electrode with an exclusion film (49, 50, 51), which excludes interferent molecules on the basis of size or charge, entrapment of ascorbate oxidase and use of a sentinel electrode for subtraction of interferent signals (24, 52, 53, 54).

A major challenge associated with implantable biosensors is the issue of calibration. Typically, *in vitro* calibration of the sensor is carried out before and after implantation in order to interpret sensor response during implantation. However, these sensors generally show a significant decay in sensitivity during implantation and therefore *in vitro* calibrations are unlikely to accurately represent the *in vivo* response of the sensor (46, 55). The loss in sensitivity is caused by fouling of the electrode surface as a result of adherence of proteins, as shown in figure 1.6, blocking catalytic sites and impeding analyte diffusion (56, 57, 58). Over long implantation times (3 days), an inflammatory response occurs, resulting in encapsulation of the sensor (29, 55, 57), which creates an issue for long-term stability. Different approaches have been taken to minimise these adverse tissue

reactions, including integration of interfaces that resist biofouling and protein adsorption, co-immobilisation of the anticoagulant heparin (59) and inclusion of nitric oxide-releasing membranes (60).

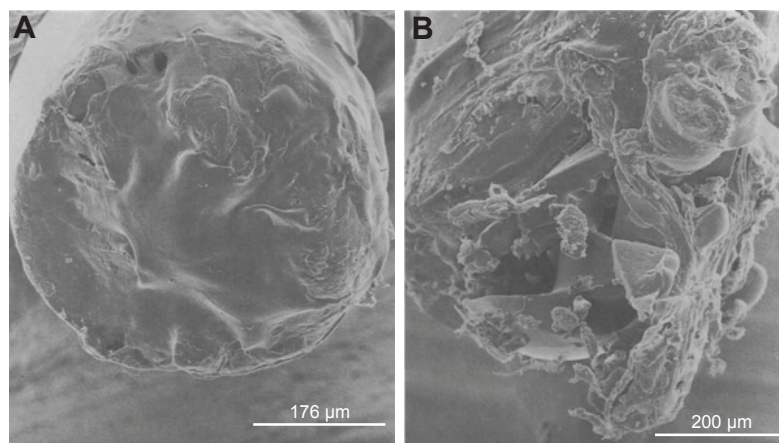


Figure 1.6: Scanning electron micrography images of tip of glucose sensors. Image taken from (29). *A.* Control sensor, soaked in glucose solution, not implanted. *B.* Non-functioning sensor after explantation.

Another possible concern for implantable sensors is that depletion of tissue oxygen, as a result of ischaemia, may affect the sensor response. Studies have shown that biosensors using glucose oxidase are insensitive to oxygen fluctuations, providing glucose concentrations are low (61). For clinical use, sterilisation of implantable biosensors without damaging the enzyme activity is also an issue (45, 62, 63).

1.4.2 Tissue sampling

An alternative approach to using implanted microsensors is to sample the ECS. Two tissue sampling methods considered here are reverse iontophoresis and microdialysis.

Reverse iontophoresis has been applied for extraction of glucose and lactate from human subjects (64). This involves application of a low electric current between two electrodes across the skin, which induces a flow of molecules across the dermis. However, poor correlation was found between blood levels and extracted levels (64). The Glucowatch used reverse iontophoresis coupled with *ex vivo* sensing for continuous glucose monitoring (65). However, the device was associated with skin irritations and was withdrawn from the market in 2008.

Alternatively, tissue sampling can be carried out using microdialysis, which is a well-established clinical technique, in part because of the availability of Food and Drug Administration (FDA)-approved and CE-marked sterile microdialysis probes. The technique is described in more detail in section 1.5.

1. INTRODUCTION

Microdialysis classically provides worse temporal and spatial resolution (typically 600 s and 0.1 mm^3 , respectively) compared with microsensors (33). However, by coupling to sensitive analytical techniques, the temporal resolution has been greatly improved (33). In addition, the tissue damage caused by insertion of the microdialysis probe is much greater than for smaller sensors (34, 35). Microdialysis results in greater flux and removal of more analyte from the tissue compared with implanted electrodes, although at lower flow rates this effect is less (see section 1.5.1).

Microdialysis can be coupled to various analytical techniques, including mass spectrometry (66), capillary electrophoresis (67, 68) and electrochemical sensors (69). This allows detection of multiple analytes in one sample with high sensitivity and selectivity. Sampling of the tissue using a semi-permeable membrane results in exclusion of large molecules such as proteins, which might otherwise foul the sensor.

A significant advantage with using microdialysis is that analysis is carried out away from the tissue, removing the need for sterility considerations. Furthermore, the dialysate samples are free of viruses and prions, so are safe to handle. This has meant that, to date, microdialysis has dominated clinical practice compared with implanted biosensors. Microdialysis will be described in more detail in the following section.

1.5 Microdialysis

A microdialysis probe consists of two lengths of concentric microbore tubing, surrounded by a semi-permeable membrane at the tip. This allows exchange of low molecular weight molecules between the probe and the extracellular fluid, according to their concentration gradients (70). The probe is continuously perfused with a physiological solution, which closely matches the ionic composition of the extracellular fluid, removing any diffusional flux of these ions. Perfusion flow rates are typically in the range of $0.1\text{-}3.0 \mu\text{l}/\text{min}$. This creates a concentration gradient across the membrane for ECF species not in the perfusate and results in diffusion of analytes from the ECF across the membrane and into the probe lumen down their concentration gradient, as shown in figure 1.7 by the pink arrows. This generates a constant flux of dialysate that can be analysed for compounds of interest.

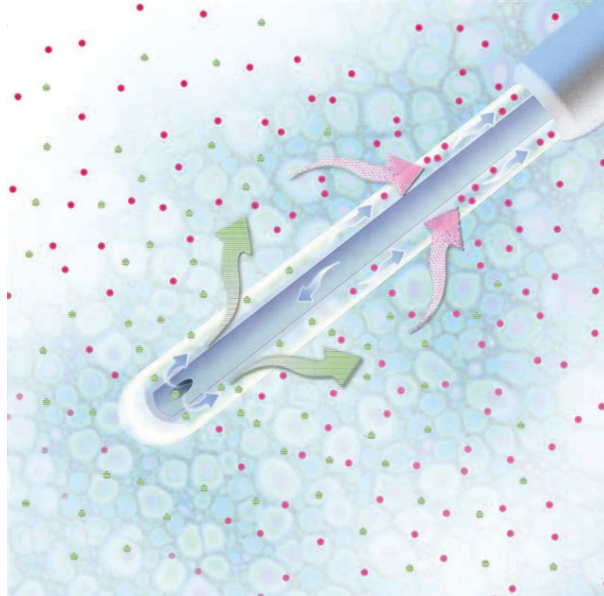


Figure 1.7: Microdialysis probe. The inner tube is perfused with a physiological solution, which flows past the semi-permeable membrane at the tip. Diffusion of molecules below the molecular weight cut-off occurs between the probe and the tissue according to concentration gradients. The dialysate stream flows out of the outlet tubing for analysis. Image from CMA Microdialysis.

1.5.1 Recovery

When a perfused microdialysis probe is placed in a sample, the analyte concentration in the dialysate (C_{out}) will be less than that in the sample (C_{ext}). The ratio is known as the relative recovery (R) and is often expressed as a percentage, as shown in equation 1.7.

$$R = \frac{C_{out} - C_{in}}{C_{ext} - C_{in}} \times 100 \quad (1.7)$$

Where C_{in} is the concentration of analyte in the perfusion medium, C_{out} is the concentration of analyte in the dialysate and C_{ext} is the concentration of analyte in the tissue.

The relative recovery depends on a number of factors, including perfusion flow rate, temperature, membrane size and molecular weight cut-off (71, 72).

The relative recovery of the microdialysis probe can be measured *in vitro* by placing the probe into a vigorously stirred solution of known concentration and measuring the concentration in the dialysate. However, this *in vitro* measurement of the relative recovery cannot simply be extended to *in vivo* measurements as molecules have to diffuse through the tortuous extracellular environment to reach the probe, compared with the unimpeded diffusion of the analyte *in vitro* (73, 74). Rates of uptake and release mechanisms also contribute to the deviation of the *in vivo* recovery from that measured *in vitro* (75, 76). This effect is demonstrated in figure 1.8.

1. INTRODUCTION

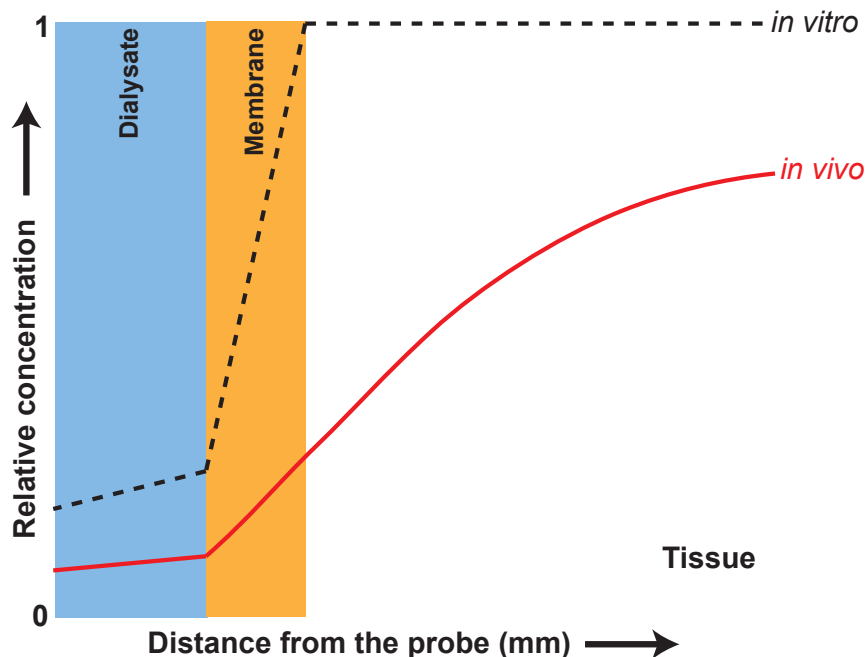


Figure 1.8: Recovery of a microdialysis probe *in vitro* and *in vivo*. The dotted line indicates the concentration profile of analytes in a well-stirred beaker. The red line indicates the concentration profile in tissue. Image adapted from (73).

Reducing the flow rate at which the probe is perfused leads to a higher relative recovery, as there is greater time for an equilibrium to be established between the solution inside the probe and the extracellular fluid. The true tissue concentration *in vivo* can be measured by setting the recovery to 100%, either by increasing the membrane size or by reducing the flow rate (73). Alternatively, a no-net-flux experiment can be used to determine the extracellular fluid concentration and the probe recovery by varying C_{in} to determine the concentration at which there is no overall movement of molecules across the probe membrane (77). However, this method assumes the recovery is constant but this is not always the case as a result of tissue damage (75, 76, 78, 79, 80, 81). Finally, the recovery can be measured in the tissue in real time using a reference compound, as has been done in the brain using urea (82).

It is possible to calculate the amount of analyte removed from the tissue by a microdialysis probe, using equation 1.8.

$$J = QC \tag{1.8}$$

Where J is the flux to the microdialysis probe, Q is the perfusion flow rate and C is the analyte concentration in the dialysate at the probe outlet.

For a probe perfused at $2 \mu\text{l}/\text{min}$ and a dialysate concentration of 1 mM , the flux is $33 \text{ pmol}/\text{s}$. The removal of analyte from the tissue by microdialysis varies with flow rate

and would be less at lower flow rates. It is interesting to compare the amount of analyte removed from the tissue using a microdialysis probe with that removed by an implanted biosensor. This can be calculated using equation 1.9.

$$J = \frac{i}{nF} \quad (1.9)$$

Where i is the current for a given concentration, n is the number of electrons per oxidised molecule of hydrogen peroxide and F is the Faraday constant.

For a typical glucose biosensor (see section 3.3), the amount of hydrogen peroxide consumed, which is assumed to be directly proportional to the amount of glucose consumed, for a 1 mM concentration is 0.927 fmol/s, which is considerably smaller than that removed using microdialysis. However, because of the differences in size of the two measurement devices, the amount of glucose per unit area enables better comparison between the two methods. Factoring in area, the microdialysis probe (0.6 mm outer diameter (OD) membrane, 10 mm length) removes 175 pmols⁻¹cm⁻², whereas the glucose biosensor removes 33.1 pmols⁻¹cm⁻². Therefore, the microdialysis sampling has a 5-times greater effect on the tissue being measured than the implanted biosensor.

1.5.2 Tissue damage

Probe insertion results in trauma to the surrounding tissue, including oedema (83), inflammation (84, 85) and gliosis (35, 83), as a result of the relatively large dimensions (clinical microdialysis probes are typically 0.6 mm OD). Studies have shown that tissue damage is affected by probe dimensions (86), material (83), sterility (87) and perfusion fluid (88).

Initial studies investigating this tissue damage showed that blood flow and glucose metabolism decreased during the first 2 hours after probe insertion but returned to near normal levels within 24 hours (89). As a result, researchers typically allow a period of stabilisation after probe insertion of 1-24 hours (33, 90).

However, recent studies have shown that ischaemic disruption is still evident 24 hours after probe implantation, although it is reduced compared with that after 4 hours (35). In fact, glial encapsulation of the microdialysis probe is still present 5 days after insertion, as shown in figure 1.9. In another study, tissue disruption was observed up to 1.4 mm away from the probe site 40 hours after probe insertion (91). Therefore, microdialysis samples injured tissue, even after a stabilisation period (35).

Interpretation of microdialysis results can be complicated by the tissue damage associated with probe insertion. The relationship between dialysate and tissue concentrations is affected by the thickness of the damaged tissue surrounding the probe (92). However,

1. INTRODUCTION

under carefully controlled conditions, microdialysis can still provide valid measurements (33, 93).

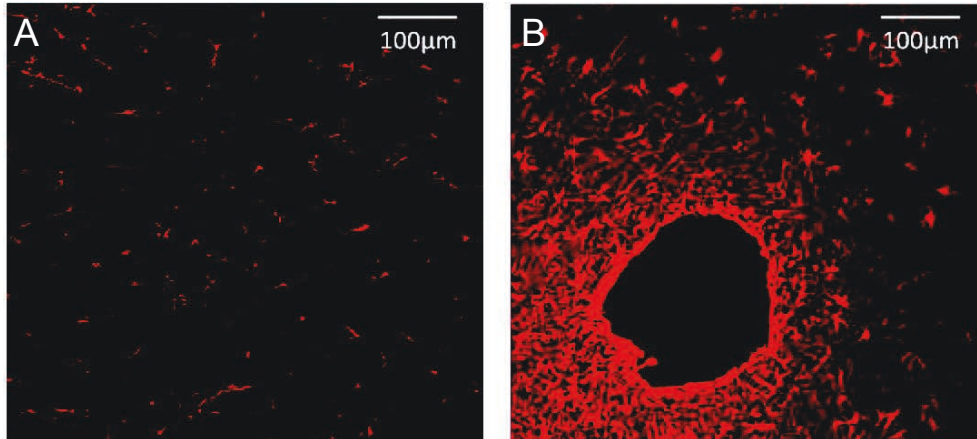


Figure 1.9: Effect of microdialysis probe on glial cells. Image taken from (94). Glial cells were stained with glial fibrillary acidic protein (GFAP) marker and were imaged using fluorescence microscopy. *A.* Brain tissue from non-implanted tissue. *B.* Tissue next to a microdialysis probe track showing glial barrier formed after 5 days of microdialysis.

1.5.3 Offline analysis

Conventional microdialysis involves discrete collection of dialysate samples into microvials for analysis offline. As a result of the low flow rates used, the time taken to collect sufficient volume per sample is typically 30-60 minutes. The sample therefore represents an average of the dialysate levels over the collection period. This method has poor temporal resolution and leads to a delay in information regarding the condition of the tissue. As a result, offline microdialysis is not suitable for resolving dynamic metabolic changes.

1.5.4 Online analysis

Online microdialysis offers many advantages over offline methods. Online analysis removes the need for separate sample collection and analysis and facilitates improved time resolution. Moreover, results can be displayed in real time, which is particularly important for providing important clinical feedback for staff during hospital monitoring.

Rapid sampling microdialysis (rsMD) has been extensively used to monitor changes in glucose and lactate levels in the brain (95, 96, 97, 98), bowel (99) and muscle (100) during surgery and postoperatively. This technique is described in more detail in section 2.3 and is used in chapters 4-7. It offers improved temporal resolution compared with offline techniques, as the dialysate flows directly into a flow injection analysis system, enabling sampling every 30 seconds.

Recent work in the Boutelle group has led to the development of microelectrode biosensors for online analysis of dialysate. These online biosensors offer improved temporal resolution compared to rsMD, as they allow continuous measurement of metabolites. Online biosensors positioned in a PDMS chip have been used in animal studies to monitor glucose and lactate in brain dialysate (69). Microelectrode biosensors are described in more detail in section 2.5 and are used in chapters 3, 5, 7 and 8.

The fairly low microdialysis flow rates used results in a lag time between the changes occurring in the tissue and their detection, as shown in figure 1.10. At a flow rate of $2 \mu\text{l}/\text{min}$ this delay is approximately 12 minutes. Laminar flow inside the long connection tubing also leads to a smearing of the concentration change, because of Taylor dispersion (101), which is best characterised by T_{90} (90% response time). The lag time and response time (T_{90}) for a concentration change in the fluid stream after it has flowed down 1 m of connection tubing is demonstrated in figure 1.10.

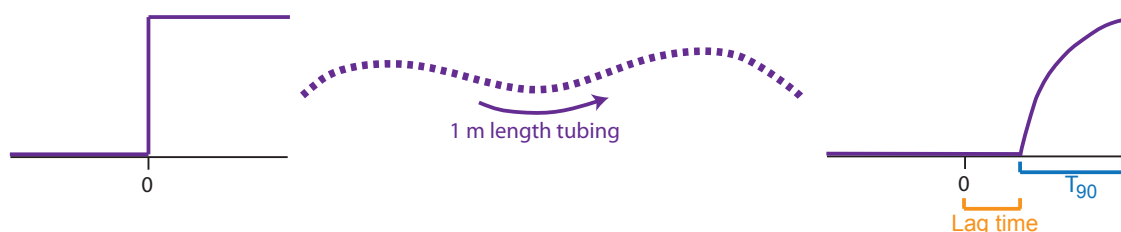


Figure 1.10: Schematic of response caused by 1 m of connection tubing. The slow flow rate used results in a lag time between the changes occurring in the tissue and their detection. Taylor dispersion causes a smearing of the concentration change, characterised by the T_{90} response.

Taylor dispersion occurs as fluid moves slower at the walls as a result of friction, leading to a non-uniform velocity profile across the cross-sectional area, as shown in figure 1.11A. This non-uniform velocity profile causes a concentration gradient perpendicular to the direction of flow, which results in diffusion of the analyte across the width of the channel, leading to smearing of the concentration step change, as shown in figure 1.11B.

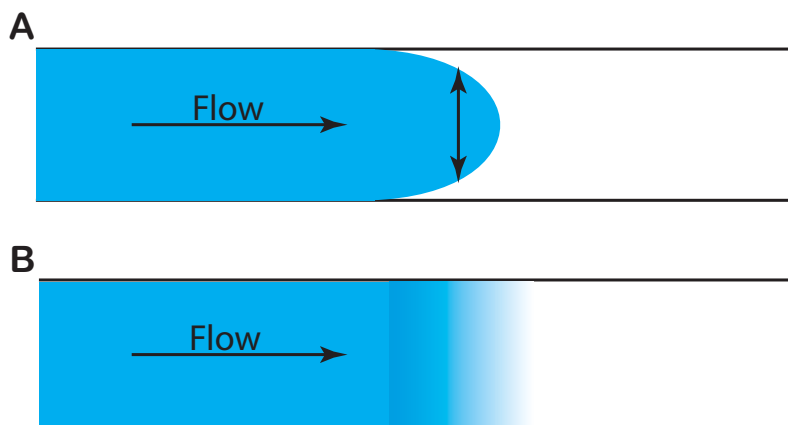


Figure 1.11: Taylor dispersion. *A.* Velocity profile of liquid flow inside the connection tubing. A concentration step change is shown from white to blue. *B.* Diffusion of analyte perpendicular to the flow leads to smearing of the step change.

1.6 Thesis outline

Common methods and materials are described in chapter 2, together with an overview of the current rsMD analysis system. Fabrication of combined needle electrodes and the method for making glucose and lactate biosensors are also described.

Chapter 3 describes the development of analysis methods used throughout this thesis from the starting point of chapter 2. The performance of the glucose and lactate biosensors is discussed. It was necessary to extend the dynamic range of the lactate biosensor to make it suitable for measuring physiological levels, therefore the addition of a diffusion-limiting polyurethane film is described. The development of an autocalibration system is discussed, which was built using LabSmith programmable components. This system can be used with both the rsMD system and online biosensors in a microfluidic chip. LabSmith components were also used to develop an in-flow enzyme addition biosensing system for glucose and lactate. This methodology was used to develop a microfluidic analysis board to monitor glucose and lactate in two dialysate streams. In proof-of-concept experiments, the in-flow enzyme addition system was implemented for more complicated analysis systems such as detection of ATP and pyruvate. Finally, a novel method of collecting dialysate samples in storage tubing for delayed analysis while retaining temporal resolution is demonstrated.

Chapter 4 describes the use of the rsMD system to monitor lactate levels in porcine kidneys during two clinical methods of cold preservation, static cold storage and hypothermic machine perfusion, and subsequent warming. Dialysate lactate levels are compared between the two preservation methods and between two regions of the kidney, the cortex and the medulla. Chapter 5 shows a series of preliminary studies extending this method-

ology to include monitoring of glucose in addition to lactate and to monitor transplant organs immediately after retrieval. Preliminary experiments are also presented in which the online rsMD system is used to evaluate factors that may affect kidney health. In addition, measurements using discarded human kidneys are described, as well as monitoring of porcine and human transplant pancreases.

In chapter 6, the rsMD system is implemented for tissue monitoring during free flap surgery, in which tissue is transplanted from one area of the body to another. Glucose and lactate levels were measured to observe tissue ischaemia when the blood supply was cut and a return to normal levels after successful re-attachment at the recipient site. Metabolite levels were also monitored afterwards during recovery in the intensive therapy unit (ITU) to identify flap failure in the crucial time period after surgery.

In chapters 7 and 8, a system to monitor subcutaneous metabolite levels in cyclists during exercise is developed. Chapter 7 describes preliminary experiments using rsMD and on-chip biosensors to define the scope of the analytical problem. In chapter 8 the development of a 3D printed microfluidic chip, which connects directly to the outlet of a microdialysis probe and incorporates glucose and lactate biosensors is discussed. Finally, a proof-of-concept study is described in which the wearable analysis system is coupled to wireless potentiostats and is implemented during cycling trials.

Chapter 9 concludes the thesis and describes possible future work.

1. INTRODUCTION

Chapter 2

Methods & materials

2.1 Electroanalytical techniques

2.1.1 Cyclic voltammetry

Cyclic voltammetry is a commonly used electrochemical technique, in which the potential at the working electrode is ramped linearly versus time, at a given scan rate. When the working electrode potential reaches a set value, the ramp is inverted and the potential is scanned in the reverse direction. Figure 2.1 shows an example of a cyclic voltammogram (CV) obtained using a platinum (Pt) disc electrode (50 μm diameter) in 1.5 mM ferrocene monocarboxylic acid solution (Fc) versus a Ag|AgCl reference electrode, at a scan rate of 10 mV/s. In this example, as the potential is scanned in the positive direction, Fc is oxidised to Fc^+ , giving rise to an increased current. As the potential becomes more positive the electrode kinetics for the oxidation reaction become more favourable and the current rises until a maximum is reached. At this potential, the current is controlled by the rate at which the species can diffuse to the electrode surface from the bulk solution. As the scan direction is reversed, Fc^+ is reduced back to Fc, as the reaction is reversible, producing a decrease in current.

For macroelectrodes, an oxidation peak in the current is observed, after which the current falls since the depletion zone around the electrode increases as oxidation proceeds, and hence the Fc molecules have further to diffuse to reach the electrode surface. A reduction peak is also observed on the reverse scan. The peak current for a macroelectrode depends on the diffusion coefficient, the bulk concentration of the electroactive species, the electrode area, the number of electrons transferred in the redox reaction and the scan rate. This is described by the Randles-Sevcik equation, given in equation 2.1.

$$i_p = (2.69 \times 10^5) n^{\frac{3}{2}} A D^{\frac{1}{2}} \nu^{\frac{1}{2}} C \quad (2.1)$$

2. METHODS & MATERIALS

Where i_p is the peak current, n is the number of electrons transferred, A is the electrode area, F is the Faraday constant, D is the diffusion coefficient, C is the concentration and ν is the scan rate. The equation assumes the solution is at 25°C.

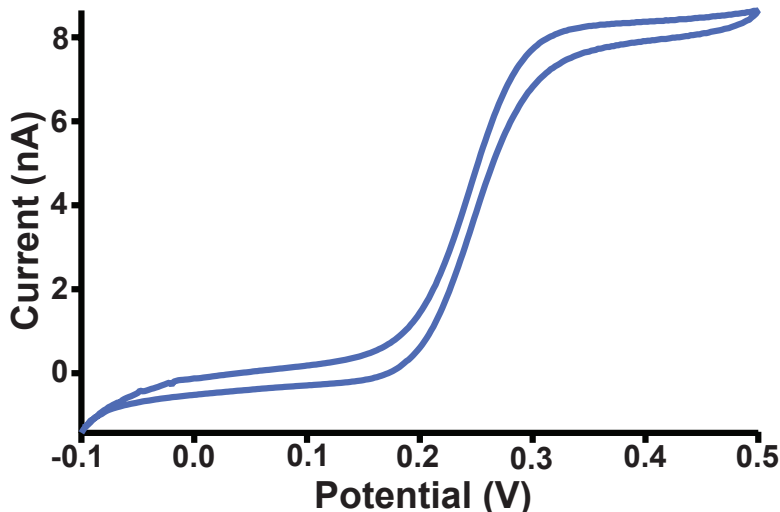


Figure 2.1: Cyclic voltammetry. A typical CV obtained using a 50 μm platinum disc electrode in 1.5 mM Fc solution, scanned at 10 mV/s from -100 mV to 500 mV.

Diffusion to a macroelectrode takes place normal to the electrode surface, and the diffusion layer is small compared with the size of the electrode. However, because of the smaller dimensions of a microelectrode, edge effects dominate and the diffusion field is hemispherical, exceeding the electrode dimensions. This leads to enhanced flux to the electrode under near steady-state conditions, so that current peaks are not observed, as shown in figure 2.1. For a microdisc electrode, with radius r , the steady-state limiting current, I_{lim} , is given by equation 2.2.

$$I_{lim} = 4nFDrC \quad (2.2)$$

CVs were carried out using a three-electrode system and in-house potentiostats and were controlled using EChem software (eDAQ, UK). In this thesis cyclic voltammetry is used to assess the electrodes and their surface characteristics, as described in section 2.5.2.

2.1.2 Amperometry

Amperometry is an electrochemical technique in which the working electrode is held at a constant potential and the resulting current is measured over time. This technique is used throughout this thesis to measure the concentration of analytes in a sample. When the rapid sampling microdialysis (rsMD) system is used, the potential is held at 0 V and the

current resulting from the reduction of Fc^+ to Fc is measured, as shown in figure 2.6. An increase in the reduction current corresponds to an increase in analyte concentration. For non-mediated biosensing mechanisms where the concentration of analyte is proportional to the concentration of its enzymatic reaction product, hydrogen peroxide, the potential is held at +0.75 V and the oxidation current is measured. An increase in the oxidation current corresponds to an increase in hydrogen peroxide and hence in analyte concentration in the sample. Amperometric techniques were carried out using a three-electrode system and in-house potentiostats and were controlled using LabChart software (ADInstruments, New South Wales, Australia).

Electropolymerisation

Electropolymerisation is an amperometric technique in which a constant potential is applied to a working electrode placed in a solution of a particular monomer to initiate a polymerisation reaction. This technique is used throughout this thesis to coat the working electrode with either a poly(phenol) film or a poly(m-phenylenediamine) (mPD) film, as described in section 2.5.3. An example of a typical electropolymerisation trace is shown in figure 2.2.

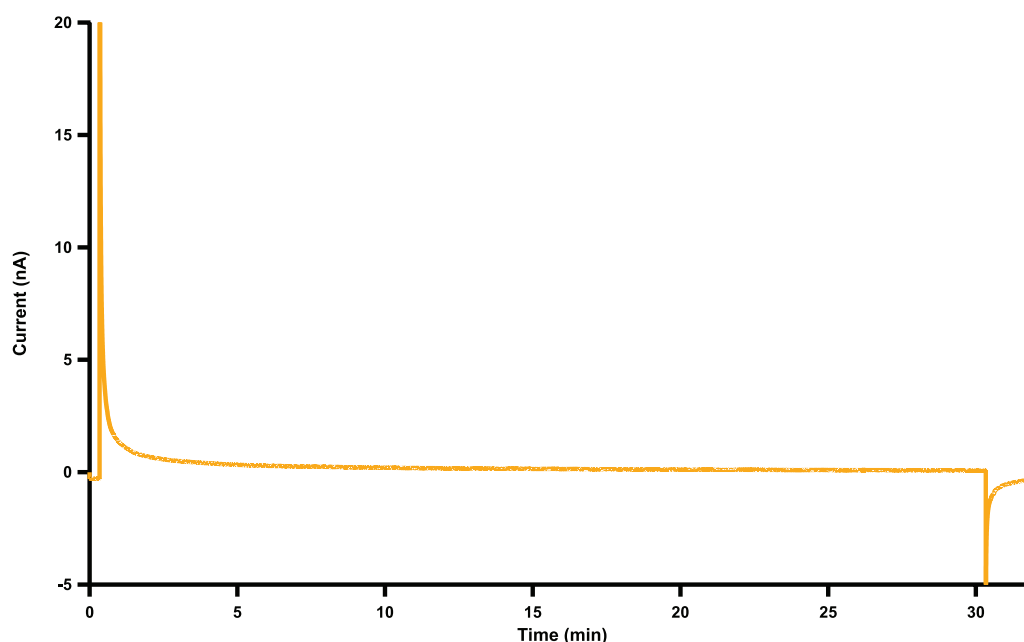


Figure 2.2: Electropolymerisation. A typical electropolymerisation trace seen during phenol polymerisation at a $50 \mu\text{m}$ platinum electrode. The electrode was placed in a solution of 50 mM phenol in PBS. The potential was held at 0 V for 20s, 0.9 V for 30 min and 0V for 1 min.

2. METHODS & MATERIALS

2.2 Microdialysis

2.2.1 Microdialysis probes

Different microdialysis probes were used for each application. A summary of the probes used is given in table 2.1. For kidney and pancreas experiments, where sterility was not an issue, flexible MAB11.35.4 animal probes (Microbiotech, Stockholm, Sweden) were used. These probes have a 6 kDa molecular weight cut-off and a 4 mm membrane length. Probes were re-used between experiments, but were checked prior to use to confirm they were functioning well (see section 4.2). Two microdialysis probes were inserted into each kidney: one into the cortex and one into the medulla. The cortex probe inlet tubing was connected to a syringe pump (CMA 400 pump, CMA Microdialysis, Stockholm, Sweden) and perfused with a physiological solution, T1 (see table 2.2 for details) at 2 $\mu\text{l}/\text{min}$. The medulla probe inlet tubing was connected to another syringe pump and perfused with T1 solution at 1 $\mu\text{l}/\text{min}$. For pancreas experiments, the probes were perfused at 2 $\mu\text{l}/\text{min}$.

Clinical microdialysis probes were used for monitoring during free flap surgery (CMA 70, MDialysis, Sweden) and during cycling (CMA 63, MDialysis, Sweden) to ensure sterility. These probes both have a 20 kDa molecular weight cut-off and a 10 mm membrane length. The probe inlet tubing was connected to a portable syringe pump (CMA 107, MDialysis, Sweden) and perfused with sterile T1 perfusion solution (MDialysis, Sweden) at 2 $\mu\text{l}/\text{min}$ for free flap surgery and at 1-5 $\mu\text{l}/\text{min}$ for cycling experiments.

Table 2.1: Summary of microdialysis probes used for each application.

	MAB11.35.4	CMA 70	CMA 63
Application	kidney/pancreas	free flap	cycling
Membrane length (mm)	4	10	10
Membrane outer diameter (mm)	0.6	0.6	0.6
Molecular-weight cut-off (kDa)	6	20	20
Membrane material	polyethersulphone	polyamide	polyarylethersulphone

2.2.2 T1 perfusion solution

T1 solution was used to perfuse the microdialysis probes to mimic the tissue ionic concentration. The composition of this solution is given in table 2.2. For human studies, sterile T1 solution (MDialysis, Sweden) was used.

2.3 Rapid sampling microdialysis (rsMD)

Table 2.2: Composition of T1 perfusion solution

Chemical	Concentration (mM)
Calcium chloride	2.3
Sodium chloride	147
Potassium chloride	4

2.3 Rapid sampling microdialysis (rsMD)

RsMD is a flow injection analysis system that combines sample collection and analysis, and allows for sampling of metabolites with high temporal resolution in real time. This system has been used clinically to monitor changes in glucose and lactate levels in the brain and the bowel during surgery and postoperatively (92, 95, 96, 97, 99).

2.3.1 Injection valve

The dialysate stream is connected to a custom-made 6-port flow injection valve (Valco, Switzerland), which injects a sample of the dialysate into a stream of mediator and through the assay at regular intervals. The flow injection valve used initially contained 200 nl sample loops but, in some cases, when this valve was not available, a 60 nl sample loop valve was used instead. However, this type of valve was found to fail after repeated use and after consultation with Valco we designed a new 100 nl dual-internal loop Cheminert valve, as shown in figure 2.3, which is more suitable for the purpose.

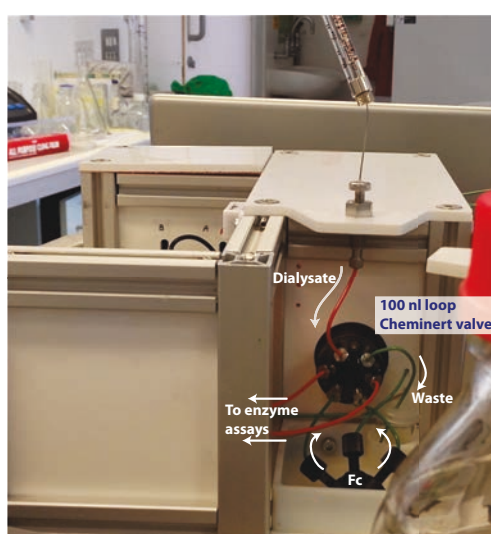


Figure 2.3: RsMD Cheminert flow injection valve. The new Cheminert valve was housed in a custom-made enclosure. The photograph shows the setup for analysis of glucose and lactate in one dialysate stream.

2. METHODS & MATERIALS

The system can be set up in two configurations depending on the application: the system can be configured to analyse one dialysate stream for two metabolites or to analyse two dialysate streams for one metabolite only.

2.3.1.1 One dialysate stream, two analytes

In this configuration, the rsMD system can be used to monitor the dialysate from one microdialysis probe for both glucose and lactate levels. The outlet of the microdialysis probe is connected to the sample loop of the 6-port internal loop valve. A high-performance liquid chromatography (HPLC) pump (Rheos 2000, Flux Instruments, Basel, Switzerland) is used to flow a filtered analysis Fc mediator solution (see table 2.5 for details) at $200 \mu\text{l}/\text{min}$ into a T-connector, which splits the stream equally into two analysis loops of the valve, as shown in figure 2.4. Every 30 seconds a dialysate sample is automatically injected alternately into one of the two analysis flow streams. Each analysis stream accelerates the dialysate through an enzyme reactor, containing the appropriate enzymes, to a downstream electrode, which detects a reduction current. The mechanism for this reaction is described in figure 2.6.

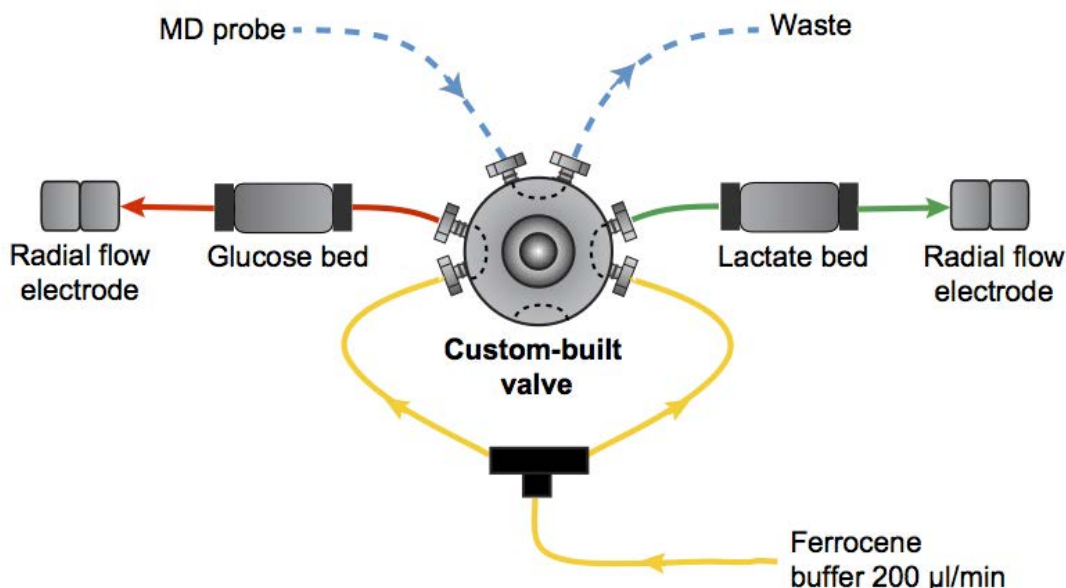


Figure 2.4: RsMD setup for measurement of glucose and lactate in one dialysate stream. The microdialysis (MD) probe outlet is connected to the sample loop of the flow injection valve. Every 30 s a dialysate sample is injected alternately into each analysis flow stream. The dialysate sample flows through an enzyme reactor that contains two consecutive membranes, the first loaded with substrate oxidase and the second with horseradish peroxidase (HRP), to a glassy carbon electrode held at 0 V. The reactions are mediated by Fc.

2.3.1.2 Two dialysate streams, one analyte

I developed this configuration for use in the transplant kidney studies (chapters 4 and 5). In this configuration, the rsMD system can be used to simultaneously measure the metabolite concentration of either glucose or lactate in two dialysate streams. In all cases where this configuration was used the metabolite that was chosen to be measured was lactate. The outlet tubing of each microdialysis probe is connected to a separate sample loop of the flow injection valve, either side of the analysis loop, as shown in figure 2.5. The Fc analysis solution is pumped by an HPLC pump at $100 \mu\text{l}/\text{min}$ into the analysis loop of the valve. Every 30 seconds a dialysate sample is injected into the analysis flow stream, alternating between the two dialysate streams. The dialysate sample is accelerated by the analysis stream through a lactate enzyme reactor to a downstream electrode that detects a reduction current, as shown in figure 2.6.

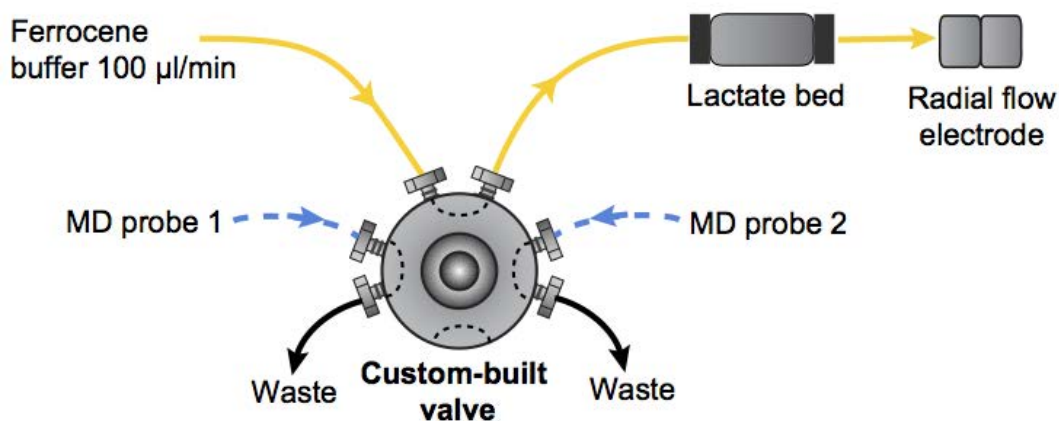


Figure 2.5: RsMD setup for measurement of lactate in two dialysate streams. The microdialysis (MD) probe outlets are connected to the flow injection valve of the rsMD system, either side of the analysis loop. Every 30 s a dialysate sample is injected into the analysis flow stream, alternating between each dialysate stream. The dialysate sample flows through an enzyme reactor that contains two consecutive membranes, the first loaded with lactate oxidase (LOx) and the second with horseradish peroxidase (HRP), to a glassy carbon electrode held at 0 V. The reaction is mediated by Fc.

2.3.2 Enzyme reactors

Dialysate samples are injected into a Fc mediator flow stream and pumped through immobilised dual-enzyme reactors to a downstream electrode for detection of glucose or lactate. These enzyme reactors consist of two nitrocellulose membranes (6 mm diameter discs) loaded with enzyme, held inside a reactor made from inline biocompatible filter components, comprising a stainless steel body and two polyether ether ketone (PEEK) filter end fittings (IDEX Health & Science, Germany).

2. METHODS & MATERIALS

To create the immobilised enzyme membranes each enzyme is dissolved in 1 ml of Fc buffer according to the concentrations given in table 2.3 and repeatedly filtered through a nitrocellulose membrane (0.025 μm pore size, 25 mm diameter, Millipore, UK) placed inside a 25 mm filter holder (Swinnex, Millipore, UK). A ring is placed inside the filter holder to create a seal, as the process of loading the enzyme into the membrane is done at high pressure. This ensures the enzyme solution passes through the membrane and does not leak out. The membrane turns a yellow/brown colour, depending on the enzyme, once it has been successfully loaded into the membrane. Several 6 mm discs are then cut from this membrane using a hole punch and are stored in the Fc buffer solution in the fridge to prevent them from drying out.

In assembling the enzyme reactors, two membranes are placed in each reactor, one loaded with the substrate oxidase enzyme (SOx), either glucose oxidase (GOx) or lactate oxidase (LOx), and one loaded with horseradish peroxidase (HRP). The SOx membrane must be placed so that it is the first membrane in the direction of flow, followed by the HRP membrane; if the membranes are placed in the wrong order the reaction will not take place.

When the dialysate sample passes through the first membrane, the SOx catalyses the oxidation of the substrate, producing hydrogen peroxide. This could be detected electrochemically but it would require high electrode potentials and would result in detection of other chemicals present in the dialysate (102). Instead, the second membrane loaded with HRP catalyses the reduction of hydrogen peroxide to water (103). The HRP is regenerated by oxidation of two Fc mediator species, producing ferrocenium ions, which are detected at the electrode by reduction, producing current peaks. The amplitude of these peaks is proportional to the concentration of substrate in the dialysate sample (due to the small sample size). The reaction sequence is shown in figure 2.6.

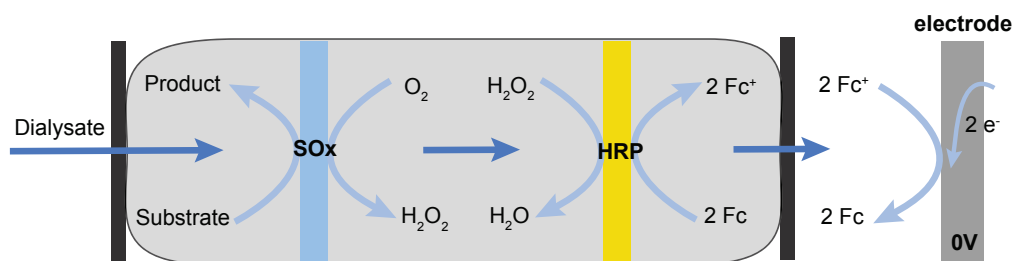


Figure 2.6: Reaction sequence occurring within the immobilised enzyme bed. The dialysate sample is mixed with the Fc and is pumped through two membranes loaded with enzyme, the first with the SOx and the second with HRP. The enzymatic reactions result in the production of 2 ferrocenium ions (Fc⁺), which are detected at the glassy carbon electrode by reduction at 0 V.

The concentration of each enzyme used to load into the enzyme membranes is given

2.3 Rapid sampling microdialysis (rsMD)

in table 2.3. All enzymes were purchased from Sekisui Diagnostics (Kent, UK).

Table 2.3: RsMD membrane enzyme concentration

Enzyme	Activity (units mg ⁻¹)	Concentration (mg ml ⁻¹)
Glucose oxidase (GOx)	244.9	1
Lactate oxidase (LOx)	37	2
Horseradish peroxidase (HRP)	224.9	0.5

2.3.3 Radial flow cell

The electrodes used for detection of the substrate consist of a three-electrode system housed inside a radial flow cell (Unijet, BASi, USA). The flow from the enzyme reactor passes through the stainless steel jet counter electrode to the 3 mm diameter glassy carbon working electrode opposite. An Ag|AgCl reference electrode is also embedded next to the working electrode. The working and counter electrodes are separated from each other by a 16 μm Teflon gasket.

2.3.4 The clinical trolley

The clinical trolley is used in the hospital to hold all the equipment required for the rsMD system. An example of the trolley used for monitoring transplant organs is shown in figure 2.7. The trolley has several shelves to hold the equipment, including the HPLC pump, PowerLab and uninterruptible power supply (UPS), as well as the necessary solutions. A box is attached to a moveable arm that holds the flow injection valve, enzyme beds and potentiostats. This also acts as a Faraday cage.

2.3.5 Calibrating the rsMD system

The system was calibrated at regular intervals by manually injecting known concentrations of glucose/lactate standards into the flow injection valve using a 100 μl Hamilton glass syringe. These injections are seen as current peaks, the amplitude of which is proportional to the concentration of substrate in the sample (due to the small sample size). A calibration curve can therefore be created, relating current to concentration for each substrate.

2. METHODS & MATERIALS

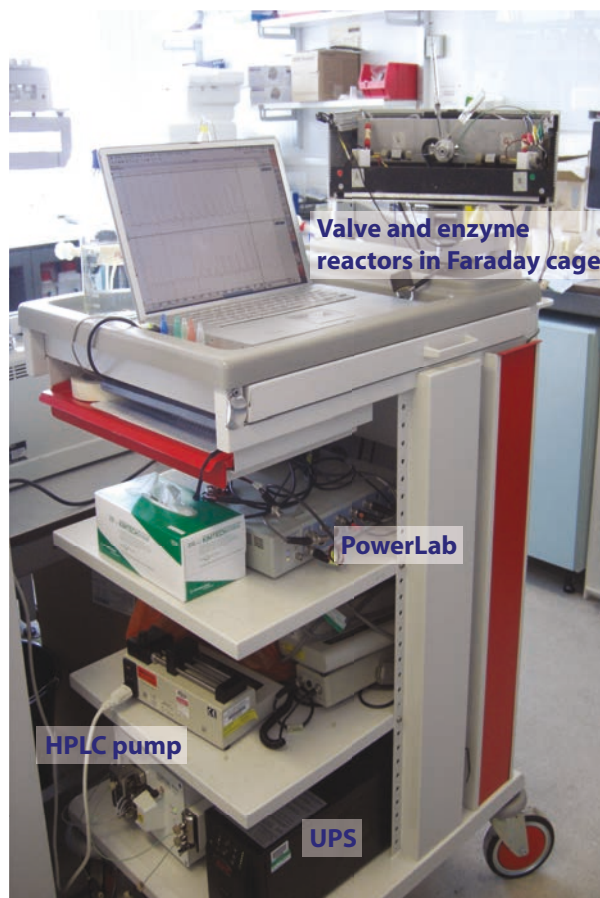


Figure 2.7: The clinical trolley. This holds all the equipment required for the rsMD system.

2.3.6 Data acquisition and analysis

Data presented in chapters 4 and 5 were collected using a PowerLab 8/30 data acquisition unit (ADInstruments, New South Wales, Australia) and Chart 5.6 software (ADInstruments, New South Wales, Australia) running on a Powerbook G4 portable computer (Apple Computers, Cupertino, CA). Data presented in chapter 6 were collected using a PowerLab 8SP and Chart 5.6 software running on a Macbook Pro portable computer. Data presented in chapter 7 were collected using a PowerLab 16/35 and LabChart 7 software running on a Macbook Pro portable computer. Although the PowerLab 8SP is compatible with LabChart 7, when run together the output voltage, which is necessary to switch the flow injection valve, is not supplied. Therefore, when using the PowerLab 8SP, it is necessary to collect data using Chart 5.6. However, when used with a PowerLab 8/30 or 16/35, LabChart 7 does apply the necessary output voltage.

Typically, reduction current peaks were inverted for convenience. Raw rsMD data were processed in MATLAB (MathWorks, USA) using algorithms previously developed in the group to remove common artefacts such as baseline ripples and spikes and to identify

2.4 Microfluidic polydimethylsiloxane (PDMS) chip fabrication

the peaks (104). The current peaks were then converted into analyte concentrations using the appropriate calibration curve. This concentration data were then exported to the graphical package Igor Pro (WaveMetrics, USA) to plot the data and to carry out statistical analysis.

2.3.7 Storage tubing

In some experiments, where online analysis was not possible, dialysate was collected in fine-bore Portex tubing (0.4 mm internal diameter, Smith Medical, UK) for offline analysis. This enabled samples to be collected while retaining temporal resolution for analysis at a later time. For flow rates of 2 $\mu\text{l}/\text{min}$, 63 minutes of dialysate could be collected per 1 m length and, at 1 $\mu\text{l}/\text{min}$, 126 minutes per 1 m length. The ends of each of these lengths of storage tubing were melted to seal them so that the dialysate samples were not lost. They were then stored in the fridge or freezer until they could be analysed. The original direction of flow was noted so that the tubing could be ‘played back’ as if in real time.

2.4 Microfluidic polydimethylsiloxane (PDMS) chip fabrication

Microfluidic chips were fabricated out of polydimethylsiloxane (PDMS, Sylgard 184, Dow Corning, USA), using a master previously fabricated in the group by photolithography. The same master can be re-used multiple times. The PDMS silicone elastomer and curing agent were thoroughly mixed in a 10:1 ratio by weight. The PDMS mixture was poured over the master to a height of approximately half a centimetre. The remaining mixture was poured into a clean petri dish and left to de-gas naturally to be used later as the base. The PDMS in the master was de-gassed using a desiccator. Any air bubbles that remained on the surface after de-gassing were gently removed by blowing air over them using a pasteur pipette. The master was cured in the oven at 65°C for 1 hour. After it had been cured, the PDMS was gently peeled off from the master and cut into single chips using a scalpel. Holes were punched into the PDMS chips for the electrodes and the connection tubing using a blunted needle (20 gauge (20 G) for 1/32” outer diameter (OD) tubing and 25 G electrodes, and 22 G for 360 OD μm tubing and 27 G electrodes). The PDMS base was partially cured at 65°C for approximately 12 minutes. This was tested using a piece of fully cured PDMS; the base should be tacky to touch so that a slight imprint is left from the piece of fully cured PDMS, but not too runny or the channels will be filled when the chips are placed on top. The chips were then placed channel-side down onto the semi-cured base. The two parts were cured together at 65°C overnight.

2.5 Microelectrode biosensors

2.5.1 Needle electrode fabrication

Combined needle electrodes developed previously in the group (69, 105) were used for placement in a miniaturised flow cell. These needle electrodes incorporate all three electrodes needed for an electrochemical cell, the working electrode (WE), the reference electrode (RE) and the counter electrode (CE), as shown in figure 2.8.

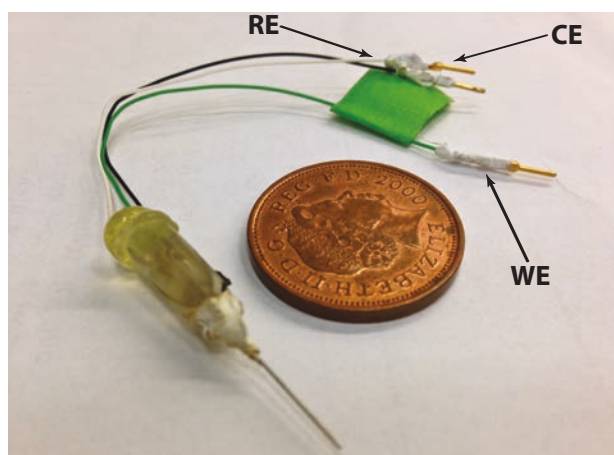


Figure 2.8: Combined needle electrode. 27 G hypodermic needle, which contains a 50 μm platinum wire for the working electrode (WE) and a 50 μm silver wire, is sealed with epoxy resin and polished flat to give disc electrodes. The silver wire is chloridised to give a Ag|AgCl reference electrode (RE) and the stainless steel needle shaft serves as the counter electrode (CE).

A 50 μm diameter polytetrafluoroethylene (PTFE) insulated platinum/iridium (90%:10%) wire (Advent Research Materials, UK) was threaded through a 27 G hypodermic needle to serve as the working electrode. A 50 μm diameter polyester insulated silver wire was also threaded through the same needle to be converted into a Ag|AgCl reference electrode. The insulation layer was removed from the ends of the wires using a small flame to expose the metal. The ends of the two wires were each connected to an electrical wire using conductive silver epoxy glue (RS Components, UK) and were cured overnight at room temperature or at 65°C for 1 hour. Crimp pins (Farnell, UK) had previously been soldered onto the other end of these electrical wires to make the connection to the potentiostats. Fast-drying epoxy adhesive (RS Components, UK) was used to secure the two wires on opposite ends of the needle barrel so as to ensure the two wires were not connected. This also ensured that the wire joins, which could be fragile, were secured inside the needle barrel. Finally, the needle was filled with epoxy resin (Robnor resins, CY1301 and HY1300) to strengthen the combined electrode and to secure the wires in place. The resin and hardener were mixed together in a 3:1 ratio by volume and sonicated to ensure

they were thoroughly mixed. The mixture was then placed in a desiccator to remove any air bubbles formed during mixing. A second hypodermic needle was connected to each needle electrode by a piece of tubing and was used to fill the internal volume of the needle with the epoxy resin, ensuring all air bubbles were removed from the needle barrel. The needles were left connected together and were secured in an upright position, with the filling needle placed slightly higher than the needle electrode to ensure the epoxy resin did not leak out before it had cured. The needles were then left to cure at room temperature for two days.

Once the epoxy resin was cured, the tip of the needle was sanded down using P1200 sandpaper (Buehler, UK) to just above the bevel of the needle to create silver and platinum disc electrodes. The blunt needle was then polished with two additional grades of sandpaper, P2500 and P4000 (Buehler, UK). For each grade of sandpaper, the electrode was held perpendicular to the paper and was moved in a figure of eight motion 50 times, before rotating the needle 90°. This process was repeated another three times. After rough polishing with the sandpaper, the electrode was then polished with alumina slurries. A 1 μm alumina slurry was used, following the same method as described for polishing with sandpaper. The electrodes were then rinsed with deionised water and sonicated for 1 minute to remove any particles from the electrode tip. This process was then repeated using a 0.3 μm and finally a 0.05 μm alumina slurry. The electrode surface was characterised with an external reference electrode using cyclic voltammetry and the polishing process was repeated until a satisfactory CV was achieved (see section 2.5.2).

To create the counter electrode, an electrical wire was wound around the outside of the hypodermic needle and secured in place using conductive silver epoxy (RS Components, UK). This was cured overnight at room temperature or at 65°C for 1 hour. As with the electrical wires for the working and reference electrodes, a crimp pin was previously soldered to the other end of the electrical wire to make the connection to the potentiostats.

Finally, in order to create the Ag|AgCl reference electrode, the tip of the needle was dipped into a potassium dichromate reference solution (BASi, US) for 3 seconds and then into a solution of diluted 37% hydrochloric acid (1 in 10 dilution) for 20 seconds to remove the oxide layer from the working and counter electrodes. The electrode tip was then thoroughly rinsed with deionised water, as the hydrochloric acid can erode the stainless steel needle shaft.

On some occasions a larger diameter working electrode was required. In this case, a 127 μm perfluoroalkoxy polymer resin (PFA)-insulated diameter platinum/iridium (90%:10%) wire (Advent Research Materials, UK) inside a slightly larger 25 G needle was used instead.

2. METHODS & MATERIALS

2.5.2 Electrode characterisation

Following fabrication, all electrodes were characterised by carrying out a CV in Fc solution. The potential applied to the working electrode was scanned from -100 mV to 500 mV, compared with a Ag|AgCl reference electrode, and the corresponding current recorded. Information about the electrode can be obtained using this technique. Electrodes were also characterised in this way each time after re-polishing.

Electrode surface characterisation

The shape of the CV, as well as the steady-state oxidation current produced, can be used to assess the area of the electrode and to verify that the electrode characteristics are satisfactory after polishing. An example of a typical CV in 1.5 mM Fc solution, at a scan rate of 10 mV/s for a 50 μm platinum disc electrode, was previously shown in figure 2.1. Using equation 2.2, the theoretical limiting current for a 50 μm disc electrode in 1.5 mM Fc is found to be 8.29 nA (D is $5.73 \times 10^{-6} \text{ cm}^2\text{s}^{-1}$ (106)). In practice, the observed current may differ from the theoretical value as a result of uneven polishing, leading to an electrode surface that is not a perfect disc or that is uneven.

On occasions, during polishing silver atoms can be transferred onto the platinum working electrode. This can be identified by performing a CV in Fc solution, as shown in figure 2.9A; if silver atoms are present on the working electrode, the CV exhibits a peak at $\pm 65 \text{ mV}$. In some cases, sonication can remove the silver atoms from the working electrode, but in most cases, re-polishing is required.

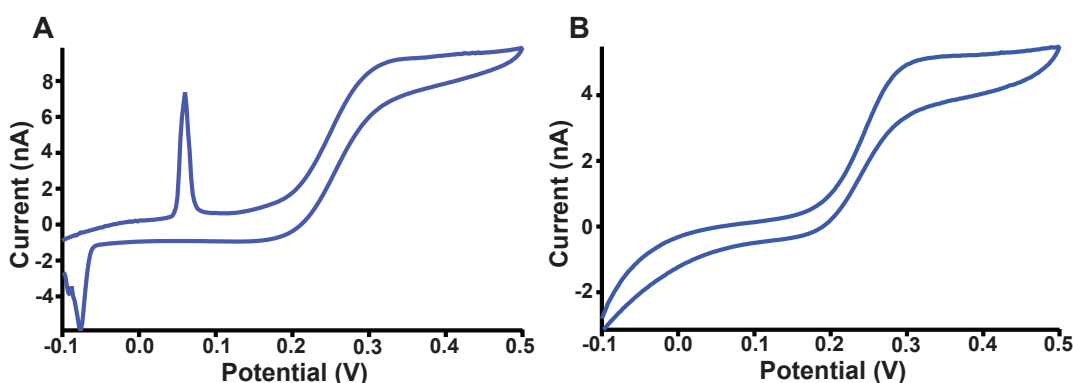


Figure 2.9: Examples of poor electrode characteristics. The working electrode potential was scanned from -100 mV to 500 mV and then reversed for a 50 μm diameter platinum disc electrode. The CVs were carried out in 1.5 mM Fc at 10 mV/s. *A.* The peaks at $\pm 65 \text{ mV}$ indicate that silver atoms are present on the working electrode. *B.* The CV has high capacitance, indicating that the electrode surface is not clean.

An example of a CV with high capacitance is shown in figure 2.9B, where there is a large difference in the current observed on the forward and backward scans. This indicates

that the electrode surface is not clean and thorough polishing is necessary to reduce the capacitance.

Reference electrode characterisation

Repeated polishing can result in removal of the Ag|AgCl layer on the silver wire, leading to an unstable reference electrode. In this case, the silver wire would need to be re-chloridised, as described in section 2.5.1. The reference electrode can be tested by performing a CV in Fc solution, as described above. As shown in figure 2.10, if the reference electrode has begun to fail, the potential at which oxidation and reduction occurs will be shifted to the right or the backward scan will cross over the forward scan.

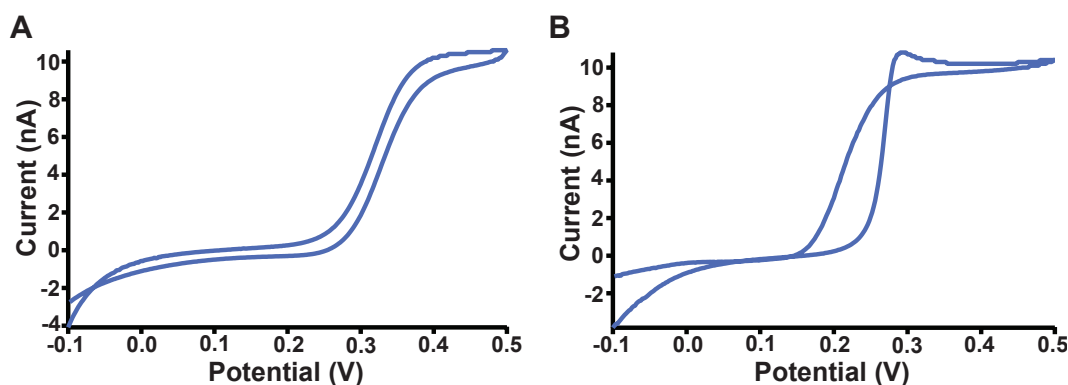


Figure 2.10: CVs obtained when the reference electrode has shifted. The working electrode potential was scanned from -100 mV to 500 mV and then reversed for a 50 μm diameter platinum disc electrode with a failed Ag|AgCl reference electrode. The CVs were carried out in 1.5 mM Fc at 10 mV/s. *A.* Oxidation and reduction peaks are shifted to higher potentials. *B.* Backward scan crosses over forward scan. Both CVs indicate that the reference electrode needs to be re-chloridised.

2.5.3 Biosensor fabrication

Glucose and lactate biosensors were created using two methods, described below. In both cases, either glucose oxidase (GOx) or lactate oxidase (LOx) was immobilised onto a combined needle electrode for selective and sensitive detection of glucose and lactate, respectively.

2.5.3.1 Poly(phenol) glucose biosensors

Glucose biosensors were initially fabricated using electropolymerisation, previously developed in the group (69). Using this method, GOx was entrapped in a poly(phenol) film on the working electrode. The electrode was placed in a solution containing 50 mM phenol and 4 mg/ml GOx (Sekisui Diagnostics, Kent, UK) in 0.01 M phosphate buffered saline (PBS, pH 7.2) and allowed to stabilise for 10 minutes. The working electrode was held at

2. METHODS & MATERIALS

0 V for 20 s and polarised to 0.9 V for 30 minutes in order to begin electropolymerisation of the film, followed by a further 1 minute at 0 V. The needle tip was gently rinsed with deionised water and stored overnight at 4°C before use. Cyclic voltammetry in Fc solution was carried out to ascertain whether the electropolymerisation had been successful. In this case, the polyphenol film should act as a barrier, preventing the Fc molecules from reaching the electrode surface to be oxidised. Therefore, the characteristic oxidation and reduction peaks should not be visible, as shown in figure 2.11.

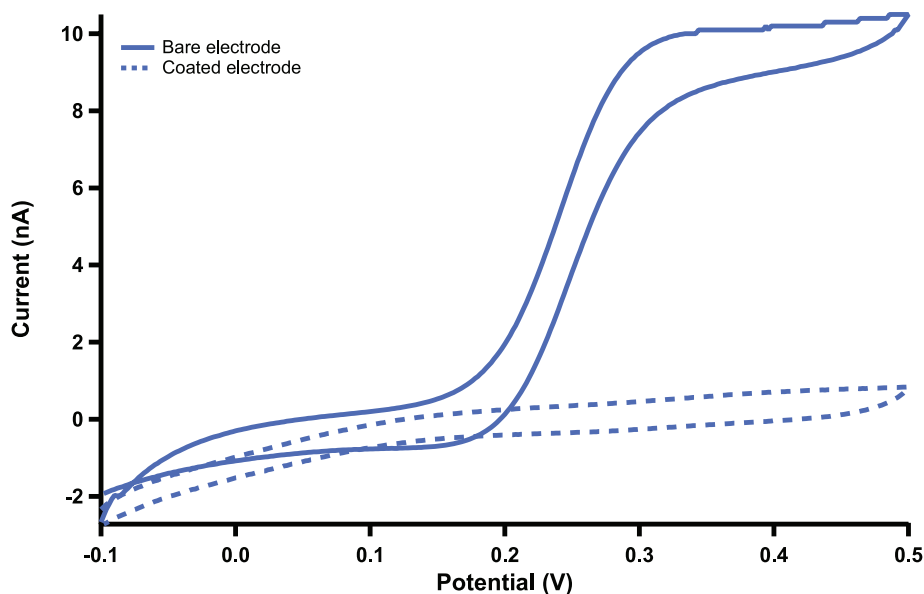


Figure 2.11: CV of a bare electrode and after coating with poly(phenol). The working electrode potential was scanned from -100 mV to 500 mV and then reversed for a 50 μm diameter platinum disc electrode. The CV was carried out in 1.5 mM Fc at 10 mV/s. The solid and dotted lines show the CVs obtained before and after coating with poly(phenol), respectively.

2.5.3.2 Hydrogel biosensors

Glucose and lactate biosensors were also fabricated by entrapment of the enzyme in a hydrogel film, using a standard method developed in the group, based on that described by Vasylieva *et al* (107, 108). Further development of this method for the applications described in this thesis is discussed in section 3.3. The working electrode was initially coated with a poly(m-phenylenediamine) (mPD) exclusion layer in order to stop any potential interferents reaching the electrode where they could be oxidised. This was done by electropolymerisation in a 100 mM solution of mPD in 0.01 M PBS (pH 7.4). The working electrode was held at 0 V for 20 s and then polarised to 0.7 V for 20 minutes for electropolymerisation to occur. The electrode was then held at 0 V for a further 5 minutes to allow the film to stabilise. The needle tip was gently rinsed with deionised water before testing that the electropolymerisation step has been successful by cyclic voltammetry in

Fc solution. If the electropolymerisation has been successful, the Fc molecules would not be able to reach the electrode surface, as they are blocked by the exclusion film, and therefore the characteristic oxidation and reduction peaks should not be seen, as shown in figure 2.12.

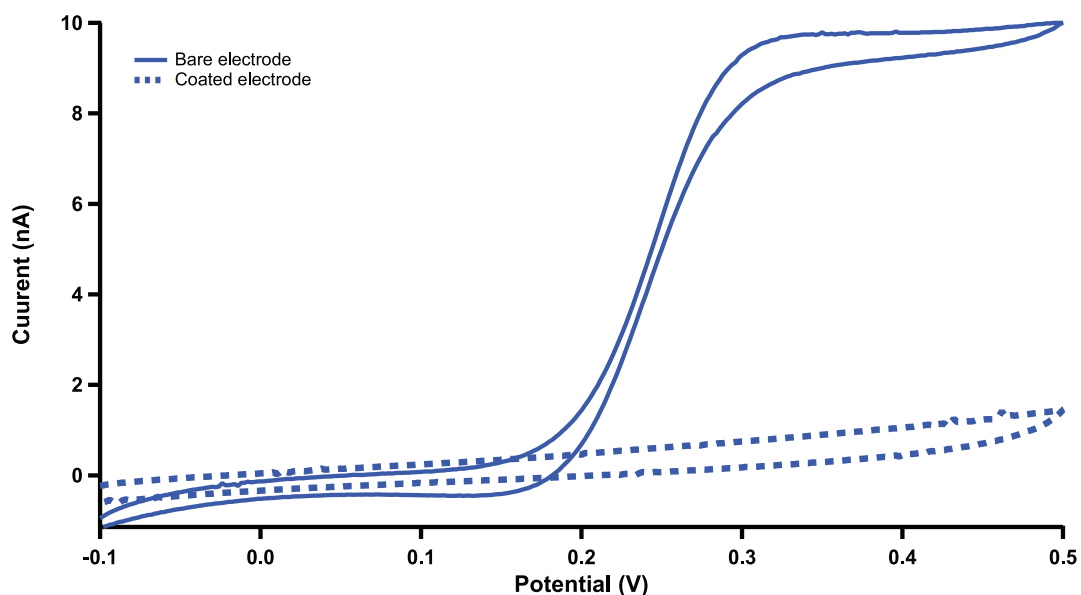


Figure 2.12: CV of a bare electrode and after coating with mPD. The working electrode potential was scanned from -100 mV to 500 mV and then reversed for a 50 μm diameter platinum disc electrode. The CV was carried out in 1.5 mM Fc at 10 mV/s. The solid and dotted lines show the CVs obtained before and after coating with mPD, respectively.

In cases where the CV prior to electropolymerisation showed high capacitance, as in the example shown in figure 2.9B, electropolymerisation tends to be unsuccessful. This emphasises the importance of thorough electrode polishing and of carrying out a CV beforehand to check the electrode surface characteristics. After successful electropolymerisation, the electrode was dipped into an enzyme hydrogel solution in 0.01 M PBS (pH 7.4) for 30 s. Table 2.4 shows the composition of this solution.

Table 2.4: Composition of enzyme hydrogel solution

Chemical	Concentration
Enzyme (GOx or LOx)	60 mg/ml
Bovine serum albumin (BSA)	30 mg/ml
Poly(ethylene glycol) diglycidyl ether (PEGDE)	60 mg/ml
Glycerol	2%

In order to use these biosensors in a microfluidic chip, it was found that they were less susceptible to damage if the hydrogel layer was only on the tip of the needle and not on

2. METHODS & MATERIALS

the sides of the needle. In order to achieve this, 5 μl of the hydrogel solution was placed on a glass slide and the needle tip was slowly brought down towards the drop until the solution came up to touch the needle, where it was held in place for 30 s. To improve the reproducibility of this step, a micro-manipulator was used to dip the needle electrodes into the hydrogel solution, as shown in figure 2.13. After dipping, the needles were secured upside down, in order to keep the film as thin as possible, at 55°C for 2 hours. Biosensors were stored at 4°C for short-term storage, and at -20°C for longer-term storage.

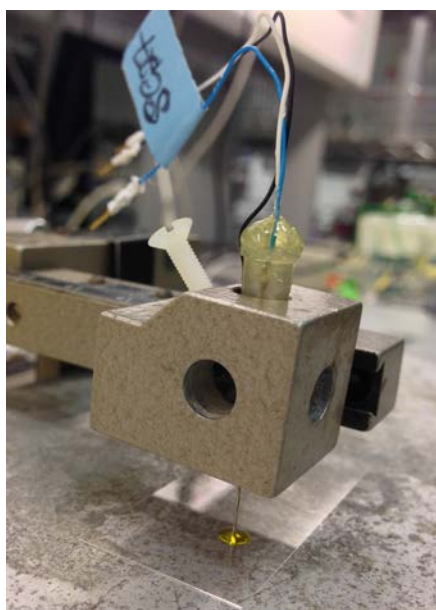


Figure 2.13: Dip-coating needle electrode in enzyme solution using micro-manipulator. The needle electrode is slowly lowered until the solution just touches the tip of the needle and is held in place for 30 s.

2.5.4 Calibrating biosensors

In all cases, biosensor characteristics were assessed by calibration. The working electrode was held at 0.75 V compared with a Ag|AgCl reference electrode using an in-house potentiostat. Data were collected using a PowerLab 8/35 data acquisition unit (ADInstruments, New South Wales, Australia) and LabChart 7 software (ADInstruments, New South Wales, Australia) running on a Macbook Pro portable computer (Apple Computers, Cupertino, CA).

Unless otherwise stated, the biosensor was placed in a 10 ml stirred solution of 0.01 M or 0.1 M PBS (pH 7.4) for glucose and lactate, respectively. The biosensors were allowed to stabilise before aliquots of a concentrated substrate solution were added using a Gilson pipette. Step changes in current corresponding to increasing substrate concentration were used to construct a calibration curve for the biosensor, which was fitted with either

a Michaelis-Menten curve or with the Hill equation in Igor Pro (WaveMetrics USA) in order to assess the kinetics of the immobilised enzyme.

2.5.5 Wireless potentiostats

In chapter 8, wireless potentiostats were used to control glucose and lactate needle electrode biosensors. These potentiostats were designed and fabricated by Mr Chu Wang. They consist of a transmitter and a receiver module, as shown in figure 2.14. The transmitter module consists of 4 layers: layer 1 contains a 2-channel potentiostat, supplying a constant -0.7 V to the reference electrode, layer 2 is the Bluetooth module (RN42, Microchip, US), layer 3 contains the analog-to-digital converters (ADS1298, Texas Instruments, US) and layer 4 contains a microprocessor (Arduino DUE development board). The receiver module contains 3 layers: layer 1 is the Bluetooth module (RN42, Microchip, US), layer 2 contains the analog-to-digital converters (DAC7634, Texas Instruments, US) and layer 3 contains a microprocessor (Arduino DUE). As such, this system is capable of wirelessly sending 16-channel data. In chapter 8, only 2 channels of data were used, but the system could be extended to include more potentiostat layers.

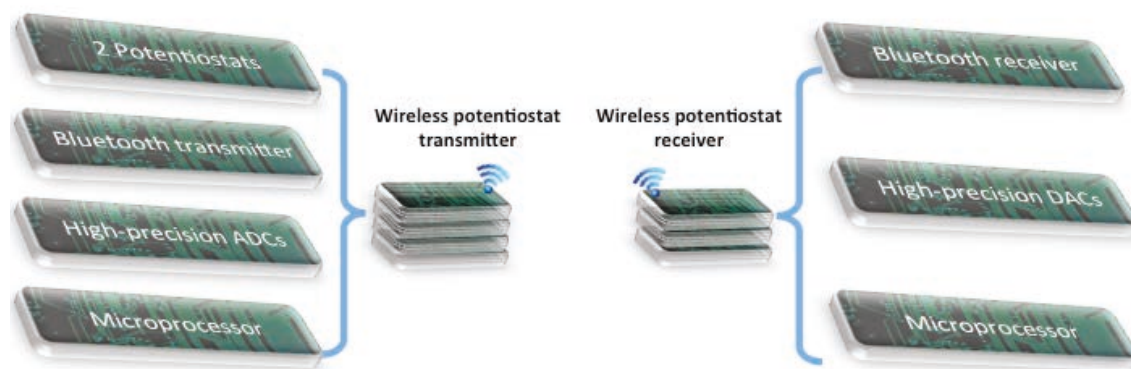


Figure 2.14: Wireless potentiostat system. The wireless potentiostats consist of a transmitter and a receiver module, both constructed in a stacked configuration. The transmitter module consists of 4 layers: 2-channel potentiostat, Bluetooth module, analog-to-digital converter and microprocessor layers. The receiver module consists of 3 layers: Bluetooth module, analog-to-digital converter and microprocessor layers. Figure courtesy of Chu Wang.

2.6 Common solutions and standards

All chemicals were obtained from Sigma-Aldrich (UK) unless otherwise stated.

2. METHODS & MATERIALS

2.6.1 Ferrocene monocarboxylic acid (Fc) buffer solution

Ferrocene monocarboxylic acid (Fc) buffer was used to mediate the enzyme reaction in the rsMD system. It was also used as a redox couple for cyclic voltammetry experiments to test electrodes and to assess their surface characteristics. The composition of this solution is given in table 2.5.

For use with the rsMD system the solution was filtered with membrane filters (0.1 μm and 0.02 μm 47 mm Anodisc, Whatman International Ltd) to remove any undissolved particles that could potentially block the fine-bore tubing. 200 μl 5-chloro-2-methyl-4-isothiazoline-3-one (Kathon CG, Rohms and Hass) per litre of Fc buffer was also added as an antibacterial agent.

Table 2.5: Composition of ferrocene monocarboxylic acid (Fc) buffer solution

Chemical	Concentration (mM)
Ferrocene monocarboxylic acid (Fc)	1.5
Ethylenediaminetetraacetic acid (EDTA)	1
Sodium citrate	100
Sodium chloride	150

2.6.2 Phosphate buffered saline

To make up 0.01 M phosphate buffered saline (PBS), 1 PBS tablet (Sigma-Aldrich, UK) was dissolved in 200 ml of deionised water. For 0.1 M PBS, the solution was made as described in table 2.6. The pH was adjusted to 7.4 using 0.1 M sodium hydroxide.

Table 2.6: Composition of 0.1 M PBS solution

Chemical	Concentration (mM)
Sodium phosphate dibasic (Na_2HPO_4)	77.4
Sodium phosphate monobasic (NaH_2PO_4)	21.2
Sodium chloride	150

2.6.3 Substrate standards

Glucose and lactate rsMD calibration standards were dissolved in deionised water or T1 physiological solution. As the sample was injected into a much larger volume of Fc buffer, the background solution was not important. For biosensor calibrations, standards were dissolved in T1 solution or in PBS.

Chapter 3

Clinical analysis system for dialysate metabolites

This chapter will describe the development of the analysis methods that will be used in this thesis, in the following chapters.

3.1 Introduction

3.1.1 Biosensors

Biosensors consist of a biorecognition element, such as an enzyme, and a transduction element, such as an electrode, typically in direct contact (45). Biosensors are classified into three categories according to their mode of operation. A brief summary of each generation will be described here.

First-generation biosensors

First-generation biosensors detect the product of the enzyme-substrate reaction directly at the electrode. For instance, a first-generation glucose biosensor is one in which glucose oxidase (GOx) is immobilised on the surface of the electrode. Glucose reacts with the enzyme producing hydrogen peroxide, which is detected at the electrode by oxidation. As a result, these biosensors require a continuous supply of oxygen. The current observed is related to the concentration of glucose and for low concentrations is proportional. The main drawback with this approach is that there are several electroactive interferent molecules, such as uric acid, ascorbic acid and acetaminophen, that could also be oxidised at the high potentials used. The hydrogel biosensors presented in section 3.3 are examples of first-generation biosensors. The in-flow enzyme addition mechanisms described in section 3.5 are examples of distributed first-generation biosensors.

3. CLINICAL ANALYSIS SYSTEM FOR DIALYSATE METABOLITES

Second-generation biosensors

Second-generation biosensors use a synthetic mediator, such as ferrocene monocarboxylic acid, to carry electrons from the enzyme to the electrode surface and to regenerate the enzyme. Using this approach, the reaction mechanism is not dependent on a constant supply of oxygen. In addition, the mediator can be selected so that it undergoes fast reaction kinetics and can be detected at a potential at which other electroactive species do not react. The enzyme reactors used in rapid sampling microdialysis (rsMD) are examples of distributed second-generation biosensors.

Third-generation biosensors

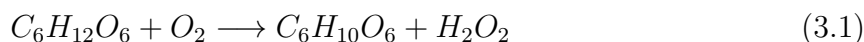
Third-generation biosensors are based on the direct transfer of electrons between the enzyme and the electrode surface. Studies of direct electron transfer approaches include using conducting organic salts such as the charge transfer complex tetrathiofulvalene-tetracyanoquinodimethane (TTF-TCNQ) (109, 110) (although there is some debate as to whether this is a true third-generation biosensor (111, 112)), redox-wired enzymes (113, 114) or oxidised boron-doped diamond electrodes (115). Direct electron transfer allows much lower potentials to be applied, which removes issues of interference. However, for most oxidase enzymes the distance between the redox centre of the enzyme and the electrode is too great for efficient tunnelling of electrons between the two.

3.1.2 Enzymes

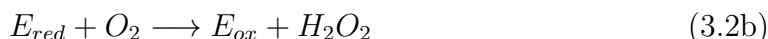
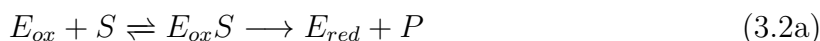
Glucose oxidase

Glucose oxidase (GOx) is a flavoprotein that catalyses the oxidation of glucose and is typically isolated from *Aspergillus niger*. It is a homodimer, consisting of two identical 80 kDa subunits, containing two non-covalently bound flavin adenine dinucleotide (FAD) coenzymes, which act as electron carriers (116). The structure at 1.9 Å is shown in figure 3.1. Its dimensions are 6.75 x 6.75 x 21.54 nm (117).

GOx catalyses the oxidation of D-glucose to D-gluconolactone, as described in equation 3.1.



The proposed mechanism for this reaction is shown in equation 3.2 (118).



Where E_{ox} and E_{red} represent the oxidised and reduced forms of the enzyme, respectively, S and P represent the substrate and product, respectively, and $E_{ox}S$ represents the enzyme-substrate complex.

The product of the reaction, hydrogen peroxide, can be electrochemically detected and its concentration is directly proportional to the concentration of glucose. The reported K_m of GOx is 30 mM, according to the Genzyme data sheet.

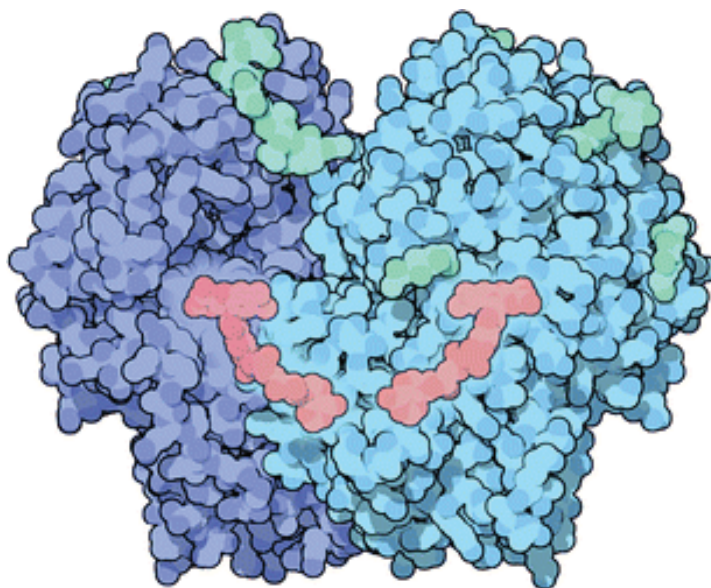


Figure 3.1: Structure of glucose oxidase. The light and dark blue regions show the two subunits and the pink regions represent the FAD coenzymes (119).

Lactate oxidase

Lactate oxidase (LOx) belongs to a family of flavin mononucleotide (FMN)-dependent α -hydroxy acid-oxidising enzymes. The structure of LOx from *Aerococcus viridans* has been solved and the active site was shown to be located around the FMN (120, 121). The asymmetric LOx unit contains 2 tightly packed tetramers, each unit of which has a molecular weight of 41 kDa and forms a biologically active unit. The dimensions of LOx are 11.73 x 13.47 x 18.56 nm (120) and the structure is shown in figure 3.2.

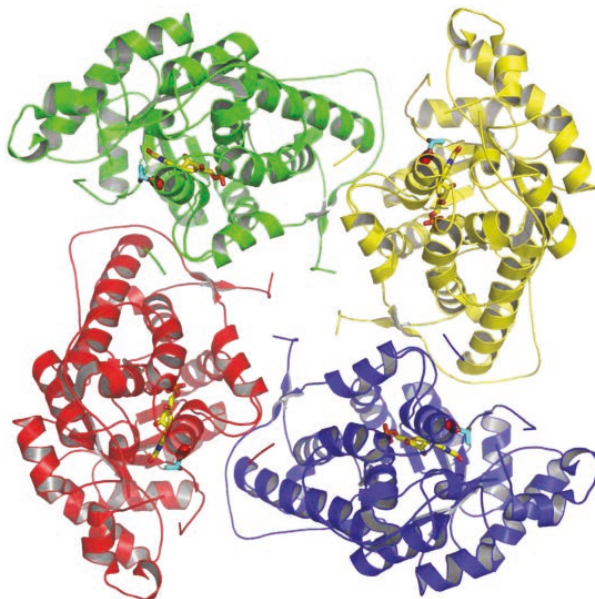
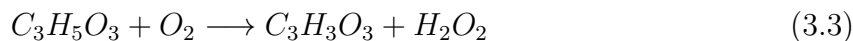
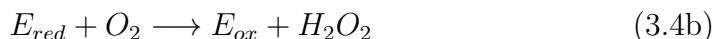


Figure 3.2: Structure of lactate oxidase. Ribbon representation of the LOx tetramer (half of the asymmetric unit), with each monomer shown in a different colour (120).

LOx catalyses the oxidation of lactate to pyruvate, as shown in equation 3.3.



The reaction mechanism is complex and has been characterised as a ping-pong mechanism (122). In this reaction scheme, the enzyme is initially reduced, converting lactate to pyruvate. The reduced form of the enzyme then reacts with an electron acceptor, O_2 , leading to the formation of hydrogen peroxide, as described in equation 3.4.



As with GOx, the concentration of hydrogen peroxide, which can be electrochemically detected, is directly related to the lactate concentration. Recombinant LOx is used in this thesis. According to the Genzyme data sheet, the reported K_m of LOx is 0.7 mM.

Horseradish peroxidase

Although not used in this chapter, horseradish peroxidase (HRP) is used throughout this thesis in the enzyme reactors used for the rsMD system, as described in section 2.3.2. HRP is a haem-containing enzyme, with dimensions of 4.03 x 6.77 x 11.7 nm (123). The structure is shown in figure 3.3.

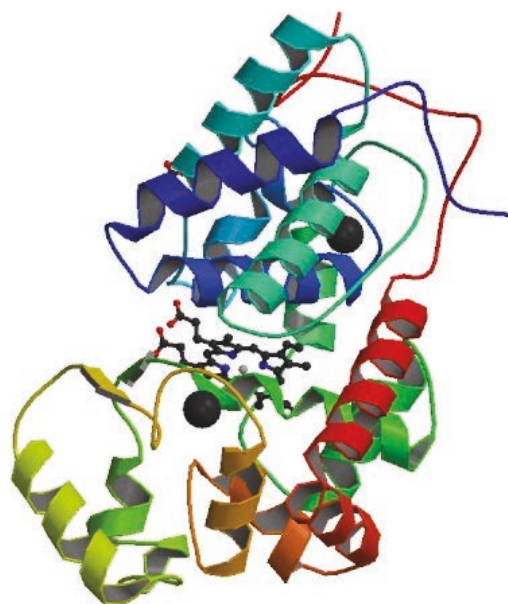


Figure 3.3: Structure of horseradish peroxidase. Ribbon representation of HRP, obtained from protein data bank (123).

The reaction mechanism is complex and is explained in detail elsewhere (124). The reaction mechanism is summarised in figure 3.4.

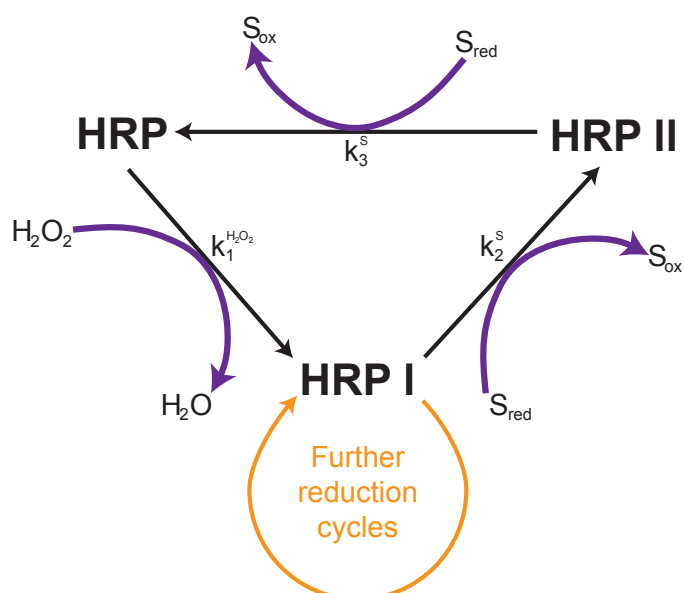


Figure 3.4: Summary of HRP mechanism. Adapted from (124). HRP reacts with hydrogen peroxide to produce HRP I, which is reduced back to HRP in two steps via HRP II by reaction with two oxidised acceptor molecules, S (*purple*). An alternative pathway is possible (*orange*) where HRP I continues to react with hydrogen peroxide by electron transfer from the protein part of the same or another HRP molecule.

3. CLINICAL ANALYSIS SYSTEM FOR DIALYSATE METABOLITES

HRP in its native state consists of a catalytic haem group containing Fe(III) and the surrounding protein. Reduction of hydrogen peroxide results in production of HRP I, with the haem group in a +5 oxidation state. Reduction of HRP I back to HRP occurs in two steps; firstly, HRP I is reduced to HRP II, which has a +4 oxidation state, after which HRP II is reduced to HRP. In total, one hydrogen peroxide reacts with HRP to give two oxidised acceptor molecules, S.

However, Sanz *et al.* have shown that the reaction of hydrogen peroxide with HRP can take place in the absence of an external substrate by transfer of electrons from the proteic part of either the same HRP molecule or another HRP molecule to the haem group (124). After the first reaction, HRP I can continuously react with hydrogen peroxide until the proteic part is unable to transfer more electrons to the haem group, which slows down the overall reaction rate. As $k_1^{\text{H}_2\text{O}_2}$ is very fast, high levels of H_2O_2 can lead to population of other activated states derived from HRP I, and hence to a reduction in efficiency of generating S_{ox} .

3.1.3 Enzyme kinetics

The activity of most enzymes can be described using Michaelis-Menten kinetics. The rate of catalysis (V) is defined as the number of moles of product formed per second. At low substrate concentrations ($[S]$), the reaction rate increases almost linearly with increasing substrate concentration. However, above a certain substrate concentration, the reaction rate begins to plateau until the maximum rate is reached (V_{max}). At this point, the reaction rate is independent of increasing substrate concentrations. The Michaelis-Menten constant, K_m , is the substrate concentration at which the reaction rate is half of its maximum value. The Michaelis-Menten formula is described in equation 3.5.

$$V = \frac{V_{max}[S]}{K_m + [S]} \quad (3.5)$$

Allosteric enzymes, which contain multiple active sites or subunits, do not obey Michaelis-Menten kinetics. For these enzymes, binding of a substrate to one active site can affect the properties of the other active sites in the same enzyme molecule. This can result in cooperative binding, in which binding of the first substrate facilitates substrate binding to other active sites. In addition, in some cases, enzyme activity can also be affected by binding of regulatory molecules to non-catalytic sites. For these enzymes, their activity can be described by the Hill equation, which is shown in equation 3.6.

$$I = \frac{V_{max}}{(1 + (\frac{K_m}{[S]}))^\alpha} \quad (3.6)$$

Where I is a measure of the reaction rate and α represents the deviation from Michaelis-Menten kinetics. When $\alpha = 1$, the Hill equation is equivalent to the Michaelis-Menten equation.

The Hill equation is widely used to fit biosensor calibration curves (125). In particular, GOx and LOx kinetics for glucose and lactate biosensors, respectively, have been shown to fit the Hill equation (126).

3.2 Autocalibration

In clinical situations, monitoring continues for long periods of time. As a result, it is critical to regularly calibrate to ensure that the results obtained are accurate. With the current systems, this requires someone to be present to calibrate the system, which is not always possible. Therefore, a system which could automatically calibrate itself would be a considerable improvement.

I have been part of group effort within the biosensors group to develop an autocalibration system using LabSmith (California, US) programmable syringe pumps and valves. The LabSmith components used are described in figure 3.5.

The devices are controlled using Windows uProcess software or C++ drivers. Automated sequences are programmed for automatic coordinated control of several devices at the same time.

The autocalibration boards developed can be integrated with the rsMD analysis system as well as with on-chip biosensors. The basic setup of the autocalibration board is the same for both analysis systems and will be described in the following section.

3. CLINICAL ANALYSIS SYSTEM FOR DIALYSATE METABOLITES








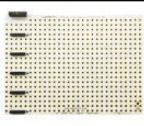



Item	Image	Icon	Specifications
Syringe pump			Volume: 20 μ l. Flow rate range: 0.2-1100 μ l/min. Step size: 0.033 μ l. Dispenses at fixed flow rate (~1% accuracy) or fixed volume (~1% accuracy).
Valve			Three-port two-position valve or four-port two-position valve. Zero dead volume. For use with 360 μ m or 1/32" OD tubing. Switch time of 0.4 s.
Valve manifold		N/A	Required to automatically control the automated valves. One manifold can control up to 4 valves.
Reservoir			1.1 ml fluid reservoir. Four ports for LabSmith CapTite one-piece fittings.
Breadboard		N/A	Integrated connectors for uDevices. 1/4" through-hole spacing for mounting valves and interconnects. Two sizes: 5-device, 185 x 132 mm. 8-device, 254 x 229 mm.
Interconnect			Interconnect tee or cross for use with 360 μ m OD capillary or 1/32" OD tubing via CapTite one-piece fittings. Interconnect unions to connect 360 μ m OD capillary to 1.32" OD tubing. Can be mounted to breadboards.
Electronic interface board (EIB)		N/A	Simultaneously operate up to 10 uDevices (valves and syringe pumps) or up to 100 devices sequentially. RS-232 interface.

Figure 3.5: LabSmith components. These components were used in the development of an autocalibration system.

3.2.1 Autocalibration board

The autocalibration board was constructed using LabSmith (California, US) components. A schematic of the setup is shown in figure 3.6.

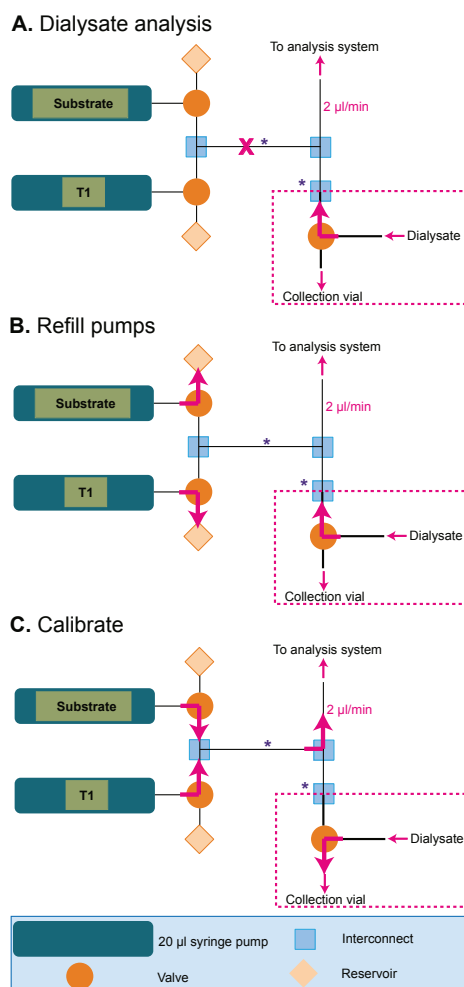


Figure 3.6: Schematic of autocalibration board. This setup would be used to calibrate on-chip biosensors. All tubing and components in the pink box are 1/32" outer diameter (OD) and the rest are 360 μ m OD. In cases where the system is used to calibrate the rsMD system, the union adaptor (labelled with a purple asterisk) would be placed between the calibration interconnect tee and the analysis system interconnect tee, as indicated with a purple asterisk, as the tubing to the rsMD system is 1/32" OD.

Dialysate analysis

As shown in figure 3.6A the dialysate flows into a three-port two-position valve, which can either be directed to a collection vial or towards the analysis system. This is an important feature as it ensures that flow through the microdialysis probe is not interrupted. The dialysate is directed towards the analysis system between calibrations. Both the calibration stream and the dialysate stream flow into an interconnect tee. In order to ensure that the liquid stream flows towards the analysis system, it is important to make sure that the alternative path is blocked. Hence, between calibrations the calibration valves are closed.

3. CLINICAL ANALYSIS SYSTEM FOR DIALYSATE METABOLITES

Refill pumps

As shown in figure 3.6B, the calibration stream is created using two 20 μl syringe pumps, one of which contains the substrate of interest and the other of which contains T1 solution (and does not contain the substrate of interest). These pumps can be programmed to refill from their respective reservoir by switching the valve towards the reservoir.

Calibrate

Once refilled, the valves can be switched so that the liquid stream is directed towards the analysis system (figure 3.6C). The solutions from the two pumps are mixed at the interconnect tee and hence the substrate is diluted depending on the mixing ratio. A multistep calibration can be carried out by varying the respective flow rates of the two pumps. For instance, if both flow at 1 $\mu\text{l}/\text{min}$, then the substrate will be diluted by 50%, but if the substrate pump flows at 0.5 $\mu\text{l}/\text{min}$ and the T1 pump flows at 1.5 $\mu\text{l}/\text{min}$, then the substrate will be diluted by 75%. When only one pump is running, the other valve is closed to ensure that flow can only be directed towards the analysis system. During calibrations, the dialysate is directed towards the collection vial.

The number of calibration steps and their duration can be varied and is determined by the purpose-written script. Steps can also be included to refill the pumps when necessary. The script can be written on a loop so that calibrations are carried out after a set length of time has elapsed. With this system, calibrations are carried out at regular intervals without the need for someone to be present. The script ensures that during calibrations the dialysate is automatically switched to a collection vial and that afterwards the dialysate is switched back towards the assay for analysis.

3.2.2 RsMD autocalibration

The autocalibration board has been implemented with the rsMD system to enable more regular calibrations. Figure 3.7 shows a schematic of the setup used.

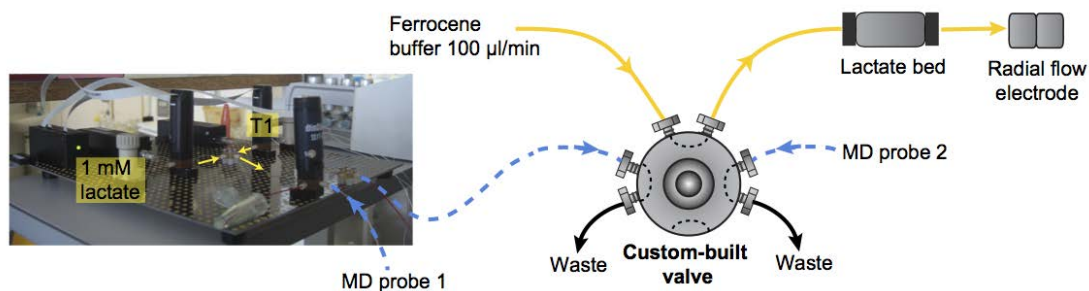


Figure 3.7: Schematic of experimental setup for rsMD autocalibration. Dialysate from microdialysis (MD) probe 1 flows into the calibration board, which is connected to a loop of the flow injection valve. Dialysate 2 is connected to another loop of the flow injection valve as normal.

In this example, the rsMD system was set up as described in section 2.3.1.2 to measure the lactate concentration in two dialysate streams. The outlet of microdialysis probe 1 was connected to the dialysate valve of the autocalibration board and fluorinated ethylene propylene (FEP) was used to connect the autocalibration board to the flow injection valve, while probe 2 was connected to another loop of the flow injection valve as normal. Figure 3.8 shows an example of a calibration carried out using this system.

3. CLINICAL ANALYSIS SYSTEM FOR DIALYSATE METABOLITES

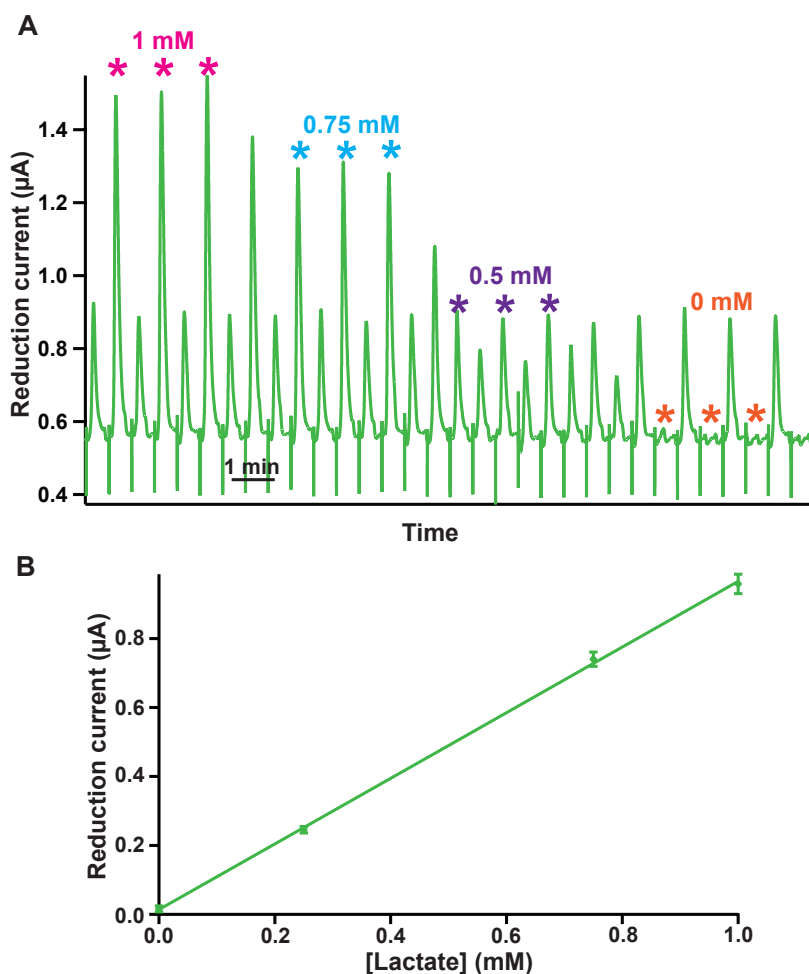


Figure 3.8: Results of rsMD lactate autocalibration. *A.* Raw data for a 4-point lactate calibration. Peaks alternate between the calibration stream (marked with an asterisk) and the second dialysate stream. *B.* Corresponding calibration curve from 0 to 1 mM, fitted with a straight line. Markers indicate the mean \pm standard deviation for each measurement ($n=3$).

During calibrations, dialysate 1 was switched to a collection vial and the calibration stream was directed to the the flow injection valve instead. As a result, peaks alternate between those for the calibration stream and those for dialysate 2. When the calibration was complete, the valves were closed and dialysate 1 was directed to the flow injection valve. The autocalibration board has also been used in exactly the same way with the rsMD system in its other configuration, as described in section 2.3.1.1, to analyse glucose and lactate (data not shown here).

3.2.3 On-chip biosensor autocalibration

The autocalibration board has been used with biosensors housed in a PDMS microfluidic chip, as shown in figure 3.9.

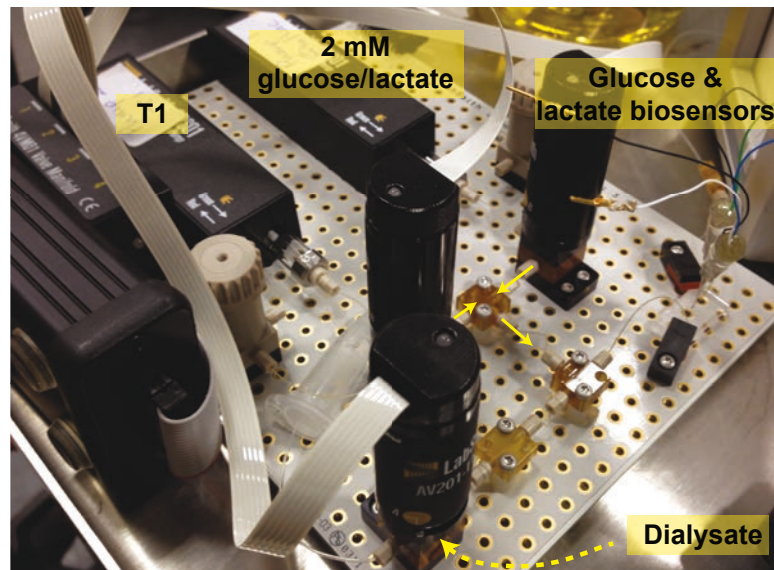


Figure 3.9: Photograph of experimental setup for on-chip biosensor autocalibration. Either the calibration stream or the dialysate is directed past glucose and lactate needle biosensors housed in a PDMS microfluidic chip.

A PDMS microfluidic chip, which housed glucose and lactate biosensors, was placed on the autocalibration board. The valves were programmed to direct either the calibration stream or the dialysate into the PDMS chip and past the biosensors. Figure 3.10 shows the raw data for a 5-point glucose and lactate calibration on-chip and figure 3.11 shows the corresponding calibration curves.

3. CLINICAL ANALYSIS SYSTEM FOR DIALYSATE METABOLITES

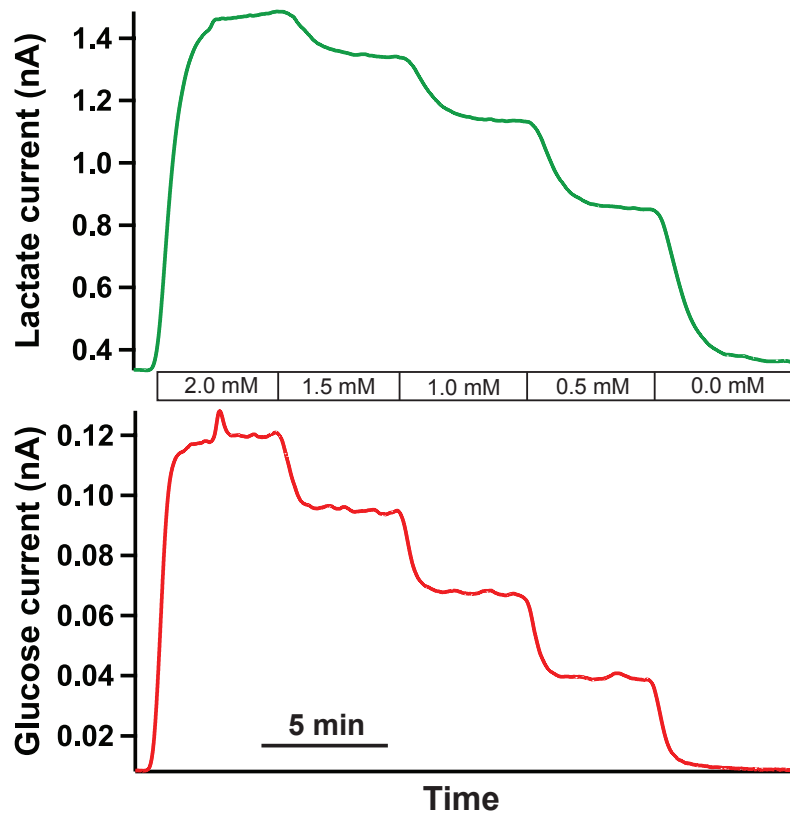


Figure 3.10: Raw data for on-chip glucose and lactate autocalibration. The red trace shows a 5-point glucose calibration and the green trace shows a 5-point lactate calibration. Steps are 2.0, 1.5, 1.0, 0.5 and 0.0 mM (indicated on the graph). The dialysate stream flows past the glucose biosensor first, followed by the lactate biosensor. These biosensors had already been used in previous experiments and therefore the measured currents do not represent typical responses for optimal biosensors.

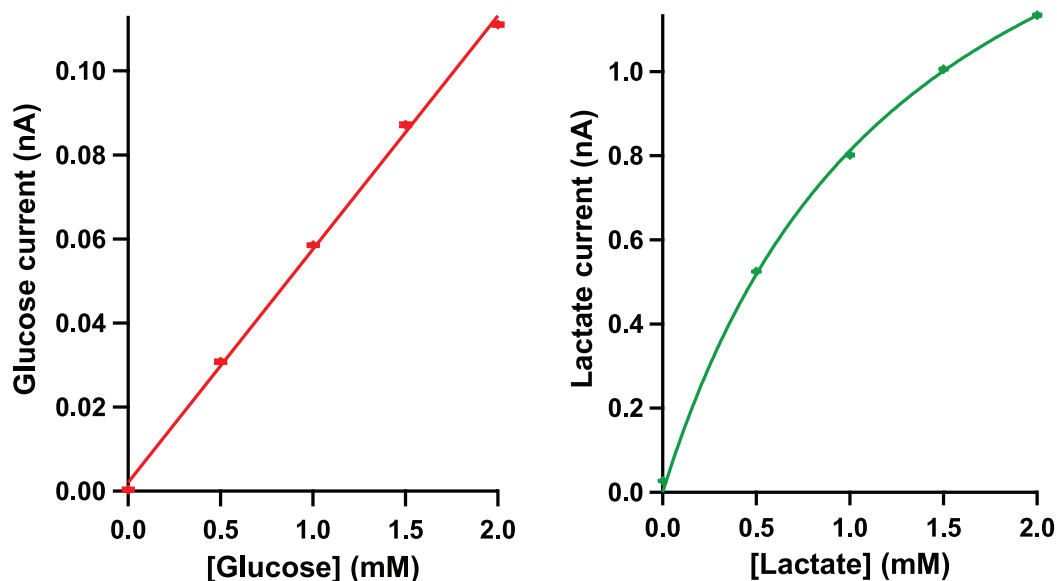


Figure 3.11: Calibration curves for on-chip autocalibration. *Left:* glucose calibration curve from 0 to 2 mM fitted with a straight line. *Right:* lactate calibration from 0 to 2 mM fitted with the Michaelis-Menten equation. Markers indicate the mean \pm standard deviation for each measurement.

3.3 Hydrogel biosensors

Hydrogel glucose and lactate biosensors were fabricated using a method adapted from that described by Vasylieva *et al.* (107, 108), as described in section 2.5.3.2. Using this method, enzyme is trapped on the electrode surface in a matrix, which is formed by the reaction of the epoxy groups in poly(ethylene glycol) diglycidyl ether (PEGDE) with the amine groups on the protein. This reaction would take approximately 48 hours to occur at room temperature, but Vasylieva *et al.* found that, by increasing the temperature to 55°C, the reaction was accelerated enough to form a stable immobilised film in 2 hours while still preserving enzymatic activity (107).

Scanning electron microscopy (SEM) was used to visualise the hydrogel film. SEM images of 15 μl GOx hydrogels (made following the same recipe as for the biosensors) are shown in figure 3.12.

3. CLINICAL ANALYSIS SYSTEM FOR DIALYSATE METABOLITES

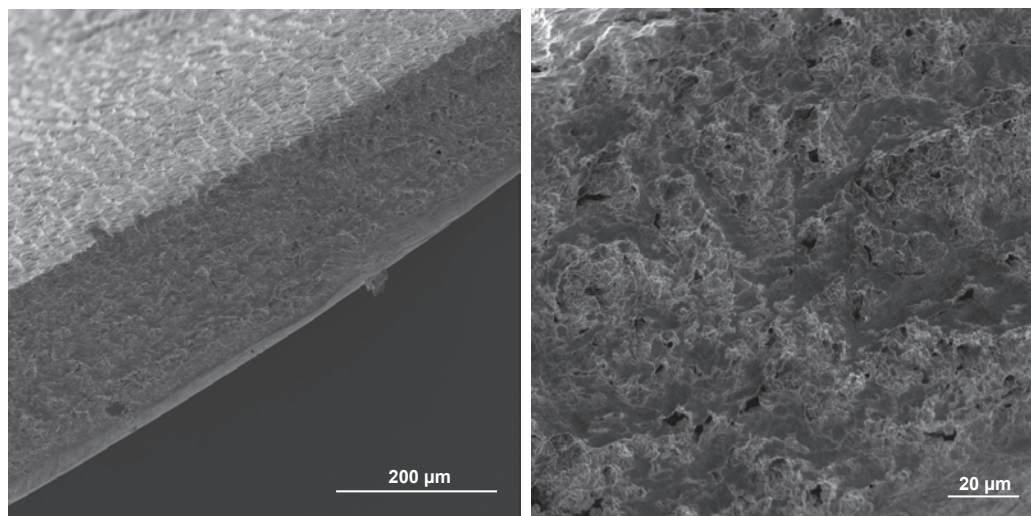


Figure 3.12: SEM images of GOx hydrogel. *Left:* Hydrogel was sliced in half to image the inner structure. *Right:* Surface of the hydrogel. Pores are visible in the hydrogel structure.

Biosensors were characterised in a well-stirred beaker containing PBS. Aliquots of a concentrated substrate solution were added using a Gilson pipette to create a step change in concentration. Typical calibration curves for glucose and lactate hydrogel biosensors are shown in figure 3.13.

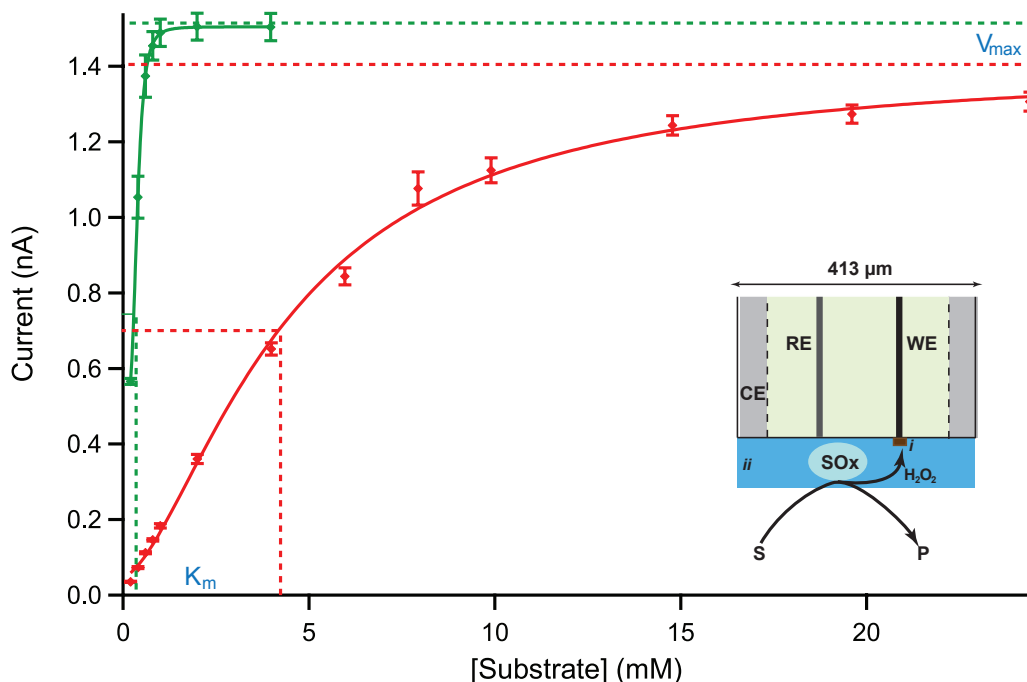


Figure 3.13: Typical hydrogel biosensor calibration curves. Calibrations were carried out in a beaker. Biosensors were held at a constant potential of +0.75 V. The green trace shows the lactate response and the red trace shows the glucose response. Mean \pm standard deviation of measurement is shown. Points fitted with the Hill equation. Dotted lines indicate V_{max} and K_m for each biosensor. *Inset:* Schematic cross-section of needle biosensor tip, comprising a platinum working electrode (WE), a Ag|AgCl reference electrode (RE) and a stainless steel counter electrode (CE), showing the layers making up the biosensor. (i) poly(m-phenylenediamine) (mPD) interference layer and (ii) substrate oxidase (SOx) entrapped in a hydrogel.

Both glucose and lactate calibration curves were fitted with the Hill equation using Igor Pro. In the example shown in figure 3.13, the V_{max} and K_m for the glucose biosensor were 1.4 ± 0.04 nA and 4.4 ± 0.23 mM, respectively (coefficient values \pm standard deviation calculated in Igor Pro). For the lactate biosensor in figure 3.13, the V_{max} and K_m were 1.5 ± 0.003 nA and 0.38 ± 0.003 mM, respectively. An overview of average glucose and lactate biosensor responses is given in table 3.1.

Table 3.1: Glucose and lactate hydrogel biosensor responses (mean \pm standard deviation).

Biosensor	Sensitivity (nA/mMcm ²)	T ₉₀ (s)	V_{max} (nA)	K_m (mM)
Glucose (n=24)	$8.5 \pm 10 \times 10^3$	6.6 ± 3.9	1.2 ± 0.5	6.6 ± 3.9
Lactate (n=30)	$4.3 \pm 3.5 \times 10^4$	5.1 ± 2.6	1.4 ± 1.3	0.38 ± 0.09

Overall, both glucose and lactate biosensors were fast to respond to changes in concentration, and displayed good sensitivity, but responses were varied. The apparent K_m of the lactate biosensor was considerably less than for the glucose biosensor, as expected

3. CLINICAL ANALYSIS SYSTEM FOR DIALYSATE METABOLITES

on the basis of the K_m of the free enzyme. The apparent K_m for the glucose biosensor was considerably less than that of the free enzyme (30 mM from Genzyme data sheet). A similar trend was also found by Vasylieva *et al.* (107) and may reflect distortion of the enzyme during immobilisation, leading to a change in the kinetics of the enzyme. Nevertheless, non-linear curve-fitting can be used to fit the calibration values and glucose levels can still be detected in the physiological range.

3.4 Extending the biosensor dynamic range

To extend the linear range of a biosensor, a diffusion-limiting membrane can be added as an outer layer, as depicted in figure 3.14. The addition of this layer inhibits mass transport to the enzyme, resulting in a response that is dependent on substrate diffusion rather than on enzyme kinetics alone. However, limiting diffusion of the substrate also results in a reduction in sensitivity. Therefore, the optimised design should be a compromise between sensitivity and dynamic range (127). Several membranes have been used to limit diffusion, including polyurethane (26, 60, 128, 129), cellulose acetate (130) and polyvinyl chloride (131).

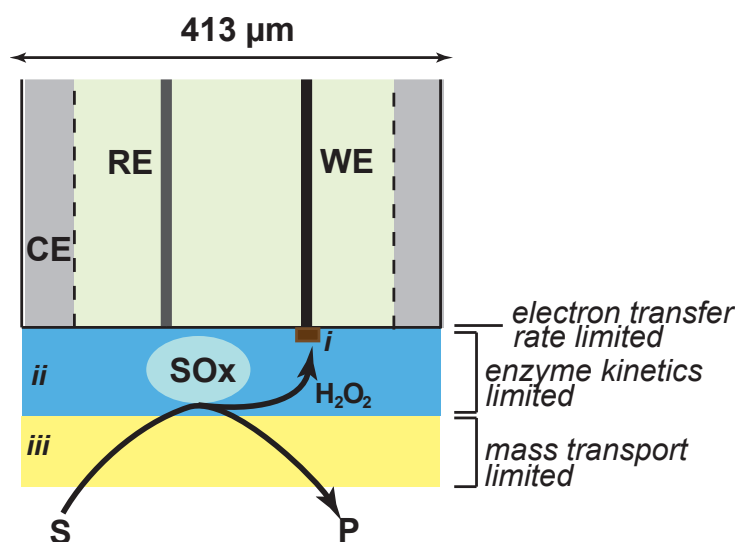


Figure 3.14: Schematic cross-section of needle biosensor tip. Layers that make up the biosensor are: (i) mPD interference layer, (ii) enzyme (SOx) entrapped in hydrogel and (iii) diffusion-limiting outer film.

The dynamic range for the lactate biosensor in particular was not suitable for the *in vivo* applications in this thesis. Therefore, an outer diffusion-limiting layer of polyurethane was incorporated, which will be described in this section.

3.4.1 Preliminary investigations

Initial experiments were conducted with 11 mg/ml polyurethane (texin 985, Bayer) dissolved in tetrahydrofuran (THF). A 10 μl drop of the polyurethane solution was placed onto a glass slide and the needle tip was slowly brought down towards the drop until the solution came up to touch the needle in order to create a thin film on the electrode. A new drop was used for each biosensor, as THF is very volatile and therefore evaporation occurred quickly. The biosensors were dried upside down for 30 minutes before a calibration was carried out. As a preliminary investigation into the effect of adding a polyurethane layer, six lactate biosensors were fabricated using the procedure described in section 2.5.3.2. Of these biosensors, two received no further treatment, two were coated with the polyurethane solution for 5 seconds and the other two for 15 seconds. The current responses to increasing beaker lactate concentrations for the six biosensors are shown in figure 3.15 and their characteristics are described in more detail in table 3.2.

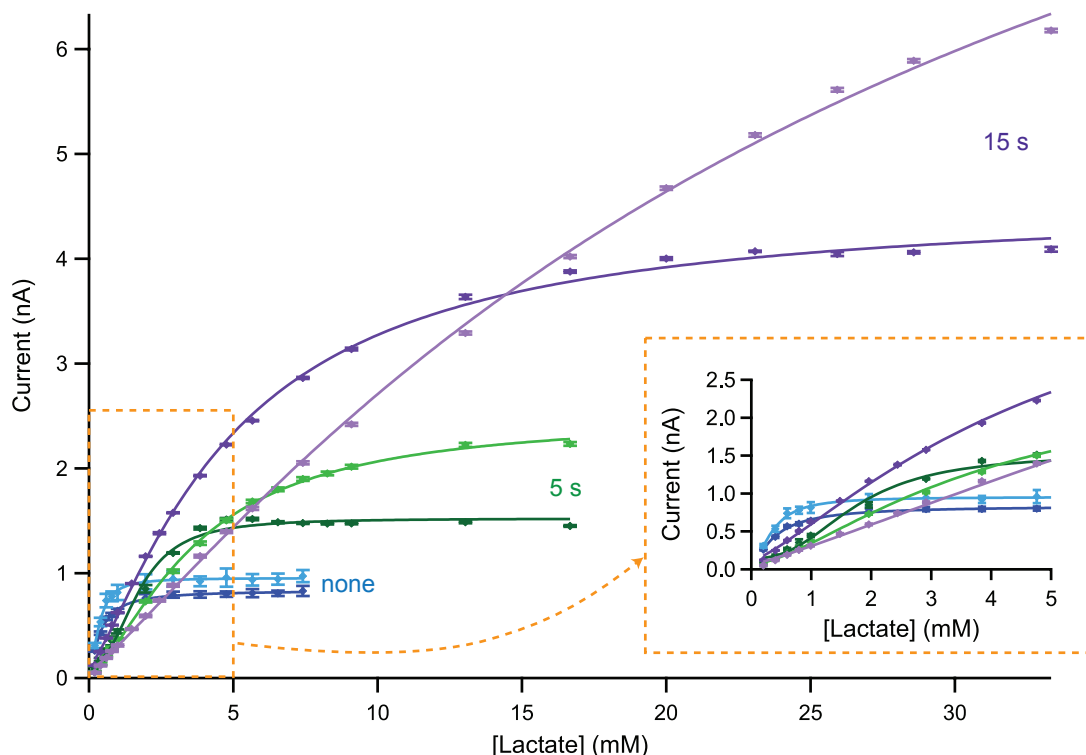


Figure 3.15: Effect of polyurethane outer layer on lactate biosensor response. Calibration curves for six lactate biosensors, carried out in a beaker. Biosensors were held at a constant potential of +0.75 V. The blue traces are for two biosensors with no polyurethane layer, the green traces are for two biosensors that were coated with the polyurethane solution for 5 s and the purple traces are for two biosensors which were coated with the polyurethane solution for 15 s. Mean \pm standard deviation of measurement is shown. Points fitted with Hill equation. *Inset:* Magnified view of the current response in the physiological range (low lactate concentrations).

3. CLINICAL ANALYSIS SYSTEM FOR DIALYSATE METABOLITES

Table 3.2: Effect of polyurethane coating time on lactate biosensor response.

Polyurethane coating time	V_{max} (nA)	K_m (mM)	Sensitivity (nA/mMcm ²)	T_{90} (s)
None	0.95 ± 0.01	0.38 ± 0.07	1.24×10^4	5.07 ± 0.76
None	0.84 ± 0.01	0.39 ± 0.09	3.62×10^4	8.80 ± 2.11
5 s	2.50 ± 0.05	3.70 ± 0.11	1.91×10^4	5.54 ± 0.25
5 s	1.52 ± 0.03	1.74 ± 0.11	2.84×10^4	5.55 ± 0.81
15 s	12.05 ± 1.15	30.60 ± 4.90	1.09×10^4	30.8 ± 2.23
15 s	4.53 ± 0.08	1.31 ± 0.06	3.74×10^4	18.8 ± 3.05

These results show that the addition of a polyurethane layer successfully extended the dynamic range of the lactate biosensors. Although, the results were variable, there seems to be a general trend that the addition of the polyurethane film caused an increase in the K_m , V_{max} , the response time and the dynamic range of the biosensor and resulted in a decrease in sensitivity. These effects were greater with longer coating times. These observations are consistent with the biosensor being diffusion-limited. The change in V_{max} was unexpected; the biosensors behaved as though there was more enzyme available. In this case, lactate biosensors were not calibrated prior to treatment with polyurethane. Therefore, the outer layer may have prevented enzyme from being lost during the calibration, which may explain why biosensors coated with polyurethane behaved as though they had a higher enzyme loading.

In order to investigate this effect, lactate biosensors were calibrated before being coated with the polyurethane solution for 15 s, after which they were calibrated again. If the effect seen previously was due to the polyurethane film preventing enzyme from being washed out during hydration of the hydrogel, then the effect would not be seen if the biosensor had already been hydrated prior to coating. Figure 3.16 shows the calibration curves for two lactate biosensors before and after coating with polyurethane.

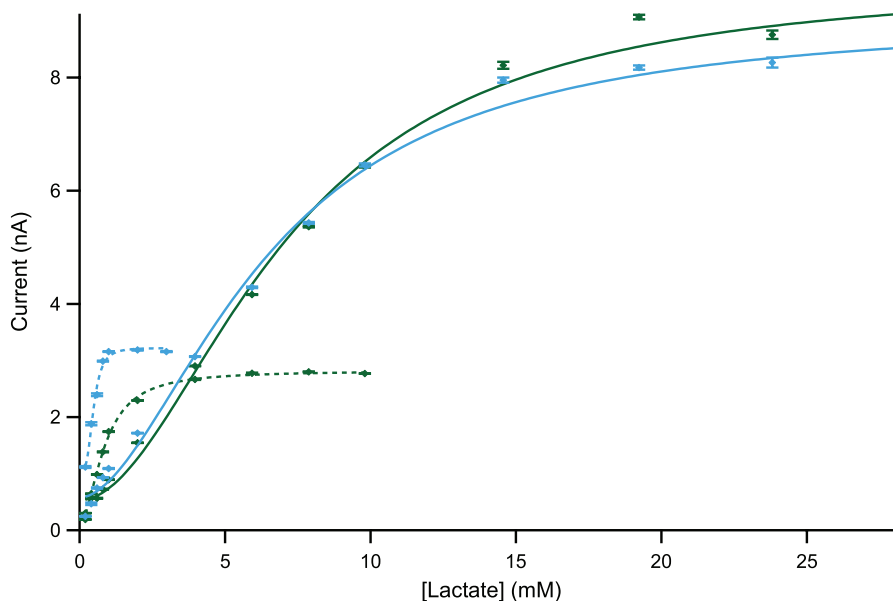


Figure 3.16: Lactate biosensor calibration before and after coating with polyurethane. Calibration curves for two lactate biosensors, carried out in a beaker. Biosensors were held at a constant potential of +0.75 V. The dotted traces show the biosensor response prior to coating with a polyurethane film and the solid traces show their response after coating with the polyurethane solution for 15 s. Mean \pm standard deviation of measurement is shown. Points fitted with the Hill equation.

These results clearly show that the higher V_{max} for polyurethane-coated electrodes was not due to the enzyme being more effectively trapped. In order to investigate what, if any, effect coating with the polyurethane solution had on the hydrogel structure, SEM was used to image the hydrogel with and without treatment with polyurethane. In order to achieve this, 15 μl drops of GOx hydrogel solution were made, were placed in the oven at 55°C for 2 hours and were stored at 4°C. Some hydrogel drops were dipped into a solution of 11 mg/ml polyurethane in THF (0.25 $\mu\text{l}/\text{ml}$, Brij 30 surfactant was also added and will be discussed later) for 15 s to mimic the biosensor treatment conditions. Others were dipped into THF only for 15 s to identify whether any structural changes observed are due to the polyurethane or the THF solution it is dissolved in. SEM images of these hydrogels are shown in figure 3.17.

As shown in figure 3.17, crystals were clearly visible on the surface of the polyurethane-coated hydrogel but were not visible on the untreated hydrogel (shown earlier in figure 3.12). These crystals were also visible when the hydrogel was dipped in just THF, suggesting that it is the THF and not the polyurethane causing this effect.

3. CLINICAL ANALYSIS SYSTEM FOR DIALYSATE METABOLITES

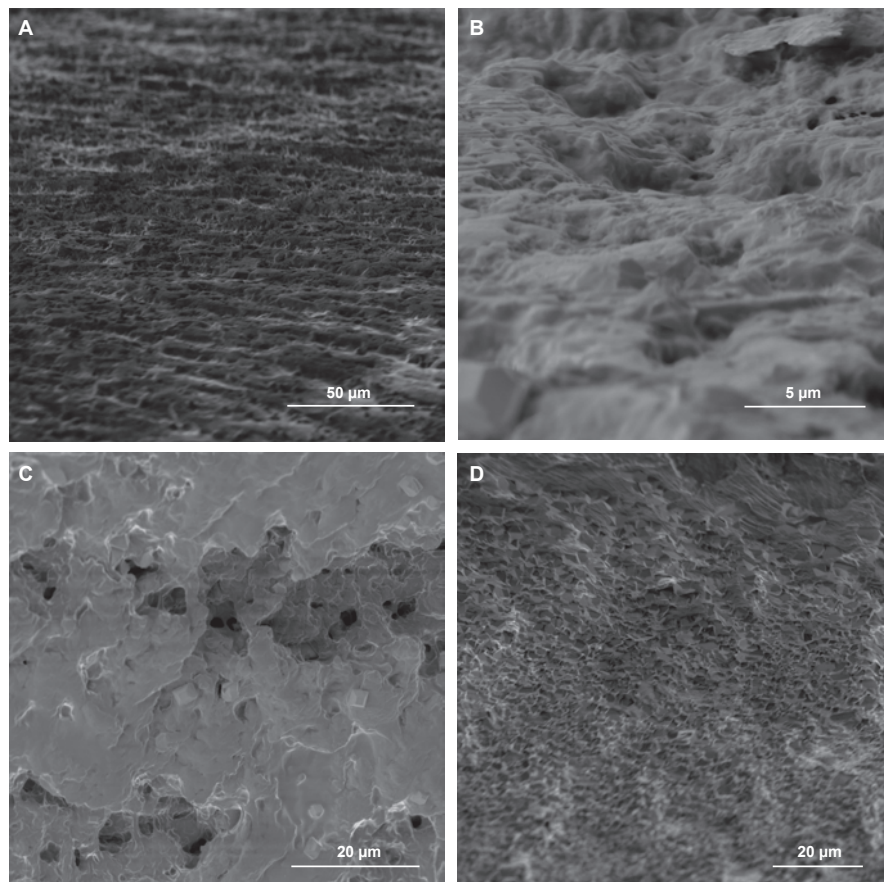


Figure 3.17: SEM images of GOx hydrogel after coating with polyurethane in THF. *A-C.* The hydrogel was dipped into 11 mg/ml polyurethane in THF for 15 s. Crystals are visible on the surface. *D.* The hydrogel was dipped into THF for 15 s. Regular crystals were formed after dipping the hydrogel in THF.

3.4.2 Effect of multiple layers of polyurethane

In order to optimise the process of coating the biosensors with polyurethane to obtain the optimal compromise between the dynamic range and the sensitivity and response time of the biosensor, the effect of adding multiple polyurethane layers was investigated. The results are shown in figure 3.18.

3.4 Extending the biosensor dynamic range

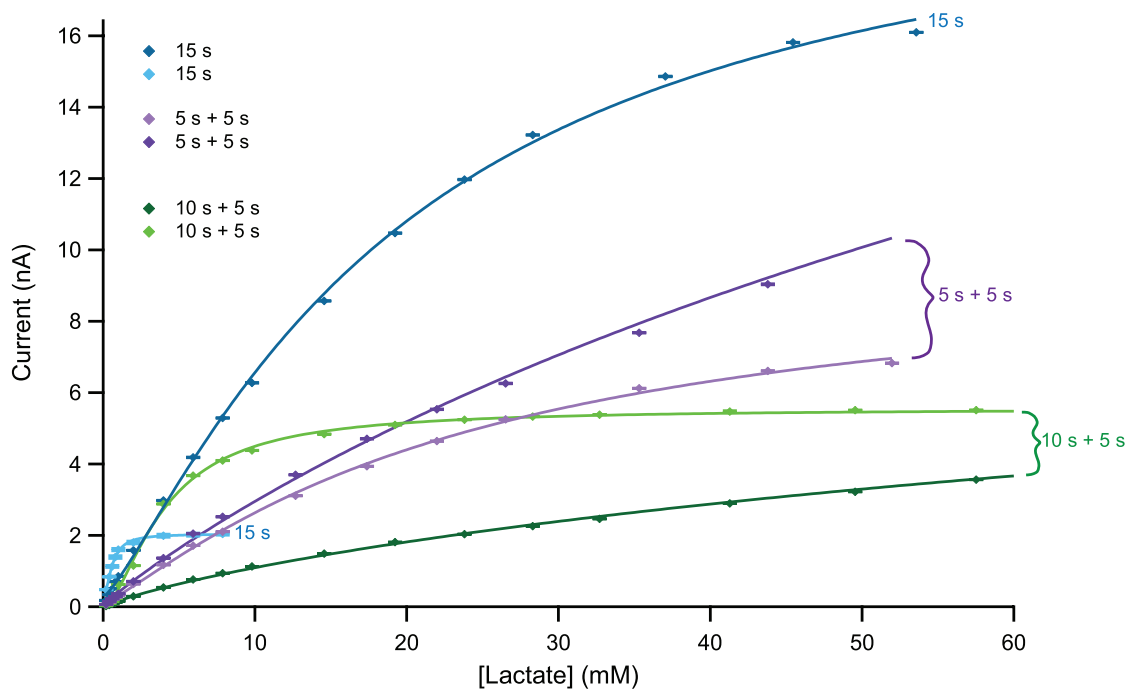


Figure 3.18: Effect of multiple layers and coating time on lactate biosensor response. Calibrations were carried out in a beaker. Biosensors were held at a constant potential of +0.75 V. Lactate biosensors were coated with polyurethane solution in either one layer for 15 s (*blue*), or in two layers for 5 s each (*purple*), or for 10 s and then 5 s (*green*). Biosensors were dried upside down at room temperature for 10 minutes in between each layer, and finally for 30 minutes. Mean \pm standard deviation of measurement is shown. Points fitted with the Hill equation. Results not shown for biosensors coated for 5 s and then 10 s as the coating was not successful.

The results obtained were variable and in some cases coating was unsuccessful. However, there is a clear trend in the results. Coating with a single layer of polyurethane for 15 s succeeded in extending the dynamic range, but only for one of the biosensors; therefore, coating with polyurethane for 15 s did not show good reproducibility. Moreover, coating with two polyurethane layers had a greater effect on the biosensor response characteristics than simply coating with a single layer and resulted in better reproducibility. However, coating with a longer first layer seemed to yield less reproducible results than when the first layer was coated for just 5 s.

3.4.3 Reproducibility

The biosensor response characteristics were extremely variable after coating with polyurethane, despite efforts to control the coating process. To address this problem, 0.25 $\mu\text{l}/\text{ml}$ of a surfactant (Brij 30, Sigma Aldrich, UK) was added into the polyurethane solution to prevent pinhole formation during solvent evaporation (26, 128, 129). In addition, the electrodes were coated with polyurethane solution using a micro-manipulator in an attempt to make

3. CLINICAL ANALYSIS SYSTEM FOR DIALYSATE METABOLITES

the coating procedure more consistent. However, the biosensors still showed considerable variability. Six lactate biosensors produced in this way were imaged under a microscope. Pictures of each are shown in figure 3.19.

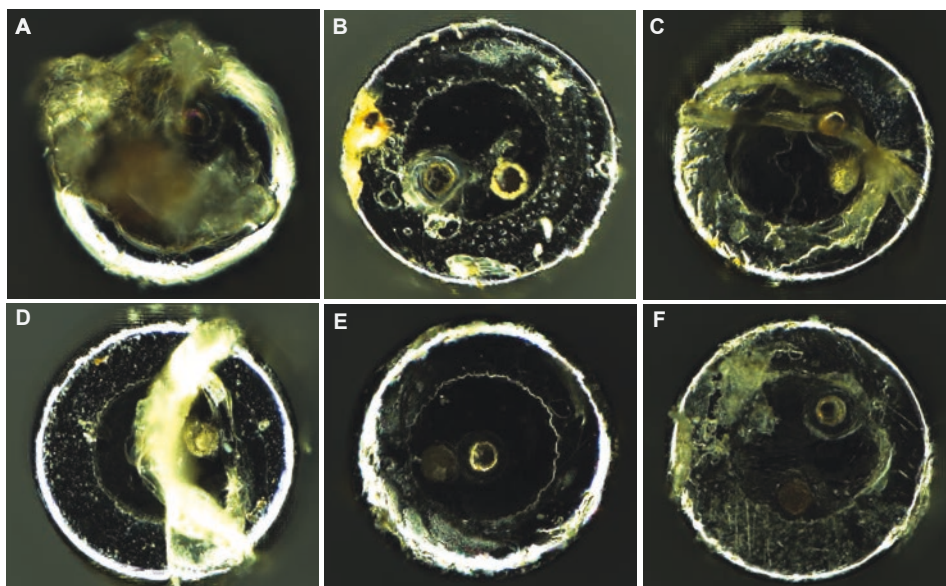


Figure 3.19: Microscope images of polyurethane-coated lactate biosensors. Images show the needle tip in each case. The two discs in the centre are the working and reference electrodes. The needle is $413 \mu\text{m}$ in diameter.

These images clearly show why the corresponding responses are variable. The biosensor shown in figure 3.19A has a large polyurethane aggregate covering almost the entire needle tip, whereas the biosensors shown in figure 3.19B-F have varying amounts of polyurethane visible, sometimes covering the working electrode. The current response of the two biosensors shown in figure 3.19A and B (representing the two extremes) are shown in figure 3.20 and are summarised in table 3.3.

For biosensor A, which had a large polyurethane aggregate at the tip, the response time was long and the sensitivity was low, compared with biosensor B, which had no large aggregates over the electrodes.

Table 3.3: Variability in lactate biosensor responses.

Biosensor	Sensitivity (nA/mMcm^2)	T_{90} (s)
A	1.5×10^3	209 ± 11.24
B	6.7×10^3	7.33 ± 0.24

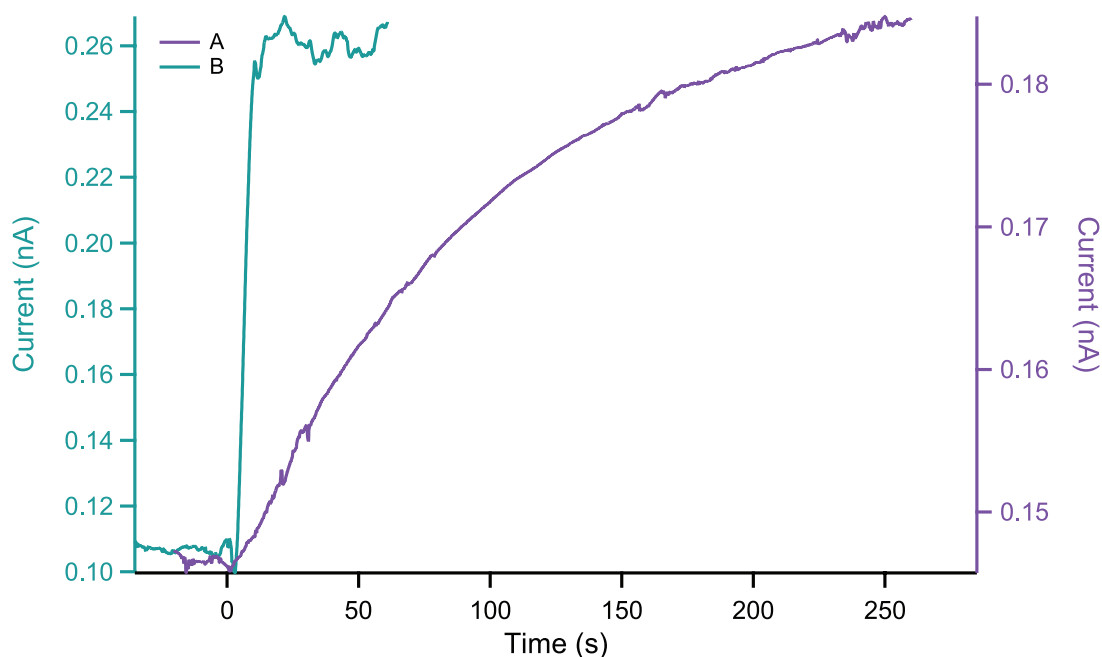


Figure 3.20: Response time of polyurethane-coated lactate biosensors. Raw data trace for a step change in lactate concentration from 2 to 4 mM in a well-stirred beaker. Time 0 is the point of injection. The two biosensors were prepared in the same way but show large variability in their responses.

3.4.4 Protocol optimisation

The variability in the polyurethane coating could be due to the method of casting the layer. As a result of the fairly small volume ($50 \mu\text{l}$) used to coat each electrode and the high volatility of THF, evaporation occurred very quickly. This meant that it was very difficult to control the process, as slight variations, for instance in the time between pipetting the drop of polyurethane solution onto a glass slide and coating the electrode, could have a large impact on the final result. To overcome this issue, the procedure was adapted so that the micro-manipulator was used to dip the needle electrode biosensor into a small glass vial containing the polyurethane solution, through a hole in the lid to prevent evaporation. However, as a result, the coating time and the polyurethane concentration had to be optimised for this new protocol as, using the previous conditions, no real change was observed in the dynamic range of the biosensors. After several attempts, the optimal biosensor response was obtained with 25 mg/ml polyurethane in THF and $0.25 \mu\text{l/ml}$ Brij 30. The biosensors were dipped into the solution twice, for 15 s each. The electrodes were allowed to dry upside down for 10 minutes in between the two layers and for 30 minutes after the final layer. Despite this optimised protocol, the response of the lactate biosensors was still found to be quite variable, therefore further optimisation is necessary.

3. CLINICAL ANALYSIS SYSTEM FOR DIALYSATE METABOLITES

This final protocol was used to fabricate biosensors for *in vivo* monitoring in chapter 8.

3.4.5 Polyurethane-coated biosensor characteristics

The same methodology was applied for glucose hydrogel biosensors as well as for lactate. An example of a typical response for a glucose and lactate biosensor fabricated using this method is shown in figure 3.21. Comparison with figure 3.13 clearly indicates that the polyurethane-coated biosensors are both mass-transport limited.

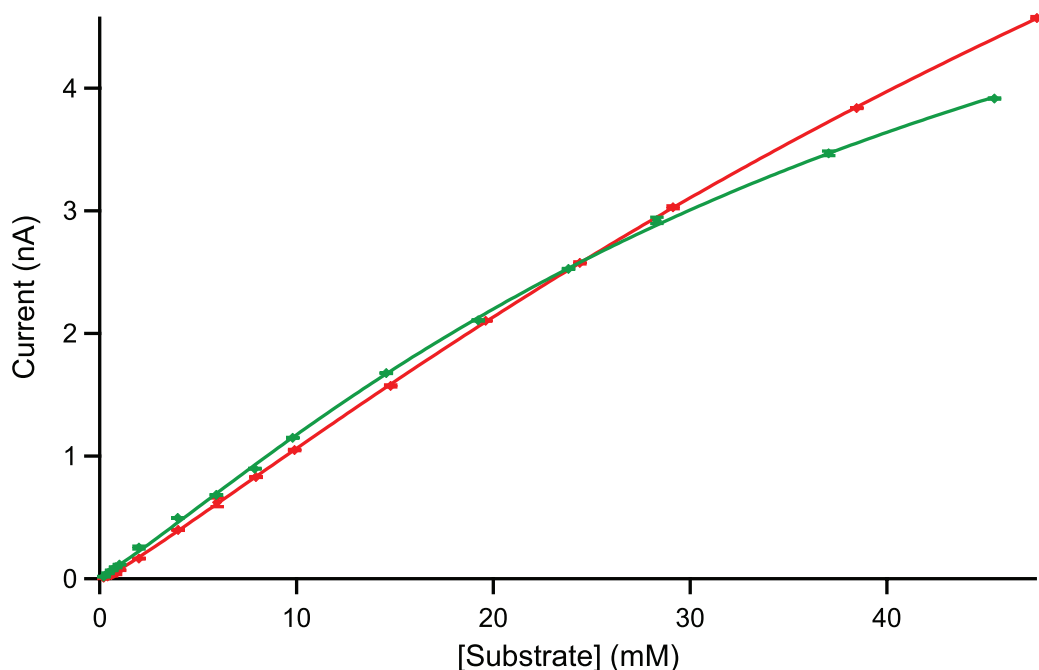


Figure 3.21: Typical polyurethane biosensor calibration curves. Calibrations were carried out in a beaker. Biosensors were held at a constant potential of +0.75 V. The green trace shows the lactate response and the red trace shows the glucose response. Mean \pm standard deviation of measurement is shown. Points fitted with the Hill equation.

The response time and sensitivity of polyurethane-coated glucose and lactate biosensors are summarised in table 3.4. The variability in both sensitivity and the T_{90} response is caused by the difficulty in controlling the thickness of the polyurethane film produced.

Table 3.4: Glucose and lactate polyurethane biosensor responses.

Biosensor	Sensitivity (nA/mMcm ²)	T_{90} (s)
Glucose (n=5)	$3.2 \pm 2.2 \times 10^3$	36.1 ± 19.6
Lactate (n=21)	$1.4 \pm 1.7 \times 10^4$	22.8 ± 11.3

3.4.6 Summary

Glucose and lactate biosensors have been adapted to include a diffusion-limiting polyurethane outer layer. This modification results in a loss in sensitivity as well as an increase in the response time of the biosensor. However, it extends the dynamic range, which, particularly for lactate sensing, allows detection within the physiological range for tissue dialysate. The method of coating the biosensors in the polyurethane layer was optimised but further optimisation is required to improve reproducibility.

3.5 In-flow enzyme addition

The advantage of combining microfluidic chips with LabSmith components is that it is possible to create a ‘homogeneous’ biosensing system. There have been limited reports of in-flow glucose and lactate enzymatic sensing, in which the enzyme is mixed with the substrate in solution (132, 133, 134). This method could be advantageous, as the activity of enzymes changes upon immobilisation as a result of structural changes that occur. Using the LabSmith programmable syringe pumps it is possible to create a biosensing system in which enzyme is automatically dosed into the dialysate stream to react with the substrate in solution. The reaction product can then be detected at a downstream electrode. This system would allow separate optimisation of the biorecognition and detection elements of the biosensing system.

3.5.1 Experimental setup

A sensing system was constructed based on the autocalibration board described in section 3.2.3. A schematic diagram of the setup is shown in figure 3.22. In addition to the calibration components, another pump and valve were incorporated for addition of the enzyme solution.

3. CLINICAL ANALYSIS SYSTEM FOR DIALYSATE METABOLITES

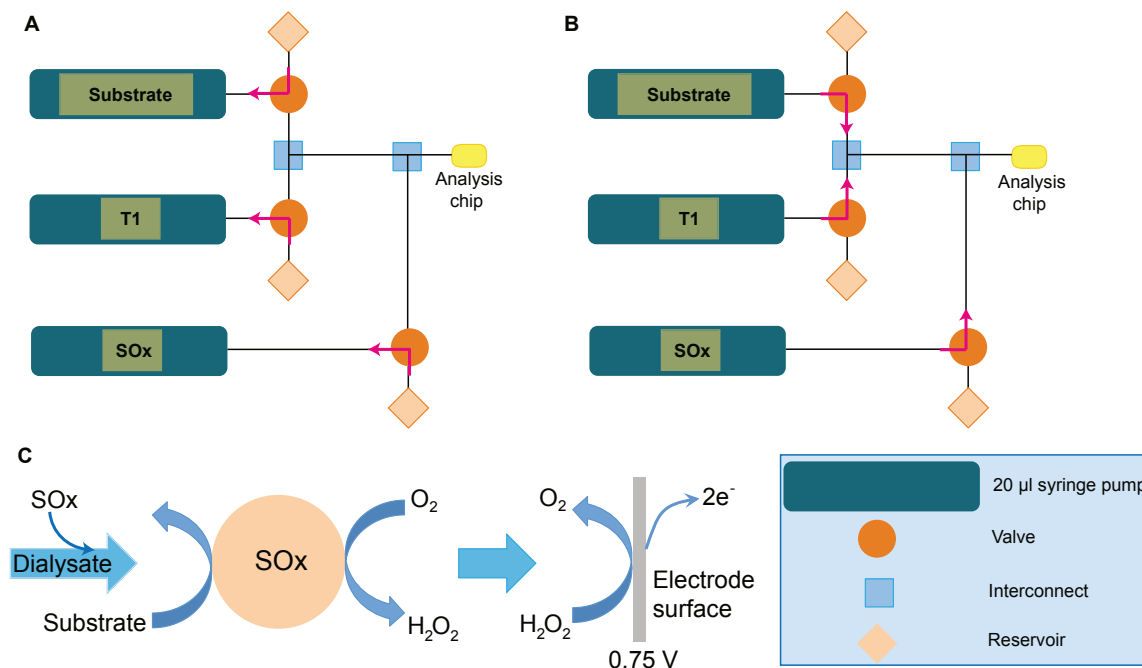


Figure 3.22: Experimental setup for dosing in enzyme for in-flow sensing. *A.* Pumps can be programmed to refill automatically by switching the valves so that the pumps can draw up new solution from their reservoirs. *B.* Valves are switched so that the calibration stream is directed towards the analysis chip. Enzyme is added into the calibration stream before it reaches the analysis stream. *C.* Substrate detection reaction mechanism. The enzyme (SOx) is added into the dialysate, where it oxidises the substrate producing hydrogen peroxide. The hydrogen peroxide is detected at a platinum electrode by oxidation.

3.5.2 Calibration

This section will describe the detection of glucose and lactate using this system. For glucose detection a solution of GOx in T1 (8.7 mg/ml) was used and for lactate detection a solution of LOx in T1 (4.2 mg/ml) was used. The enzyme stream flowed at 0.5 μ l/min and the calibration stream flowed at 2 μ l/min, giving a total flow rate of 2.5 μ l/min at the electrode. An example of a 5-point glucose calibration from 5 to 0 mM is shown in figure 3.23. This figure also shows typical calibration curves for glucose and lactate using this system.

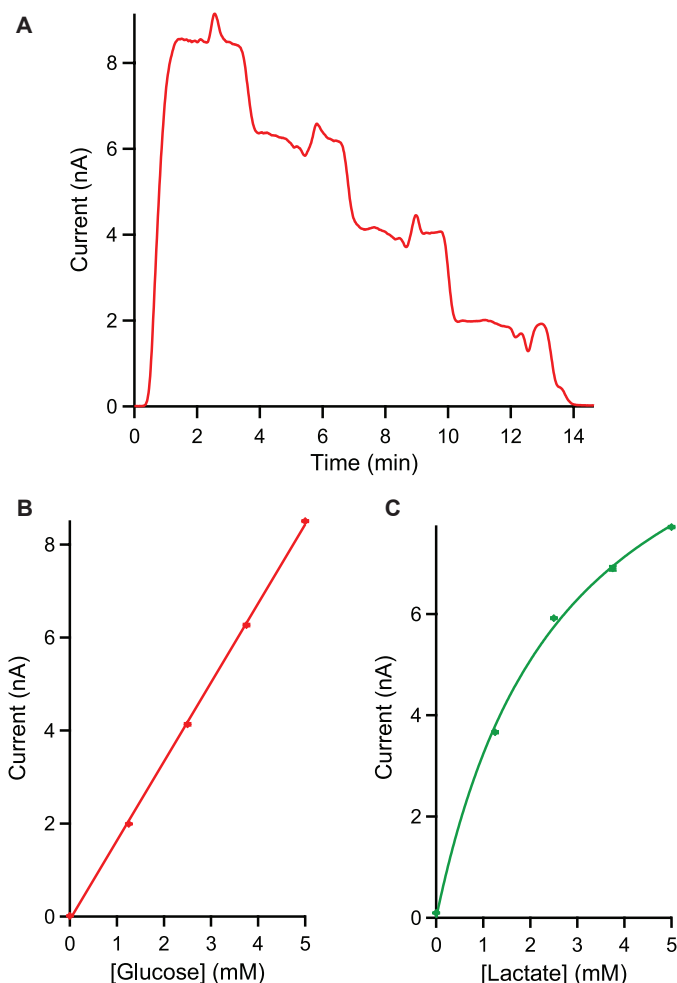


Figure 3.23: Glucose and lactate calibrations using in-flow sensing system. *A.* Raw data for a 5-point glucose calibration from 5 to 0 mM at 2 $\mu\text{l}/\text{min}$ using a 50 μm platinum disc electrode. Steps were 5, 3.75, 2.5, 1.25 and 0 mM. *B.* Corresponding glucose calibration curve fitted with a straight line. *C.* Lactate calibration curve for a 5-point calibration from 5 to 0 mM using a 50 μm platinum disc electrode. Points fitted with the Michaelis-Menten equation. Mean \pm standard deviation of measurement given. Enzyme (GOx 8.7 mg/ml or LOx 4.2 mg/ml) flow rate was 0.5 $\mu\text{l}/\text{min}$.

For both glucose and lactate, the currents observed were considerably higher than those observed with the hydrogel biosensors for the same size electrode. For these calibrations, the glucose biosensing system had a sensitivity of $5.8 \times 10^5 \text{ nA}/\text{mMcm}^2$ and the lactate biosensing system had a sensitivity of $1.5 \times 10^4 \text{ nA}/\text{mMcm}^2$, which are considerably higher than for the hydrogel biosensors. Furthermore, the dynamic range of the lactate biosensing system was extended compared with the lactate hydrogel biosensors, but not to the extent of the polyurethane-coated biosensors. Using these conditions, only 300 μl of enzyme solution would be used for 10 hours of continuous monitoring.

In this system, although the enzyme is substrate-specific, the electrode is not, it simply

3. CLINICAL ANALYSIS SYSTEM FOR DIALYSATE METABOLITES

detects the product of the in-flow reaction, which is the same for both the glucose and the lactate reaction mechanisms. Therefore, care was taken throughout to ensure that all components used for one enzyme were kept separate from those used for the other to prevent cross-contamination.

3.5.3 Stability

A gradual loss of sensitivity was observed over time; this could be due to enzyme degradation or a result of the enzyme adhering to the electrode surface and blocking the active sites. In order to investigate this, repeated calibrations were carried out with a 1-hour pause in between. The results for the glucose system are shown in figure 3.24A. There was a considerable loss in sensitivity from 1.2×10^5 nA/mMcm² to 1.9×10^3 nA/mMcm² over 12.5 hours. This experiment was repeated with a poly(phenol)-coated electrode to investigate whether the film would protect against electrode fouling, if this was the cause of the gradual loss in sensitivity. The results are shown in figure 3.24B, and figure 3.24C compares the sensitivity over time for the uncoated and poly(phenol)-coated electrode.

The loss in sensitivity was much less for the poly(phenol)-coated electrode. This suggests that the sensitivity loss over time was caused by the enzyme adhering to the electrode surface and that the poly(phenol) film provides some protection against this. Furthermore, the poly(phenol) film provided a crucial screening layer to prevent oxidation of other species present in the dialysate (105). There was still some loss in sensitivity over time for the coated electrode, as the sensitivity decreased from 1.1×10^5 nA/mMcm² to 4.3×10^4 nA/mMcm² over 35 hours. However, as shown in figure 3.24C, the system was able to operate continuously for more than 35 hours. A similar trend was observed for the lactate sensing system.

To investigate whether this loss in sensitivity was caused by enzyme degradation over time, after running the system overnight, the enzyme solution was replaced with newly made solution. Even with fresh enzyme solution, the sensitivity remained the same. Therefore, this sensitivity loss is probably caused by enzyme adherence onto the electrode, but this effect is greatly reduced by the poly(phenol) film. This illustrates the need to regularly calibrate during long periods of monitoring.

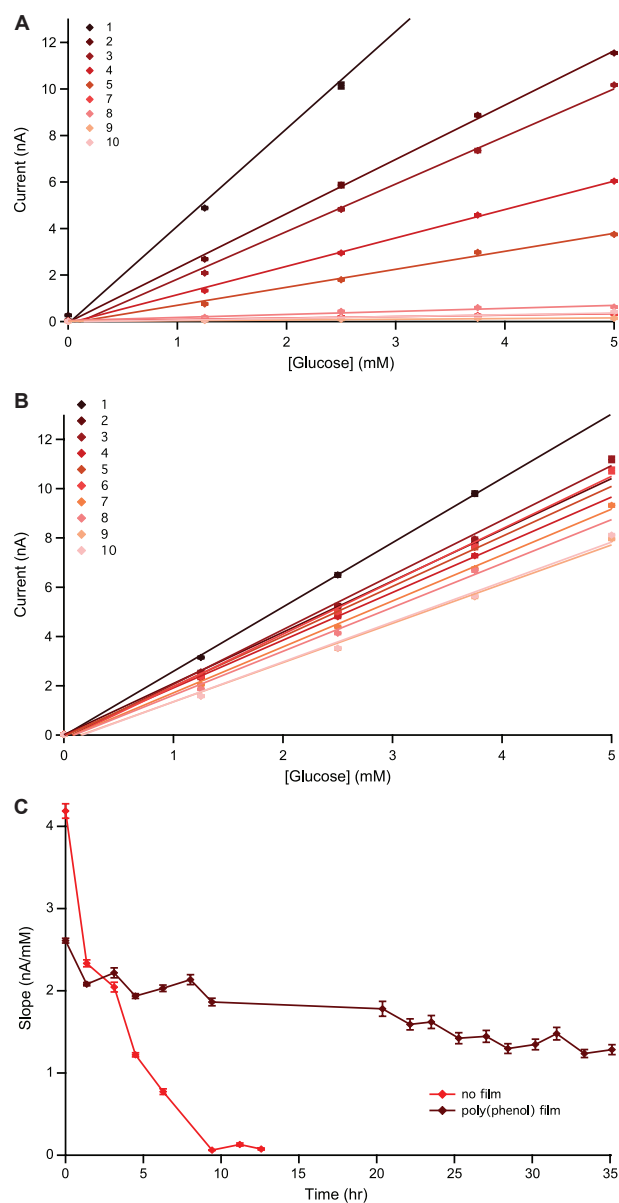


Figure 3.24: Repeated glucose calibrations with and without poly(phenol) film on electrode. The script was programmed to carry out a 5-point glucose calibration followed by a 1-hour pause and was then repeated. Calibrations were carried out using an uncoated *A.* and poly(phenol)-coated *B.* 50 μm platinum disc electrode. *C.* Sensitivity decreased over time for both the coated and the uncoated electrodes, but the effect was much greater for the uncoated electrode. Mean \pm standard deviation of measurement given.

3.5.4 Script optimisation

Initially the pumps were programmed to push at a set flow rate until they had dispensed a certain volume of liquid. At each stage, the script waited until all pumps had dispensed their programmed volumes until it moved on to the next step. The pumps are designed to accurately deliver a fixed volume of liquid. In order to do this the pump mechanism

3. CLINICAL ANALYSIS SYSTEM FOR DIALYSATE METABOLITES

slows as it nears its end point to avoid dispensing too much. However, this affected the overall flow rate and resulted in some pumps finishing before the rest, which caused flow artefacts in the signal. In particular, this was a problem if the enzyme pump finished first, as this resulted in a temporary fall in the signal until the pump restarted.

To overcome this issue and to reduce the flow artefacts, the script commands were changed so that the pumps were instead programmed to push at a set flow rate for a certain length of time. This meant that the flow rate was constant and all pumps finished simultaneously. A comparison of a 5-point calibration carried out using the two alternative scripts is shown in figure 3.25. Although there were artefacts in both traces, they were less exaggerated for the script in which the time and flow rate were set, rather than the volume and the flow rate.

In addition, care was taken to regularly flush the system with deionised water and with methanol water (1:1), as artefacts were more evident if the pumps had not been properly cleaned. On occasions, the inside of the glass syringes were also manually cleaned.

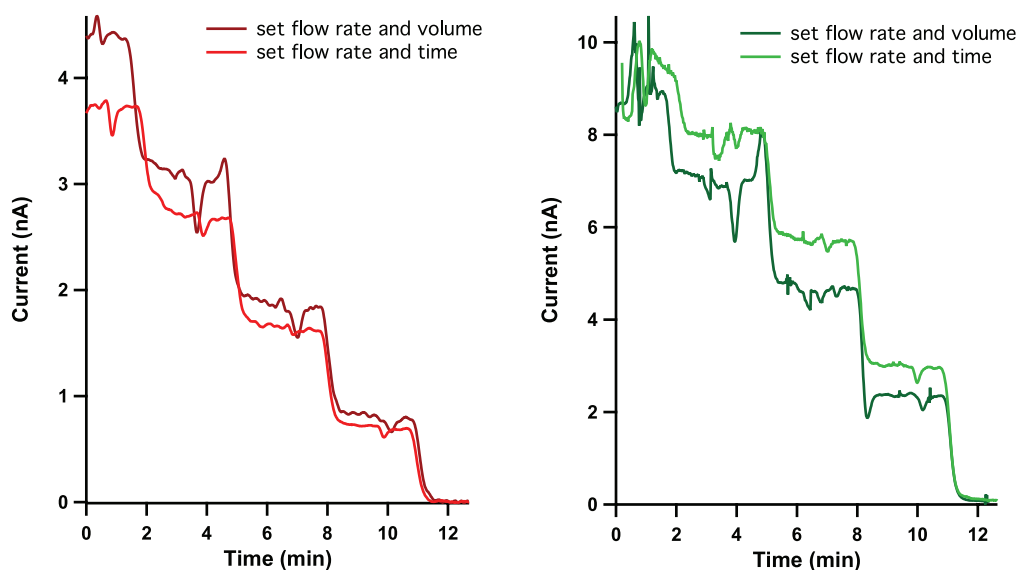


Figure 3.25: Effect of script on glucose and lactate response. Raw data for a 5-point calibration from 2 to 0 mM for glucose (*red*) and lactate (*green*) at 2 $\mu\text{l}/\text{min}$. The darker traces show the response if the script is written in terms of flow rate and volume and the lighter traces show the response if the script is written in terms of flow rate and time. Enzyme (GOx 8.7 mg/ml or LOx 4.2 mg/ml) flowed at 0.5 $\mu\text{l}/\text{min}$. Total flow rate was 2.5 $\mu\text{l}/\text{min}$.

Enzyme optimisation

The precise control offered by the LabSmith components could provide an ideal method of optimising the enzyme concentration and flow rate. As a proof of concept, an optimisation board was developed and an experiment was carried out to demonstrate whether it was

possible to determine the optimal enzyme concentration and flow rate for the analysis system in this way. The automated optimisation board was set up as shown in figure 3.26.

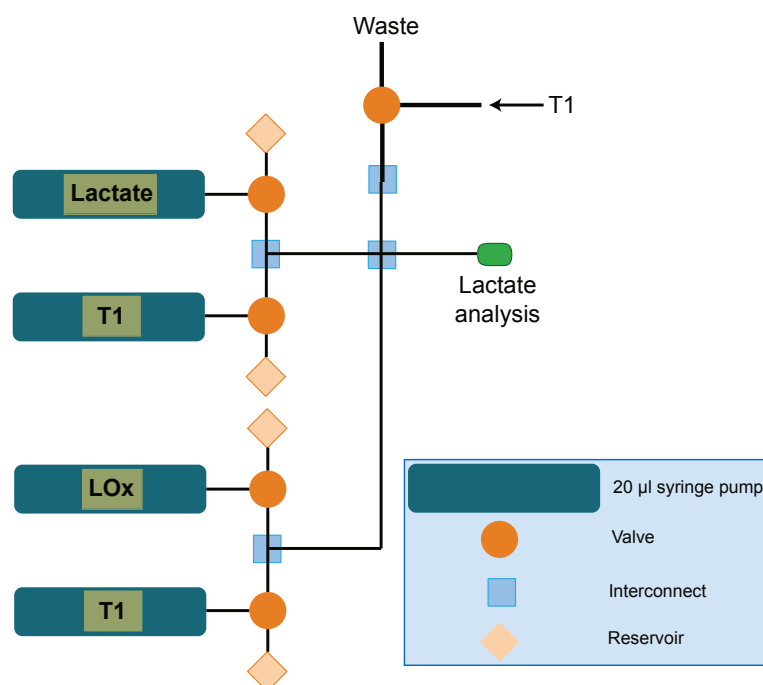


Figure 3.26: Automated board for enzyme optimisation. The board consisted of two calibration systems to dilute the enzyme and the substrate. It also contained another valve to flow T1 through the PDMS chip, when the pumps were refilling, to stop air being introduced.

The design of the optimisation board essentially consisted of two calibration boards. One was to vary the substrate concentration for each different enzyme condition, keeping the total substrate flow rate constant. The other calibration board enabled the enzyme concentration to be varied independently of flow rate. A script was written that carried out a 5-point lactate calibration for a fixed enzyme concentration at different enzyme flow rates. This process was repeated for different enzyme concentrations. When the script was complete, it looped back to the beginning and repeated.

The results of the proof-of-concept experiment for lactate optimisation are summarised in figure 3.27.

3. CLINICAL ANALYSIS SYSTEM FOR DIALYSATE METABOLITES

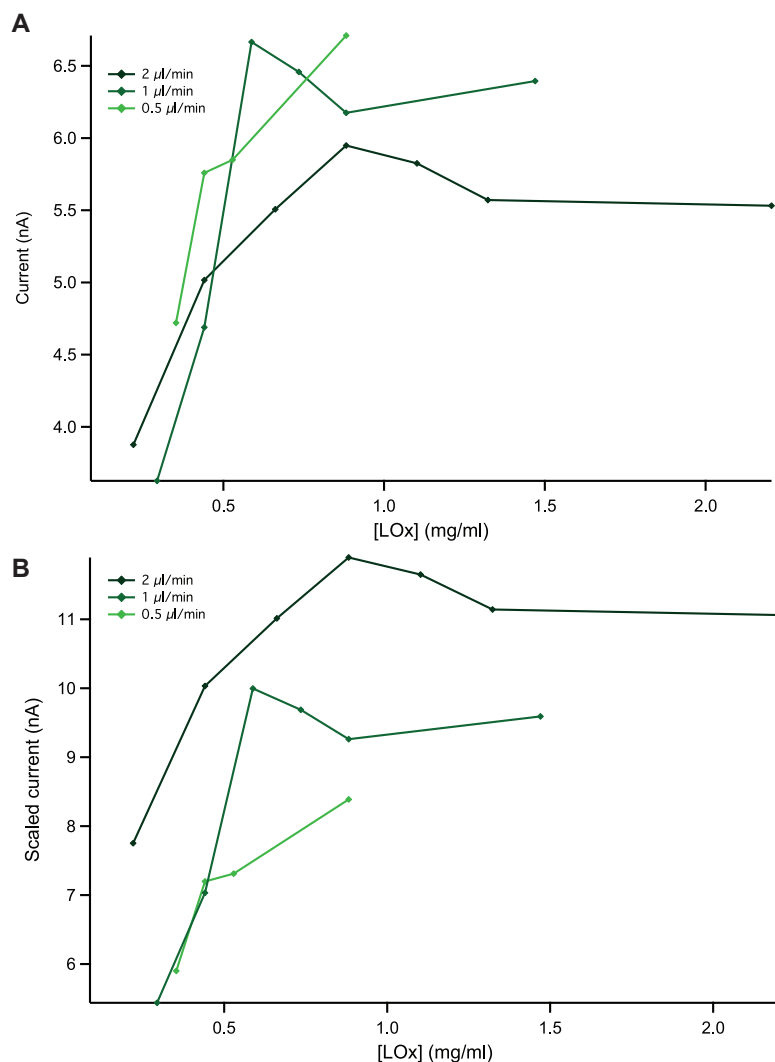


Figure 3.27: Results of LOx optimisation. *A.* Current response for 2 mM lactate mixed with varying concentrations of enzyme at 0.5, 1 and 2 $\mu\text{l}/\text{min}$. *B.* Current scaled to take into account dilution of lactate due to varying enzyme flow rate and therefore the total flow rate. Current has been multiplied by the dilution factor. In both graphs, enzyme concentration in the final volume is given. Results for 0.75 $\mu\text{l}/\text{min}$ have been omitted as there were insufficient points to identify trends.

As shown earlier, there is a gradual loss in sensitivity over time, therefore this approach produced very variable results. However, despite this variability, there does appear to be a trend for LOx. As shown in figure 3.27A, as the enzyme concentration increased, the current increased. However, above a certain enzyme concentration the response reached a plateau.

As a result of the nature of the experimental protocol, increasing the enzyme flow rate also had the effect of diluting the lactate concentration in the total flow. Therefore, figure 3.27B has been scaled to show what the current response would have been without this dilution effect. On the basis of these results, it appears that optimal currents would

be obtained by flowing the enzyme at $2 \mu\text{l}/\text{min}$ and hence delivering more enzyme per minute, but the substrate is diluted more and therefore the observed current is lower than for slower flow rates. This indicates that optimal currents could be achieved by flowing slower but with a more concentrated enzyme stock solution.

Further work is needed to improve the optimisation protocol. The steps should be carried out in a random order so as to reduce systematic bias in the results caused by electrode fouling over time. Moreover, the flow rates should be separately varied for each enzyme concentration so that the experiment does not have to be run for as long in one go, which should reduce variability.

3.5.5 In-flow enzyme addition - donor kidney analysis board

As part of the project to monitor dialysate metabolites in transplant kidneys (see chapters 4 and 5) a system was required that would allow two metabolites to be monitored in two organs. Therefore, an analysis system was built that used in-flow enzyme addition to detect glucose and lactate in two dialysate streams. This system has the advantage that it allows optimisation of the enzyme flow to create a system suitable for this application. A schematic of the setup for this analysis system is shown in figure 3.28.

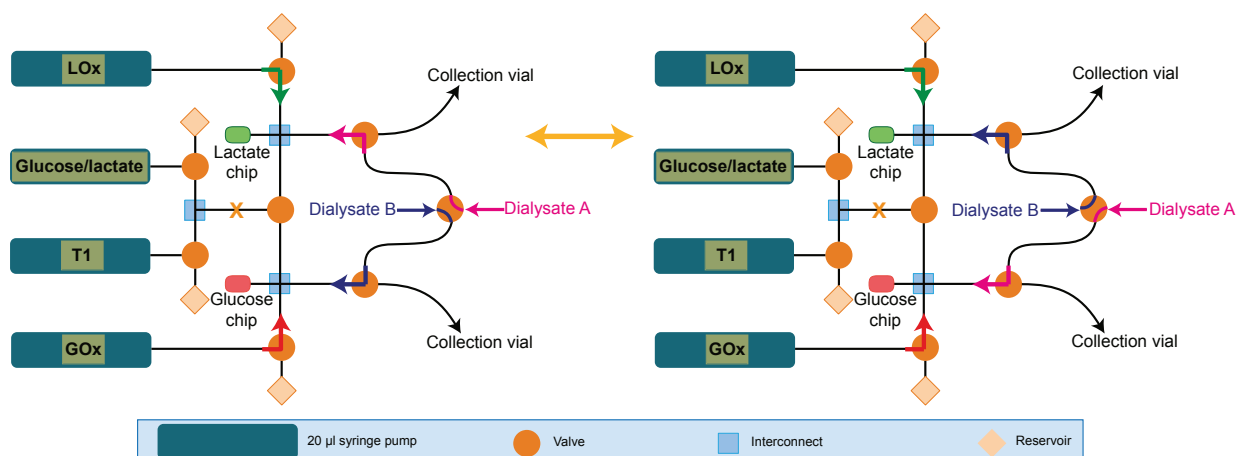


Figure 3.28: Schematic of analysis system to monitor two analytes in two donor kidneys. Dialysate A is directed towards the lactate chip and mixes with LOx, while dialysate B is directed towards the glucose chip and mixes with GOx. The dialysate valve is switched so that dialysate A is then analysed for glucose and B for lactate. The dialysate valve is programmed to switch between the two dialysate streams every 2-3 minutes. The calibration valves are closed throughout.

The system consists of the calibration components and a separate pump and valve for each enzyme stream. It also incorporates a two-position four-port valve, which provides the means to direct two dialysate streams at the same time so that each stream could be directed alternately between the two analysis chips. As shown in figure 3.28, glucose

3. CLINICAL ANALYSIS SYSTEM FOR DIALYSATE METABOLITES

was measured in one dialysate stream, while lactate was measured in the other, then the valve switched position and directed each dialysate stream into the other analysis chip. The board was fully automated to run unattended for long periods of time. Figure 3.29 shows an excerpt of raw data, using the system to analyse two different sample streams simultaneously.

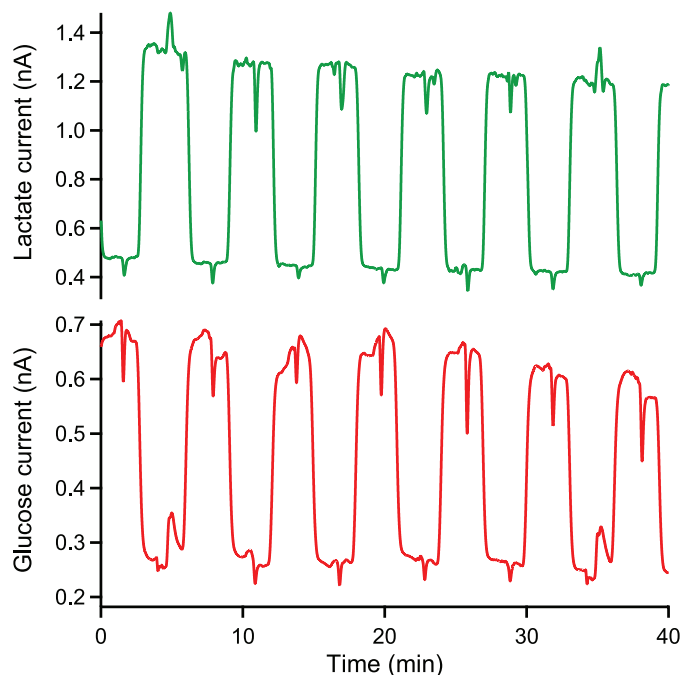
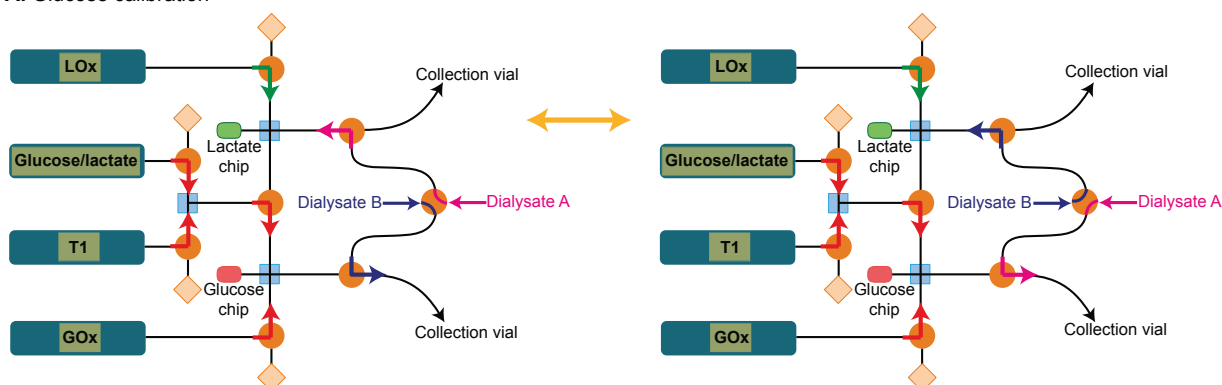


Figure 3.29: Measurement of glucose and lactate in two sample streams. Raw data showing the analysis system switching between two sample streams, 1.0 and 0.5 mM, every 3 minutes. Glucose (*red*) is measured in one sample stream while lactate (*green*) is measured in the other.

The step length was varied to investigate the minimum length required for each step in order for a stable level to be reached before the valve switched. The minimum step length was found to be 2 minutes.

It was important to incorporate the autocalibration components into the design so that regular calibrations could be carried out during long periods of monitoring. These calibrations could be set up to automatically occur at regular intervals. Each dialysate stream flowed into a valve so that the stream could be diverted to a collection vial during calibrations. This ensured that flow through the probe was never interrupted. With this setup, the glucose and lactate analysis systems were calibrated separately. During calibration of one analyte, measurement of the other analyte in the two dialysate streams alternately was still possible. One dialysate stream was diverted to a collection vial, while the other was analysed and the valve automatically switched between the two dialysate streams.

A. Glucose calibration



B. Lactate calibration

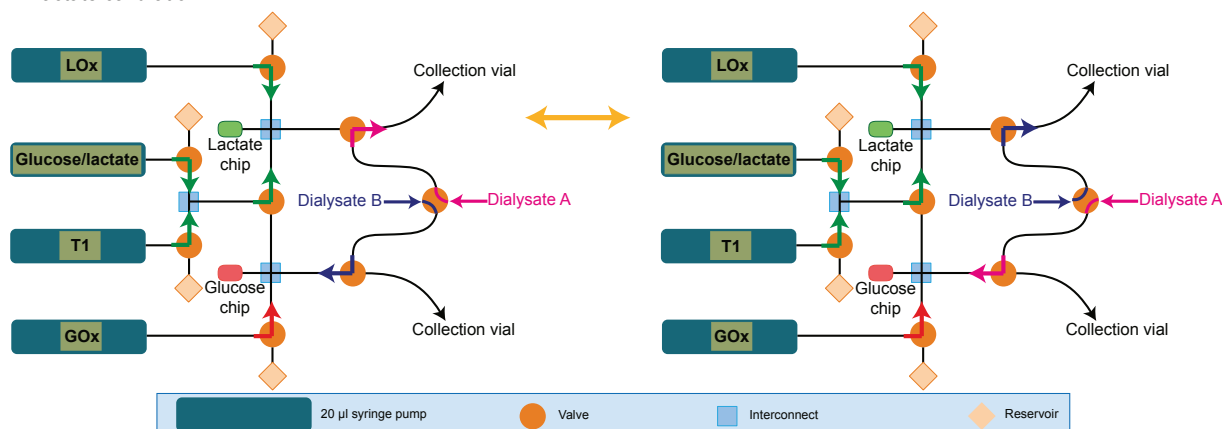


Figure 3.30: Calibration of microfluidic analysis board. *A.* Configuration during glucose calibration. Changing the flow rates of the two pumps varies the overall concentration of analyte in the calibration stream. While glucose is calibrating, lactate can still be alternately detected in both dialysate streams by switching the dialysate valve. The dialysate stream not being analysed is switched to a collection vial. *B.* Configuration during lactate calibration. The dialysate valve is switched so that glucose can be alternately detected in both dialysate streams during lactate calibrations. The dialysate stream not being analysed is switched to a collection vial.

An analysis algorithm was written in Matlab to automatically process the data. This involved separating the data for each dialysate stream and converting the detected currents into concentrations for each analyte using the relevant calibration.

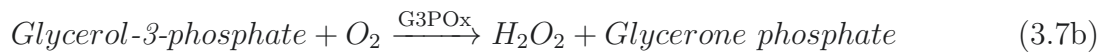
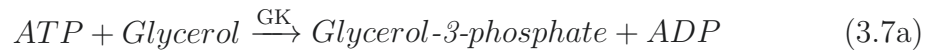
3.5.6 ATP detection

The method of dosing enzyme into the dialysate has been shown for glucose and lactate. This method is ideal for more complicated systems, such as those involving multiple enzymes, as it allows the reaction to be carried out in sequence, consecutively adding enzymes. It also allows optimisation of each step individually.

ATP would be a useful biomarker to measure in transplant kidneys, as it would provide

3. CLINICAL ANALYSIS SYSTEM FOR DIALYSATE METABOLITES

additional information about whether the energy demands of the tissue are being met. Two mechanisms have been reported for enzymatic detection of ATP. The first involves the use of two enzymes, hexokinase and GOx (105). In the presence of ATP, hexokinase converts glucose to glucose-6-phosphate, which cannot react with GOx, therefore, as the concentration of ATP increases, the glucose signal decreases. However, this system is also glucose sensitive, and is therefore not ideal for a situation in which glucose levels may vary. An alternative mechanism uses a two enzyme cascade (135), as shown in equation 3.7.



As a proof of concept, a system was set up to detect ATP by consecutively dosing in glycerol kinase (GK) and glycerol-3-phosphate oxidase (G3POx). For the reaction to depend only on ATP concentration, the glycerol concentration needs to be high enough to saturate the GK (>0.5 mM) (135). This can be achieved by dissolving the GK in a high concentration of glycerol. Figure 3.31 shows the experimental setup used to detect ATP.

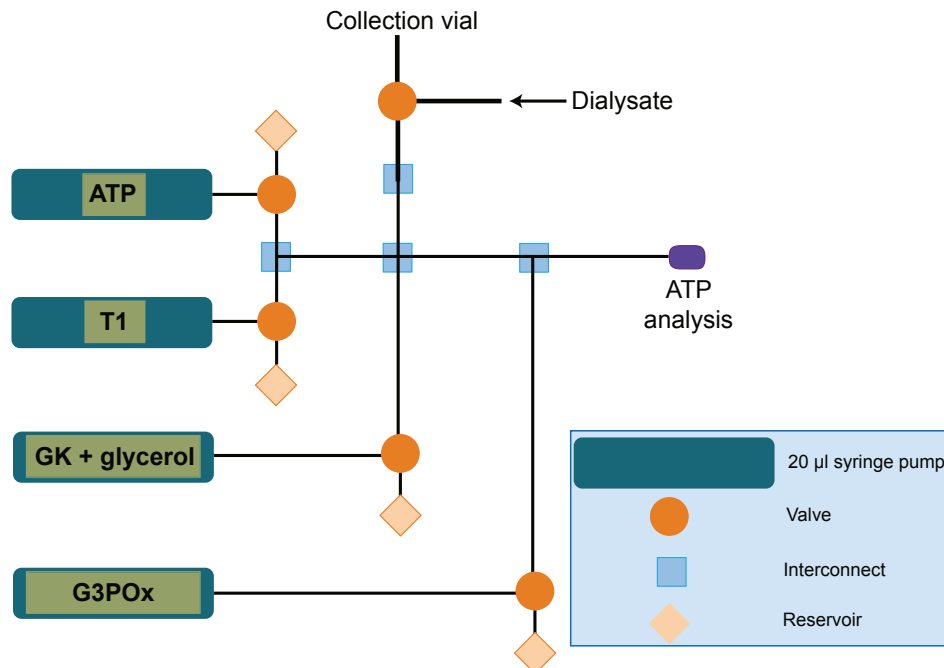


Figure 3.31: Schematic of analysis system to measure dialysate ATP. The board was set up as for glucose or lactate detection, with the calibration components and a dialysate valve. In addition, two enzyme pumps were incorporated, which would add in GK (6.25 mg/ml) and glycerol (5 mM) first and then G3POx (6.55 mg/ml) downstream. The reaction mixture flowed into the PDMS analysis chip, which contained a 50 μm platinum poly(phenol)-coated disc electrode. Both enzyme solutions flowed at 0.5 $\mu\text{l}/\text{min}$.

The glycerol solution was diluted 5 times when it was added into the dialysate stream, therefore a higher initial concentration than necessary was used to ensure that when diluted the concentration was still sufficient to saturate the GK. For this preliminary experiment, the enzyme activities used were 1:1 (250 U/ml), but in the future this could be optimised to improve the overall sensitivity of the system.

An example of a 5-point calibration from 100 to 0 μM is shown in figure 3.32, together with the corresponding calibration curve. Although the detected currents were low, each 25 μM step was clearly visible. Figure 3.32C shows the results of a preliminary experiment to measure the ATP concentration in a sample of kidney dialysate. During haemoperfusion of a porcine kidney, cortical dialysate was collected into a 1 m length of storage tubing, as described in section 4.2.4, which was frozen until analysis was possible, and run through the ATP analysis system at a later time. It was possible to detect ATP in the kidney dialysate using this method. ATP levels were fairly stable and very low.

3. CLINICAL ANALYSIS SYSTEM FOR DIALYSATE METABOLITES

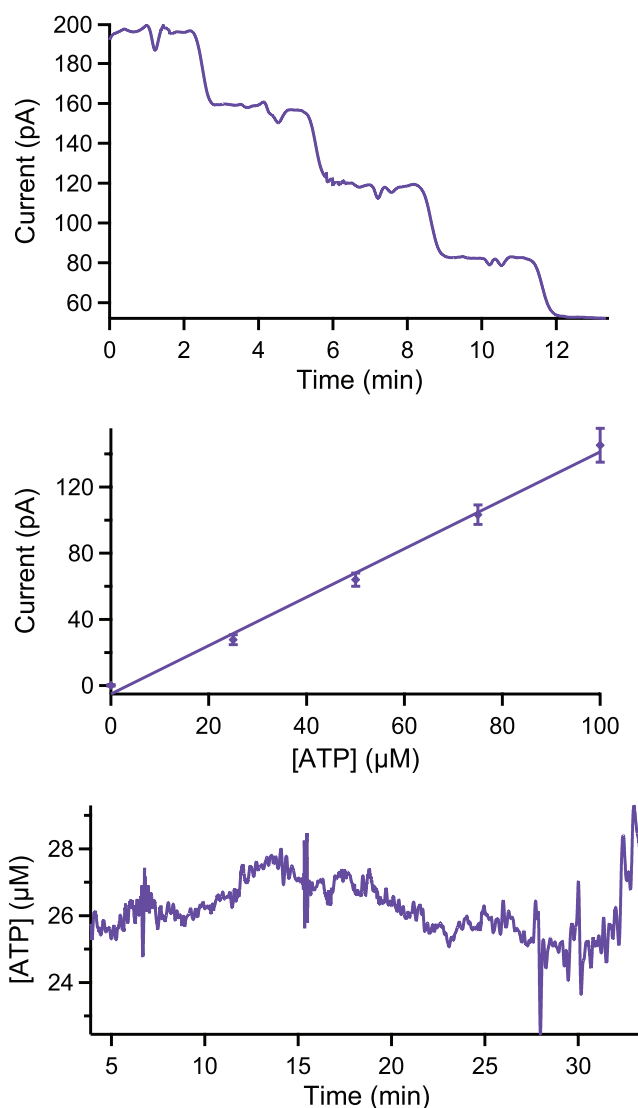


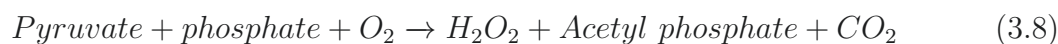
Figure 3.32: ATP detection using in-flow enzyme addition. *A.* 5-point ATP calibration. Steps are 100, 75, 50, 25 and 0 μM . *B.* ATP calibration curve from 0-100 μM . Markers represent the mean \pm standard deviation for each measurement and are fitted with a straight line. *C.* ATP levels in kidney dialysate, collected in storage tubing and analysed at a later time. Dialysate was collected and analysed at 2 $\mu\text{l}/\text{min}$. Data are smoothed with a Savitsky-Golay 201-point filter. GK (6.25 mg/ml) and glycerol (5 mM) were dosed in first, followed by G3POx (6.55 mg/ml) downstream, the dialysate then flowed into a PDMS analysis chip, which contained a 50 μm platinum poly(phenol)-coated disc electrode. Both enzyme solutions flowed at 0.5 $\mu\text{l}/\text{min}$.

3.5.7 Pyruvate detection

Detection of pyruvate is another situation in which this methodology could prove useful. Detection of pyruvate requires only one enzyme, pyruvate oxidase (POx), but this enzyme needs an additional cofactor, thiamine pyrophosphate (TPP), to work effectively. Previous work has also shown that the presence of Mg^{2+} can enhance its catalytic activity (136).

3.5 In-flow enzyme addition

However, the optimal concentration of these cofactors varies greatly in the literature (137, 138, 139). The reaction mechanism is summarised in equation 3.8.



Previous attempts within the group to make a pyruvate biosensor have been unsuccessful, possibly as a result of denaturing of the enzyme during immobilisation. The in-flow enzyme addition system could be suitable for pyruvate detection, as the enzyme is ‘free’ and therefore undamaged by immobilisation. It also provides an ideal means to easily optimise each component individually. Preliminary experiments were carried out in collaboration with Dr Michelle Rogers to investigate whether pyruvate could be measured using this methodology and whether the system could be used to optimise each of the components.

The board used to detect pyruvate is shown in figure 3.33.

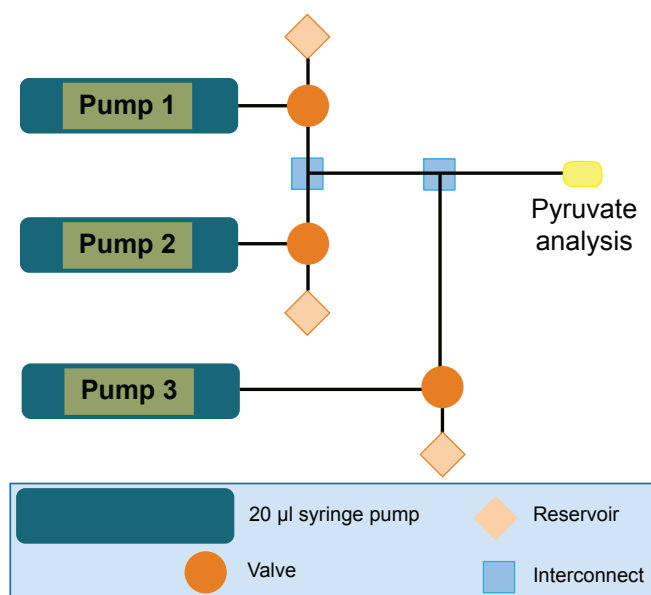


Figure 3.33: Schematic of analysis system for pyruvate detection. The board consisted of the calibration components and an additional pump for the enzyme/cofactor mixture. For cofactor optimisation, the calibration board was used to vary the concentration of each cofactor individually, keeping the concentration of pyruvate, the other cofactor and POx constant.

Using this setup, it was possible to detect pyruvate levels, as shown in figure 3.34. Cofactor concentrations were initially chosen on the basis of previous research in the group (136). After dilution, the concentration of Mg^{2+} was 12 mM and that of TPP was 1 mM. These cofactors were mixed with 30 mg/ml of POx (300 U/mg) and flowed at 0.5 $\mu\text{l}/\text{min}$. Using these initial concentrations the purple calibration curve in figure 3.34D was obtained. The board was then used to optimise the cofactor concentrations to increase the

3. CLINICAL ANALYSIS SYSTEM FOR DIALYSATE METABOLITES

detection sensitivity. The results are shown in figure 3.34. Each cofactor was individually varied using the calibration board, while concentrations of pyruvate, POx and the other cofactor were kept constant.

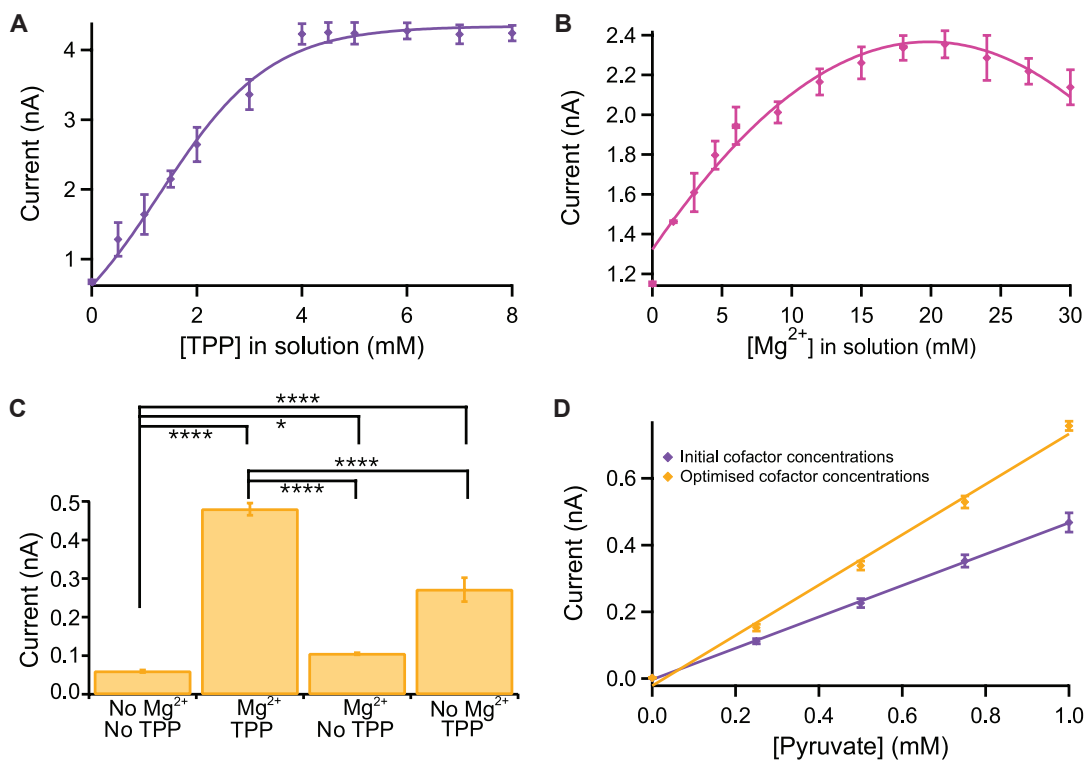


Figure 3.34: Pyruvate detection and optimisation. *A.* The concentration of TPP was varied using the calibration system and the resulting current recorded for a fixed pyruvate concentration. The optimal concentration was found to be 6 mM, which corresponded to 4.8 mM in the final volume, factoring in dilution. *B.* The concentration of Mg²⁺ was varied using the calibration system and the resulting current recorded for a fixed pyruvate concentration. The optimal concentration was found to be 21 mM, which corresponded to 16.8 mM in the final volume, factoring in dilution. *C.* There was a significant improvement in current response following addition of each of the optimised cofactors for 0.5 mM pyruvate. Tested using a Mann-Whitney U Test. Significance: * $p < 0.05$ and **** $p < 0.0001$. *D.* Calibration curves before and after optimisation. Markers represent the mean \pm standard deviation for each measurement and are fitted with a straight line. Sensitivity was improved with optimisation of the cofactor concentrations.

The results show a clear relationship between the concentration of each cofactor and the current obtained. On the basis of these results, the optimal cofactor concentrations were selected. The pyruvate calibration was repeated using the same electrode and is represented by the yellow trace in figure 3.34D. Optimisation of the cofactor concentrations resulted in an increase in sensitivity from 0.47 nA/mM to 0.75 nA/mM.

3.5.8 Conclusion

In-flow enzyme addition provides a biosensing system that has excellent sensitivity, especially compared with immobilised biosensors. It is easy to use, and does not require as much skill in fabrication. Moreover it is very quick to set up as enzyme can be weighed out in advance and stored in the freezer until needed. When required, it is ready to use once T1 has been added. Preliminary experiments have demonstrated the usefulness of this method for optimisation of the biosensing system, as well as for more complex systems such as multiple enzyme mechanisms or enzymes that are difficult to immobilise. Both in-flow and conventional immobilised biosensing systems have been shown to be stable for long periods of monitoring.

However, this system would not be suitable for a wearable application because of the size of the syringe pumps and valves. Although measurement of multiple analytes in one dialysate stream has been demonstrated it results in discrete measurements, whereas, using immobilised biosensors, continuous measurement of multiple analytes in one dialysate stream is possible.

In summary, as each system has its advantages and disadvantages it is likely that each would be suitable for different applications.

3.6 Dialysate collection in storage tubing

Linder *et al.* described a technique for storing and delivering reagents by filling flexible polyethylene tubing with a sequence of plugs of fluid, which they labelled a ‘cartridge’ (140). The authors used air spacers to separate reagents and to prevent mixing. They found that, using tubing with 0.38 mm inner diameter (ID), the reagent plugs were not affected by physical movement. In microdialysis, if the dialysate stream is not analysed online, it has to be collected into microvials for delayed analysis, creating discrete samples with poor temporal resolution. This technique of using fine-bore tubing to store samples without mixing could provide a means to collect dialysate for offline analysis while retaining temporal resolution. This section will describe initial experiments to validate this methodology and to investigate the stability of dialysate collected and stored in this way.

3.6.1 Validation

To validate this methodology, an experiment was carried out in which two microdialysis probes were inserted into the same region of a porcine kidney *ex vivo*, following the methodology described in chapter 4, perfused at 1 $\mu\text{l}/\text{min}$. One dialysate stream was analysed online using the rsMD system (section 2.3.1.2), while the dialysate from the second probe was collected into a length of fine-bore polyethylene tubing (0.4 mm ID, 6

3. CLINICAL ANALYSIS SYSTEM FOR DIALYSATE METABOLITES

m). Once the online experiment was complete, the stored dialysate was pumped through the analysis system at $2 \mu\text{l}/\text{min}$, effectively ‘playing back’ the liquid stream collected during the experiment. The results of this experiment, comparing results from delayed analysis to those from real-time analysis, are presented in figure 3.35.

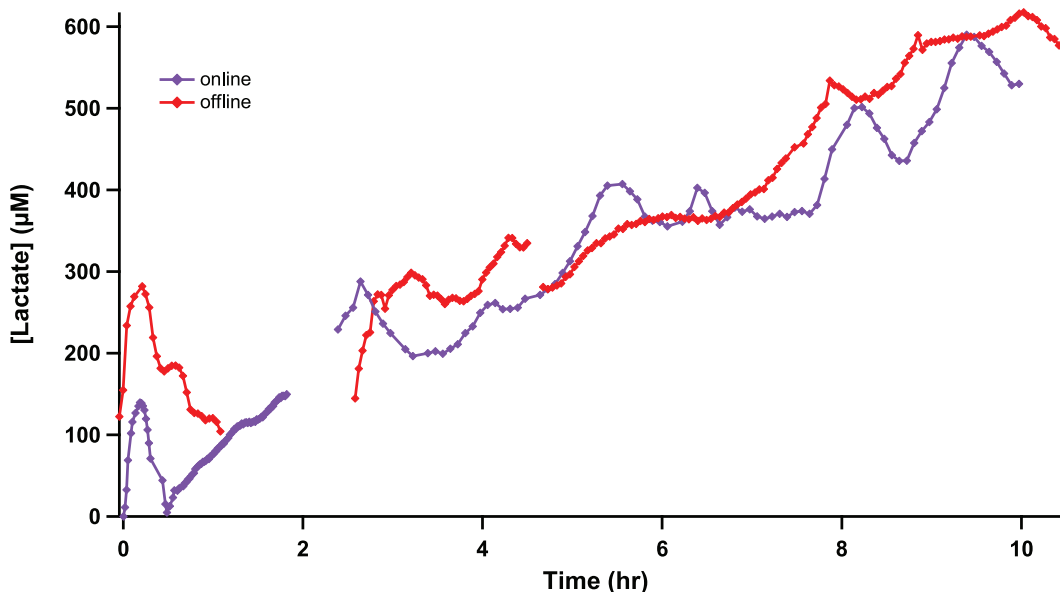


Figure 3.35: Validation of collection in storage tubing for delayed analysis. The purple trace shows the dialysate lactate concentration analysed online using rsMD. The red trace shows the lactate level in the dialysate from a second microdialysis probe, which was collected in storage tubing and analysed at a later time using rsMD. Results have been time-aligned.

There is some temporal smearing in the offline data but, critically, the levels obtained by the two methods are in close agreement. Furthermore, the mean difference between the two probes was $24.7 \pm 62.5 \mu\text{M}$ ($n=69$). This validation experiment demonstrates that dialysate can be collected and stored in lengths of tubing and analysed at a later time while retaining temporal resolution.

3.6.2 Stability

Further experiments were conducted to investigate the stability of dialysate samples over time in lengths of storage tubing and to establish the best method of storing the samples.

Preparation of filled storage tubing

In order to investigate the stability of filled storage tubing over time, the first step was to produce a batch of identical samples. The initial idea was to use a microdialysis probe and to switch it between beakers of different lactate concentrations, thus creating a step-change in dialysate lactate concentration, which could be collected into lengths of

3.6 Dialysate collection in storage tubing

storage tubing attached to the outlet of the microdialysis probe. Multiple sample tubes were produced using the same microdialysis probe to remove variations resulting from differences in probe recovery.

To investigate the variability between sample tubes produced using the same microdialysis probe, an experiment was carried out in which a microdialysis probe was placed into a well-stirred beaker of 1 mM lactate solution. A 1 m length of storage tubing was connected to the outlet of each microdialysis probe. After 20 minutes the probe was moved to a second beaker containing 2 mM lactate solution, and after a further 20 minutes it was moved back to the 1 mM lactate beaker, where it remained for a final 20 minutes. When the storage tubing had been filled, the ends were heated with a wax pen and pinched to seal them. The sample tubes were analysed straightaway using the rsMD system (described in section 2.3.1.2) at $2 \mu\text{l}/\text{min}$. The current peaks recorded were converted into lactate concentrations based on calibrations. Four sample tubes were made consecutively from one microdialysis probe. The results obtained for all four sample tubes are shown in figure 3.36.

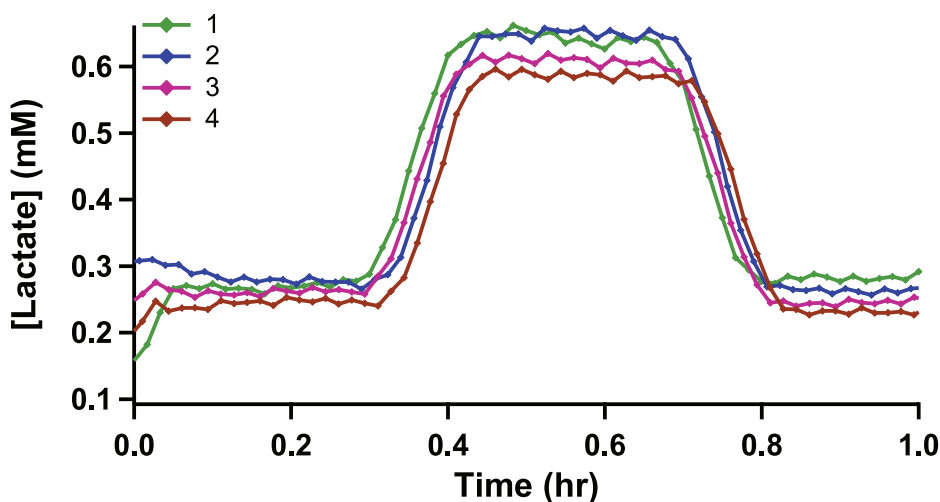


Figure 3.36: Dialysate collected from one microdialysis probe in multiple storage tubes.

A microdialysis probe, perfused with T1 at $2 \mu\text{l}/\text{min}$, was placed into stirred beakers of 1 mM, 2 mM and finally 1 mM lactate solution for 20 minutes each. A 1 m length of storage tubing was connected to the end of the microdialysis probe to collect the dialysate. The sample tube was analysed at $2 \mu\text{l}/\text{min}$ using rsMD, giving a reading every minute for each dialysate stream. This process was repeated four times, creating four consecutive sample tubes. Results are smoothed with a 9-point Savitsky-Golay filter.

As demonstrated in figure 3.36, it was possible to detect clear step changes in concentration using this methodology. Results obtained from multiple storage tubes produced using this microdialysis probe show some variability in the absolute values, but the per-

3. CLINICAL ANALYSIS SYSTEM FOR DIALYSATE METABOLITES

centage change is constant and reproducible. However, microdialysis probes can fail, as demonstrated in figure 3.37.

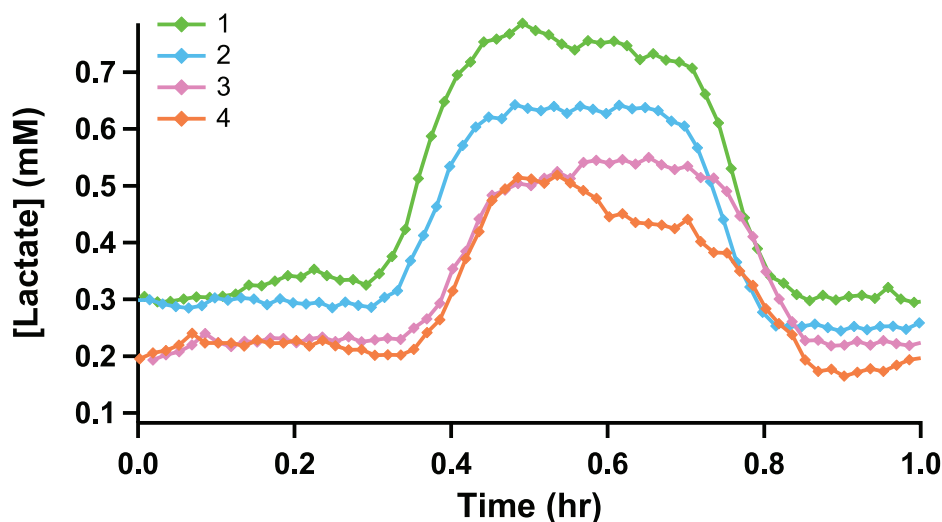


Figure 3.37: Variability in dialysate collected from one microdialysis probe in multiple storage tubes. A microdialysis probe, perfused with T1 at $2 \mu\text{l}/\text{min}$, was placed into stirred beakers of 1 mM, 2 mM and finally 1 mM lactate solution for 20 minutes each. A 1 m length of storage tubing was connected to the end of the microdialysis probe to collect the dialysate. The sample tube was analysed at $2 \mu\text{l}/\text{min}$ using rsMD, giving a reading every minute for each dialysate stream. This process was repeated four times, creating four consecutive sample tubes. Results are smoothed with a 9-point Savitsky-Golay filter.

The results obtained in figure 3.37 showed considerable variability. One possible explanation for this could be that the membrane was damaged, leading to variability in recovery. An alternative explanation could be that the tubing caused back pressure, which resulted in the membrane leaking. However, the total volume collected from the probe after 1 hour of perfusion with deionised water, with different sample tubes attached to the outlet, was measured and was found to be less than expected in all cases. This indicates that the variability was caused by the probe membrane leaking and not as result of the addition of the sample tube. As this is unpredictable, it was concluded that it was not possible to make reproducible sample tubes using microdialysis probes.

An alternative system was constructed that used syringe pumps and LabSmith programmable valves to inject a controlled volume of glucose/lactate standards into the storage tubes. Figure 3.38 shows the setup used to fill the lengths of tubing.

As LabSmith components are designed to precisely manipulate volumes of fluid, this setup ensured that each sample tube would be identical to the others. The system was set up so that two sample tubes could be filled at once and was programmed to run automatically.

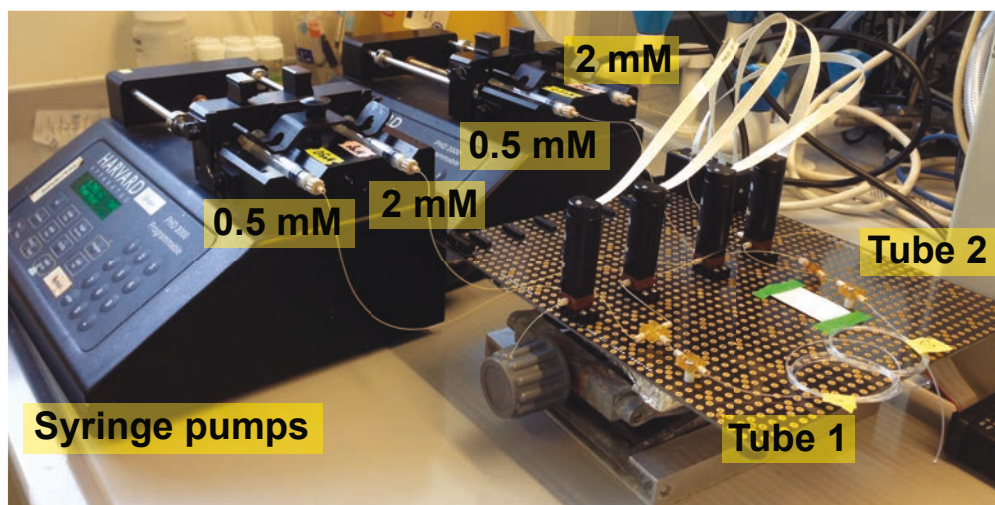


Figure 3.38: Experimental setup used to fill lengths of storage tubing. Two glucose/lactate standards (0.5 and 2 mM) were pumped at $8 \mu\text{l}/\text{min}$ using Harvard syringe pumps. The pumps flowed into LabSmith three-port two-position valves, which directed the stream either into the length of storage tubing or into a waste vial. Two sample tubes were simultaneously filled.

Stability at -80°C

To produce the sample tubes, the system directed 2 mM glucose/lactate standard at $8 \mu\text{l}/\text{min}$ into a 1 m length of storage tubing. After a 5-minute pause, the 2 mM stream was directed to a waste vial and the 0.5 mM stream was switched in to the sample tube instead. After another 5-minute pause, the streams were switched again. This created a sample tube containing three sections of 2, 0.5 and 2 mM glucose/lactate standard. Unfortunately, as a result of technical issues with the rsMD system, it was not possible to analyse samples on day 0, as was intended. The storage tubes were kept in the freezer at -80°C for 72 days before being analysed for glucose and lactate using the rsMD system (described in section 2.3.1.1). Figure 3.39 shows the results.

3. CLINICAL ANALYSIS SYSTEM FOR DIALYSATE METABOLITES

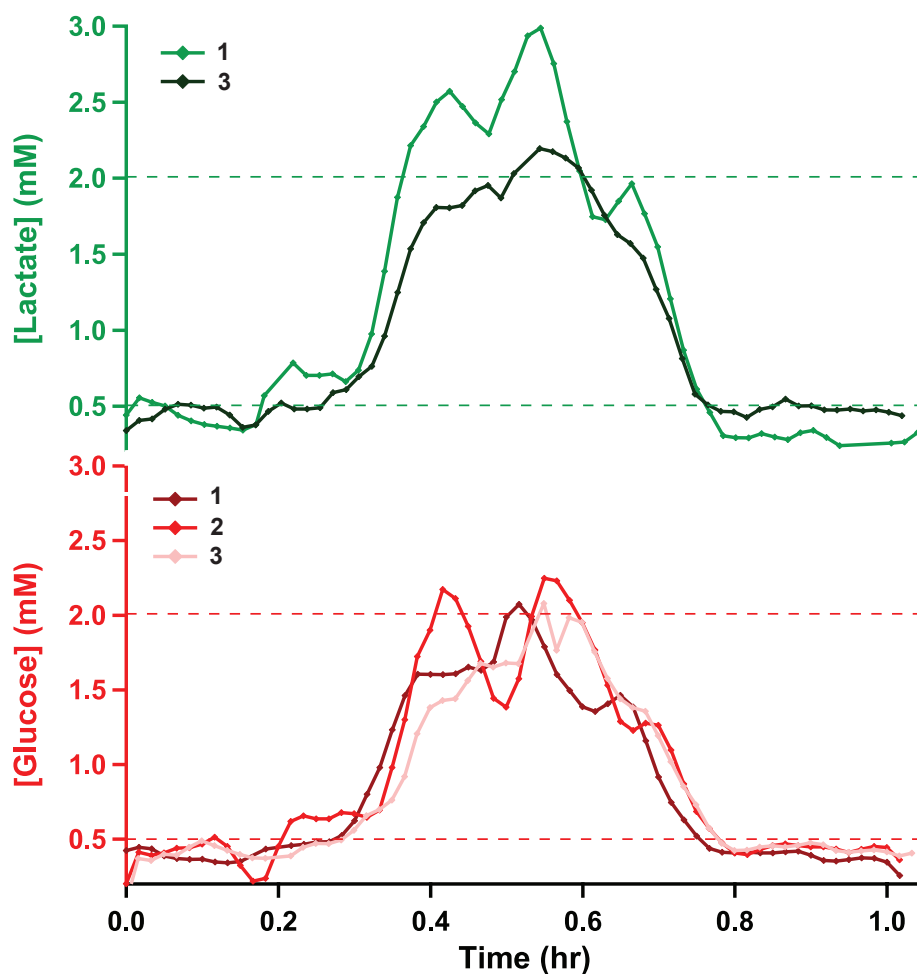


Figure 3.39: Sample storage tubes kept at -80°C . Three repeats were analysed at $2\ \mu\text{l}/\text{min}$ using the rsMD system, which gave a reading every minute for each metabolite. As a result of problems with the lactate assay during analysis of storage tube 2, it was only possible to measure glucose levels. Dotted lines indicate the concentrations used to fill the tubes.

These results show that, even after 72 days in the freezer, the temporal resolution was retained in all three storage tubes. At 2 mM, levels appear to be quite variable. This is probably caused by ripples in the baseline (from fluctuations in the high-performance liquid chromatography (HPLC) pump flow rate) overlapping with the peaks and distorting their shape. This effect leads to regular fluctuations in both metabolites, as seen here. The glucose/lactate standards that were used to fill the storage tubes were also frozen in vials at -80°C for 72 days. Samples of these standards were injected into the glucose and lactate assays to verify that their levels had not changed over time. The levels were compared with those obtained during the calibration and were found to be comparable.

3.6.3 Summary

This investigation has demonstrated that lengths of fine-bore storage tubing can be used to collect dialysate for delayed analysis while retaining temporal resolution. For long term storage, sample tubes can be kept at -80°C and are stable for at least 72 days in these conditions.

3.7 Conclusion

In summary, this chapter shows the development of various analysis methods that will be applied throughout the thesis.

This chapter has introduced an autocalibration board, which can be used with both the rsMD analysis system and with on-chip biosensors. The system allows calibrations to be carried out at regular intervals without the need for someone to be present.

In addition, two biosensing systems have been described for glucose and lactate detection. The first sensing system presented was glucose and lactate biosensors, which consist of enzyme entrapped in a hydrogel layer. In order to extend the linear range of these biosensors, a polyurethane diffusion-limiting layer was also incorporated. The second biosensing system involved in-flow enzyme addition using LabSmith microfluidic components. The system allows separate optimisation of factors influencing biorecognition and detection. The system was also demonstrated for more complex systems.

Finally, a method of collecting dialysate in lengths of storage tubing while retaining temporal resolution has been investigated and was shown to be feasible for offline dialysate collection and delayed analysis. The method was validated against the online analysis method and good agreement was shown between the two methods.

3. CLINICAL ANALYSIS SYSTEM FOR DIALYSATE METABOLITES

Chapter 4

Transplant organ viability assessment: Part I

This chapter will describe the use of rapid sampling microdialysis to monitor transplant kidneys in the period after organ retrieval, as a potential method for assessing their viability prior to transplantation. This work was carried out in collaboration with Mr Karim Hamaoui and Prof. Vassilios Papalois. In this chapter, online assessment of transplant kidneys during two clinical preservation methods and subsequent warming will be presented. Chapter 5 will follow on from this work, extending the analysis system for use with human organs and for preliminary analysis of transplant pancreases.

4.1 Introduction

4.1.1 The kidney

Kidneys are key regulatory organs that serve several vital bodily functions. They filter the blood, removing metabolic waste products and foreign chemicals, and excrete them in the urine. Kidneys also serve homeostatic functions, including regulation of water and electrolytes, maintenance of acid-base balance and acting as a site of gluconeogenesis, producing glucose for release to the rest of the body. In addition, the kidneys are responsible for production of a number of hormones, including erythropoietin, as well as the enzyme renin. The structure of the kidney is shown in figure 4.1.

4. TRANSPLANT ORGAN VIABILITY ASSESSMENT: PART I

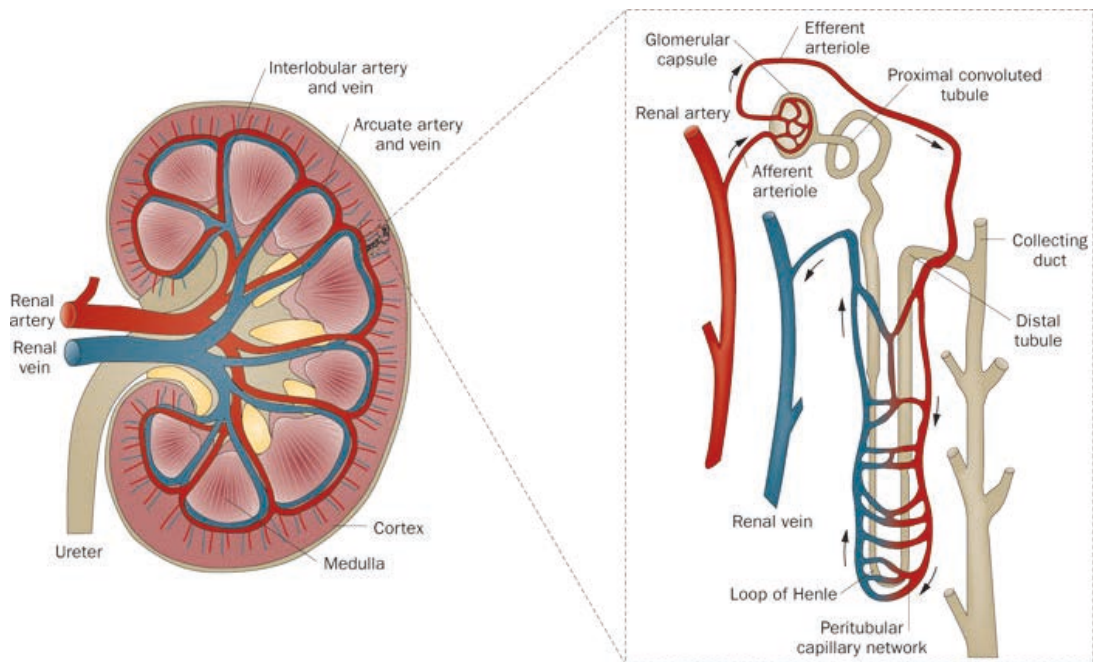


Figure 4.1: Structure of the kidney. *Left:* The kidney comprises an outer region, the cortex, and an inner region, the medulla. *Right:* The basic functional unit of the kidney is the nephron, which extends from the cortex to the medulla (141).

The basic functional unit of the kidney is the nephron, which is responsible for water and electrolyte regulation by blood filtration, reabsorption and excretion. Each kidney contains approximately 1 million nephrons. The nephron consists of a renal corpuscle, which is the initial filtering component and is located in the cortex, and the renal tubule, in which substances can be added or removed and which extends from the cortex into the medulla. The fluid at the end of each nephron combines into medullary collecting ducts, which drain into the renal pelvis, and the fluid eventually exits the kidney as urine.

4.1.2 Kidney transplantation

Kidney transplantation is the preferred treatment for end-stage renal failure, as it improves quality of life and is more cost-effective compared with dialysis (142). However, there is a severe shortage in the number of donor kidneys available for transplantation. For instance, between 2013-2014 there were 5881 patients on the active waiting list for a kidney transplant in the UK and only 3256 kidney transplants were actually carried out (including those from living donors) (143). Moreover, the median waiting time for a kidney transplant is 1114 days for an adult patient and, in 2008, only 19% of patients received a transplant within 1 year of registration on the national transplant list (143). Clinical practice is limited by the shortage of donor organs, the quality of these organs and the inability to assess their viability before transplantation (144, 145).

The majority of deceased-donor kidneys are retrieved from donation-after-brain-death (DBD) donors, whose hearts were beating prior to organ retrieval. However, in order to expand the pool of available donor organs, particularly given the reduction in DBD donors in recent years (146), alternative sources of organs have been sought and there is increasing interest in the use of marginal donor organs, such as those from donation-after-circulatory-death (DCD) donors. In fact, over the last decade, the number of kidney transplants from DCD donors has increased from 6.5% of all kidney transplants performed in 2003-2004 to 25% in 2013-2014 (143, 147). Marginal organs are under-utilised as the traditional preservation method of static cold storage is ineffective in such cases, leading to increased incidence of primary non-function (148). DCD donors are classified according to Maastricht categories (142, 149, 150), which are:

Table 4.1: Maastricht categories of DCD donors

Category	Definition	Classification
Type I	Dead on arrival	Uncontrolled
Type II	Unsuccessful resuscitation	Uncontrolled
Type III	Awaiting cardiac arrest	Controlled
Type IV	Cardiac arrest after brain-stem death	Controlled
Type V	Unexpected cardiac arrest in intensive care	Uncontrolled

The crucial difference between controlled and uncontrolled DCDs is the length of warm ischaemia time (WIT) and hence the duration of warm ischaemic injury endured by the kidney prior to organ preservation. In the controlled situation, WIT is typically 10-15 minutes; however, in the uncontrolled situation, WIT could be 30-60 minutes (142). Studies have shown that DCD kidneys have a higher rate of primary non-function, as well as a higher incidence of delayed graft function (DGF), probably as a result of increased warm ischaemic injury (142, 151). However, in terms of long-term graft survival, no significant difference has been shown between DBD and DCD kidneys (151, 152), demonstrating the potential of using these under-utilised organs to expand the donor pool. Studies have shown it is more important to consider other factors that may affect the outcome for DCD kidneys than for DBD kidneys (142, 152), for instance that the use of DCD organs from older donors leads to significantly worse outcomes (153).

In addition to increasing the use of DCD donor kidneys, another solution to the shortage of transplant kidneys is to reduce the discard rate of organs from expanded criteria donors (ECD). Donors are classified as ECD if they are aged 60 years or older or if they are aged between 50 and 59 years and meet 2 of the following criteria: history of hypertension, serum creatinine level greater than 1.5 mg/dl (132.6 μ M) and cerebrovascular cause of death (154). One study showed that the risk of graft failure after an ECD kidney transplant was 70% higher than from a non-ECD transplant (154). However, ECD

4. TRANSPLANT ORGAN VIABILITY ASSESSMENT: PART I

transplants have been shown to be beneficial compared with transplant candidates who remained on dialysis (155).

4.1.3 Renal ischaemia

Ischaemia is an unavoidable outcome of donor organ retrieval as a result of the cessation of blood flow to the kidney. As described in section 1.3, this leads to tissue glucose and oxygen deprivation, leading to a switch from aerobic to anaerobic metabolism in order to meet the energy requirements of the cells. However, the quantity of high-energy phosphates produced by anaerobic metabolism cannot meet the energy demands of the tissue, resulting in ATP depletion and loss of metabolic activity, which in turn initiates a cascade of cellular damage.

Ischaemic injury is an important determinant of transplantation success and can lead to poor outcomes (156, 157). Hypothermia is itself detrimental to the tissue as it can result in altered tissue integrity (158). Organs can tolerate moderate periods of cold ischaemia or a short period of warm ischaemia without significant damage, but prolonged cold ischaemia, particularly when combined with warm ischaemia, increases the severity of the reperfusion injury (159, 160). This is because the inhibited cellular metabolism during hypothermia prevents any reparative processes occurring after warm ischaemic injury (158). As a result, particularly in the case of DCD organs that may have been subjected to longer WIT, CIT should be kept as short as possible in order to reduce the resulting ischaemic injury (156, 160, 161).

Reperfusion is the effector phase of ischaemic injury. During reperfusion, repair and regeneration occur at the same time as cell death (159) and the ultimate fate of the organ is determined by the balance between tissue damage caused by ischaemia-reperfusion injury (IRI) and the regenerative processes occurring (162).

4.1.4 Clinical preservation methods

The primary objective of renal tissue preservation is to maintain the viability of the donor organ between retrieval and implantation to ensure a functional organ upon transplantation (148, 159). The preservation technique must preserve the organ for sufficient time to allow for transportation and for tissue typing and matching (163). In order to limit ischaemic damage during preservation, donor kidneys are stored under hypothermic conditions, as the organ's metabolic rate can be reduced by 1.5-2-fold for every 10°C fall in temperature (164, 165). This reduction in metabolic activity minimises ATP depletion and slows the resulting processes that lead to ischaemic injury (165, 166). In addition, use of a preservation solution in combination with hypothermia can inhibit cell swelling and acidosis, and

could further extend the preservation period (167, 168) There are currently two preservation methods that are clinically approved for kidney storage: static cold storage (SCS) and hypothermic machine perfusion (HMP).

Static cold storage (SCS)

SCS is the most widely used kidney preservation method in current clinical practice because of its simplicity (159). During SCS, the donor kidneys are flushed with a preservation solution and then stored statically on ice until implantation (148, 169). Using SCS, kidneys from standard donors can be stored for up to 24 hours (170); however, for preservation of kidneys from DCDs, SCS is inadequate (148).

Hypothermic machine perfusion (HMP)

In HMP the donor kidney is continuously perfused with a pulsatile flow of cold preservation solution at low pressure, which simulates metabolism by providing the tissue with oxygen and metabolic substrates and by removing waste products. The preservation solution also serves to minimise hypothermically induced cell swelling and oedema and to buffer intracellular acidosis (167). HMP has been shown to be beneficial for prolonged preservation times (171). Moreover, HMP allows for administration of protective agents, for sampling of the perfusate and for monitoring of several perfusion parameters in order to assess organ viability (172). Although studies have shown that perfusion dynamics alone are not a reliable marker of organ viability (173, 174, 175). The pulsatile flow simulates cardiac pressure and has been shown to improve preservation (176, 177). Studies have also shown that kidney preservation using HMP allows for extended storage of up to 24 to 30 hours (159, 171), which would enable more time for organ transplantation and tissue matching.

Since the 1970s, there has been an ongoing debate as to which of the two clinical preservation methods is superior. Many large-scale studies comparing the two techniques failed to find any benefit of HMP compared with SCS (178, 179) and, as a result, SCS became more widely used because of its low cost and simplicity compared with the high cost and technical expertise required for HMP (163, 180). However, over the last decade there has been a renewed interest in HMP as it is believed to reduce the rate of DGF, which has been linked to poor outcomes (181). In randomised studies in which one donor kidney of a pair was stored using SCS and the other using HMP, results have shown that the risk of delayed function of a transplanted kidney (graft) was significantly reduced with HMP stored kidneys and that graft survival after 1 year was significantly higher for donor kidneys that were preserved using HMP compared with SCS (169, 182). In particular,

4. TRANSPLANT ORGAN VIABILITY ASSESSMENT: PART I

there is evidence to suggest that HMP can be beneficial for preservation of ischaemically damaged kidneys from DCD donors when compared with SCS (180, 183, 184, 185).

4.1.5 Viability assessment

As a result of expanding the donor pool to include the use of marginal organs, such as ECD and DCD organs, there is an emerging need for better viability testing prior to transplantation in order to identify organs that are at risk of a poor outcome. Organ assessment may aid clinicians in deciding whether to accept or to discard a donor organ prior to transplantation, as well as allowing for possible intervention to improve the outcome. The period of time between retrieval and transplantation, in which organs are preserved, provides a unique opportunity to assess the health of the renal tissue.

In 2013-2104, the median CIT for kidney-only transplants from DBD donors was 14.4 hours (interquartile range 11.4-17.9 hours) and for DCD donors was 13.3 hours (interquartile range 10.6-16.4 hours). In 2013, 1556 kidneys were offered for donation from DBD donors, only 92% of which were actually retrieved and only 87% were transplanted, as a result of unsuitability of the donors or organs in the other cases. Furthermore, of the 1076 kidneys offered for donation from DCD donors, only 96% were actually retrieved and only 83% were transplanted, either because of donor age or organ unsuitability (143). These statistics show that 13-17% of potential kidneys are discarded because of concerns about their suitability for transplantation. Furthermore the long period of time between organ retrieval and transplantation could provide an ideal opportunity for viability assessment and intervention. As well as improving graft survival, the ability to assess viability prior to transplantation could reduce this discard rate without compromising outcome (186).

Despite this, there are currently no accepted indicators of kidney viability and potential post-operative organ function prior to transplantation; transplantation is the only definitive test of graft viability (187, 188, 189). Several biochemical and ischaemic injury markers have been quantified in the renal effluent (for instance calcium ions, heart fatty acid-binding protein and glutathione S-transferase) (190, 191, 192); however, their use is limited and their ability to predict kidney function *in vivo* is controversial (145, 192, 193). Additionally, a study by Baicu *et al.* showed that changes in kidney metabolism were not detected using biochemical analyses of renal artery effluent and that interstitium biochemical profiles might provide a better indicator of viability and suitability for transplantation (194).

Microdialysis has been used in a limited number of cases as a tool for organ assessment during SCS (195, 196, 197) and HMP (194) and has shown promise as it provides an early indication of metabolic changes. Microdialysis has been used in several studies to monitor metabolic changes occurring in human livers after transplantation (198, 199, 200, 201);

however, as yet no such studies after renal transplantation in humans have been conducted, although microdialysis has been used to monitor human kidneys in patients undergoing nephrectomies as a result of cancer (202). As there is currently no definitive measure of function, some viable organs will inevitably be unnecessarily rejected.

In recent years there has been growing interest in the use of normothermic perfusion, as the perfused organ is metabolically active, which allows for functional viability assessments to be carried out in an attempt to predict post-transplant outcome (203, 204, 205). Moreover, normothermic perfusion has been found to recover function of severe ischaemically damaged kidneys (158, 206).

4.1.6 Lactate and the kidney

Lactate is an end-product of anaerobic glycolysis, formed by the conversion of pyruvate by lactate dehydrogenase, and as such is a key marker of tissue hypoxia and ischaemia. However, the physiology of lactate in the kidney is complex and differs between the cortex and the medulla (207, 208). The kidney can be considered as two separate organs (as shown in figure 4.1) because of differences in the distribution of enzymes along the nephron, resulting in a functional partition across the kidney (209, 210). As a result, the kidney comprises an intricate cortico-medullary glucose-lactate recycling system. Glucose utilisation predominantly occurs in the medulla, where glycolysis occurs, generating lactate and energy. The cortex then takes up lactate released from the medulla and other systemic sources for oxidation and energy production and for gluconeogenesis, producing glucose, which is released for medullary and systemic use (208, 210, 211, 212). The complexity of lactate metabolism within the kidney means that care needs to be taken when interpreting results. In fact, one study has shown that the medulla produces lactate despite an adequate supply of oxygen and metabolic substrates (213). Furthermore, glucose production in the cortex has been found to increase during acidosis (207, 209) and only fails during marked reductions in renal blood flow (207).

Several studies have used perfusate lactate during HMP as a biomarker of renal ischaemic injury and have found that higher perfusate lactate levels are associated with the risk of DGF (214, 215). In addition, lactate dehydrogenase, which converts pyruvate to lactate and vice versa, has also been studied in the perfusate and has been shown to be associated with primary and delayed function and even graft failure (215). However, measuring lactate in the perfusate does not provide site-specific information of renal metabolism. Since lactate physiology in the kidney is so complex, this analysis technique is too simplistic. Microdialysis allows individual sampling of local lactate levels in both the cortex and the medulla in order to gain a more accurate understanding of the metabolic state of the two distinct regions during preservation.

4.1.7 Aims

In this initial study our aims were two-fold:

1. To assess the feasibility of using rapid sampling microdialysis (rsMD) for continuous monitoring of lactate in the renal cortex during organ preservation in a porcine model.
2. To compare the effects of the two preservation techniques, SCS and HMP, on renal metabolism during preservation and subsequent warming.

4.2 Methodology for kidney studies

In this chapter and chapter 5, a number of studies were conducted using rsMD as a method of monitoring transplant organs. In all cases, the method of organ retrieval was the same and, although experimental protocols varied between studies, the sample analysis methodology was largely the same throughout. This section will describe the aspects of the experiments that were the same throughout the transplant organ studies.

4.2.1 Organ retrieval

Porcine kidneys were retrieved from a local abattoir by clinicians and were immediately flushed with cold preservation solution, either University of Wisconsin (Viaspan, Bristol-Myers Squibb Pharmaceuticals Ltd, Dublin, Ireland) solution (UW) or Soltran, depending on the study, until the effluent was clear. After flushing, the organs were stored in the flushing solution and transported on ice to the laboratory.

4.2.2 Microdialysis probe insertion

MAB 11.35.4 microdialysis probes (Royem Scientific, UK) with a 4 mm membrane and a 6 kDa molecular weight cut-off were used for these studies. The renal capsule was removed and a 21 G tunnelling needle was used to make two holes in each kidney, one superficially in the cortex and one placed deeper, perpendicular to the medulla. Once the needle was removed, a microdialysis probe was carefully placed inside the hole and the tubing was secured to the side of the container using tape. Figure 4.2 shows the two microdialysis probes positioned inside a porcine kidney.

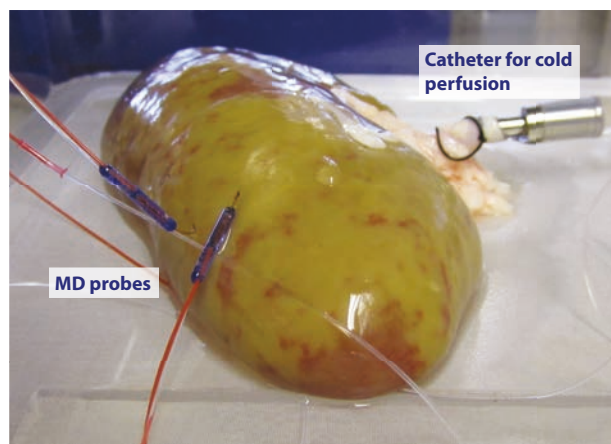


Figure 4.2: Photograph of porcine kidney with two microdialysis (MD) probes inserted.

A probe recovery experiment was carried out prior to insertion to verify that the probe was functioning well. This was carried out by placing the microdialysis probe membrane into a solution of a known lactate solution. The probe was left in place until steady-state lactate peaks were obtained. The peak amplitude was compared with that of a manual injection of the lactate standard into the valve in order to calculate a ratio of the two.

4.2.3 Online rsMD analysis system

The probe was perfused prior to insertion into the kidney to ensure it was functioning well. This was done by flowing T1 solution through the inlet, using a syringe pump (CMA 400 pump, CMA Microdialysis, Stockholm, Sweden) at a rate of $2 \mu\text{l}/\text{min}$. This flow rate was chosen to minimise the delay in the dialysate reaching the analyser whilst maximising the recovery of the probe; slower flow rates would have resulted in an increased recovery but would have increased the lag time. The outlet tubing of the probe was connected to the rsMD analysis system described in section 2.3.1.2. In most cases, the probe outlet tubing was extended using fluorinated ethylene propylene (FEP) fine-bore tubing (0.12 mm ID, Royem Scientific, UK) and tubing adaptors in order to reach the analysis system. Using this system, two kidneys could be simultaneously monitored. Every 30 seconds a dialysate sample was injected through the lactate assay, alternately from each kidney, as shown in figure 4.3. On some occasions, the valve switching frequency was reduced to every 150 seconds.

4. TRANSPLANT ORGAN VIABILITY ASSESSMENT: PART I

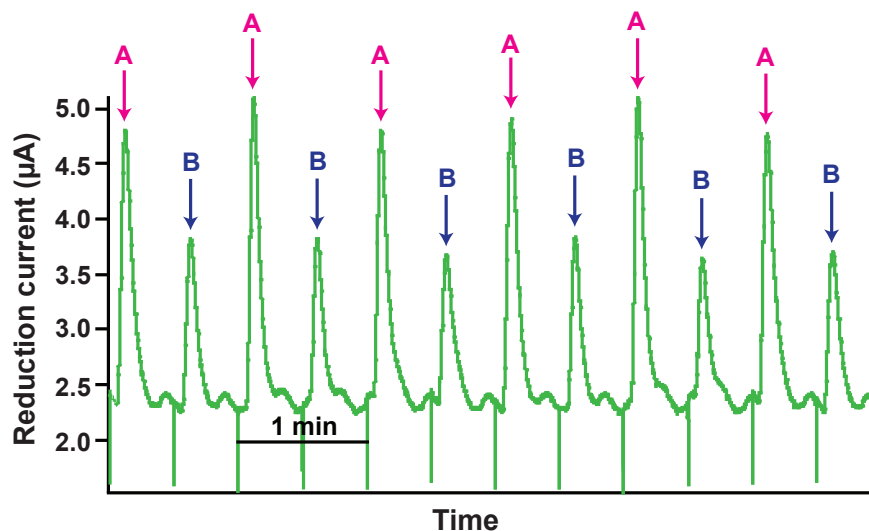


Figure 4.3: Extract of raw data current peaks for alternating kidneys. A sample is analysed for lactate levels every 30 s. Peaks alternate between the two kidneys and the height is proportional to the concentration of lactate in the sample.

4.2.4 Delayed analysis using storage tubing

In cases where a second microdialysis probe was placed into the medulla of the kidney, the dialysate from this probe was collected into lengths of tubing for analysis at a later time. The probe was connected to a syringe pump in the same way as for the online analysis and was perfused with T1 solution at a flow rate of $1 \mu\text{l}/\text{min}$. This lower flow rate was chosen to increase the probe recovery and to reduce the length of storage tubing required. Usually this would increase the time delay between the probe and the assay but this was not an issue in this case as the samples were analysed later. The outlet of the probe was connected to a length of coiled storage tubing (fine-bore polyethylene tubing, 0.4 mm inner diameter; Smiths Medical, UK; 13 m for SCS experiments and 6 m for HMP) primed with T1 solution. These lengths of storage tubing were labelled so that the direction of flow was known and were attached to the probe outlet using tubing adaptors. Once filled, the ends of the storage tubing were melted to seal them, so that the dialysate samples were not lost, and the tubes were stored in the freezer until analysis was possible.

At the end of the kidney monitoring experiment, during which one probe for each kidney was assayed online, the stored dialysate from the second probe was then pumped into the online assay, effectively ‘playing back’ the online liquid stream collected during the experiment. To do this, the ends of the coiled tubings that had been connected to the probes were detached and connected to a syringe pump and perfused with T1 solution at a flow rate of $2 \mu\text{l}/\text{min}$, while the other end of each of the coiled tubings was connected

to two separate sample loops of the valve, either side of the analysis loop, as before, allowing the data to be analysed with temporal resolution. The dialysate was analysed as described above for the online assay. Sometimes the time was slightly distorted during offline analysis, possibly because of the presence of air bubbles in the tubing. These differences, as well as differences in flow rate and delay, were accounted for to compare these results to the online results, as shown in figure 4.4.

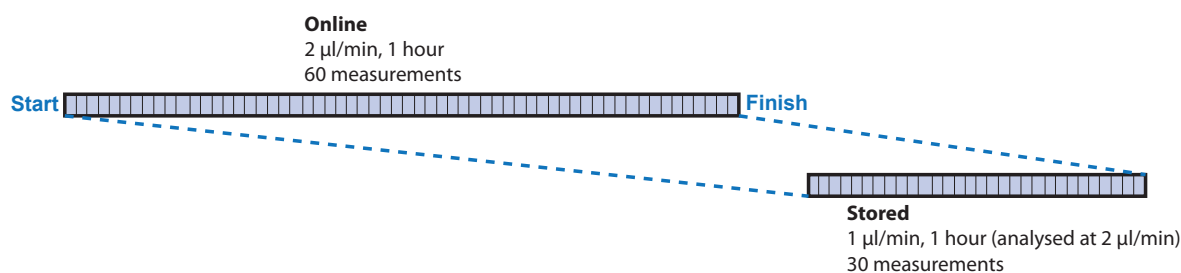


Figure 4.4: Schematic comparison between the online and stored analysis methods. Online analysis was carried out at 2 $\mu\text{l}/\text{min}$, giving 60 measurements in 1 hour. Stored samples were collected at 1 $\mu\text{l}/\text{min}$ and analysed at 2 $\mu\text{l}/\text{min}$, giving 30 measurements in 1 hour.

4.2.5 Data analysis and statistical analysis

The recorded current peaks were separated in Matlab (R2011b, MathWorks, US) to produce individual results for each kidney. The data were despiked using algorithms developed for the purpose of removing artefacts caused by valve movement (104). If necessary, a purpose-written derippling algorithm was applied to the data to remove periodic baseline ripples caused by fluctuations in the HPLC pump flow, which occur between the peaks of interest and can overlap with the peaks, distorting their shape and height in slow variations. Figure 4.5 shows the results of applying the derippling algorithm to a section of data.

4. TRANSPLANT ORGAN VIABILITY ASSESSMENT: PART I

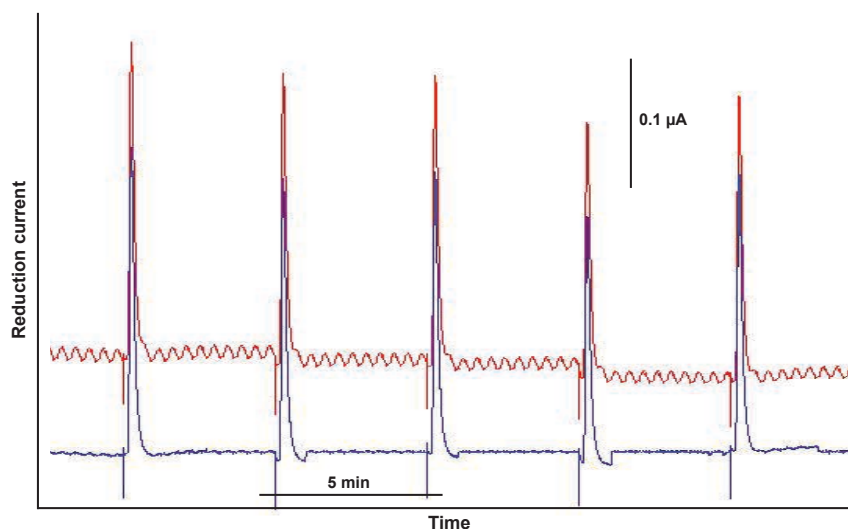


Figure 4.5: Derippling algorithm. Results of applying the derippling algorithm to a section of data. The red trace shows the data before derippling and the blue trace shows the derippled data.

The current peaks were converted into concentrations based on calibrations (using different concentrations of lactate) carried out before, during and after each experiment. The results were smoothed using a Savitsky-Golay filter over 21 points and adjusted to correct for the transit time between the microdialysis probe and the analysis system. Concentrations reported are dialysate concentrations and are not corrected for the unknown *in vivo* probe recovery. A summary of the data analysis process is given in figure 4.6.

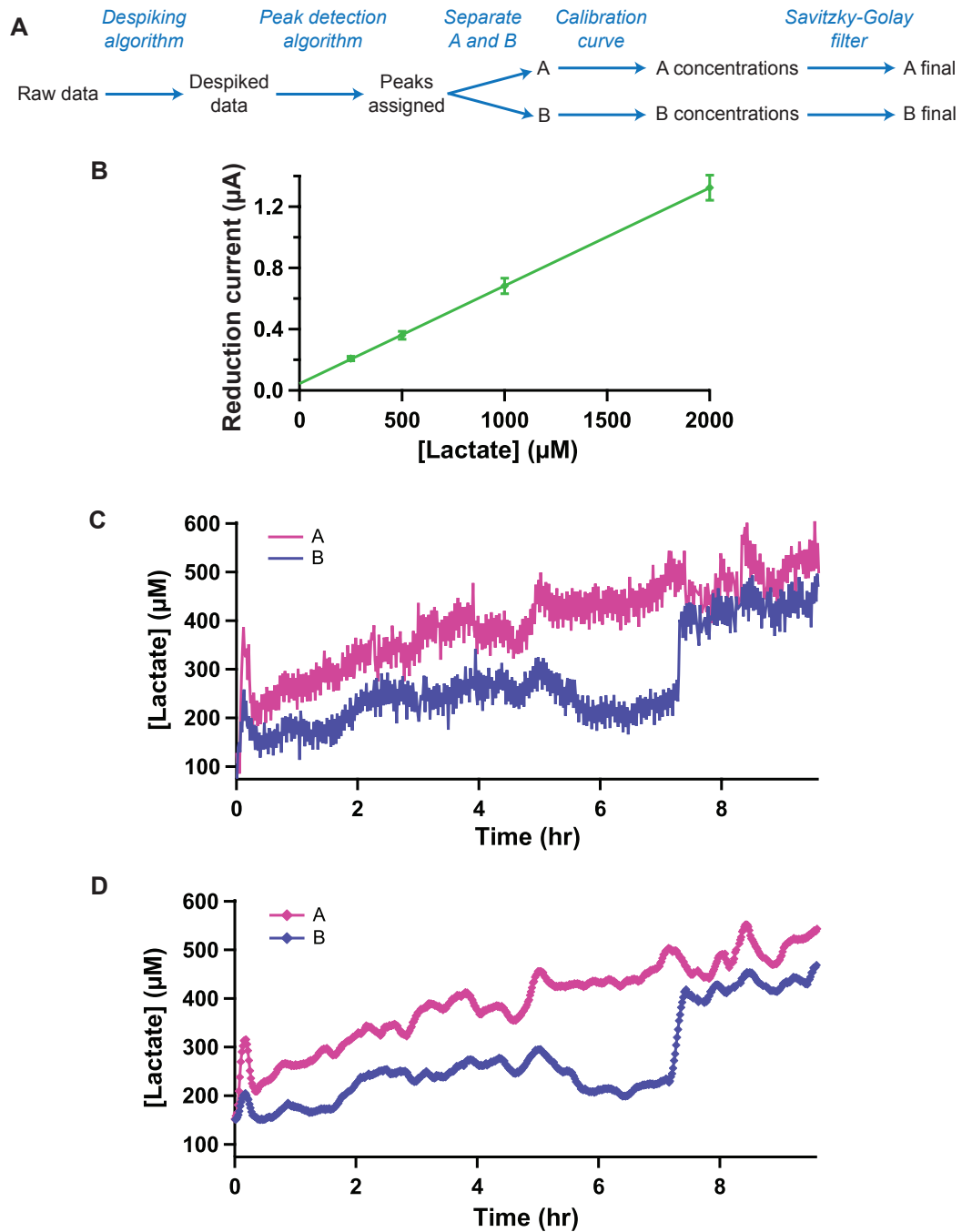


Figure 4.6: Data analysis protocol. *A.* Summary of steps involved in data analysis process. *B.* Current response of the lactate assay to increasing lactate concentrations manually injected into the flow injection valve. Markers indicate a mean \pm standard deviation ($n=6$) current for each lactate standard injected into the assay with a best-fit line through these points. *C.* Example of processed data for a pair of kidneys. Current peaks were separated for kidneys A and B and converted into concentrations in Matlab using the calibration curve. *D.* Final results, smoothed with a 21-point Savitsky-Golay filter.

4. TRANSPLANT ORGAN VIABILITY ASSESSMENT: PART I

Calibration stability

Calibrations were initially carried out at the start and the end of each experiment, but calibration drifts were observed to varying degrees over the course of each experiment. To account for this, a linear change in assay sensitivity over time was assumed and both calibrations were factored into the analysis to a differing degree depending on the time corresponding to each data point. However, in cases where there was a considerable shift in calibration sensitivity over the course of the experiment, this analysis methodology had a significant effect on the shape of the trace, as shown in figure 4.7.

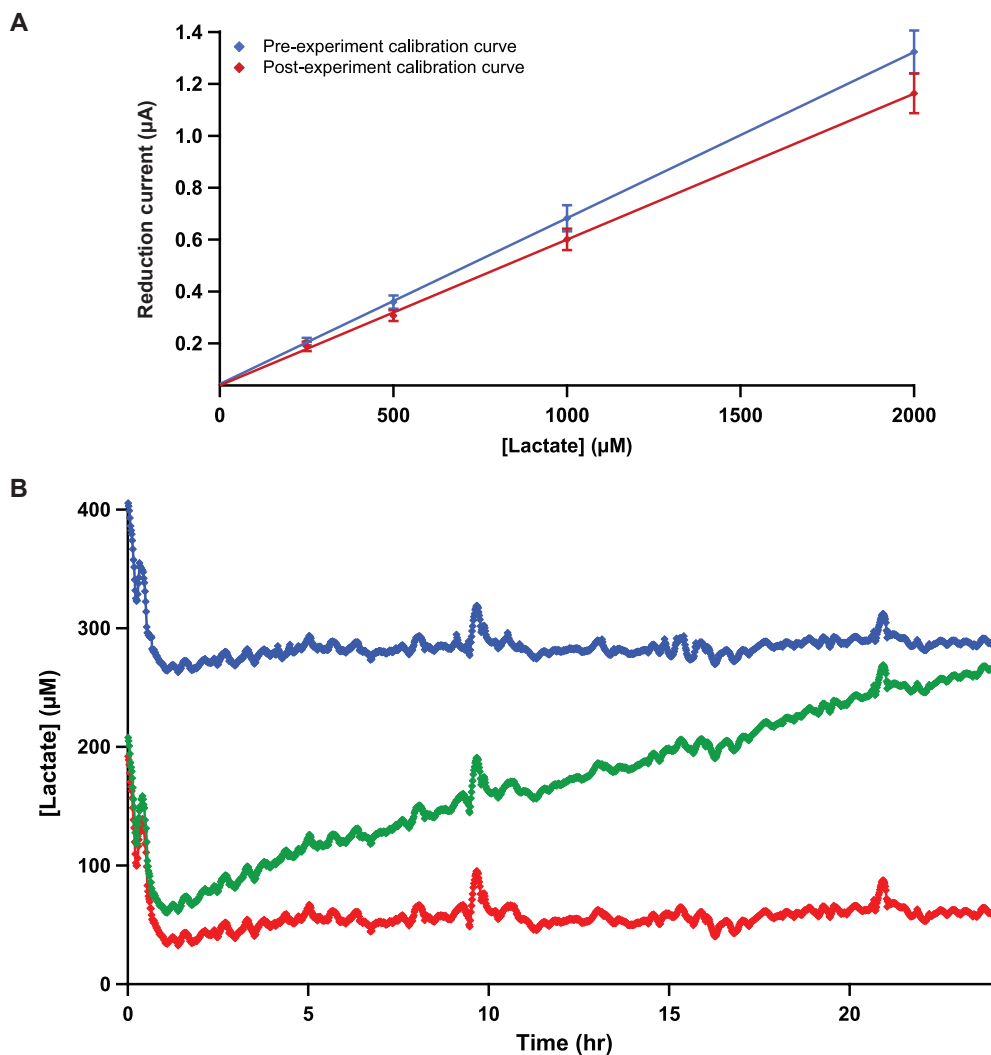


Figure 4.7: Calibration drift over an experiment. *A.* The blue line represents a calibration carried out before starting the experiment and the red line represents a calibration carried out at the end of the experiment. Markers indicate the mean \pm standard deviation ($n=6$) current for each lactate standard injected into the assay with a best-fit line through these points. *B.* Effect of calibration drift on the analysed results is shown. The red line is calculated using the pre-experiment calibration, the blue line using the post-experiment calibration and the green line is a combination of the two, which considerably affects the overall trend.

4.3 Methodology for comparing renal preservation methods

Observation of this calibration drift led to a change in the experimental protocol to include more regular calibrations to ensure the accuracy of the results obtained. A summary of the adapted experimental protocol for SCS and HMP is shown in section 4.3.1 in figure 4.8. On the basis of this observation, an automatic calibration system was later developed (as described in section 3.2.2) to improve the reliability of the results obtained.

For intra-preservation group comparisons, statistical tests were done using the paired Wilcoxon signed-rank test (two-tail) while the Mann-Whitney U test (two-tail) was used for inter-preservation group comparisons. Significance was taken to be $p < 0.05$. For comparison, lactate levels are represented graphically using box plots showing the median and interquartile range, with whiskers showing the 10th and 90th percentiles. Levels quoted in the following sections represent the median value of each group for a specific time point.

4.3 Methodology for comparing renal preservation methods

This section will describe an initial feasibility study to investigate whether rsMD could be used to monitor donor organs in the period after retrieval and before transplantation. Lactate profiles of porcine kidneys preserved using two clinical preservation methods, SCS and HMP, were compared in order to determine possible differences.

4.3.1 Experimental protocol

After retrieval and arrival at the hospital, kidneys underwent either a further 24 hours of SCS or 10 hours of HMP. Ten kidneys underwent 24 hours of SCS (mean temperature 3.5°C) in the original flushing solution, while another ten underwent 10 hours of HMP (mean temperature 7.8°C) on a Waters Medical Systems RM3 perfusion machine, perfused with UW solution. All efforts were made to keep conditions constant prior to preservation. The experimental protocol for the two preservation techniques is described in more detail in the following sections.

A clinical decision was made to use UW solution (Viaspan, Bristol-Myers Squibb Pharmaceuticals Ltd, Dublin, Ireland) for both HMP and SCS preservation to remove differences in preservation solution as a source of variability. In clinical practice, UW solution is used for SCS preservation but the Belzer-MPS variant, which contains glucose, is used for preservation by HMP, although studies have suggested that UW solution may be superior to the Belzer-MPS variant for ischaemically damaged kidneys (216).

Following 24 hours of SCS or 10 hours of HMP, preservation support was stopped abruptly and each kidney was allowed to warm passively for 2 hours to room temperature

4. TRANSPLANT ORGAN VIABILITY ASSESSMENT: PART I

in order to detect changes in lactate concentrations occurring as a result of increasing tissue temperature and ischaemic cellular injury. This was a massive challenge for the kidneys to test their reaction to the rewarming injury and the potential effect of each preservation method on the reaction of the kidney to the challenge.

Dialysate lactate levels were measured throughout the entire protocol in both the cortex and the medulla for each kidney. Cortical dialysate was analysed online in real time, while medullary dialysate was collected into lengths of storage tubing and analysed offline at a later time.

Figure 4.8 describes the main steps of the experimental protocol.

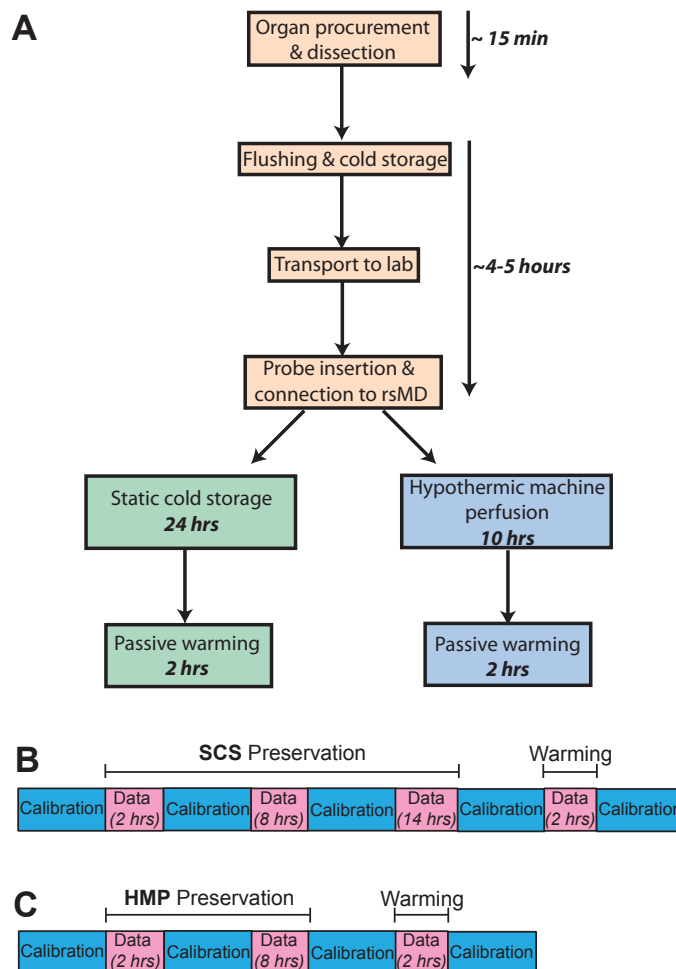


Figure 4.8: Experimental protocol for the two preservation groups. *A.* Overall, 20 kidneys were monitored using this protocol, 10 during 24 hours of SCS and 2 hours of subsequent warming, and 10 during 10 hours of HMP and 2 hours of subsequent warming. *B.* Timeline indicates the calibration protocol throughout monitoring for SCS experiments. *C.* Timeline indicates the calibration protocol throughout monitoring for HMP experiments.

4.3.1.1 Static cold storage

During preservation by SCS, kidneys were placed into a plastic box and were partially submerged in UW solution. They were then placed on ice in an insulated box, as shown in figure 4.9. Microdialysis probes were inserted into the cortex of each kidney for online analysis and into the medulla for collection and delayed analysis. A temperature probe (Thermalert TH-5, Physitemp, Clifton, USA) was also inserted into one of the kidneys to simultaneously monitor the tissue temperature. The kidneys were continuously monitored for 24 hours, after which time they were removed from the ice and allowed to warm for 2 hours. Five pairs of kidneys (n=10) were monitored during SCS, 9 of which were monitored during an additional 2 hours of passive warming to ambient temperature. For this group, the mean WIT was 15 ± 2.7 min (n=10).

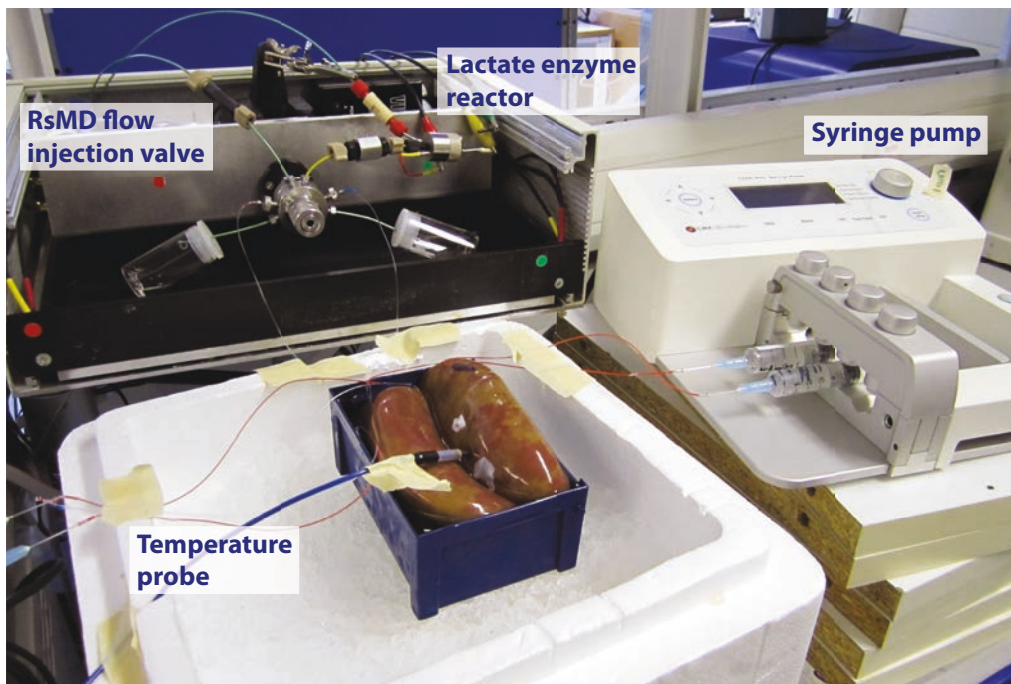


Figure 4.9: Experimental setup for static cold storage preservation. The two kidneys were placed on ice in an insulated box. Two microdialysis probes were placed in each kidney and perfused using a syringe pump. A temperature probe was also placed in one of the kidneys. The dialysate outflow from one probe in each kidney flowed into the rsMD analysis system for simultaneous online measurement of lactate in two kidneys.

4.3.1.2 Hypothermic machine perfusion

During HMP, each kidney was placed onto a separate RM3 perfusion machine (Waters Medical Systems, Rochester, USA), as shown in figure 4.10. Microdialysis probes were inserted into the cortex of each kidney for online analysis and into the medulla for collection and delayed analysis, after which, perfusion commenced. This involved pumping cold UW

4. TRANSPLANT ORGAN VIABILITY ASSESSMENT: PART I

preservation solution, in a pulsatile manner, through the renal artery of each kidney. The kidneys were continuously monitored for 10 hours, after which time a temperature probe was inserted into one and perfusion was stopped. The kidneys were allowed to warm for 2 hours and were monitored throughout. Three pairs and four individual kidneys (n=10) were monitored during HMP and subsequent warming. For this group, the mean WIT was 15.4 ± 1.7 min and the mean CIT prior to beginning perfusion was 4 ± 0.5 hours (n=10). Perfusion parameters measured by the perfusion machine, such as temperature, flow rate and vascular resistance, were monitored throughout. Systolic perfusion pressure was adjusted hourly in the first four hours and regulated to 40 mmHg; after 4 hours no further changes were made to the perfusion parameters.

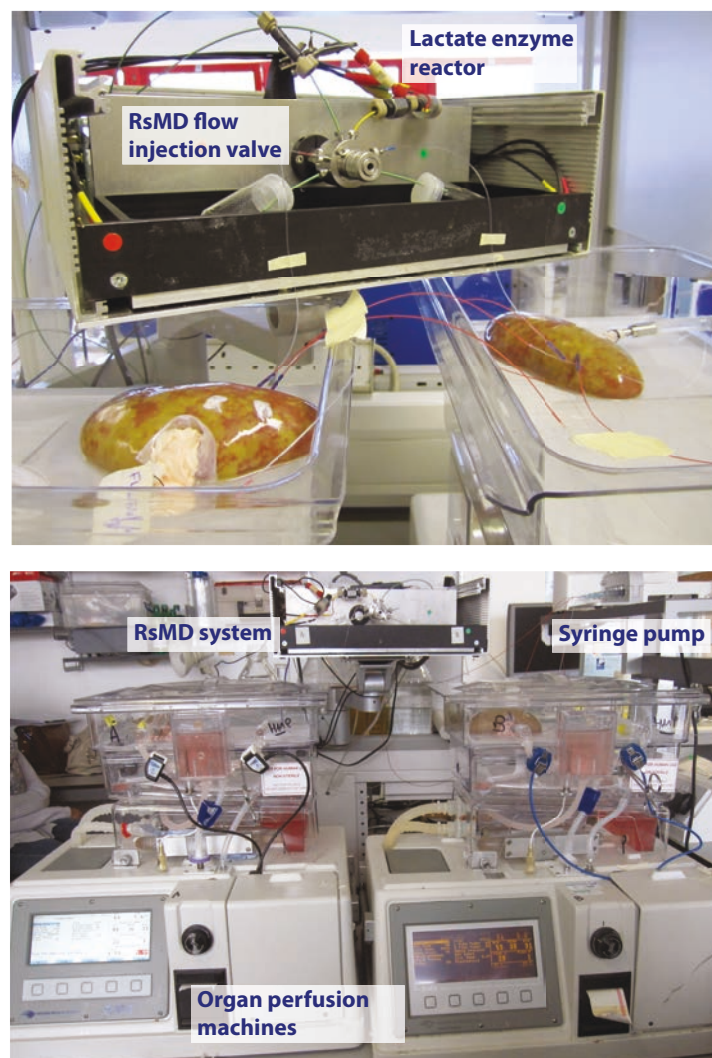


Figure 4.10: Experimental setup for preservation by HMP. Each kidney was placed on a perfusion machine, which pumped it with cold preservation solution in a pulsatile manner. Two microdialysis probes were placed in each kidney and perfused using a syringe pump. The dialysate outflow from one probe in each kidney flowed into the rsMD analysis system for simultaneous online measurement of lactate in two kidneys.

HMP cooling efficiency

In HMP, the organs are cooled from the inside by perfusion with a cold preservation medium. This mechanism of cooling is very different to that of SCS, in which the organs are cooled by the surrounding ice. In order to gain an understanding of the cooling efficiency of HMP, the temperature of the perfusate going into and out of the kidney was measured, as well as the tissue temperature, with and without additional cooling, as shown in figure 4.11.

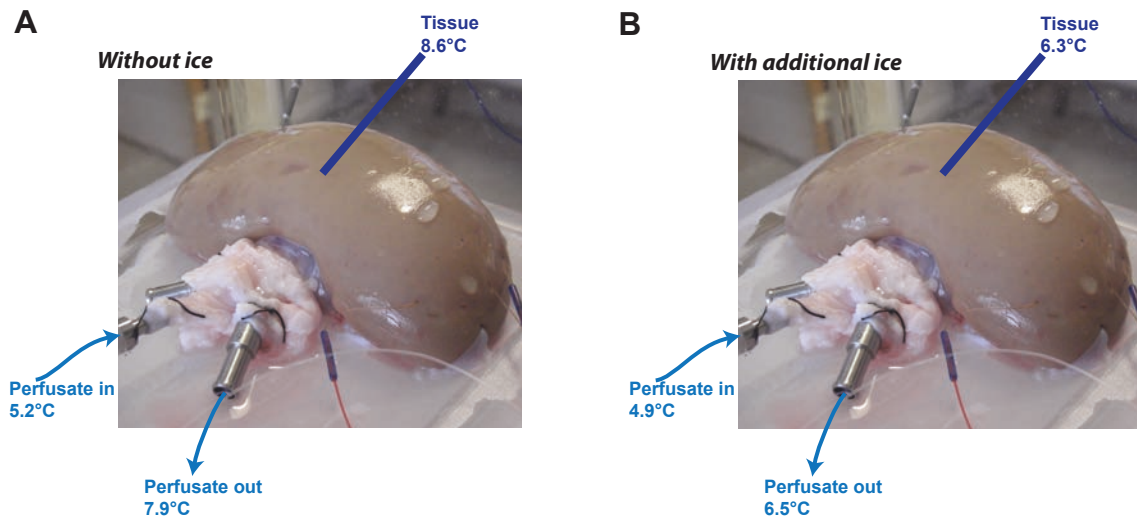


Figure 4.11: Effect of additional cooling during HMP. A. Without additional cooling, the warmer tissue caused the perfusate temperature to rise by 2.7°C B. With additional ice around the kidney, the perfusate temperature rose by only 1.6°C.

These results show that cooling by HMP is ineffective without additional ice around the kidney because the perfusate temperature increased by 2.7°C as it was pumped through the relatively warm tissue. By contrast, when ice blocks were placed around the kidney to provide additional cooling from the outside, the tissue temperature decreased, reducing the warming effect of the kidney on the perfusate to a 1.6°C increase. In a clinical situation, HMP is typically carried out at temperatures of 4-6°C (217). However, in our experimental model, the current system was inadequate at maintaining these low tissue temperatures as a result of the effect of the warm surroundings during preservation. To more closely replicate the clinical situation, additional ice packs were placed around the kidney when necessary.

In reality, maintaining these cold temperatures during HMP proved complex; ice packs could not be placed directly on the kidney, as the pressure would have affected the perfusion dynamics. Instead, a frame was built to hold the ice packs, which could be placed around the kidney. Submerging the kidney in cold perfusion solution may have been a

more effective means of cooling but this was not possible with the current system. Moreover, with the current system the cooling efficiency is limited by perfusion dynamics; if the kidney is not well perfused then the cooling effect of the cold perfusion medium on the tissue will be less.

4.4 Results: during preservation

4.4.1 SCS cortex and medulla

Preservation by SCS was conducted at temperatures as low as possible and efforts were made to maintain a constant temperature throughout. The mean temperature throughout the preservation period was $3.5 \pm 1.8^{\circ}\text{C}$ (n=10).

Figure 4.12 shows the dialysate lactate concentration in the cortex for kidneys preserved using SCS. Box plots also show median concentrations at key time intervals during the 24-hour period. Sets of paired kidneys tended to display very similar trends to one another over the course of the preservation, as shown in figure 4.12, where similar colours represent pairs of kidneys.

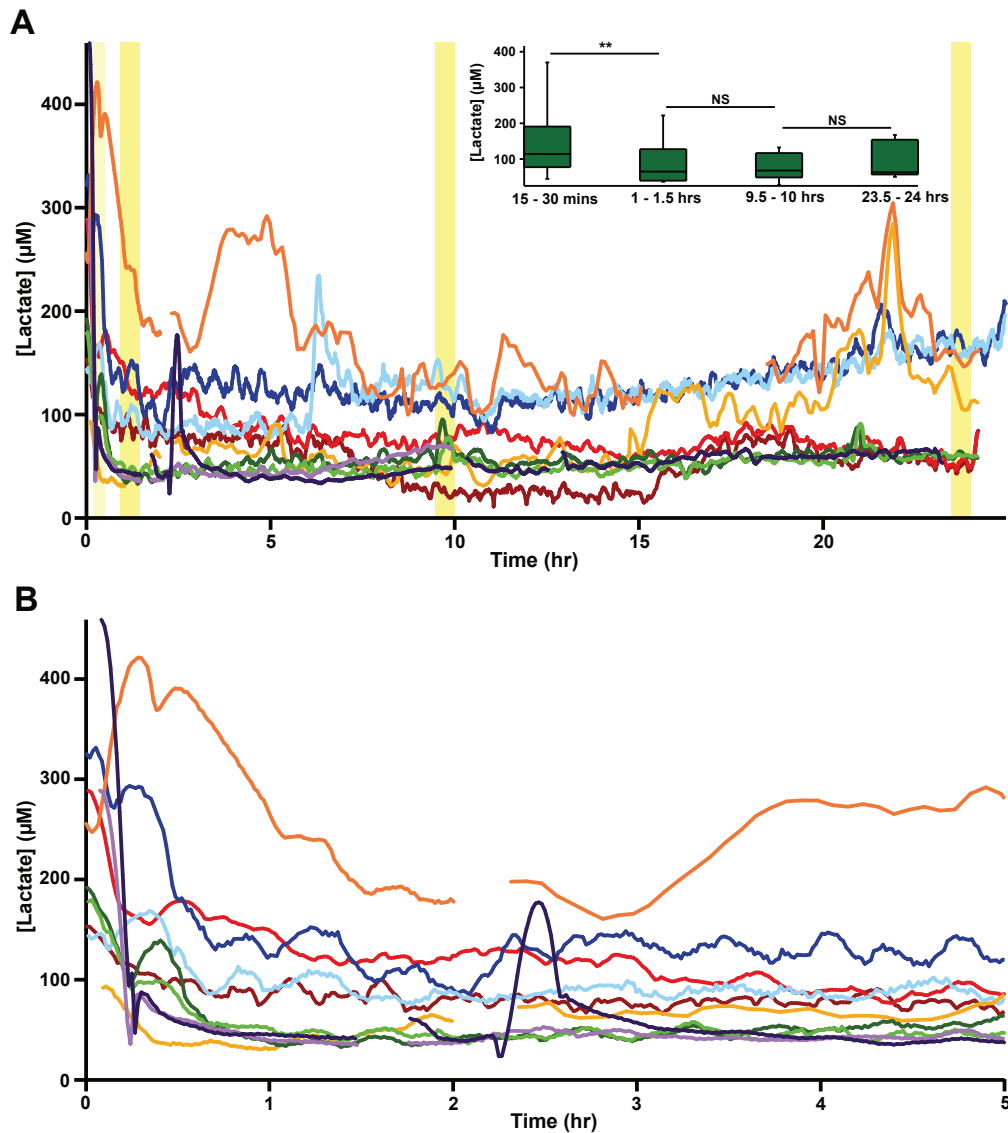


Figure 4.12: Dialysate cortical lactate profiles during SCS. *A.* Dialysate lactate levels over 24 hours are shown. *B.* Magnified view of the first 5 hours of preservation shown. Each line represents real-time data of an individual kidney with a point every minute (every 5 minutes in 2 cases, for the section from 2 hours to end) smoothed with a Savitsky-Golay 21-point filter. Similar colours indicate pairs of kidneys (red, orange, green, blue and purple). Gaps in the data correspond to mid-experiment calibrations. *Inset:* Median lactate concentrations of SCS kidneys at 4 key time intervals during the 24 hours of preservation, shown here for clarity and evaluated in more detail in figure 4.22. Shaded regions indicate the data window averaged to give the data presented in the box plots. Box plots show median levels and interquartile range. Whiskers indicate 10th and 90th percentiles. Significance: ** $p < 0.01$, NS=not significant.

In all cases, lactate levels began high and decreased to a near steady state after 1.5 hours of preservation, as shown in figure 4.12B. Paired statistical analysis, using a Wilcoxon signed-rank test to compare the change in lactate concentration between the mean level at 15-30 minutes and that at 1-1.5 hours, showed a significant decrease in the

4. TRANSPLANT ORGAN VIABILITY ASSESSMENT: PART I

dialysate lactate concentration from a median of 114 to 65 μM in this period. However, it is not clear, whether the initially high lactate concentrations seen were an experimental artefact, as a result of handling of the kidney and of probe insertion. Typically, tissue stabilisation following probe insertion has been found to occur within 12 minutes of probe insertion (99), suggesting that, in this case, additional factors contributed to this effect, as levels took longer to decrease to a stable value. After 1.5 hours, levels remained low and no further changes were seen overall, as levels at 24 hours were still a median of 63 μM , although individual fluctuations were still observed. Statistical analysis to compare the mean levels at 1-1.5 hours to those at 23.5-24 hours into preservation showed no significant change in the lactate levels.

The microdialysis probes were not secured in position inside the kidney and, as a result, movement could lead to a temporary spike in dialysate lactate levels. An example of this effect is shown in figure 4.13, where a kidney in which the microdialysis probe was moved slightly is compared with one in which no movement occurred. When the probe remains stationary, the tissue immediately surrounding the membrane becomes depleted of lactate as a result of diffusion across the probe membrane. If a disturbance causes the probe to move at all, the membrane will then come into contact with tissue that has not been depleted in this way, causing a temporary increase in the lactate detected. Interestingly, the time-scale of the increase and its return to normal levels is comparable with the spike seen initially during SCS, suggesting that this may also have been an effect of probe stabilisation. As a result, care had to be taken throughout these experiments to avoid any unnecessary probe movement.

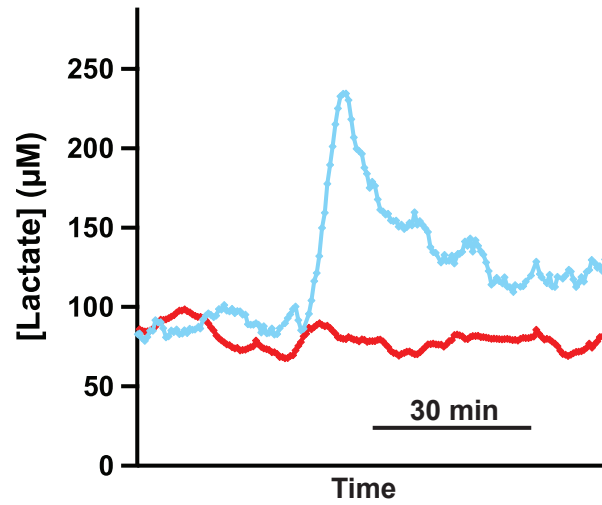


Figure 4.13: Concentration artefact caused by microdialysis probe movement. Lactate concentration change caused by movement of implanted microdialysis probe in the kidney (*light blue*) compared with results from a kidney in which no such probe movement occurred (*red*).

In contrast to the trends observed in the cortex, there was no significant change in medullary lactate levels during the 24 hours of SCS, as shown in figure 4.14 (traces not shown here).

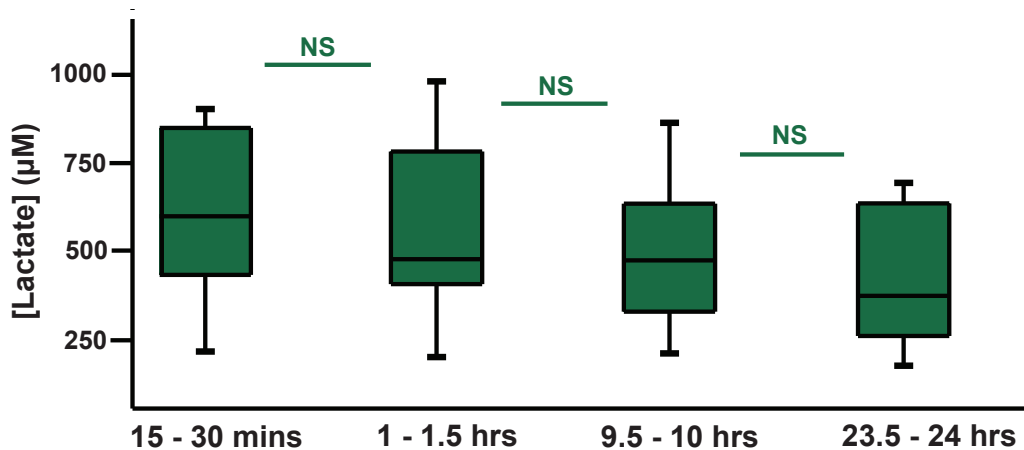


Figure 4.14: Dialysate medullary lactate profiles during SCS. Box plots show medullary lactate concentrations of SCS kidneys at 4 key time intervals during the 24 hours of preservation. Box plots show median levels and interquartile range. Whiskers indicate 10th and 90th percentiles. Significance: NS=not significant.

4. TRANSPLANT ORGAN VIABILITY ASSESSMENT: PART I

4.4.2 HMP cortex and medulla

As with SCS, efforts were made to keep temperatures low and consistent during preservation by HMP. As described earlier, temperatures were higher for this preservation method, as cold perfusion was less efficient at effectively cooling the kidney than storage on ice. The mean temperature throughout the HMP preservation period was $7.8 \pm 1.9^\circ\text{C}$ ($n=10$), as measured in the perfusate by the perfusion machine. As discussed in section 4.3.1.2, we subsequently found that cooling was poor using HMP and as a result real tissue temperatures would have been even higher.

Figure 4.15 shows the dialysate lactate concentration in the cortex for kidneys preserved using HMP. Box plots also show median concentrations at key time intervals during the 10-hour period. In this case, the matching between pairs of kidneys was not as good as with the SCS group. This is likely to be because in these experiments each kidney was perfused on a separate perfusion machine that, in retrospect, did not cool the organs efficiently in ambient laboratory temperatures.

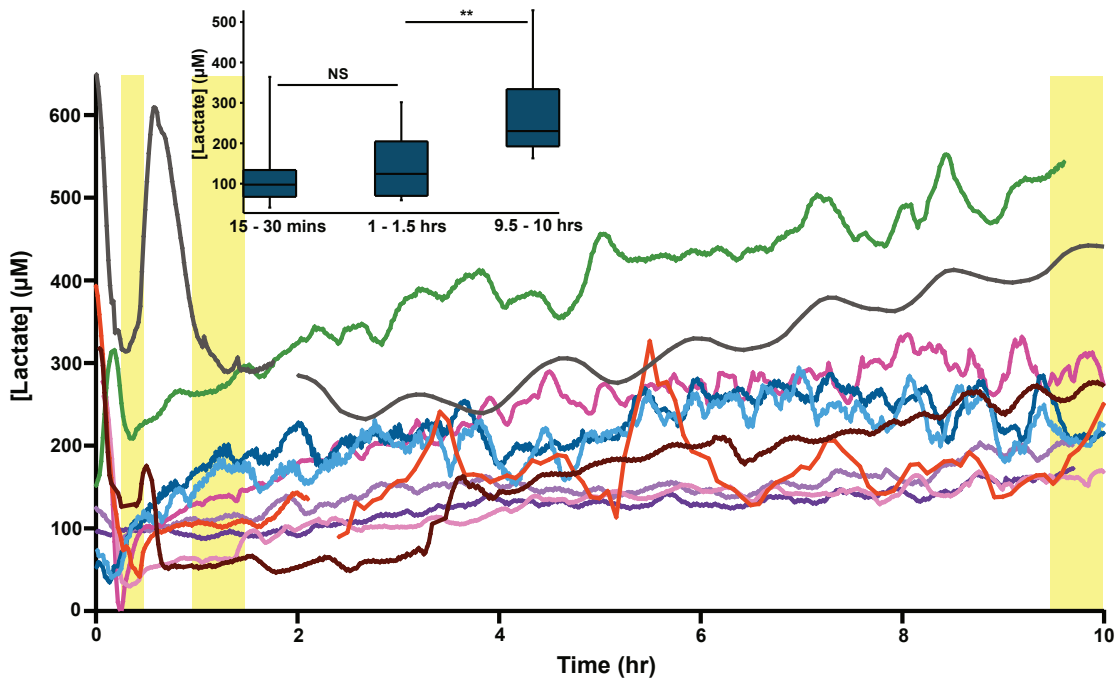


Figure 4.15: Dialysate cortical lactate profiles during HMP. Each line represents real-time data of an individual kidney with a point every minute (every 5 minutes in 2 cases, for section from 2 hours to end) smoothed with a Savitsky-Golay 21-point filter. Similar colours indicate pairs of kidneys (blue, purple and pink). The green, red, brown and grey traces represent single kidneys. Gaps in the data correspond to mid-experiment calibrations. *Inset:* Median lactate concentrations of SCS kidneys at 3 key time intervals during the 10 hours of preservation, shown here for clarity and evaluated in more detail in figure 4.22. Shaded regions indicate the data window averaged to give the data presented in the box plots. Box plots show median levels and interquartile range. Whiskers indicate 10th and 90th percentiles. Significance: ** $p < 0.01$, NS=not significant.

For these kidneys, the initial trend varied; in some cases the lactate began high and then decreased sharply and in other cases the lactate concentration began low. The average lactate concentration between 15-30 minutes for each kidney (median 98 μM) was compared with that between 1-1.5 hours (median 124 μM) using a Wilcoxon signed-rank test, which showed no significant change. After the initial period, dialysate lactate concentrations steadily rose over the course of the experiment. Further statistical analysis to compare the average lactate concentration between 1-1.5 hours into cold perfusion for each kidney to that between 9.5-10 hours (median 230 μM) showed a significant increase.

The overall trend in medullary lactate levels was the same as for the cortex, as shown in figure 4.16 (individual traces not shown). As seen in the cortex, medullary lactate levels also remained stable during the initial 1.5 hours of preservation, with no significant change during this time, followed by a significant increase over the remaining preservation time.

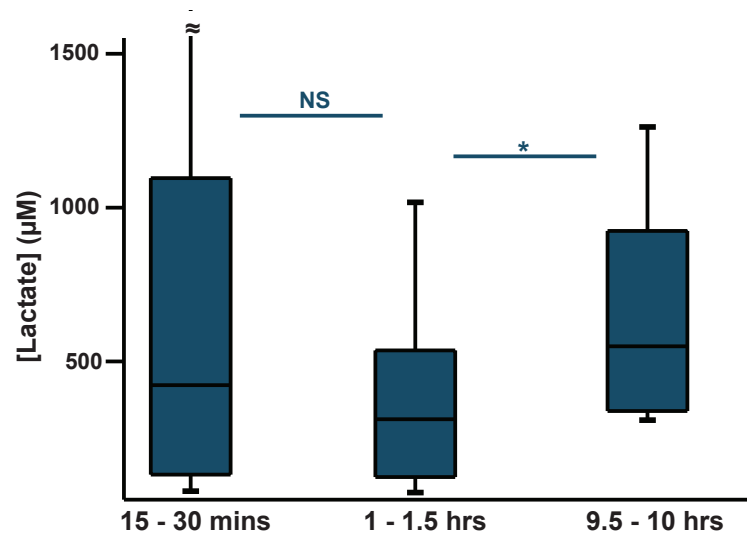


Figure 4.16: Dialysate medullary lactate profiles during HMP. Box plots show medullary lactate concentrations of HMP kidneys at 3 key time intervals during the 10 hours of preservation. Box plots show median levels and interquartile range. Whiskers indicate 10th and 90th percentiles. Significance: * $p < 0.05$, NS=not significant.

4.5 Results: during passive warming

4.5.1 SCS warming

After 24 hours of SCS, kidneys were removed from the ice and allowed to warm to ambient temperature for 2 hours. The lactate levels in the cortex and the medulla were measured throughout this time. Figure 4.17 shows how the dialysate lactate concentration in the cortex changed over this period of warming compared with the pre-warming levels.

4. TRANSPLANT ORGAN VIABILITY ASSESSMENT: PART I

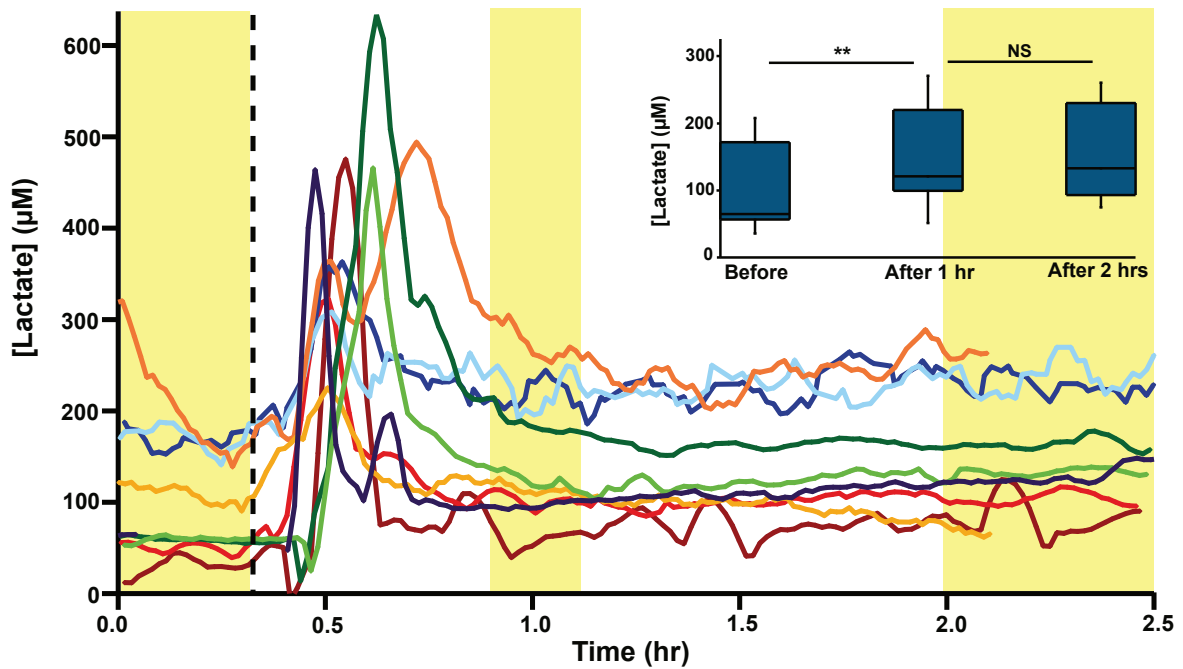


Figure 4.17: Dialysate cortical lactate profiles during passive warming after SCS. After 24 hours of preservation, kidneys were removed from the ice and allowed to warm passively to ambient temperature. The dotted line indicates when warming began. Each line represents real-time data of an individual kidney with a point every minute, smoothed with a Savitsky-Golay 11-point filter. Similar colours indicate pairs of kidneys (red, orange, green and blue). *Inset:* Median lactate concentrations of SCS kidneys at 3 key time intervals during the 2 hours of passive warming are shown here for clarity and evaluated in more detail in figure 4.24. Shaded regions indicate the data window averaged to give the data presented in the box plots. Box plots show median levels and interquartile range. Whiskers indicate 10th and 90th percentiles. Significance: ** p<0.01, NS=not significant.

As shown in figure 4.17, there was an initial peak in cortical lactate levels on cessation of cold storage, which then decreased to a stable level within 1 hour, with levels significantly higher after 1 hour of warming (median 121 μM) compared with pre-warming levels (median 65 μM). However, no further increase was seen after 2 hours of warming (median 133 μM) even though the temperature continued to increase. Maximum lactate levels were detected almost immediately after the onset of warming (median 11 min, n=9).

By contrast, medullary lactate levels showed a different trend to that of the cortex. As shown in figure 4.18, there was a significant increase in the lactate concentration during the first hour of warming (median 644 μM) compared with pre-warming levels (median 381 μM) and there was no further change after another hour of warming (median 667 μM), despite the temperature continuing to increase. This trend is similar to that of the cortex, but in this region, no initial peak in lactate was observed upon commencing warming (traces not shown). Moreover, the median time to maximum lactate levels after

the onset of warming was much longer in the medulla than in the cortex (median 120 minutes, n=9).

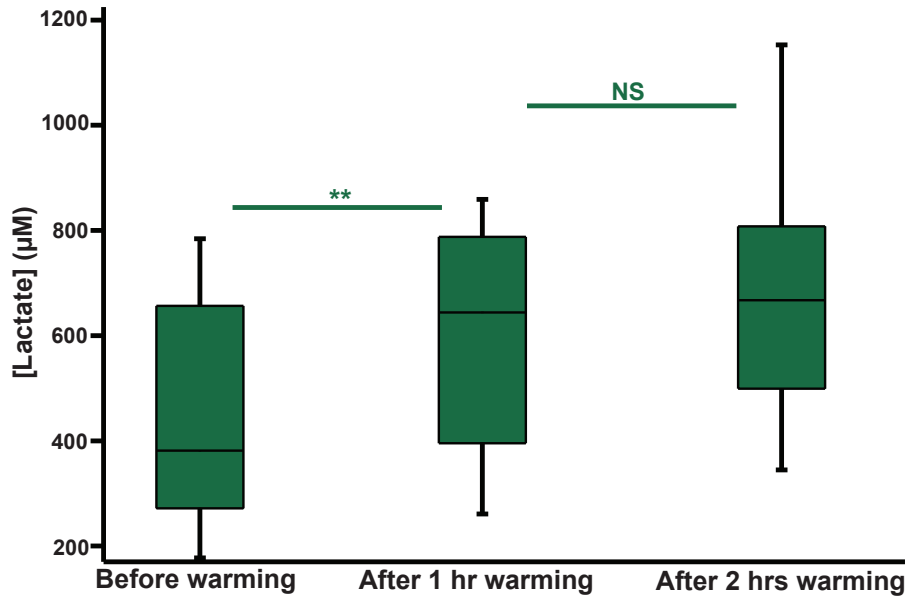


Figure 4.18: Dialysate medullary lactate levels during passive warming after SCS. Box plots show medullary lactate concentrations of SCS kidneys at 3 key time intervals during the 2 hours of passive warming to ambient temperature. Box plots show median levels and interquartile range. Whiskers indicate 10th and 90th percentiles. Significance: ** p<0.01, NS=not significant.

4.5.2 HMP warming

After 10 hours of HMP, perfusion was stopped and kidneys were allowed to warm to ambient temperature for 2 hours. Figure 4.19 shows the cortical lactate concentration during 2 hours of passive warming compared with pre-warming levels.

4. TRANSPLANT ORGAN VIABILITY ASSESSMENT: PART I

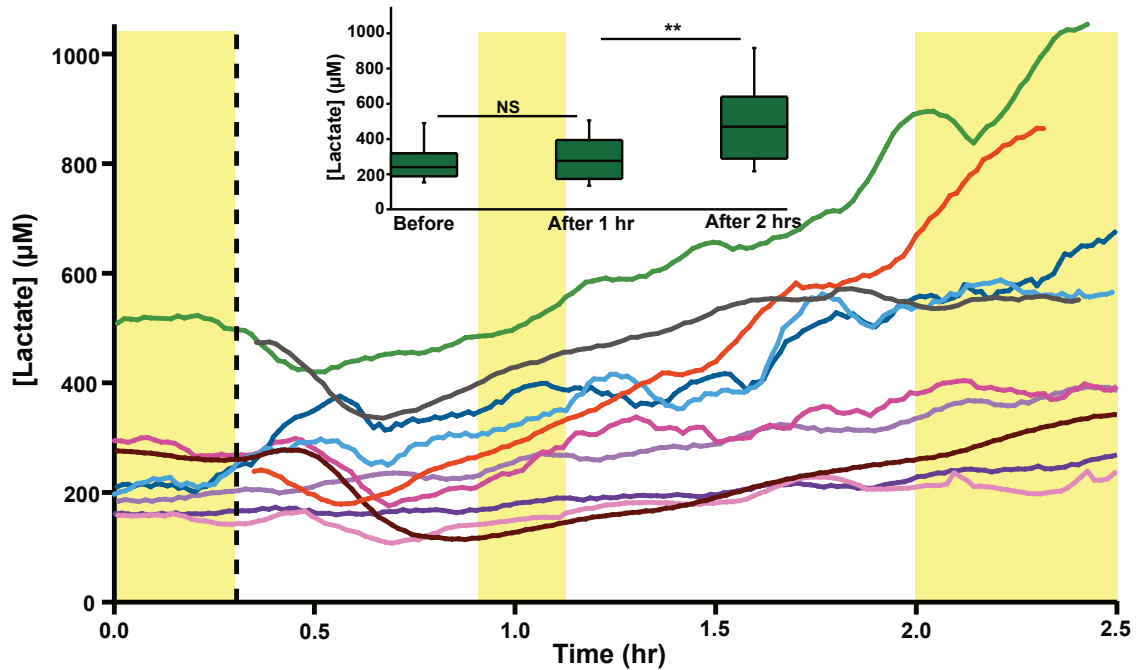


Figure 4.19: Dialysate cortical lactate profiles during passive warming after HMP. After 10 hours of preservation, perfusion was stopped and kidneys were allowed to warm passively to ambient temperature. The dotted line indicates when warming began. Each line represents real-time data of an individual kidney with a point every minute, smoothed with a Savitsky-Golay 21-point filter. Similar colours indicate pairs of kidneys (blue, purple and pink). *Inset:* Median lactate concentrations of HMP kidneys at 3 key time intervals during the 2 hours of passive warming are shown here for clarity and evaluated in more detail in figure 4.24. Shaded regions indicate the data window averaged to give the data presented in the box plots. Box plots show median levels and interquartile range. Whiskers indicate 10th and 90th percentiles. Significance: ** $p < 0.01$, NS=not significant.

As shown in figure 4.19, cortical lactate levels significantly increased after 2 hours of passive warming (median 470 μM) compared with pre-warming levels (median 241 μM). For this group, the time to maximum detected lactate was significantly longer than for the SCS group (median 120 min, $n=10$), as there was no initial peak.

In order to passively warm the kidneys after HMP, as well as subjecting the kidneys to increasing temperatures, perfusion was also stopped. The increase in lactate seen during this warming phase could therefore have been due to the cessation of perfusion, resulting in the accumulation of lactate that had previously been washed out. To test this theory, after 10 hours of HMP, one kidney was warmed for 2 hours while perfusion continued. This was achieved by replacing the ice, which normally cools the perfusion solution, with water at room temperature and allowing the perfusion solution to warm to ambient temperature as it circulated. Figure 4.20 shows the cortical lactate profile for this kidney during the 2 hours of warm perfusion. The lactate profile for this kidney is very similar to those of the

other HMP kidneys, which were warmed without perfusion, suggesting that the lactate increase during warming is not because of cessation of perfusion but is due to the effect of the increasing temperature.

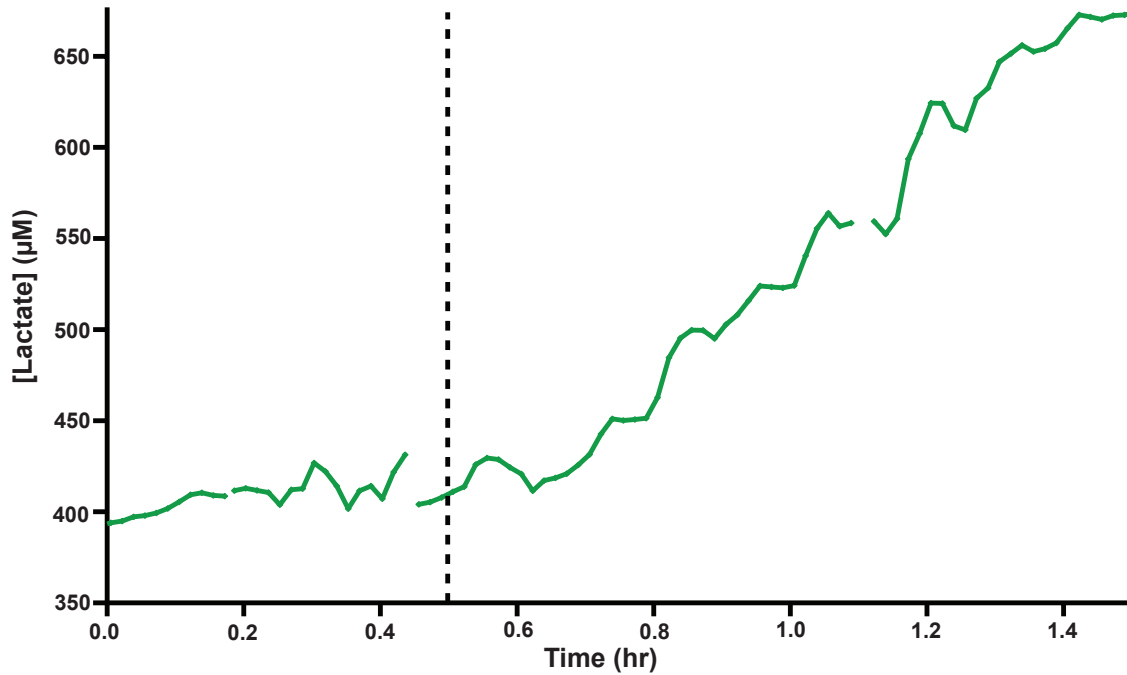


Figure 4.20: Dialysate cortical lactate profile during warm perfusion after HMP. After 10 hours of HMP, the ice was removed from the perfusion machine and the perfusate was allowed to warm to ambient temperature. The kidney was continuously perfused for the following 2 hours. The dotted line indicates when warming began.

In this case, medullary lactate profiles showed a similar trend to that of the cortex (traces not shown). As shown in figure 4.21, there was no significant increase in medullary lactate levels during the first hour of warming (median $629 \mu\text{M}$) compared with pre-warming levels (median $517 \mu\text{M}$); however, levels significantly increased after 2 hours of passive warming (median $926 \mu\text{M}$). In the medullary region, the median time to maximum lactate levels after the onset of warming was similar to the cortical region (median 98 minutes, $n=10$).

4. TRANSPLANT ORGAN VIABILITY ASSESSMENT: PART I

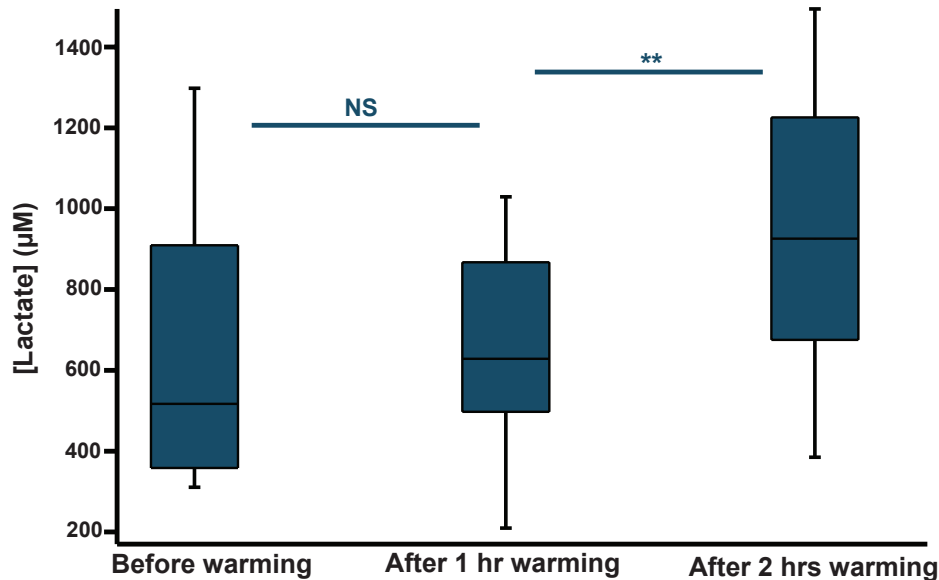


Figure 4.21: Dialysate medullary lactate levels for HMP kidneys during passive warming. Box plots show medullary lactate concentrations of HMP kidneys at 3 key time intervals during the 2 hours of passive warming to ambient temperature. Box plots show median levels and interquartile range. Whiskers indicate 10th and 90th percentiles. Significance: ** $p < 0.01$, NS=not significant.

4.6 Comparison of preservation methods

4.6.1 During preservation

Figure 4.22 shows a comparison of the mean cortical lactate levels in kidneys stored using the two preservation methods at key time points. Important differences can be identified between the lactate profiles for the two preservation methods. Over the initial 1.5 hours of preservation there was no significant difference in the lactate profiles of kidneys stored by the two techniques, despite the difference in storage temperature. However, after 10 hours of preservation, the lactate levels of HMP stored kidneys were dramatically higher (median 230 μM , $n=10$) than for those stored by SCS (median 68 μM , $n=9$).

4.6 Comparison of preservation methods

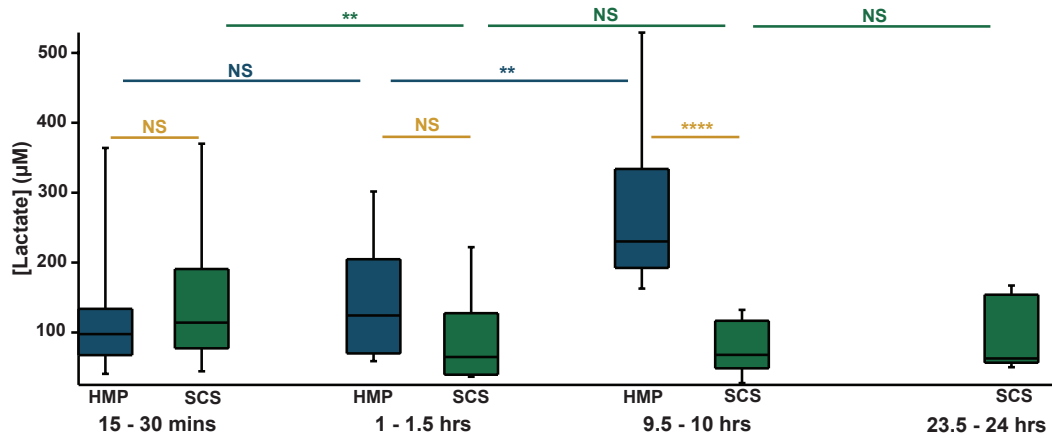


Figure 4.22: Dialysate cortical lactate levels for kidneys undergoing SCS and HMP. Box plots show cortical lactate concentrations of HMP kidneys (n=10) and SCS kidneys (n=10) at key time intervals during the 10 and 24 hours of preservation, respectively. Box plots show median levels and interquartile range. Whiskers indicate 10th and 90th percentiles. Significance: ** p<0.01, **** p<0.0001, NS=not significant.

By contrast, in the medulla, there was no significant difference in lactate levels between the two preservation methods over 10 hours of preservation, as shown in figure 4.23.

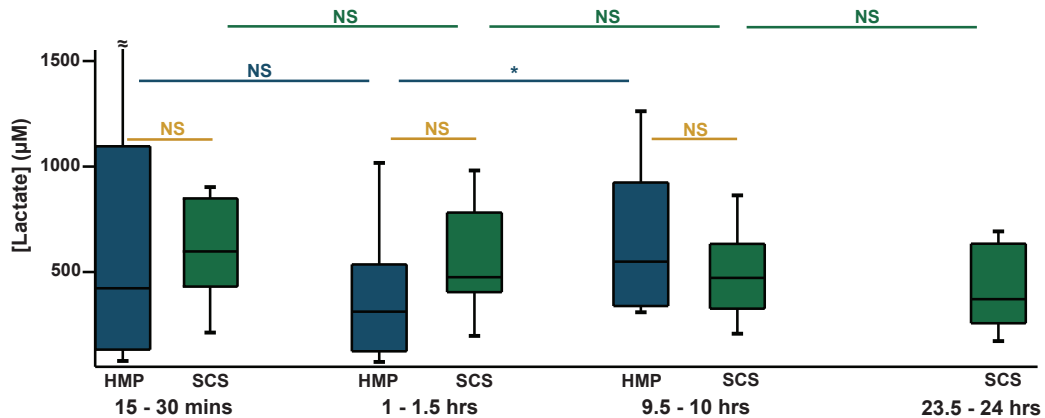


Figure 4.23: Dialysate medullary lactate levels for kidneys undergoing SCS and HMP. Box plots show medullary lactate concentrations of HMP kidneys (n=10) and SCS kidneys (n=10) at key time intervals during the 10 and 24 hours of preservation, respectively. Box plots show median levels and interquartile range. Whiskers indicate 10th and 90th percentiles. Significance: * p<0.05, NS=not significant.

4.6.2 During warming

The mean increase in temperature during 2 hours of warming was similar for kidneys stored using the two preservation methods (median increase: SCS 13.2°C, interquartile

4. TRANSPLANT ORGAN VIABILITY ASSESSMENT: PART I

range 11.6-13.3°C, n=9; HMP 11.1°C, interquartile range 10.1-11.4°C, n=10). Furthermore, there was no significant difference between the final temperature after 2 hours of warming for the two groups; for SCS stored kidneys the final median temperature was 17.1°C and for HMP stored kidneys the final median temperature was 17.9°C.

In both preservation groups, there was a significant increase in cortical lactate levels after 2 hours of passive warming, as shown in figure 4.24. However, the increase in lactate during the warming phase was significantly higher for kidneys that had been preserved by HMP (median 143 μM) compared with those that had been preserved by SCS (median 56 μM). Additionally, the cortical lactate profiles of SCS stored kidneys during warming were very different to those of HMP stored kidneys, with levels peaking a median of 11 minutes compared with 120 minutes after the onset of warming, respectively.

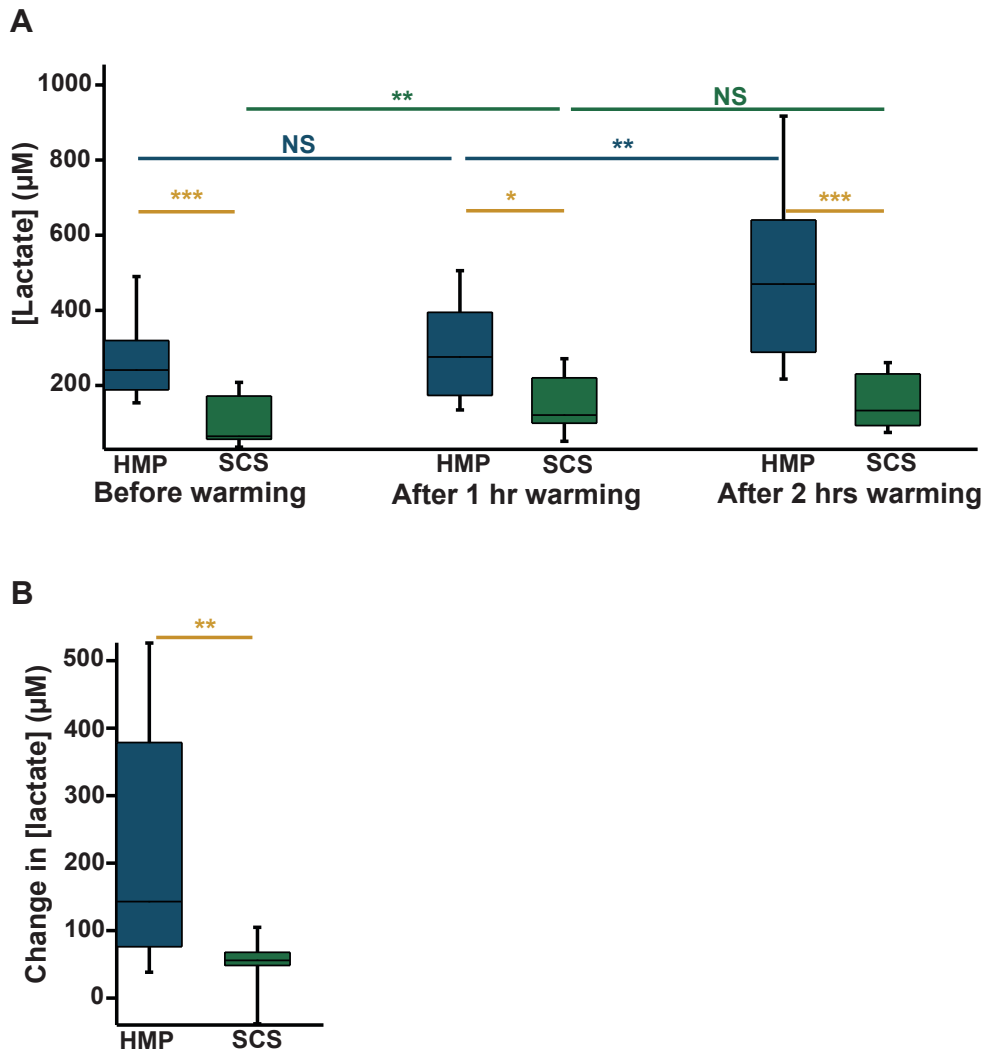


Figure 4.24: Dialysate cortical lactate levels during passive warming after SCS or HMP. *A.* Box plots show cortical lactate concentrations of HMP kidneys (n=10) and SCS kidneys (n=9) at key time intervals during the 2 hours of passive warming following preservation. *B.* Comparison of cortical lactate increase over the 2 hours of warming for the two preservation groups. Box plots show median levels and interquartile range. Whiskers indicate 10th and 90th percentiles. Significance: * p<0.05, ** p<0.01, *** p<0.001, NS=not significant.

Medullary lactate levels also significantly increased after 2 hours of warming, as shown in figure 4.25. However, in contrast to the cortical region, there was no significant difference in the medulla between the magnitude of the increase for the two preservation groups. The medullary lactate profiles of kidneys stored using the two preservation methods were very similar, with lactate levels peaking after a median of 120 minutes for SCS stored kidneys and after a median of 98 minutes for HMP stored kidneys.

4. TRANSPLANT ORGAN VIABILITY ASSESSMENT: PART I

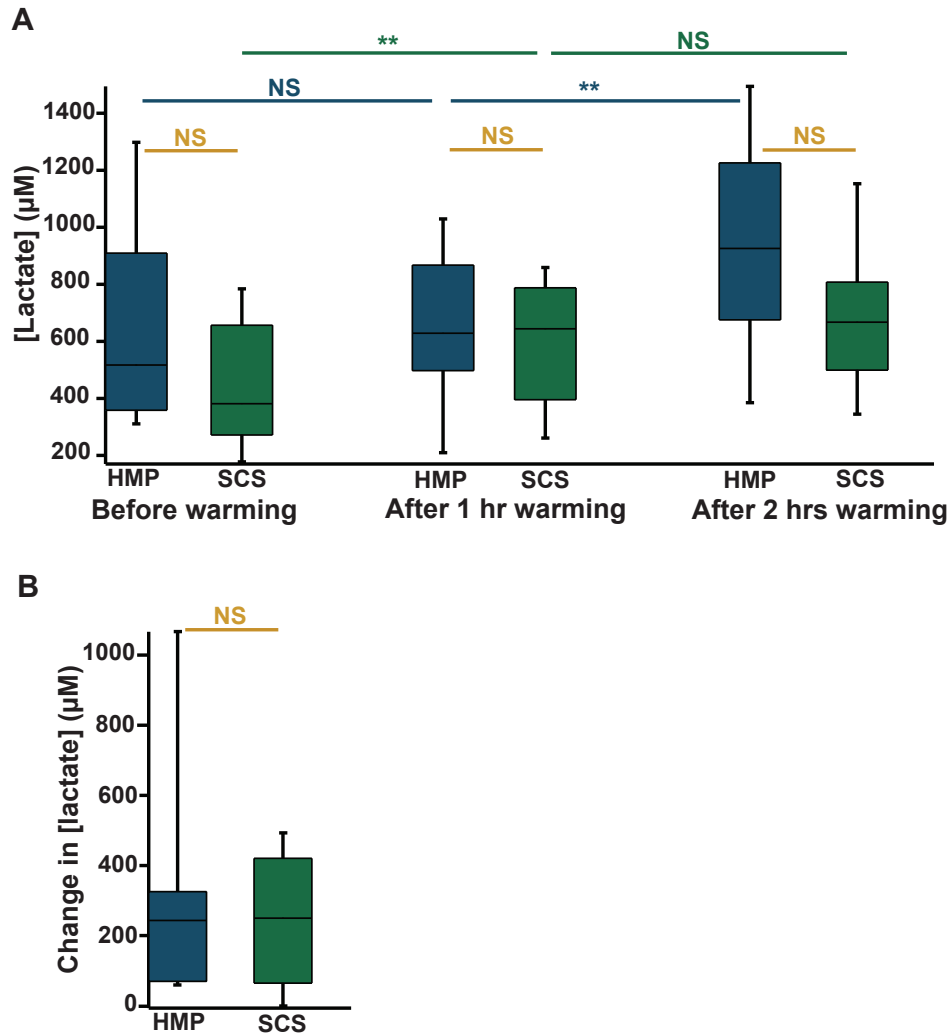


Figure 4.25: Dialysate medullary lactate levels during passive warming after SCS or HMP. *A.* Box plots show medullary lactate concentrations of HMP kidneys (n=10) and SCS kidneys (n=9) at key time intervals during the 2 hours of passive warming following preservation. *B.* Comparison of medullary lactate increase over the 2 hours of warming for the two preservation groups. Box plots show median levels and interquartile range. Whiskers indicate 10th and 90th percentiles. Significance: ** p<0.01, NS=not significant.

Area-under-the-curve (AUC) analysis of the lactate profiles during the initial 40 minutes of warming was carried out and was compared with an assumed linear increase using a one-sample t-test (two-tail) to test whether the data were significantly different from a linear increase. Results of this analysis are shown in figure 4.26. For SCS stored kidneys, cortical lactate levels showed a highly significant positive AUC, whereas medullary levels showed a significant negative AUC. For kidneys preserved by HMP, AUC values were not significantly different from zero in either cortical or medullary regions.

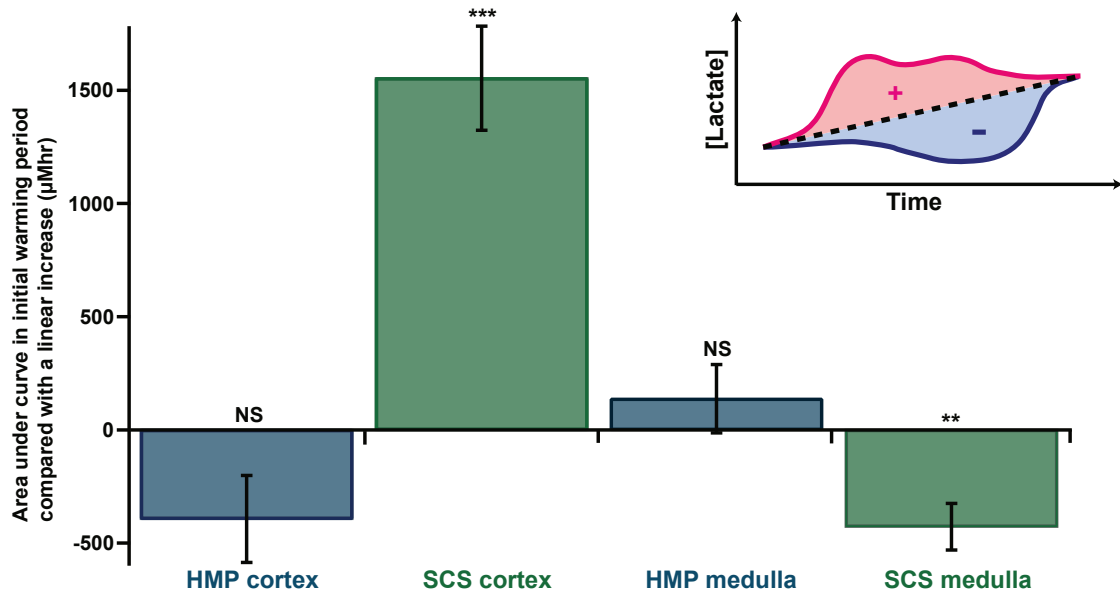


Figure 4.26: Area-under-the-curve analysis of kidney lactate profiles during warming. The lactate profile during the initial 40 minutes of passive warming was compared with a linear increase model for the cortex and the medulla in the two preservation groups. Histograms show mean difference, error bars indicate the standard error. Significance: ** $p < 0.01$, *** $p < 0.001$, NS=not significant. *Inset:* Diagram showing how the area-under-the-curve analysis was carried out. A straight line was used to join the levels before warming and after 40 minutes of warming for each kidney. This linear increase was subtracted from the actual data. If the difference was not significantly different from 0 then the increase was effectively linear, if it was positive then it represented a peak (example shown in pink) and if it was negative it represented a trough (example shown in blue).

Is the AUC change in SCS kidneys an artefact caused by probe movement?

In this experimental protocol, in order to warm the SCS stored kidneys, they first had to be physically removed from the ice. As shown in figure 4.13, any movement of the probe can result in artefacts in the signal, which are similar in shape to those seen on commencing warming in the cortex of SCS stored kidneys. In order to rule out that the cortical warming trend for SCS stored kidneys was a result of probe movement, an experiment was conducted in which the kidneys were allowed to warm to room temperature without the need to remove them from the ice box. In order to achieve this a shelf was constructed inside the ice box onto which the kidneys were placed. At the end of preservation, the ice was melted by addition of room temperature water and the water drained out through a hole at the bottom of the box. As the kidneys were placed on a shelf inside the ice box, the varying ice level did not cause the kidneys to move at all. Figure 4.27 shows the cortical lactate profile for a kidney that was not moved upon warming compared with a ‘typical’ kidney, which was moved. The initial peak in lactate that was previously seen at

4. TRANSPLANT ORGAN VIABILITY ASSESSMENT: PART I

the onset of warming was seen even when the kidney was not moved, implying that the peak is not an artefact caused by prove movement but a real physiological change.

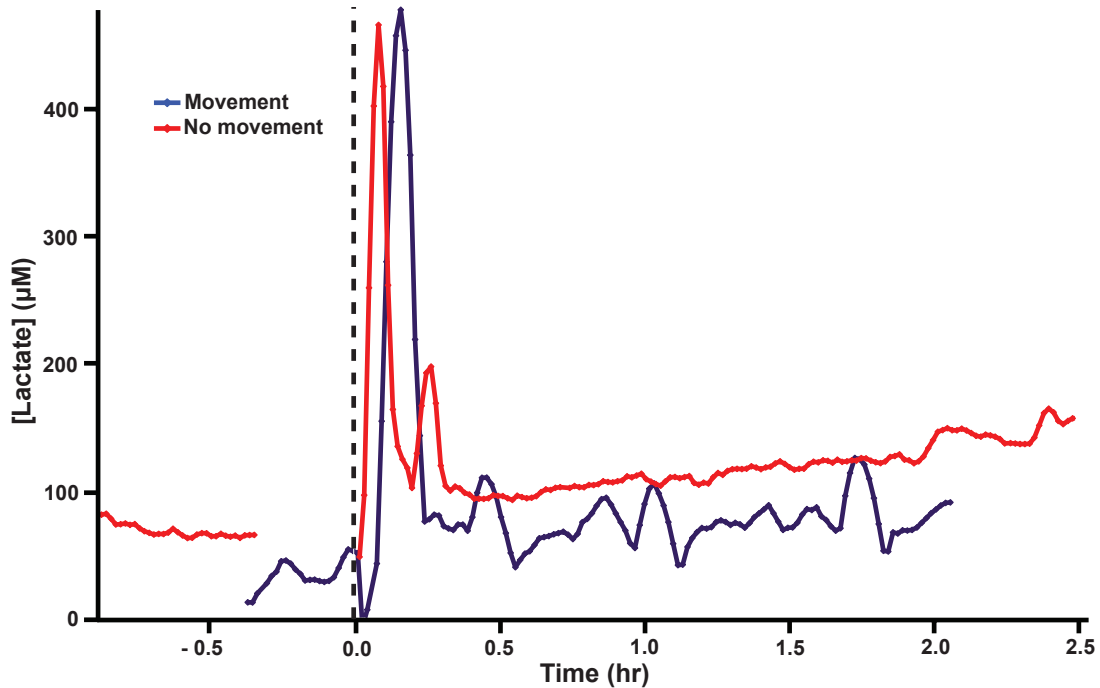


Figure 4.27: Cortical lactate profiles during warming, with and without movement. Cortical lactate concentrations during 2 hours of passive warming following 24 hours of SCS are shown. The purple trace represents the cortical warming profile for a ‘typical’ kidney, which was moved during the warming phase and the red trace represents a kidney that was warmed without any movement. Traces have been time-aligned and time 0 (*dotted line*) indicates when warming began.

Is the difference between SCS and HMP kidneys upon warming caused by differences in CIT?

In our study, markedly different lengths of cold preservation were used between the SCS and HMP groups. These times were chosen to mimic clinical situations in our institution; when kidneys are preserved using HMP, total CIT is usually kept below 20 hours, while kidneys preserved using SCS may be subjected to longer CIT as a result of transportation considerations. However because of logistical constraints more than 10 hours of HMP was not feasible as the perfusion machine needed to be constantly topped up with ice. As the kidneys were collected at 6am and the laboratory was locked at 11pm, longer times were not possible. As a result, it was critical to identify whether the different warming profiles seen for the two preservation groups were a result of these differences in CIT. Figure 4.28 shows a pair of kidneys, one of which was stored on ice for 10 hours, to mimic the HMP situation, while the other was stored on ice for 24 hours, as was the case for the rest of SCS group. Moreover, care was taken not to move either kidney during warming.

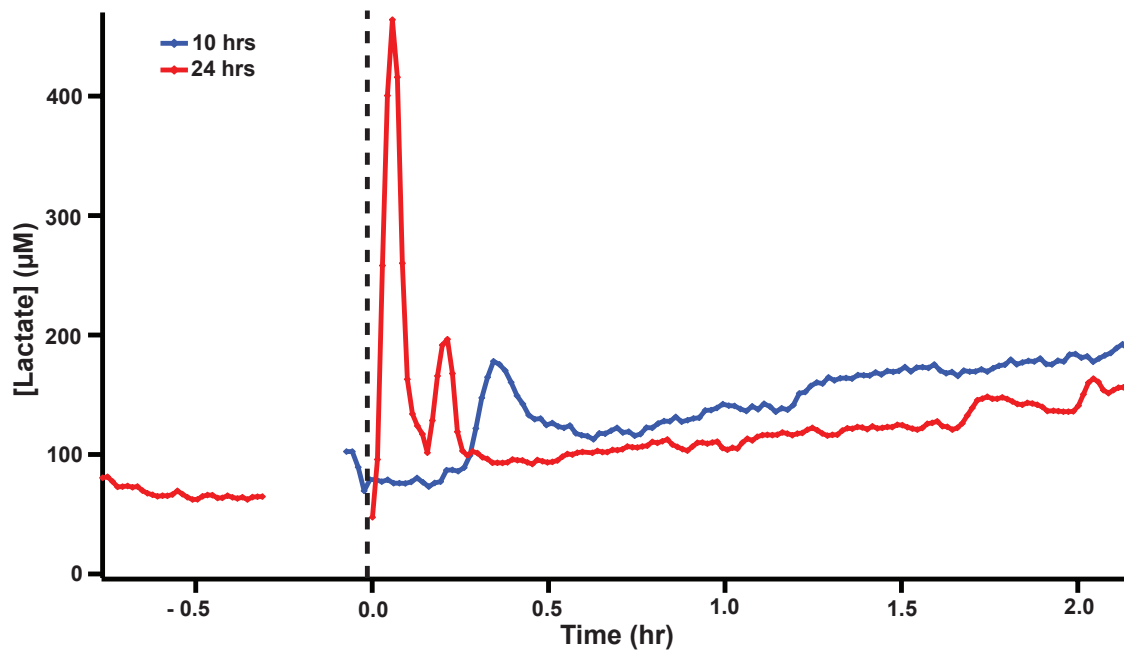


Figure 4.28: Cortical lactate profiles during warming, after varying lengths of SCS. Cortical lactate concentrations during 2 hours of passive warming following 24 (*red*) and 10 (*blue*) hours of SCS are shown. Traces have been time-aligned and time 0 (*dotted line*) indicates when warming began. In both cases, care was taken not to move either kidney during warming.

The pair of kidneys should have been of a similar health before retrieval and were subjected to the same WIT and CIT prior to preservation. In this comparison, at the end of preservation the kidney that was stored for 10 hours should have been healthier than the one that was stored for 24 hours. The kidney that had been subjected to SCS for 10 hours showed a similar trend to that seen for kidneys stored on ice for 24 hours, with an initial peak at the onset of warming. Interestingly, however, the magnitude of this peak was considerably less than for its pair, which was stored for longer on ice. In addition, the peak seemed to be delayed compared with the kidney subjected to a longer CIT. In this respect, the kidney stored on ice for the shorter 10 hours more closely resembled the HMP kidneys than the kidney stored on ice for 24 hours, as the maximum lactate concentration was observed at the end of warming for HMP kidneys. This preliminary result suggests that the difference in cortical lactate seen during warming between the two preservation groups is not simply a result of the differing CIT but an effect brought about by the storage method itself. The results suggest that, for SCS, the size and the timing of the peak could provide some indication of kidney health; however, more experiments would need to be carried out to reach any firm conclusions regarding this.

4. TRANSPLANT ORGAN VIABILITY ASSESSMENT: PART I

4.7 Cortex versus medulla

For both HMP and SCS, the lactate concentration in the medulla was significantly higher than in the cortex at all selected time points throughout preservation. For convenience, values from figures 4.24 and 4.25 are summarised in table 4.2.

Table 4.2: Summary of median cortical and medullary values during SCS and HMP (n=10), compared using Wilcoxon signed-rank test (two-tail), * p<0.05, ** p<0.01, **** p<0.0001.

Time-point	[Lactate] _{Cortex} (μM)	[Lactate] _{Medulla} (μM)	Significance
SCS			
15 - 30 min	114	600	****
1 - 1.5 hr	64.9	478	****
9.5 - 10 hr	68.0	474	****
23.5 - 24 hr	62.9	374	**
HMP			
15 - 30 min	97.6	425	**
1 - 1.5 hr	124	315	*
9.5 - 10 hr	230	551	**

As described in section 4.2, the use of storage tubing for collection of the medullary dialysate and the use of online analysis for the cortical dialysate required the microdialysis flow rate used for the two regions to be different, with 2 $\mu\text{l}/\text{min}$ used for the cortex and 1 $\mu\text{l}/\text{min}$ for the medulla. As a result, we would expect the probe recovery to be higher in the medulla than in the cortex. In order to ascertain whether higher probe recovery is the cause of the higher levels of lactate observed in the medulla, a ratio of the average cortical and medullary lactate concentrations at each time point was taken. SCS and HMP groups were treated separately, as the difference in temperature between the two preservation groups may also have had an effect on probe recovery (197). The mean medulla/cortex ratio was 7.2 ± 5.7 (n=39) for the SCS kidneys and 5.0 ± 6.4 (n=27) for the HMP kidneys. For each individual kidney there was considerable variation in the ratio over the course of the preservation period. If the difference in magnitude in the two regions was simply a recovery effect, we would expect the ratio to be constant for each kidney. Moreover, for a probe placed in a beaker containing a stirred solution of lactate, the concentration of lactate in the dialysate at 1 $\mu\text{l}/\text{min}$ was 1.9 times that at 2 $\mu\text{l}/\text{min}$. Therefore, the difference between cortical and medullary lactate concentrations was considerably higher than the recovery difference *in vitro* for the two flow rates. Alternatively, to investigate this effect, we could consider the number of moles recovered by the probe per second at each flow rate. So, for the *in vitro* beaker experiment previously described, the ratio of the number of moles recovered by the probe at 1 $\mu\text{l}/\text{min}$ to that at 2 $\mu\text{l}/\text{min}$ was 0.95

but, *in vivo*, this ratio was 2.54 and 1.65 for the SCS and HMP groups, respectively. These results suggest that the differences observed in the cortex and the medulla were not caused by probe recovery effects alone and that lactate levels in the medulla really were higher than those in the cortex. However, it is difficult to make any firm conclusions regarding the size of this difference.

4.8 Discussion

This chapter has described the use of rsMD to identify key differences in renal metabolism during preservation using the two clinical methods, SCS and HMP, as well as during subsequent warming. The lactate profiles of kidneys stored using the two preservation methods showed significant differences, both during preservation and during the warming phase.

Preservation phase

As a result of the washout effect provided by HMP, it was initially assumed that tissue lactate levels in HMP preserved kidneys would be lower than in SCS preserved kidneys, with levels predicted to progressively rise as lactate accumulation occurred during SCS. However, interestingly in this study the reverse was found; after the initial hour of SCS, cortical lactate levels remained low and stable, while lactate levels in HMP preserved kidneys progressively increased. The stable lactate levels observed during SCS appear to contradict previous findings in the literature (195, 218).

Typically, in clinical practice, HMP is carried out at temperatures between 4-6°C, while SCS is performed at lower temperatures between 2-4°C (217, 219). On the basis of this, experimental protocols in this study were designed to mimic clinical practice as closely as possible to enable clinical translation of the data generated. However, as a result of this, in addition to the inefficiency of HMP cooling, SCS kidneys were typically stored on average 4.6°C lower than HMP kidneys. As a result, local glycolytic activity may have been limited in SCS stored kidneys because of the lower temperatures slowing cellular function and leading to a reduction in energy demand and metabolism rates. Furthermore, in contrast to SCS, kidneys preserved by HMP were subjected to sustained pulsatile perfusion, which in turn allowed buffering of intracellular and extracellular acidosis, as well as removal of metabolic products. Hence, for SCS stored kidneys the local glycolytic activity may also have been limited by a finite supply of glucose and ATP precursors, as well as by the inhibitory effect of acidosis on glycolysis rates.

However, as described in section 4.1.6, lactate metabolism in the kidney is complex. One theory for the increasing lactate levels observed during HMP is that the perfusion circuit provides the possibility for removal of local metabolic products from one part of

4. TRANSPLANT ORGAN VIABILITY ASSESSMENT: PART I

the kidney and for redistribution throughout the organ as the perfusate is recycled. As a result, local transport and distribution of glucose and lactate between the cortex and the medulla could be re-established, which in the cortex could facilitate low levels of glucose and energy production in the presence of oxygen, as well as further glycolysis in the medulla.

To test this theory further, a preliminary study to test the glucose and lactate levels of HMP perfusate samples was carried out. Effluent samples were taken at the start of HMP, and then after 3, 6 and 10 hours. The samples were stored at -80°C and were analysed at a later date using the rsMD system described in section 2.3.1.1. Each sample was manually injected into the system until 6 peaks were obtained for each of glucose and lactate. Figure 4.29 shows data from perfusate analysis of two HMP kidneys.

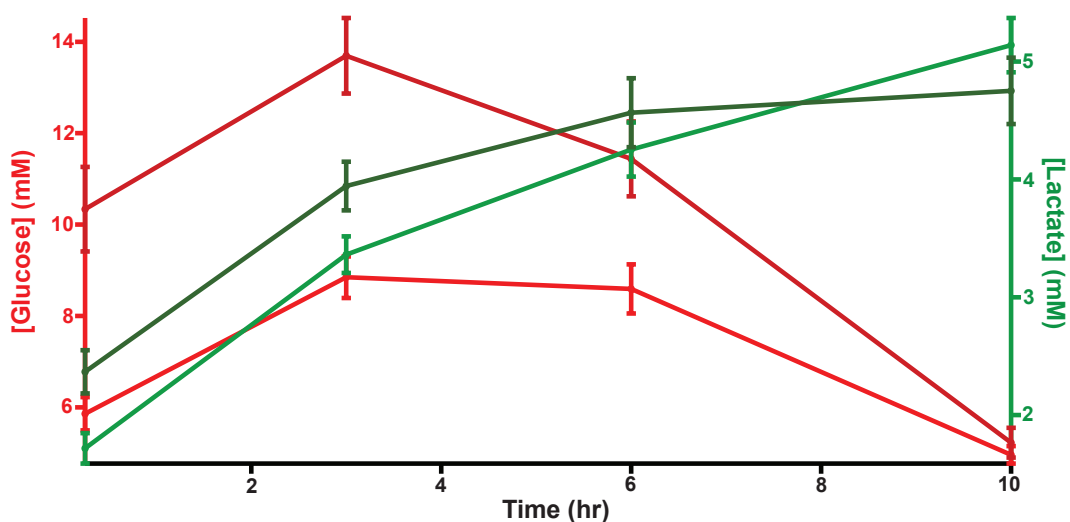


Figure 4.29: Analysis of renal effluent metabolite concentrations during HMP. Perfusate lactate (*green*) and glucose (*red*) concentrations during 10 hours of HMP for two kidneys are shown. The darker and lighter colours indicate the two kidneys. Samples of effluent were manually injected into the rsMD analysis system and converted to concentrations on the basis of calibrations. Markers indicate mean \pm standard deviation ($n=6$) of sample injections. Lactate increased during HMP, while glucose peaked after several hours and declined until the end of perfusion.

For these kidneys, perfusate lactate levels increased throughout HMP preservation, while perfusate glucose levels increased over the initial 3 hours of perfusion and decreased over the remaining preservation period. The increase in glucose observed during the initial 3 hours of perfusion suggests that cortical gluconeogenesis was occurring, resulting in the local production of glucose (207, 220). As the perfusate was recycled, this glucose could be transported to the medulla, facilitating further glycolysis and resulting in the increasing lactate levels seen in both the tissue and the perfusate. Moreover, the higher

levels of lactate detected in the medulla, compared with the cortex further support this explanation.

In summary, HMP enables re-establishment of glucose-lactate recycling within the kidney, as well as delivery of low levels of oxygen and nutrients in the perfusate, which may be sufficient to facilitate resumption of a certain degree of inherent physiological function. However, as SCS kidneys were not perfused, these benefits were not provided, which may explain the different lactate profiles observed between the two preservation modalities.

Warming phase

The warming phase of the experimental protocol was designed to test the reaction of the kidney to an extreme challenge and to investigate how kidneys preserved by SCS and HMP are affected by this reaction. As temperatures increased, the type of ischaemia the kidneys were subjected to changed from hypothermic to sub-normothermic, resulting in further, more deleterious cell damage and death, which corresponds to the increased lactate levels observed. The initial spike in lactate levels seen in the cortex of SCS preserved kidneys in the first 30-40 minutes of warming could have been caused by a surge in the limited metabolic activity of the kidneys and in anaerobic glycolysis brought about by the sudden temperature increase. Furthermore, the subsequent decrease in lactate to lower stable levels could represent surviving cortical cells with minimal metabolic activity. By contrast, HMP preserved kidneys showed a gradual increase in cortical lactate over 2 hours of warming. In this case, any contribution from the medulla would be negligible, as without continued perfusion, glucose-lactate recycling would not be possible. Therefore, the progressive lactate increase observed for HMP preserved kidneys during warming is probably due to increased anaerobic glycolysis and may represent similar cell damage to that observed in the SCS group but over a protracted period of time. The time over which the cell damage occurs may indicate the ability of the kidneys to tolerate the warming insult, suggesting that preservation by HMP provides some protection for the kidneys.

With respect to their function and metabolic activity, the medulla and the cortex can be considered as physiologically distinct entities (207, 220, 221). In contrast to the cortex, kidneys preserved by HMP and SCS showed similar trends in medullary lactate levels during preservation. Moreover, there was no significant difference in the observed medullary lactate profiles of SCS and HMP kidneys during passive warming, suggesting that any protective effects offered by HMP may dominate in the cortex.

4.8.1 Our results in the context of other microdialysis studies of renal metabolism

In recent years there has been a growing interest in the use of microdialysis as a tool for monitoring transplant organs during preservation, but studies are still limited (194, 195, 196, 197). Moreover, these studies were all conducted using conventional microdialysis, in which samples were collected in vials and analysed at discrete intervals (every 20 min - 2 hr), resulting in poor temporal resolution.

In the first renal study during *ex vivo* preservation, Baicu *et al.* used microdialysis to determine the efficacy of perfusate supplementation during HMP (194). The authors quantified pyruvate levels in the renal effluent as well as in the interstitial fluid and concluded that measuring changes in the interstitial fluid provides a better means of assessing organ viability than in the effluent alone.

Keller *et al.* monitored dialysate cortical lactate levels during a fairly short CIT of 2 hours and observed a decrease in lactate (197). This decrease in lactate concentration was expected, as microdialysis monitoring began prior to recovery; therefore, the decrease represents the onset of cold storage causing local metabolism to slow. In the same study, the authors used arterial clamping to induce postoperative ischaemia in a porcine model of renal transplantation and observed a significant increase in both lactate and the lactate/glucose ratio within 30 minutes of clamping. However, the time to detection was limited by their sampling rate; it is possible that using a higher sampling rate metabolic changes could have been detected even earlier. However, in their later study (195), Keller *et al.* demonstrated increasing cortical lactate levels during 24 hours of SCS, in contrast to our findings.

In a recent study by Fonouni *et al.*, the effect of differing lengths of SCS was investigated during anastomosis and reperfusion in a porcine transplant model using microdialysis (196). Interestingly, in kidneys that had been subjected to 24 hours of SCS, the authors observed an immediate rise in lactate levels on reperfusion, which peaked and then declined. These lactate profiles during WIT are very similar to those observed in our study of SCS kidneys during warming; however, as a result of the superior temporal resolution of our rsMD system, we were better able to resolve these changes, and to determine the duration and the concentration change of the warming peak. For kidneys that were subjected to a shorter CIT of 6 hours, the authors observed a more gradual increase in lactate during WIT, which resembles the lactate profiles we observed in HMP kidneys during warming. These results suggest that the warming profile of HMP kidneys in our study represents those of less ischaemically damaged kidneys (6 hrs CIT). However, Fonouni *et al.* noted an eventual peak in lactate during reperfusion in the kidneys that had been subjected to a shorter CIT, supporting the preliminary results shown in figure 4.28,

which suggested that the size and the timing of the warming peak could provide some indication of the health of the organ after SCS.

Several studies have used microdialysis to monitor *in situ* clamping of renal arteries to instigate ischaemia (197, 222, 223). In all cases, cortical lactate levels increased while glucose levels decreased, which is expected during an ischaemic event as anaerobic metabolism dominates. In addition, microdialysis has been used in a study to detect varying degrees of vascular thrombosis in a porcine transplant model (224). In this study, the authors found no significant difference in the lactate/pyruvate ratio between groups with varying degrees of thrombosis; however, glucose levels varied significantly, with levels highest in the control group.

4.8.2 Limitations and future work

In this study, online microdialysis has provided preliminary insights into the biochemical processes occurring while a donor kidney is stored *ex vivo*, suggesting a possible explanation for clinical differences between the two preservation methods, as well as for the observed protective role of HMP in donor kidneys (169, 225, 226).

However, in order to determine the potential of this technique in the assessment of transplant organs prior to transplantation, it is necessary to correlate observed lactate profiles with some measure of functional outcome. This would ideally be carried out using a transplant model or using an *ex vivo* isolated reperfusion model to simulate revascularisation and reperfusion. Additionally, to test viability assessment, organs with varying degrees of ischaemic injury should be investigated in order to compare the lactate profiles of successful and unsuccessful transplants.

The ability to monitor the tissue metabolism of a donor organ in real time, prior to transplantation, has the potential to provide important information regarding organ viability. However, it is necessary to measure multiple biomarkers (such as glucose, pyruvate, ATP and glycerol) in addition to lactate in order to gain a better understanding of the complex processes occurring.

An inherent limitation to this study was that organ monitoring only commenced once the organs were brought to the laboratory. As a result, no data were recorded for the critical time that included animal death, organ recovery, organ flushing and initial CIT during transportation. Information during this period could provide additional insights, as it would provide a baseline level from which to compare any changes, as well as to provide additional information on the processes occurring in the donor organ. With the current system, monitoring of the donor organ was not possible outside the laboratory because of the size of the analysis system; however, if this system could be miniaturised then earlier monitoring would be possible. Alternatively, the dialysate sample could be

4. TRANSPLANT ORGAN VIABILITY ASSESSMENT: PART I

collected into a length of storage tubing and ‘played back’ with temporal resolution at a later time.

This study has demonstrated the feasibility of using rsMD to measure kidney cortical and medullary metabolic profiles during preservation and subsequent warming. Furthermore, this technique has been used to identify differences in the lactate profiles of kidneys stored using two different clinical preservation methods. This analysis system could therefore be used as a tool for investigating other factors affecting organ viability. The following chapter will describe the use of this methodology in preliminary experiments to investigate several factors that could potentially affect organ outcome.

Chapter 5

Transplant organ viability assessment: Part II

The previous chapter demonstrated the feasibility of using rapid sampling microdialysis (rsMD) to monitor transplant organs as a potential tool for viability assessment and described a study comparing porcine kidneys stored using the two different clinical preservation methods, hypothermic machine perfusion (HMP) and static cold storage (SCS). The study prompted several questions and highlighted areas where the methodology could be improved. This chapter will describe a series of preliminary experiments addressing questions arising from the previous chapter, as well as developments to the analysis system. In addition, it will show initial experiments extending the technology for use with human organs and transplant pancreases.

5.1 Monitoring kidneys immediately after retrieval

In the previous chapter, monitoring of donor kidneys was only possible once the organ had been transported to the laboratory, approximately 4-5 hours after organ retrieval. This was identified as a weakness, as it was not possible to gather information about metabolite levels during this critical time period.

In order to collect data for this initial phase immediately after organ removal, a portable system was required to collect dialysate for delayed analysis, while still maintaining temporal resolution. In a proof-of-concept study, the microdialysis probe was inserted at the abattoir immediately after receipt of the organ (after 45 min warm ischaemia time (WIT)) and dialysate was collected into a 5 m length of storage tubing, as described in section 4.2.4. The microdialysis probe was perfused with T1 physiological solution at 2 $\mu\text{l}/\text{min}$, starting before probe insertion, using a portable microdialysis pump (CMA 107, MDialysis, Sweden). It was necessary to hold the probe in place, as demonstrated in figure 4.13; however, the means of achieving this was not trivial, as the kidney was

5. TRANSPLANT ORGAN VIABILITY ASSESSMENT: PART II

fully submerged in preservation solution and care had to be taken not to compress the soft tubing of the microdialysis probe. After several attempts with various methods, the probe was successfully held in place during transportation using a mesh sock. Figure 5.1 shows the setup for portable collection of cortical dialysate.

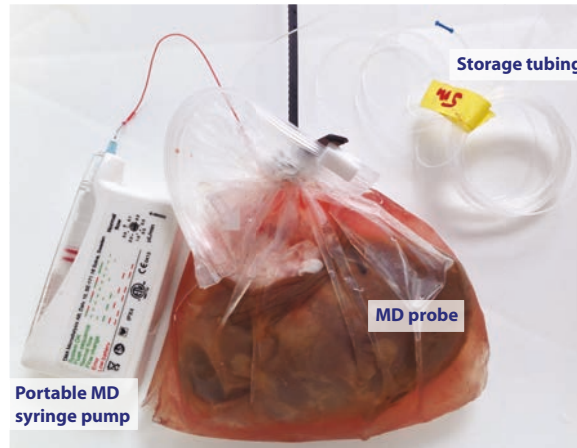


Figure 5.1: Experimental setup for portable collection of dialysate in storage tubing. The microdialysis (MD) probe was perfused with T1 solution at $2 \mu\text{l}/\text{min}$ using a portable syringe pump. The probe was held in place inside the kidney using a mesh sock. The dialysate was collected into a 5 m length of storage tubing for delayed analysis.

The initial cortical lactate levels are shown in figure 5.2. The trace starts after 45 minutes WIT. Interestingly, cortical lactate levels were very low at this early stage, suggesting that local glucose supplies had been exhausted. However, as only one kidney was monitored using this methodology, it is not possible to draw any firm conclusions without further investigation. The initial peak is probably due to tissue stabilisation following probe insertion, which usually occurs after 10-15 minutes (99). The peak at 2.5 hours is of unknown origin but coincides with arrival at the laboratory and therefore could be movement related.

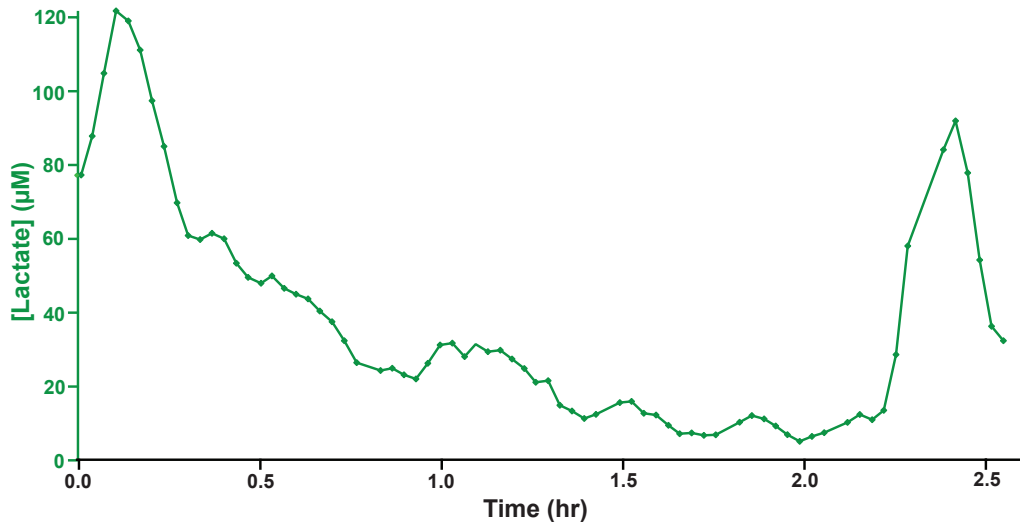


Figure 5.2: Dialysate cortical lactate profile immediately after organ retrieval. A microdialysis probe was inserted into the porcine kidney immediately after retrieval of the organ at the abattoir (WIT 45 min). The probe was perfused with a portable microdialysis pump at $2 \mu\text{l}/\text{min}$ and dialysate was collected into a length of storage tubing. The dialysate was analysed offline at $4 \mu\text{l}/\text{min}$ using the rsMD system.

5.2 Varying cold ischaemia time

In the previous chapter, a one-off experiment to investigate the effect of differing lengths of cold ischaemia time (CIT) was described. Results showed a difference in the cortical lactate profiles following different lengths of CIT, possibly as a result of differing renal health. This section will describe further investigations into this effect. For the current study, pairs of kidneys were used to control for other factors that might impact kidney health. For each pair, kidney A was perfused immediately after reaching the laboratory (short CIT), whereas kidney B was stored on ice for a further 48 hours prior to monitoring (long CIT). In a clinical situation, kidneys that had been subjected to 48 hours of CIT would not normally be transplanted as extended CIT leads to poor outcome, therefore these kidneys should represent unhealthy organs (160).

5.2.1 Experimental protocol

Two pairs of porcine kidneys were retrieved from the local abattoir, in this case with a WIT of 45 minutes. The kidneys were flushed with Soltran (Baxter Healthcare, UK) as there had been a recall of Viaspan University of Wisconsin (UW) solution (Bristol-Myers Squibb Pharmaceuticals Ltd, Dublin, Ireland) because of contamination. After retrieval and arrival at the laboratory, one of each pair of kidneys underwent 10 hours

5. TRANSPLANT ORGAN VIABILITY ASSESSMENT: PART II

of hypothermic machine perfusion (HMP) on a Waters Medical Systems RM3 perfusion machine, followed by 2 hours of warm reperfusion. The second of each pair of kidneys was stored on ice for 48 hours prior to undergoing a further 10 hours of HMP, followed by 2 hours of warm reperfusion. In both cases, HMP was carried out with in-house UW solution (based on the Belzer-MPS variant) and reperfusion was carried out with warm Krebs-Henseleit buffer (Sigma-Aldrich, UK), which was continuously pumped with oxygen. Figure 5.3 describes the main steps of the experimental protocol. Microdialysis probes were removed after HMP and replaced at the start of reperfusion, as the kidneys had to be moved between the two phases to prepare the perfusion machines for reperfusion.

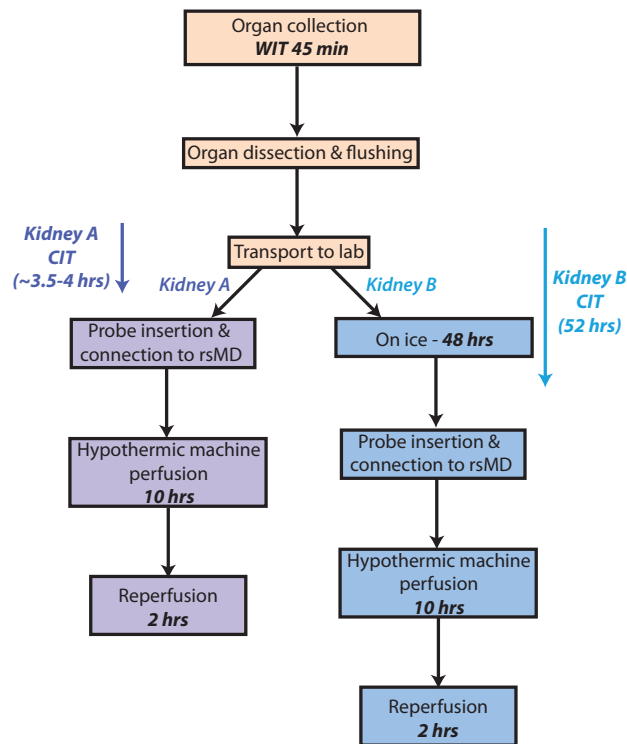


Figure 5.3: Experimental protocol for varying the length of CIT. Two pairs of kidneys were monitored using this protocol, one of each pair was subjected to 10 hours of HMP followed by 2 hours of warm reperfusion, while the second of each pair was subjected to 48 hours of storage on ice, followed by 10 hours of HMP and 2 hours of reperfusion.

In this study, a microdialysis probe, perfused at $2 \mu\text{l}/\text{min}$, was inserted into the cortex of each kidney prior to commencing HMP. Dialysate was simultaneously analysed online in real time for two kidneys using the rsMD system, as described in section 4.2.3. Concentrations referred to throughout are dialysate concentrations, which depend on the probe recovery, and not absolute tissue concentrations. A temperature probe (IT-14, Physitemp) was inserted into each kidney and was connected to an in-house temperature sensor, developed elsewhere in the group, which consisted of a T-type thermocouple con-

trolled by a chip with ice-point compensation and which incorporated multiple channels so that both kidneys could be simultaneously monitored.

5.2.2 Results

For both long and short CIT kidneys, HMP was conducted at temperatures as low as possible and efforts were made to maintain a constant temperature throughout. The mean temperature of the two short CIT kidneys, 1A and 2A, throughout HMP was $5.0 \pm 0.1^\circ\text{C}$ (n=409) and $4.8 \pm 1.0^\circ\text{C}$ (n=408), respectively. For the two long CIT kidneys, 1B and 2B, the mean temperature throughout HMP was $4.4 \pm 0.7^\circ\text{C}$ (n=436) and $6.0 \pm 1.0^\circ\text{C}$ (n=436), respectively. After HMP, both sets of kidneys were subjected to continued perfusion with a warm reperfusion solution at body temperature. The mean temperature for the short CIT kidneys, 1A and 2A, during reperfusion was $37.8 \pm 2.2^\circ\text{C}$ (n=115) and $38.2 \pm 0.9^\circ\text{C}$ (n=99), respectively. For the two long CIT kidneys, 1B and 2B, the mean reperfusion temperature was $29.7 \pm 3.9^\circ\text{C}$ (n=128) and $33.6 \pm 1.7^\circ\text{C}$ (n=123), respectively. This failure to achieve body temperature for the long CIT kidneys reflects their poorer tissue perfusion.

For the short CIT group, the mean CIT prior to HMP was 3.5 ± 0.35 hours, whereas for the long CIT group, the mean CIT prior to HMP was 52 hours. Figure 5.4 shows the dialysate cortical lactate concentrations for both sets of kidneys.

5. TRANSPLANT ORGAN VIABILITY ASSESSMENT: PART II

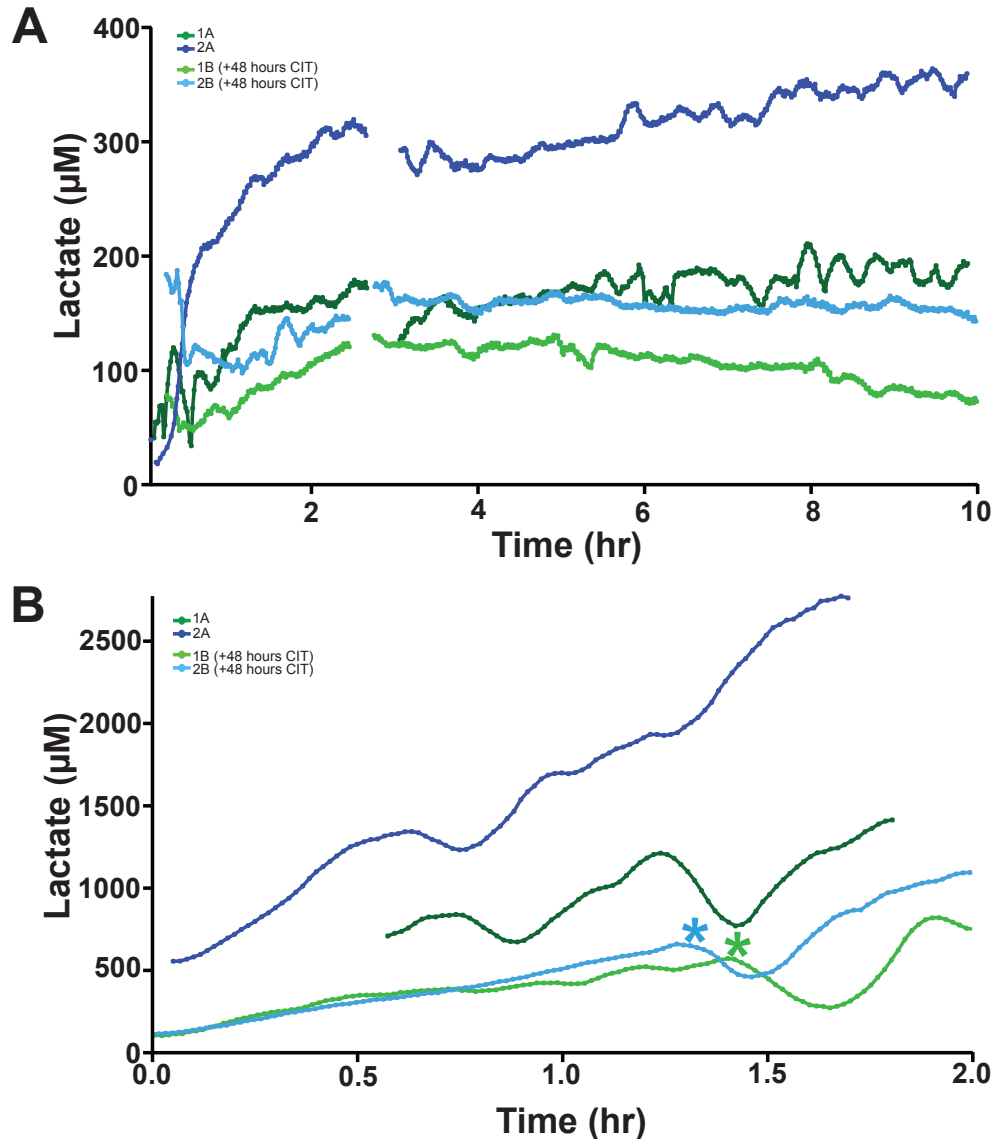


Figure 5.4: Dialysate cortical lactate profiles for kidneys undergoing HMP after varying amounts of CIT. Two pairs of kidneys were retrieved, 1 of each pair was perfused immediately after reaching the laboratory, while the other was stored on ice for an additional 48 hours before being perfused for 10 hours. *A.* Shows the cortical lactate profiles of each kidney during 10 hours of HMP. *B.* Shows the cortical lactate profile of each kidney during a further 2 hours of warm reperfusion. For the kidneys subjected to longer CIT, perfusion was stopped for a period of about 10 minutes while the machines were recalibrated during reperfusion, the start of which is marked with an asterisk. Each line represents real-time data of an individual kidney with a point every minute, smoothed with a Savitsky-Golay 21-point filter. The green and blue traces represent each pair of kidneys; the darker of each corresponds to the shorter CIT kidney.

In all cases, lactate trends observed during HMP were in close agreement with those previously observed, with lactate levels increasing as HMP progressed. However, after about 2 hours of preservation, lactate levels in the long CIT kidneys began to gradually decrease (5.4A light blue and light green traces), in contrast to the usual trend observed

during HMP (5.4A dark blue and dark green traces). Moreover, for both pairs of kidneys, higher cortical lactate levels were observed for the kidney that had been subjected to shorter CIT prior to HMP. This suggests that higher lactate levels during HMP correspond to healthier, more viable kidneys, as it demonstrates that these kidneys had resumed some degree of normal physiological metabolism. Moreover, it supports the argument made in chapter 4 that the higher cortical lactate levels observed in HMP preserved kidneys correspond to healthier organs compared with SCS preserved kidneys.

In contrast to previous studies in which kidneys were passively warmed to ambient temperature following HMP, in this case kidneys were continuously perfused at constant body temperature with a reperfusion solution (Krebs-Henseleit buffer). Despite these marked differences, the trends in cortical lactate observed during this post-HMP period show clear similarities to previous studies, with levels increasing almost linearly over the 2-hour period (5.4B). The absolute concentration of lactate was considerably higher for the reperfused kidneys that had been subjected to shorter CIT (5.4B dark blue and green traces) compared with those subjected to longer CIT (5.4B light blue and green traces). The increased lactate levels observed during reperfusion for kidneys subjected to shorter CIT, and therefore that were more healthy than those subjected to longer CIT, are most likely the result of a higher level of anaerobic metabolism in these kidneys. A certain degree of aerobic metabolism should have been resumed during the reperfusion phase, as kidneys were supplied with nutrients and oxygen in the reperfusion medium. Therefore, the increased lactate levels seen during reperfusion in all kidneys suggests that anaerobic metabolism still dominated, possibly because there was insufficient oxygen delivery to meet the high energy requirements at the increased temperatures. The higher lactate levels seen for kidneys subjected to shorter CIT seems counter-intuitive but, as only two pairs of kidneys were monitored in this preliminary study, it is not possible to draw any firm conclusions.

5.2.3 Discussion

Preliminary data comparing cortical lactate profiles in kidneys that had been subjected to different lengths of CIT, and therefore that had incurred varying amounts of ischaemic injury, show similar trends to those previously observed. Kidneys subjected to shorter CIT displayed higher cortical lactate levels compared with those subjected to longer CIT, suggesting that higher lactate levels during HMP correspond to healthier, more viable tissue. These results differ from those observed by Fonouni *et al.*, who observed higher lactate levels after longer CIT; however, in contrast to our study, the authors measured lactate levels during SCS (196). As shown in the previous chapter, cortical lactate profiles

for kidneys preserved by HMP and SCS are significantly different, which may explain this discrepancy.

5.3 Measuring multiple metabolites

On the basis of the results of analysing kidney effluent during preservation it was concluded that it would be valuable to be able to measure glucose in addition to lactate in the transplant organ. This would facilitate a better understanding of the physiological processes occurring and would enable calculation of the lactate/glucose ratio, which removes artefacts caused by probe recovery (92). With the current system it is not possible to simultaneously monitor two metabolites in two organs. However, when carrying out delayed analysis of dialysate samples collected in storage tubing, the rsMD system can be reconfigured (for details see section 2.3.1.1) so that glucose and lactate can be measured in each sample.

In the proof-of-concept study described in section 5.1, glucose was measured in the collected dialysate in addition to lactate. Figure 5.5 shows the cortical levels of both metabolites during this time period.

As described earlier, dialysate lactate levels were very low during this time period. In addition, glucose levels were very low, but fairly stable after the initial stabilisation period. The lactate/glucose ratio decreased over the initial 2 hours, possibly because of a reduction in anaerobic activity caused by hypothermic conditions. However, towards the end of monitoring, the lactate/glucose ratio increased, because of an increase in dialysate lactate levels while glucose levels remained stable. The ratio of the two metabolites provides a clear indicator of tissue health, uncomplicated by probe artefacts.

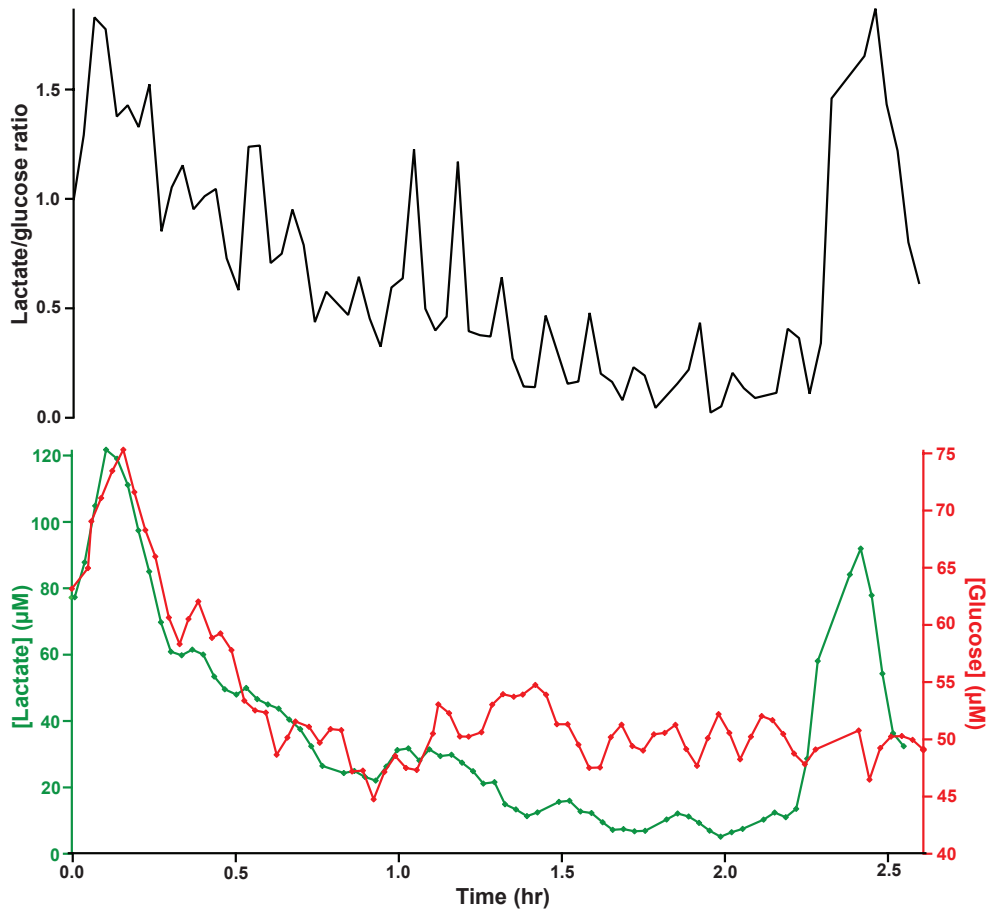


Figure 5.5: Dialysate cortical lactate and glucose profile immediately after organ retrieval. A microdialysis probe was inserted into kidney 1A immediately after retrieval of the organ at the abattoir. The probe was perfused with a portable microdialysis pump at $2 \mu\text{l}/\text{min}$ and the dialysate was collected into a length of storage tubing. The dialysate was analysed offline at $4 \mu\text{l}/\text{min}$ using the rsMD system for glucose (*red*) and lactate (*green*). The top trace (*black*) shows the corresponding lactate/glucose ratio.

Glucose biosensors

Using the current rsMD system, it is only possible to measure glucose in addition to lactate in two organs during delayed analysis. Therefore, a new system was required that enabled the simultaneous online measurement of multiple analytes in two organs. As a first step towards this, a preliminary experiment was carried out on one pair of kidneys to investigate possible differences in glucose levels in addition to lactate levels during various lengths of CIT (lactate levels shown earlier in figure 5.4). This also served as a proof-of-concept study in the design of a portable analysis system for transplant organs. Lactate levels were analysed using rsMD as described in section 5.2.1. Glucose levels were measured using a poly(phenol) glucose biosensor, as described in section 2.5.3.1, housed in a PDMS microfluidic chip. The experimental setup is shown in figure 5.6.

5. TRANSPLANT ORGAN VIABILITY ASSESSMENT: PART II

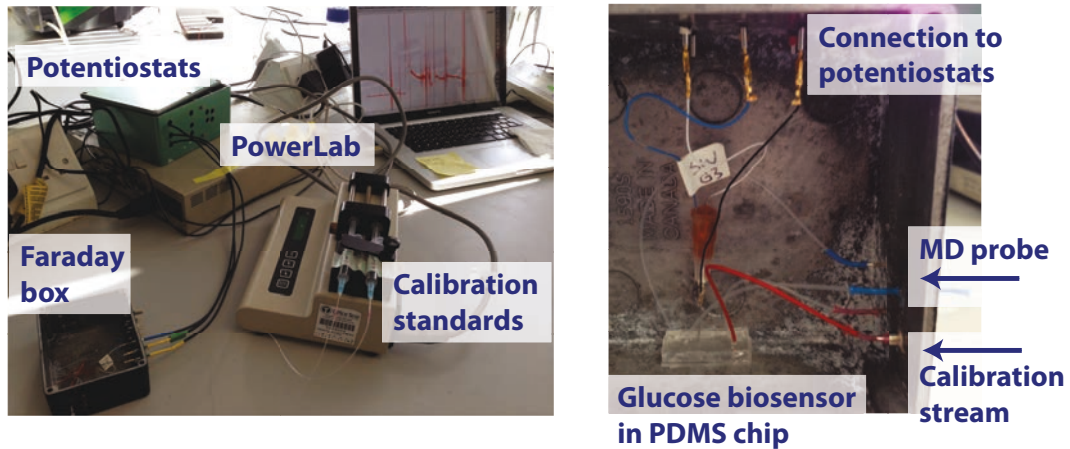


Figure 5.6: Experimental setup for glucose biosensor in microfluidic chip. The glucose biosensor was positioned in a PDMS chip, placed inside a Faraday cage. The glucose biosensor measured the concentration of glucose in the dialysate stream as it flowed past.

For each kidney, a second microdialysis probe was inserted into the cortex and was perfused with T1 solution at $2 \mu\text{l}/\text{min}$. The outlet of the probe was extended using 1 m of low-volume fluorinated ethylene propylene (FEP) tubing (0.12 mm ID, Royem Scientific, UK) in order to reach the microfluidic chip. The glucose biosensor was held at 0.75 V using in-house potentiostats and measured the concentration of glucose in the dialysate stream as it flowed past. Differences in delay were accounted for during analysis so that the results could be time-aligned with the lactate results obtained using rsMD.

Figure 5.7 shows the cortical lactate and glucose levels during HMP for kidney 1A, which was perfused immediately after reaching the laboratory, and for 1B, which was subjected to 48 hours CIT prior to HMP.

As a result of technical issues during monitoring, glucose data was only obtained for the second half of HMP. Preliminary data show that, in addition to dialysate lactate levels being higher during HMP, glucose levels were also higher for the kidney subjected to a shorter CIT compared with its pair. This result suggests that the shorter CIT kidney, which would have incurred less ischaemic injury than the kidney stored on ice for 48 hours, maintained more of its capacity for gluconeogenesis than its pair. These results are in agreement with the study conducted by Fonouni *et al.*, in which kidneys that had been stored on ice for 6 hours showed higher glucose levels at the end of cold storage than those that had been stored on ice for 24 hours (196). However, further experiments would need to be conducted to validate these results. The combination of glucose biosensors with rsMD enabled simultaneous monitoring of glucose and lactate in each kidney, providing more information on the health of the organ.

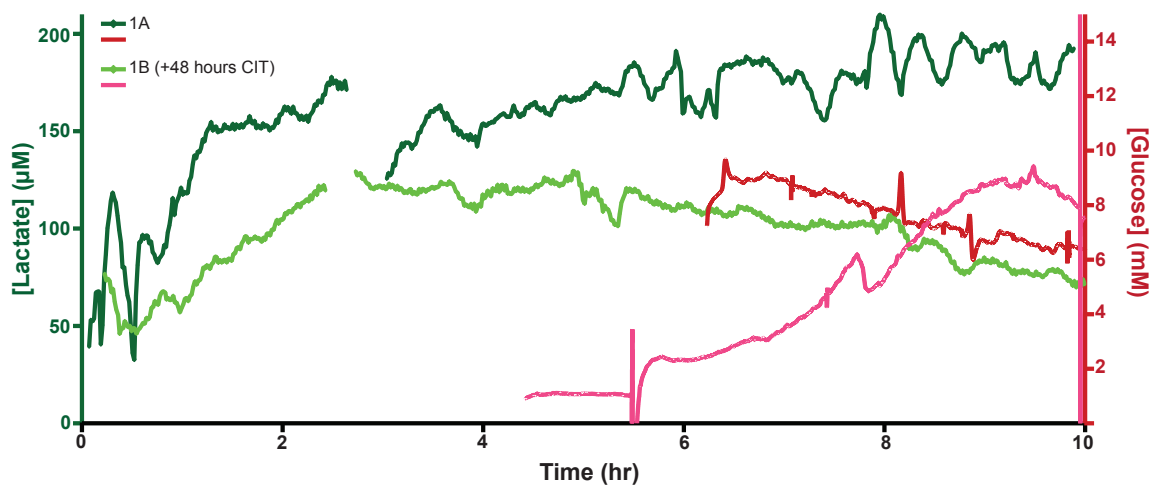


Figure 5.7: Dialysate cortical metabolite levels for kidneys undergoing HMP after varying CIT length. Two pairs of kidneys were retrieved and 1 of each pair was perfused immediately after reaching the laboratory (A), while the other was stored on ice for 48 hours (B), after which time both were subjected to 10 hours of HMP. Lactate (*green*) results were recorded by rsMD and glucose (*red*) results were measured using a poly(phenol) glucose biosensor in a PDMS microfluidic chip. The darker of each colour corresponds to the shorter CIT.

5.4 Online analysis of discarded human kidneys

We were given the opportunity to monitor discarded human kidneys, which had been donated to scientific research, when they were made available to the clinical team.

5.4.1 Case study 1

One kidney was donated from a female donor, aged between 65-70 years old. The organ was not suitable for transplantation as the donor had hydronephrosis, a condition in which the kidney becomes swollen, because of a build up of urine. The donor organ was subjected to 20 minutes of warm ischaemia, after which it was flushed with preservation solution and stored on ice before monitoring began. CIT prior to monitoring was approximately 16.5 hours.

The discarded kidney underwent 5 hours of HMP with in-house UW solution (Belzer-MPS variant), followed by 2 hours of warm reperfusion with oxygenated Krebs-Henseleit buffer. Two microdialysis probes, perfused with T1 at $2 \mu\text{l}/\text{min}$, were inserted into the kidney, one superficially into the cortex and the other into the medullary region. In this case, as only one kidney was retrieved, the online rsMD system was reconfigured so that both glucose and lactate could be measured in the cortex in real time, as described in section 2.3.1.1. The dialysate from the medullary probe was collected into storage tubing

5. TRANSPLANT ORGAN VIABILITY ASSESSMENT: PART II

(8 m), as described in section 4.2.4, for delayed analysis of both glucose and lactate at 2 $\mu\text{l}/\text{min}$, using the same rsMD system used for the online measurements. A temperature probe (Thermalert TH-5, Physitemp) was also inserted into the kidney to simultaneously monitor tissue temperature during each stage.

Cortical levels

Figure 5.8 shows cortical glucose and lactate levels during 5 hours of HMP. The trend in lactate levels shows close agreement with that observed during porcine kidney HMP, suggesting that porcine kidneys are a good model for human kidneys. Cortical lactate levels steadily increased during HMP, while glucose levels initially increased and then seemed to stabilise after 1 hour of perfusion. Figure 5.8 also shows the lactate/glucose ratio, which increased throughout HMP.

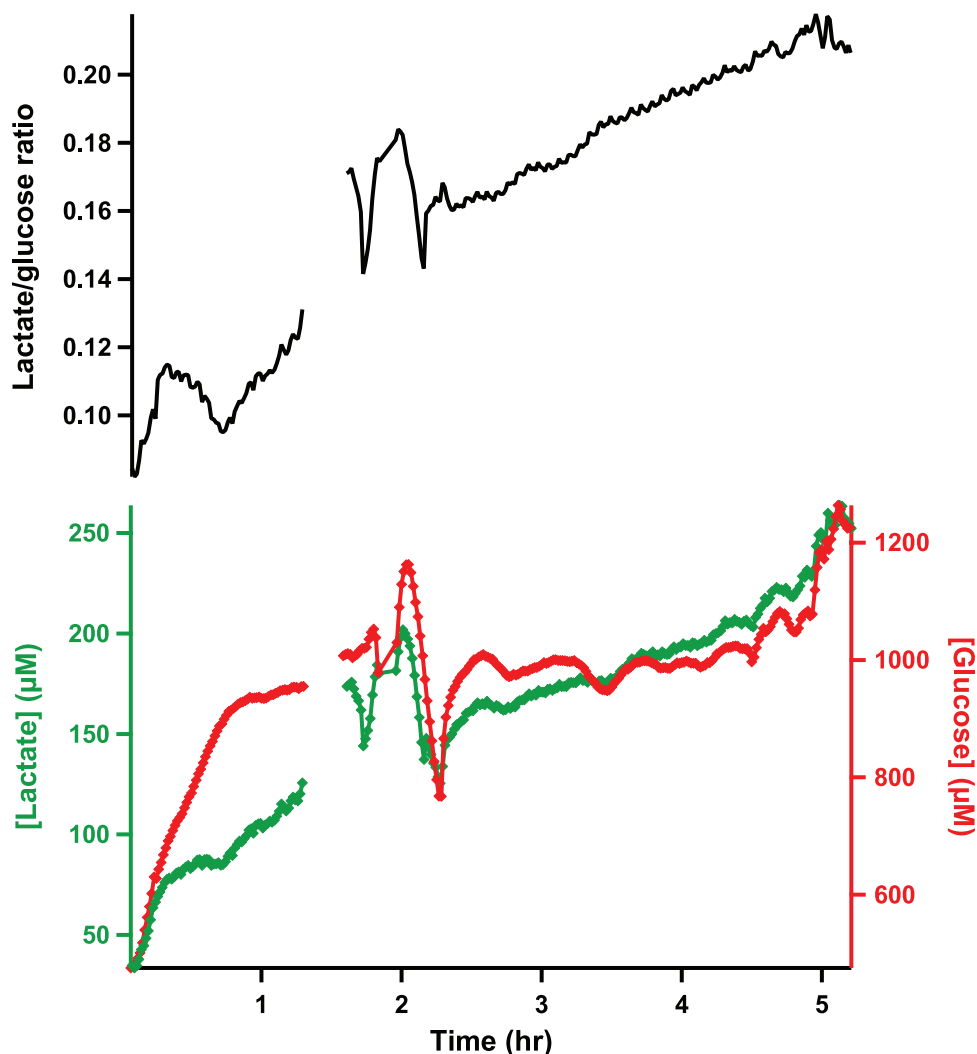


Figure 5.8: Dialysate cortical metabolite levels in a human kidney during HMP. The green trace shows dialysate lactate concentrations, the red trace shows dialysate glucose concentrations and the black trace shows the corresponding lactate/glucose ratio. Data were obtained in real time using rsMD, with a point every minute for each metabolite.

The cortical glucose and lactate levels, as well as the lactate/glucose ratio during the reperfusion phase, are shown in figure 5.9. During reperfusion, glucose levels decreased steeply, while lactate levels continued to increase. This classic signature of ischaemia suggests that, despite the provision of nutrients and oxygen during reperfusion, anaerobic metabolism still dominated. There is a large peak in glucose levels, midway through reperfusion but this is completely removed when considering the lactate/glucose ratio at this point. This demonstrates that the change is an artefact, probably caused by a change in microdialysis probe recovery, and exemplifies the importance of monitoring multiple metabolites in order to provide more reliable data. However, this is not usually possible as in most cases it is necessary to simultaneously monitor two kidneys, and therefore, using

5. TRANSPLANT ORGAN VIABILITY ASSESSMENT: PART II

the rsMD system, only one metabolite can be monitored. This is clearly a limitation of rsMD.

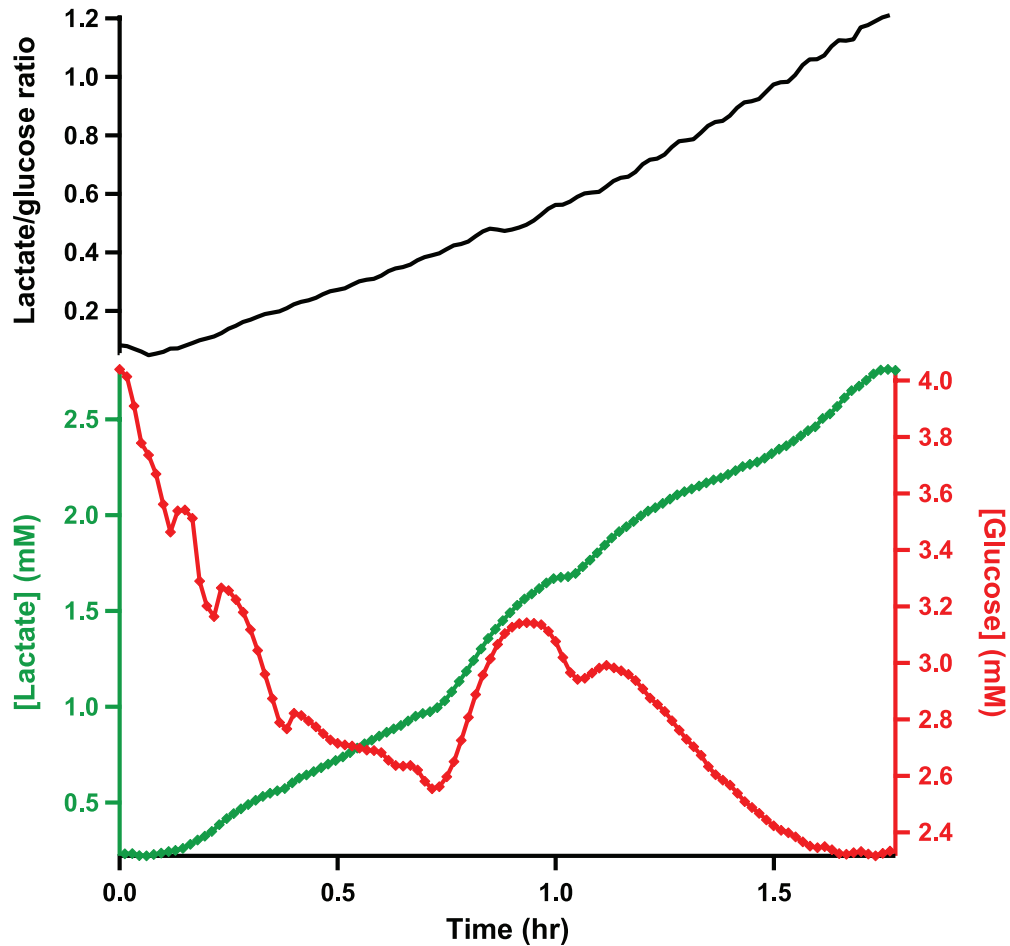


Figure 5.9: Dialysate cortical metabolite levels in a human kidney during reperfusion. The green trace shows dialysate lactate concentrations, the red trace shows dialysate glucose concentrations and the black trace shows the corresponding lactate/glucose ratio during warm reperfusion. Data were obtained in real time using rsMD, with a point every minute for each metabolite.

Medullary levels

Medullary metabolite levels during HMP and subsequent reperfusion are shown in figure 5.10.

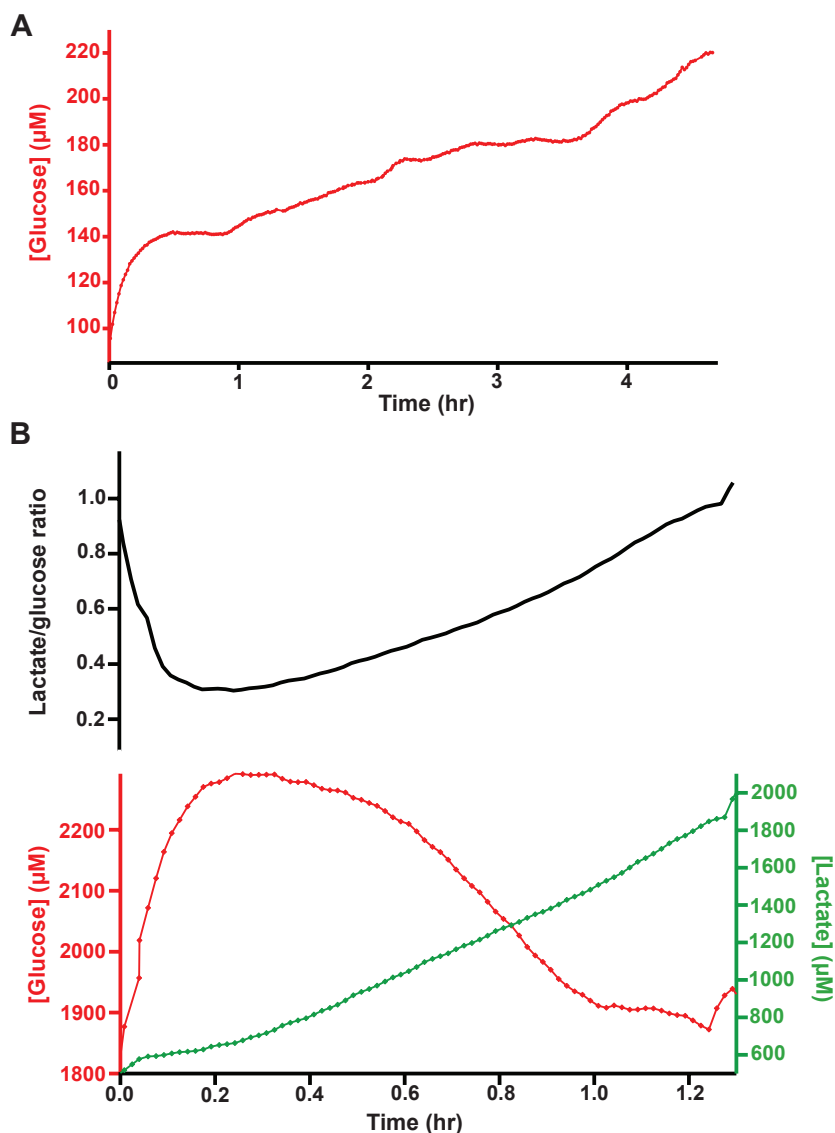


Figure 5.10: Dialysate medullary metabolite levels in a human kidney during HMP and reperfusion. Dialysate was collected into storage tubing at $2 \mu\text{l}/\text{min}$ and analysed offline using the rsMD system at $2 \mu\text{l}/\text{min}$. *A.* Medullary dialysate glucose concentration during HMP is shown. Dialysate medullary lactate levels were too low to detect. *B.* Levels during warm reperfusion are shown. The green trace shows dialysate lactate concentrations, the red trace shows dialysate glucose concentrations and the black trace shows the corresponding lactate/glucose ratio. Dialysate was collected into storage tubing and analysed at a later time using the rsMD system.

During HMP (figure 5.10A), medullary glucose levels were considerably lower than in the cortex (figure 5.8). As discussed in section 4.1.6, this was expected because of the capacity of the cortex to generate glucose. However, medullary lactate levels were too low to reliably detect. As both glucose and lactate were measured and glucose could be detected we know that the probe was functioning properly. The low medullary lactate levels were an unexpected result, as in the previous studies with porcine kidneys medullary

5. TRANSPLANT ORGAN VIABILITY ASSESSMENT: PART II

lactate levels were found to be significantly higher than cortical lactate levels at all time points throughout preservation and subsequent warming. This possibly signifies that the organ was not functioning normally, leading to a breakdown of the renal lactate-glucose recycling system and, hence, to an insufficient supply of glucose for anaerobic glycolysis to occur in the medulla. During reperfusion (figure 5.10B), there was an initial increase in medullary glucose levels, after which a similar trend was observed to that seen in the cortex (figure 5.9), with glucose levels steadily decreasing while lactate levels increased. The magnitude of the changes occurring in the medulla was less than in the cortex, suggesting that this region was less affected by the ischaemic insult.

5.4.2 Case study 2

A pair of kidneys were retrieved from a 59-year old male donor. One organ was not suitable for transplantation because of glomerulosclerosis and microthrombosis (B), while the other was suitable for transplantation but no suitable recipient could be found in time (A). Both organs were flushed with preservation solution and stored on ice for 78 hours prior to monitoring.

This experiment was carried out in collaboration with Mr. Karim Hamaoui, who was investigating the effect of treating donor kidneys with a novel synthetic protein (PTL004), which is thought to prevent thrombosis upon reperfusion. As part of the study, kidneys were monitored during haemoperfusion after treatment with the protein to evaluate whether there were any differences in the lactate profiles of kidneys that had been treated with the novel protein compared with non-treated controls. As it was possible, in chapter 4, to distinguish differences between kidneys stored by different preservation techniques using rsMD, this analysis system could prove a useful tool for evaluating novel interventions that could improve organ viability.

In a pilot study of a pancreatic thrombosis model by the group developing the synthetic protein, treatment was found to improve perfusion dynamics compared with non-treated controls (data not published). PTL004 is a fusion protein, consisting of an anticoagulant head and an endothelial-binding myristoyl tail. The tail was designed to facilitate binding and tethering of the protein to the endothelial cell membranes. Proteins with similar tethering tails have been shown to localise to capillary endothelial cell membranes in animal kidney models (227). The anticoagulant head of the protein is derived from the direct binding thrombin inhibitor hirudin, which has been found to inhibit thrombosis (227). The group developing the proteins hypothesises that targeting anti-coagulation to the vessel wall will exert a local rather than a systemic effect, which could be more effective in preventing thrombosis.

Experimental protocol

The experimental protocol was designed by the clinical team and is shown in figure 5.11.

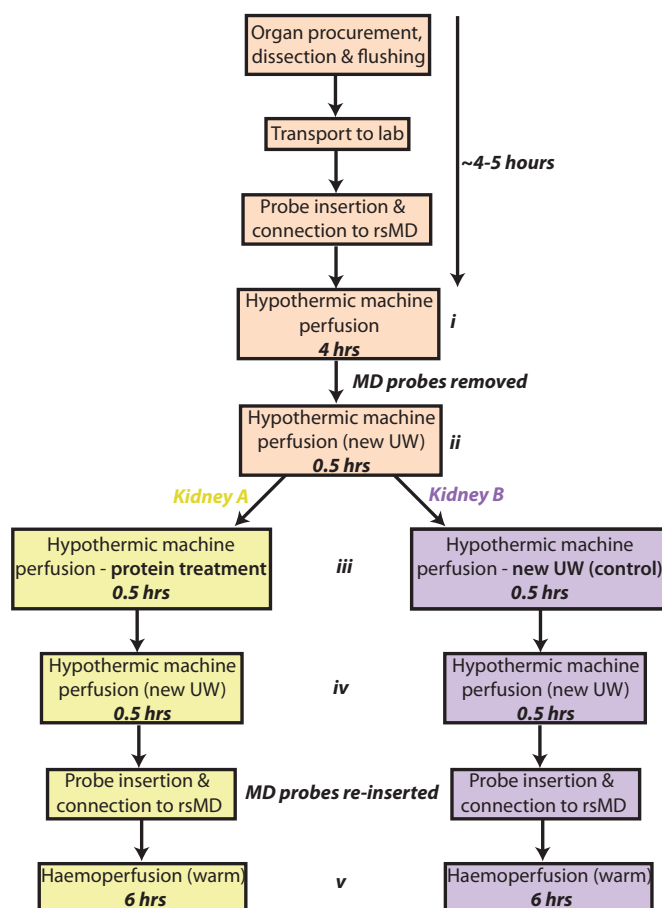


Figure 5.11: Experimental protocol for investigating the effect of protein treatment.

Pairs of kidneys were monitored using this protocol, one of each pair was treated with the novel protein (PTL004), while the other acted as its control. (i) Both kidneys were subjected to HMP for 4 hours to condition the organ, (ii) both kidneys were subjected to a further 0.5 hours of HMP with fresh UW solution, (iii) kidney A was subjected to 0.5 hours of HMP with UW containing PTL004, while kidney B was subjected to 0.5 hours of HMP with fresh UW, (iv) both kidneys were subjected to 0.5 hours of HMP with fresh UW solution to completely wash out the proteins, (v) and finally both kidneys were perfused with blood at body temperature for 6 hours.

For the haemoperfusion phase, the kidneys were perfused with pig blood from the local abattoir as human blood was not available. For this case, two microdialysis probes, perfused with T1 at $2 \mu\text{l}/\text{min}$, were inserted into each kidney, one superficially into the cortex and the other into the medullary region, prior to commencing HMP. After the initial 4 hours of HMP, probes were removed and re-inserted for the haemoperfusion phase. Cortical dialysate was simultaneously analysed online in real time for the two kidneys using the rsMD system, as described in section 4.2.3. The dialysate from the

5. TRANSPLANT ORGAN VIABILITY ASSESSMENT: PART II

medullary probe was collected into storage tubing (5 m for HMP phase and 7 m for haemoperfusion phase), as described in section 4.2.4, and frozen at -80°C until it could be analysed. As medullary samples were analysed at a later time the rsMD analysis system was reconfigured and the samples were run through the analysis system separately so that each sample could be analysed for glucose as well as for lactate levels. The stored samples were run through the rsMD analysis system at $2\ \mu\text{l}/\text{min}$ using the same rsMD system described in section 2.3.1.1. A temperature probe (IT-14, Physitemp) was also inserted into each kidney and the temperature of both kidneys was measured simultaneously using our in-house temperature sensor (briefly described in section 5.2.1) to monitor the tissue temperature at the same time. Figure 5.12 shows the experimental setup.

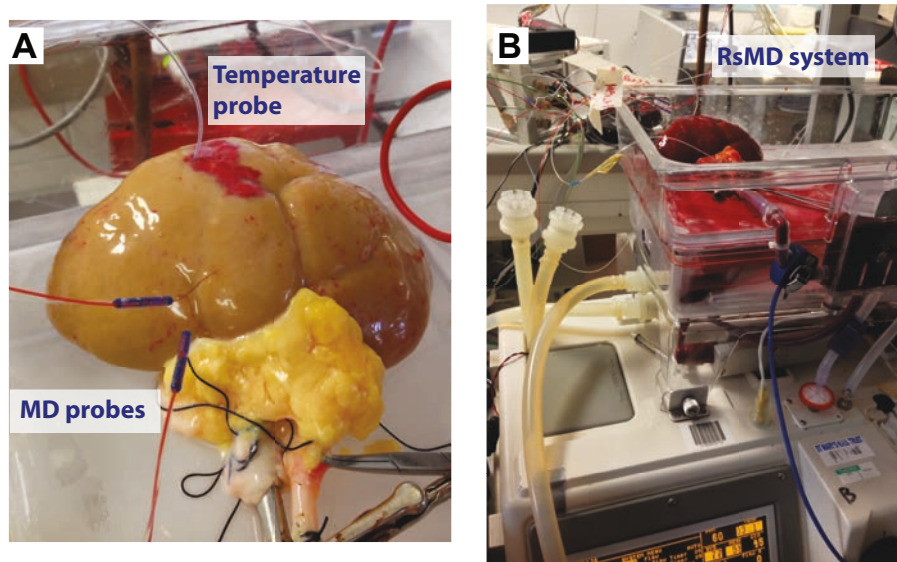


Figure 5.12: Experimental setup for perfusion of human kidney. *A.* The discarded human kidney was placed on a perfusion machine and pumped with cold preservation solution in a pulsatile manner. A temperature probe and two microdialysis (MD) probes were inserted into the kidney. *B.* After cold perfusion, the kidney was perfused at body temperature with porcine blood. The dialysate outflow from the cortical probe flowed into the rsMD analysis system for online measurement of glucose and lactate in real time.

Cortex

Figure 5.13 shows cortical glucose and lactate levels during the HMP and haemoperfusion phases. As a result of technical issues lactate levels were only recorded for kidney B during the initial part of HMP and for kidney A during the last part of HMP. However, lactate levels were recorded in both kidneys during haemoperfusion.

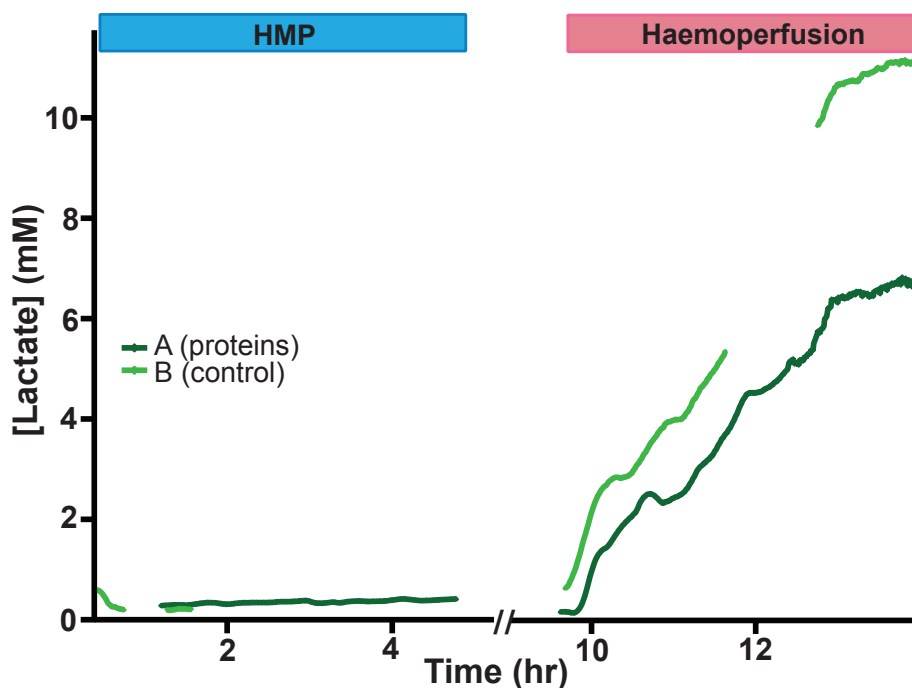


Figure 5.13: Dialysate cortical lactate profiles during haemoperfusion in human kidneys with and without protein pretreatment. Both kidneys were subjected to 4 hours of HMP, after which kidney A (*dark green*) was treated with protective proteins and kidney B (*light green*) acted as the control. Following protein treatment, both kidneys were perfused at body temperature. Each line represents real-time data of an individual kidney with a point every minute, smoothed with a Savitsky-Golay 21-point filter.

The trend in cortical lactate levels shows close agreement with that observed during porcine kidney HMP; however, despite the prolonged CIT for these kidneys, lactate levels during HMP were relatively high. During haemoperfusion, cortical lactate levels steadily increased and the non-treated kidney showed considerably higher cortical lactate levels during the haemoperfusion phase than its treated pair. However, in this case, the control kidney was rejected from transplantation due to microthrombosis and therefore it is not possible to say whether the difference in the lactate profiles of the two kidneys was because of treatment with the novel protein. Despite this, these results do suggest that the higher lactate levels observed during haemoperfusion do correspond to a less healthy donor organ.

Medulla

The medullary levels of lactate and glucose in the two kidneys during HMP and haemoperfusion are shown in figure 5.14.

5. TRANSPLANT ORGAN VIABILITY ASSESSMENT: PART II

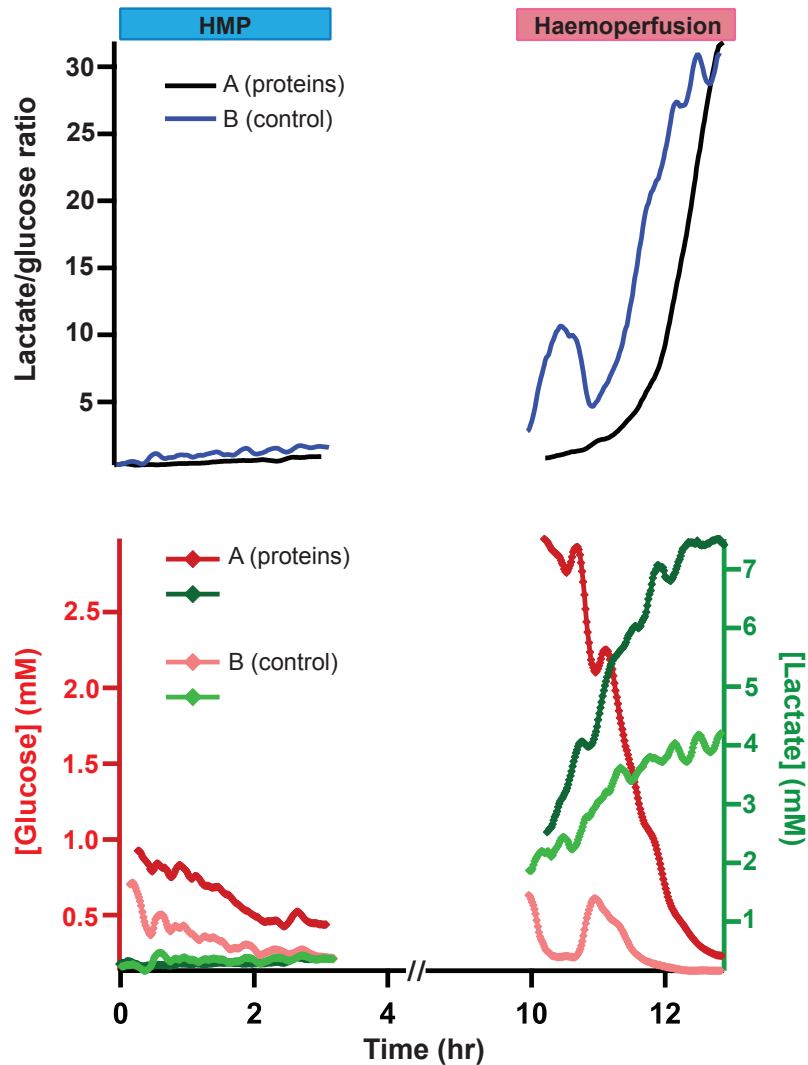


Figure 5.14: Dialysate medullary lactate profiles during haemoperfusion in human kidneys with and without protein pretreatment. Both kidneys were subjected to 4 hours of HMP, after which kidney A (*dark green*) was treated with protective proteins and kidney B (*light green*) acted as the control. Following protein treatment, both kidneys were perfused at body temperature. Dialysate was collected into storage tubing at $2 \mu\text{l}/\text{min}$ and analysed offline using the rsMD system also at $2 \mu\text{l}/\text{min}$. The green traces show dialysate lactate concentrations and the red traces show dialysate glucose concentrations, the darker corresponding to kidney A, which was treated with proteins, and the lighter corresponding to kidney B, which acted as the control. The black (*kidney A*) and blue (*kidney B*) traces show the corresponding lactate/glucose ratio.

During HMP, medullary lactate levels for the two kidneys were similar, but kidney A had considerably higher medullary glucose levels than kidney B. Both kidneys showed a similar trend, with lactate levels gradually increasing during HMP and glucose levels gradually decreasing, presumably as a result of local glycolysis.

During haemoperfusion, medullary lactate levels displayed a similar trend to that observed in the cortex, with levels steeply increasing initially, before beginning to plateau.

However, the effect of treatment on each pair was opposite in the medulla and the cortex, with medullary levels higher for the treated kidney than for the non-treated kidney. We would expect to see higher lactate levels in the medulla compared with the cortex, as the medulla is the primary site of glycolysis in the kidney. Therefore, the higher lactate levels observed in the treated kidney suggest that for this kidney the medulla is more glycolytically active. Medullary glucose levels were also higher for the treated kidney. This could simply be explained by the fact that even during HMP (before treatment) medullary glucose levels were higher for the treated kidney, possibly because this kidney was less damaged than its pair. Nonetheless, the medullary glucose levels decreased more steeply for the treated kidney compared with the non-treated kidney, which is consistent with the recovery of glycolytic enzymes improving the glucose consumption rate.

The medullary lactate/glucose ratio for the two kidneys is also shown in figure 5.14 during HMP and haemoperfusion. The lactate/glucose ratio is highest for kidney B during HMP, suggesting that this kidney was less healthy at the offset. During haemoperfusion, the lactate/glucose ratio increased steeply for both kidneys, with the increase in the treated kidney slightly delayed compared with the control.

5.5 Treatment with protective proteins

To further investigate the effect of protective proteins, the experiment described in section 5.4.2 was repeated with porcine kidneys. This also ensured that both kidneys would be of comparable health prior to treatment to enable a more reliable comparison.

In this study, two pairs of porcine kidneys were monitored. Each pair was subjected to the protocol described in figure 5.11, where A was treated with the novel protein and B acted as its control. A microdialysis probe, perfused at $2 \mu\text{l}/\text{min}$, was inserted into the cortex of each kidney prior to commencing HMP. After the initial 4 hours of HMP, probes were removed and re-inserted for the haemoperfusion phase. Dialysate was analysed online in real time simultaneously for two kidneys using the rsMD system, as described in section 4.2.3. A temperature probe (IT-14 or Thermalert TH-5, Physitemp) was also inserted into one of the kidneys to simultaneously monitor the tissue temperature.

5.5.1 Results

As a result of technical issues, lactate concentrations in kidneys 1PA and B were not monitored during the initial HMP phase. However, kidneys 2PA and B showed comparable lactate concentrations during the HMP stage (data not shown). Figure 5.15 shows the dialysate cortical lactate levels for the two pairs of kidneys during haemoperfusion. In

5. TRANSPLANT ORGAN VIABILITY ASSESSMENT: PART II

the case of kidney 2PB, the plateau in lactate levels was because of assay gain saturation at higher lactate levels.

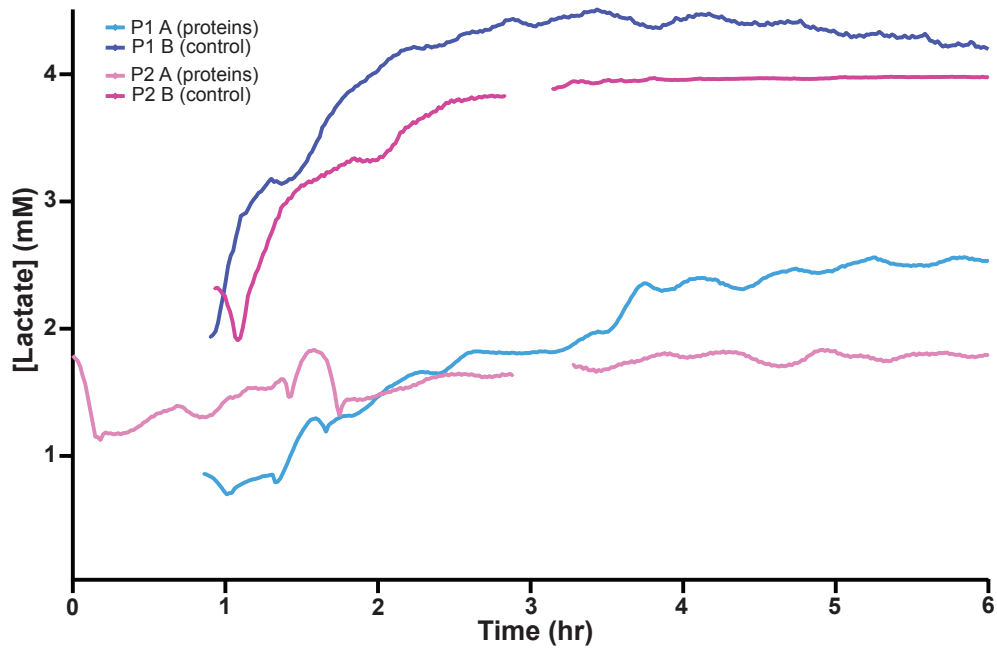


Figure 5.15: Dialysate cortical lactate profiles of kidneys undergoing haemoperfusion with and without protein pretreatment. Two pairs of kidneys were retrieved, one of each pair was treated with a novel synthetic protein (PTL004), while the other acted as the control. Each line represents real-time data of an individual kidney with a point every minute, smoothed with a Savitsky-Golay 21-point filter. The pink and blue traces represent each pair of kidneys, the lighter of each corresponding to the kidney treated with the novel protein.

In all four porcine kidneys, lactate concentrations during haemoperfusion were considerably higher than levels seen during passive warming or even during warm perfusion with a synthetic reperfusion solution, indicating that haemoperfusion enables a greater degree of metabolic activity to be resumed. For both pairs of kidneys, the kidney that had been pretreated with the novel protein (PTL004) displayed considerably lower cortical lactate levels during haemoperfusion than its non-treated control, which is in agreement with results from human kidneys monitored using the same protocol. The lactate levels initially increased before stabilising after about 3 hours. Haemoperfusion should enable resumption of a degree of aerobic metabolism, as the blood should allow for delivery of sufficient oxygen and glucose to the tissue. Therefore, the higher levels of cortical lactate observed in the non-treated control kidneys suggests that these kidneys were less healthy than their treated pairs, as anaerobic metabolism still dominated, possibly as a result of thrombosis upon reperfusion impairing the delivery of nutrients to the organ. However,

it is not possible to draw any firm conclusions on the basis of these results, as further experiments would need to be conducted to confirm these preliminary findings.

5.5.2 Discussion

Vascular thrombosis is a major complication that can lead to graft loss after renal transplantation. Despite surgical and clinical advancements, the incidence of vascular thrombosis still remains fairly high (228). It is vital that diagnosis and intervention is early to improve graft quality and early graft survival rate (229, 230). When vascular thrombosis is suspected, the diagnosis is confirmed clinically by Doppler flow examination (231). However, there is a delay in the time between graft injury and detection of pathological changes using this technique (224). Therefore, there is a need for more sensitive and continuous monitoring techniques that can enable early detection and possible intervention (223). Moreover, interventions that could potentially prevent vascular thrombosis upon reperfusion would be invaluable.

Microdialysis has been used after human liver transplantation to detect complications as a result of thrombosis (201) and has also been used in several porcine transplantation models to detect ischaemia caused by arterial and venous occlusions (222, 223, 232), as well as in conditions in which the graft is prone to vascular thrombosis after transplantation (224). Furthermore, our previous studies have shown that rsMD is particularly sensitive to metabolic differences between preserved kidneys. Therefore, rsMD was used to monitor kidneys that had been treated with a novel synthetic protein, thought to protect the organ from thrombosis upon reperfusion, to evaluate the effectiveness of the proteins.

Our results suggest that treatment with the novel protein (PTL004) provides some protection from vascular thrombosis upon reperfusion, as the lower lactate levels seen in these kidneys is indicative of less ischaemia. In addition, the higher medullary glucose seen in the treated human kidney is consistent with the study of Fonouni *et al.*, in which glucose levels were lower for more congested kidneys. These results are only preliminary and further experiments need to be conducted before any firm conclusions can be made. However, perfusion dynamics showed higher perfusion flow indices and higher renal blood flow in the treated kidneys compared with the controls, indicating that the treated kidneys were healthier than the controls.

5.6 Online analysis of transplant pancreases

A proof-of-concept study was carried out to investigate whether this technology could also be applied to monitor donor pancreases. In this study, preliminary experiments were

5. TRANSPLANT ORGAN VIABILITY ASSESSMENT: PART II

conducted with porcine pancreases to evaluate the effect of a 5-hour ‘reconditioning’ phase during preservation, as well as the effect of different lengths of CIT.

5.6.1 Introduction

The pancreas is a key organ, involved in both the endocrine and the digestive systems. In its role in the digestive system, the pancreas secretes pancreatic juice, which contains digestive enzymes (including proteases, amylase and lipase), which are responsible for aiding digestion of food and absorption of nutrients in the intestines. The pancreas also contains approximately 1 million cell clusters called islets of Langerhans, which are responsible for performing the endocrine functions of the pancreas. The islets secrete hormones, including insulin, glucagon and somatostatin, which regulate metabolism in the body.

There are currently three methods of solid organ pancreas transplantation. The most common method is simultaneous pancreas-kidney (SPK) transplantation, in which the pancreas is transplanted at the same time as a kidney. Another method is pancreas-after-kidney (PAK) transplantation, in which a pancreas is transplanted to a patient who has previously undergone a kidney transplantation. Pancreas transplantations carried out either at the same time as or after a kidney transplantation are performed on patients with end-stage renal disease, secondary to type 1 or type 2 diabetes (233, 234). The least common method is pancreas transplant alone (PTA), in which just the pancreas is transplanted, in most cases to a diabetic patient with normal renal function. This is normally only performed in patients with life-threatening hypoglycaemic unawareness (233), although it has been suggested as a possible treatment option for patients who have had a total pancreatectomy following a benign tumour or chronic pancreatitis (235). In addition, for patients with severe hypoglycaemia, isolated islet transplantations can be carried out.

Over the last decade, there has been a significant increase in the number of patients on the active waiting list for PTA, SPK and islet transplants, with numbers increasing from 132 in 2005 to 270 in 2014 (143). Of these 270 patients on the active waiting list last year, 201 were awaiting an SPK procedure, 26 a PTA procedure and 33 a pancreatic islet transplantation. The median waiting time for an adult patient is 392 days and between 2010-2011 34% of patients received a transplant within 1 year of registering on the national waiting list. Pancreas transplants are considerably less common than kidney transplants; between 2013-2014, a total of 246 deceased donor pancreas transplants were carried out, 76% of which were SPK transplants, 11% were pancreas-only transplants (PTA or PAK) and 13% were islet transplants (143). For patients with type 1 diabetes, evidence suggests that the SPK procedure prolongs patient survival rates beyond that of a kidney-only

transplantation (236); the 5- and 10-year patient survival rates for SPK transplantations are 87% and 70%, respectively (237). Furthermore, pancreas transplantation can significantly improve the quality of life for patients with type 1 diabetes (238), particularly compared with kidney transplantation alone, for patients with diabetic end-stage renal disease (239, 240).

As with kidney transplantation, there is an emerging need to expand the donor pool to meet the demands for pancreas transplants. As a result, expanded criteria donor (ECD) organs such as those from donation-after-circulatory-death (DCD) donors are being increasingly used. These organs have usually been subjected to a greater degree of ischaemic insult prior to recovery. Of the 246 pancreas transplants carried out last year, 203 were from donation-after-brain-death (DBD) donors and represented 26% of pancreases that were offered for donation from this donor group and 43 were from DCD donors and represented 8% of the organs offered for donation from this group of donors; this is because of concerns regarding the suitability of the donor or the organ itself. In 2013-2014, the median CIT for pancreas transplants from DBD donors was 10.6 hours (interquartile range 9.0-12.8 hours) and for DCD donors was 10.2 hours (interquartile range 8.6-11.6 hours) (143).

The most common method of preservation for donor pancreases is SCS; however, an optimal preservation solution to counteract the detrimental effects of cold ischaemic injury has yet to be determined (241). Some studies have shown that pancreas preservation by HMP can extend the storage time to 24 hours (242, 243). However, lower perfusion pressures than those normally used for kidney perfusion were used in these cases in order to avoid endothelial cell damage. Preservation by HMP has been shown to cause oedema, which Taylor *et al.* found to be beneficial for islet isolation, significantly improving the yield (145, 242). However, oedema is likely to be detrimental for whole-organ transplants (241).

With the increasing use of pancreases from DCD organs, there is a clear need for a method of assessing organ viability before transplantation (241), as well as for monitoring the graft following transplantation in order to target interventions where necessary (233). A study by Kitano *et al.* showed the feasibility of using microdialysis to monitor local pharmacokinetics or biomarkers in the pancreas (244). Furthermore, Blind *et al.* demonstrated that microdialysis could be used *in vivo* to detect ischaemic events in the pancreas, even when no systemic markers of ischaemia were observed (245).

Our aim was to extend the system developed for monitoring transplant kidneys, in order to determine whether this technology would be feasible for monitoring transplant pancreases as well.

5. TRANSPLANT ORGAN VIABILITY ASSESSMENT: PART II

5.6.2 Methodology for pancreas studies

After retrieval and arrival at the laboratory, pancreases underwent either 24 hours (n=4) or 48 hours (n=1) of SCS. Following SCS, four pancreases were subjected to an additional 5 hours of HMP on a Waters Medical Systems RM3 perfusion machine at 30-50 mmHg, perfused with in-house Belzer-UW solution, with added mannitol (60.4 mM) to reduce oedema, in an attempt to 'recondition' the tissue. After cold preservation, all 5 pancreases were perfused with oxygenated blood at body temperature for 2 hours. All efforts were made to keep conditions constant prior to preservation. Figure 5.16 describes the main steps of the experimental protocol.

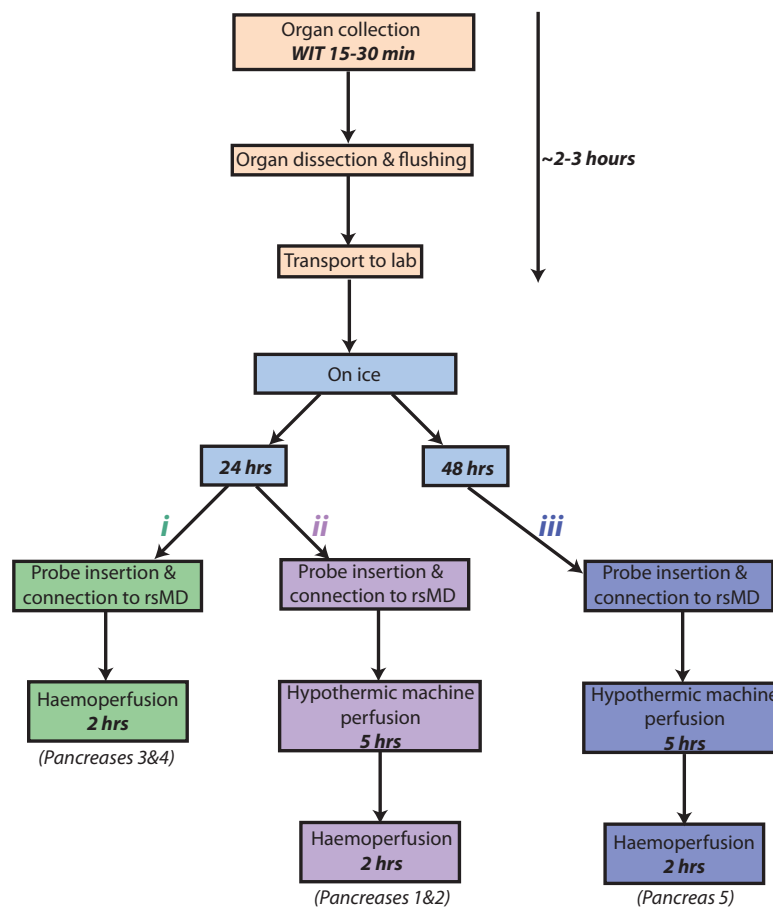


Figure 5.16: Experimental protocol for transplant pancreases. Pancreases were stored on ice for 24 hours and (i) monitored during 2 hours of haemoperfusion, (ii) monitored during 5 hours of HMP and 2 hours of subsequent haemoperfusion or (iii) stored on ice for 48 hours and monitored during 5 hours of HMP and 2 hours of subsequent haemoperfusion.

During haemoperfusion, any pancreatic juice that was produced was drained from the organ through a foley catheter. After about 30 minutes of haemoperfusion, glucose was added into the blood so that the total concentration was 22 mM to stimulate the

5.6 Online analysis of transplant pancreases

pancreas and to test how well it was functioning. Blood measurements were also taken using a commercial hospital analyser to check the concentration of glucose in the blood.

A MAB 11.35.4 microdialysis probe (Royem Scientific, UK) with a 4 mm membrane and a 6 kDa molecular weight cut-off, perfused at $2 \mu\text{l}/\text{min}$ with T1 solution, was inserted into the pancreas using a 21 G tunnelling cannula inserted in the opposite direction to the probe. A microdialysis probe was carefully placed inside the needle and then the needle was removed, leaving the probe in place. The tubing was secured to the side of the container using tape. Probes were temporarily removed between HMP and haemoperfusion phases as the perfusion machines had to be prepared for the next stage. Figure 5.17 shows the microdialysis probe positioned inside a porcine pancreas and the experimental setup.

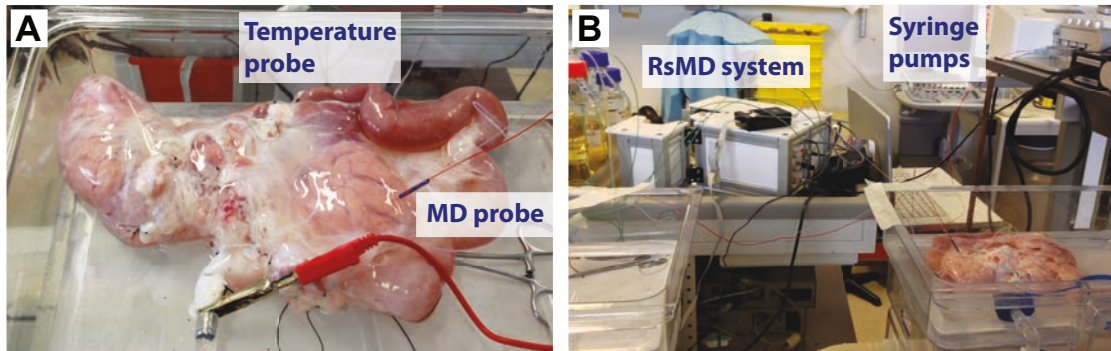


Figure 5.17: Experimental setup for perfusion of porcine pancreases. *A.* The porcine pancreas was placed on a perfusion machine and pumped with cold preservation solution in a pulsatile manner. A temperature probe and a microdialysis (MD) probe were inserted into the pancreas. *B.* The microdialysis probe was perfused at $2 \mu\text{l}/\text{min}$ using a syringe pump and the dialysate outflow flowed into the rsMD system for real-time analysis.

For pancreases 1-4, dialysate was analysed online in real time simultaneously for two organs using the rsMD system, as described in section 2.3.1.2. For pancreas 5, the system was rewired, as described in section 2.3.1.1, so that glucose and lactate could be simultaneously measured. Concentrations referred to throughout are dialysate concentrations, which depend on the probe recovery, and not absolute tissue concentrations. A temperature probe (IT-14, Physitemp) was inserted into each pancreas and was connected to our in-house temperature sensor (described briefly in section 5.2.1).

5.6.3 Porcine pancreases

Two studies were conducted, the first to investigate the effect of adding a 5-hour ‘reconditioning’ phase of cold HMP after storage on ice and the second to investigate the effect of the length of CIT. Table 5.1 summarises the WIT and CIT for each pancreas.

5. TRANSPLANT ORGAN VIABILITY ASSESSMENT: PART II

Table 5.1: Porcine pancreas WIT and CIT.

Pancreas	WIT (min)	CIT (min)
1	15	27.0
2	15	27.0
3	30	26.5
4	30	26.0
5	30	49.5

Results for the 5 pancreases studied using rsMD are shown in figure 5.18. Dialysate lactate levels were successfully detected for all five pancreases. Levels observed were broadly similar and provide a predictive range of dialysate levels for isolated pancreases.

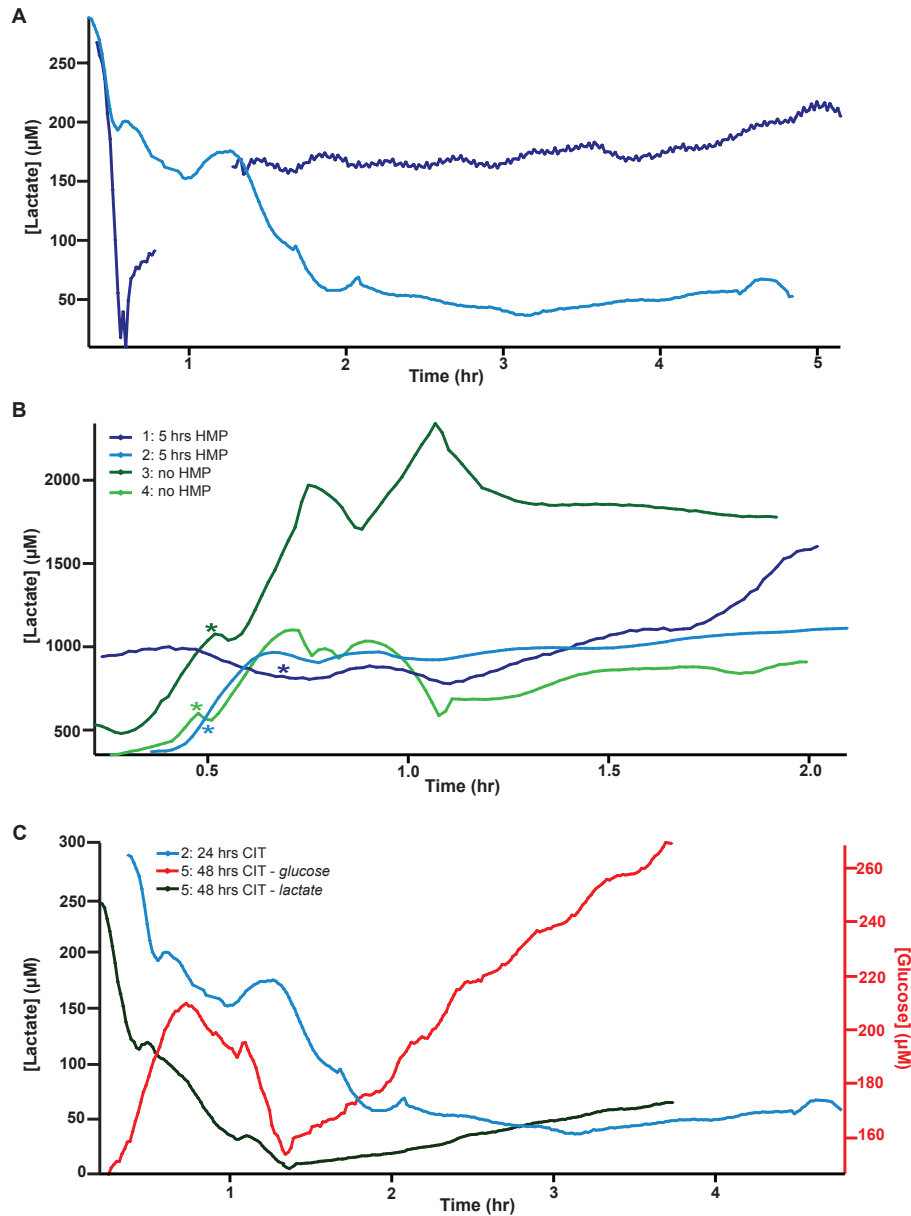


Figure 5.18: Dialysate metabolite levels for porcine pancreases. *A.* Dialysate lactate concentrations for two pancreases during 5 hours of HMP, following 24 hours of SCS, are shown. *B.* Dialysate lactate levels for pancreases during haemoperfusion after either 24 hours of SCS and 5 hours of HMP (*blue*) or after 24 hours of SCS (*green*) are shown. The asterisk indicates the point at which glucose was added into the blood to stimulate the pancreas. *C.* Dialysate glucose (*red*) and lactate (*green*) levels for a pancreas during HMP following 48 hours of SCS compared with lactate levels of a pancreas during HMP following 24 hours of SCS (*blue*) are shown. Data were obtained in real time using rsMD, with a dialysate measurement every 30 s.

Effect of adding a 5-hour ‘reconditioning’ phase before haemoperfusion

Figure 5.18A shows the dialysate lactate concentration of pancreases 1 and 2 during the ‘reconditioning’ HMP phase. Temperatures were comparable for pancreases 1 and 2 during HMP; the average temperature for pancreas 1 was 7.2 ± 1.2 °C ($n=103$) and for pancreas

5. TRANSPLANT ORGAN VIABILITY ASSESSMENT: PART II

2 was 8.0 ± 0.9 °C (n=105).

Upon haemoperfusion, all four pancreases displayed signs of oedema and did not perfuse well. Moreover, none of the organs produced bile or pancreatic juice nor was there any swelling of the small bowel. These observations indicated that the pancreases were not functioning as they should be, possibly as a result of the long CIT. Average temperatures for the four organs were slightly more variable during haemoperfusion, because of the poor perfusion (29.1 ± 3.4 °C, n=4).

Result observations:

- During HMP (figure 5.18A), stable lactate levels were obtained, which were broadly similar to those observed in kidneys during cold preservation.
- The two pancreases showed opposite trends in the first 1-2 hours of HMP; however, after 2 hours the lactate levels in both remained stable.
- For pancreases 2, 3 and 4, the lactate concentration increased upon haemoperfusion (figure 5.18B). Lactate levels were initially considerably higher for pancreas 1.
- When glucose was added to the blood (30 minutes into haemoperfusion, indicated by an asterisk in figure 5.18B), dialysate lactate levels increased before decreasing slightly and stabilising after 1 hour. However, in pancreas 1, no change was observed upon addition of glucose, possibly suggesting that this pancreas was less healthy than the other three.
- After addition of glucose, a sample of perfusate was taken and analysed using a blood analyser. For pancreas 3, the glucose level was 33.6 mM, which is considerably higher than it should have been. This was attributed to oedema reducing the total volume of blood in the circuit and hence increasing the concentration. This difference may explain the higher levels of lactate observed for this pancreas.

Effect of the length of CIT

Figure 5.18C shows the glucose and lactate levels for a pancreas undergoing 5 hours of HMP following 48 hours of storage on ice, compared with the lactate levels for pancreas 2, which was stored on ice for 24 hours. In this case the pancreas perfused very poorly; in fact, hardly any perfusate was flowing out of the vein because of worsening oedema and swelling. Extra UW had to be added to the circuit after 1 hour of perfusion in order to maintain sufficient levels of perfusate. Finally, the experiment was terminated early because of the poor condition of the organ. As a result of the poor perfusion, the average temperature during HMP was higher at 9.9 ± 1.1 °C.

Result observations:

- During HMP, the trend in lactate levels was similar for the two pancreases, with levels decreasing over the first 1-2 hours and then stabilising. However, initially, considerably lower lactate levels were observed in the pancreas that had been subjected to a longer CIT.
- Overall, glucose levels were seen to increase during HMP. Interestingly, as the organ was ischaemic, we would expect to see a decrease in glucose levels, which has been shown in other studies (245). The increasing glucose levels and the relatively stable lactate level suggests that metabolic activity had ceased as a result of the poor health of the organ.

From these results it is not possible to draw any firm conclusions regarding the benefit of adding a ‘reconditioning’ HMP phase to the preservation protocol or regarding the effect of the length of CIT on the pancreas; further experiments would need to be conducted to ascertain this.

5.6.4 Online analysis of human pancreases

On two occasions discarded human pancreases were made available to the clinical team and we were given the opportunity to use our analysis system to monitor them during preservation and reperfusion. The same protocol was used to insert the microdialysis probes as described previously for the porcine pancreases. A temperature probe (IT-14, Physitemp) was also inserted into each pancreas during each stage. Figure 5.19 shows a human pancreas with a microdialysis probe and a temperature probe inserted.

Each pancreas was stored on ice before being subjected to 5 hours of HMP with in-house Belzer-UW solution, followed by 2 hours of reperfusion with warm oxygenated Krebs-Henseleit buffer (Sigma-Aldrich, UK). As with the porcine pancreases, the microdialysis probes were removed between the HMP and the reperfusion stages.

5. TRANSPLANT ORGAN VIABILITY ASSESSMENT: PART II

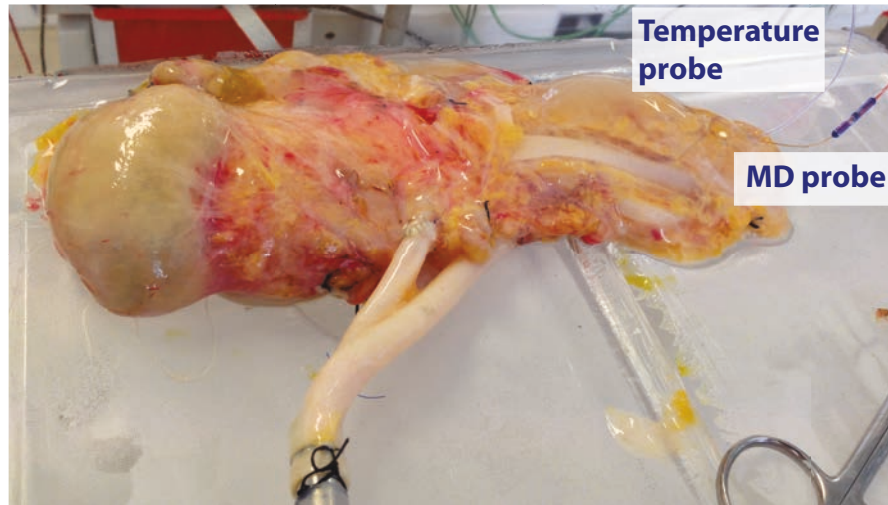


Figure 5.19: Experimental setup for perfusion of a discarded human pancreas. The discarded human pancreas was placed on a perfusion machine and pumped with cold preservation solution in a pulsatile manner. A temperature probe and a microdialysis probe (MD) were inserted into the pancreas. The microdialysis probe was perfused at $2 \mu\text{l}/\text{min}$ and the dialysate was analysed in real time using the rsMD system.

Case study 1

In this case no information was available about the donor. The organ was offered for transplantation and was matched with a recipient, but the recipient was not fit for surgery and by that time the CIT was too long to match the organ to another recipient. The pancreas was stored on ice for 57 hours before HMP commenced. Figure 5.20 shows the glucose and lactate dialysate levels during HMP and subsequent reperfusion.

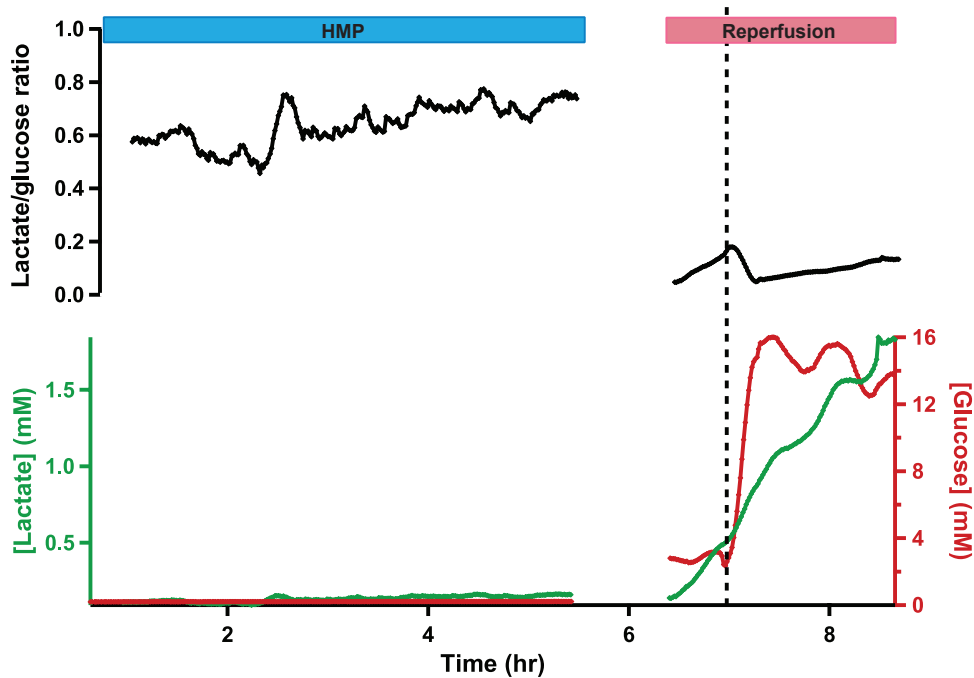


Figure 5.20: Dialysate metabolite levels in human pancreas 1 during HMP and reperfusion. The red trace shows dialysate glucose levels, the green trace shows dialysate lactate levels and the black trace shows the lactate/glucose ratio during HMP and subsequent warm reperfusion with oxygenated Krebs-Henseleit buffer. Data were obtained in real time using rsMD, with a point every minute for each metabolite. The dotted line indicates the point at which additional glucose was added into the reperfusion solution, making the final concentration 22 mM.

During HMP, both glucose and lactate levels in the dialysate remained very low, although they did slightly increase. Dialysate glucose levels were higher during reperfusion, probably as a result of the fact that the Krebs-Henseleit buffer contains glucose whereas the Belzer-UW does not. Dialysate lactate levels were also higher and increased during reperfusion, presumably because of increased glycolysis as a result of warmer temperatures and the supply of glucose. The dotted line indicates the point at which additional glucose was added into the reperfusion solution in order to stimulate the pancreas. This corresponded to a sharp increase in dialysate glucose levels and a continued increase in dialysate lactate levels. The lactate/glucose ratio remained fairly stable during HMP and dropped during reperfusion as a result of the increased glucose supply. In contrast to the porcine pancreases, this pancreas produced a considerable amount of pancreatic juice during the reperfusion phase.

Case study 2

This pancreas was donated by a 62-year old man. The organ tested positive for Epstein-Barr virus and was atherosclerotic. The organ was offered for transplantation but was refused on the basis of the donor age and the presence of atherosclerotic plaques. The

5. TRANSPLANT ORGAN VIABILITY ASSESSMENT: PART II

pancreas was stored on ice for 25 hours before HMP commenced. In this case, only lactate was measured as a porcine pancreas was simultaneously monitored. Lactate levels during HMP were too low to detect but figure 5.21 shows the dialysate lactate levels during subsequent reperfusion. The asterisk indicates the point at which additional glucose was added into the reperfusion medium to make the final concentration 22 mM.

In this case, the pancreas perfused poorly and no outflow was observed from the vein during reperfusion because of increasing oedema. However, the organ produced a considerable amount of pancreatic juice and the duodenum visibly swelled because of this production. The reperfusion was terminated early as a result of the poor perfusion characteristics. During reperfusion, lactate levels increased; however, levels were considerably lower than normally observed in tissue during the reperfusion phase.

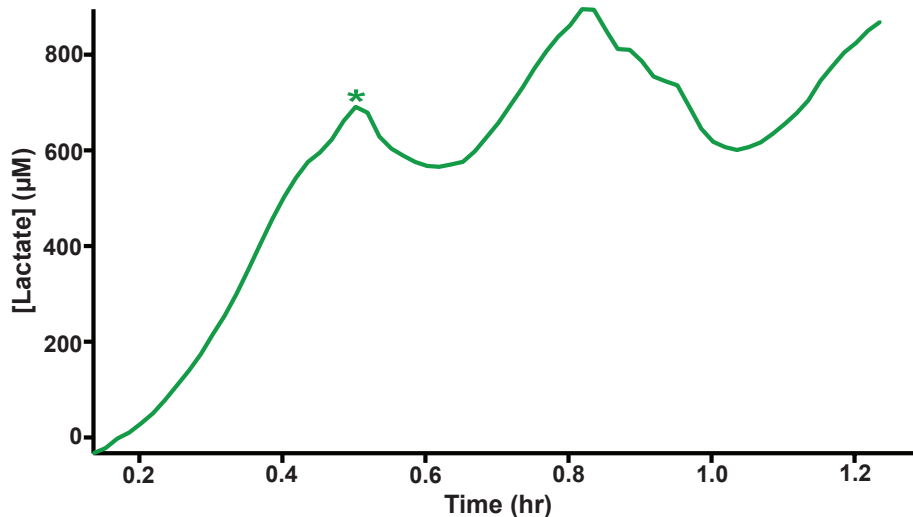


Figure 5.21: Dialysate lactate levels in human pancreas 2 during reperfusion. The pancreas was perfused with oxygenated Krebs-Henseleit buffer at body temperature. Data were obtained in real time using rsMD, with a point every minute. The asterisk indicates the point at which additional glucose was added into the reperfusion solution, making the final concentration 22 mM.

5.6.5 Discussion

These preliminary results suggest that rsMD could have potential for monitoring other transplant organs such as pancreases. As a result of the long CIT used in all cases all organs displayed poor perfusion parameters and therefore represented unhealthy organs. It would be interesting to carry out similar experiments with healthy pancreases in order to make comparisons.

5.7 Miniaturised analysis system

In a clinical situation the analysis system would need to be portable so that it could travel with the transplant organ. Therefore, a proof-of-concept study was carried out using the analysis system described in section 3.5.5 to simultaneously monitor a human and a porcine pancreas (the board was designed for use with a pair of kidneys but, as kidneys were not available at this point, it was tested with pancreases instead). The system enables measurement of both glucose and lactate in two dialysate streams. It also incorporates an autocalibration function for long periods of monitoring. In this case, the board was used during a 2-hour reperfusion phase, in which the porcine pancreas was perfused with oxygenated blood at room temperature, while the human pancreas was perfused with oxygenated Krebs-Henseleit buffer at body temperature. Figure 5.22 shows the experimental setup.

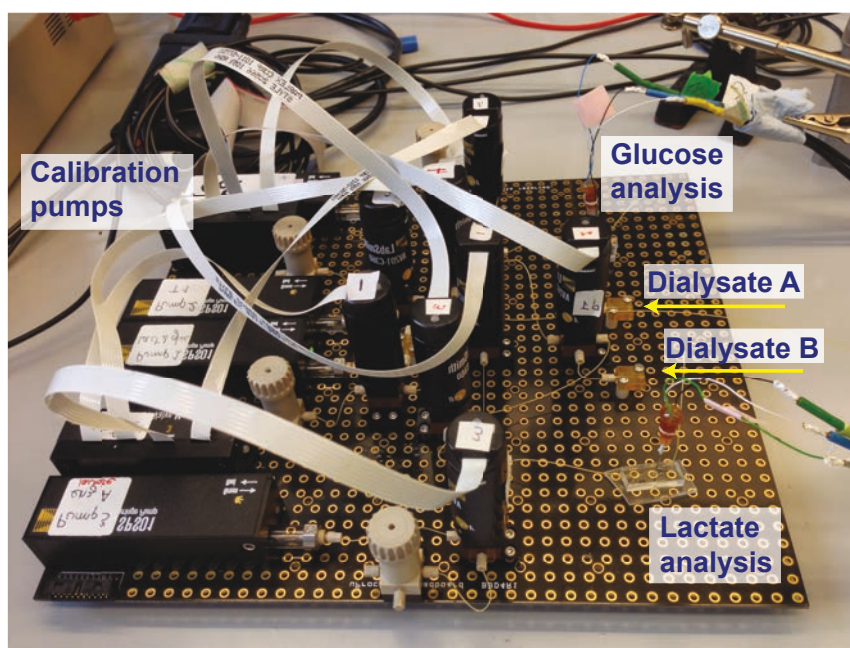


Figure 5.22: Experimental setup for glucose and lactate measurement in two dialysate streams. Two 125 μm platinum disc electrodes coated with poly(phenol), held at 0.75 V, were housed in separate PDMS chips. For lactate analysis, lactate oxidase (LOx) was dosed in to the dialysate stream, and for glucose analysis, glucose oxidase (GOx) was added in. The enzyme reacted with the substrate in solution and the reaction product, hydrogen peroxide, was detected at the electrode by oxidation, as it flowed past. The analysis system measured glucose in one dialysate stream and lactate in the other, and switched at regular intervals between the two.

Although the system can be set up to switch automatically between the two dialysate streams, it was used here in an early stage of development and therefore switching was carried out manually. An excerpt of raw data is shown in figure 5.23 and the analysed

5. TRANSPLANT ORGAN VIABILITY ASSESSMENT: PART II

data for the two pancreases is shown in figure 5.24. An average for each data section has been calculated to enable easier identification of trends. The averaged data is shown in figure 5.25.

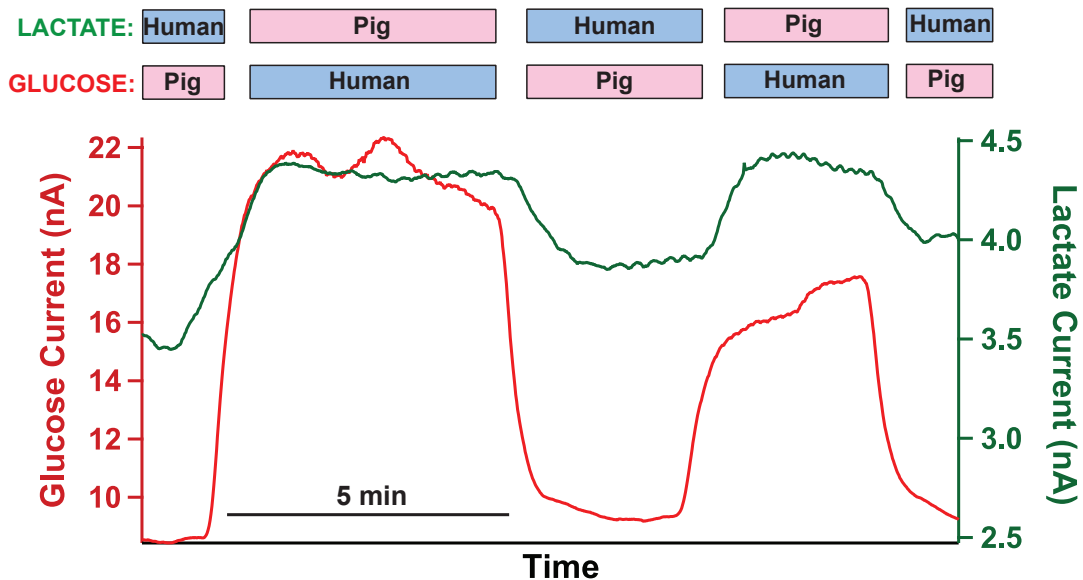


Figure 5.23: Raw data showing glucose and lactate levels alternating between two dialysates. The red trace shows the glucose current and the green trace shows the lactate current. Labels above indicate which dialysate stream these levels correspond to.

The dotted lines in figures 5.24 and 5.25 indicate the point at which glucose was added into the perfusion medium to make the total concentration 22 mM. This corresponded to a clear increase in glucose and lactate levels in the porcine pancreas (5.24A and 5.25A). The trend for the human pancreas (5.24B and 5.25B) was less clear, but glucose levels did increase following this. In addition, perfusion of the human pancreas was terminated early because of the poor perfusion characteristics and increasing oedema. This can clearly be seen in the results, as both glucose and lactate levels dropped to zero. RsMD was also carried out on these pancreases to detect dialysate lactate levels. However, separate microdialysis probes were used for each analysis system and, as the pancreases were poorly perfused, the respective levels cannot be compared in this case.

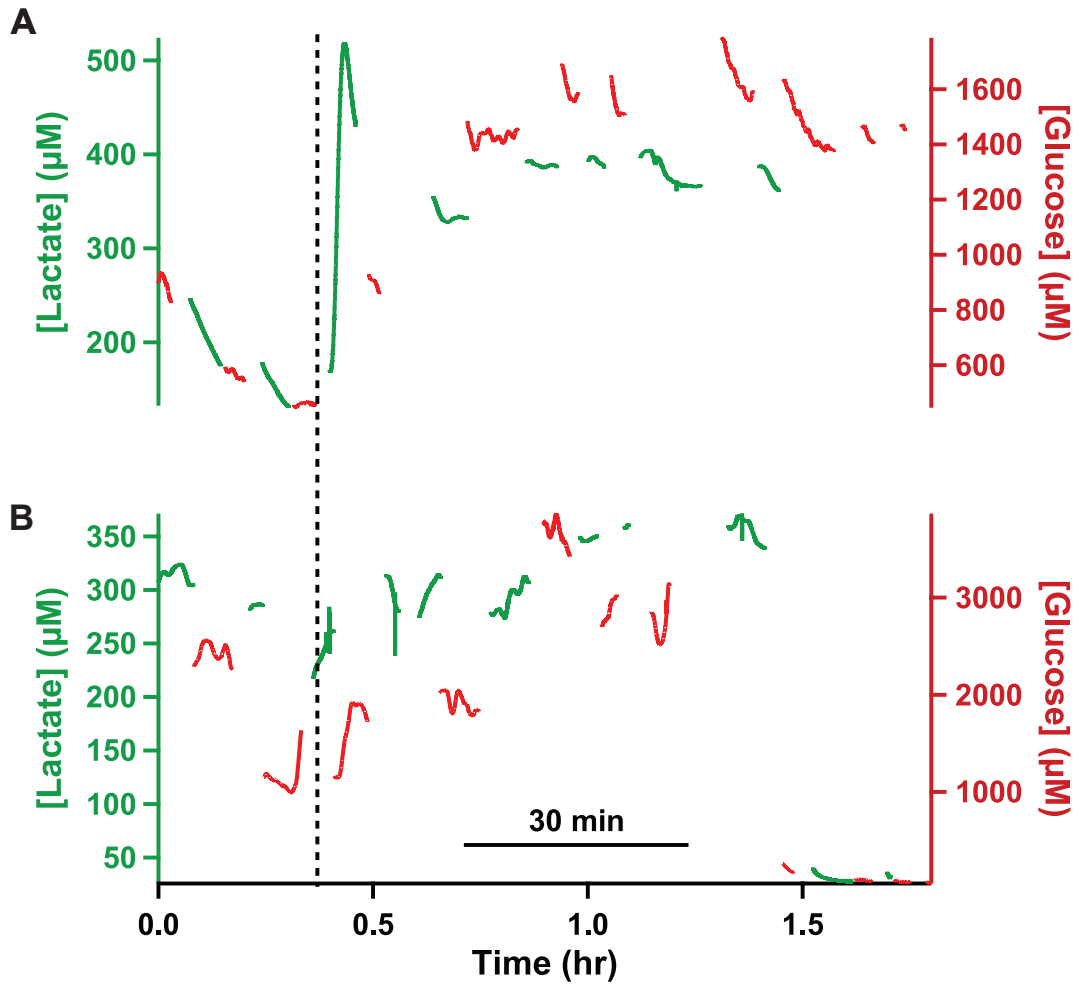


Figure 5.24: Dialysate metabolite levels for porcine and human pancreases. Red traces correspond to glucose levels and green to lactate levels in *A.* porcine and *B.* human pancreases during reperfusion at body temperature with oxygenated Krebs-Henseleit buffer and oxygenated blood, respectively. The dotted line indicates when glucose was added into the perfusion medium, making the total concentration 22 mM.

5. TRANSPLANT ORGAN VIABILITY ASSESSMENT: PART II

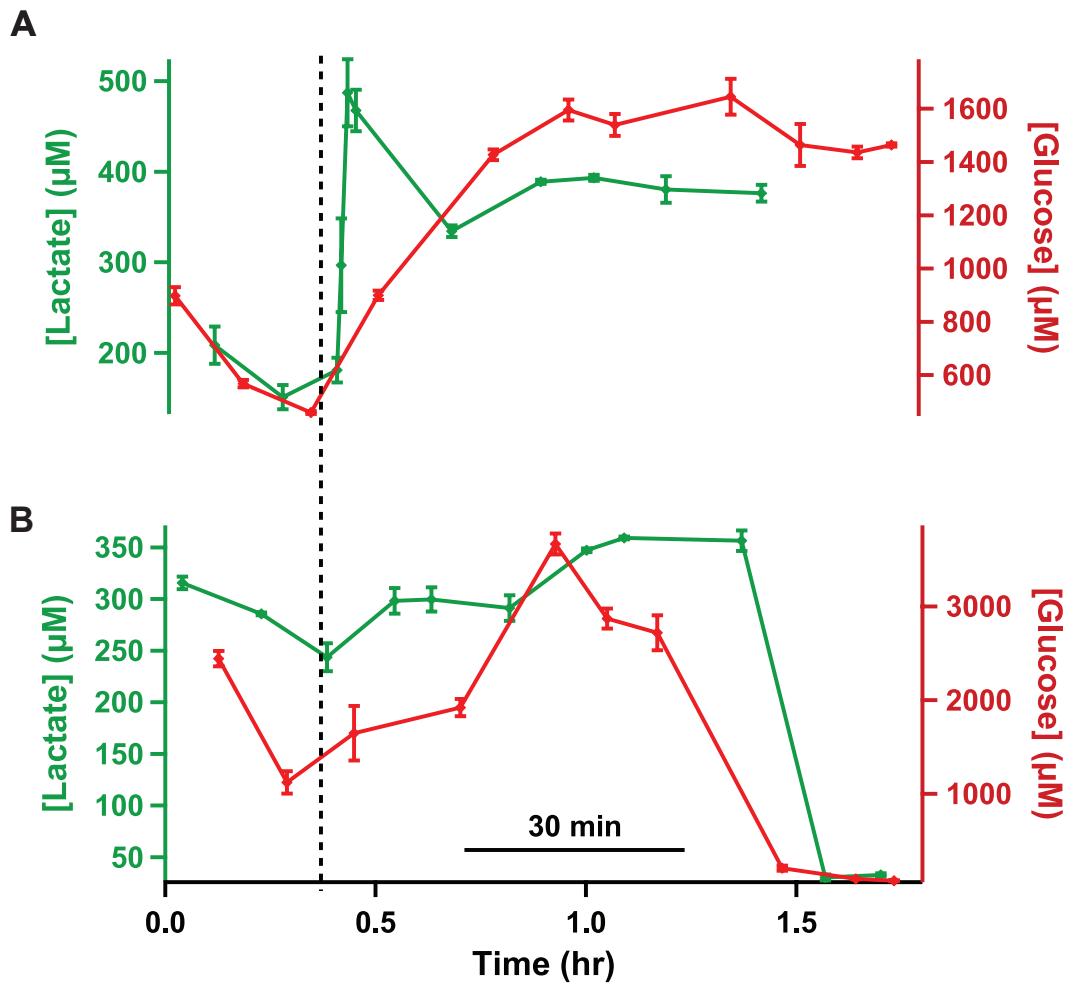


Figure 5.25: Average dialysate metabolite levels for porcine and human pancreases. Average dialysate glucose and lactate levels were recorded using the miniaturised system. Red traces correspond to glucose levels and green to lactate levels in *A.* porcine and *B.* human pancreases during reperfusion at body temperature with oxygenated Krebs-Henseleit buffer and oxygenated blood, respectively. The dotted line indicates when glucose was added into the perfusion medium, making the total concentration 22 mM. Markers are mean \pm standard deviation for each section of data.

The results show that it was possible to measure glucose and lactate in the two dialysate streams simultaneously, and clear differences between them could be detected. Each section had good temporal resolution; however, as switching was fairly infrequent, analysis was not continuous. Further development of the system enabled automatic switching to be carried out at 2 minute intervals (as described in section 3.5.5). This improvement would provide results close to those obtained using rsMD, which was found to be sufficient for the fairly slow changes occurring during preservation. Automatic switching would also enable analysis to be carried out using purpose-written algorithms in Matlab, providing data averages for a given time window. Future experiments are required to validate results obtained using the miniaturised system against those obtained

using the rsMD system.

5.8 Conclusion

In summary, this chapter brings together a collection of proof-of-concept experiments with human and porcine kidneys and pancreases. We have shown that:

- RsMD has been used to monitor kidneys subjected to differing lengths of CIT. Preliminary results show that higher lactate levels during HMP correspond to healthier, more viable tissue.
- RsMD has been applied to evaluate whether a novel protein, which prevents thrombosis upon reperfusion of the kidney, can provide the organ with protection during preservation. Initial results suggest that treatment with the novel protein has a protective effect on the kidney, as results from organs that were treated with the protein were indicative of less ischaemia than for the controls.
- The analysis methodology has been extended to facilitate monitoring immediately after organ retrieval at the abattoir by collecting dialysate into lengths of storage tubing for delayed analysis.
- Glucose has been shown to provide valuable information in addition to lactate regarding the metabolic state of the organ. Glucose levels have been measured in addition to lactate in dialysate that was collected in storage tubing and analysed at a later time.
- Glucose biosensors in microfluidic chips were used to measure glucose in real time, in addition to lactate, in a separate dialysate stream.
- A miniaturised system that can simultaneously measure glucose and lactate in two dialysate streams has been tested as a proof of concept.
- Use of these analysis techniques has been extended for discarded human kidneys, as well as for both porcine and discarded human pancreases.

Further work on a fully automated miniaturised analysis system is required to facilitate measurement of multiple metabolites in dialysate streams in transit.

5. TRANSPLANT ORGAN VIABILITY ASSESSMENT: PART II

Chapter 6

Online monitoring during free flap surgery

This chapter will describe the use of rapid sampling microdialysis for online monitoring during free flap surgery as a potential tool for early detection of flap failure. This work was carried out as part of a Boutelle lab team, in collaboration with Prof. Peter Brennan in the Department of Oral and Maxillofacial Surgery at Queen Alexandra Hospital in Portsmouth.

6.1 Introduction

Free flap surgery involves transplantation of healthy tissue, with or without bone, together with its blood supply from one site of the body to another. During the procedure, the blood vessels are first clamped, then cut at the donor site and microsurgery is used to reconnect the blood supply at the recipient site by rejoining blood vessels (anastomosis). The procedure is performed to reconstruct or to close large defects in the recipient site, for example, for breast reconstruction or for head and neck reconstruction following tumour removal.

Success rates of free flap surgery are reported to be greater than 95% (246, 247). However, successful reconstruction is dependent on continuous blood flow to the tissue through the arterial anastomosis and on outflow through the venous anastomosis. As the tissue is disconnected from the blood flow at the donor site, an initial period of ischaemia is inevitable. Once the blood supply is re-established at the recipient site, reperfusion of the flap occurs. However, complications such as thrombosis, resulting in occlusion of the artery and/or vein, can lead to a secondary phase of flap ischaemia (248, 249, 250, 251). The second ischaemic insult is not as well tolerated by the flap as the first and can eventually lead to flap failure (252).

6. ONLINE MONITORING DURING FREE FLAP SURGERY

Of the flaps that fail, 82.3% show signs of vascular compromise within the first 24 hours after surgery and 95.6% show signs within the first 72 hours (253). Therefore, the first 72 hours represent a critical time period in which close observation is necessary in order to improve salvage outcomes. Early detection of flap compromise is essential for successful flap salvage (254).

Free flaps are currently monitored using clinical assessment, including flap colour, texture, temperature, capillary refill time and turgor, as well as pricking the flap with a needle to assess bleeding (255). However, these techniques are not suitable for buried flaps, as they cannot be easily accessed. As a result, the rate of failure for buried flaps is significantly greater than for non-buried flaps (256). In recent years, other techniques, including invasive and non-invasive Doppler monitoring as well as microdialysis, have gained interest as tools to assess the flap health (257, 258, 259, 260).

Conventional microdialysis has been used as a tool to detect flap failure both during surgery and post-operatively and has been suggested to be particularly valuable for monitoring intraoral (261, 262) and buried flaps (263, 264), which are inaccessible to conventional assessment techniques (260). Microdialysis was able to detect flap ischaemia earlier than clinical assessment (261), allowing for earlier surgical intervention. In all cases, interstitial glucose and lactate were found to be sensitive markers of tissue ischaemia, with glucose levels decreasing and lactate levels increasing during an ischaemic event. Rojdmarm *et al.* found that glucose, lactate and glycerol levels were slower to return to baseline levels after repeated ischaemic episodes than after just one episode (265). All studies to date have been conducted using conventional microdialysis, in which discrete samples are taken and typically analysed at hourly intervals. As early detection of flap ischaemia is crucial, this monitoring technique could be even more useful if the delay could be still further reduced (264).

6.2 Methodology

6.2.1 Surgical procedure and microdialysis probe insertion

Patient consent was obtained prior to surgery and all procedures were approved by the local ethics committee. Two surgical teams operated on the patient simultaneously: one team removed the tumour from the recipient site, while another team raised the flap at the donor site. Prior to flap detachment at the recipient site, a sterile microdialysis probe (CMA 70 MDialysis, Sweden, 10 mm membrane length, 20 kDa molecular weight cut-off) was inserted subcutaneously using a tunnelling needle and was sutured in place around the hard plastic cover (cut to length for each flap, leaving the membrane exposed). A photograph showing a microdialysis probe inserted into a flap is given in figure 6.1.

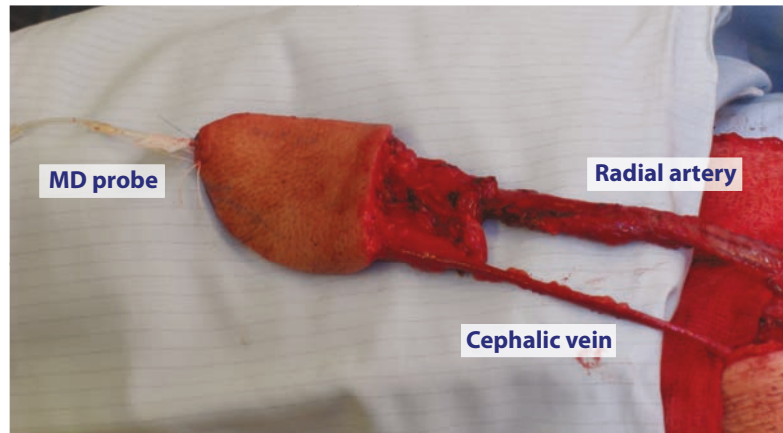


Figure 6.1: Microdialysis probe inserted into a radial forearm flap. The microdialysis (MD) probe was inserted subcutaneously and sutured in place prior to flap detachment from the blood supply.

The probe was perfused with sterile T1 solution (MDialysis, Sweden) at $2 \mu\text{l}/\text{min}$ using a portable pump (CMA 107, MDialysis, Sweden) prior to insertion and the inlet was extended using a luer-lock extension set (150 cm, 0.4 ml internal volume, Alaris Medical Systems, UK) so that the pump could be placed away from the sterile area. Levels of glucose and lactate were measured until stable baseline values were obtained, prior to flap detachment. Typically, the vasodilator papaverine was applied to blood vessels topically to maximise internal blood volume, after which the blood vessels were clamped and cut, creating the free flap. The microdialysis probe remained inserted and in most cases remained connected to the online analysis system as the flap was moved from the donor site to the recipient site. Surgery to reconstruct the recipient site was carried out as well as anastomosis of the artery. Once arterial blood flow was confirmed, the artery was clamped again and the venous anastomosis was performed. After the blood vessels were reconnected at the recipient site, all clamps were removed. The patient was transferred to the intensive therapy unit (ITU) once surgery was complete, where monitoring continued overnight for a further 12-16 hours before the microdialysis probe was removed.

6.2.2 Online analysis system

The probe outlet was extended using 1 m of low-volume fluorinated ethylene propylene (FEP) tubing (Royem Scientific, UK) to reach the clinical trolley. In order to do this, the vial holder was removed from the probe outlet, leaving about 1 cm of tubing on the end, which was connected to the FEP tubing using a tubing adaptor. The other end of the vial holder was trimmed so that just the needle was left, which was connected to the

6. ONLINE MONITORING DURING FREE FLAP SURGERY

probe outlet tubing. The FEP extension tubing was initially primed with T1 solution so that it was possible to check that the solution was flowing out through the probe as soon as it was connected. Once this was confirmed, the end of the FEP tubing was connected to the analysis system, which was housed on a clinical trolley, as shown in figure 6.2.

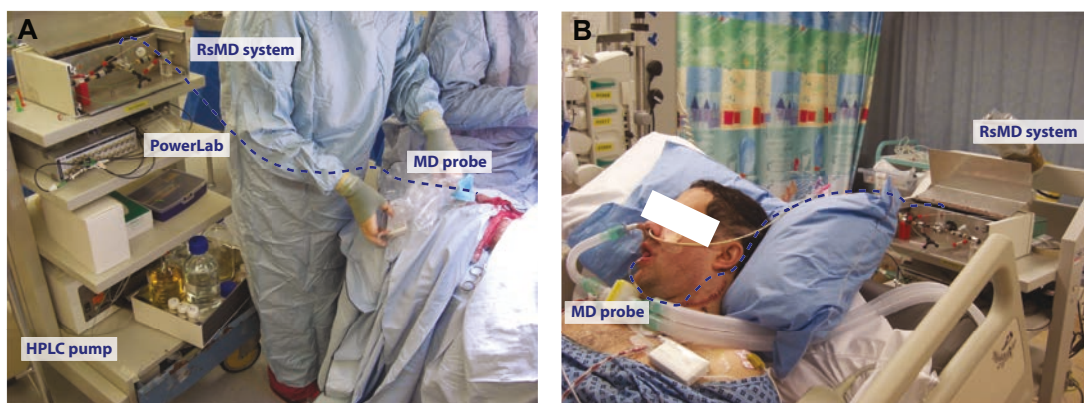


Figure 6.2: Clinical trolley for online monitoring. *A.* Photograph showing the microdialysis (MD) probe inserted into the flap prior to detachment, connected to the rapid sampling microdialysis (rsMD) trolley. *B.* The probe remained in place after surgery was complete so that monitoring could continue overnight in the ITU.

The outlet tubing of the probe was connected to the rapid sampling microdialysis (rsMD) analysis system described in section 2.3.1.1. Every 30 seconds, a dialysate sample was injected alternately through either a glucose or a lactate assay, giving a measurement every minute for each metabolite. As a result of the long extension tubing used, the delay from the microdialysis probe to the rsMD system was about 15 minutes. Events were recorded in real time as they were communicated by the surgeons; as a result, timings are approximate.

6.2.3 Delayed analysis using storage tubing

Data from each surgery are of high value, therefore it was necessary to have a method of obtaining data even when online analysis was not possible. To achieve this, the method of collecting dialysate in a length of storage tubing for delayed analysis was used as a back-up for circumstances when online analysis was not possible. As described in section 4.2.4, the dialysate was collected into lengths of Portex tubing (0.4 mm ID, Smiths Medical, UK), retaining temporal resolution for analysis at a later time. Using a flow rate of 2 $\mu\text{l}/\text{min}$, 63 minutes of dialysate could be collected per 1 m of tubing.

Figure 6.3 shows raw data from a case in which this back-up collection method was used because technical issues with the analysis system meant that online analysis was not possible. After the surgery, the storage tubing was stored at 4°C until analysis was

possible. During the collection time the probe fell out of the tissue (timing indicated by the dotted line). The decreasing glucose and lactate peaks shown in figure 6.3 correspond to this event, showing that temporal resolution was retained using this method of dialysate collection and delayed analysis.

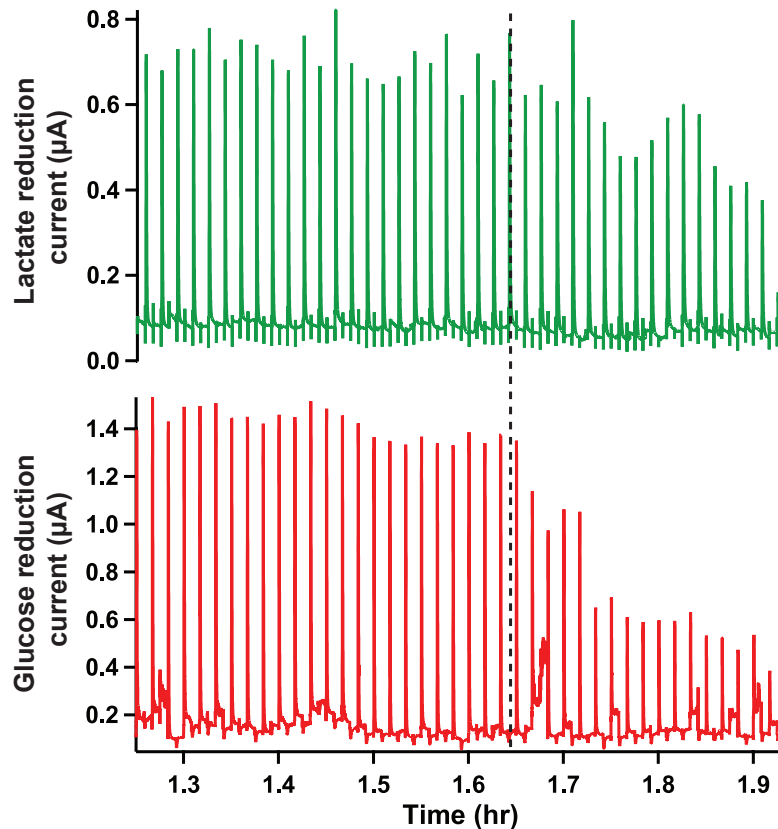


Figure 6.3: Raw data from dialysate collected into storage tubing during surgery. The dialysate was collected into a length of storage tubing and analysed using rsMD at a later time. The red peaks correspond to glucose levels and the green peaks to lactate levels. The probe fell out of the tissue during collection, corresponding to the decrease in both glucose and lactate dialysate levels (indicated by the dotted line).

6.2.4 Data and statistical analysis

The recorded current peaks were analysed in Matlab (R2011b, MathWorks, US). The peaks were despiked using purpose-written algorithms (104) and converted into concentrations on the basis of calibrations carried out at regular intervals throughout monitoring. The results were adjusted to correct for the transit time between the microdialysis probe and the analysis system. The Mann-Whitney U test (two-tail) was used to test for significance between metabolite levels at key time points. Significance was taken to be $p < 0.05$.

6. ONLINE MONITORING DURING FREE FLAP SURGERY

6.2.5 Sterility considerations

A major challenge in carrying out online analysis during surgery was the issue of sterility. In the operating theatre, a sterile zone exists directly around the patient. The microdialysis probe and perfusion solution are both sterile, but the microdialysis pump and the connection tubing are not. In order to overcome this problem, a sterile camera drape (a long polyethylene tube) was used, as shown in figure 6.4. This allowed non-sterile equipment such as the microdialysis pump and connection tubing to be placed inside the tube. As the outside of the drape was sterile, it could be placed close to the patient without the risk of contamination. However, this made it very difficult to make any adjustments to the probe connections or to the pump once they had been placed inside the drape, as it was not possible to touch the outside without compromising the sterile barrier.

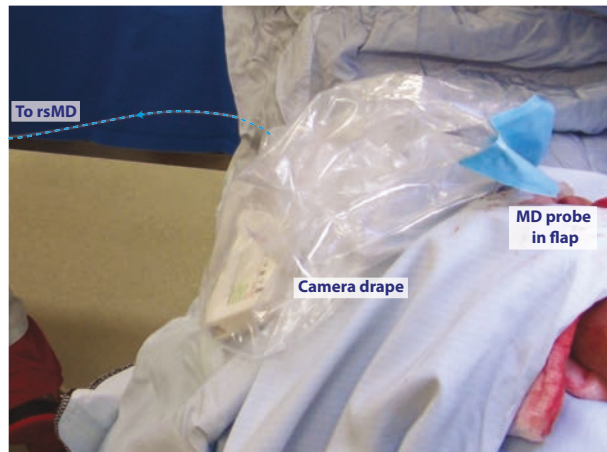


Figure 6.4: Photograph of non-sterile equipment inside camera drape. The microdialysis (MD) pump and connection tubing were placed inside the camera drape. The outside of the camera drape was sterile so that it could be placed in the sterile area during surgery.

6.3 Results

Overall, the cohort consisted of 15 cases. Unfortunately, technical issues with the analysis system meant that online data could not be collected for 3 of these cases. Dialysate was collected in storage tubing for 1 case but shortly afterwards the probe fell out so monitoring was stopped. In addition, it was not possible to collect data for 5 of the cases as a result of the probe being positioned incorrectly, being damaged during insertion or because of difficulties in reliably attaching the probe to small flaps, causing it to fall out. Monitoring of 7 cases was successfully carried out. Data will be presented for these patients, showing dialysate metabolite levels during surgery and in the ITU.

6.3.1 Case study 1

Figure 6.5 shows dialysate metabolite levels during surgery for a 39-year old man undergoing a procedure using a radial forearm flap to rebuild part of the tongue, which was removed because of a carcinoma.

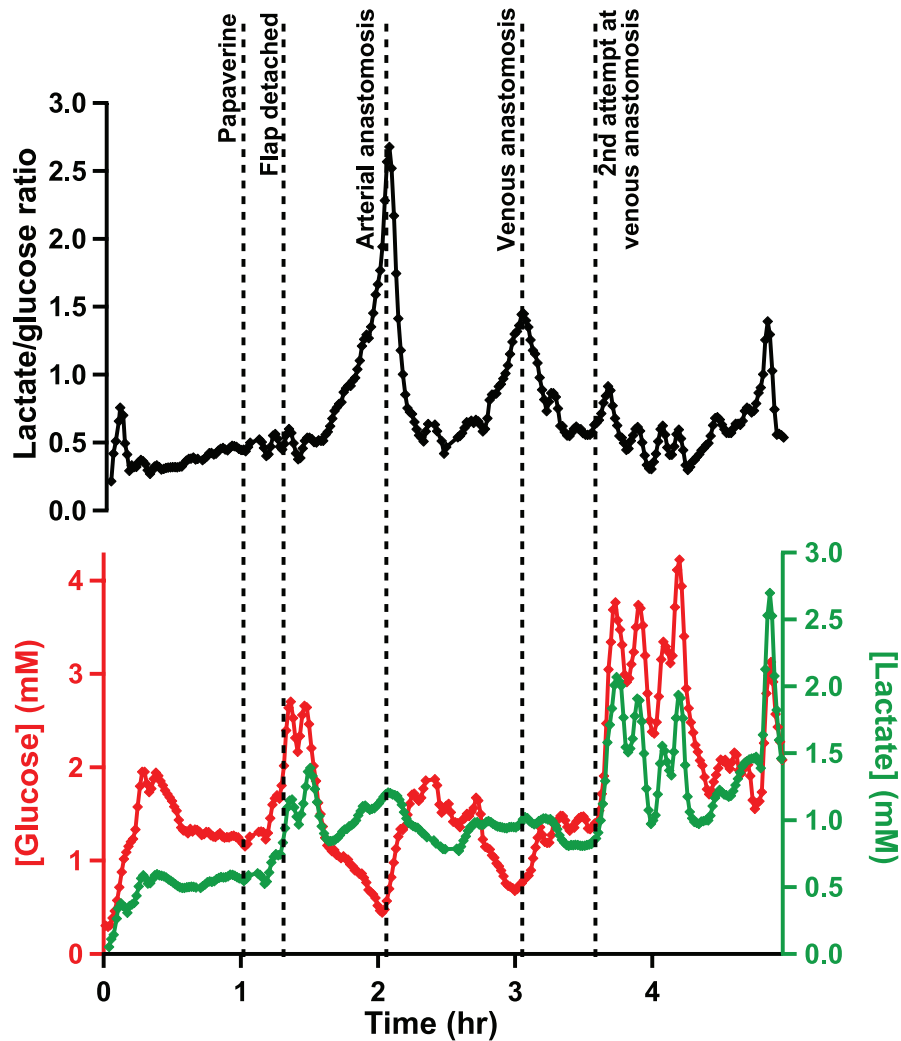


Figure 6.5: Dialysate metabolite levels during free flap surgery for patient 1. The green trace shows dialysate lactate concentrations, the red trace shows dialysate glucose concentrations and the black trace shows the corresponding lactate/glucose ratio. Data were obtained in real time using rsMD, with a point every minute for each metabolite, and were smoothed with a Savitsky-Golay 7-point filter. Time 0 represents the probe insertion point and dotted lines indicate key events during the surgery as relayed by the surgical team.

Dialysate baseline levels of glucose and lactate were 1.25 ± 0.04 ($n=10$) and 0.58 ± 0.01 ($n=10$), respectively. Before detaching the flap, the surgeons topically applied a vasodilator, papaverine, to the tissue. This caused an increase in both dialysate glucose and lactate levels, presumably because of an increase in local blood flow. As both metabolites

6. ONLINE MONITORING DURING FREE FLAP SURGERY

changed in the same direction, this increase can be attributed to a transient change in probe recovery (92). To guard against such artefacts, the ratio of the two metabolites was also calculated. Application of papaverine caused no change in the lactate/glucose ratio, indicating that this increase was due to a change in probe recovery efficiency. Following detachment of the flap, dialysate glucose levels decreased while lactate levels increased, indicating that the tissue was ischaemic. This was also reflected in the lactate/glucose ratio, which increased steeply when the blood supply to the flap was disconnected.

Dialysate glucose levels rapidly increased upon successful anastomosis, with levels rising to 1.77 ± 0.11 (n=10) within 11 minutes. Lactate levels were slower to change and remained stable for 7 minutes before gradually decreasing to 0.88 ± 0.06 mM (n=10), a level slightly higher than baseline. Following arterial anastomosis, checks were performed to ensure that blood was flowing into the tissue, after which the vessels were clamped again and the venous anastomosis was carried out. It may be the lack of local blood flow that caused the slow change in lactate levels following the arterial anastomosis, as the lactate was not efficiently cleared. The lactate/glucose ratio fell rapidly following arterial anastomosis, indicating that the ischaemia was alleviated. However, shortly afterwards, signs of ischaemia were observed, with dialysate glucose levels decreasing and lactate levels increasing. Although, the magnitude of the change was smaller than with the initial ischaemic episode. These changes coincided with an increase in the lactate/glucose ratio, which fell rapidly once the venous anastomosis had been performed because of a rapid rise in glucose and a delayed fall in dialysate lactate levels. A large and rapid increase in both glucose and lactate levels was observed upon anastomosis of the second vein. However, no changes were observed in the lactate/glucose ratio, suggesting that this was a probe recovery effect rather than a metabolic change. In this case, the lactate/glucose ratio was a clear marker of local tissue ischaemia and proved more reliable than considering either metabolite alone.

Following surgery, the patient was transferred to the ITU overnight. Metabolite levels were monitored for 14 hours in the ITU and the results are shown in figure 6.6.

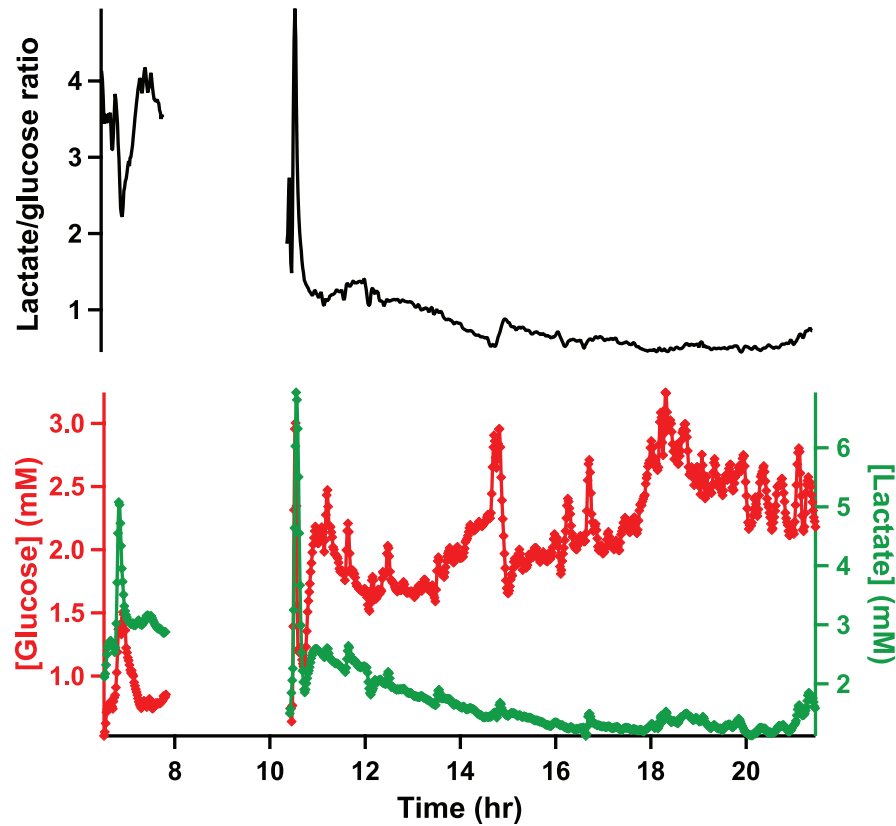


Figure 6.6: Dialysate metabolite levels in the ITU after free flap surgery for patient 1. The green trace shows dialysate lactate concentrations, the red trace shows dialysate glucose concentrations and the black trace shows the corresponding lactate/glucose ratio. Data were obtained in real time using rsMD, with a point every minute for each metabolite, and were smoothed with a Savitsky-Golay 7-point filter. Time 0 represents the probe insertion point before surgery.

Over the 14 hours that the flap was monitored in the ITU, glucose levels steadily increased to 2.17 ± 0.09 mM ($n=10$), while lactate levels steadily decreased to 1.24 ± 0.05 mM ($n=10$). These levels were still different to baseline levels (approximately double); however, this may reflect differences in local blood supply at the recipient site compared with at the donor site. However, the lactate/glucose ratio steadily decreased over the period of monitoring in the ITU, returning to baseline levels. Clinical parameters indicated that the flap reconstruction was successful.

6.3.2 Case study 2

Figure 6.7 shows dialysate metabolite levels during surgery for a male undergoing a procedure in which tissue from the fibia was used to reconstruct part of the jawbone.

6. ONLINE MONITORING DURING FREE FLAP SURGERY

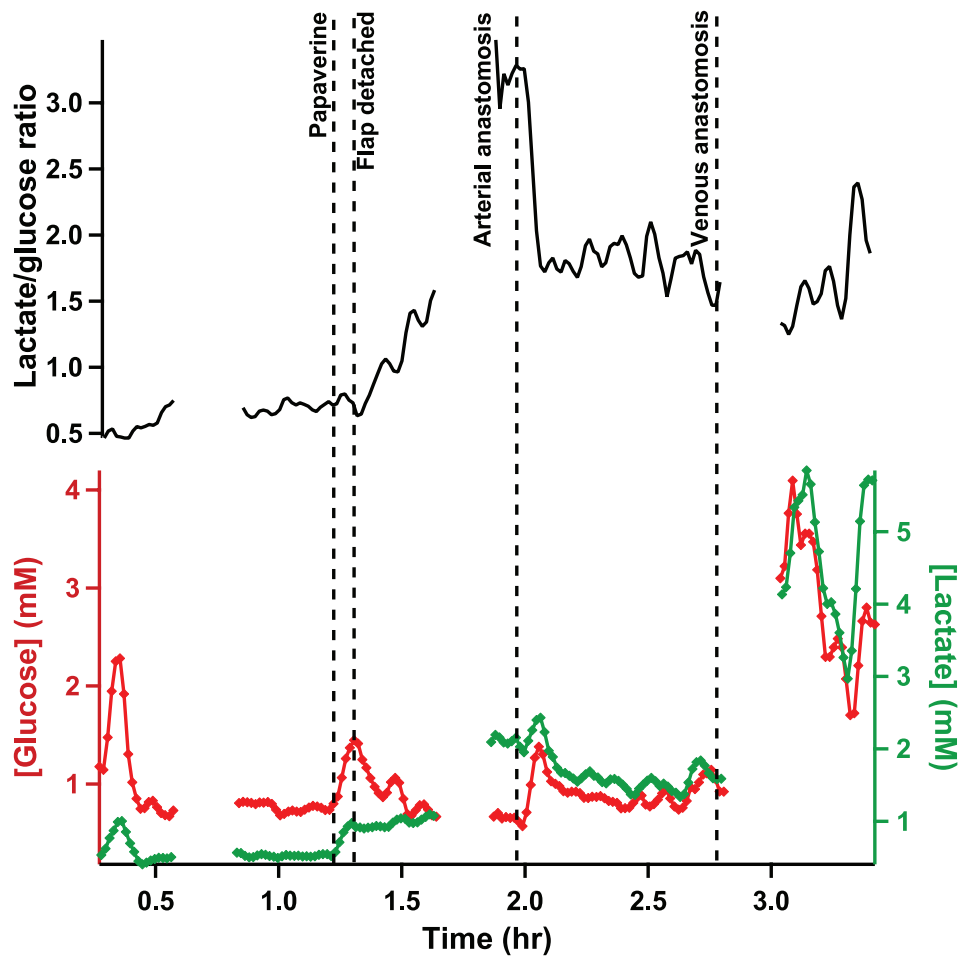


Figure 6.7: Dialysate metabolite levels during free flap surgery for patient 2. The green trace shows dialysate lactate concentrations, the red trace shows dialysate glucose concentrations and the black trace shows the corresponding lactate/glucose ratio. Data were obtained in real time using rsMD, with a point every minute for each metabolite, and were smoothed with a Savitsky-Golay 7-point filter. Time 0 represents the probe insertion point and dotted lines indicate key events during the surgery as relayed by the surgical team.

Prior to flap detachment, baseline glucose and lactate levels were 0.72 ± 0.04 mM ($n=10$) and 0.52 ± 0.02 mM ($n=10$), respectively. As with the previous case, topical application of papaverine caused a local increase in both glucose and lactate levels, but no change in the ratio of the two metabolites was observed, indicating that this was a probe recovery effect. Upon detachment of the flap from the blood supply at the donor site, dialysate glucose levels rapidly decreased, followed by a delayed and more gradual increase in dialysate lactate levels, as seen with the previous case. These changes coincided with a dramatic increase in the lactate/glucose ratio. Upon successful arterial anastomosis, the lactate/glucose ratio rapidly decreased, although it did not return to baseline levels at this point. Dialysate glucose levels increased and lactate levels began to decrease following

arterial anastomosis. After anastomosis of the vein, the local levels of both glucose and lactate dramatically increased. These changes were not observed in the lactate/glucose ratio, suggesting that this was an artefact rather than a real change.

Following surgery, the patient was transferred to the ITU where monitoring continued. Unfortunately, because of a technical problem with the analysis system, data were only recorded for the first 3 hours of monitoring in the ITU. Figure 6.8 shows dialysate metabolite levels in the ITU after surgery.

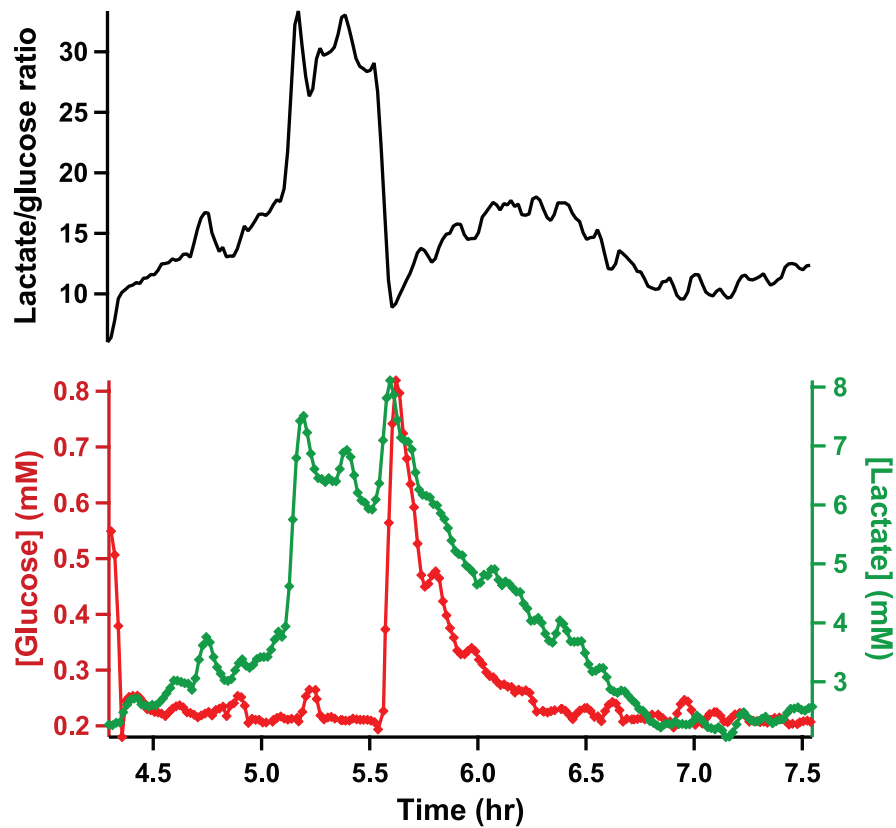


Figure 6.8: Dialysate metabolite levels in the ITU after free flap surgery for patient 2. The green trace shows dialysate lactate concentrations, the red trace shows dialysate glucose concentrations and the black trace shows the corresponding lactate/glucose ratio. Data were obtained in real time using rsMD, with a point every minute for each metabolite, and were smoothed with a Savitsky-Golay 7-point filter. Time 0 represents the probe insertion point before surgery. Data recorded correspond to 6:30pm-10:00pm.

Both glucose and lactate levels were considerably lower in the ITU than at the end of surgery; however, the lactate/glucose ratio was dramatically higher. One hour into monitoring in the ITU, large and rapid increases in lactate followed by glucose were observed, resulting in a dramatic increase in the lactate/glucose ratio. It is not clear what these changes correspond to but the metabolite levels and their ratio returned to the levels they had been at the start of monitoring in the ITU. The elevated lactate/glucose

6. ONLINE MONITORING DURING FREE FLAP SURGERY

ratio suggests that there may have been a problem with this flap but it is difficult to say as levels were not monitored for long enough after surgery. Clinical observations the following morning suggested that the flap reconstruction had been successful.

6.3.3 Case study 3

Figure 6.9 shows dialysate metabolite levels during surgery and in the ITU for a female undergoing a procedure to transfer a radial flap from the left forearm to the neck.

Dialysate baseline levels of glucose and lactate prior to detachment of the flap were 0.86 ± 0.02 mM (n=10) and 0.31 ± 0.05 (n=10), respectively. As previously described, topical application of papaverine resulted in a local increase in both glucose and lactate dialysate levels, but no change was observed in the lactate/glucose ratio, indicating that this was a probe recovery artefact. Following detachment of the flap, the characteristic signature of decreasing glucose levels and increasing lactate levels was observed at the same time as an increasing lactate/glucose ratio. Upon anastomosis of the artery, a rapid transient decrease in the lactate/glucose ratio was observed. However, shortly after, the ratio began to increase again because of a local decrease in glucose and an increase in lactate levels, indicating a second ischaemic event. Upon successful venous anastomosis, the levels of both glucose and lactate increased, as observed with the previous cases; however, no overall change in the lactate/glucose ratio was observed at this stage.

After surgery the patient was transferred to the ITU overnight, where monitoring continued. However, because of technical issues with the analysis system, data were only recorded for the first hour in the ITU. Dramatic changes in both glucose and lactate were observed in the ITU; however, although the lactate/glucose ratio continued to increase overall, its value was small (about 1.5-2.0 *c.f.* figure 6.8 where the ratio was about 30). Unfortunately, as data were not recorded for the remaining time in the ITU, it was not possible to observe whether metabolite levels returned to normal. However, clinical observations the following morning indicated that the surgery had been a success.

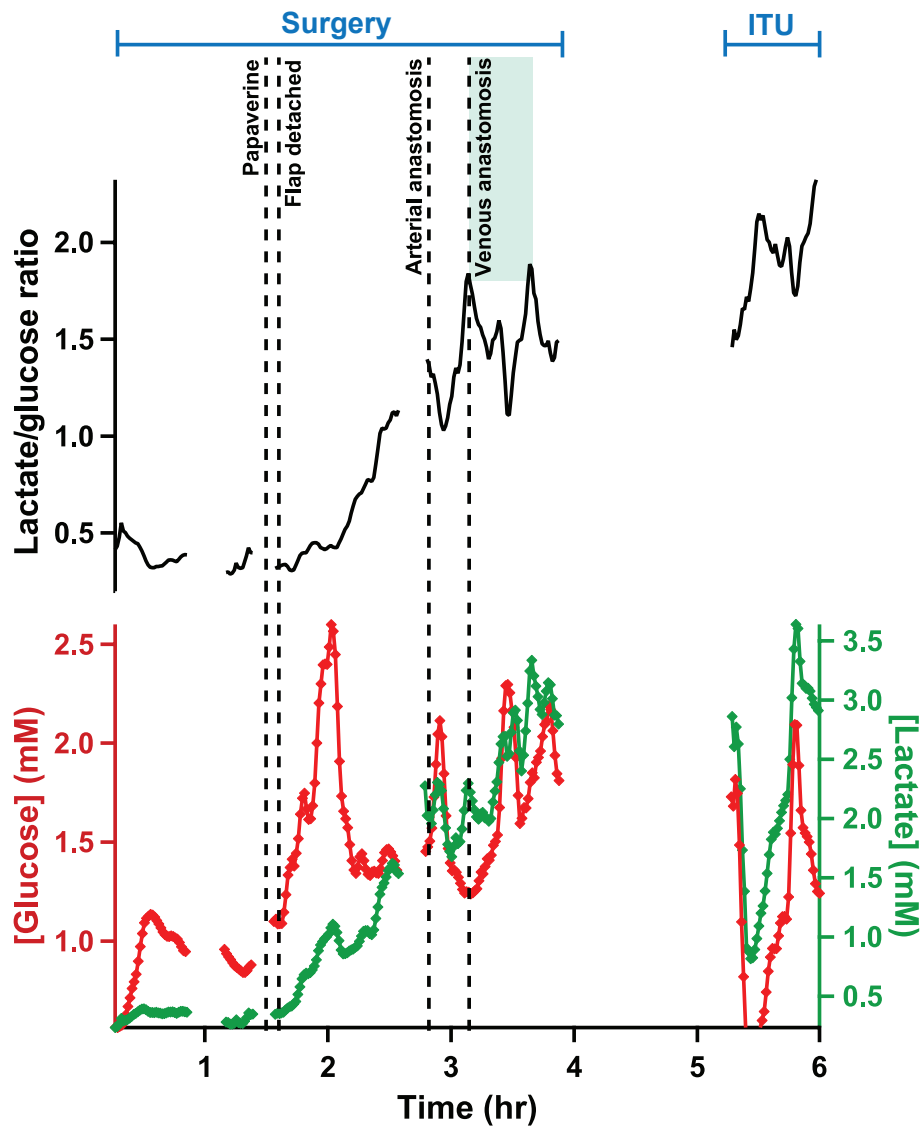


Figure 6.9: Dialysate metabolite levels during free flap surgery and in the ITU for patient 3. The green trace shows dialysate lactate concentrations, the red trace shows dialysate glucose concentrations and the black trace shows the corresponding lactate/glucose ratio. Data were obtained in real time using rsMD, with a point every minute for each metabolite, and were smoothed with a Savitsky-Golay 7-point filter. The blue box represents a block of time over which the venous anastomosis was being carried out. Time 0 represents the probe insertion point and dotted lines indicate key events during the surgery as relayed by the surgical team.

6.3.4 Case study 4

Figure 6.10 shows dialysate metabolite levels during surgery and in the ITU for a male undergoing a radial free flap procedure to rebuild part of the tongue.

6. ONLINE MONITORING DURING FREE FLAP SURGERY

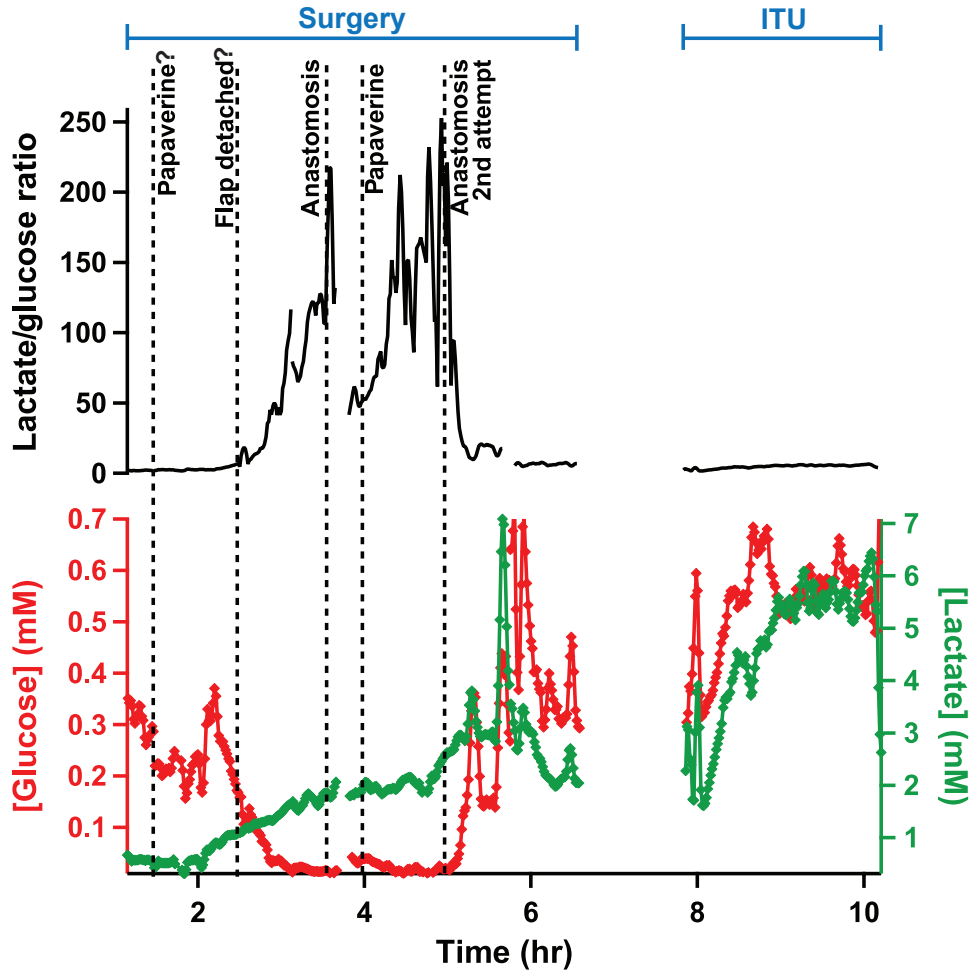


Figure 6.10: Dialysate metabolite levels during free flap surgery and in the ITU for patient 4. The green trace shows dialysate lactate concentrations, the red trace shows dialysate glucose concentrations and the black trace shows the corresponding lactate/glucose ratio. Data were obtained in real time using rsMD, with a point every minute for each metabolite, and were smoothed with a Savitsky-Golay 7-point filter. Time 0 represents the probe insertion point and dotted lines indicate key events during the surgery as relayed by the surgical team. ‘?’ indicates uncertainty in LabChart comments.

Baseline dialysate levels of glucose and lactate before the tissue was detached from the donor site were 0.30 ± 0.04 mM ($n=10$) and 0.57 ± 0.01 mM ($n=10$), respectively, which is a low concentration of glucose compared with other cases. As observed with previous cases, upon detachment of the flap from its blood supply, glucose levels steeply decreased, whereas lactate levels increased more gradually. These changes coincided with a rapid increase in the lactate/glucose ratio. In this case, the local glucose levels decreased to extremely low levels (0.02 ± 0.003 mM, $n=10$), resulting in a lactate/glucose ratio that was considerably higher than that observed in previous cases. For this procedure, the surgeons did not communicate when the individual arterial and venous anastomoses took place.

However, after the blood supply had been fully connected at the recipient site, the typical anastomosis signature changes were not observed in the metabolite levels, with glucose levels remaining very low at 0.03 ± 0.01 mM ($n=10$) and the lactate levels remaining high at 1.98 ± 0.09 mM ($n=10$). Moreover, although the lactate/glucose ratio did decrease, the levels remained elevated at 59.5 ± 9.7 ($n=10$) and began to increase again. Upon further investigation by the surgical team, the veins were found to be congested. Blood clots were removed and the blood vessels were reconnected at the recipient site. After successful anastomosis, the dialysate glucose level rose rapidly to 0.32 ± 0.03 mM, while the dialysate lactate level rose slightly before gradually decreasing. The dialysate lactate concentration at the end of surgery was 2.10 ± 0.1 mM.

Following surgery, the patient was transferred to the ITU where monitoring continued overnight. Unfortunately, because of technical issues with the analysis system overnight, only 2 hours of data were recorded in the ITU. Both glucose and lactate levels increased and remained high in the ITU, but no change was observed in the lactate/glucose ratio. These changes can therefore be attributed to a probe recovery artefact. On the basis of clinical inspection of the flap the following morning, the surgeons concluded that the flap reconstruction had been a success.

Figure 6.11 shows the metabolite levels at key time points to emphasise the changes.

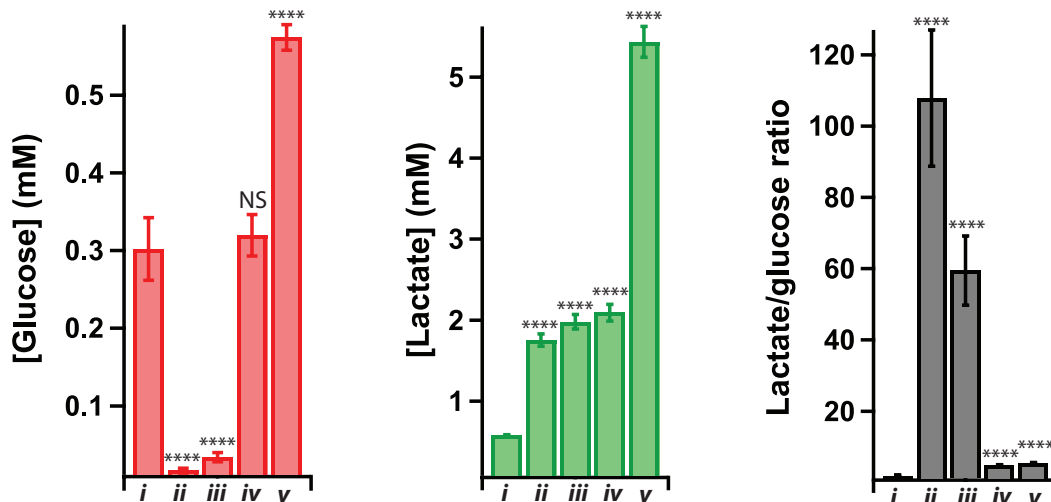


Figure 6.11: Histograms showing dialysate metabolite levels at key time points. Dialysate glucose levels are shown in red, dialysate lactate levels in green and the lactate/glucose ratio in black at (*i*) baseline, (*ii*) after flap detachment, (*iii*) after first (unsuccessful) anastomosis attempt, (*iv*) after second (successful) anastomosis attempt and (*v*) after 2 hours in the ITU. A Mann-Whitney U test was used to assess changes compared with baseline at each stage ($n=10$). NS=not significant, **** $p<0.0001$.

These histograms clearly show that, after the first anastomosis attempt (*iii*) the tissue

6. ONLINE MONITORING DURING FREE FLAP SURGERY

was still ischaemic, as glucose levels remained significantly lower than baseline and the lactate/glucose ratio remained significantly higher. However, upon successful anastomosis (*iv*) the glucose levels returned to baseline levels and the lactate/glucose level dramatically decreased, although it was still higher than baseline. The local lactate concentration increased throughout the monitoring time, further emphasising the value of considering the ratio of the two metabolites as opposed to either metabolite alone.

6.3.5 Case study 5

Figure 6.12 shows dialysate metabolite levels during surgery for a male undergoing a procedure using a radial free flap to rebuild part of the tongue.

Prior to flap detachment, baseline dialysate glucose and lactate levels were 1.12 ± 0.07 mM (n=10) and 0.51 ± 0.05 mM (n=10), respectively. As previously described, topical application of the vasodilator, papaverine, caused an increase in dialysate lactate and glucose levels but no change in the lactate/glucose ratio. Upon detachment of the flap from the blood supply at the donor site, glucose levels fell to 0.92 ± 0.09 mM (n=10), followed by a delayed increase in dialysate lactate levels to 2.93 ± 0.05 mM (n=10). These changes were accompanied by a steep increase in the lactate/glucose ratio. As the venous anastomosis was carried out soon after the arterial anastomosis, the second ischaemic event was not clear in this case. However, as the surgeons were finishing up they accidentally cut the artery, causing it to leak, as indicated in figure 6.12. The timing of this event is approximate but it coincided with another increase in the lactate/glucose ratio, presumably because the blood flow to the flap had been compromised, causing it to become ischaemic.

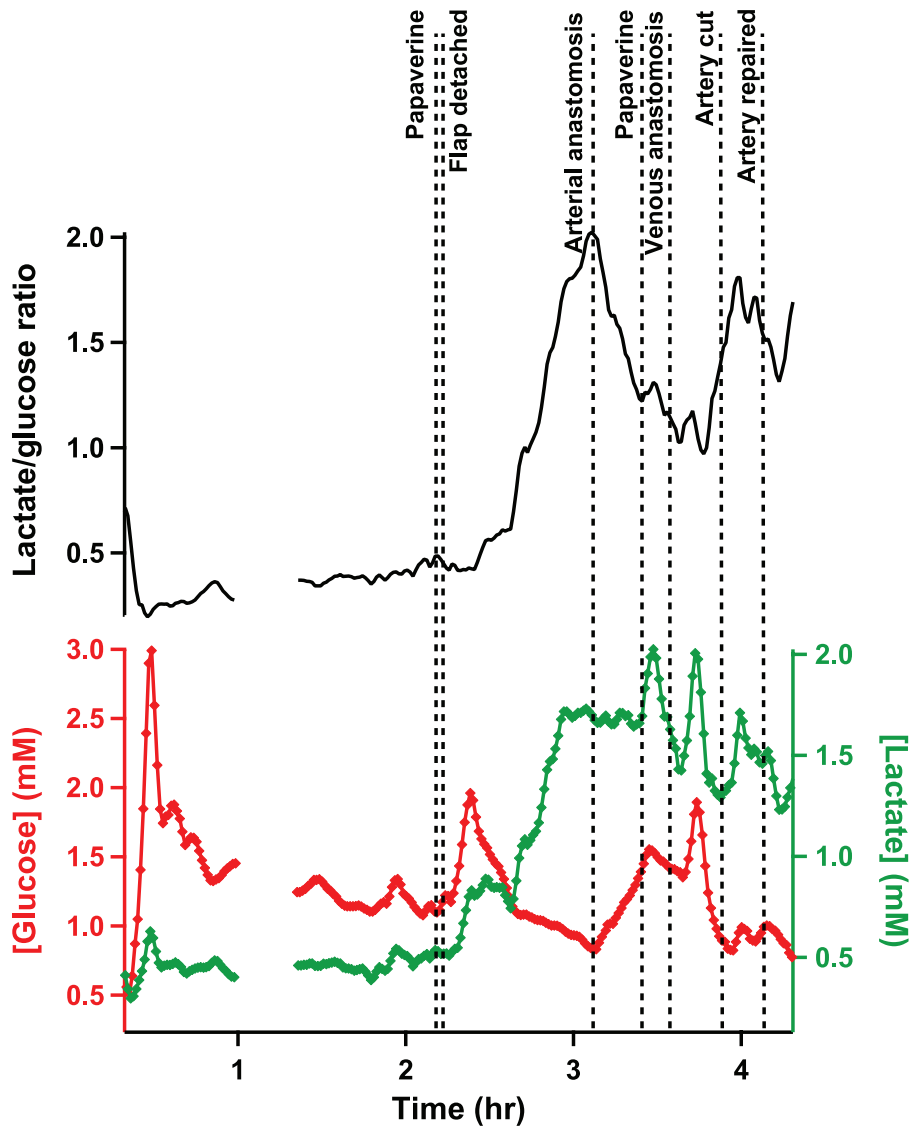


Figure 6.12: Dialysate metabolite levels during free flap surgery for patient 5. The green trace shows dialysate lactate concentrations, the red trace shows dialysate glucose concentrations and the black trace shows the corresponding lactate/glucose ratio. Data were obtained in real time using rsMD, with a point every minute for each metabolite, and were smoothed with a Savitsky-Golay 7-point filter. Time 0 represents the probe insertion point and dotted lines indicate key events during the surgery as relayed by the surgical team.

Following surgery, the patient was moved to the ITU where monitoring continued for a further 16 hours. Figure 6.13 shows dialysate metabolite levels overnight in the ITU following the surgery.

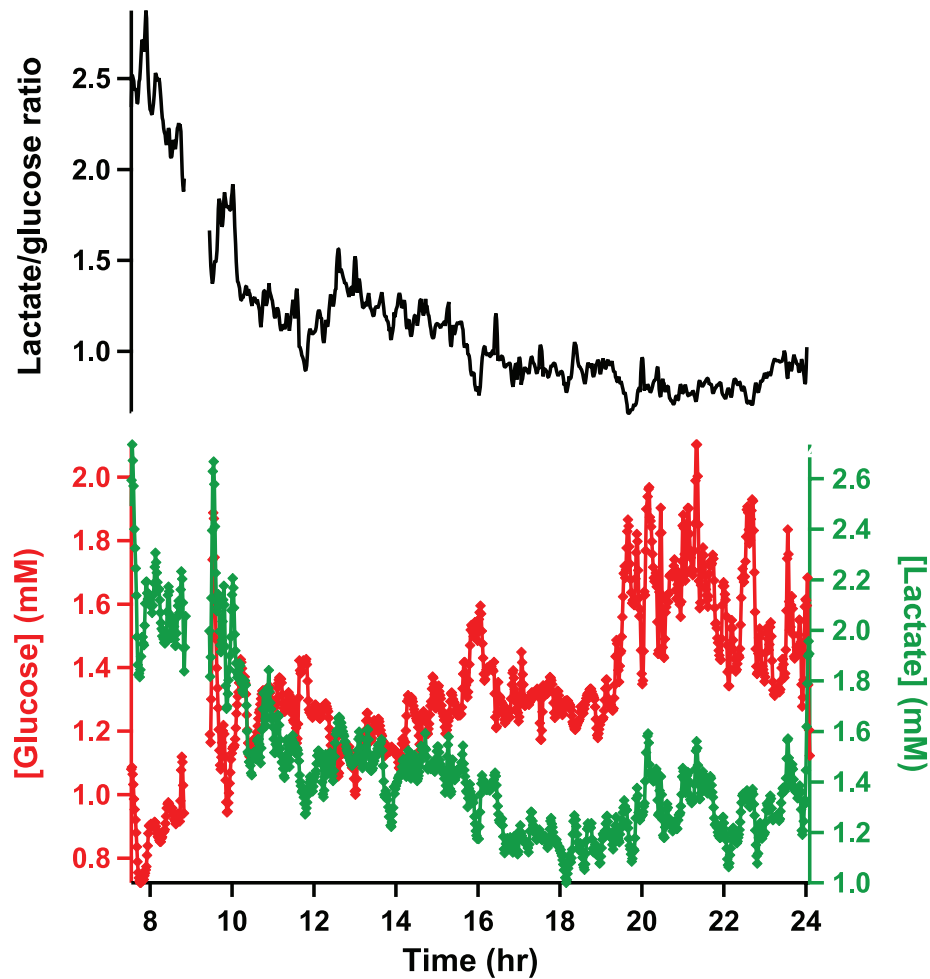


Figure 6.13: Dialysate metabolite levels in the ITU after free flap surgery for patient 5. The green trace shows dialysate lactate concentrations, the red trace shows dialysate glucose concentrations and the black trace shows the corresponding lactate/glucose ratio. Data were obtained in real time using rsMD, with a point every minute for each metabolite, and were smoothed with a Savitsky-Golay 7-point filter. Time 0 represents the probe insertion point during surgery.

Dialysate glucose levels steadily increased over the monitoring period in the ITU, with levels at 1.5 ± 0.12 mM ($n=10$) after 16 hours in the ITU. However, dialysate lactate levels steadily decreased overnight in the ITU, with levels at 1.40 ± 0.06 ($n=10$) after 16 hours of monitoring. The lactate/glucose ratio also steadily decreased, indicating that the health of the tissue was improving. The surgeons concluded that the flap reconstruction had been successful after clinical examination of the tissue the following morning.

6.3.6 Case study 6

Figure 6.14 shows dialysate metabolite levels during surgery for a 47-year old man undergoing a procedure in which tissue and bone from the fibia were used to reconstruct the jaw.

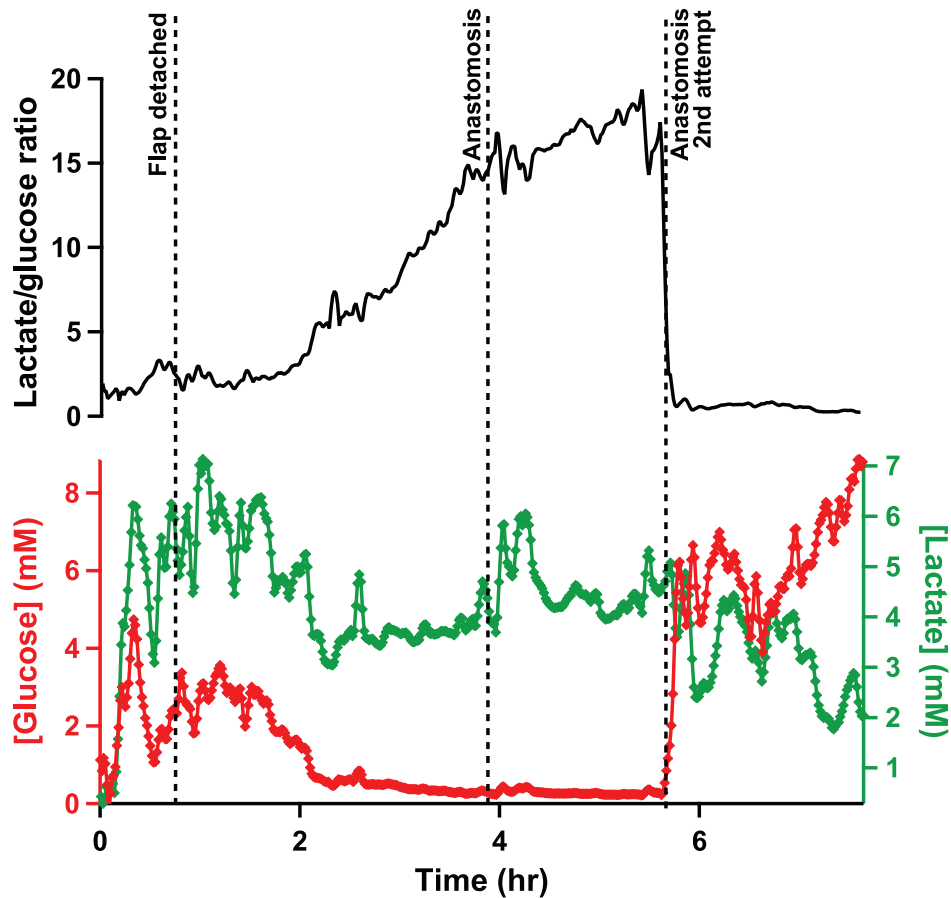


Figure 6.14: Dialysate metabolite levels during free flap surgery for patient 6. The green trace shows dialysate lactate concentrations, the red trace shows dialysate glucose concentrations and the black trace shows the corresponding lactate/glucose ratio. Data were obtained in real time using rsMD, with a point every minute for each metabolite, and were smoothed with a Savitsky-Golay 7-point filter. Time 0 represents the probe insertion point and dotted lines indicate key events during the surgery as relayed by the surgical team.

Baseline levels of glucose and lactate were 1.49 ± 0.37 mM ($n=10$) and 5.14 ± 1.00 mM, respectively; this is an unusually high concentration for lactate. As with the previous cases, detachment of the flap from the donor site resulted in a decrease in glucose concentration and an increase in the lactate/glucose ratio. Even after arterial and venous anastomosis at the recipient site, the glucose levels continued to decrease, while lactate levels continued to increase. The lactate/glucose ratio clearly shows this trend, with the ratio continuing to increase even after anastomosis, and is indicative of unsuccessful reperfusion of the flap. This fact was communicated to the surgeons. Upon further investigation, the surgeons discovered that there were blood clots in the vessels, preventing the blood flowing into and out of the flap and hence causing it to be ischaemic. The patient was thrombolysed to remove the clots and the anastomosis was carried out again. After the second attempt at anastomosis, the glucose levels increased considerably from 0.26 ± 0.01

6. ONLINE MONITORING DURING FREE FLAP SURGERY

mM (n=10) to 5.64 ± 0.83 mM (n=10). As observed in previous cases, the lactate levels were slower to change, although levels did decrease following successful anastomosis. The trend can be most clearly identified in the lactate/glucose ratio, which fell steeply from 17.25 ± 0.40 (n=10) to 0.64 ± 0.27 (n=10).

Following surgery, the patient was transferred to the ITU where monitoring continued overnight for a further 12 hours. Metabolite levels were monitored overnight following the surgery and dialysate levels are shown in figure 6.15.

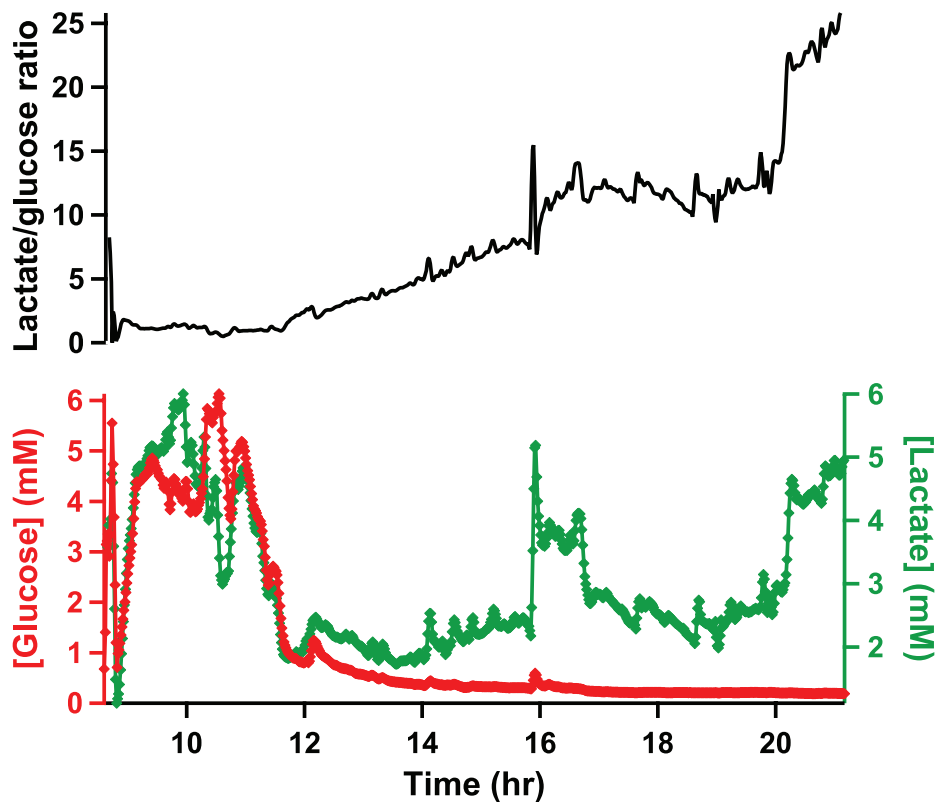


Figure 6.15: Dialysate metabolite levels in the ITU after free flap surgery for patient 6. The green trace shows dialysate lactate concentrations, the red trace shows dialysate glucose concentrations and the black trace shows the corresponding lactate/glucose ratio. Data were obtained in real time using rsMD, with a point every minute for each metabolite, and were smoothed with a Savitsky-Golay 7-point filter. Time 0 represents the probe insertion point during surgery.

After 2 hours of monitoring in the ITU, dialysate glucose levels began to decrease to 0.20 ± 0.002 mM (n=10) and lactate levels began to increase to 4.83 ± 0.13 mM (n=10). Moreover, the lactate/glucose ratio gradually increased over the 12 hours and was 24.83 ± 0.82 when monitoring was stopped. These levels suggested that the flap was ischaemic and that further surgery was required. However, at this stage clinical observations indicated that the flap was healthy. At a later time, after microdialysis monitoring had stopped, the surgeons became concerned about the flap on the basis of clinical parameters and decided

to re-operate as the flap had failed. Later tests revealed that this patient had a rare blood condition that caused clots to form. Online monitoring using rsMD enabled the flap failure to be detected before the problem could be identified by conventional clinical parameters, which would have allowed earlier intervention.

6.3.7 Case study 7

Figure 6.16 shows dialysate metabolite levels before the probe was detached in surgery and later in the ITU for a 64-year old female undergoing a flap procedure using a radial forearm flap to reconstruct the cheek.

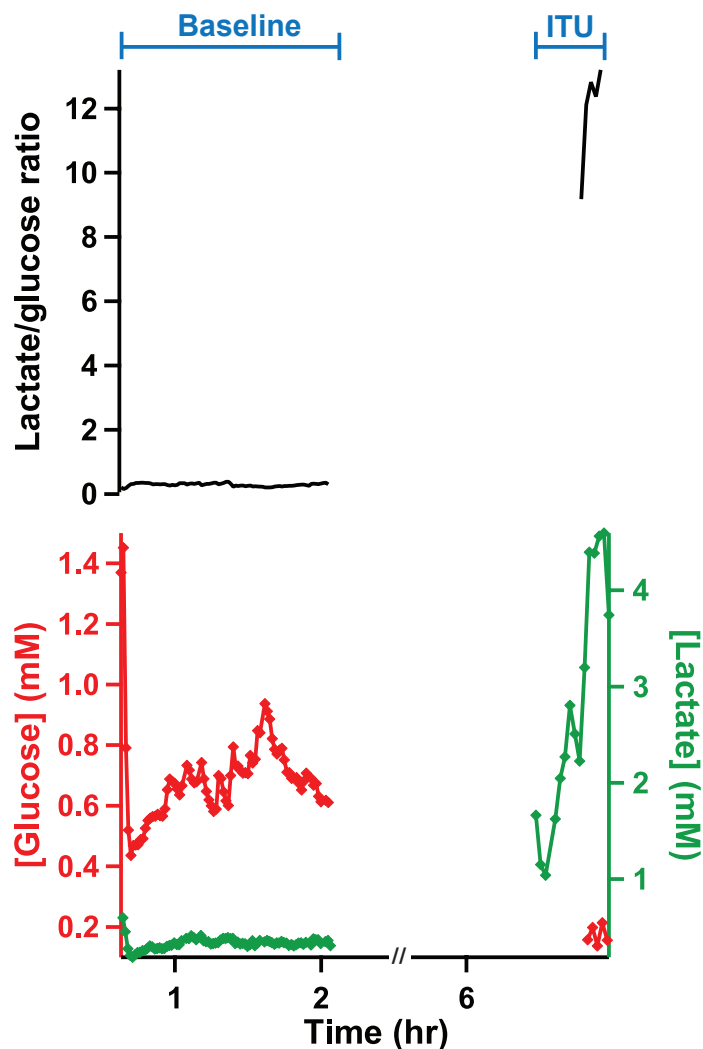


Figure 6.16: Dialysate metabolite baseline levels and levels in the ITU for patient 7. The green trace shows dialysate lactate concentrations, the red trace shows dialysate glucose concentrations and the black trace shows the corresponding lactate/glucose ratio. Data were obtained in real time using rsMD, with a point every minute for each metabolite, and were smoothed with a Savitsky-Golay 7-point filter. Time 0 represents the probe insertion point.

6. ONLINE MONITORING DURING FREE FLAP SURGERY

Initial baseline levels were measured during surgery, prior to flap detachment. Dialysate glucose and lactate levels were 0.69 ± 0.02 mM (n=10) and 0.33 ± 0.02 mM (n=10), respectively. However, as the flap was moved from the donor site to the recipient site, the probe fell out of the flap. The surgery was at a time-critical stage once the flap was disconnected from the blood supply and therefore a replacement probe could not be inserted until the end of surgery. As a result, data were not obtained until the patient had been moved to the ITU. At this point, glucose peaks were initially too low to reliably detect and the concentration was estimated to be 0.17 ± 0.03 mM (n=5). In addition, dialysate lactate levels were considerably higher than baseline levels at 3.47 ± 0.98 mM (n=10) and were rising steeply, as was the lactate/glucose ratio. Comparison with baseline levels before surgery allows us to conclude that this is a further example of a flap failure. Upon clinical inspection of the flap, the surgeons concluded that there was no pulse and decided to re-operate. During the second surgery, the surgeons were unable to successfully reconnect the blood supply to the flap and because of the complicated nature of the case, microdialysis monitoring was stopped.

6.4 Discussion

These results have demonstrated the feasibility of using rsMD to detect flap failure in real time both during surgery and later in the ITU. Of the 7 cases presented, in cases 1, 2 and 3 the operation went as planned with a successful outcome. In case 5, the anastomosis was successful but the artery was cut after the anastomosis and was subsequently repaired. Cases 4 and 6 demonstrated intermittent failure during surgery, which was corrected. Case 4 went on to have a successful outcome after surgery. However, in case 6, the flap went on to later fail again in the ITU. Case 7 also shows an example of flap failure after surgery, in the ITU.

Average dialysate glucose and lactate levels were 0.92 ± 0.40 mM and 1.14 ± 1.77 mM respectively, (n=7). This gives us a range of expected metabolite values for healthy tissue under these microdialysis conditions. In all cases, a similar metabolic pattern was observed in the dialysate upon onset of flap ischaemia.

After detachment of the flap the dialysate glucose levels decreased, while dialysate lactate levels increased. The average change in glucose and lactate dialysate levels compared with baseline was -0.31 ± 0.58 and $+0.91 \pm 1.30$ mM (n=6). These changes corresponded to an increase in the lactate/glucose ratio (mean $+20.16 \pm 42.11$ mM, n=6, $p < 0.5$ using Wilcoxon signed-rank test (two-tail)). Ischaemia caused by arterial and venous occlusion, two common causes of flap failure, could be individually identified.

Successful anastomosis resulted in an increase in dialysate glucose levels, a decrease in dialysate lactate levels and a decrease in the lactate/glucose ratio. The average change

in glucose and lactate dialysate levels compared with pre-anastomosis levels was $+1.70 \pm 2.04$ and $+0.44 \pm 1.64$ mM, respectively ($n=6$). The average change in the lactate/glucose ratio compared with pre-anastomosis levels was -19.56 ± 41.04 mM ($n=6$). By contrast, the average change in glucose and lactate dialysate levels compared with pre-anastomosis levels for unsuccessful anastomoses was -0.02 ± 0.06 and $+0.51 \pm 0.41$ mM, respectively ($n=2$) and the average change in the lactate/glucose ratio was $+21.38 \pm 38.18$ mM ($n=2$).

Compared with baseline levels, the average change in glucose and lactate dialysate levels upon successful anastomosis was $+1.39 \pm 1.72$ and $+1.35 \pm 2.18$ mM, respectively ($n=6$) and the average change in the lactate/glucose ratio was $+0.60 \pm 1.78$ ($n=6$). Compared with baseline levels, the average dialysate glucose and lactate changes for an unsuccessful flap was -0.75 ± 0.68 and $+0.38 \pm 1.45$ mM, respectively ($n=2$) and the lactate/glucose ratio was $+8.25 \pm 69.71$ mM ($n=2$). Although a clear trend can be seen from these results, the changes were not significant using a Wilcoxon signed-rank test (two-tail) as a result of the small sample size.

Using this technique it was possible to clearly distinguish between successful and unsuccessful flap reconstructions both during surgery and post-operatively. Histograms summarising the metabolite levels at key time points are shown in figure 6.17 for a successful (case 1) and unsuccessful case (case 6).

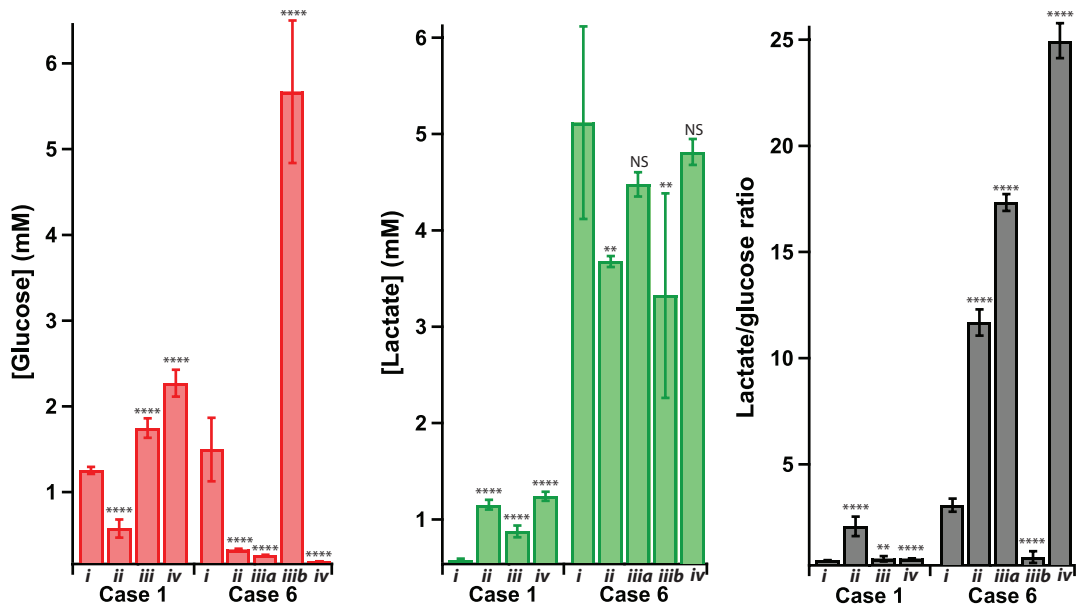


Figure 6.17: Dialysate metabolite levels at key time points for cases 1 and 6. Dialysate glucose levels are shown in red, dialysate lactate levels in green and the lactate/glucose ratio in black at (i) baseline, (ii) after flap detachment, (iii) after anastomosis, for case 6 (iii-a) was an unsuccessful attempt and (iii-b) was successful, and (iv) after monitoring overnight in the ITU. A Mann-Whitney U test was used to assess changes compared with baseline at each stage ($n=10$). NS=not significant, ** $p<0.01$, **** $p<0.0001$.

6. ONLINE MONITORING DURING FREE FLAP SURGERY

For case 1, the glucose levels decreased upon flap detachment, which corresponded to an increase in the lactate/glucose ratio. However, after successful anastomosis the levels recovered and glucose levels increased even more in the ITU. This is the signature of a successful flap. For case 6, although the profile starts off the same, upon reconnection, no change in the glucose levels was observed and the lactate/glucose ratio continued to increase. At this point the surgeons attempted to redo the anastomosis, resulting in a temporary increase in the dialysate glucose levels and a decrease in the lactate/glucose ratio, similar to the signature for the successful flap. However, these changes were not permanent as monitoring in the ITU shows that the glucose levels decreased and the lactate/glucose ratio increased again. These results indicate that the flap was compromised, as was later discovered by clinical assessment, and demonstrate the signature for an unsuccessful flap. Using rsMD, we were able to detect signs of flap failure much earlier than conventional methods allowed.

Glucose appears to be a more sensitive marker than lactate, as changes occurred more rapidly; however, the changes are harder to identify when only considering glucose or lactate trends individually, as opposed to considering them together. The lactate/glucose ratio proved to be a considerably more sensitive and reliable marker of tissue health than either metabolite alone, as it was not affected by flow or recovery artefacts, and as a result it eliminated artefacts caused by drugs such as vasodilators.

In summary, these results have shown that it is feasible to monitor dialysate metabolite levels during free flap surgery and afterwards in the ITU as a marker of flap health. Changes observed in the dialysate glucose and lactate levels and the lactate/glucose ratio correspond extremely well with events as relayed by the surgical team. Using online rsMD it was possible to detect flap failure in surgery and in the ITU.

As a result of the small number of cases monitored and the variability between them, further studies are required in order to carry out a full statistical analysis and to draw firm conclusions. Greater reliability is required in attaching the microdialysis probe to small flaps to prevent it falling out. Furthermore, a challenge during surgical monitoring was the difficulty in positioning the clinical trolley close enough to the patient to minimise the analysis delay whilst keeping out of the way of the surgical teams during a busy and stressful procedure. A miniaturised wireless system that could be placed in a sterile container at the patient bedside would eliminate this problem and would reduce the delay time further still, as the long connection tubing would not be needed, allowing closer to real-time measurements. A step towards this goal can be seen in chapter 8.

Chapter 7

Athlete monitoring: the bioanalytical problem

This chapter and chapter 8 describe the development of a wearable biosensing system for monitoring subcutaneous energy metabolites in cycling athletes, in collaboration with Prof. Guang-Zhong Yang, as part of the ESPRIT project. This chapter presents the rationale and the relevant literature for the use of wearable sensors in exercise monitoring. A series of measurements are presented starting with delayed analysis of samples collected online in storage tubing, through to real-time analysis using rapid sampling microdialysis (rsMD) and online biosensors. This chapter aims to define the bioanalytical problem for the eventual development of a wearable biosensing system, which will be described in detail in chapter 8.

7.1 Introduction

Research into wearable sensors is a rapidly growing area, with many new technologies emerging that can provide the wearer with real-time information about their health and fitness (266, 267, 268). Miniaturised wearable chemical/biochemical sensors have been developed for detection of analytes in various different bodily fluids, including sweat (269, 270), tears (271, 272), saliva (273, 274) and interstitial fluid (275, 276).

In particular, there has been considerable interest in wearable sensors that can assess athlete performance. Until recently, developments in wearable sensors have mainly focused on measurement of vital signs such as heart rate and electrocardiography, but chemical/biochemical sensors can provide important information in addition to these physical parameters (267, 277). Real-time information can allow athletes to assess their training effectiveness, to make appropriate adjustments and to track improvements on an individual level.

7. ATHLETE MONITORING: THE BIOANALYTICAL PROBLEM

Measurement of lactate and glucose is particularly interesting as it can provide important information about tissue oxygenation levels. During intense exercise, low tissue oxygen levels result in a switch from aerobic to anaerobic metabolism to meet the energy demands of the body. Anaerobic metabolism results in an increase in lactate and an increased consumption of glucose, as anaerobic processes are less efficient than aerobic processes (described in section 1.3). At low or moderate levels of exercise, the body is able to clear the lactate that is produced so that exercise can continue. However, at high intensities of exercise, the amount of lactate produced exceeds the amount that the body is capable of clearing, resulting in an accumulation of excess lactate, which leads to fatigue. Therefore, lactate is a particularly important biomarker for sports monitoring, as it can be used as a measure of how hard the body is working (278). This in turn enables athletes to modulate their effort to avoid causing themselves damage as a result of over-training or to train their body to increase its efficiency in clearing excess lactate.

Metabolite monitoring of athletes is usually carried out in the blood, using commercial finger-prick blood analysers. Although blood measurements provide important information about body metabolite levels, these analysers are impractical for continuous monitoring. The analysers take discrete measurements, therefore samples have to be taken regularly in order to obtain good temporal information, which results in constant interruptions during the activity period. Moreover, even with repeated measurements, the temporal resolution is not sufficient to observe dynamic changes in metabolite levels.

An autonomous portable device that allows continuous monitoring of metabolite levels in real time would present significant advantages over the discrete blood measurements that are currently used. Biosensors that can continuously measure lactate levels in sweat in real time have recently received considerable interest as they offer a non-invasive monitoring method (270, 279). However, levels observed depend on the site of measurement and there is some debate regarding the correlation between sweat and blood lactate levels as studies have shown that lactate in sweat is simply a result of sweat-gland metabolism (280). Moreover, these devices can be affected by humidity (268) and it is not possible to obtain baseline levels before exercise using this method, as these devices rely on the presence of sweat to connect the electrochemical cell.

Metabolite measurement in saliva has also been investigated as a non-invasive alternative to blood measurement (268, 281). Kim *et al.* proposed a non-invasive mouthguard biosensor for continuous measurement of salivary lactate (281). However, the device was not tested with humans.

Continuous monitoring of tissue metabolites using microdialysis has also been proposed (282, 283). Poscia *et al.* adapted the GlucoDay[®] device, which uses microdialysis to measure subcutaneous glucose levels in real time, for measurement of subcutaneous lactate (282). A preliminary study demonstrated the feasibility of using the device for a

human subject. However, this system only gives a data point every 3 minutes. Therefore, for dynamic changes during exercise, its temporal resolution is limited. Implantable needle biosensors that incorporate lactate oxidase have also been developed for subcutaneous measurement of lactate levels during exercise (37). However, sterilisation may affect the activity of the enzyme and therefore the sensitivity of the sensor.

Although it would be preferable to use a non-invasive or minimally invasive method of monitoring, microdialysis is particularly attractive as Food and Drug Administration (FDA)-approved, CE-marked sterile probes are available that can be used for human subjects. When coupled with an online analysis system, microdialysis can provide good time resolution that is ideal for resolving dynamic changes during exercise (5, 33).

More generally, development of a wearable device to measure metabolite levels in dialysate could have huge potential for clinical microdialysis applications. Exercising athletes are likely to display a large range of metabolite concentrations and will be physically moving. Therefore, a wearable device that is feasible for exercising athletes should also be feasible in a clinical situation.

In this chapter and chapter 8 I describe the development of a wearable microfluidic device that uses microdialysis to sample the subcutaneous tissue and glucose and lactate biosensors to continuously measure changes in dialysate metabolite levels during and after exercise. As a first approach, preliminary experiments are presented using existing technologies to define the scope of the analytical problem and to obtain a clear picture of the necessary requirements for the final device. In particular, as lactate levels increase during exercise it is important to identify the range that the lactate biosensors are required to detect in; the dynamic range can be extended if necessary, as described in chapter 3. Chapter 8 follows on from these preliminary experiments, describing the development of a proof-of-concept wearable device using exercising athletes to demonstrate its feasibility.

7.2 Sample collection in storage tubing for delayed analysis

For preliminary experiments, dialysate samples were collected into lengths of fine-bore storage tubing and analysed for glucose and lactate levels at a later date. This enabled cycling trials to be carried out without the need for the probe to be connected to the large clinical trolley during exercise. In this initial set of experiments preliminary information was gathered in order to investigate the feasibility of monitoring tissue metabolite levels during cycling using this methodology, as well as to determine the typical magnitude and timescale of any changes for design of the new analysis system. It also served to define

7. ATHLETE MONITORING: THE BIOANALYTICAL PROBLEM

a strict protocol for further experiments, including selection of the appropriate perfusion flow rate.

7.2.1 Microdialysis procedure

All procedures were approved by the local ethics committee and microdialysis probes were implanted by a qualified clinician. Prior to probe insertion, the skin was cleaned with alcohol wipes, after which an anaesthetic cream (EMLA, APP Pharmaceuticals) was applied. After 45-60 minutes, the anaesthetic cream was removed and an ice pack was applied for 5 minutes to further numb the area. A sterile microdialysis probe (CMA 63, MDialysis, Sweden) with a 10 mm membrane length and a 20 kDa molecular weight cut-off was inserted subcutaneously into the lower back using the tunnelling needle and introducer supplied and secured in place using a sterile dressing. The probe was perfused with sterile T1 perfusion solution (MDialysis, Sweden) using a portable syringe pump (CMA 107, MDialysis, Sweden) prior to insertion. A luer-lock extension set (150 cm, 0.4 ml internal volume, Alaris Medical Systems, UK) was used to extend the inlet tubing of the probe so that the pump could be placed at a distance from the cyclist so as not to be in the way.

7.2.2 Sample collection and analysis

As described in section 4.2.4, dialysate samples were collected and stored in tubing for delayed analysis. Lengths of 0.4 mm inner diameter (ID) Portex tubing (Smiths Medical, UK) were primed with T1 solution and were attached to the outlet of the probe to collect the dialysate. These lengths of storage tubing were labelled so that the direction of flow was known and were attached to the probe outlet using interconnect tees and fittings (LabSmith, US), as shown in figure 7.1. This enabled the tubing to be securely attached with minimum dead volume and to be easily taken off and replaced with new tubing as necessary. Once filled, the ends of the storage tubing were melted to seal them, so that the dialysate samples were not lost and the tubes were stored in the freezer until analysis was possible.

The stored dialysate was analysed at a later time by flowing the samples through the rsMD analysis system described in section 2.3.1.1. Using this system, a dialysate sample was injected through either a glucose or a lactate assay every 30 seconds. In this way the collected samples were effectively ‘played back’ as if in real time, with retention of temporal resolution.

7.2 Sample collection in storage tubing for delayed analysis

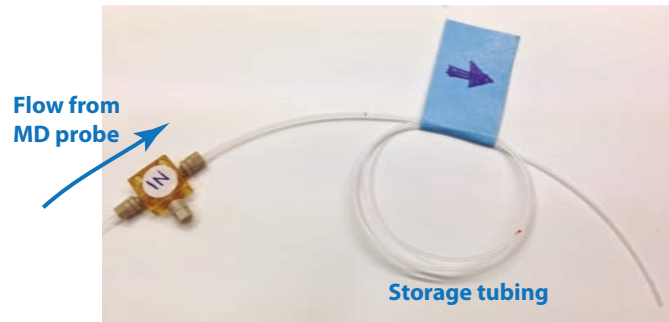


Figure 7.1: Online sample collection in storage tube. Collection tubing attached to the microdialysis (MD) probe outlet using LabSmith interconnect tees and fittings to reduce the dead volume and to allow easy changeover between subsequent tubes.

7.2.3 Experimental protocol

The cycling protocol was designed by the ESPRIT sensors team to include varying levels of exercise to investigate whether any correlation exists between tissue glucose and lactate levels and exercise intensity. The protocol used is shown in figure 7.2A, with approximate rotations per minute (rpm) indicated at each stage. Although the general protocol was followed in all cases, the exact rotation speeds were tailored to the fitness level of each cyclist, as it was important that they were able to complete the whole protocol.

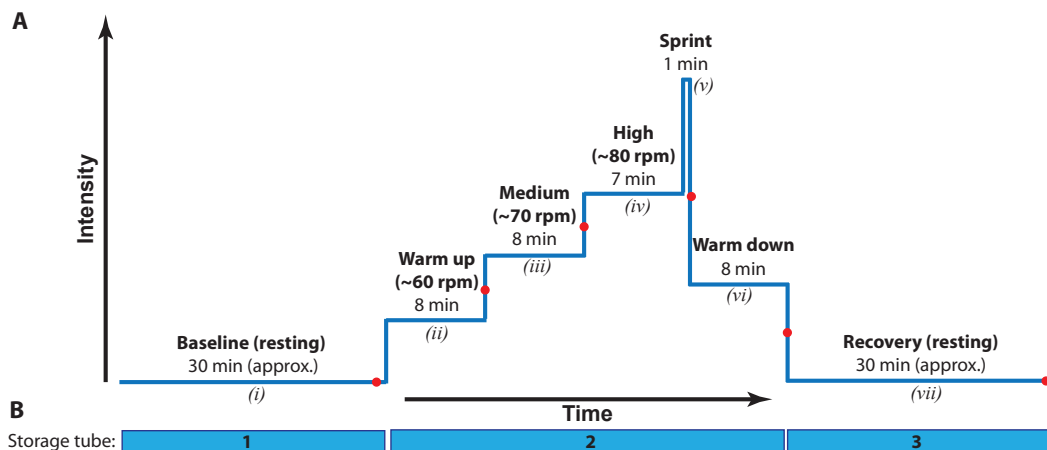


Figure 7.2: Schematic diagram showing the experimental protocol. A. Tissue levels were monitored during an initial resting period, followed by cycling at 4 levels of increasing rpm, a period of warming down and a final period of resting. Red dots indicate when blood samples were taken. B. Dialysate was consecutively collected into three sample tubes for the three phases: baseline (1), exercise (2) and recovery (3).

For each experiment, dialysate samples were collected in three lengths of tubing, one for each of the three sections: baseline, cycling and recovery, as shown in figure 7.2B.

7. ATHLETE MONITORING: THE BIOANALYTICAL PROBLEM

These lengths of tubing were each long enough to hold 45 minutes of dialysate; for probe perfusion at $5 \mu\text{l}/\text{min}$ this was 1.79 m and at $1 \mu\text{l}/\text{min}$ this was 0.358 m. The experimental setup is shown in figure 7.3.

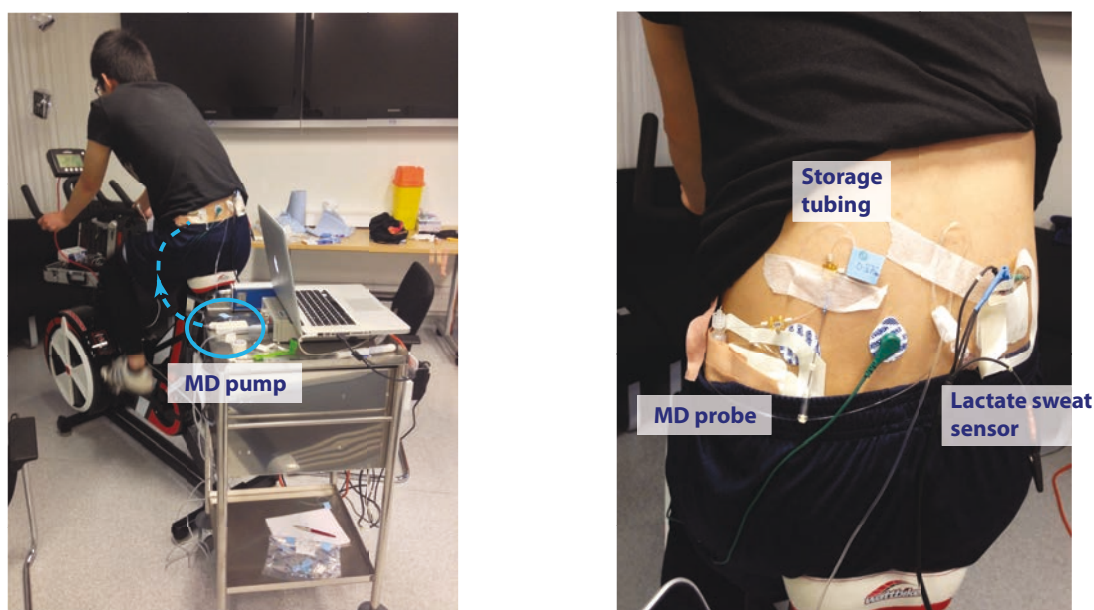


Figure 7.3: Experimental setup. The microdialysis (MD) probe was inserted subcutaneously into the lower back. The probe outlet was connected to a length of storage tubing for sample collection. The microdialysis pump was placed out of the way. A lactate sweat sensor, developed by Dr Salzitsa Anastasova was also placed on the lower back for comparison between tissue and sweat measurements.

In between each stage, cycling was temporarily interrupted to obtain a measure of glucose and lactate levels in the blood (timings indicated by red dots in figure 7.2A). This was carried out using a finger-prick test and commercial analysers. A saliva sample was also collected at the same time for analysis of lactate levels at a later date. Monitoring of lactate levels in sweat was also performed by Dr Salzitsa Anastasova, in order to identify any apparent trends between levels in tissue, blood, saliva and sweat, however these findings will not be discussed here.

7.2.4 Microdialysis resolution enhancement

In a process analogous to that used in chapter 4.2.4, storage tubing was used to break the link between collection and analysis time. This allowed us to take advantage of the fact that using delayed analysis, the stored sample can be analysed at a slower flow rate than that at which it was collected, which in turn improves the temporal resolution. For

7.2 Sample collection in storage tubing for delayed analysis

example, using the rsMD analysis system, glucose and lactate measurements are obtained every minute. Therefore, by collecting dialysate at $5 \mu\text{l}/\text{min}$ and running the sample back at the lower flow rate of $1 \mu\text{l}/\text{min}$, 5 measurements could be obtained per minute of collected dialysate, giving readings every 12 s. This concept is demonstrated in figure 7.4.

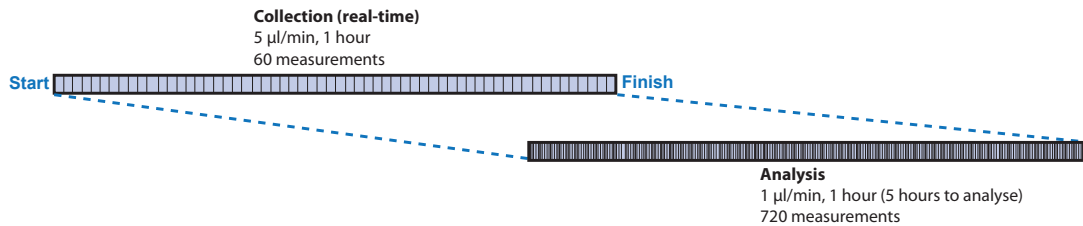


Figure 7.4: Schematic comparison of temporal resolution at different flow rates. Samples were collected at $5 \mu\text{l}/\text{min}$, which would give 60 glucose and lactate measurements in 1 hour if it was also analysed at this flow rate. If the analysis flow rate is slowed down to $1 \mu\text{l}/\text{min}$, 720 measurements can be obtained per hour of collected dialysate.

7.2.5 Offline results at $5 \mu\text{l}/\text{min}$

Dialysate glucose and lactate levels, as well as the ratio of the two, during the cycling protocol are shown in figure 7.5 for a preliminary experiment using a flow rate of $5 \mu\text{l}/\text{min}$, with the approximate timings of the exercise phases indicated. As a result of time constraints, in this case, the cycling protocol did not include the final warm-down phase and only consisted of a short period of recovery.

7. ATHLETE MONITORING: THE BIOANALYTICAL PROBLEM

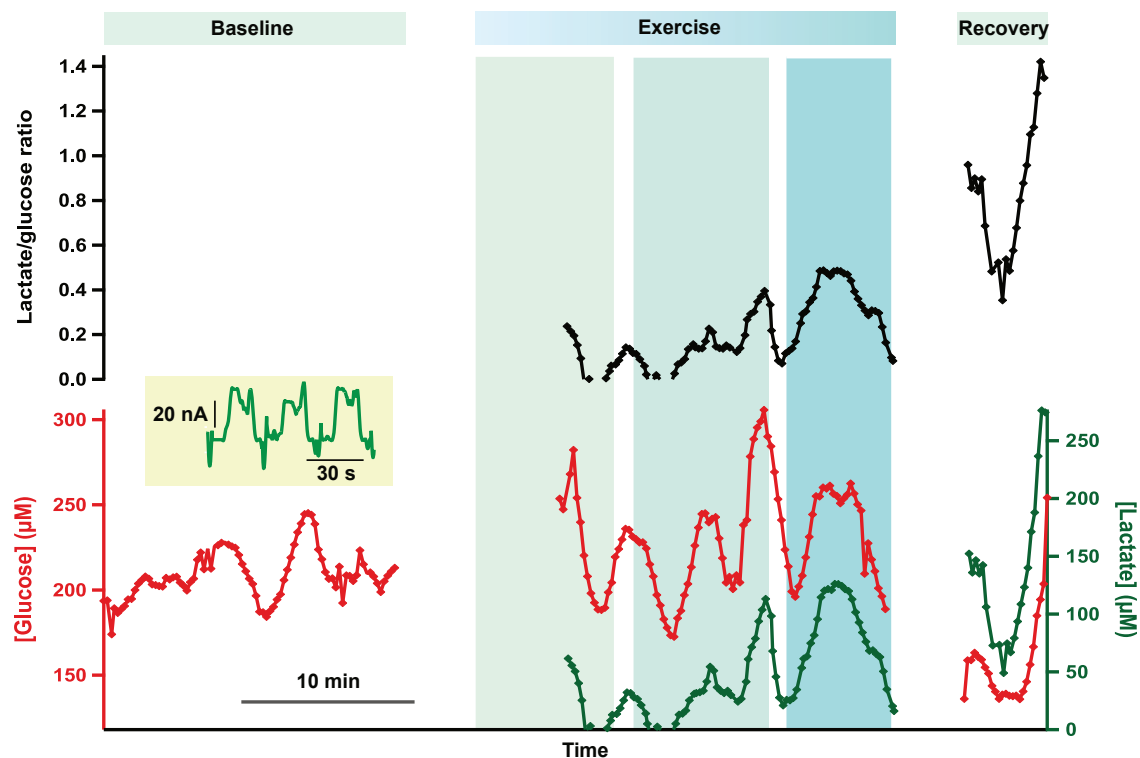


Figure 7.5: Results at 5 $\mu\text{l}/\text{min}$: dialysate metabolite levels during the cycling protocol. The green trace shows dialysate lactate concentrations, the red trace shows dialysate glucose concentrations and the black trace shows the corresponding lactate/glucose ratio. Data were collected in storage tubing at 5 $\mu\text{l}/\text{min}$ and analysed using rsMD at 1 $\mu\text{l}/\text{min}$, with a point every minute for each metabolite, corresponding to a point every 12 s in real time. The sections highlighted in blue indicate the three phases of exercise, of increasing intensity. Lactate levels were too low to reliably detect in the baseline phase. *Inset:* Exemplar lactate peaks during the baseline phase, almost indistinguishable from baseline ripple.

In this preliminary experiment, a relatively fast microdialysis flow rate of 5 $\mu\text{l}/\text{min}$ was used to maximise possible time resolution and to reduce the risk of high lactate concentration, which would be beyond the dynamic range of the assay. The faster flow rate succeeded in improving the time resolution, giving a data point every 12 seconds, but it reduced the probe recovery to the extent that the lactate signal during the baseline phase was too low to reliably detect. Therefore, a lower flow rate was chosen for further experiments.

As a result of the high time resolution, it was possible to detect dynamic, fast-changing events during the exercise period, which could be linked to the brief pauses where the cyclist stopped exercising for blood measurements to be taken. These findings indicated that it was necessary to adapt the protocol to remove these pauses, as they affected the results obtained.

During the exercise phase, lactate concentrations were measurable. Preliminary re-

7.2 Sample collection in storage tubing for delayed analysis

sults show that the lactate and lactate/glucose ratio both rose during increasing levels of exercise intensity and continued to rise even after exercise had stopped. These results highlighted the importance of monitoring for a longer period of time following exercise, as levels were still changing dramatically; it would be interesting to investigate this effect further.

As a result of a technical issue in the sample analysis, the first 5 minutes of the exercise sample were lost. At times, the length of data obtained varied from that expected, suggesting that the time was slightly distorted using this method. This made assignment of events complicated.

Microdialysis flow rate

As described in section 1.5.1, the recovery of the microdialysis probe is dependent on the rate at which it is perfused; a higher flow rate leads to larger sample volumes and greater mass extraction, but also to lower probe recovery and hence to lower dialysate concentration. It was found that a probe flow rate of 5 $\mu\text{l}/\text{min}$ was too high in the preliminary experiment, causing basal lactate levels to be too low to reliably detect.

To determine the appropriate microdialysis flow rate to use for further experiments, at which probe recovery would be high enough to enable reliable detection of basal lactate levels, baseline samples collected at 5, 2 and 1 $\mu\text{l}/\text{min}$ were compared. The results are presented in figure 7.6.

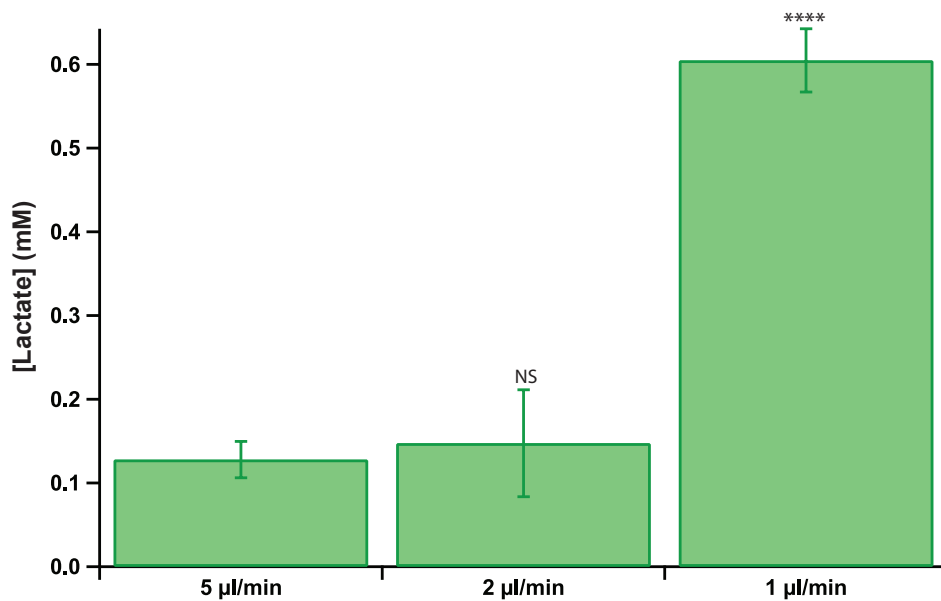


Figure 7.6: Choice of microdialysis flow rate. Baseline dialysate lactate levels collected at 1, 2 and 5 $\mu\text{l}/\text{min}$. Histograms represent mean \pm standard deviation, $n=10$ for 1 and 5 $\mu\text{l}/\text{min}$ and $n=3$ for 2 $\mu\text{l}/\text{min}$. A Mann-Whitney U test was used to compare levels with that at 5 $\mu\text{l}/\text{min}$. NS=not significant, **** $p<0.0001$.

7. ATHLETE MONITORING: THE BIOANALYTICAL PROBLEM

As shown in figure 7.6, basal lactate levels were very low at both 5 and 2 $\mu\text{l}/\text{min}$. In fact, Matlab tends to overestimate peak height at these low levels so concentrations are likely to be even lower than shown here. However, at 1 $\mu\text{l}/\text{min}$, baseline levels were considerably higher and much easier to detect and analyse.

7.2.6 Offline results at 1 $\mu\text{l}/\text{min}$

Example 1

For a second experiment, the probe perfusion flow rate was reduced to 1 $\mu\text{l}/\text{min}$ in order to increase the probe recovery and therefore increase the concentration of lactate in the samples so that levels could easily be detected. As shown in figure 7.7, dialysate lactate levels were high enough to be successfully detected, even during the baseline phase, confirming that 1 $\mu\text{l}/\text{min}$ was a suitable flow rate to use here. The time resolution was still improved during analysis by halving the flow rate at which the samples were collected so that a measurement could be made every 30 seconds of collected data.

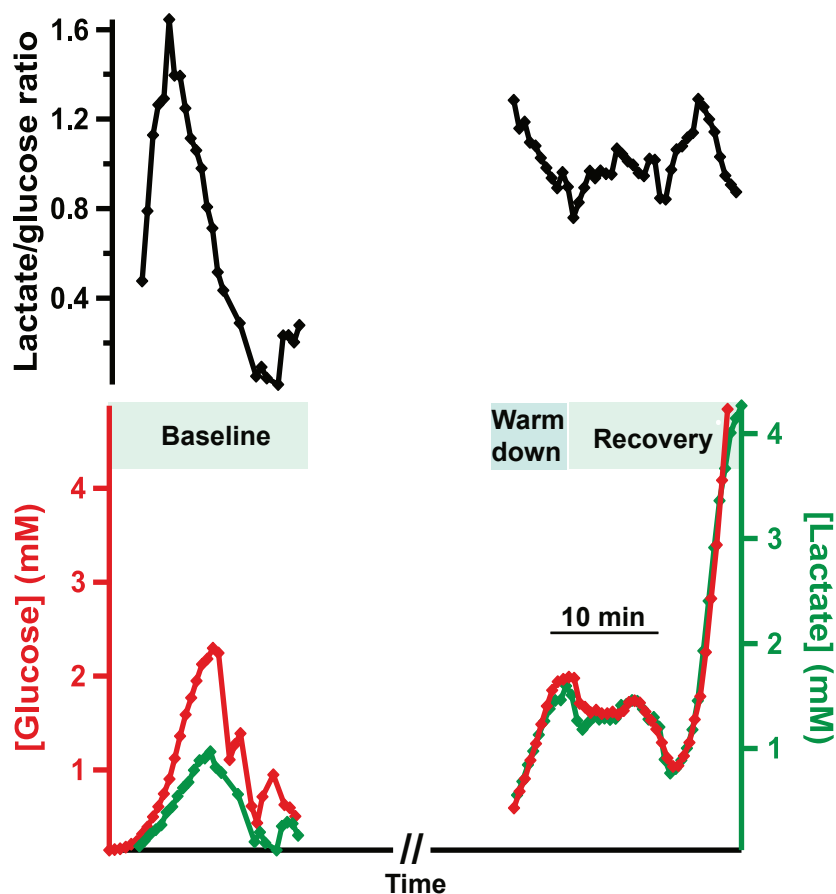


Figure 7.7: Example 1 at 1 $\mu\text{l}/\text{min}$: dialysate metabolite levels during the cycling protocol. The green trace shows dialysate lactate concentrations, the red trace shows dialysate glucose concentrations and the black trace shows the corresponding lactate/glucose ratio. Data were collected in storage tubing at 1 $\mu\text{l}/\text{min}$ and analysed using rsMD at 0.5 $\mu\text{l}/\text{min}$, with a point every minute for each metabolite, corresponding to a point every 30 s in real time.

However, in this case the cyclist was setting up the bike during the baseline phase and, as a result of this movement, the lactate and glucose levels during this period were not stable. Tissue metabolite levels are likely to vary between different people, therefore it is critical to measure a resting baseline level to act as a control with which to compare levels during the varying levels of exercise. Therefore, for future experiments, the bike was set up prior to probe insertion and the cyclists were asked to remain seated until a baseline level had been measured.

In addition, technical issues were encountered during the sample analysis, as the storage tubing became disconnected from the flow injection valve and the sample drained out. As a result, the exercise section of the data was lost. Sample loss is an inherent disadvantage with this methodology; if the samples were analysed in real time, issues could be identified as they happen and if necessary, sampling could be carried out for

7. ATHLETE MONITORING: THE BIOANALYTICAL PROBLEM

longer. However, if problems occur when samples are analysed offline, then data may be irrecoverably lost.

Towards the end of the recovery phase, both glucose and lactate levels rose steeply, possibly because of movement of the probe. However, this dramatic change was not seen in the lactate/glucose ratio, exemplifying the importance of calculating the ratio. Moreover, this result indicated that the probe needed to be placed more securely for future experiments.

Example 2

Figure 7.8 shows the results from another experiment carried out at $1 \mu\text{l}/\text{min}$.

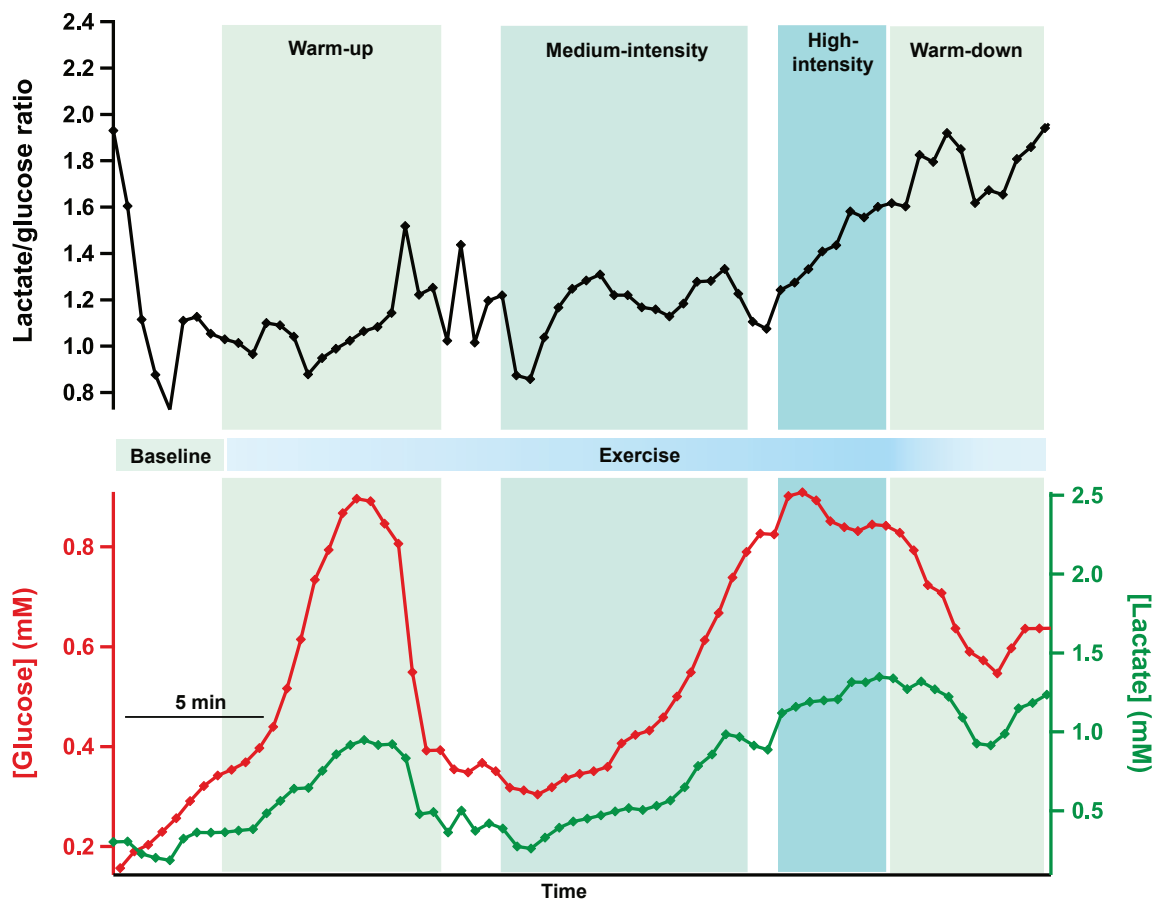


Figure 7.8: Example 2 at $1 \mu\text{l}/\text{min}$: dialysate metabolite levels during the cycling protocol. The green trace shows dialysate lactate concentrations, the red trace shows dialysate glucose concentrations and the black trace shows the corresponding lactate/glucose ratio. Data were collected in storage tubing at $1 \mu\text{l}/\text{min}$ and analysed using rsMD at $0.5 \mu\text{l}/\text{min}$, with a point every minute for each metabolite, corresponding to a point every 30 s in real time.

Unfortunately the data from the baseline storage tubing were lost during sample analysis, but a short section remained at the beginning of the exercise phase storage tubing.

7.2 Sample collection in storage tubing for delayed analysis

The data obtained during the exercise phase show good temporal resolution, with clear changes visible. Preliminary results show that lactate and the lactate/glucose ratio increased during exercise. At the end of the warm-up phase, lactate levels appear to have dropped. However, using the storage tubes for sample collection and delayed analysis appears to have caused a volume error, resulting in some distortion of the time, making event assignment difficult. Therefore, it is possible that the phases indicated in figure 7.8 have been shifted.

The data presented here are an example of a cyclist who was not physically able to complete the full protocol. In addition, in this case the probe came out slightly so that the membrane was not fully inserted under the skin. As a result, the levels could actually have been considerably higher if the full sampling area had been in contact with the tissue. This would have resulted in very high levels of tissue lactate, suggesting that tissue lactate levels may be linked to fitness. However, it also emphasised the importance of ensuring the probe was well secured.

In this particular case, it is unlikely that a steady speed was maintained at each level as the cyclist was struggling to maintain the pace. This highlights the need to improve the protocol to incorporate a means of aligning the data with some measure of the cyclist's exertion. In addition, it was not possible to draw any conclusions regarding subcutaneous metabolite levels during recovery as insufficient time was allowed for collection of dialysate during the recovery phase; however, the results show that the lactate/glucose ratio continued to increase during the warm-down phase, indicating the importance of extending the protocol to include monitoring of a longer period of recovery after exercise.

7.2.7 Preliminary conclusions

Although it was possible to collect dialysate in storage tubing for delayed analysis, the method did not prove suitable for this application because of the fast-changing events that occur and the difficulty in assigning exact timings to these events; instead, future experiments were carried out with online analysis so that events could be noted as they occurred. However, on the basis of these initial experiments it was possible to make improvements to the experimental protocol in order to improve the quality of the data obtained. In order to quantify the exercise intensity to aid interpretation of the results, it would be useful to also have some measure of the cyclist's heart rate throughout the protocol. On the basis of these preliminary experiments it was possible to define the expected range of dialysate glucose and lactate concentrations, which are 0.2-5.0 mM and 0.2-4.0 mM, respectively.

7.3 Online analysis of dialysate

The next stage towards the development of a wearable device was to move to online analysis in a microfluidic chip. The first step in achieving this was to validate the biosensors to ensure they were capable of detecting the physiological levels of subcutaneous glucose and lactate. In the following experiments, the lactate and glucose biosensors were positioned in a PDMS chip, upstream of the rsMD system, so that the dialysate would first flow past the online biosensors and then on to the rsMD system, enabling comparison of the results obtained using the online biosensors with those obtained using the gold-standard rsMD analysis system.

7.3.1 Configuring the online system

The choice of biosensors was informed by the preliminary results obtained in section 7.2.6. On the basis of these results, the expected physiological range of dialysate glucose and lactate with these microdialysis conditions is 0.2-5.0 mM and 0.2-4.0 mM, respectively. The hydrogel biosensors described in section 3.3 are capable of detecting glucose in this predicted range. However, the dynamic range of the lactate hydrogel biosensors would not be sufficient for this application. Therefore, it was necessary to coat the lactate biosensors with polyurethane in order to extend their dynamic range. As described in section 3.4, addition of an outer polyurethane layer results in a decrease in sensitivity but an increase in the dynamic range. The sensitivity of the polyurethane-coated lactate biosensors was still sufficient for the predicted levels. The effect of the addition of an outer polyurethane layer is demonstrated in figure 7.9.

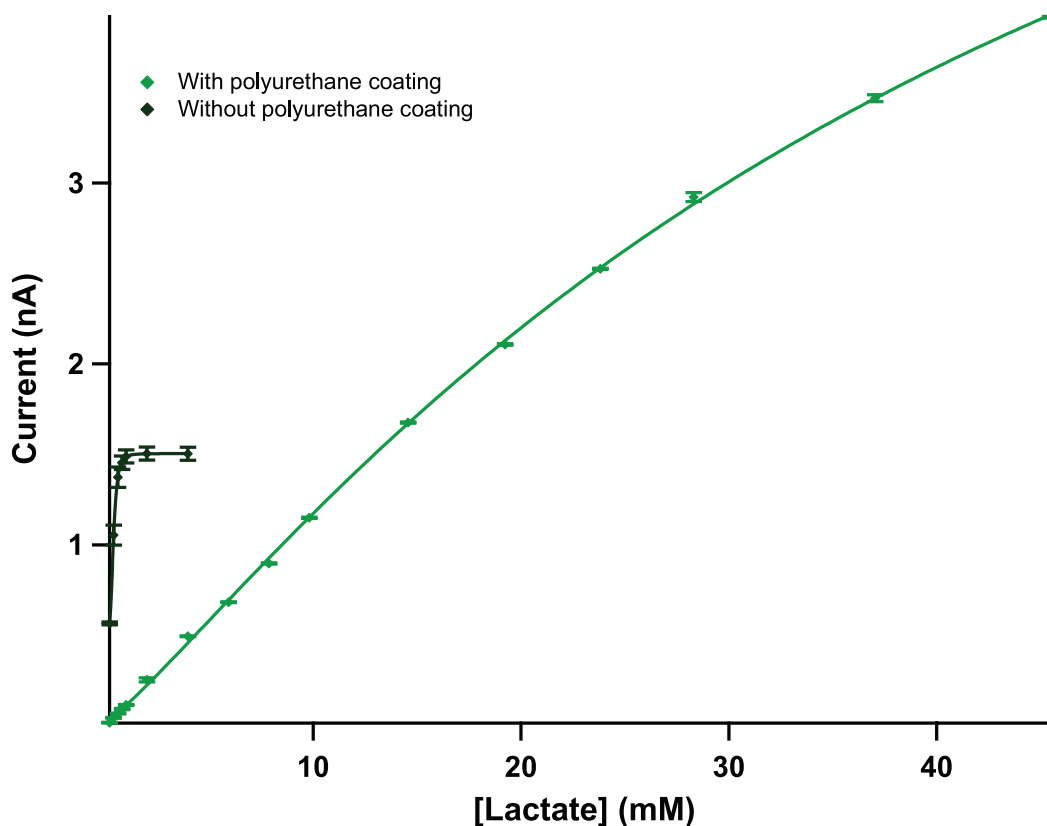


Figure 7.9: Dynamic range of lactate biosensors. Comparison of response of polyurethane-coated (*light green*) and uncoated (*dark green*) lactate biosensors to injections of lactate standard. Calibrations were carried out in a beaker. Biosensors were held at a constant potential of +0.75 V. Mean \pm standard deviation of measurement is shown. Points fitted with the Hill equation.

In order to allow simultaneous measurement of dialysate glucose and lactate levels using both rsMD and on-chip biosensors, the dialysate passed first through a PDMS microfluidic chip containing glucose and lactate 50 μm disc electrode hydrogel biosensors, then into a 100 nl sample loop of the rsMD flow injection valve. The analysis system is shown in figure 7.10.

The outlet of the probe was extended using 1 m of low-volume fluorinated ethylene propylene (FEP) tubing (0.12 mm ID, Royem Scientific, UK) in order to reach the clinical trolley. In order to do this, the vial holder was removed from the probe outlet, leaving about 1 cm of tubing on the end, which was connected to the FEP tubing using a tubing adaptor. The other end of the vial holder was trimmed so that just the needle was left, which was connected to the probe outlet tubing. The FEP extension tubing was initially primed with T1 solution so that it was possible to check that the solution was flowing out through the probe as soon as it was connected. Once this was confirmed, the end of the FEP tubing was connected to the analysis system. As a result of the long extension tubing and the low flow rate used, the delay from the microdialysis probe to the online

7. ATHLETE MONITORING: THE BIOANALYTICAL PROBLEM

biosensors was 26 minutes and to the rsMD system was 34 minutes.

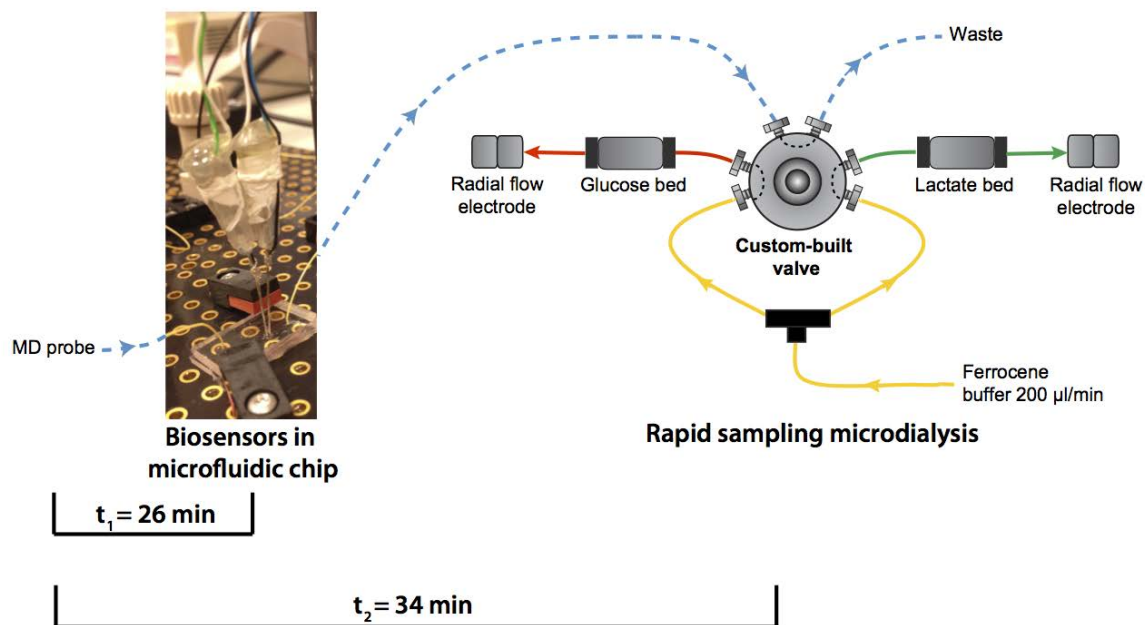


Figure 7.10: Online analysis experimental setup. The microdialysis probe flowed first into a PDMS microfluidic chip containing 50 μm disc electrode hydrogel glucose and lactate biosensors and then into the flow injection valve of the rsMD system. The delay between the microdialysis (MD) probe and the online biosensors (t_1) was 26 min and the delay between the microdialysis probe and the rsMD system (t_2) was 34 min at 1 $\mu\text{l}/\text{min}$.

The biosensors and rsMD system were initially calibrated using a LabSmith autocalibration board, as described in section 3.2.3. In this case, 5 steps were carried out using T1 solution and a 2 mM glucose/lactate solution. Using this autocalibration board it was possible to calibrate both analysis systems simultaneously. An example of a 5-point calibration of the two systems from 2-0 mM is shown in figure 7.11; the calibration stream flowed first through the online biosensors and then into the rsMD system.

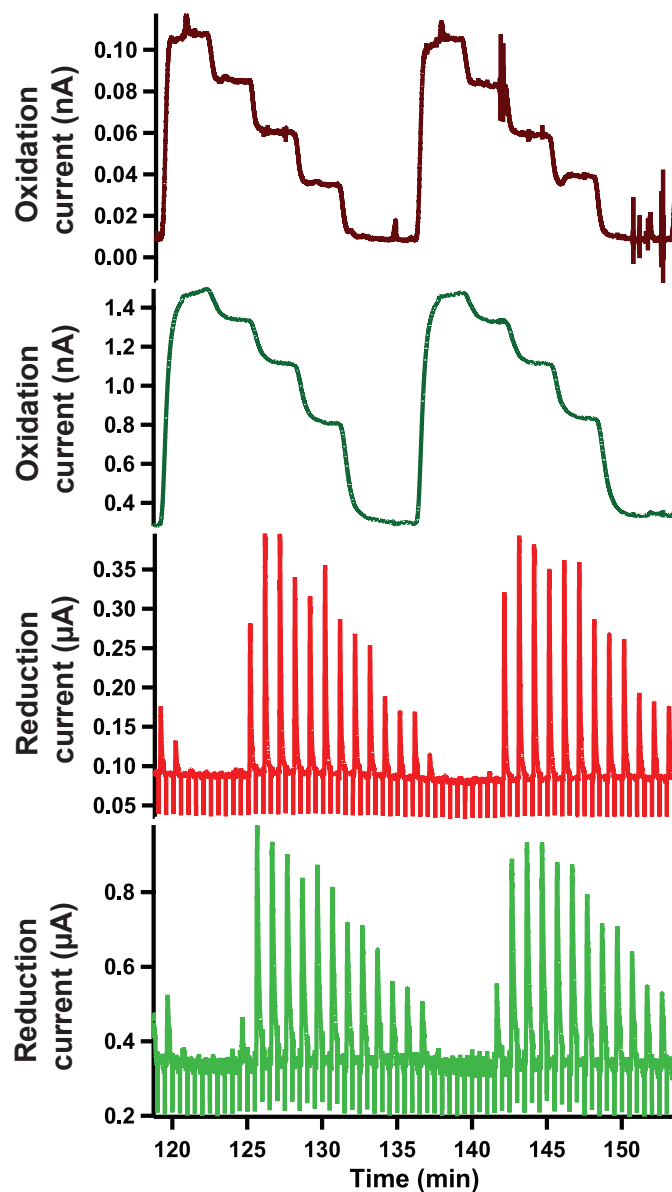


Figure 7.11: A 5-point calibration of the two online analysis systems. The calibration stream flowed through the microfluidic chip containing the glucose and lactate biosensors and then into the rsMD analysis system, leading to a short delay between the calibrations for the two systems. The top two traces show the calibration steps for the glucose (*red*) and lactate (*green*) online biosensors, and the bottom two traces show the inverted reduction peaks for glucose (*red*) and lactate (*green*) obtained using the rsMD system. The calibration steps are 2.0, 1.5, 1.0, 0.5 and 0.0 mM.

All the equipment was housed on a clinical trolley, placed next to the exercise bike. A photograph of the experimental setup is shown in figure 7.12.

7. ATHLETE MONITORING: THE BIOANALYTICAL PROBLEM

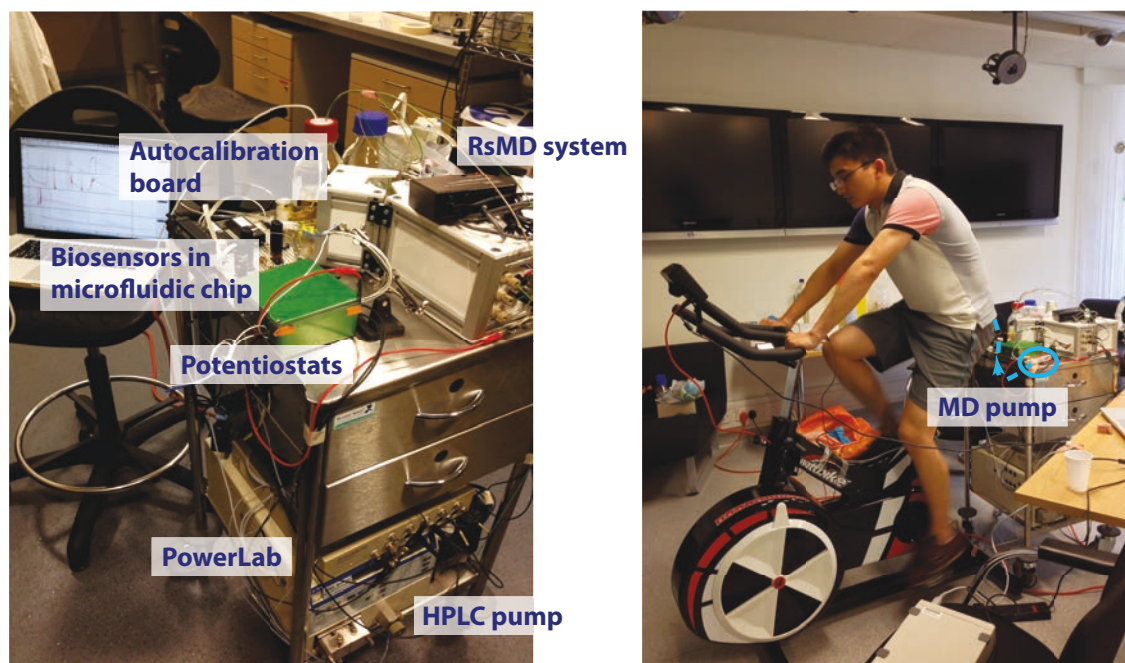


Figure 7.12: The clinical trolley for online analysis. The microdialysis (MD) probe outlet was extended to reach the clinical trolley, which held all the equipment for the on-chip biosensor and rsMD systems and was placed beside the exercise bike to monitor dialysate glucose and lactate levels during cycling.

7.3.2 Improved experimental protocol

The experimental protocol was improved on the basis of the preliminary results. For these experiments, blood and saliva samples were taken without the cyclist stopping between stages so as to avoid interrupting the exercise. In addition, the length of the recovery time was extended and the bike was set up prior to commencing exercise, so that during the baseline period the cyclist could remain seated in order to obtain stable baseline levels, uncomplicated by movement. A heart rate monitor chest belt (Suunto[®] dual chest belt, Finland), which wirelessly linked with the exercise bike, was worn and parameters from the bike, such as heart rate and rpm, were recorded from the exercise bike during cycling in order to quantify the exercise intensity to correlate with the metabolite results observed.

7.3.3 Results: rsMD

A total of three cyclists were monitored using this methodology. Results obtained using the gold-standard rsMD system are discussed in this section.

7.3.3.1 Cyclist 1

Figure 7.13A demonstrates the parameters that can be recorded from the exercise bike in order to quantify the exercise intensity; heart rate and rpm for the cycling phase, corresponding to the data section between the dotted lines in figure 7.13B, are shown for this cyclist. Dialysate glucose and lactate levels, as well as the ratio of the two, during the complete cycling protocol are shown in figure 7.13B. Tissue dialysate and blood levels of glucose and lactate at key time points during the cycling protocol are summarised in table 7.1.

7. ATHLETE MONITORING: THE BIOANALYTICAL PROBLEM

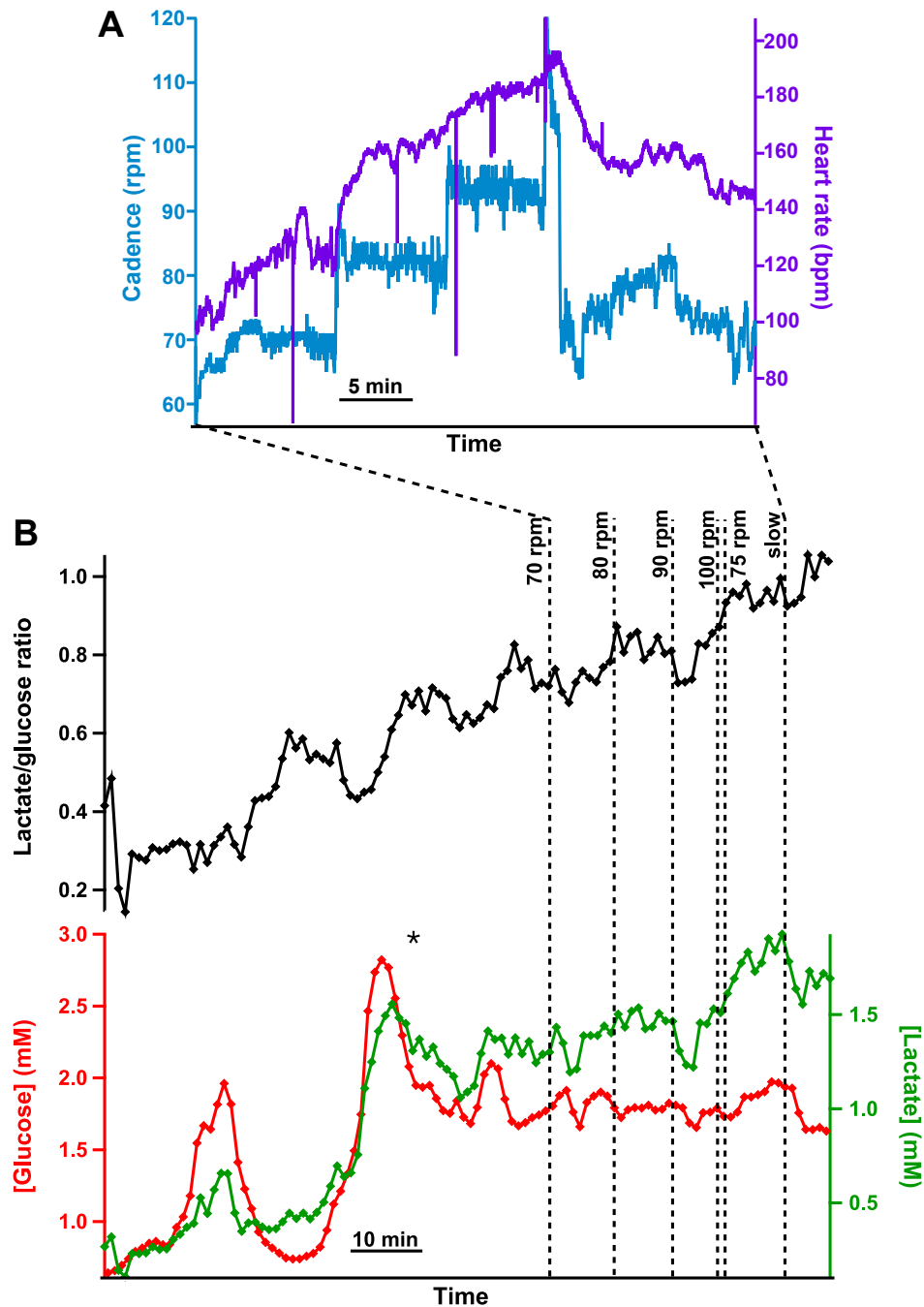


Figure 7.13: Dialysate metabolite levels and recorded exercise parameters for cyclist 1. *A.* The blue trace shows rpm and the purple trace shows heart rate during the cycling phase of the protocol. A heart rate monitor chest belt, which wirelessly links with the exercise bike, was worn and data were recorded in real time. *B.* The green trace shows dialysate lactate concentrations, the red trace shows dialysate glucose concentrations and the black trace shows the corresponding lactate/glucose ratio. Data were obtained in real time using rsMD, with a point every minute for each metabolite.

An initial peak in both dialysate glucose and lactate levels was seen following probe insertion. The period of time for tissue stabilisation following probe insertion has previ-

7.3 Online analysis of dialysate

Table 7.1: Subcutaneous levels of lactate and glucose levels compared with blood levels for cyclist 1 before, during and after exercise. A Mann-Whitney U test was used to assess changes compared to baseline at each stage. NS=not significant, * $p < 0.05$, ** $p < 0.01$.

Stage	[Glucose] (mM)		[Lactate] (mM)	
	Tissue dialysate	Blood	Tissue dialysate	Blood
Baseline	1.8 ± 0.17 (n=10)	3.8	1.3 ± 0.05 (n=10)	1.0
After 8 min 70 rpm	1.9 ± 0.06 (NS, n=3)	3.9	1.4 ± 0.03 (*, n=3)	2.4
After 8 min 80 rpm	1.8 ± 0.03 (NS, n=3)	4.1	1.5 ± 0.04 (**, n=3)	5.1
After 7 min 90 rpm & sprint	1.8 ± 0.07 (**, n=3)	5.4	1.7 ± 0.08 (**, n=3)	16.1
After warm-down	1.6 ± 0.01 (NS, n=3)	4.7	1.7 ± 0.03 (**, n=3)	8.3

ously been reported to be 10-15 minutes (99), which is consistent with these results. This increase is removed when considering the ratio of the two metabolites and is therefore an artefact. This participant had not eaten for several hours prior to monitoring and consequently his blood glucose levels were low, as can be seen in table 7.1; the asterisk in figure 7.13B indicates the point at which he ate a small amount of food in order to ensure he could complete the exercise protocol. Unfortunately, this may have complicated the baseline levels, as this coincides with a large peak in the measured glucose and lactate levels as well as a steady increase in the lactate/glucose ratio.

During exercise, the glucose and lactate levels seemed to remain fairly stable, with a slight increase in lactate levels. This corresponded to a stepwise increase in the lactate/glucose ratio as the exercise intensity increased, showing that this is a more sensitive marker of the subcutaneous changes occurring. As the exercise intensity was reduced, the ratio continued to increase. From the glucose and lactate traces, this can be attributed to an increase in the local lactate levels, despite a coincident small increase in local glucose levels. The recovery period was only monitored for a short time in this case, but the initial trend seems to indicate a continued rise in the lactate/glucose ratio, again emphasising the value of this way of representing the data. Monitoring during the recovery period needs to be extended in order to gain more information on the changes occurring during this phase.

In contrast to the fairly stable tissue glucose levels observed, blood glucose levels seemed to increase, even during intense exercise, which was unexpected; however, this could possibly be due to the participant eating immediately prior to this, which could have complicated the results. In contrast to the small increase observed for tissue lactate, blood lactate levels showed a dramatic rise with increasing exercise intensity, followed by a decrease as the cyclist slowed down. This decrease was not seen in the tissue dialysate levels.

7. ATHLETE MONITORING: THE BIOANALYTICAL PROBLEM

7.3.3.2 Cyclist 2

Subcutaneous dialysate levels of glucose and lactate during the cycling protocol are shown in figure 7.14 for cyclist 2. Table 7.2 summarises tissue and blood metabolite levels at key time points throughout the monitoring period.

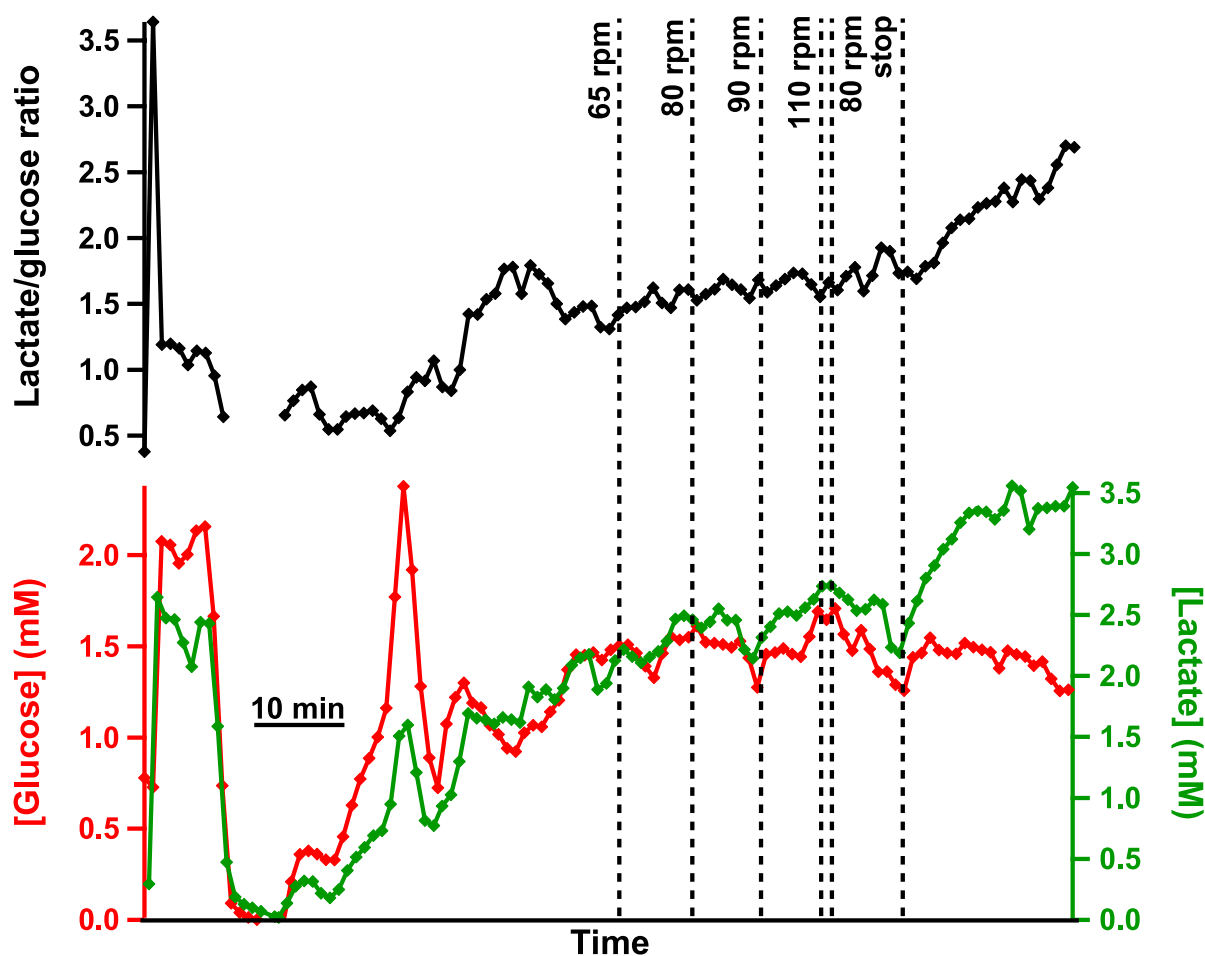


Figure 7.14: Dialysate metabolite levels during the cycling protocol for cyclist 2. The green trace shows dialysate lactate concentrations, the red trace shows dialysate glucose concentrations and the black trace shows the corresponding lactate/glucose ratio. Data were obtained in real time using rsMD, with a point every minute for each metabolite.

As with the previous data, an initial peak in both glucose and lactate was seen immediately after probe insertion, which was cancelled out by considering the lactate/glucose ratio. A second spike in glucose and lactate was seen during the baseline period, which was also removed by calculating the ratio of the two metabolites, indicating that this was also an artefact.

7.3 Online analysis of dialysate

Table 7.2: Subcutaneous levels of lactate and glucose levels compared with blood levels for cyclist 2 before, during and after exercise. A Mann-Whitney U test was used to assess changes compared to baseline at each stage. NS=not significant, * $p < 0.05$, ** $p < 0.01$.

Stage	[Glucose] (mM)		[Lactate] (mM)	
	Tissue dialysate	Blood	Tissue dialysate	Blood
Baseline	1.4 ± 0.16 (n=10)	5.5	2.0 ± 0.14 (n=10)	1.7
After 8 min 65 rpm	1.6 ± 0.04 (NS, n=3)	5.4	2.5 ± 0.02 (*, n=3)	3.2
After 8 min 90 rpm & sprint	1.6 ± 0.07 (**, n=3)	5.4	2.7 ± 0.03 (**, n=3)	11.7
After 10 min recovery	1.5 ± 0.01 (NS, n=3)	5.2	3.3 ± 0.01 (**, n=3)	12.3

During the exercise period, blood and tissue glucose levels remained fairly stable, while lactate increased in both the tissue and the blood. The magnitude of this lactate increase was much larger in the blood than on a local tissue level. One possible explanation for this could be that in order to meet the increased demands of the tissue during exercise, the local blood supply would have increased and acted as a sink, removing excess lactate from the tissue. During exercise, there was a slight increase in the lactate/glucose ratio, in a stepwise manner. As the level of exercise decreased, the glucose and lactate levels also decreased, but the ratio continued to increase.

In the recovery period after exercise, the glucose levels remained fairly stable, while the lactate levels increased, as did the lactate/glucose ratio. Even after 10 minutes of recovery, the tissue and blood lactate levels continued to increase. However, in this case the percentage change was largest in the tissue, suggesting that the decreased local blood supply on cessation of exercise lessened this sink effect. Although a longer period of recovery was monitored in this case, it would be interesting to monitor for longer still to see when these levels return to normal.

7.3.3.3 Cyclist 3

For the third cyclist monitored using this methodology, the recovery period was extended in order to increase our understanding of the local changes occurring following exercise. Dialysate glucose and lactate levels and their ratio over the full monitoring period are shown in figure 7.15. Blood and tissue metabolite levels at key moments during the cycling protocol are summarised in table 7.3.

7. ATHLETE MONITORING: THE BIOANALYTICAL PROBLEM

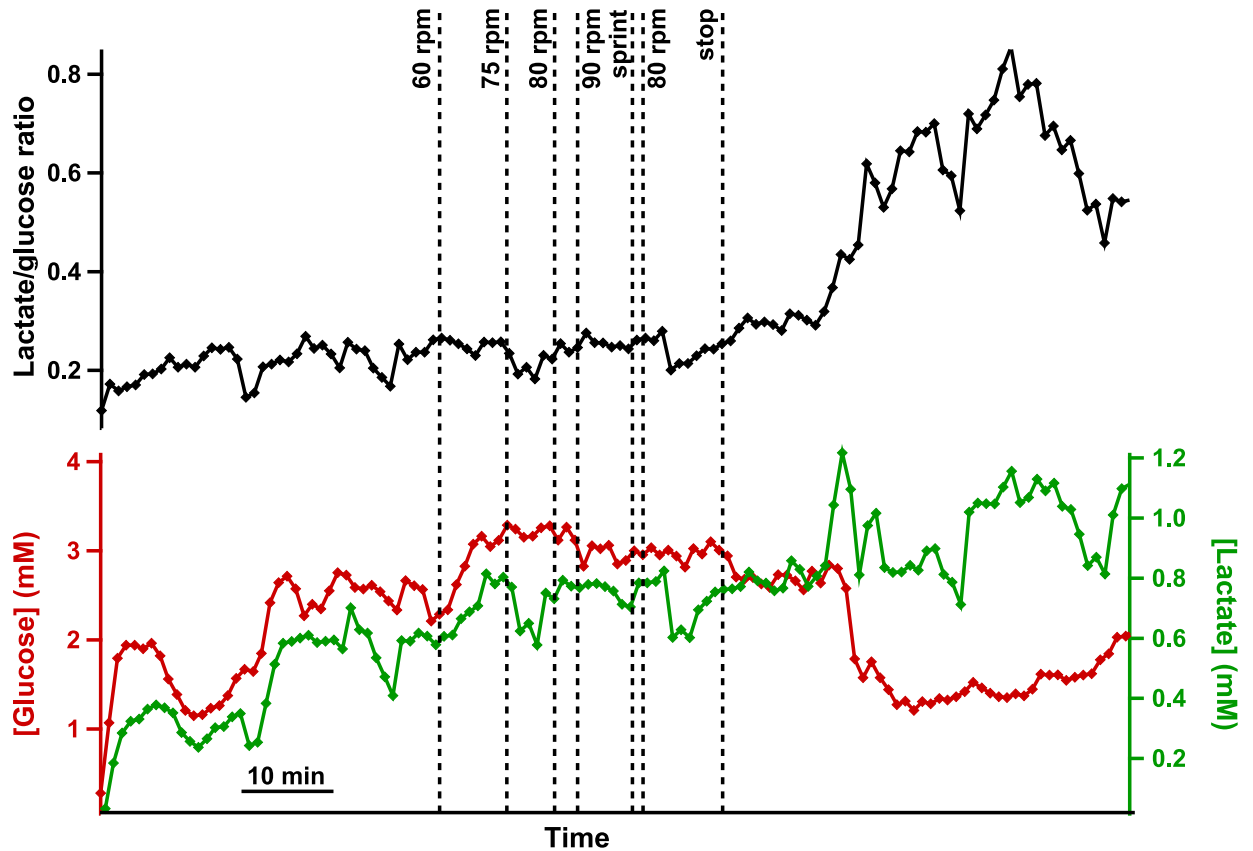


Figure 7.15: Dialysate metabolite levels during the cycling protocol for cyclist 3. The green trace shows dialysate lactate concentrations, the red trace shows dialysate glucose concentrations and the black trace shows the corresponding lactate/glucose ratio. Data were obtained in real time using rsMD, with a point every minute for each metabolite.

Table 7.3: Subcutaneous levels of lactate and glucose levels compared with blood levels for cyclist 3 before, during and after exercise (ND indicates level below detection limit). A Mann-Whitney U test was used to assess changes compared to baseline at each stage. * $p < 0.05$, ** $p < 0.01$.

Stage	[Glucose] (mM)		[Lactate] (mM)	
	Tissue dialysate	Blood	Tissue dialysate	Blood
Baseline	2.6 ± 0.11 (n=10)	6.2	0.6 ± 0.08 (n=10)	ND
After 6 min 80 rpm	3.2 ± 0.09 (**, n=3)	5.0	0.8 ± 0.03 (**, n=3)	1.7
After 8 min 90 rpm & sprint	3.0 ± 0.05 (**, n=3)	5.3	0.8 ± 0.03 (**, n=3)	9.6
After 10 min recovery	2.7 ± 0.01 (*, n=3)	5.2	0.8 ± 0.02 (**, n=3)	3.2

A small peak in both glucose and lactate levels can be seen at the start of monitoring. As this effect is not evident in the lactate/glucose ratio, it can be attributed to a tissue stabilisation effect following probe insertion.

In this data set, there was a small increase in tissue glucose levels after some exercise, although this slightly decreased after further exercise and even further still after the cyclist had rested. This could be due to an initial increase in the supply of glucose locally, followed by an increased usage, in order to meet the extra energy demands of the tissue. Blood glucose decreased from baseline levels, although it remained fairly stable during increasing exercise intensity and resting. In this case, tissue lactate levels remained fairly stable, with a slight increase compared with baseline after intense exercise and even after 10 minutes of resting. Changes in blood lactate levels were much more marked, with a large increase as exercise intensity increased. Interestingly, in this case, blood lactate levels dramatically decreased after 10 minutes of resting, although they continued to rise in the tissue.

During exercise, the lactate/glucose ratio remained fairly stable, despite small fluctuations in the individual metabolite levels; this marker is a much clearer indicator of the overall trends than either metabolite alone. The stability of the lactate/glucose ratio during increasing exercise intensity could serve as an indicator of the ability of the body to regulate its response during intense exercise in order to meet the extra energy demands. In this case, as exertion increased the local blood supply was sufficient to maintain local glucose levels and to remove excess lactate.

After about 10 minutes of resting, there was a sharp decrease in the local glucose levels and an increase in lactate levels, leading to a steep increase in the lactate/glucose ratio. One possible explanation for this could be that the blood supply had returned to normal, reducing the local glucose delivery, while local usage remained elevated. After resting for half an hour, the lactate/glucose ratio began to return to normal. The time needed for levels to return to normal could possibly serve as a marker of fitness.

7.3.3.4 Summary

Histograms summarising average metabolite levels for each cyclist at the main stages during the cycling protocol are shown in figure 7.16.

7. ATHLETE MONITORING: THE BIOANALYTICAL PROBLEM

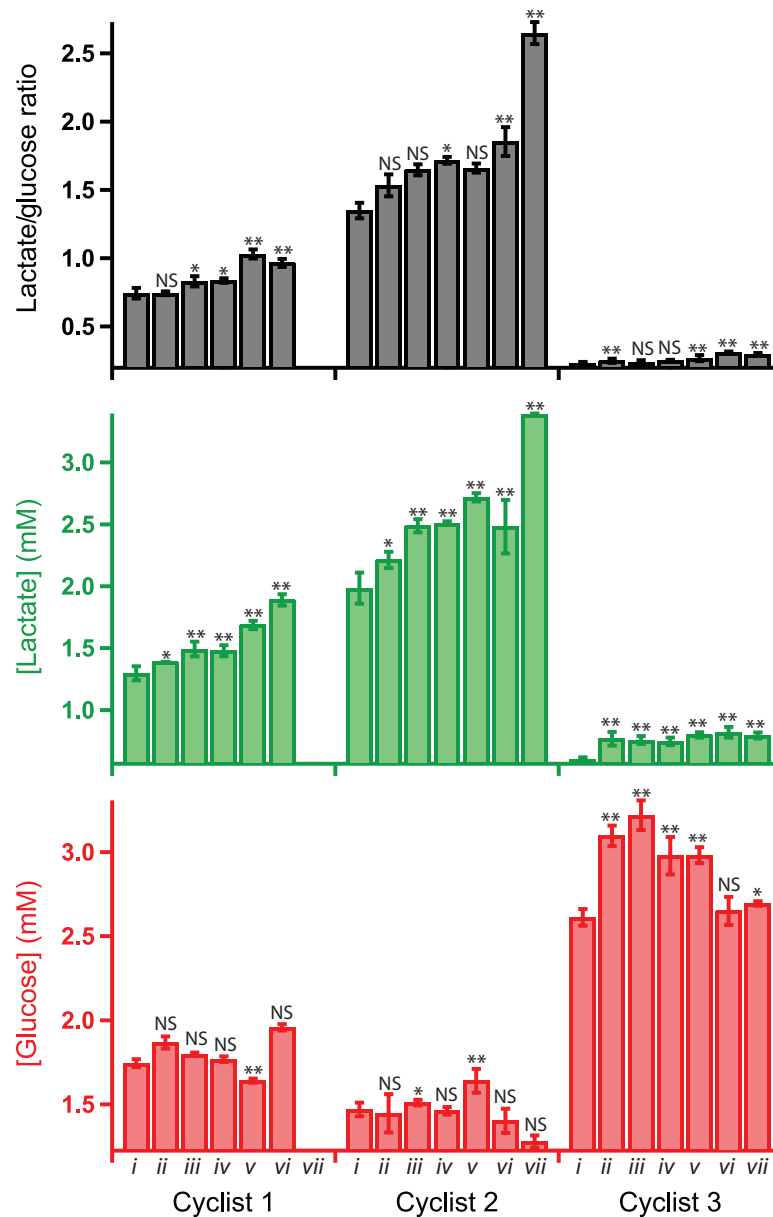


Figure 7.16: Dialysate levels during key points in cycling protocol. Dialysate lactate levels are shown in green, dialysate glucose levels in red and the lactate/glucose ratio in black for each of the three cyclists at (i) baseline, (ii) midway through warm-up stage, (iii) midway through medium-intensity stage, (iv) midway through high-intensity stage, (v) after sprint, (vi) after warm-down stage and (vii) after 10 min recovery, where data available. Time points correspond to labels in the cycling protocol in figure 7.2. A Mann-Whitney U test was used to assess changes compared to baseline at each stage (n=3, except baseline where n=10). NS=not significant, * p<0.05, ** p<0.01.

There is a clear trend in the local lactate concentration, with levels elevated after intense exercise and remaining so even after exercise has stopped. However, the glucose trend is less clear across all three cases. The lactate/glucose ratio showed a similar trend to that of lactate, with levels rising after intense exercise and remaining higher than baseline even after exercise had stopped. The magnitude of the lactate/glucose ratio for cyclist

3 is much lower than that for the other two cyclists and levels did not seem to change much during exercise. Interestingly, after a longer recovery time than is represented here, the ratio dramatically increased (see figure 7.15). As this was the only case in which the recovery period was extended it is not possible to draw conclusions from this result, but it suggests that this would be an interesting period to monitor for future studies.

7.3.4 Results: online biosensors

Dialysate was analysed online using two methodologies, as described in section 7.3.1. The dialysate flowed through a microfluidic chip containing glucose and lactate biosensors and then to the rsMD system, enabling comparison of the online biosensor results with that of the gold-standard rsMD analysis system. As a result of technical problems, only two of the three cyclists were monitored using both methodologies. A comparison of the results obtained for the two methods is shown in this section.

Dialysate levels obtained simultaneously using rsMD and online biosensors during two cycling protocols are shown in figures 7.17 and 7.18. The results have been time-aligned for comparison.

The absolute concentrations obtained were slightly different for the two methods, although levels were in fairly close agreement. One cause of variability between the two analysis methods could be that the biosensors are more susceptible to movement. In particular, when the cyclist got on and off the bike, the sensors could have been knocked and moved within the channel. This could have led to changes in the sensitivity of the sensors and hence the calculated concentrations could be inaccurate. In addition to this, these biosensors are flow rate dependent and are calibrated at $1 \mu\text{l}/\text{min}$. However, if the flow rate coming from the probe was less than this, possibly as a result of partially occluded tubing or of pressure on the membrane inside the tissue, this could have led to inaccurate interpretation of the results. The measured lag time generally differs to that calculated, therefore there may be a discrepancy between the specified and the actual flow rates. For the rsMD assays, which are not flow dependent, because of the nature of the flow injection system, this would result in an error in the lag time but not in the observed current, which could lead to differences between the two methods.

Despite the slight discrepancy in the absolute values obtained using the two methods, the overall trends are in close agreement, with many of the main features evident in both sets of data. Moreover, results obtained using the online biosensors showed better time resolution as individual features were more resolved.

7. ATHLETE MONITORING: THE BIOANALYTICAL PROBLEM

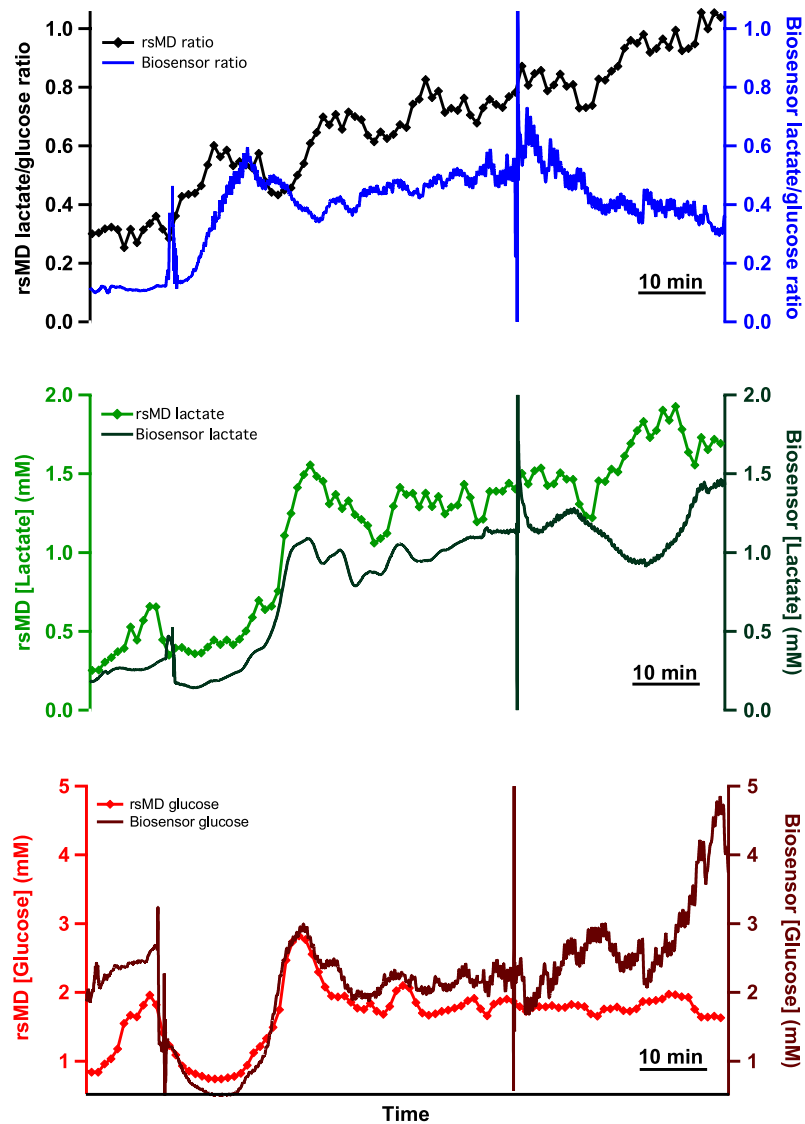


Figure 7.17: Dialysate metabolite levels for cyclist 1 obtained by rsMD and online biosensors. The light green and light red traces show dialysate lactate and glucose concentrations, respectively, obtained using rsMD. The black trace shows the corresponding lactate/glucose ratio obtained using the rsMD system. Data were obtained in real time, with a point every minute for each metabolite. The dark green and burgundy traces show dialysate lactate and glucose concentrations, respectively, measured using online biosensors. The blue trace shows the corresponding lactate/glucose ratio obtained using online biosensors. Data were obtained in real time and are smoothed with a Savitsky-Golay 201-point filter. All data has been time-aligned for comparison.

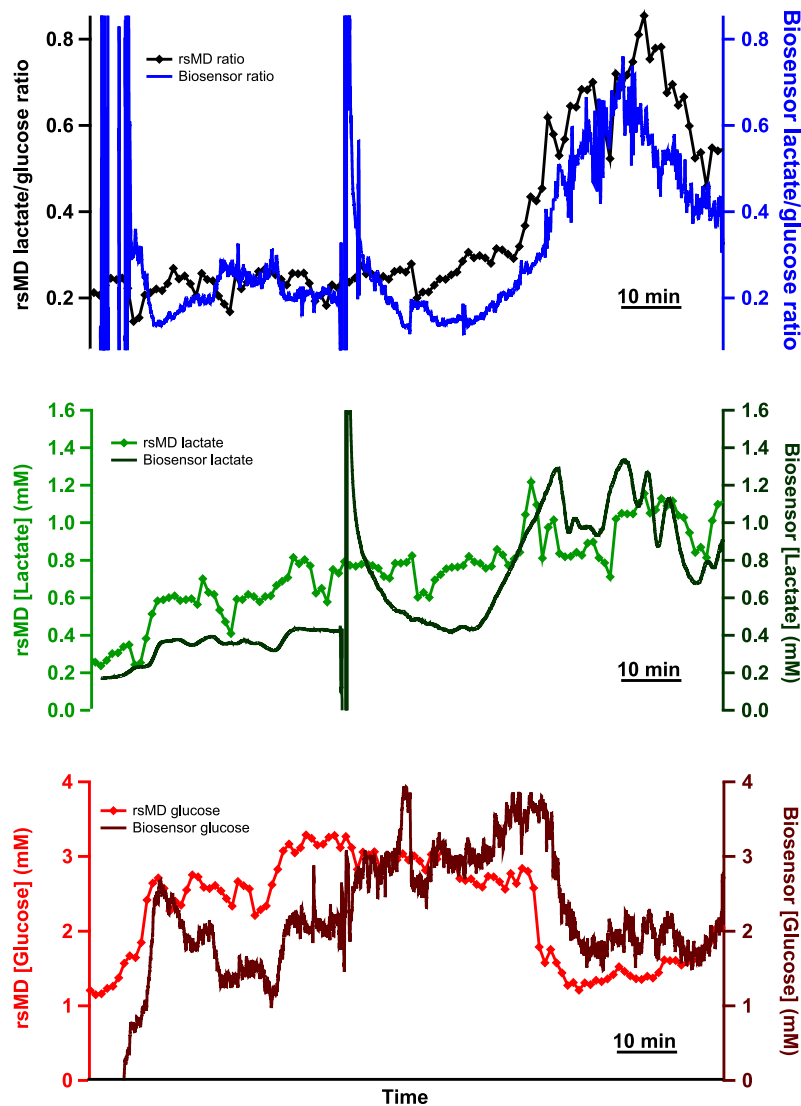


Figure 7.18: Dialysate metabolite levels for cyclist 3 obtained by rsMD and online biosensors. The light green and light red traces show dialysate lactate and glucose concentrations, respectively, obtained using rsMD. The black trace shows the corresponding lactate/glucose ratio obtained using the rsMD system. Data were obtained in real time, with a point every minute for each metabolite. The dark green and burgundy traces show dialysate lactate and glucose concentrations, respectively, measured using online biosensors. The blue trace shows the corresponding lactate/glucose ratio obtained using online biosensors. Data were obtained in real time and are smoothed with a Savitsky-Golay 201-point filter. All data has been time-aligned for comparison.

7.3.5 Conclusion

This chapter described a preliminary study to specify the characteristics necessary for a wearable device to monitor cycling athletes. In conclusion, it was possible to detect dialysate metabolite levels during the baseline resting phase and in response to increasing

7. ATHLETE MONITORING: THE BIOANALYTICAL PROBLEM

exercise intensity using a microdialysis flow rate of 1 $\mu\text{l}/\text{min}$. Online analysis proved much more suitable for subcutaneous monitoring of glucose and lactate levels in real time as it enabled events to be assigned as they happened.

This preliminary study has enabled a strict protocol to be defined for future monitoring experiments in order to improve the quality of the data obtained. For instance, it is important that during the initial resting period the cyclist remains still so that stable baseline levels can be measured. In addition, the regular stops to take blood measurements during exercise led to fluctuations in the data; therefore, blood measurements need to be taken without interrupting the exercise. These results have also demonstrated the need to extend the monitoring time after exercise has stopped as data observed in this time may provide information about the fitness of the athlete and their ability to recover after intense exercise.

Preliminary results with on-chip biosensors have shown that glucose biosensors and polyurethane-coated lactate biosensors are able to detect glucose and lactate levels in human dialysate samples. There were some discrepancies between the absolute values measured by the online biosensors and the rsMD system but levels were similar and general trends were in close agreement.

However, there are several limitations with the current monitoring system. The delay between the changes occurring in the tissue and the analysis system was relatively long as a result of the length of outlet tubing that was needed to reach the clinical trolley holding the analysis system and the low flow rates used. Ideally the data needs to be as close to real-time as possible; this delay could be substantially reduced if the analysis system could be placed nearer to the outlet of the microdialysis probe. The soft PDMS chip would be impractical as a wearable device as movement of the athlete during exercise could result in repositioning of the biosensors inside the microfluidic channel, which would make it necessary to re-calibrate the system. Moreover, biosensors are currently positioned inside the channel using manual judgement, which can be very difficult; it is time-consuming as it involves trial-and-error, it could damage the biosensor and it requires experience. Therefore, for a robust wearable device, the biosensors would need to be easily and reproducibly secured in place inside the channel without leaks occurring.

The current method of connecting the probe outlet to the analysis system, as described in section 7.3.1, was difficult to do without piercing the tubing with the needle, especially under time pressure. Therefore, the wearable device would need to be designed to incorporate an easy and reproducible connection to the microdialysis probe. In addition, the measured lag time was not equal to that calculated, possibly due to a discrepancy in the microdialysis flow rate. An additional benefit of a wearable system that can be placed close to the probe outlet is that this should reduce the back pressure on the membrane, if this is the cause of the discrepancy.

Chapter 8

Athlete monitoring: a wireless microfluidic device

This chapter follows on from chapter 7 and presents the development of a wearable microfluidic device that integrates with a commercial microdialysis probe and incorporates glucose and lactate biosensors for online monitoring of tissue metabolites during cycling. The requirements of the device design were informed by the preliminary studies discussed in chapter 7.

8.1 Introduction

8.1.1 Wearable microfluidic device

Initial results from online monitoring of subcutaneous dialysate glucose and lactate levels before, during and after exercise have shown that this methodology could provide important information about an athlete's performance during physical activity, and about their ability to recover afterwards. However, the system presented in chapter 7 is large and impractical for this application; it can only be used if the athlete is stationary and, because of its size, a long length of connection tubing has to be used to feed the dialysate into the analysis system, leading to a delay in obtaining the data, as well as causing smearing of the response as a result of Taylor dispersion. The delay between the microdialysis probe and the analysis system can be greatly reduced if the analysis system is miniaturised and developed into a wearable device, enabling closer to real-time measurement. This would also make the system more practical and more versatile for sports monitoring.

The use of microfluidic devices combined with microdialysis has proved popular, as they are able to reliably manipulate the small sample volumes produced during continuous microdialysis sampling (284, 285). Microfluidic devices have conventionally been

8. ATHLETE MONITORING: A WIRELESS MICROFLUIDIC DEVICE

fabricated using rapid prototyping methods, such as soft lithography. PDMS-based microfluidic devices in particular have proved popular because of their ease of fabrication and their ability to make an effective seal. PDMS chips have been extensively used within our group to house biosensors for online dialysate analysis (69, 286). In clinical use, the PDMS-needle biosensor system is placed on a clinical trolley near the patient and requires 1 m of connection tubing between the probe and the analysis system. At 1 $\mu\text{l}/\text{min}$, this long connection tubing leads to a 26 minute lag time before analysis and a smeared temporal response as a result of Taylor dispersion (101).

The needle-PDMS biosensor system involves manual positioning of the needle electrode biosensor inside the PDMS chamber. This can be very difficult; if the biosensor is placed too near the bottom of the chip, no current response is observed, but, if the biosensor is recessed, slow diffusion of the analyte results in a long response time (286). Furthermore, this system is not suitable for a wearable device as movement during exercise could lead to repositioning of the biosensor in the microfluidic channel. These observations necessitate the development of a robust device that can be placed close to the microdialysis probe outlet and that incorporates biosensors as easily replaceable modules, reproducibly and securely positioning them in the correct position inside the channel.

In recent years, the use of 3D printing for the fabrication of microfluidic devices has proved popular (287, 288, 289, 290, 291) as it enables fabrication of a rigid and re-usable microfluidic device in one step (292). A significant advantage of 3D printing is the dimensional control it offers, enabling integration of the printed device with commercially available components (287). Moreover, 3D printing enables a flexible, modular approach to the design of the device, facilitating fabrication of a multi-component system. Each part can be designed to meet exact requirements and design modifications can be made in an iterative manner, allowing modifications to be made quickly and easily and for their influence on the device performance to be evaluated (287, 292).

Erkal *et al.* recently described the fabrication of 3D printed microfluidic devices with integrated electrodes that could be removed and re-used (287). The electrodes were housed inside commercial flangeless fitting nuts, which could be threaded into microfabricated receiving ports on the device.

On this basis, 3D printing is an ideal fabrication method for the development of the microfluidic wearable platform, as it facilitates the design and the fabrication of a custom microfluidic device that can be directly integrated with the outlet of a clinical microdialysis probe. In addition, it allows modular incorporation of biosensors securely and reproducibly inside the microfluidic channel, without the need for adhesives, allowing them to be removed for repolishing and re-use.

This chapter describes the development of a 3D printed microfluidic device that combines directly with a clinical microdialysis probe. The device incorporates removable

needle type biosensors and can be used for continuous online monitoring of dialysate metabolite levels.

8.1.2 Device requirements

On the basis of the initial experiments carried out in chapter 7, a clearer picture of the requirements for a robust wearable device were obtained. These are listed below.

- Easy and reliable connection to commercially available microdialysis probe outlet
- Reproducible placement of biosensors in flow stream
- Biosensors held securely in place, without leaking
- Removable biosensors so that they can be repolished and re-used
- Fast response time of biosensors to concentration changes
- Easy connection to calibration board

A diagram summarising the requirements for our microfluidic device is shown in figure 8.1. Design and fabrication of the wearable microfluidic device was carried out in collaboration with Dr Vincenzo F. Curto and Prof. Guang-Zhong Yang, and rendering of the 3D designs in SolidWorks[®] were made in collaboration with Mr Carlo A. Seneci. Several 3D printed designs were tested before all device requirements were met. This section will describe these designs in detail.

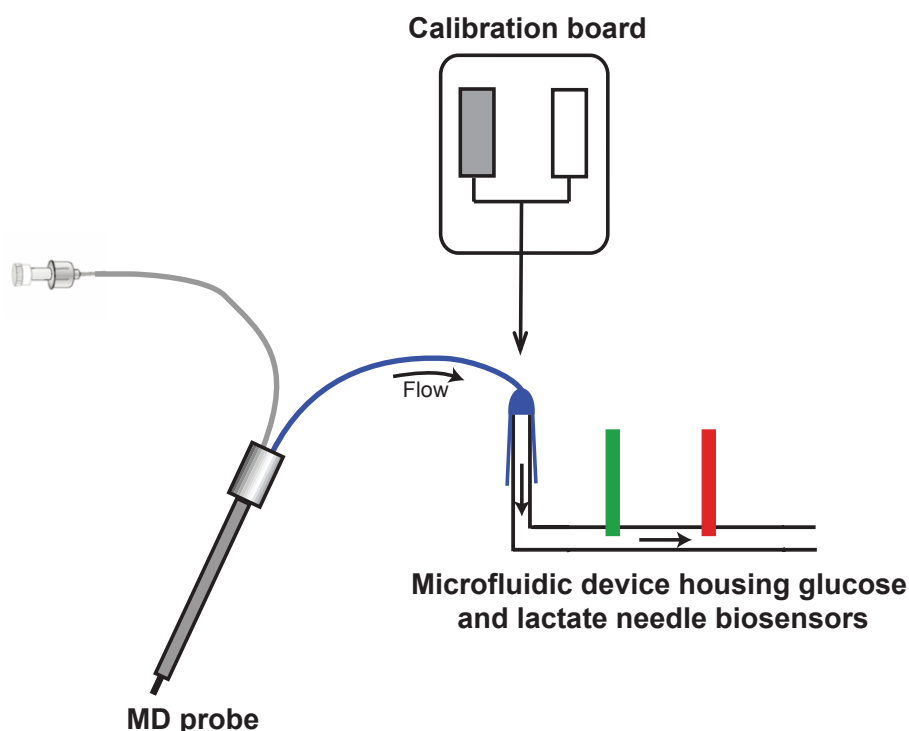


Figure 8.1: Schematic of wearable microfluidic device. The microfluidic device will connect to the outlet of the microdialysis (MD) probe and will hold a glucose and a lactate biosensor securely in position inside the channel. It will also allow easy connection to the calibration board.

8.2 Design and fabrication of microfluidic device

Devices were designed using SolidWorks[®] 2014, which creates parts as .STL files.

For this work, two different 3D printers were used for fabrication of the microfluidic platform. The microfluidic chip was printed using an ULTRA[®] 3SP[™] 3D printer, which has a resolution of 100 μm in the x- and y-axes and between 25-100 μm in the z-axis, depending on the parameters set. However, in reality the printer resolution is determined by the voxel dimension and the material used during fabrication. The ABS 3SP[™] White resist was used for fabrication of all versions of the microfluidic chip, as it allows printing of components that are dimensionally and mechanically stable. However, as a result of shrinkage during polymerisation, the dimensions observed were smaller than those specified in the design of the microfluidic channel. It was determined that a tolerance of about 100 μm should be factored in to the design of any components printed in this way.

The biosensor holders fabricated in design 1 of the microfluidic device were also printed using ABS 3SP[™] White resist and the ULTRA[®] 3SP[™] 3D printer. However, the biosensor holders employed for designs 2-4 were printed using the Objet260 Connex[™] 3D printer. This printer was chosen in this case, because of its ability to simultaneously

print both hard and soft plastics onto the same component. In this case, VeroWhitePlus (RGD835) and TangoBlack (FLX973) were used for printing of the rigid and soft parts, respectively.

8.3 Microfluidic device: design 1

Commercially available clinical microdialysis probes have a vial holder at the outlet, into which a microvial can be connected for sample collection in conventional microdialysis, as shown in figure 8.2. Our custom microfluidic device was based around this concept and was designed so that the microfluidic chip would slot into the vial holder instead of the microvial to allow easy connection to the microdialysis probe. In order to achieve this, the microfluidic chip was designed and printed with an L-shape, the vertical arm of which was designed to mimic the geometry of the microvial, to ensure a good fit with the probe outlet holder, as shown in figure 8.3. The microfluidic inlet port was also designed so that it could incorporate the rubber insert from the microvial to take advantage of this easy and leak-free connection approach. The connection between the microfluidic chip and the probe outlet worked very well, with no leaks occurring over hours of operation.

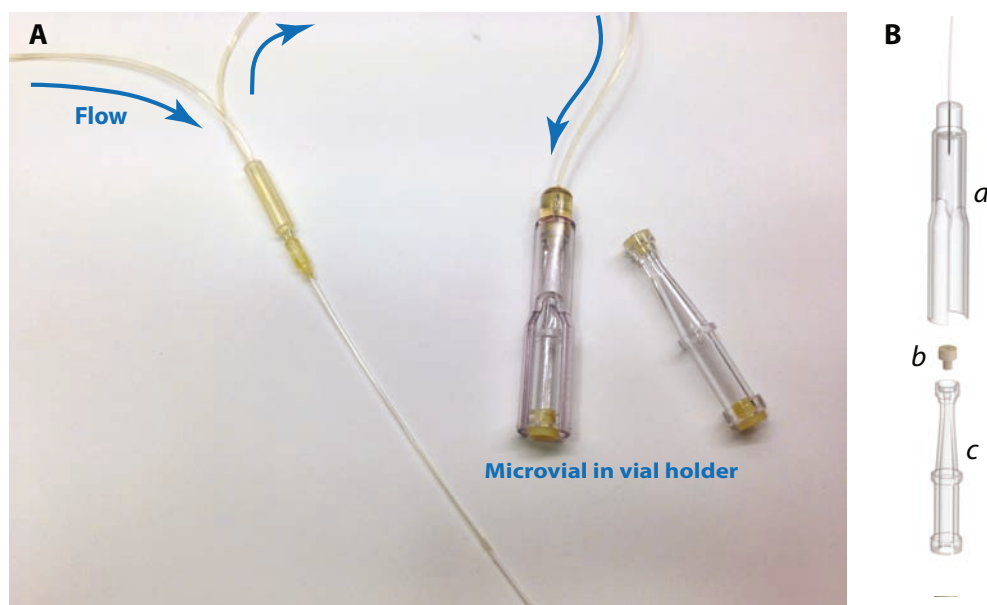


Figure 8.2: Conventional setup of commercial microdialysis probe. *A.* A microvial is inserted into the vial holder at the probe outlet to collect the dialysate sample. *B.* Schematic showing the probe outlet holder (*a*), the rubber insert of the microvial (*b*) and the microvial (*c*).

A major challenge with the design of a rigid microfluidic device is the issue of incorporating and securing the biosensors in the correct position inside the microfluidic channel without any leaks occurring. The horizontal arm of the microfluidic chip was used for

8. ATHLETE MONITORING: A WIRELESS MICROFLUIDIC DEVICE

integration of the biosensors. As it was necessary to integrate two separate needle biosensors, one for glucose and the other for lactate sensing, into the microfluidic chip, two round openings were printed onto the top wall of the microfluidic channel, creating a compact device. In the initial design, attempts were made to integrate the biosensors using commercially available fittings that could be tightened to secure the electrode in place inside the microfluidic chip and to prevent leaks occurring (287). This method also ensured that, because of the design of the microfluidic chip, the sensors could be held in a fixed position, which was defined by the fitting.

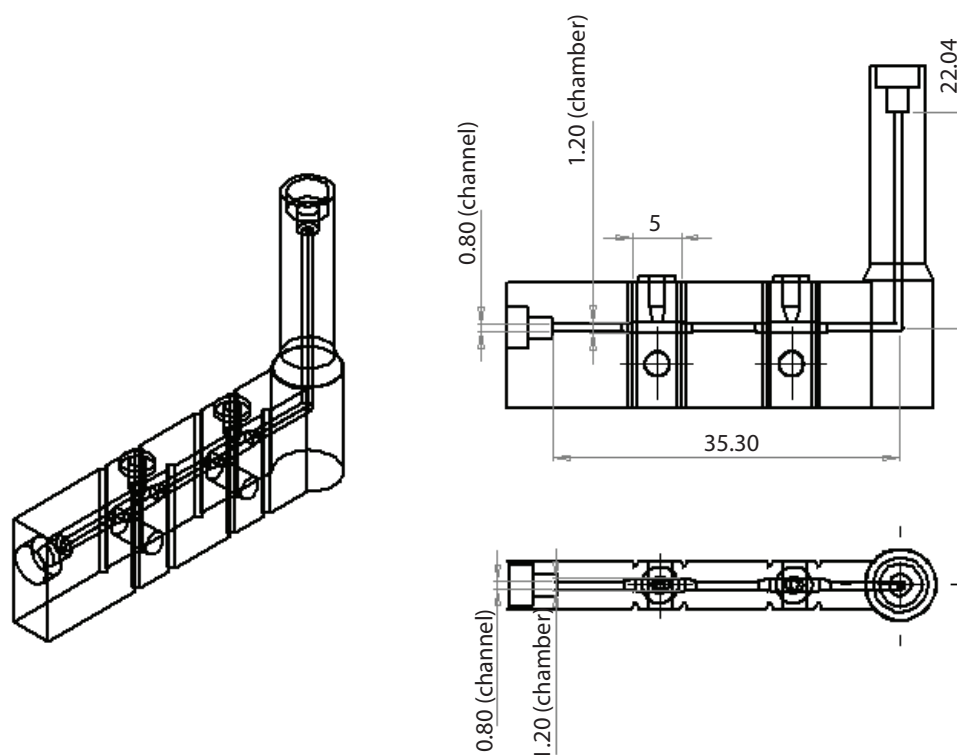


Figure 8.3: Schematic diagram of design 1 of microfluidic chip. *Left* shows 3D diagram of microfluidic chip. *Right (top)* shows side view of microfluidic chip and *Right (bottom)* shows top view of microfluidic chip with key dimensions of microfluidic channel and electrode chamber given in mm.

LabSmith fitting holder

The needle electrodes were secured in place inside the microfluidic chip using 1/32" LabSmith one-piece fittings (360 μm inner diameter (ID)), which successfully gripped the electrode when tightened. The height of the channel inside the microfluidic chip was designed such that, when tightened, the tip of the fitting would be positioned in the middle of the channel. The needles were placed inside the fitting so that the tip was flush with the end of the fitting and were held in place with parafilm, as shown in figure 8.4. The dimensions were determined by the size of the fittings and as such were relatively large, as

shown in figure 8.3. Therefore, two slightly wider chambers (1.2 mm) were incorporated into the microfluidic channel at the two biosensor insertion locations to accommodate the fittings while maintaining smaller dimensions for the rest of the channel (0.8 mm) in order to reduce the overall volume of the device. The receiving ports, into which the fittings would be inserted, were originally printed as hollow cylinders and the threads for the fittings were made later using a thread taper (M2.5). Erkal *et al.* used commercially available fittings to integrate electrodes into a 3D printed microfluidic device, in which the threads were printed onto the receiving port. However, because of the small size of our sensor, a 1/32" fitting was required and the threads were too small (2-56 UNC) to be printed.

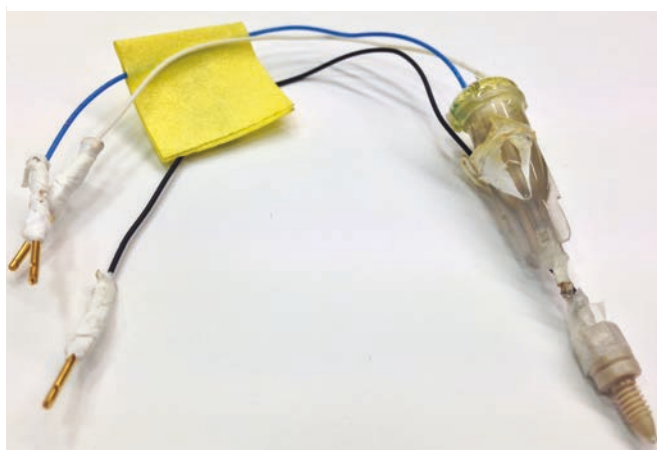


Figure 8.4: Needle electrode placed inside LabSmith one-piece fitting. The needle was positioned so that the tip was flush with the end of the fitting. Parafilm stabilised the construct.

The electrode was polished until a satisfactory cyclic voltammogram (CV) was obtained and then secured in place inside the fitting so that the needle tip was flush with the end of the fitting. It was important to secure the fitting in place before carrying out any further functionalisation of the electrode as the process of inserting the needle into the fitting might otherwise have damaged the enzyme layer and the poly(*m*-phenylenediamine) (mPD) film. Once the fitting was secured in place, the electrode was coated with the mPD and enzyme layers, as described in section 2.5.3.2. The lactate biosensor was also coated with a further polyurethane layer to extend its detection range. These biosensors showed good calibration curves when tested in a stirred beaker (data not shown), proving that it was possible to fabricate biosensors inside the fittings.

When flushing the microfluidic chip, liquid was initially found to leak around the fittings, even when fully tightened. This occurred because the fitting did not grip the electrode securely enough as it was not possible to incorporate a conical receiving port into the microfluidic chip. This issue was addressed by wrapping polytetrafluoroethylene

8. ATHLETE MONITORING: A WIRELESS MICROFLUIDIC DEVICE

(PTFE) thread seal tape around the fittings and also around the needle before it was inserted into the fitting. With repeated tightening and loosening, the parafilm stabilising the construct was not sufficient to hold the fittings in place and they began to come loose from the electrodes, so that the position of the electrode inside the channel was no longer well defined.

Custom electrode holder

To overcome the issue of electrode movement, a custom electrode holder was designed (figure 8.5). The fitting was still used to make a seal with the microfluidic chip but it was held inside the holder to stabilise the construct. Using this design, the electrode was threaded through the holder first and then through the fitting (same as previously), which slotted into place inside the holder (figure 8.5B). The inside of the holder was designed to have a hexagonal shape, as shown in figure 8.5C, mimicking the shape of the fitting, so that it could be used to tighten the fitting inside the microfluidic chip.

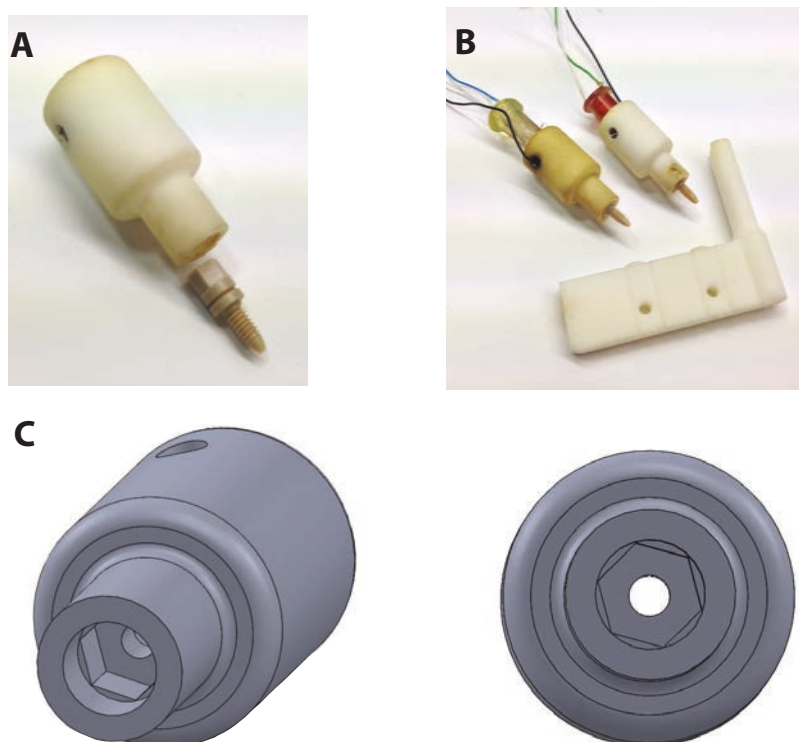


Figure 8.5: Design 1 of the microfluidic device with electrode holders. *A.* The fitting was secured in place inside the electrode holder. *B.* The needle electrode was threaded through the electrode holder and then through the fitting. The electrode secured inside the holder could then be screwed into the microfluidic device. *C. Left* 3D representation of the holder into which the one-piece fitting was secured. *Right* Bottom view of electrode holder to show the hexagonal shape that could be used to tighten the one-piece fitting.

Grub screws were used to hold the fitting (with electrode) in place inside the holder

so that the needle tip was flush with the end of the fitting, as shown in figure 8.5. The counter electrode lead was threaded out through a hole in the side of the holder.

An initial test was carried out to check the response time of lactate and glucose biosensors inside the microfluidic chip. This was carried out using a LabSmith calibration board, as described in section 3.2.3. A vial holder was removed from the end of a microdialysis probe and connected to a short piece of fluorinated ethylene propylene (FEP) tubing (2 cm) using a tubing adaptor. This in turn was connected to the outlet tubing of the calibration board using a union adaptor (LabSmith, US) to connect the two different size tubings with minimal dead volume. This allowed the device to be reliably connected to either a microdialysis probe or to the calibration board.

At 1 $\mu\text{l}/\text{min}$, the T_{90} response time of the lactate sensor, which was placed first in the direction of flow, to a step change in concentration from 0 to 4 mM was 664 ± 3 s ($n=3$), and that of the glucose sensor, which was placed after the lactate sensor, was 761 ± 17 s ($n=3$). This response time proved far too long for this application and was attributed to the relatively large internal volume of the microfluidic chip, leading to smearing of the concentration step change, as described in the following section 8.6. In this design, the channel height was determined based on the dimensions of the fitting in order to keep the fitting and therefore the sensor in the middle of the channel. Therefore, it was not possible to reduce the channel size any further using this fitting. In addition, this approach did not provide a satisfactory seal with the microfluidic chip, causing leaks to occur. For later versions of the microfluidic device, custom-made electrode holders were designed and fabricated, which allowed the electrode to be secured in place inside the microfluidic channel without the need for the fitting.

8.4 Microfluidic device: design 2

The use of 3D printing to design and fabricate the device enabled it to be made using a modular approach, consisting of separate parts integrated together. Using this method, each part of the device could be designed to meet its own individual requirements. The means of connecting the microfluidic chip to the microdialysis probe remained the same for the second design, as this worked well and provided an easy and leak-free connection between the two. However, the design for the electrode holders needed to be adapted in order to reduce the internal volume of the device and to provide a better seal between the electrode holder and the microfluidic chip.

The electrode holders were designed so that the needle tip protruded from the end and the needle was secured in place using two grub screws. The needle position inside the holder could be varied depending on the length of the needle, which can change after repeated polishing of the electrode. This ensured that the needle tip was at a fixed distance

8. ATHLETE MONITORING: A WIRELESS MICROFLUIDIC DEVICE

from the end of the electrode holder and at a fixed height inside the microfluidic channel. The design of the microfluidic chip was also adapted so that the holder and therefore the biosensor could be guided into position; two pegs on the sides of the electrode holder threaded into helical guiding slots on the top wall of the microfluidic chip and locked into place, precisely positioning the needle tip inside the channel. Details of the microfluidic chip design are shown in figure 8.6. Integration of the biosensors into the microfluidic chip using this approach ensured that the overall packaging of the microfluidic device was compact, but it limited the minimum width of the microfluidic channel, as it had to fit the 27 G needle (outer diameter (OD) = ca. $413 \mu\text{m}$) biosensors.

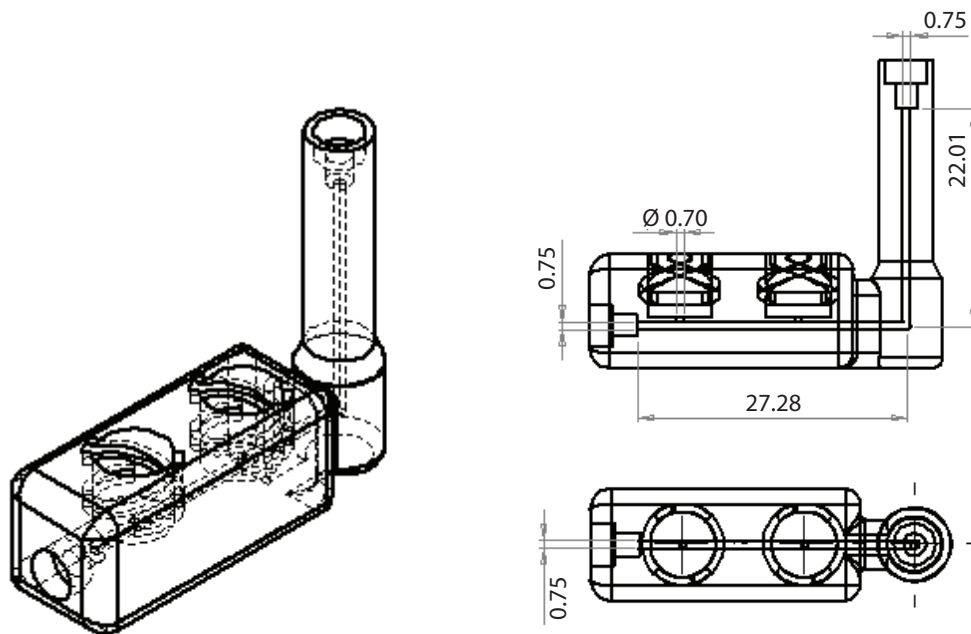


Figure 8.6: Schematic diagram of design 2 of microfluidic chip. *Left* shows 3D diagram of microfluidic chip. *Right (top)* shows side view of microfluidic chip and *Right (bottom)* shows top view of microfluidic chip, with key dimensions of microfluidic channel given in mm.

The holder was printed using an Objet260 ConnexTM 3D printer, capable of printing both hard and soft plastic on the same component. This enabled the base of the holder to be printed using a soft, compressible plastic, providing a good seal between the holder and the microfluidic chip and preventing potential leaks. In this case VeroWhitePlus (RGD835) and TangoBlack (FLX973) were used for printing of the rigid and soft parts, respectively. As shown in figure 8.7, the soft part of the electrode holder had a truncated cone shape (OD= 6.2 mm and H=1.3 mm) in order to guarantee a good seal between the electrode holder and the microfluidic chip. Initially, a cylindrical shaped soft part was tested. However, this led to incorrect positioning of the needle biosensor, as the soft part expanded radially in the x-y direction when compressed.

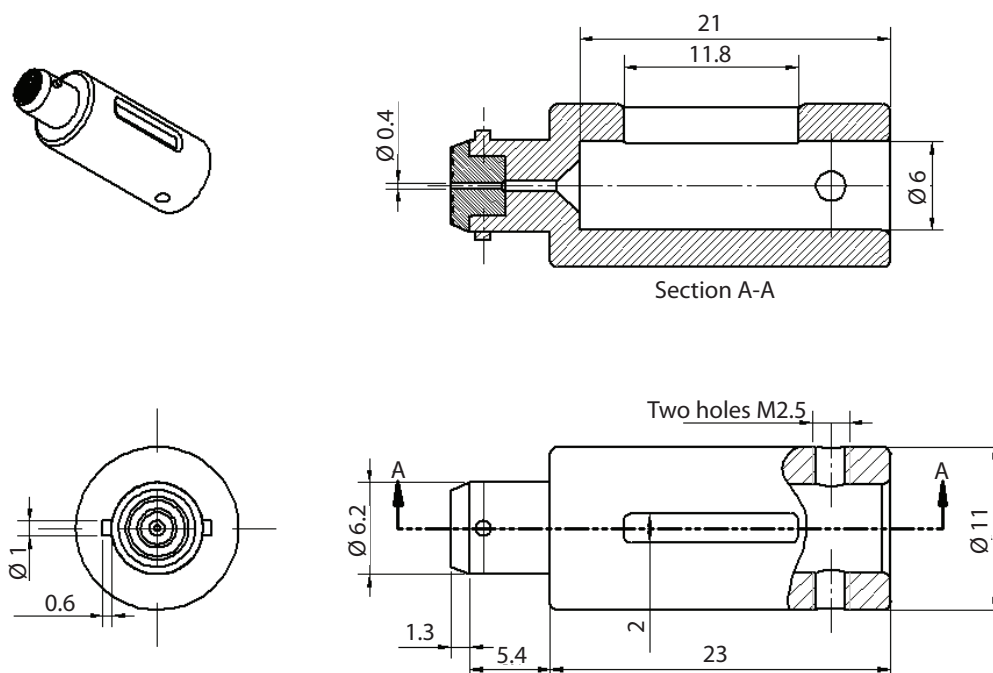


Figure 8.7: Detailed schematic of needle holder. The needle holder has a soft, compressible plastic at the tip, which can form a seal with the microfluidic chip. Pegs at the side of the holder are used to guide the holder and therefore the electrode into place inside the microfluidic channel. The needle electrode was placed inside the holder and two grub screws (M2.5) were tightened to fix the electrode in place. A slot was added to the side so that the counter electrode wire could be threaded through. All measurements given are in mm.

Using this methodology, many holders could be printed in one run of the 3D printer and kept as spares, and each holder could be used multiple times. However, it was found that, after repeated use, the soft plastic no longer formed a good seal with the microfluidic chip, causing leaks to occur. A picture of the needle holder and the microfluidic chip is shown in figure 8.8.

In order to allow precise positioning of the needle electrode inside the channel, an additional cross-sectional cut-out of the microfluidic chip was printed (figure 8.9). Using this cut-out, it was possible to visualise the electrode inside the channel under a microscope, enabling the sensors to be precisely secured inside the holders so that the tip of the biosensor was at the correct height inside the microfluidic channel.

Once a satisfactory CV was achieved, the electrode was placed inside the holder so that the needle protruded as far out as possible. The electrodes were then functionalised by coating with an mPD film and an enzyme layer, as described in section 2.5.3.2. The lactate biosensor was also coated with a further polyurethane layer to extend its detection range. The sensors were then precisely positioned inside the holders under a microscope, using the cross-sectional cut-out to determine the appropriate distance from the end of the holder that would set the tip of the biosensor at the desired height inside the channel. The

8. ATHLETE MONITORING: A WIRELESS MICROFLUIDIC DEVICE

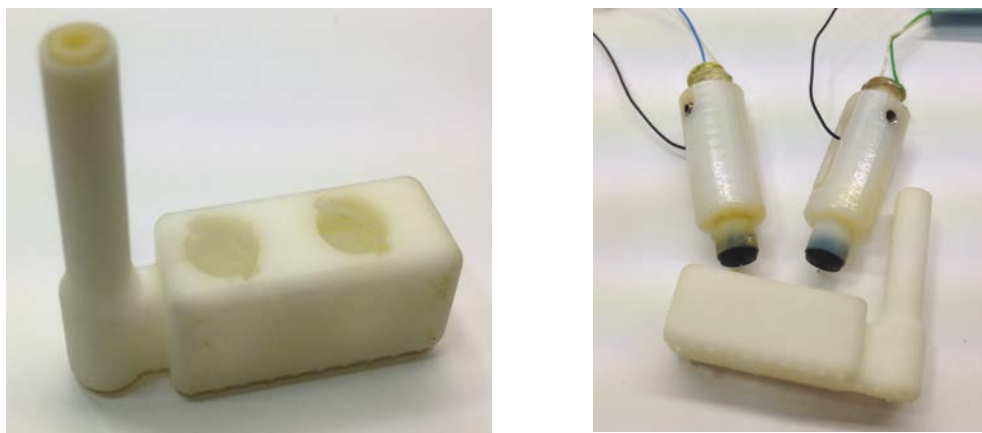


Figure 8.8: Design 2 of the microfluidic chip with electrode holders. *A.* The microfluidic chip was adapted so that the new electrode holders could be guided and locked into place. *B.* The needle electrodes were secured in position inside the electrode holders so that the tip protruded a fixed distance. Two holders could be screwed into the microfluidic chip.

sensors were secured in place inside the holder. As the soft plastic is compressed when the holder is locked into place this is the most accurate method of positioning the electrode inside the channel; it would not be sufficient just to fix the electrode a set distance from the end of the holder each time, as the position of the electrode inside the channel would be altered depending on the compressibility of the soft plastic.

For this design, the T_{90} response time of a lactate sensor to a step change from 2 to 0 mM at $1 \mu\text{l}/\text{min}$ was measured with the electrode positioned both in the middle of the channel and also near the bottom to investigate the best position for the sensor inside the channel. When the sensor was in the middle of the channel, the T_{90} response time was $254 \pm 8.7 \text{ s}$ ($n=3$). When the sensor was at the bottom of the channel the T_{90} response time was much shorter at $175 \pm 4.9 \text{ s}$ ($n=2$). This shorter response time can be attributed to a higher linear flow rate past the electrode (figure 8.9C). Approximate calculations indicate an additional 11% occlusion of the cross-sectional area between an electrode positioned halfway and one positioned two-thirds of the way down the channel (figure 8.9C). On the basis of this result, the channel dimensions were re-designed to reduce the channel height and therefore to reduce the response time.

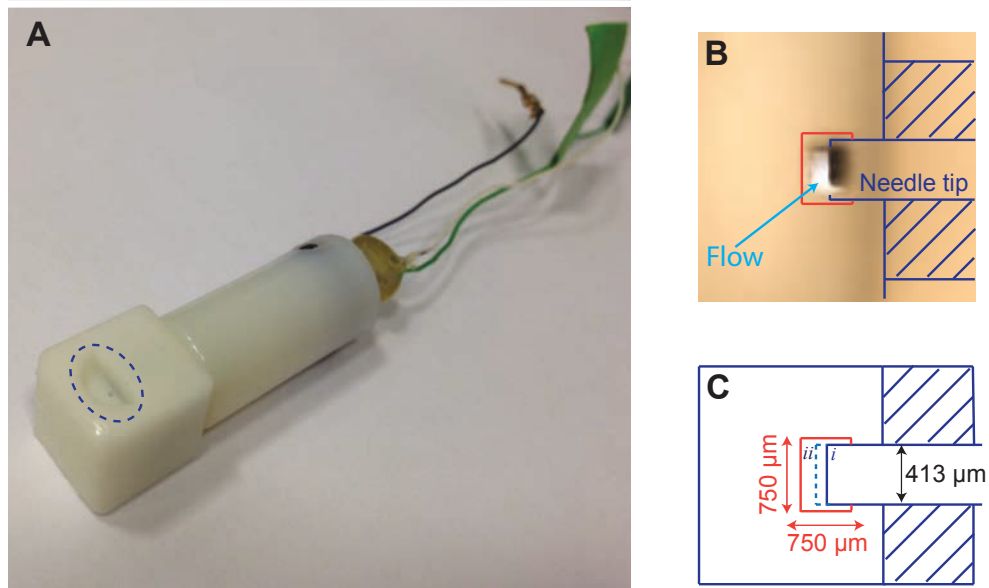


Figure 8.9: Cross-sectional cut-out of the microfluidic chip. For electrode positioning inside the microfluidic channel. *A.* The electrode holder, containing the needle biosensor, can be inserted into the cut-out part, as with the microfluidic chip. The needle position inside the channel can be visualised under a microscope so that the needle position can be adjusted and secured in place once the desired height has been achieved. *B.* Close-up image of the circled region in *A.* Shows the needle biosensor positioned in the middle of the channel. Direction of flow is perpendicular to the page. *C.* Schematic representation of the needle position inside the channel, (i) halfway down and (ii) two-thirds down from the top. Not drawn to scale.

8.5 Microfluidic device: design 3

The use of 3D printing for device fabrication allowed design changes to be made and implemented quickly, enabling the device to be adapted iteratively, until optimal features were obtained. In design 3, the following alterations were made:

- The nominal channel height was reduced from $750\ \mu\text{m}$ to $550\ \mu\text{m}$ to reduce the response time of the biosensors.
- The internal volume was reduced by cutting off the right angle (figure 8.10) and directly joining the two arms of the device and by reducing the length of the probe connection arm.

8. ATHLETE MONITORING: A WIRELESS MICROFLUIDIC DEVICE

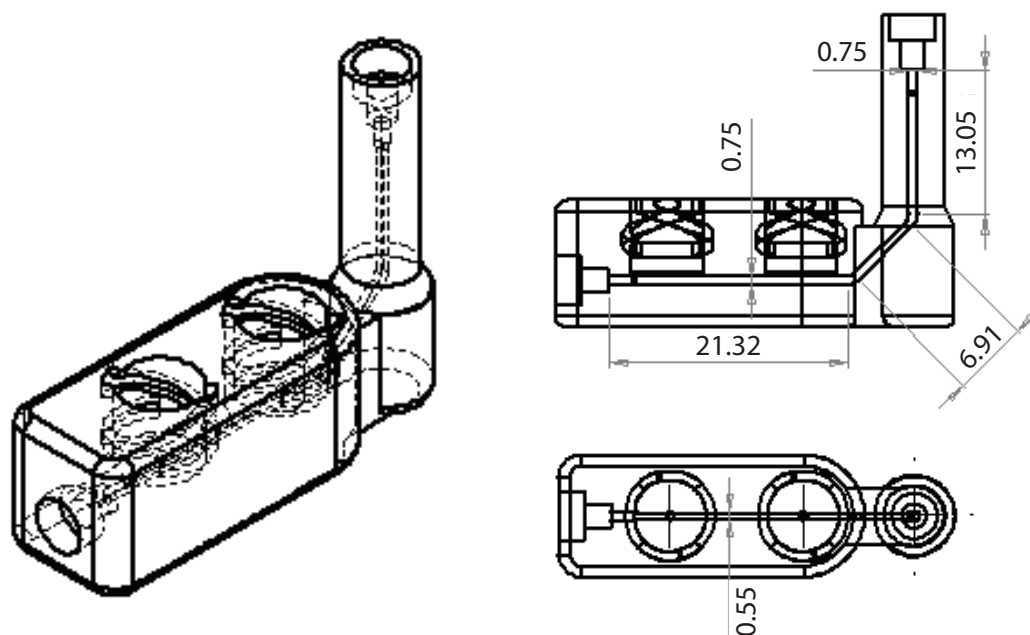


Figure 8.10: Schematic diagram of design 3 of microfluidic chip. *Left* shows 3D diagram of microfluidic chip. *Right (top)* shows side view of microfluidic chip and *Right (bottom)* shows top view of microfluidic chip, with key dimensions of microfluidic channel given in mm.

However, because of the shortened inlet structure on this design, the microfluidic chip no longer fit well inside the probe outlet holder, which meant that the needle was not able to fully pierce the rubber inlet, causing a build up of pressure and the probe membrane to leak. This problem could be overcome by modifying the outer shape of the inlet structure so that it could fit fully inside the probe outlet holder.

Using this microfluidic chip with the calibration board, the T_{90} response time of a lactate sensor to a step change from 0 to 2 mM at $1 \mu\text{l}/\text{min}$ with the sensor positioned near the bottom of the channel was $228 \pm 12 \text{ s}$ ($n=3$). Despite the reduced internal volume, this response time was actually slightly longer than for the previous design, but, this could be due to this lactate sensor being slower to respond to the concentration changes than the previous sensor.

In order to determine the optimal position of the sensor inside the channel, the position of both sensors was varied together. The T_{90} response time and change in current for a step change from 0 to 4 mM glucose and lactate was measured for comparison. The results are shown in table 8.1.

For the lactate biosensor, the T_{90} response decreased as the electrode was positioned further down the channel, occluding the channel more, as expected. The current observed for the lactate biosensor when it was positioned in the middle or at the bottom of the channel was the same, suggesting that, to a certain extent, the biosensor was not affected

8.6 Effect of channel size on biosensor response

Table 8.1: Effect of electrode position on biosensor response time (n=2). Fraction indicates the position of the electrode in the channel from the top.

Position	Glucose		Lactate	
	T ₉₀ (s)	Current (nA)	T ₉₀ (s)	Current (nA)
Bottom (3/4)	298 ± 3.5	0.80 ± 0.03	188 ± 7.1	0.96 ± 0.21
Middle (1/2)	266 ± 1.8	0.30 ± 0.01	171 ± 5.3	0.97 ± 0.03
Top (1/4)	283 ± 3.9	0.38 ± 0.03	226 ± 10.8	0.38 ± 0.06

by differences in flow, possibly as a result of the polyurethane outer film. However, the current was lower when the biosensor was positioned at the top of the channel, where linear flow rate would have been lowest. By contrast, the glucose biosensor showed more variability with electrode position, although it is not clear why.

These results indicate that the position of the electrode inside the channel has a huge impact on the sensor response. For uncoated biosensors, the results suggest that electrode positioning has a considerable effect on the observed response, but that near the bottom of the channel is optimal. For a polyurethane-coated biosensor, as long as the electrode is positioned past the middle of the channel then it appears to be invariant to flow. However, response time suggests the middle is preferable. The flow invariance of the polyurethane-coated biosensor presents a strong argument for its addition to both glucose and lactate biosensors, as it is difficult to accurately position the electrode and, without a polyurethane coating, the position seems to become critically important. As shown in section 3.4, the addition of the polyurethane layer results in a decrease in sensitivity compared with uncoated biosensors. However, the sensors were sensitive enough for this application (figure 8.14) and hence were implemented for all further designs.

8.6 Effect of channel size on biosensor response

The results from design 3 of the microfluidic chip showed that the response time was still relatively long. In order to investigate the effect of the microfluidic channel dimensions on the response time of the sensors, three different sizes of microfluidic channels were tested. These microfluidic channels had different height and width dimensions, which were: (1) 520 x 520 μm , (2) 750 x 550 μm and (3) 1000 x 550 μm (W x H). Allowing for shrinking of the material during the printing process, channel 1 was designed to include two slightly wider microfluidic chambers at the two needle biosensor insertion locations, as shown in figure 8.12, in order to prevent issues with biosensor placement. Smaller channels were also attempted but these were found to be blocked when tested.

Figure 8.11 shows the normalised current response for a glucose biosensor to a step change from 0 to 4 mM at 1 $\mu\text{l}/\text{min}$ for the different channel dimensions. In each case,

8. ATHLETE MONITORING: A WIRELESS MICROFLUIDIC DEVICE

the sensor was positioned in the middle of the channel. In reality, the channel dimensions were smaller than those specified in the design, as shrinking occurs during the printing process. Therefore, cross-sections of each channel were measured using a microscope to determine the actual dimensions of the channels. The measured dimensions are given in the table in figure 8.11.

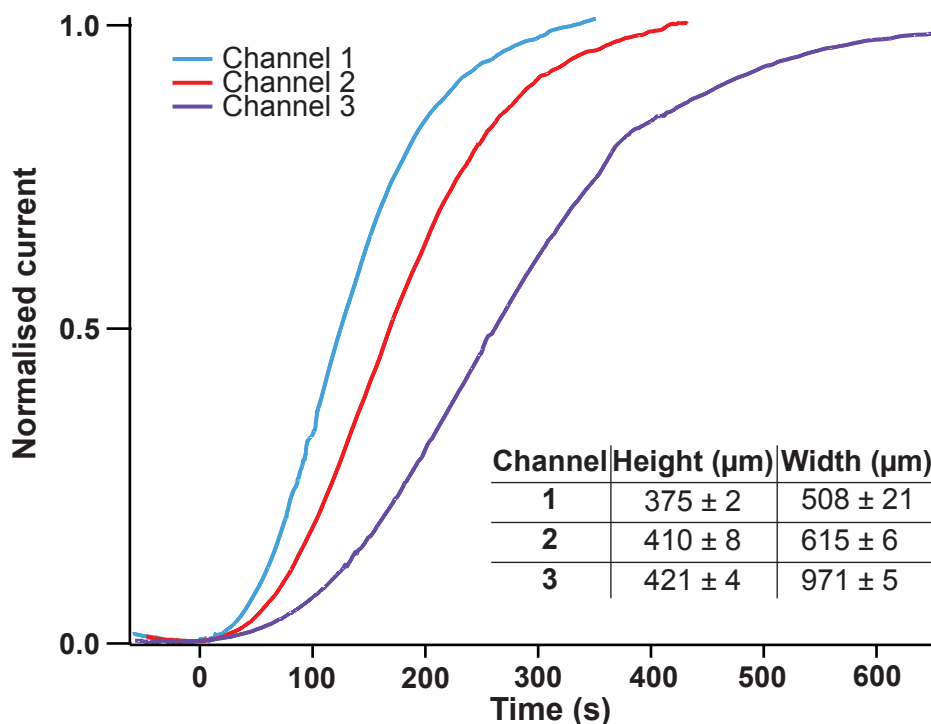


Figure 8.11: Comparison of concentration step change in different size channels. Normalised current response of a polyurethane-coated glucose biosensor placed in the middle of each channel to a concentration change from 0 to 4 mM at $1 \mu\text{l}/\text{min}$ in three different microfluidic channels. The actual channel sizes are shown in the table inset ($n=3$).

The T_{90} responses of glucose and lactate biosensors for each microfluidic channel are summarised in table 8.2.

Table 8.2: Effect of channel dimensions on T_{90} response of polyurethane-coated glucose and lactate biosensors in the microfluidic channel (glucose $n=3$, lactate $n=2$).

Channel	Glucose	Lactate
	T_{90} (s)	T_{90} (s)
1	208 ± 0.28	194 ± 15
2	267 ± 0.30	227 ± 7.0
3	398 ± 0.35	286 ± 6.9

Laminar flow inside the connection tubing and the microfluidic channel leads to a smearing of the concentration change as a result of Taylor dispersion (101), as described in

section 1.5.4. As figure 8.11 demonstrates, the response time of the sensor to a step change in concentration is reduced by decreasing the channel size. The fastest response time was observed in channel 1 ($520 \times 520 \mu\text{m}$). In addition, as previously shown, variability in current was observed with different channel sizes because of variation in the linear flow rate. However, there was no clear trend as these experiments were challenging to control because of the roughness of the walls and the difficulty in precisely positioning the biosensor reproducibly.

8.7 Microfluidic device: design 4

Taking all the design improvements from designs 1-3 into account, a final device was designed and fabricated. The fastest response time was observed in the $520 \times 520 \mu\text{m}$ channel, therefore these dimensions were chosen for the final device. It was also necessary to remove the curved channel and to change to a right-angle design, as the curve would not be smooth at this resolution. In this design, the outer shape of the inlet structure was modified so that the shorter structure could fit inside the vial holder, as this had been an issue in the previous version of the microfluidic chip. 3D drawings of the design with key dimensions are shown in figure 8.12 and a detailed schematic of the final design of the microfluidic chip is shown in figure 8.13.

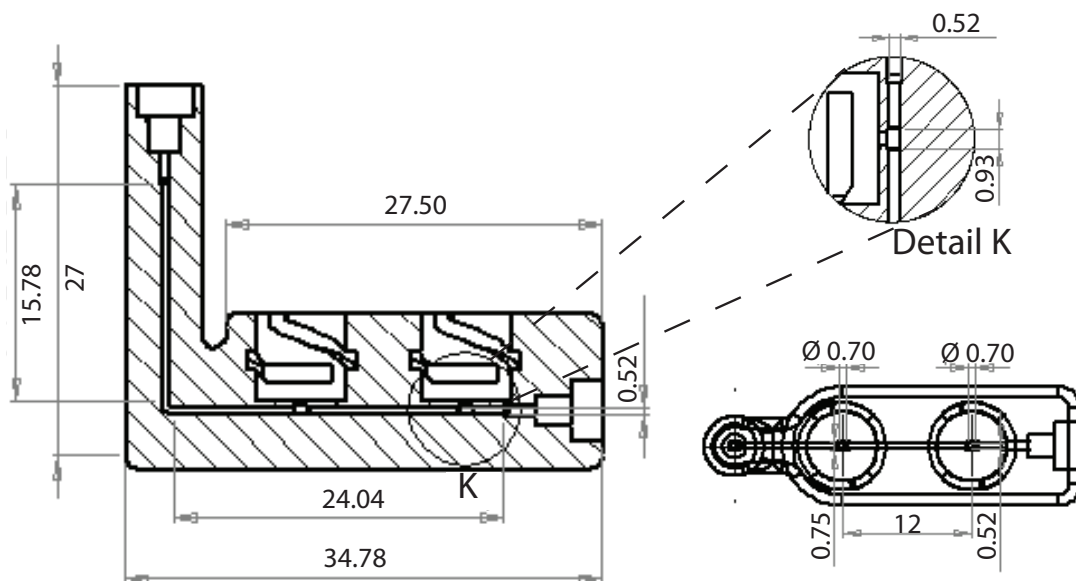


Figure 8.12: Schematic drawings of design 4 of microfluidic chip. *Left* shows side view of microfluidic chip. *Right (top)* shows close-up of the microfluidic chamber into which the needle biosensor is inserted and *Right (bottom)* shows top view of microfluidic chip. Key dimensions of microfluidic channel given in mm.

8. ATHLETE MONITORING: A WIRELESS MICROFLUIDIC DEVICE

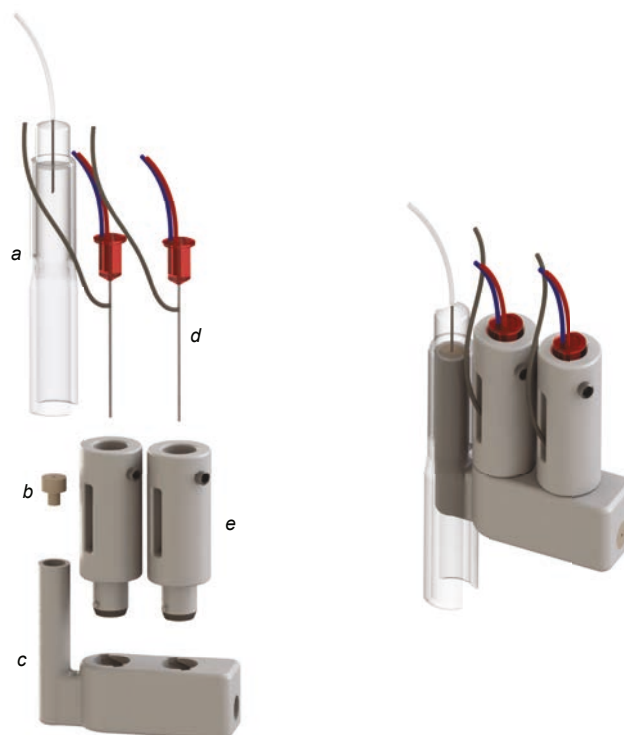


Figure 8.13: Schematic representation of modular microfluidic device. The microfluidic device connects into the vial holder (*a*) at the probe outlet using the rubber insert (*b*) from a microvial. The microfluidic chip (*c*) houses two needle biosensors (*d*), each of which are fixed in place inside a needle holder (*e*) that slots into the microfluidic chip, creating a seal.

On the basis of the specified dimensions, the internal volume up to the first biosensor was approximately $2.70 \mu\text{l}$ and on the basis of the measured dimensions, it was approximately $1.91 \mu\text{l}$.

In order to verify that this system was capable of detecting physiologically relevant concentrations of glucose and lactate levels in the dialysate, the system was calibrated online at $1 \mu\text{l}/\text{min}$ from 0 to 10 mM. Figure 8.14A shows the typical current response of a polyurethane-coated lactate sensor to changes in lactate concentration when it is placed in the middle of the microfluidic channel. In figure 8.14B, the results for a glucose and lactate biosensor were fitted with the Michaelis-Menten equation and the enzyme parameters are shown in table 8.3. These data demonstrate that the biosensing system has good sensitivity to glucose and lactate, with increasing levels of substrate resulting in clear current changes. Moreover, the biosensors show a good dynamic range that is suitable for physiological monitoring.

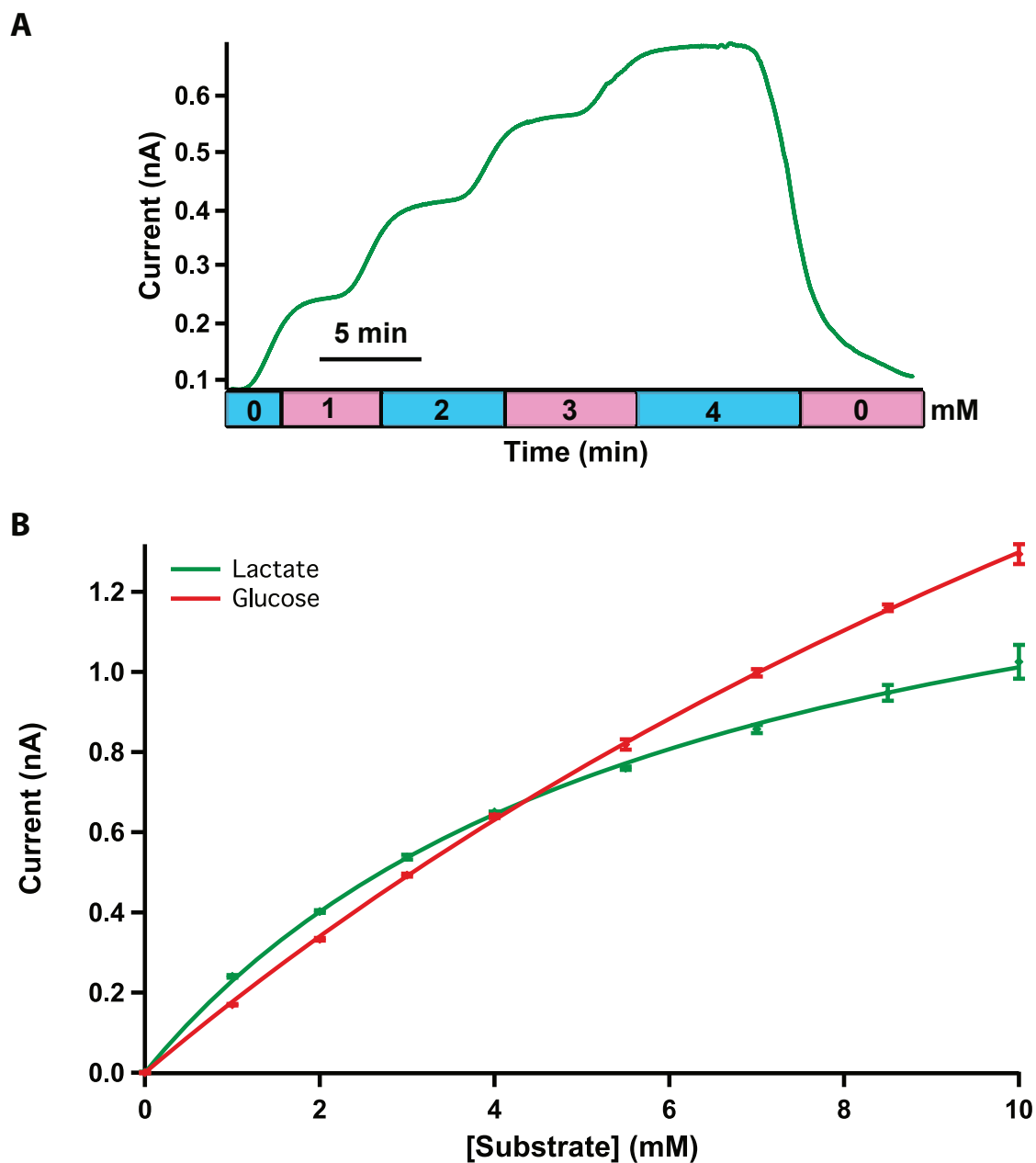


Figure 8.14: Typical biosensor calibration curves in the microfluidic device. *A.* Raw data for a typical 5-point lactate calibration from 0 to 4 mM; steps are 0, 1, 2, 3 and 4 mM. *B.* Typical calibration curves for 50 μm polyurethane-coated glucose and lactate biosensors in the microfluidic device at 1 $\mu\text{l}/\text{min}$. Mean \pm standard deviation of measurement shown. Points fitted with the Michaelis-Menten equation.

Table 8.3: Biosensors characteristics at 1 $\mu\text{l}/\text{min}$ inside microfluidic channel (n=6).

	V_{max} (nA)	K_m (mM)
Glucose	4.40 ± 0.14	23.9 ± 1.01
Lactate	1.63 ± 0.03	6.12 ± 0.26

8. ATHLETE MONITORING: A WIRELESS MICROFLUIDIC DEVICE

It was important to compare the new microfluidic analysis platform with that of the previous rapid sampling microdialysis (rsMD) ‘gold-standard’ system to assess differences in the lag time and the time resolution of the two methods. In order to do this, two expired CMA 70 brain microdialysis probes were placed in a well-stirred beaker of T1 solution and subjected to changes in beaker lactate and glucose concentrations. The microdialysis probes were perfused at 1 $\mu\text{l}/\text{min}$ with CMA 107 microdialysis syringe pumps and aliquots of 0.5 M glucose and lactate standard were added to the beaker to increase the concentration. The outlet of one microdialysis probe was connected directly to the microfluidic device. The outlet of the second microdialysis probe was extended using 1 m of low-volume FEP tubing, as in previous *in vivo* experiments, and connected to the flow injection valve of the rsMD analysis system. In both analysis systems, Taylor dispersion causes smearing of the step changes, as shown in figure 8.15.

Comparison of the response time of the two systems indicates that the smearing effect is greater for the rsMD system than for the microfluidic biosensing system as a result of the long connection tubing necessary to reach the clinical trolley. In addition to comparing the temporal resolution, it was necessary to consider the lag time for the two systems. This lag time is the delay between the changes occurring at the probe membrane and the biosensing system. For the rsMD system, at 1 $\mu\text{l}/\text{min}$ the total delay was found to be 24.0 ± 1.21 minutes (n=2), of which approximately 11 minutes were due to the outlet tubing of the microdialysis probe, as opposed to the extension tubing. For the microfluidic device, also at 1 $\mu\text{l}/\text{min}$, the total delay for the lactate biosensor, which was placed first in the direction of flow, was found to be 14.6 ± 0.68 minutes (n=3), and for the glucose biosensor, which was placed second in the direction of flow, was found to be 16.8 ± 0.66 minutes (n=3). However, in this case, the major cause of this delay was the outlet tubing of the microdialysis probe, which contributed approximately 11 minutes of the total delay; custom-order microdialysis probes could be purchased with a shorter probe outlet, which would reduce the delay further still.

The two biosensors were positioned consecutively in the flow stream, hence the 2.2 minute delay between the response of the two sensors to a dialysate concentration change. This is compared to a predicted delay of 2.28 minutes at 1 $\mu\text{l}/\text{min}$ based on an estimation of the volume between the two sensors (separation distance: 12 mm; measured channel dimensions: 375 x 508 μm).

These results demonstrate that the microfluidic device offers a considerable improvement in the lag time compared with the previous analysis system, as the ability to connect the microfluidic chip directly to the microdialysis probe removes the need for long connection tubing.

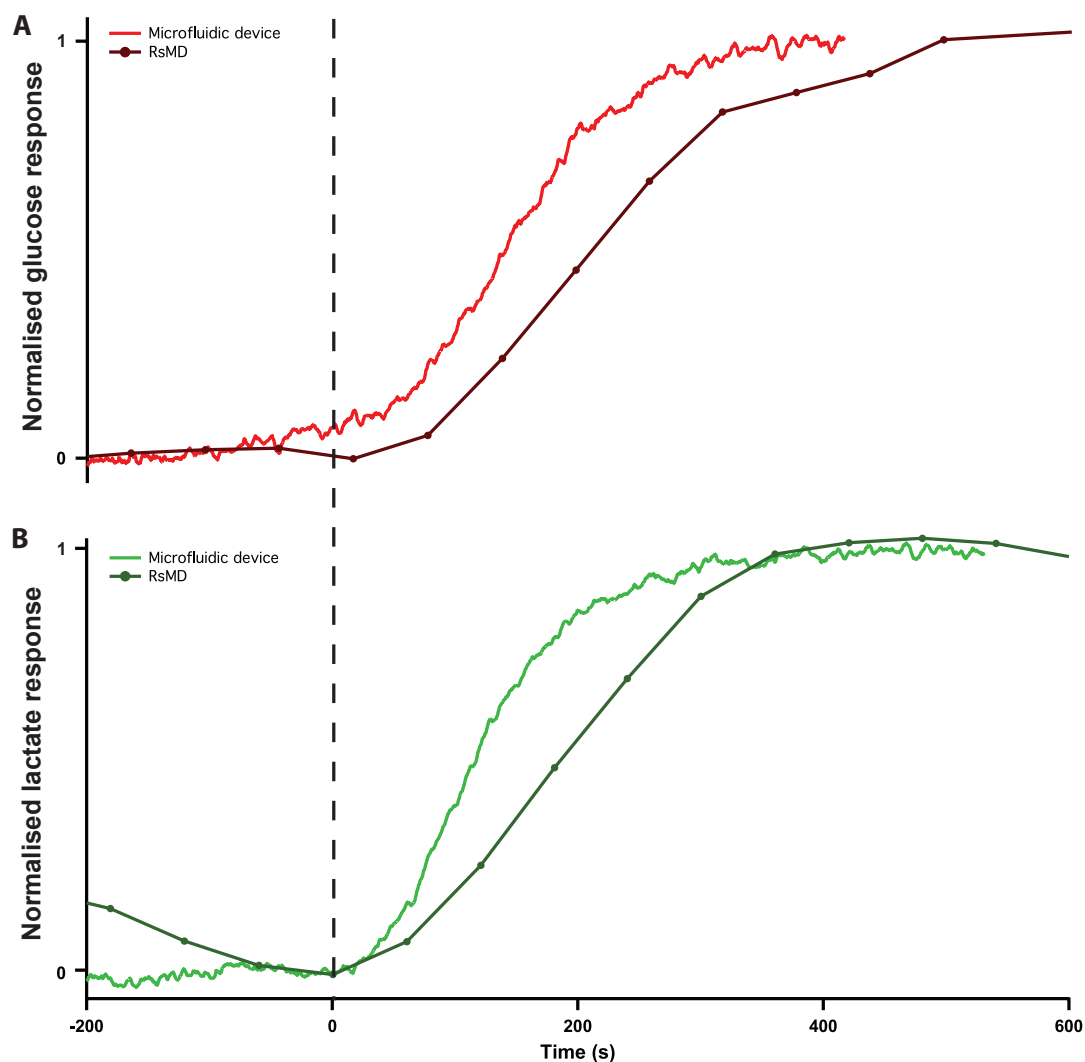


Figure 8.15: Response of rsMD compared with microfluidic device. Comparison of rsMD response and biosensor response in microfluidic analysis system to a step change in dialysate concentration. Microdialysis probes were perfused at $1 \mu\text{l}/\text{min}$ in a vigorously stirred beaker of T1 solution. The concentration was changed by adding aliquots of glucose/lactate standard to the beaker. The normalised response is plotted for *A.* glucose and *B.* lactate. The lag time between the probe and the beaker differed between the two analysis systems; for comparison purposes, they have been time-aligned here.

In conclusion, the microfluidic analysis system greatly reduces the time delay in detecting changes occurring in the tissue, as the long connection tubing is no longer necessary. This in turn also reduces the effect of Taylor dispersion on the signal, leading to less smearing of the sensor response and improved signal resolution.

8.8 Cycling trials with wearable device

Once the microfluidic device had been validated *in vitro*, a proof-of-concept study was carried out using the 3D printed microfluidic chip, housing glucose and lactate needle biosensors, as a wearable device for online measurement of subcutaneous metabolite levels during cycling training. Data will be presented from two cyclists.

8.8.1 Microdialysis procedure

The same procedure was used for insertion of the microdialysis probe as described for previous cycling trials. In brief, an anaesthetic cream (EMLA, APP Pharmaceuticals) was applied to the skin of the lower back 45 minutes prior to probe insertion. An ice pack was also placed on the skin 5 minutes before probe insertion to further numb the area, after which a sterile microdialysis probe (CMA 63, 10 mm membrane length, 20 kDa molecular weight cut-off) was inserted subcutaneously, using the tunnelling needle and introducer supplied, and was secured in place with 3MTM single-coated conformable incise medical tape. All procedures were approved by the local ethics committee and microdialysis probes were implanted by a qualified clinician. The probe was perfused with sterile T1 perfusion solution (MDialysis, Sweden) at 1 $\mu\text{l}/\text{min}$ using a portable syringe pump (CMA 107, MDialysis, Sweden) prior to insertion. A luer-lock extension set (150 cm, 0.4 ml internal volume, Alaris Medical Systems, UK) was used to extend the inlet tubing of the probe so that the pump could be placed away from the exercise bike. In the final design of the microfluidic device, the pump would either be incorporated into a pocket in the cyclist's clothing or in a pouch worn around the waist.

8.8.2 Online analysis using wearable device

Once it was confirmed that solution was successfully flowing out of the probe, the microfluidic analysis system was connected to the probe outlet holder and secured to the lower back, as shown in figure 8.16. The dialysate flowed into the microfluidic device, which housed 50 μm glucose and lactate disc electrode hydrogel biosensors. The solution passed the lactate biosensor first, followed by the glucose biosensor. Both glucose and lactate biosensors were coated with polyurethane in order to protect against any flow variations that could occur, affecting mass transport conditions; for the lactate biosensor, this also extended the dynamic range.

For these trials, the biosensors were controlled by an in-house wireless two-channel potentiostat (briefly described in section 2.5.5), designed and fabricated by Mr Chu Wang, which were housed in a saddlebag on the exercise bike. The potentiostat used is fairly large (10.5 x 6.0 x 5.0 cm LxWxH) compared with the microfluidic device and is not yet small

enough to be integrated into a fully wearable system. However, the wireless potentiostat was used here as a proof of concept for the final miniaturised device. Additionally, the wireless link replaced the electrical isolation barrier usually provided by a >0.5 m length of microdialysis outlet tubing.

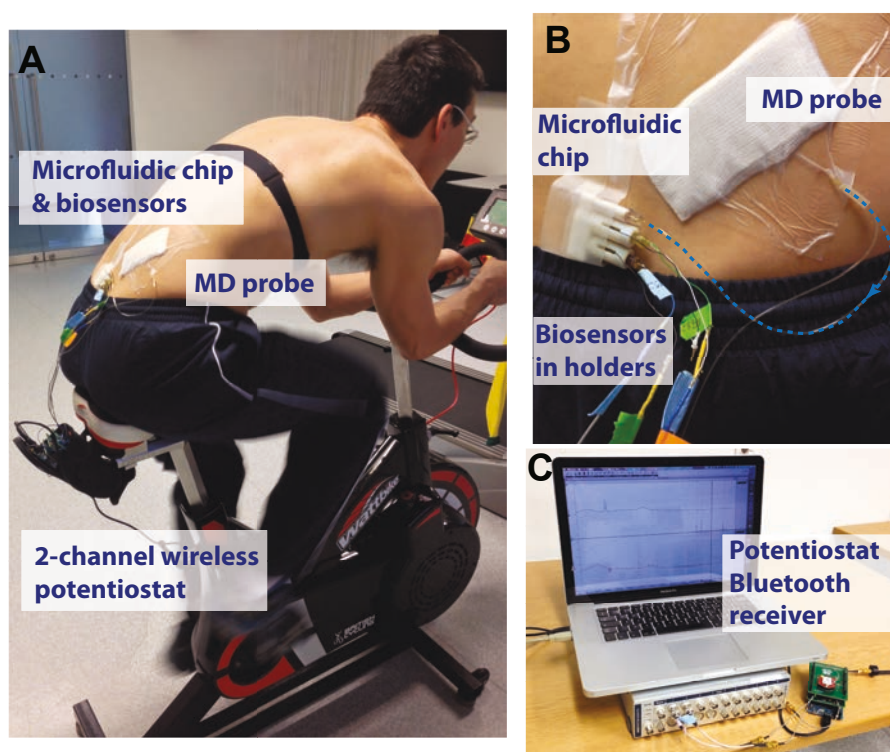


Figure 8.16: Wearable microfluidic device with wireless potentiostats during cycling protocol. *A.* Photograph of microfluidic device worn by cyclist during exercise. The biosensors were connected to wireless potentiostats, which were housed in a saddlebag attached to the bike. *B.* The dialysate flowed into the microfluidic chip, housing the glucose and lactate biosensors, which was worn during cycling. *C.* The potentiostat linked wirelessly with the receiver module.

8.8.3 Monitoring protocol

The protocol that was optimised in the previous chapter was used for this proof-of-concept study. Briefly, baseline dialysate glucose and lactate levels were measured following probe insertion prior to exercise. Levels after probe implantation were variable as a result of the trauma of insertion. Typically, tissue stabilisation following probe insertion occurs after 12 minutes (99), therefore, baseline levels were monitored for at least 30 minutes following probe implantation to allow sufficient time to obtain a stable level. The exercise phase consisted of three levels of increasing intensity, followed by a short sprint and a period of warming down. Finally, dialysate glucose and lactate levels were monitored during the recovery period following exercise. As previously described, a heart rate monitor chest

8. ATHLETE MONITORING: A WIRELESS MICROFLUIDIC DEVICE

belt (SuuntoTM, Finland), which wirelessly links with the exercise bike, was worn and data from the bike (Wattbike, UK), such as heart rate and rotations per minute (rpm), were recorded. In addition, blood levels of glucose and lactate were measured at specific time points throughout the protocol for comparison with tissue levels (time points indicated in figure 8.19).

8.8.4 Results

Results obtained from two cyclists monitored using the miniaturised microfluidic analysis system coupled to wireless potentiostats will be discussed in this section.

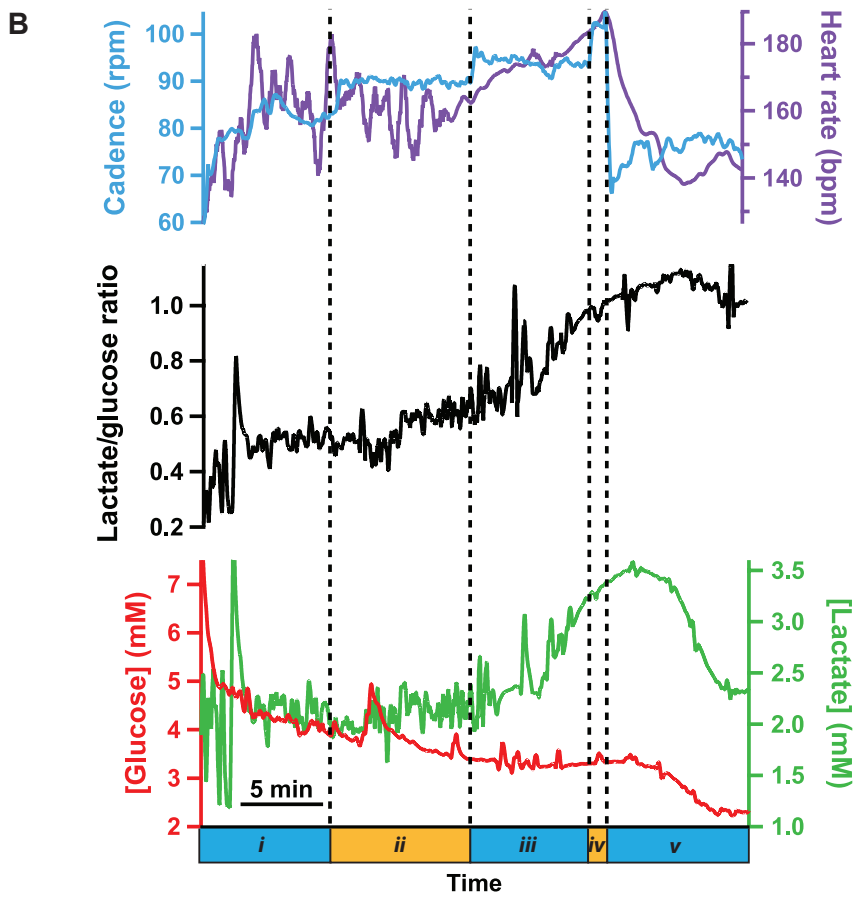
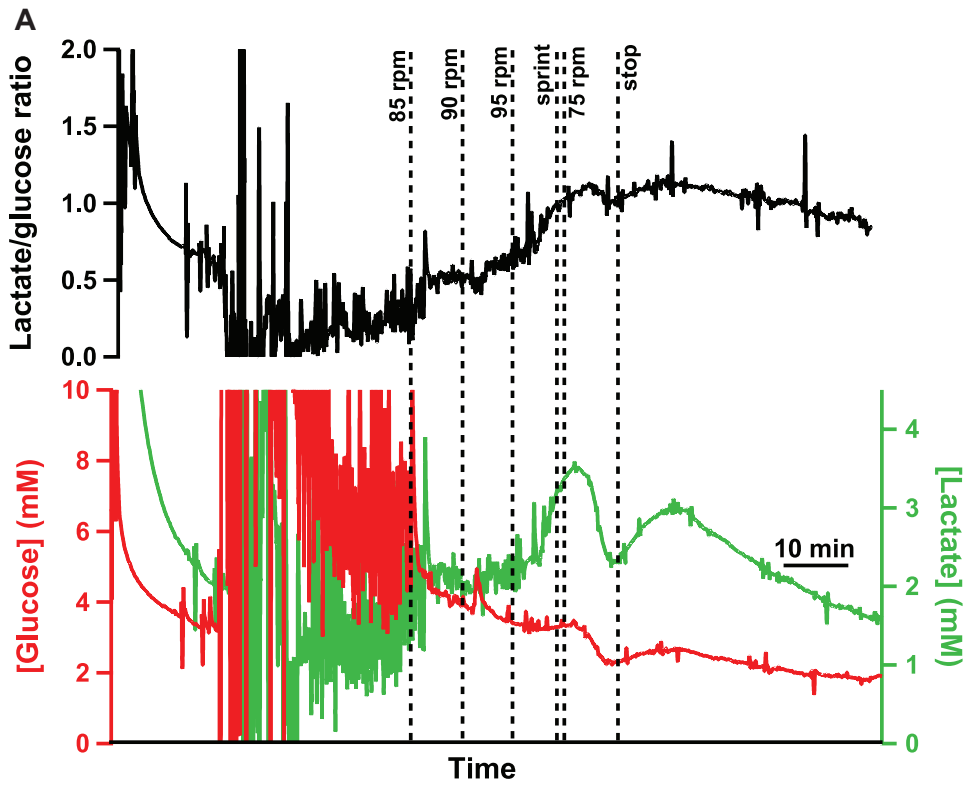
Cyclist 1

Subcutaneous dialysate glucose and lactate levels are presented in figure 8.17A for cyclist 1. The metabolite levels during the exercise phase are shown in more detail in figure 8.17B together with data recorded from the exercise bike showing heart rate and rpm, to quantify the exercise intensity. The lactate/glucose ratio was also calculated to guard against possible changes in probe recovery, as in previous cycling studies this was found to be a more sensitive marker of tissue changes than either metabolite alone.

In this case, the glucose and lactate levels in the baseline period were particularly noisy, even after filtering. This was due to the fact that, for the initial period, the battery was going flat. Once it had been replaced the noise was greatly reduced. Use of the lactate/glucose ratio is particularly useful at this point, as the noise is cancelled out to a certain degree and therefore levels are clearer. At the start of exercise (sections *i* and *ii*) the heart rate data were variable as there was insufficient sweat to ensure good contact between the skin and the electrodes.

Figure 8.17: Dialysate metabolite levels during the cycling protocol for cyclist 1. *A.* Over the whole protocol. *B.* During the exercise phase. The green trace shows dialysate lactate concentrations, the red trace shows dialysate glucose concentrations and the black trace shows the corresponding lactate/glucose ratio, measured using online biosensors in the microfluidic device. Data were obtained in real time and are smoothed with a Savitsky-Golay 401-point filter (to filter out noise). Data are time-aligned. Dotted lines indicate the stages of varying intensity during the protocol: *i.* 85 rpm, *ii.* 90 rpm, *iii.* 95 rpm, *iv.* sprint, *v.* 75 rpm.

8.8 Cycling trials with wearable device



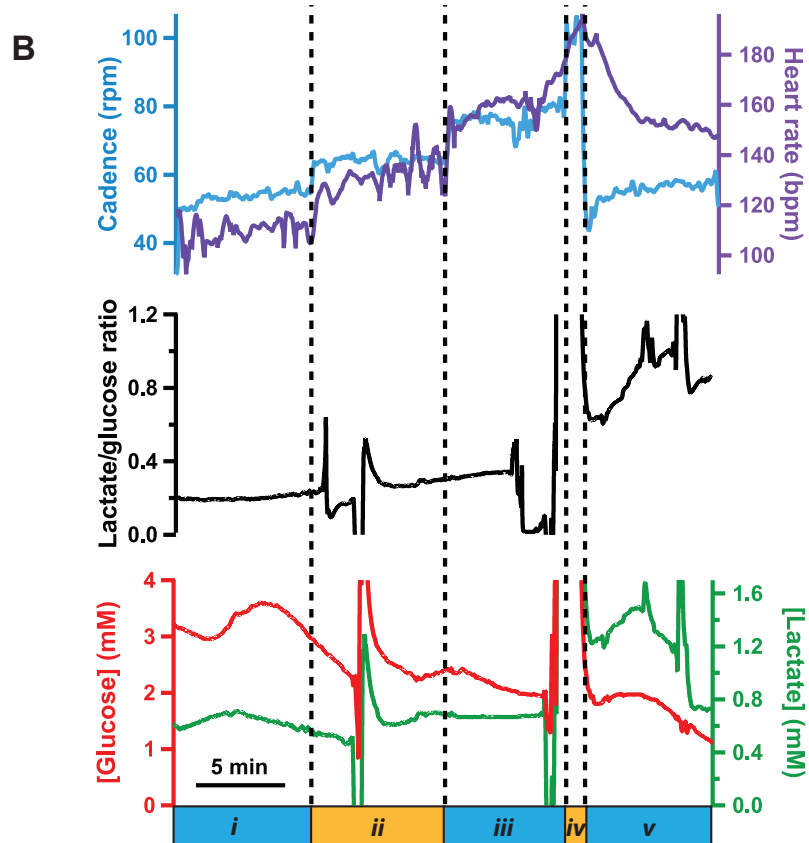
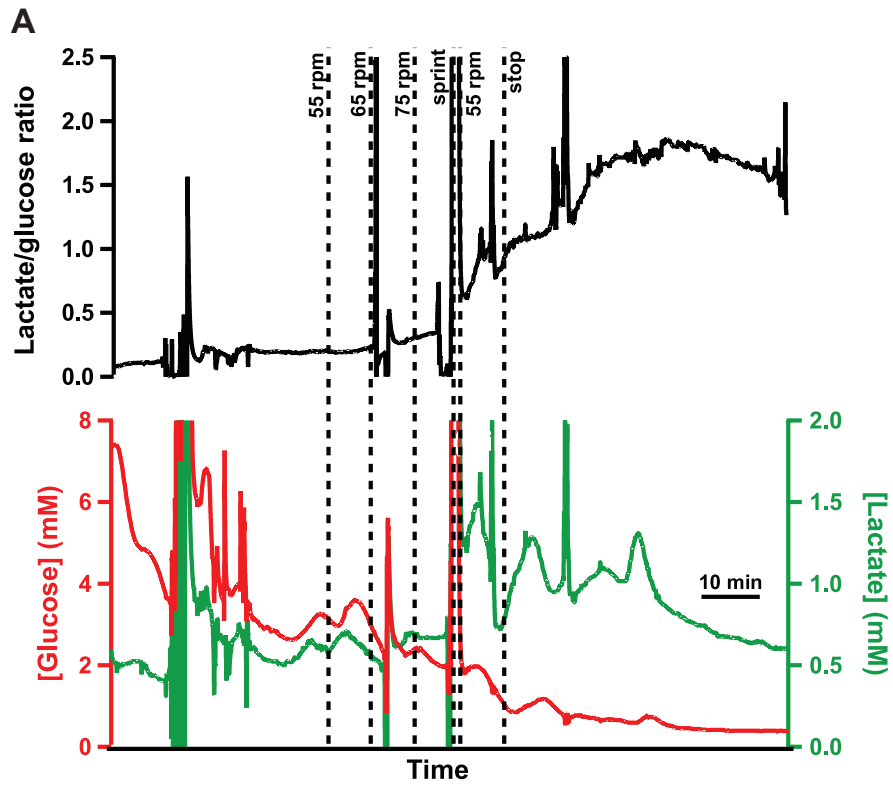
8. ATHLETE MONITORING: A WIRELESS MICROFLUIDIC DEVICE

Baseline dialysate glucose and lactate levels were 6.02 ± 1.08 mM and 1.81 ± 0.33 mM, respectively (mean \pm standard deviation over 30 second time period) prior to commencing exercise. Subcutaneous dialysate glucose levels decreased with increasing cycling intensity and continued to decrease even after 50 minutes of resting. By contrast, subcutaneous lactate levels initially increased when exercise commenced but remained fairly stable for the first two stages of the cycling protocol. By the third stage of the exercise regime, local lactate levels began to increase, peaking immediately after the sprint and gradually decreasing once cycling had stopped. After 50 minutes of resting, subcutaneous dialysate glucose and lactate levels were 1.84 ± 0.05 mM and 1.67 ± 0.03 mM, respectively. The lactate/glucose ratio increased when cycling commenced and rose more steeply with increasing exercise intensity. The lactate/glucose ratio continued to increase even after exercise had stopped and gradually began to decrease during the recovery phase.

Cyclist 2

Subcutaneous glucose and lactate levels for the second cyclist over the whole protocol are shown in figure 8.18A, and in more detail during the exercise phase in figure 8.18B. Spikes in the data were caused by biosensor leads becoming briefly disconnected during vigorous exercise. As a result, the lactate/glucose ratios at these points are inaccurate.

Figure 8.18: Dialysate metabolite levels during the cycling protocol for cyclist 2. *A.* Over the whole protocol. *B.* During the exercise phase. The green trace shows dialysate lactate concentrations, the red trace shows dialysate glucose concentrations and the black trace shows the corresponding lactate/glucose ratio, measured using online biosensors in the microfluidic device. Data were obtained in real time and are smoothed with a Savitsky-Golay 201-point filter. Data are time-aligned. Dotted lines indicate the stages of varying intensity during the protocol: i. 55 rpm, ii. 65 rpm, iii. 75 rpm, iv. sprint, v. 55 rpm.



8. ATHLETE MONITORING: A WIRELESS MICROFLUIDIC DEVICE

Prior to starting exercise, baseline dialysate glucose and lactate levels were 2.67 ± 0.02 mM and 0.52 ± 0.001 mM, respectively (mean \pm standard deviation over 30-second time period). Subcutaneous glucose levels decreased in an almost stepwise manner with increasing exercise intensity. Local glucose levels were driven down further still, even after 50 minutes of resting. At this stage, glucose levels appeared to stabilise but at a level that was considerably lower than baseline. By contrast, subcutaneous lactate levels increased when exercise began and rose more steeply with increasing exercise intensity, peaking immediately after the sprint. Dialysate lactate levels remained high for about half an hour in the post-exercise period and then gradually decreased. In contrast to the previous case study, in which lactate levels began to drop relatively quickly after cycling had stopped, in this case lactate levels took longer to decrease. The lactate/glucose ratio increased when cycling began and rose more steeply with increasing exercise intensity. Interestingly, the lactate/glucose ratio continued to increase considerably, even after exercise had stopped, for much longer than with the previous case. After 50 minutes of resting, dialysate glucose and lactate levels were 0.39 ± 0.002 mM and 0.67 ± 0.005 mM, respectively. As discussed in the previous chapter with cyclists monitored using the rsMD analysis system, the length of time required for levels to decrease following exercise could serve as a marker of fitness level and could suggest that cyclist 1 was better able to recover after intense exercise than cyclist 2. In the baseline period in particular, the lactate/glucose ratio successfully removed variations that were present in both metabolites, giving a much clearer indication of real changes occurring in the tissue.

Overall summary

An overview of the dialysate glucose and lactate levels and the lactate/glucose ratio at the main stages of the cycling protocol for the two cyclists is shown in figure 8.19. Levels are also compared with blood readings that were taken simultaneously.

The overall trends in tissue glucose and lactate levels are similar for the two cyclists, although the absolute concentrations appear to be quite different. This variability could be due to a number of factors such as differences between the individuals, differences in probe recovery or variations in the probe placement. Differences caused by probe recovery are removed by considering the lactate/glucose ratio, allowing for a clearer comparison between the two cyclists. Despite this, there are still marked differences in the lactate/glucose ratio trend between the two cyclists.

Although both cyclists showed the same overall trends during increasing exercise intensity, with the lactate/glucose ratio increasing throughout, there was a noticeable difference in the post-exercise recovery phase. For cyclist 2, the lactate/glucose ratio continued to increase significantly, even after 50 minutes of resting, whereas for cyclist 1, the ratio had begun to decrease at this stage, although it was still significantly higher than baseline.

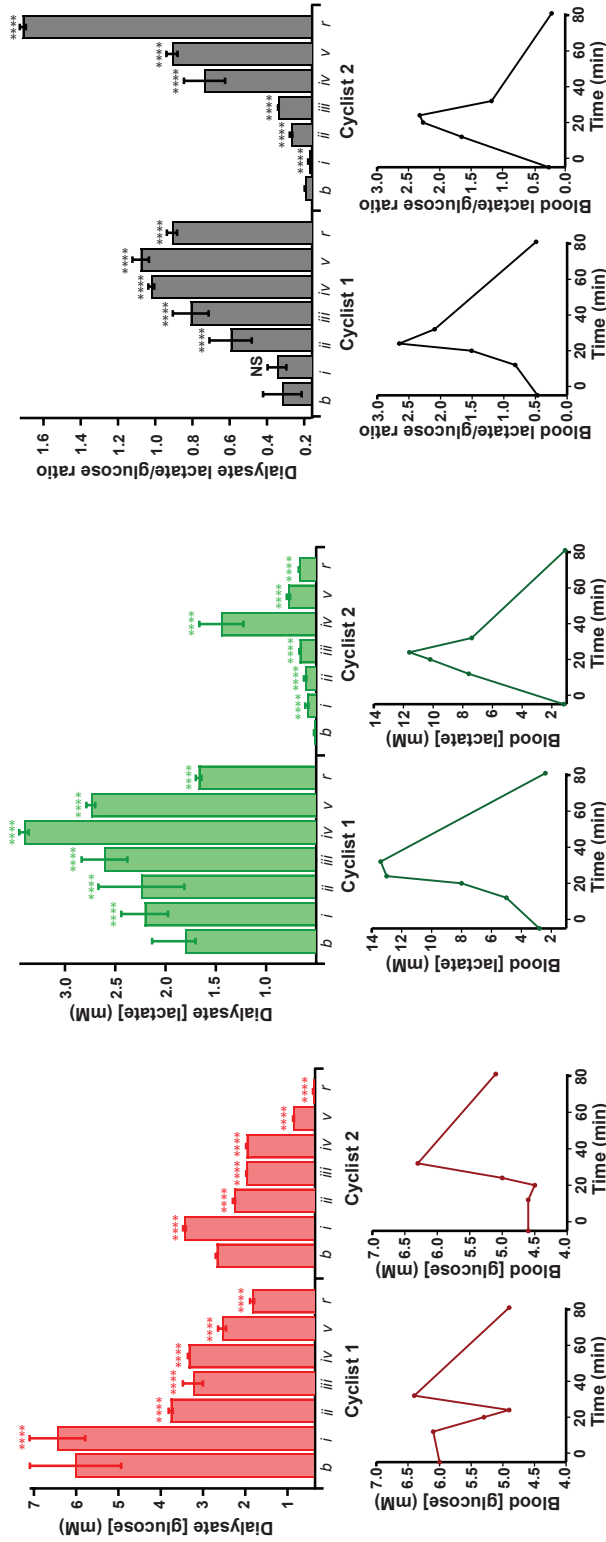


Figure 8.19: Dialysate and blood metabolite levels at key points in cycling protocol. Dialysate glucose levels are shown in red, dialysate lactate levels in green and the lactate/glucose ratio in black for each cyclist at (b) baseline, (i) midway through warm-up (4 min), (ii) midway through medium-intensity (12 min), (iii) midway through high-intensity (20 min), (iv) end of sprint (24 min), (v) end of warm-down (32 min) and (r) after 50 min of recovery (81 min). Cycling begins at time 0. Levels correspond to those used to label exercise phases in figures 8.17 and 8.18. A Mann-Whitney U test was used to assess changes compared with baseline at each stage (n=500). NS=not significant, **** p<0.0001. Blood metabolite levels are also plotted against time. Samples were taken at times corresponding to b, ii, iii, iv, v and r.

8. ATHLETE MONITORING: A WIRELESS MICROFLUIDIC DEVICE

These local differences in the trends in metabolite levels could give some indication of the fitness of the cyclist and of their ability to recover following intense exercise.

Trends in glucose did not correlate between tissue and blood in either case, although trends in tissue lactate correlated fairly closely with blood lactate trends. The trend in the lactate/glucose ratio followed that of the blood, with the ratio increasing as exercise intensity increased. However, the trends differed after the point of maximum exertion; at this point the blood lactate/glucose ratio decreased and in both cases had returned to baseline levels by the end of monitoring. By contrast, the tissue lactate/glucose ratio continued to increase in the case of cyclist 2 even after 50 minutes of resting and had only slightly decreased after 50 minutes of resting in the case of cyclist 1, suggesting that the tissue had not fully recovered despite blood levels having returned to normal. These results demonstrate the potential merit of measuring tissue metabolic changes as an alternative to blood for elite athlete performance monitoring.

8.9 Conclusion

In conclusion, a viable wearable microfluidic device that can be combined directly with a commercial microdialysis probe has been successfully engineered. The system incorporates biosensors that are easily and reproducibly positioned inside the channel and that can be removed, repolished and re-used.

3D printing provides a powerful tool to progress from a concept, through optimisation, to the final device. Moreover, this fabrication method provides the dimensional control to design a system that can be integrated with commercial components, providing the ability to make a connection to the microdialysis probe without connection tubing or adaptors, which are usually necessary.

However, in addition to the many advantages associated with fabrication using 3D printing there are also many challenges. As shrinkage occurs during the printing process, the device dimensions do not match those specified in the design. The discrepancy between the measured and specified dimensions was found to be more than the quoted precision of the printer. Moreover, the channel roughness can lead to irreproducibility in the sensor responses. This effect is greater as the channel dimensions are reduced.

In a proof-of-concept study, the microfluidic platform was used as a wearable device for subcutaneous monitoring of dialysate glucose and lactate levels in cyclists during exercise. The system was capable of resolving the metabolic changes occurring during exercise. Furthermore, the miniaturised device could have potential in other microdialysis applications, such as bedside monitoring, which could reduce the long lag times that are associated with the long connection tubing usually necessary.

Chapter 9

Conclusions and future work

9.1 Overview

The aim of this thesis was to develop and to implement online biosensing systems for real-time monitoring of tissue metabolism using microdialysis as a tissue sampling technique. In chapters 2 and 3, a number of new and generally applicable methodologies were developed in the course of this challenging research. These include:

- **Autocalibration**

An autocalibration system was developed based on commercially available programmable syringe pumps and valves. The system was used with rapid sampling microdialysis (rsMD) and online biosensors to automatically carry out regular calibrations. This is essential during long periods of monitoring, as it allows meaningful interpretation of results obtained.

- **New conventional biosensors**

Glucose and lactate hydrogel biosensors were developed using a combined needle electrode. In order to extend their dynamic range, optimisation of a protocol for coating the biosensor with a diffusion-limiting polyurethane film was carried out. This coating also resulted in a decrease in sensitivity and an increase in the response time of the sensor, therefore a compromise between these factors and extension of the dynamic range was necessary.

- **Distributed biosensors**

An alternative biosensing system was developed, which employed automated microfluidic syringe pumps and valves to manipulate calibration and dialysate streams and to dose enzyme into the flow stream. The enzyme reacted with the substrate in flow and the reaction product, hydrogen peroxide, was detected at a downstream

9. CONCLUSIONS AND FUTURE WORK

poly(phenol)-coated 50 μm platinum disc electrode housed in a PDMS chip. The system was demonstrated in detail for detection of glucose and lactate. Proof-of-concept detection of ATP and pyruvate was also demonstrated using this technique.

- **Storage tubes for microdialysis**

A method of collecting dialysate in lengths of storage tubing for delayed analysis while retaining temporal resolution was developed. This method was validated and showed good agreement with online results. The sample tubes were found to be stable during long-term storage at -80°C .

This collection of technologies was then refined for use in a number of tissue monitoring challenges. These included:

- **Porcine kidneys during cold preservation and ischaemic rewarming (in chapter 4)**

An online system for simultaneous monitoring of lactate levels in two transplant kidneys has been developed. Microdialysis was used to sample the cortical tissue and was coupled to the rsMD analysis system that was reconfigured for this application. In order to monitor two regions of each kidney simultaneously, dialysate from a second microdialysis probe placed in the renal medulla was collected into lengths of storage tubing for delayed analysis. Porcine kidneys were monitored during either 24 hours of static cold storage (SCS) or 10 hours of hypothermic machine perfusion (HMP) and 2 hours of subsequent passive warming to ambient temperature. Significant differences in the cortical lactate profiles were identified for kidneys stored using the two clinical preservation groups, both during preservation and warming. Cortical lactate levels were significantly higher for HMP stored kidneys after 10 hours of warming, and these kidneys showed a significantly larger increase in lactate levels on warming. Analysis of the renal effluent during HMP points towards re-establishment of complex glucose-lactate recycling within the kidney upon perfusion as the cause of these differences.

- **Human kidneys and pancreases (in chapter 5)**

This analysis methodology was extended to monitor discarded human kidneys, as well as both porcine and human pancreases during preservation. In addition, the system was developed to allow measurement of glucose as well as lactate both through delayed analysis using the conventional rsMD setup or through the use of glucose biosensors. RsMD was used to monitor paired kidneys subjected to different lengths of cold ischaemia time (CIT) to attempt to compare organs of different health. The kidney subjected to a shorter CIT, and that was presumably more healthy, displayed

higher dialysate lactate levels during preservation and a larger increase in lactate during reperfusion. The effect of treatment of porcine and human kidneys with a novel protein, thought to prevent thrombosis upon reperfusion, was evaluated using the rsMD system and preliminary results show that dialysate lactate levels during haemoperfusion were higher for the control kidney. A length of storage tubing was used to collect dialysate in the early stages, immediately after organ retrieval, for delayed analysis of glucose and lactate levels. A preliminary experiment showed that dialysate glucose and lactate levels were very low during transport from the abattoir to the laboratory. A miniaturised microfluidic system has also been tested, which uses in-flow enzyme addition and downstream poly(phenol)-coated platinum disc electrodes to detect glucose and lactate in two kidneys simultaneously.

- **Free flap surgery (in chapter 6)**

Real-time monitoring of tissue ischaemia was carried out during free flap surgery and afterwards in the intensive therapy unit (ITU). Using this technique it was possible to clearly distinguish between successful and unsuccessful flap reconstructions both during surgery and post-operatively. Using rsMD, signs of flap failure were detected much earlier than conventional methods allowed. The lactate/glucose ratio was shown to be a considerably more sensitive and reliable marker of tissue health than either glucose or lactate alone as it was not affected by flow artefacts caused by drugs such as vasodilators.

- **Athlete monitoring (in chapter 7)**

The development of a wearable device for subcutaneous monitoring of tissue metabolites during cycling has been presented. A Food and Drug Administration (FDA)-approved microdialysis probe was used to sample the subcutaneous tissue and was coupled to online biosensing systems. Initial investigations were carried out using rsMD to define the scope of the problem in terms of requirements for the microfluidic device and for the biosensors. These experiments also served to improve the experimental protocol and to determine the microdialysis flow rate required to obtain detectable levels of glucose and lactate in the dialysate. Preliminary experiments used storage tubing to collect the dialysate while retaining temporal resolution for delayed analysis. However, this method did not prove suitable for the fast-changing events occurring in the tissue. Instead, online analysis using rsMD was coupled to biosensors housed in a microfluidic chip to verify that they were capable of detecting metabolite levels within the physiological range. Online analysis proved much more suitable for subcutaneous monitoring of glucose and lactate levels in real time, as it enabled events to be assigned as they happened. However, the lag time caused

9. CONCLUSIONS AND FUTURE WORK

by the long connection tubing and the low flow rates that were necessary was not ideal.

In the final data chapter 8, ideas from the whole thesis culminate in the presentation of a new 3D printed wireless biosensor system. This microfluidic chip was designed to connect directly to the microdialysis probe outlet holder and enabled integration of two needle biosensors in custom-made holders. The design progression and optimisation is presented and the effect of reducing the channel size on the response time of the biosensors is demonstrated. The final wearable design was compared with the current rsMD system (set up in the usual way with 1 m of connection tubing between the microdialysis probe and the analysis system) and the lag time was found to be considerably improved. In addition, the effect of smearing of concentration changes caused by Taylor dispersion was reduced using the microfluidic device. Proof-of-concept experiments using the microfluidic device coupled with wireless potentiostats to monitor cycling athletes are presented. As discussed for real-time analysis of free flaps, the lactate/glucose ratio provided the most sensitive marker of metabolic changes occurring in the tissue.

9.2 Future work

Biosensing systems

Although in most cases the dynamic range of the hydrogel biosensors was successfully extended by addition of the polyurethane film, there was a large degree of variability and in some cases the coating was unsuccessful. To improve the reproducibility of the polyurethane-coated hydrogel biosensors, further optimisation of the coating protocol, in terms of the number of layers and the dipping time, is required. Alternatively, other diffusion-limiting layers could be investigated to improve the success rate. Additionally, investigation of the biosensor stability over time is necessary as it would allow biosensors to be made in advance and stored until required. For the in-flow enzyme addition system, further work on optimisation of the enzyme concentration and flow rate for detection of glucose and lactate is necessary. Steps varying enzyme concentration and flow rate should be carried out in a random order to reduce systematic bias. Optimisation of the enzyme conditions should improve the sensitivity of the system.

Monitoring transplant organs

Initial experiments have shown that monitoring tissue metabolism in real time during organ preservation can provide important information regarding the health of the organ. However, in order to assess the potential of this technique for viability assessment, it

is necessary to correlate these findings with some measure of functional outcome. Organs subjected to different degrees of ischaemic injury could be studied to compare the metabolic profiles of healthy and unhealthy organs. Alternatively the study could be extended to monitor organs during a transplantation model, as this is the most robust method of testing organ function.

These results have shown the importance of measuring multiple metabolites and of using ratiometric analysis to increase the reliability of the results obtained. Therefore, it is necessary to extend the system to measure glucose in addition to lactate. In addition, it would be interesting to monitor dialysate ATP levels to gain a better understanding of whether the energy demands of the tissue are being met. Proof-of-concept results were demonstrated for detection of ATP, but optimisation of the system is necessary. For transplant kidneys, the final analysis system could also include a means of testing renal function. One example would be giving a bolus of inulin to the perfused kidney. Inulin should be completely removed from the perfusate in a properly functioning kidney, therefore measurement of inulin in the urine would provide a measure of glomerular filtration rate and hence renal function. Work on this is currently being undertaken in the Boutelle group. The consensus in the literature is that no one marker alone can be used to reliably assess organ viability, therefore, measurement of multiple analytes could facilitate development of a viability score, taking several factors into account.

Initial work to miniaturise the analysis system has been demonstrated, but further development is required. This would enable the system to be portable and to travel with the transplant organ between donor and recipient sites. It would also facilitate monitoring at an earlier stage after organ retrieval. The system should incorporate an autocalibration system to improve the reliability of the results. In addition, a method of controlling the temperature of the analysis system is also necessary if it is to travel with the organ on ice, as this would affect the kinetics of the system.

Finally, development of a flat microdialysis probe that could sit on the surface of the organ would be useful. This would be less invasive and in addition would be less susceptible to movement, which was a problem using a conventional concentric probe. Studies have shown that a microdialysis probe placed on the organ surface can allow early detection of ischaemia (218, 293, 294).

Monitoring during free flap surgery

A major drawback with the rsMD system is the long lag time between changes occurring in the tissue at the microdialysis probe membrane and when they are detected at the analysis system. This lag time is caused by the 1 m length of fine-bore tubing that is needed to connect the microdialysis probe outlet to the large clinical trolley housing the analysis system. Furthermore, the large trolley is impractical during surgery when space

9. CONCLUSIONS AND FUTURE WORK

is limited. The issues of delay and space could be greatly reduced by using a miniaturised wearable analysis system based on microfluidics and online biosensors, similar to that used for monitoring cyclists during training. Wireless potentiostats would also be necessary for the wearable device. As it would be nearer to the patient, the wearable device would need to be housed in a sterile container during surgery. For monitoring in the ITU for long periods of time, it would also be necessary to incorporate an autocalibration system into the final device. Currently, research in the group is being carried out to develop an ‘intelligent’ autocalibration system, which can track changes in biosensor sensitivity over time and make decisions regarding calibration frequency accordingly. This would be extremely useful in this situation to improve the reliability of the results during long periods of monitoring.

Wearable platform for cyclist monitoring during exercise

The wearable microfluidic platform developed for subcutaneous monitoring of cyclists during exercise shows considerable improvements in terms of lag time and dispersion compared with the rsMD system, but this is limited by the length of the outlet tubing of the commercially available microdialysis probe. The lag time could be reduced to just a few minutes if the microdialysis probe were to be customised so that the outlet tubing was shorter. The effect of reducing the channel size on the biosensor response to a step change in concentration has been demonstrated, but the width of the channel is limited by the diameter of the needle electrode in the current system. If the electrodes were redesigned so that this was no longer the limiting factor, it may be possible to reduce the channel size further still and to improve the sensor response time as a result. However, this may be beyond the capabilities of the 3D printer. Miniaturisation of the wireless potentiostats is also necessary for the final system so that they can be incorporated into the final wearable device.

Bibliography

- [1] EVA SYKOVÁ AND CHARLES NICHOLSON. **Diffusion in brain extracellular space.** *Physiological reviews*, **88**(4):1277–340, October 2008. 23, 24
- [2] CHARLES NICHOLSON AND EVA SYKOVÁ. **Extracellular space structure revealed by diffusion analysis.** *Trends in Neurosciences*, **21**(5):207–215, 1998. 24
- [3] DAVID W PAUL AND JULIE A STENKEN. **A Review of Flux Considerations for in Vivo Neurochemical Measurements.** *The Analyst*, pages 3709–3730, 2015. 25
- [4] LULU XIE, HONGYI KANG, QIWU XU, MICHAEL J CHEN, YONGHONG LIAO, MEENAKSHISUNDARAM THIYAGARAJAN, JOHN O DONNELL, DANIEL J CHRISTENSEN, JEFFREY J ILIFF, TAKAHIRO TAKANO, RASHID DEANE, AND MAIKEN NEDERGAARD. **Sleep Drives Metabolite Clearance from the Adult Brain.** *Science*, **342**:6156, 2013. 26
- [5] K N SCHULTZ AND R T KENNEDY. **Time-resolved microdialysis for in vivo neurochemical measurements and other applications.** *Annual review of analytical chemistry*, **1**:627–661, 2008. 28, 221
- [6] CHRISTIAN RUMMEL, CHRISTOPH ZUBLER, GERHARD SCHROTH, JAN GRALLA, KETY HSIEH, EUGENIO ABELA, MARTINUS HAUF, NIKLAUS MEIER, RAJEEV K VERMA, ROBERT H ANDRES, ARTO C NIRKKO, AND ROLAND WIEST. **Monitoring cerebral oxygenation during balloon occlusion with multichannel NIRS.** *Journal of cerebral blood flow and metabolism*, **34**(2):347–56, February 2014. 28
- [7] ERIC YI SUN, RALPH WEISSELEDER, AND LEE JOSEPHSON. **Continuous analyte sensing with magnetic nanoswitches.** *Small*, **2**(10):1144–7, October 2006. 29
- [8] K V LARIN, M S ELEDRISEI, M MOTAMEDI, AND R O ESENALIEV. **Non-invasive blood glucose monitoring with optical coherence tomography. A pilot study in human subjects.** *Diabetes care*, **25**(12), 2002. 29
- [9] VERONIKA V SAPOZHNIKOVA, ROMAN V KURANOV, INGA CICENAITE, RINAT O ESENALIEV, AND DONALD S PROUGH. **Effect on blood glucose monitoring of skin pressure exerted by an optical coherence tomography probe.** *Journal of biomedical optics*, **13**(2):021112, 2008. 29
- [10] SCOTT A HILDERBRAND AND RALPH WEISSELEDER. **Near-infrared fluorescence: application to in vivo molecular imaging.** *Current opinion in chemical biology*, **14**(1):71–9, February 2010. 29
- [11] VASILIS NTZIACHRISTOS. **Fluorescence molecular imaging.** *Annual review of biomedical engineering*, **8**:1–33, January 2006. 29
- [12] VASILIS NTZIACHRISTOS, CHRISTOPH BREMER, AND RALPH WEISSELEDER. **Fluorescence imaging with near-infrared light: new technological advances that enable in vivo molecular imaging.** *European radiology*, **13**(1):195–208, January 2003. 29
- [13] MARY K BALACONIS AND HEATHER A CLARK. **Biodegradable optode-based nanosensors for in vivo monitoring.** *Analytical chemistry*, **84**(13):5787–93, July 2012. 29
- [14] KELVIN BILLINGSLEY, MARY K BALACONIS, J MATTHEW DUBACH, NING ZHANG, ED LIM, KEVIN P FRANCIS, HEATHER A CLARK, AND GLUCOSE-DERIVED BORONATE ESTER. **Fluorescent Nano-Optodes for Glucose Detection.** *Analytical chemistry*, **82**(9):3707–3713, 2010. 29
- [15] SARAH M BUCK, YONG-EUN LEE KOO, ED PARK, HAO XU, MARTIN A PHILBERT, MURPHY A BRASUEL, AND RAOUL KOPELMAN. **Optochemical nanosensor PEBBLEs: photonic explorers for bioanalysis with biologically localized embedding.** *Current opinion in chemical biology*, **8**(5):540–6, October 2004. 29
- [16] YONG-EUN LEE KOO, RODNEY AGAYAN, MARTIN A PHILBERT, ALNAWAZ REHEMTULLA, BRIAN D ROSS, AND RAOUL KOPELMAN. **Photonic Explorers Based on Multifunctional Nanoplatforms : In Vitro and In Vivo Biomedical Applications.** In *New Approaches in Biomedical Spectroscopy*, pages 200–218. 2007. 29
- [17] HAO XU, JONATHAN W. AYLOTT, AND RAOUL KOPELMAN. **Fluorescent nano-PEBBLE sensors designed for intracellular glucose imaging.** *The Analyst*, **127**(11):1471–1477, October 2002. 29
- [18] HAO XU, JONATHAN W AYLOTT, RAOUL KOPELMAN, TERRY J MILLER, AND MARTIN A PHILBERT. **A Real-Time Ratiometric Method for the Determination of Molecular Oxygen Inside Living Cells Using Sol - Gel-Based Spherical Optical Nanosensors with Applications to Rat C6 Glioma.** *Analytical chemistry*, **73**(17):4124–4133, 2001. 29
- [19] YONG-EUN LEE KOO, YOUFU CAO, RAOUL KOPELMAN, SANG MAN KOO, MURPHY BRASUEL, AND MARTIN A PHILBERT. **Real-time measurements of dissolved oxygen inside live cells by organically modified silicate fluorescent nanosensors.** *Analytical chemistry*, **76**(9):2498–505, May 2004. 29
- [20] MURPHY BRASUEL, RAOUL KOPELMAN, TERRY J. MILLER, RON TJALKENS, AND MARTIN A. PHILBERT. **Fluorescent Nanosensors for Intracellular Chemical Analysis: Decyl Methacrylate Liquid Polymer Matrix and Ion-Exchange-Based Potassium PEBBLE Sensors with Real-Time Application to Viable Rat C6 Glioma Cells.** *Analytical Chemistry*, **73**(10):2221–2228, May 2001. 29
- [21] HEATHER A. CLARK, RAOUL KOPELMAN, RON TJALKENS, AND MARTIN A. PHILBERT. **Optical Nanosensors for Chemical Analysis inside Single Living Cells. 2. Sensors for pH and Calcium and the Intracellular Application of PEBBLE Sensors.** *Analytical Chemistry*, **71**(21):4837–4843, November 1999. 29
- [22] YONG-EUN KOO LEE, RON SMITH, AND RAOUL KOPELMAN. **Nanoparticle PEBBLE sensors in live cells and in vivo.** *Annual review of analytical chemistry*, **2**:57–76, January 2009. 29
- [23] JOHN P. LOWRY, ROBERT D. O'NEILL, MARTYN G. BOUTELLE, AND MARIANNE FILLENZ. **Continuous Monitoring of Extracellular Glucose Concentrations in the Striatum of Freely Moving Rats with an Implanted Glucose Biosensor.** *Journal of Neurochemistry*, **70**(1):391–396, November 1998. 30
- [24] JASON J BURMEISTER, FRANCOIS POMERLEAU, MICHAEL PALMER, BRIAN K DAY, PETER HUETTL, AND GREG A GERHARDT. **Improved ceramic-based multisite microelectrode for rapid measurements of L-glutamate in the CNS.** *Journal of neuroscience methods*, **119**:163–171, 2002. 30
- [25] FIACHRA B BOLGER, STEPHEN B MCHUGH, RACHEL BENNETT, JENNIFER LI, KEITA ISHIWARI, JENNIFER FRANCOIS, MICHAEL W CONWAY, GARY GILMOUR, DAVID M BANNERMAN, MARIANNE FILLENZ, MARK TRICKLEBANK, AND JOHN P LOWRY. **Characterisation of carbon paste electrodes for real-time amperometric monitoring of brain tissue oxygen.** *Journal of neuroscience methods*, **195**(2):135–142, 2011. 30

BIBLIOGRAPHY

- [26] BAZHANG YU, NATHAN LONG, YVONNE MOUSSY, AND FRANCIS MOUSSY. **A long-term flexible minimally-invasive implantable glucose biosensor based on an epoxy-enhanced polyurethane membrane.** *Biosensors & bioelectronics*, **21**(12):2275–82, June 2006. 30, 78, 83
- [27] MICHELLE L STEPHENS, FRANCOIS POMERLEAU, PETER HUETTL, GREG A GERHARDT, AND ZHIMING ZHANG. **Real-time glutamate measurements in the putamen of awake rhesus monkeys using an enzyme-based human microelectrode array prototype.** *Journal of neuroscience methods*, **185**(2):264–72, January 2010. 30
- [28] N. SACHEDINA AND J. C. PICKUP. **Performance assessment of the Medtronic-MiniMed Continuous Glucose Monitoring System and its use for measurement of glycaemic control in Type 1 diabetic subjects.** *Diabetic Medicine*, **20**(12):1012–1015, December 2003. 30
- [29] JC PICKUP, DJ CLAREMONT, AND GW SHAW. **Responses and calibration of amperometric glucose sensors implanted in the subcutaneous tissue of man.** *Acta Diabetologica*, **30**:143–148, 1993. 30, 31
- [30] TODD M. GROSS AND JOHN J. MASTROTOTARO. **Efficacy and Reliability of the Continuous Glucose Monitoring System.** *Diabetes Technology & Therapeutics*, **2**(supplement 1):19–26, December 2000. 30
- [31] B FELDMAN, R BRAZG, S SCHWARTZ, AND RICHARD WEINSTEIN. **A Continuous Glucose Sensor Based on Wired Enzyme Technology Results from a 3-Day Trial in Patients with Type 1 Diabetes.** *Diabetes Technology & Therapeutics*, **5**(5):769–779, 2003. 30
- [32] V POITOUT, D MOATTI-SIRAT, G REACH, Y ZHANG, G S WILSON, F LEMONNIER, AND J C KLEIN. **A glucose monitoring system for on line estimation in man of blood glucose concentration using a miniaturized glucose sensor implanted in the subcutaneous tissue and a wearable control unit.** *Diabetologia*, **36**:658–663, 1993. 30
- [33] C J WATSON, B J VENTON, AND R T KENNEDY. **In vivo measurements of neurotransmitters by microdialysis sampling.** *Analytical chemistry*, **78**(5):1391–1399, 2006. 30, 32, 35, 36, 221
- [34] J L PETERS, L H MINER, A C MICHAEL, AND S R SESACK. **Ultrastructure at carbon fiber microelectrode implantation sites after acute voltammetric measurements in the striatum of anesthetized rats.** *Journal of neuroscience methods*, **137**(1):9–23, 2004. 30, 32
- [35] A JAQUINS-GERSTL AND A C MICHAEL. **Comparison of the brain penetration injury associated with microdialysis and voltammetry.** *Journal of neuroscience methods*, **183**(2):127–135, 2009. 30, 32, 35
- [36] JOHN P LOWRY, MARTYN G BOUTELLE, AND MARIANNE FILLENZ. **Measurement of brain tissue oxygen at a carbon paste electrode can serve as an index of increases in regional cerebral blood flow.** *Journal of neuroscience methods*, **71**(2):177–182, 1997. 30
- [37] ANNA-MARIA SPEHAR-DELEZE, SALZITSA ANASTASOVA, JONATHAN POPPLEWELL, AND PANKAJ VADGAMA. **Extreme Physiological State: Development of Tissue Lactate Sensor.** *2012 Ninth International Conference on Wearable and Implantable Body Sensor Networks*, pages 17–21, May 2012. 30, 221
- [38] GAIA ROCCHITTA, OTTAVIO SECCHI, MARIA DOMENICA ALVAU, DONATELLA FARINA, GIANFRANCO BAZZU, GIAMMARIO CALIA, ROSSANA MIGHELLI, MARIA SPERANZA DESOLE, ROBERT D O'NEILL, AND PIER A SERRA. **Simultaneous telemetric monitoring of brain glucose and lactate and motion in freely moving rats.** *Analytical chemistry*, **85**(21):10282–8, November 2013. 30
- [39] PIER ANDREA SERRA, GIULIA PUGGIONI, GIANFRANCO BAZZU, AND GIAMMARIO CALIA. **Design and Construction of a Distributed Sensor NET for Biotelemetric Monitoring of Brain Energetic Metabolism using Microsensors and Biosensors.** In PIER ANDREA SERRA, editor, *Biosensors*, number February. 2010. 30
- [40] C A CORDEIRO, M G DE VRIES, W NGABI, P E OOMEN, T I F H CREMERS, AND B H C WESTERINK. **In vivo continuous and simultaneous monitoring of brain energy substrates with a multiplex amperometric enzyme-based biosensor device.** *Biosensors & bioelectronics*, **67**:677–86, May 2015. 30
- [41] F MOUSSY, J HARRISON, DARRYL W O'BRIEN, AND RAY V RAJOTTE. **Performance of Subcutaneously Implanted Needle-Type Glucose Sensors Employing.** *Analytical chemistry*, **65**(4):2072–2077, 1993. 30
- [42] JOHN P LOWRY, MICHAEL R RYAN, AND ROBERT D O NEILL. **Behaviourally induced changes in extracellular levels of brain glutamate monitored at 1 s resolution with an implanted biosensor.** *Analytical Communications*, **35**:87–89, 1998. 30
- [43] SU-YOUNE CHANG, INYONG KIM, MICHAEL P MARSH, DONG PYO JANG, SUN-CHUL HWANG, JAMIE J VAN GOMPEL, STEPHAN J GORERS, CHRISTOPHER J KIMBLE, KEVIN E BENNETT, PAUL A GARRIS, CHARLES D BLAHA, AND KENDALL H LEE. **Wireless fast-scan cyclic voltammetry to monitor adenosine in patients with essential tremor during deep brain stimulation.** *Mayo Clinic proceedings*, **87**(8):760–5, August 2012. 30
- [44] PAUL E.M. PHILLIPS AND R.MARK WIGHTMAN. **Critical guidelines for validation of the selectivity of in-vivo chemical micro-sensors.** *TrAC Trends in Analytical Chemistry*, **22**(8):509–514, September 2003. 30
- [45] GEORGE S WILSON AND RAEANN GIFFORD. **Biosensors for real-time in vivo measurements.** *Biosensors & bioelectronics*, **20**(12):2388–403, June 2005. 30, 31, 61
- [46] GEORGE S WILSON AND MALIKA AMMAM. **In vivo biosensors.** *The FEBS journal*, **274**(21):5452–61, November 2007. 30
- [47] GEORGE S WILSON AND MICHAEL A JOHNSON. **In-Vivo Electrochemistry: What Can We Learn about Living Systems?** *Chemical reviews*, **108**:2462–2481, 2008. 30
- [48] JOSEPH WANG. **In vivo glucose monitoring: towards 'Sense and Act' feedback-loop individualized medical systems.** *Talanta*, **75**(3):636–41, May 2008. 30
- [49] JOHN P LOWRY, MADDALENA MIELE, ROBERT D O'NEILL, MARTYN G BOUTELLE, AND MARIANNE FILLENZ. **An amperometric glucose-oxidase/poly(o-phenylenediamine) biosensor for monitoring brain extracellular glucose: in vivo characterization in the striatum of freely-moving rats.** *Journal of neuroscience methods*, **79**(1):65–74, 1998. 30
- [50] ROBERT D O'NEILL, JOHN P LOWRY, GAIA ROCCHITTA, COLM P MCMAHON, AND PIER A SERRA. **Designing sensitive and selective polymer / enzyme composite biosensors for brain monitoring in vivo.** *Trends in Analytical Chemistry*, **27**(1):78–88, 2008. 30
- [51] FINBAR O. BROWN AND JOHN P. LOWRY. **Microelectrochemical sensors for in vivo brain analysis: an investigation of procedures for modifying Pt electrodes using Nafion.** *The Analyst*, **128**(6):700, 2003. 30
- [52] F MOUSSY, D J HARRISON, D W O'BRIEN, AND R V RAJOTTE. **Performance of subcutaneously implanted needle-type glucose sensors employing a novel trilayer coating.** *Analytical chemistry*, **65**:2072–2077, 1993. 30
- [53] O M SCHUVAILO, O O SOLDATKIN, A LEFEBVRE, R CESPUGLIO, AND A P SOLDATKIN. **Highly selective microbiosensors for in vivo measurement of glucose, lactate and glutamate.** *Analytica chimica acta*, **573-574**:110–6, July 2006. 30

- [54] YIBAI HU AND GEORGE S. WILSON. **A Temporary Local Energy Pool Coupled to Neuronal Activity: Fluctuations of Extracellular Lactate Levels in Rat Brain Monitored with Rapid-Response Enzyme-Based Sensor.** *Journal of Neurochemistry*, **69**(4):1484–1490, November 2002. 30
- [55] MARTIJN GERRITSEN, JOHN A. JANSEN, ALEXANDER KROS, ROELAND J. M. NOLTE, AND JOS A. LUTTERMAN. **Performance of Subcutaneously Implanted Glucose Sensors: A Review.** *Journal of Investigative Surgery*, **11**(3):163–174, January 1998. 30
- [56] RAEANN GIFFORD, JOSEPH J KEHOE, SANDRA L BARNES, BORIS A KORNLAYEV, MICHAIL A ALTERMAN, AND GEORGE S WILSON. **Protein interactions with subcutaneously implanted biosensors.** *Biomaterials*, **27**(12):2587–98, April 2006. 30
- [57] NATALIE WISNIEWSKI, F. MOUSSY, AND W. M. REICHERT. **Characterization of implantable biosensor membrane biofouling.** *Fresenius J Anal Chem*, **366**(6-7):611–621, March 2000. 30
- [58] PATRICK A. TRESKO AND BRENT D. WINSLOW. **The Challenge of Integrating Devices into the Central Nervous System.** *Critical Reviews in Biomedical Engineering*, **39**(1):29–44, 2011. 30
- [59] NATALIE WISNIEWSKI AND MONTY REICHERT. **Methods for reducing biosensor membrane biofouling.** *Colloids and Surfaces B: Biointerfaces*, **18**(3-4):197–219, October 2000. 31
- [60] AHYEON KOH, DANIEL A RICCIO, BIN SUN, ALEXIS W CARPENTER, SCOTT P NICHOLS, AND MARK H SCHOENFISCH. **Fabrication of nitric oxide-releasing polyurethane glucose sensor membranes.** *Biosensors & bioelectronics*, **28**(1):17–24, October 2011. 31, 78
- [61] BLANAID M DIXON, JOHN P LOWRY, AND ROBERT D O NEILL. **Characterization in vitro and in vivo of the oxygen dependence of an enzyme / polymer biosensor for monitoring brain glucose.** *Journal of neuroscience methods*, **119**:135–142, 2002. 31
- [62] PLAMEN ATANASOV AND EBTISAM WILKINS. **In vivo rechargeable glucose biosensors.** *Sensors and Actuators B: Chemical*, **36**(1-3):435–447, October 1996. 31
- [63] P.U ABEL AND T VON WOEDTKE. **Biosensors for in vivo glucose measurement: can we cross the experimental stage.** *Biosensors and Bioelectronics*, **17**(11-12):1059–1070, December 2002. 31
- [64] TAK S CHING AND PATRICIA CONNOLLY. **Simultaneous transdermal extraction of glucose and lactate from human subjects by reverse iontophoresis.** *International Journal of Nanomedicine*, **3**(2):211–223, 2008. 31
- [65] THE DIABETES RESEARCH IN CHILDREN (DIRECNET) STUDY GROUP. **Accuracy of the GlucoWatch G2 Biographer and the Continuous Glucose Monitoring System During Hypoglycemia.** *Diabetes care*, **27**(3):1–5, 2004. 31
- [66] PENG SONG, NEIL D HERSHEY, OMAR S MABROUK, THOMAS R SLANEY, AND ROBERT T KENNEDY. **Mass spectrometry "sensor" for in vivo acetylcholine monitoring.** *Analytical chemistry*, **84**(11):4659–64, June 2012. 32
- [67] MENG WANG, GREGORY T ROMAN, MAURA L PERRY, AND ROBERT T KENNEDY. **Microfluidic Chip for High Efficiency Electrophoretic Analysis of Segmented Flow from a Microdialysis Probe and in Vivo Chemical Monitoring.** *Analytical chemistry*, **81**(21):9072–9078, 2009. 32
- [68] PRADYOT NANDI, DHARA P DESAI, AND SUSAN M LUNTE. **Development of a PDMS-based microchip electrophoresis device for continuous online in vivo monitoring of microdialysis samples.** *Electrophoresis*, **31**(8):1414–22, April 2010. 32
- [69] MICHELLE L ROGERS, DELPHINE FEUERSTEIN, CHI LENG LEONG, MASATOSHI TAKAGAKI, XIZE NIU, RUDOLF GRAF, AND MARTYN G BOUTELLE. **Continuous Online Microdialysis Using Microfluidic Sensors: Dynamic Neurometabolic Changes during Spreading Depolarization.** *ACS Chemical Neuroscience*, **4**:799–807, 2013. 32, 37, 52, 55, 250
- [70] URBAN UNGERSTEDT AND C PYCOCK. **Functional Correlates of Dopamine Neurotransmission.** *Bulletin der Schweizerischen Akademie der Medizinischen Wissenschaften*, **30**(1-3):44–45, 1974. 32
- [71] JULIE A STENKEN. **Methods and issues in microdialysis calibration.** *Analytica chimica acta*, **379**(3):337–358, 1999. 33
- [72] JULIE A STENKEN, CRAIG E LUNTE, Z SOUTHARD, MARYLEE, AND LARS STAHL. **Factors That Influence Microdialysis Recovery. Comparison of Experimental and Theoretical Microdialysis Recoveries in Rat Liver.** *Journal of pharmaceutical sciences*, **86**(8):958–966, 1997. 33
- [73] MG BOUTELLE AND M FILLENZ. **Clinical Microdialysis: The Role of On-line Measurement and Quantitative Microdialysis.** *Acta neurochirurgica. Supplement*, **67**:13–20, 1996. 33, 34
- [74] HELENE BENVENISTE, ANKER JON HANSEN, AND NIELS SAABYE OTTOSEN. **Determination of Brain Interstitial Concentrations by Microdialysis.** *Journal of Neurochemistry*, **52**(6):1741–1750, June 1989. 33
- [75] PETER M BUNGAY, PAIGE NEWTON-VINSON, WANDA ISELE, PAUL A GARRIS, AND JOSEPH B JUSTICE. **Microdialysis of dopamine interpreted with quantitative model incorporating probe implantation trauma.** *Journal of Neurochemistry*, **86**(4):932–946, 2003. 33, 34
- [76] HUA YANG, JENNIFER L PETERS, AND ADRIAN C MICHAEL. **Coupled Effects of Mass Transfer and Uptake Kinetics on In Vivo Microdialysis of Dopamine.** *Journal of Neurochemistry*, **71**(2):684–692, 1998. 33, 34
- [77] P LONNROTH, P A JANSSON, B B FREDHOLM, AND U SMITH. **Microdialysis concentration of intercellular adenosine in subcutaneous tissue in humans.** *American Journal of Physiology*, **256**(29):E250–E255, 1989. 34
- [78] YI LU, JENNIFER L PETERS, AND ADRIAN C MICHAEL. **Direct Comparison of the Response of Voltammetry and Microdialysis to Electrically Evoked Release of Striatal Dopamine.** *Journal of Neurochemistry*, **70**(2):584–593, 1998. 34
- [79] JENNIFER L PETERS AND ADRIAN C MICHAEL. **Modeling Voltammetry and Microdialysis of Striatal Extracellular Dopamine: The Impact of Dopamine Uptake on Extraction and Recovery Ratios.** *Journal of Neurochemistry*, **70**(2):594–603, 1998. 34
- [80] KEVIN C CHEN. **Evidence on extracellular dopamine level in rat striatum: implications for the validity of quantitative microdialysis.** *Journal of Neurochemistry*, **92**(1):46–58, 2005. 34
- [81] KEVIN C CHEN. **Preferentially impaired neurotransmitter release sites not their discreteness compromise the validity of microdialysis zero-net-flux method.** *Journal of Neurochemistry*, **92**(1):29–45, 2005. 34
- [82] E RONNE-ENGSTROM, K G CESARINI, P ENBLAD, G HESSELAGER, N MARKLUND, P NILSSON, K SALCI, L PERSSON, AND L HILLERED. **Intracerebral microdialysis in neurointensive care: the use of urea as an endogenous reference compound.** *Journal of neurosurgery*, **94**(3):397–402, 2001. 34
- [83] H BENVENISTE AND N H DIEMER. **Cellular reactions to implantation of a microdialysis tube in the rat hippocampus.** *Acta Neuropathologica*, **74**:234–238, 1987. 35

BIBLIOGRAPHY

- [84] M N WOODROOFE, G S SARNA, M WADHWA, G M HAYES, A J LOUGHLIN, A TINKER, AND ML CUZNER. **Detection of interleukin-1 and interleukin-6 in adult rat brain, following mechanical injury, by in vivo microdialysis: evidence of a role for microglia in cytokine production.** *Journal of Neuroimmunology*, **33**:227–236, 1991. 35
- [85] JULIE STENKEN, MARTIN CHURCH, CAROLYN GILL, AND GERALDINE CLOUGH. **How Minimally Invasive is Microdialysis Sampling? A Cautionary Note for Cytokine Collection in Human Skin and other Clinical Studies.** *The AAPS journal*, **12**(1):73–78, 2010. 35
- [86] D H SZAROWSKI, M D ANDERSEN, S RETTERER, A J SPENCE, AND M ISAACSON. **Brain responses to micro-machined silicon devices.** *Brain Research*, **983**:23–35, 2003. 35
- [87] FANG ZHOU, JOAN F BRADDOCK, YONG HU, XIONGWEI ZHU, RUDY J CASTELLANI, MARK A SMITH, AND KELLY L DREW. **Microbial origin of glutamate, hibernation and tissue trauma: an in vivo microdialysis study.** *Journal of neuroscience methods*, **119**:121–128, 2002. 35
- [88] J ROS, N PECINSKA, B ALESSANDRI, H LANDOLT, AND M FILLENZ. **Lactate Reduces Glutamate-Induced Neurotoxicity in Rat Cortex.** *Journal of Neuroscience Research*, **794**:790–794, 2001. 35
- [89] H. BENVENISTE, J. DREJER, A. SCHOUSBOE, AND N. H. DIEMER. **Regional Cerebral Glucose Phosphorylation and Blood Flow After Insertion of a Microdialysis Fiber Through the Dorsal Hippocampus in the Rat.** *Journal of Neurochemistry*, **49**(3):729–734, September 1987. 35
- [90] M SANTIAGO AND B H C WESTERINK. **Characterization of the in vivo release of dopamine as recorded by different types of intracerebral microdialysis probes.** *Archives of Pharmacology*, **342**:407–414, 1990. 35
- [91] KIMBERLY L CLAPP-LILLY, ROSALINDA C ROBERTS, LAWRENCE K DUFFY, KATHERINE P IRONS, YONG HU, AND KELLY L DREW. **An ultrastructural analysis of tissue surrounding a microdialysis probe.** *Journal of neuroscience methods*, **90**(2):129–142, 1999. 35
- [92] MARK C PARKIN, SARAH E HOPWOOD, MARTYN G BOUTELLE, AND ANTHONY J STRONG. **Resolving dynamic changes in brain metabolism using biosensors and on-line microdialysis.** *TrAC Trends in Analytical Chemistry*, **22**(8):487–497, 2003. 35, 45, 162, 202
- [93] AMINA S KHAN AND ADRIAN C MICHAEL. **Invasive consequences of using micro-electrodes and microdialysis probes in the brain.** *TrAC Trends in Analytical Chemistry*, **22**(8):503–508, 2003. 36
- [94] ANDREA JAQUINS-GERSTL, ZHAN SHU, JING ZHANG, YANSHENG LIU, STEPHEN G WEBER, AND ADRIAN C MICHAEL. **Effect of Dexamethasone on Gliosis, Ischemia, and Dopamine Extraction during Microdialysis Sampling in Brain Tissue.** *Analytical chemistry*, **83**(20):7662–7667, 2011. 36
- [95] M PARKIN, S HOPWOOD, D A JONES, P HASHEMI, H LANDOLT, M FABRICIUS, M LAURITZEN, M G BOUTELLE, AND A J STRONG. **Dynamic changes in brain glucose and lactate in pericontusional areas of the human cerebral cortex, monitored with rapid sampling on-line microdialysis: relationship with depolarisation-like events.** *Journal of cerebral blood flow and metabolism*, **25**(3):402–413, 2005. 36, 45
- [96] DELPHINE FEUERSTEIN, ANDREW MANNING, PARASTOO HASHEMI, ROBIN BHATIA, MARTIN FABRICIUS, CHRISTOS TOLIAS, CLEMENS PAHL, MAX ERVINE, ANTHONY J STRONG, AND MARTYN G BOUTELLE. **Dynamic metabolic response to multiple spreading depolarizations in patients with acute brain injury: an online microdialysis study.** *Journal of cerebral blood flow and metabolism*, **30**(7):1343–1355, 2010. 36, 45
- [97] R BHATIA, P HASHEMI, A RAZZAQ, M C PARKIN, S E HOPWOOD, M G BOUTELLE, AND A J STRONG. **Application of rapid-sampling, online microdialysis to the monitoring of brain metabolism during aneurysm surgery.** *Neurosurgery*, **58**(4):313–321, 2006. 36, 45
- [98] D A JONES, M C PARKIN, H LANGEMANN, H LANDOLT, AND S E HOPWOOD. **On-line monitoring in neurointensive care Enzyme-based electrochemical assay for simultaneous, continuous monitoring of glucose and lactate from critical care patients.** *Journal of Electroanalytical Chemistry*, **539**:243–252, 2002. 36
- [99] S DEEBA, E P CORCOLES, G B HANNA, B G HANNA, P PARESKEVAS, O AZIZ, M G BOUTELLE, AND A DARZI. **Use of rapid sampling microdialysis for intraoperative monitoring of bowel ischemia.** *Diseases of the colon and rectum*, **51**(9):1408–13, September 2008. 36, 45, 132, 156, 239, 271
- [100] M L ROGERS, P A BRENNAN, C L LEONG, S A N GOWERS, T ALDRIDGE, T K MELLOR, AND M G BOUTELLE. **Online rapid sampling microdialysis (rsMD) using enzyme-based electroanalysis for dynamic detection of ischaemia during free flap reconstructive surgery.** *Analytical and bioanalytical chemistry*, **405**(11):3881–3888, 2013. 36
- [101] GEOFFREY TAYLOR. **Dispersion of soluble matter in solvent flowing slowly through a tube.** *Proceedings of the Royal Society of London. Series A, Mathematical and Physical Sciences*, **219**(1137):186–203, 1953. 37, 250, 264
- [102] M G BOUTELLE, L K FELLOWS, AND C COOK. **Enzyme packed bed system for the on-line measurement of glucose, glutamate, and lactate in brain microdialysate.** *Analytical chemistry*, **64**(17):1790–1794, 1992. 48
- [103] MARK H SMIT AND ANTHONY E G CASS. **Cyanide detection using a substrate-regenerating peroxidase-based biosensor.** *Analytical chemistry*, **62**(22):2429–2436, 1990. 48
- [104] D FEUERSTEIN, K H PARKER, AND M G BOUTELLE. **Practical methods for noise removal: applications to spikes, non-stationary quasi-periodic noise, and baseline drift.** *Analytical chemistry*, **81**(12):4987–4994, 2009. 51, 121, 199
- [105] BHAVIK ANIL PATEL, MICHELLE ROGERS, TALIA WIEDER, DANNY O'HARE, AND MARTYN G BOUTELLE. **ATP microelectrode biosensor for stable long-term in vitro monitoring from gastrointestinal tissue.** *Biosensors & bioelectronics*, **26**(6):2890–6, February 2011. 52, 90, 98
- [106] P N BARTLETT AND K F E PRATT. **A study of the kinetics of the reaction between ferrocene monocarboxylic acid and glucose oxidase using the rotating-disc electrode.** *Journal of Electroanalytical Chemistry*, **397**:53–60, 1995. 54
- [107] NATALIA VASYLIEVA, BOGDAN BARNYCH, ANNE MEILLER, CAROLINE MAUCLER, LOREDANO POLLEGIONI, JIAN-SHENG LIN, DANIEL BARBIER, AND STÉPHANE MARINESCO. **Covalent enzyme immobilization by poly (ethylene glycol) diglycidyl ether (PEGDE) for microelectrode biosensor preparation.** *Biosensors and Bioelectronics*, **26**:3993–4000, 2011. 56, 75, 78
- [108] ALESSANDRO VIGGIANO, STÉPHANE MARINESCO, FRÉDÉRIC PAIN, ANNE MEILLER, AND HIRAC GURDEN. **Reconstruction of field excitatory post-synaptic potentials in the dentate gyrus from amperometric biosensor signals.** *Journal of neuroscience methods*, **206**:1–6, 2012. 56, 75
- [109] GOLAM FARUQUE KHAN, MASAKI OHWA, AND WOLFGANG WERNET. **Design of a Stable Charge Transfer Complex Electrode for a Third-Generation Amperometric Glucose Sensor.** *Analytical chemistry*, **68**(17):2939–2945, 1996. 62
- [110] FRANCESCO PALMISANO, PIER GIORGIO ZAMBONIN, DIPARTIMENTO CHIMICA, VIA ORABONA, DIEGO CENTONZE, MAURIZIO QUINTO, AND PRODUZIONI ALIMENTARI. **Glucose Biosensor Based on Overoxidized Poly (pyrrole)/Tetrathiafulvalene - Tetracyanoquinodimethane Composite.** *Analytical chemistry*, **74**(23):5913–5918, 2002. 62

- [111] P N BARTLETT. **Some Studies of Electrodes Made From Single-Crystals of TTF.TCNQ.** *Journal of Electroanalytical Chemistry*, **300**:175–189, 1991. 62
- [112] J.J. KULYS. **Enzyme electrodes based on organic metals.** *Biosensors*, **2**(1):3–13, 1986. 62
- [113] LING YE, J MARTIN HIMMERLE, ARJEN J J OLSTHOORN, SCHUHMANN HANS-LUDWIG SCHMIDT, JOHANNIS A DUINE, AND ADAM HELLERT. **High Current Density Wired Quinoprotein Glucose Dehydrogenase Electrode.** *Analytical chemistry*, **65**(4):4–7, 1993. 62
- [114] YU-CHEN TSAI, SHIH-CI LI, AND JIE-MING CHEN. **Cast Thin Film Biosensor Design Based on a Nafion Backbone, a Multivalled Carbon Nanotube Conduit, and a Glucose Oxidase Function.** *Langmuir*, **21**(15):3653–3658, 2005. 62
- [115] JING WU AND YANG QU. **Mediator-free amperometric determination of glucose based on direct electron transfer between glucose oxidase and an oxidized boron-doped diamond electrode.** *Analytical and bioanalytical chemistry*, **385**(7):1330–5, August 2006. 62
- [116] R WILSON AND APF TURNER. **Review article Glucose oxidase: an ideal enzyme.** *Biosensors and Bioelectronics*, **7**:165–185, 1992. 62
- [117] GERD WOHLFAHRT, SUSANNE WITT, JÖRG HENDLE, DIETMAR SCHOMBURG, HENRYK M. KALISZ, AND HANS-JÜRGEN HECHT. **1.8 and 1.9Å resolution structures of the *Penicillium amagasakiense* and *Aspergillus niger* glucose oxidases as a basis for modelling substrate complexes.** *Acta Crystallographica Section D Biological Crystallography*, **55**(5):969–977, May 1999. 62
- [118] SATOSHI NAKAMURA AND YASUYUKI OGURA. **Action Mechanism of Glucose Oxidase of *Aspergillus niger*.** *The Journal of Biochemistry*, **63**(3):308–316, 1968. 62
- [119] CHUN MING WONG, KWUN HEI WONG, AND XIAO DONG CHEN. **Glucose oxidase: natural occurrence, function, properties and industrial applications.** *Applied microbiology and biotechnology*, **78**(6):927–38, April 2008. 63
- [120] MAKIO FURUICHI, NOBUHIRO SUZUKI, BALASUNDARESAN DHAKSHNAMOORHTY, HIROTAKA MINAGAWA, RYOSUKE YAMAGISHI, YUTA WATANABE, YUKARI GOTO, HIROKI KANEKO, YOSHIHITO YOSHIDA, HIROTAKA YAGI, IWAO WAGA, PENMETCHA K R KUMAR, AND HIROSHI MIZUNO. **X-ray structures of *Aerococcus viridans* lactate oxidase and its complex with D-lactate at pH 4.5 show an alpha-hydroxyacid oxidation mechanism.** *Journal of molecular biology*, **378**(2):436–46, April 2008. 63, 64
- [121] INGAR LEIROS, ELLEN WANG, TONNI RASMUSSEN, ESKO OKSANEN, HEIDI REPO, STEFFEN B PETERSEN, PIIRKKO HEIKINHEIMO, AND EDWARD HOUGH. **The 2.1 Å structure of *Aerococcus viridans* L-lactate oxidase (LOX).** *Acta crystallographica. Section F, Structural biology and crystallization communications*, **62**(Pt 12):1185–90, December 2006. 63
- [122] K MAEDA-YORITA, K AKI, H SAGAI, H MISAKI, AND V MASSEY. **L-Lactate oxidase and L-lactate monooxygenase: Mechanistic variations on a common structural theme.** *Biochimie*, **77**:631–642, 1995. 64
- [123] GUNNAR I BERGLUND, GUNILLA H CARLSSON, ANDREW T SMITH, HANNA SZOKE, ANETTE HENRIKSEN, AND JANOS HAJDU. **The catalytic pathway of horseradish peroxidase at high resolution.** *Nature*, **417**(May):463–468, 2002. 64, 65
- [124] VANESA SANZ, SUSANA DE MARCOS, JUAN R CASTILLO, AND JAVIER GALBA. **Application of Molecular Absorption Properties of Horseradish Peroxidase for Self-Indicating Enzymatic Interactions and Analytical Methods.** *Journal of the American Chemical Society*, **127**:1038–1048, 2005. 65, 66
- [125] I. A. BORISOV, A. V. LOBANOV, A. N. RESHETILOV, AND B. I. KURGANOV. **Quantitative analysis of the calibration dependences for biosensors.** *Applied Biochemistry and Microbiology*, **36**(3):215–220, May 2000. 67
- [126] DIMITRA G GEORGANOPOULOU, ROBERT CARLEY, DEBORAH A JONES, AND MARTYN G BOUTELLE. **Development and comparison of biosensors for in-vivo applications.** *Faraday Discussions*, **116**(0):291–303, 2000. 67
- [127] DIBAKAR BHATTACHARYYA AND ALLAN DA BUTTERFIELD, editors. **New Insights into Membrane Science and Technology: Polymeric and Biofunctional Membranes: Polymeric and Biofunctional Membranes. Vol. 8.** Elsevier, 2003. 78
- [128] JAKUB TRZEBINSKI, SANJIV SHARMA, ANNA RADOMSKA-BOTELHO MONIZ, KOSTIS MICHELAKIS, YANGYANG ZHANG, AND ANTHONY E G CASS. **Microfluidic device to investigate factors affecting performance in biosensors designed for transdermal applications.** *Lab on a chip*, **12**(2):348–52, January 2012. 78, 83
- [129] NING WANG, KRISHNA BURUGAPALLI, WENHUI SONG, JUSTIN HALLS, FRANCIS MOUSSY, ASIM RAY, AND YUDONG ZHENG. **Electrospun fibro-porous polyurethane coatings for implantable glucose biosensors.** *Biomaterials*, **34**(4):888–901, January 2013. 78, 83
- [130] STEPHEN F WHITE, IBTISAM E TOTTHILL, JEFFREY D NEWMAN, AND ANTHONY P F TURNER. **Development of a mass-producible glucose biosensor and flow-injection analysis system suitable for on-line monitoring during fermentations.** *Analytica chimica acta*, **321**:165–172, 1996. 78
- [131] RASA PAULIUKAITE, MONIKA SCHOENLEBER, PANKAJ VADGAMA, AND CHRISTOPHER M A BRETT. **Development of electrochemical biosensors based on sol-gel enzyme encapsulation and protective polymer membranes.** *Analytical and bioanalytical chemistry*, **390**(4):1121–31, February 2008. 78
- [132] BYEONG-UI MOON, SANDER KOSTER, KLAAS J C WIENTJES, RADO-SAW M KWAPISZEWSKI, ADELBERT J M SCHOONEN, BEN H C WESTERINK, AND ELISABETH VERPOORTE. **An Enzymatic Microreactor Based on Chaotic Micromixing for Enhanced Amperometric Detection in a Continuous Glucose Monitoring Application.** *Analytical chemistry*, **82**(16):6756–6763, 2010. 87
- [133] D.G. PIJANOWSKA, A.J. SPRENKELS, W OLTHUIS, AND P BERGVELD. **A flow-through amperometric sensor for micro-analytical systems.** *Sensors and Actuators B: Chemical*, **91**(1-3):98–102, June 2003. 87
- [134] S BOHM, D PIJANOWSKA, W OLTHUIS, AND P BERGVELD. **A flow-through amperometric sensor based on dialysis tubing and free enzyme reactors.** *Biosensors & Bioelectronics*, **16**:391–397, 2001. 87
- [135] ENRIQUE LLAUDET, SONJA HATZ, MAGALI DRONIOU, AND NICHOLAS DALE. **Microelectrode Biosensor for Real-Time Measurement of ATP in Biological Tissue.** *Analytical chemistry*, **77**(10):3267–3273, 2005. 98
- [136] DEBORAH A JONES. **Development of a pyruvate assay for neurochemical studies.** Technical report, Department of Chemistry, Kings College London, 1996. 100, 101
- [137] K IKEBUKURO, RYOKO NISHIDA, HIROYUKI YAMAMOTO, YOSHIKO ARIKAWA, H NAKAMURA, M SUZUKI, I KUBO, T TAKEUCHI, AND I KARUBE. **A novel biosensor system for the determination of phosphate.** *Journal of Biotechnology*, **48**:67–72, 1996. 101
- [138] MD. AMINUR RAHMAN, DEOG-SU PARK, SEUNG-CHEOL CHANG, CALUM J. MCNEIL, AND YOON-BO SHIM. **The biosensor based on the pyruvate oxidase modified conducting polymer for phosphate ions determinations.** *Biosensors and Bioelectronics*, **21**(7):1116–1124, January 2006. 101
- [139] M MASCINI AND F MAZZEL. **Amperometric sensor for pyruvate with immobilized pyruvate oxidase.** *Analytica chimica acta*, **192**:9, 1987. 101

BIBLIOGRAPHY

- [140] VINCENT LINDER, SAMUEL K SIA, AND GEORGE M WHITESIDES. **Reagent-loaded cartridges for valveless and automated fluid delivery in microfluidic devices.** *Analytical chemistry*, **77**(1):64–71, January 2005. 103
- [141] I. MIMURA AND M NANGAKU. **The suffocating kidney: tubulointerstitial hypoxia in end-stage renal disease.** *Nature Reviews Nephrology*, 2010. 112
- [142] N R BROOK AND M L NICHOLSON. **Kidney transplantation from non heart-beating donors.** *The Surgeon*, **1**(6):311–322, 2003. 112, 113
- [143] **NHSBT Organ Donation and Transplantation Activity Report 2013-2014.** Technical report, 2014. 112, 113, 116, 178, 179
- [144] S D ST PETER, C J IMBER, AND P J FRIEND. **Liver and kidney preservation by perfusion.** *Lancet*, **359**(9306):604–613, 2002. 112
- [145] M J TAYLOR AND S C BAICU. **Current state of hypothermic machine perfusion preservation of organs: The clinical perspective.** *Cryobiology*, **60**(3 Suppl):S20–35, 2010. 112, 116, 179
- [146] LUKE R DEVEY, PETER J FRIEND, JOHN L R FORSYTHE, LISA L MUMFORD, AND STEPHEN J WIGMORE. **The use of marginal heart beating donor livers for transplantation in the United kingdom.** *Transplantation*, **84**(1):70–4, July 2007. 113
- [147] **NHSBT Organ Donation and Transplantation Activity Report 2003-2004.** Technical report, 2004. 113
- [148] C Y LEE AND M J MANGINO. **Preservation methods for kidney and liver.** *Organogenesis*, **5**(3):105–112, 2009. 113, 114, 115
- [149] ANA I SANCHEZ-FRUCTUOSO, DOLORES PRATS, JAIME TORRENTE, CRISTINA FERN ANDEZ, AND ALBERTO BARRIENTOS. **Renal Transplantation from Non-Heart Beating Donors: A Promising Alternative to Enlarge the Donor Pool.** *J Am Chem Soc Nephrology*, **11**:350–358, 2000. 113
- [150] G KOOTSTRA, J H C DAEMEN, AND A P A OOMEN. **Categories of non-heart-beating donors.** *TRANSPLANTATION PROCEEDINGS*, **27**(5):2893–2894, October 1995. 113
- [151] M RENGEL, J KANTER, M PUERTA, F ANAYA, M RODRIGUEZ, AND E VERDE. **Kidney transplantation with grafts from non-heart-beating donors.** *Transplantation proceedings*, **38**(3):890–1, April 2006. 113
- [152] R M WIJNEN, M H BOOSTER, B M STUBENITSKY, J DE BOER, E HEINEMAN, AND G KOOTSTRA. **Outcome of transplantation of non-heart-beating donor kidneys.** *Lancet*, **345**(8957):1067–70, April 1995. 113
- [153] R HATTORI, S OHSHIMA, Y ONO, T FUJITA, T KINUKAWA, AND O MATSUURA. **Long-term outcome of kidney transplants from non-heart-beating donors: multivariate analysis of factors affecting graft survival.** *Transplantation proceedings*, **31**(7):2847–50, November 1999. 113
- [154] FRIEDRICH K PORT, JENNIFER L BRAGG-GRESHAM, ROBERT A METZGER, DAWN M DYKSTRA, BRENDA W GILLESPIE, ERIC W YOUNG, FRANCIS L DELMONICO, JAMES J WYNN, ROBERT M MERION, ROBERT A WOLFE, AND PHILIP J HELD. **Donor characteristics associated with reduced graft survival: an approach to expanding the pool of kidney donors.** *Transplantation*, **74**(9):1281–6, November 2002. 113
- [155] AKINLOLU O OJO, JULIE A HANSON, CHIKE N OKECHUKWU, ROBERT A WOLFE, ALAN B LEICHTMAN, LAWRENCE Y AGODOA, BRUCE KAPLAN, AND FRIEDRICH K PORT. **Survival in Recipients of Marginal Cadaveric Donor Kidneys Compared with Other Recipients and Wait-Listed Transplant Candidates.** *J Am Chem Soc Nephrology*, **12**:589–597, 2001. 114
- [156] PETER J MORRIS, RACHEL J JOHNSON, SUSAN V FUGGLE, MARK A BELGER, J DOUGLAS BRIGGS, AND H L A TASK. **Analysis of factors that affect outcome of primary cadaveric renal transplantation in the UK.** *The Lancet*, **354**:1147–1152, 1999. 114
- [157] DOMINIC M SUMMERS, RACHEL J JOHNSON, JOANNE ALLEN, SUSAN V FUGGLE, DAVID COLLETT, CHRISTOPHER J WATSON, AND J ANDREW BRADLEY. **Analysis of factors that affect outcome after transplantation of kidneys donated after cardiac death in the UK: a cohort study.** *The Lancet*, **376**(9749):1303–1311, 2010. 114
- [158] LAUREN BRASILE, BART M STUBENITSKY, MAURITS H BOOSTER, SUSANNE LINDELL, D ARANEDA, CORINNE BUCK, J BRADFELD, CARL E HAISCH, AND GAUKE KOOTSTRA. **Overcoming severe renal ischemia: the role of ex vivo warm perfusion.** *Transplantation*, **73**(6):897–901, 2002. 114, 117
- [159] M KOSIERADZKI AND W ROWINSKI. **Ischemia/Reperfusion Injury in Kidney Transplantation: Mechanisms and Prevention.** *Transplantation Proceedings*, **40**(10):3279–3288, 2008. 114, 115
- [160] SARAH A HOSGOOD, ATUL BAGUL, BIN YANG, AND MICHAEL L NICHOLSON. **The relative effects of warm and cold ischemic injury in an experimental model of nonheartbeating donor kidneys.** *Transplantation*, **85**(1):88–92, January 2008. 114, 157
- [161] J E LOCKE, D L SEGEV, D S WARREN, F DOMINICI, C E SIMPKINS, AND R A MONTGOMERY. **Outcomes of kidneys from donors after cardiac death: implications for allocation and preservation.** *American journal of transplantation : official journal of the American Society of Transplantation and the American Society of Transplant Surgeons*, **7**(7):1797–807, July 2007. 114
- [162] P BOROS AND J S BROMBERG. **New cellular and molecular immune pathways in ischemia/reperfusion injury.** *American journal of transplantation : official journal of the American Society of Transplantation and the American Society of Transplant Surgeons*, **6**(4):652–8, April 2006. 114
- [163] B M STUBENITSKY, M H BOOSTER, A P NEDERSTIGT, J K KIEVIT, R W JACOBS, AND G KOOTSTRA. **Kidney preservation in the next millenium.** *Transplant international : official journal of the European Society for Organ Transplantation*, **12**(2):83–91, 1999. 114, 115
- [164] G J FUHRMAN AND F A FUHRMAN. **Oxygen consumption of animals and tissues as a function of temperature.** *J Gen Physiol.*, **42**(4):715, 1959. 114
- [165] MICHAEL J TAYLOR. **Biology of Cell Survival in the Cold: The Basis for Biopreservation of Tissues and Organs.** In *Advances in biopreservation*, pages 15–62. 2006. 114
- [166] MICHAEL J TAYLOR. **Hypothermic Blood Substitution: Special Considerations for Protection of Cells during ex vivo and in vivo Preservation.** *Transfusion Medicine and Hemotherapy*, **34**(4):226–244, 2007. 114
- [167] SIMONA C BAICU, MICHAEL J TAYLOR, AND KELVIN G M BROCKBANK. **The role of preservation solution on acid-base regulation during machine perfusion of kidneys.** *Clinical transplantation*, **20**(1):113–21, 2005. 115
- [168] SIMONA C BAICU AND MICHAEL J TAYLOR. **Acid-base buffering in organ preservation solutions as a function of temperature: new parameters for comparing buffer capacity and efficiency.** *Cryobiology*, **45**(1):33–48, August 2002. 115
- [169] C MOERS, J M SMITS, MARK-HUGO J MAATHUIS, J TRECKMANN, F VAN GELDER, B P NAPIERALSKI, M VAN KASTEROP-KUTZ, J J VAN DER HEIDE, J P SQUIFFLET, E VAN HEURN, G R KIRSTE, A RAHMEL, HENRI G D LEUVENINK, A PAUL, J PIRENNE, AND RUTGER J PLOEG. **Machine Perfusion or Cold Storage in Deceased-Donor Kidney Transplantation.** *New England Journal of Medicine*, **360**(1):7–19, 2009. 115, 153

- [170] G M COLLINS, MARIA BRAVO-SHUGARMAN, AND P I TERASAKI. **Kidney preservation for transportation: Initial Perfusion and 30 Hours' Ice Storage.** *The Lancet*, **294**(7632):1219–1222, December 1969. 115
- [171] F O BELZER, B S ASHBY, P F GULYASSY, AND M POWELL. **Successful seventeen-hour preservation and transplantation of human-cadaver kidney.** *The New England journal of medicine*, **278**(11):608–10, 1968. 115
- [172] N MATSUNO, K KOZAKI, H DEGAWA, Y NARUMI, N SUZUKI, K KIKUCHI, M UCHIYAMA, K KUBOTA, E SAKURAI, M KOZAKI, AND T NAGAO. **A useful predictor in machine perfusion preservation for kidney transplantation from non-heart-beating donors.** *Transplantation Proceedings*, **32**(1):173–174, 2000. 115
- [173] C J SONNENDAY, M COOPER, E KRAUS, F GAGE, C HANDLEY, AND R A MONTGOMERY. **The hazards of basing acceptance of cadaveric renal allografts on pulsatile perfusion parameters alone.** *Transplantation*, **75**(12):2029–2033, 2003. 115
- [174] I JOCHMANS, C MOERS, J M SMITS, H G D LEUVENINK, J TRECKMANN, A PAUL, A RAHMEL, J-P SQUIFFLET, E VAN HEURN, D MONBALIU, R J PLOEG, AND J PIRENNE. **The prognostic value of renal resistance during hypothermic machine perfusion of deceased donor kidneys.** *American journal of transplantation*, **11**(10):2214–20, October 2011. 115
- [175] I JOCHMANS AND J PIRENNE. **Graft quality assessment in kidney transplantation: not an exact science yet!** *Current opinion in organ transplantation*, **16**(2):174–179, 2011. 115
- [176] J A ADAMS, M J MANGINO, J BASSUK, P KURLANSKY, AND M A SACKNER. **Regional blood flow during periodic acceleration.** *Critical care medicine*, **29**(10):1983–1988, 2001. 115
- [177] I R HUTCHESON AND T M GRIFFITH. **Release of endothelium-derived modulated both by frequency relaxing factor is and amplitude of pulsatile flow.** *American Journal of Physiology - Heart and Circulatory Physiology*, **261**(1):H257–H262, 1991. 115
- [178] EA CLARK, PI TERASAKI, G OPELZ, AND MR MICKEY. **No Title.** *New England Journal of Medicine*, **291**(21):1099–1102, 1974. 115
- [179] G OPELZ AND PI TERASAKI. **Kidney preservation: perfusion versus cold storage- 1975.** *Transplantation Proceedings*, **8**(1):121–125, 1976. 115
- [180] JEREMY P WIGHT, JIM B CHILCOTT, MIKE W HOLMES, AND NAOMI BREWER. **Pulsatile machine perfusion vs. cold storage of kidneys for transplantation: a rapid and systematic review.** *Clinical transplantation*, **17**(4):293–307, August 2003. 115, 116
- [181] SRI G YARLAGADDA, STEVEN G COCA, RICHARD N FORMICA, EMILIO D POGGIO, AND CHIRAG R PARIKH. **Association between delayed graft function and allograft and patient survival: a systematic review and meta-analysis.** *Nephrology, dialysis and Transplant Association - European Renal Association*, **24**(3):1039–47, March 2009. 115
- [182] JÜRGEN TRECKMANN, CYRIL MOERS, JACQUELINE M. SMITS, ANJA GALLINAT, MARK HUGO J MAATHUIS, MARGITTA VAN KASTEROP-KUTZ, INA JOCHMANS, JAAP J. HOMAN VAN DER HEIDE, JEAN PAUL SQUIFFLET, ERNEST VAN HEURN, GÜNTER R. KIRSTE, AXEL RAHMEL, HENRI G D LEUVENINK, JACQUES PIRENNE, RUTGER J. PLOEG, AND ANDREAS PAUL. **Machine perfusion versus cold storage for preservation of kidneys from expanded criteria donors after brain death.** *Transplant International*, **24**:548–554, 2011. 115
- [183] R J STRATTA, P S MOORE, A C FARNEY, J ROGERS, E L HARTMANN, A REEVES-DANIEL, M D GAUTREAUX, S S ISKANDAR, AND P L ADAMS. **Influence of pulsatile perfusion preservation on outcomes in kidney transplantation from expanded criteria donors.** *Journal of the American College of Surgeons*, **204**(5):873–874, 2007. 116
- [184] N VAZIRI, R THUILLIER, F D FAVREAU, M EUGENE, S MILIN, N P CHATAURET, T HAUET, AND B BARROU. **Analysis of machine perfusion benefits in kidney grafts: a preclinical study.** *Journal of translational medicine*, **9**:15, 2011. 116
- [185] J H C DAEMEN, B. DE VRIES, A P A OOMEN, J DEMEESTER, AND G KOOTSTRA. **Effect of machine perfusion preservation on delayed graft function in non-heart-beating donor kidneys - early results.** *Transplant International*, **10**:317–322, 1997. 116
- [186] S BALUPURI, ALAN STRONG, NICK HOERNICH, CHRIS SNOWDEN, MOSTAFA MOHAMED, DEREK MANAS, JOHN KIRBY, AND DAVID TALBOT. **Machine perfusion for kidneys: how to do it at minimal cost.** *Transplant International*, **14**(2):103–107, 2001. 116
- [187] TIM C VAN SMAALEN, E R PIETER HOOGLAND, AND L W ERNEST VAN HEURN. **Machine perfusion viability testing.** *Current opinion in organ transplantation*, **18**(2):168–73, April 2013. 116
- [188] CYRIL MOERS, OANA C VARNAV, ERNEST VAN HEURN, INA JOCHMANS, GÜNTER R KIRSTE, AXEL RAHMEL, HENRI G D LEUVENINK, JEAN-PAUL SQUIFFLET, ANDREAS PAUL, JACQUES PIRENNE, WIM VAN OEVEREN, GERHARD RAKHORST, AND RUTGER J PLOEG. **The value of machine perfusion perfusate biomarkers for predicting kidney transplant outcome.** *Transplantation*, **90**(9):966–73, November 2010. 116
- [189] GAUKE KOOTSTRA. **The asystolic, or non-heartbeating, donor.** *Transplantation*, **63**(7):917–921, 1997. 116
- [190] M M POLYAK, B O ARRINGTON, W T STUBENBORD, S KAPUR, AND M KINKHABWALA. **Prostaglandin E1 influences pulsatile preservation characteristics and early graft function in expanded criteria donor kidneys.** *The Journal of surgical research*, **85**(1):17–25, July 1999. 116
- [191] J K KIEVIT, A P NEDERSTIGT, A P OOMEN, M A JANSSEN, L SCHOOT, AND G KOOTSTRA. **Release of alpha-glutathione S-transferase (alpha GST) and pi-glutathione S-transferase (pi GST) from ischemic damaged kidneys into the machine perfusate—relevance to viability assessment.** *Transplantation proceedings*, **29**(8):3591–3, December 1997. 116
- [192] MUHAMMED A GOK, MAURICE PELSERS, JAN F C GLATZ, BRIAN K SHENTON, ROBERT PEASTON, CHRIS CORNELL, AND DAVID TALBOT. **Use of two biomarkers of renal ischemia to assess machine-perfused non-heart-beating donor kidneys.** *Clinical chemistry*, **49**(1):172–5, January 2003. 116
- [193] SIMONA C BAICU, MICHAEL J TAYLOR, AND KELVIN G M BROCKBANK. **Modulating biochemical perturbations during 72-hour machine perfusion of kidneys: Role of preservation solution.** *Cryobiology*, **54**(1):114–120, 2007. 116
- [194] SIMONA C BAICU, PATRICIA M SIMMONS, LIA H CAMPBELL, MICHAEL J TAYLOR, AND KELVIN G M BROCKBANK. **Interstitial fluid analysis for assessment of organ function.** *Clinical transplantation*, **18 Suppl 1**:16–21, January 2004. 116, 152
- [195] A K KELLER, C KIERULF-LASSEN, U MØ LDRUP, B M BIBBY, AND B JESPERSEN. **Messengers of Renal Graft Quality During Warm and Cold Ischemia: A Porcine Microdialysis Study.** *Transplantation Proceedings*, **45**(3):1172–1177, 2013. 116, 149, 152
- [196] HAMIDREZA FONOUNI, PARVIN JARAHIAN, MORVA TAHMASBI RAD, MOHAMMAD GOLRIZ, ALIREZA FARIDAR, MAJID ESMAEILZADEH, MOHAMMADREZA HAFEZI, STEPHAN MACHER-GOEPFINGER, THOMAS LONGERICH, BERK ORAKCIOGLU, OLIVER W SAKOWITZ, CAMELIA GAROUSSI, AND ARIANEB MEHRABI. **Evaluating the effects of extended cold ischemia on interstitial metabolite in grafts in kidney transplantation using microdialysis.** *Langenbeck's Archives of Surgery*, **398**(1):87–97, 2013. 116, 152, 161, 164

BIBLIOGRAPHY

- [197] ANNA KRARUP KELLER, TROELS MUNCH JORGENSEN, KRISTIAN RAVLO, TORBEN KAER NIELSEN, L HENNING OLSEN, AND LARS B STOLLE. **Microdialysis for detection of renal ischemia after experimental renal transplantation.** *The Journal of urology*, **182**(4 Suppl):1854–9, October 2009. 116, 148, 152, 153
- [198] MICHAEL A. SILVA, DOUGLAS A. RICHARDS, SIMON R. BRAMHALL, DAVID H. ADAMS, DARIUS F. MIRZA, AND NICK MURPHY. **A Study of the Metabolites of Ischemia-Reperfusion Injury and Selected Amino Acids in the Liver Using Microdialysis during Transplantation.** *Transplantation*, **79**(7):828–835, April 2005. 116
- [199] MICHAEL A SILVA, NICK MURPHY, DOUGLAS A RICHARDS, STEPHEN J WIGMORE, SIMON R BRAMHALL, JOHN A C BUCKELS, DAVID H ADAMS, AND DARIUS F MIRZA. **Interstitial lactic acidosis in the graft during organ harvest, cold storage, and reperfusion of human liver allografts predicts subsequent ischemia reperfusion injury.** *Transplantation*, **82**(2):227–33, July 2006. 116
- [200] G NOWAK, J UNGERSTEDT, J WERNERMAN, U UNGERSTEDT, AND B-G ERICZON. **Clinical experience in continuous graft monitoring with microdialysis early after liver transplantation.** *The British journal of surgery*, **89**(9):1169–75, September 2002. 116
- [201] L WAELEGAARD, E B THORGERSEN, P D LINE, A FOSS, T E MOLLNES, AND T I TNNESSEN. **Microdialysis monitoring of liver grafts by metabolic parameters, cytokine production, and complement activation.** *Transplantation*, **86**(8):1096–1103, 2008. 116, 177
- [202] KYLE J WELD, KRISTIN EVEARITT, PATRICIA DIXON, AND R DUANE CEPEDAS. **Effects of ischemia on human renal interstitial fluid metabolites.** *The Journal of urology*, **181**(2):878–83, February 2009. 117
- [203] SRIKANTH P REDDY, JENS BROCKMANN, AND PETER J FRIEND. **Normothermic Perfusion: A Mini-Review.** *Transplantation*, **87**(5):631–632 10.1097/TP.0b013e3181995e83, 2009. 117
- [204] THOMAS VOGEL, JENS G BROCKMANN, CONSTANTIN COUSSIOS, AND PETER J FRIEND. **The role of normothermic extracorporeal perfusion in minimizing ischemia reperfusion injury.** *Transplantation Reviews*, **26**(2):156–162, 2012. 117
- [205] SARAH A HOSGOOD, ADAM D BARLOW, PHILLIP J YATES, MAARTEN G J SNOEIJIS, ERNEST L W VAN HEURN, AND MICHAEL L NICHOLSON. **A pilot study assessing the feasibility of a short period of normothermic preservation in an experimental model of non heart beating donor kidneys.** *The Journal of surgical research*, **171**(1):283–90, November 2011. 117
- [206] A BAGUL, S A HOSGOOD, M KAUSHIK, M D KAY, H L WALLER, AND M L NICHOLSON. **Experimental renal preservation by normothermic resuscitation perfusion with autologous blood.** *The British journal of surgery*, **95**(1):111–8, January 2008. 117
- [207] RINALDO BELLOMO. **Bench-to-bedside review: Lactate and the kidney.** *Critical care*, **6**(4):1–5, 2002. 117, 150, 151
- [208] G WIRTHENSOHN AND W G GUDER. **Renal Substrate Metabolism.** *Physiological reviews*, **66**(2), 1986. 117
- [209] HA KREBS. **Renal Gluconeogenesis.** *Advances in enzyme regulation*, **24**(2), 1963. 117
- [210] WG GUDER AND BD ROSS. **Enzyme distribution along the nephron.** *Kidney international*, **26**:101–111, 1984. 117
- [211] SYLVIA BARTLETT, JOSEPH ESPINAL, PETER JANSSENST, AND BRIAN D ROSS. **The influence of renal function on lactate and glucose metabolism.** *Biochemical Journal*, **219**:73–78, 1984. 117
- [212] GEORGE A BROOKS, H DUBOUCHAUD, M BROWN, JP SICURELLO, AND E BUTZ. **Role of mitochondrial lactate dehydrogenase and lactate oxidation in the intracellular lactate shuttle.** *Proceedings of the National Academy of Sciences*, **96**:1129–1134, 1999. 117
- [213] JULIUS J COHEN. **Is the function exclusively of the renal papilla coupled to an anaerobic pattern of metabolism ?** *American Journal of Physiology*, **236**:F423–F431, 1979. 117
- [214] M KOSIERADZKI, R DANIELEWICZ, A KWIATKOWSKI, W P POLAK, M WSZOA, S FESOOWICZ, G MICHALAK, W LISIK, AND I WE. **Early Function of Kidneys Stored by Continuous Hypothermic Pulsatile Perfusion Can Be Predicted Using a New Viability Index .** *Transplantation proceedings*, **34**:541–543, 2002. 117
- [215] RONIK S BHANGOO, ISAAC E HALL, PETER P REESE, AND CHIRAG R PARIKH. **Deceased-donor kidney perfusate and urine biomarkers for kidney allograft outcomes: a systematic review.** *Nephrology, dialysis, transplantation : official publication of the European Dialysis and Transplant Association - European Renal Association*, **27**(8):3305–14, August 2012. 117
- [216] SUSANNE L LINDELL, PHILIPPE COMPAGNON, MARTIN J MANGINO, AND JAMES H. SOUTHARD. **UW Solution for Hypothermic Machine Perfusion of Warm Ischemic Kidneys.** *Transplantation*, **79**(10):1358–1361, May 2005. 125
- [217] MICHAL WSZOLA, ARTUR KWIATKOWSKI, PIOTR DIUWE, PIOTR DOMAGAA, LUKASZ GÓRSKI, RAFAL KIESZEK, ANDRZEJ BERMAN, AGNIESZKA PERKOWSKA-PTASISKA, MAGDA DURLIK, LESZEK PCZEK, AND ANDRZEJ CHMURA. **One-year results of a prospective, randomized trial comparing two machine perfusion devices used for kidney preservation.** *Transplant international : official journal of the European Society for Organ Transplantation*, **26**(11):1088–96, November 2013. 129, 149
- [218] ANNA KRARUP KELLER, TROELS MUNCH JORGENSEN, KRISTIAN RAVLO, TORBEN KAER NIELSEN, L HENNING OLSEN, AND LARS B STOLLE. **Microdialysis for Detection of Renal Ischemia After Experimental Renal Transplantation.** *The Journal of Urology*, **182**(4, Supplement):1854–1859, 2009. 149, 283
- [219] SCOT D HENRY AND JAMES V GUARRERA. **Protective effects of hypothermic ex vivo perfusion on ischemia/reperfusion injury and transplant outcomes.** *Transplantation reviews (Orlando, Fla.)*, **26**(2):163–75, April 2012. 149
- [220] NOËL CANO. **Bench-to-bedside review: glucose production from the kidney.** *Critical care*, **6**(4):317–321, 2002. 150, 151
- [221] THOMAS L PALLONE, ZHONG ZHANG, AND KRISTIE RHINEHART. **Physiology of the renal medullary microcirculation.** *American journal of renal physiology*, **284**(2):F253–F266, 2003. 151
- [222] ANNA KRARUP KELLER, TROELS MUNCH JORGENSEN, L HENNING OLSEN, AND LARS B STOLLE. **Early detection of renal ischemia by in situ microdialysis: an experimental study.** *The Journal of urology*, **179**(1):371–5, January 2008. 153, 177
- [223] ANNA K KELLER, TROELS M JØ RGENSEN, DORTHE M VITTRUP, ULRIK K KJERKEGAARD, BENTE JESPERSEN, SØREN R P KRAG, BO M BIBBY, AND LARS B STOLLE. **Fast detection of renal ischemia in transplanted kidneys with delayed graft function-an experimental study.** *Transplantation*, **95**(2):275–9, January 2013. 153, 177
- [224] HAMIDREZA FONOUNI, MORVA TAHMASBI RAD, MOHAMMAD GOLRIZ, ALIREZA FARIDAR, MAJID ESMAEILZADEH, PARVIN JARAHIAN, MOHAMMADREZA HAFEZI, SHADI JAFARIEH, STEPHAN MACHER-GOEPFINGER, THOMAS LONGERICH, BERK ORAKCIOGLU, OLIVER SAKOWITZ, JAN SCHMIDT, AND ARIANEB MEHRABI. **Using microdialysis for early detection of vascular thrombosis after kidney transplantation in an experimental porcine model.** *Nephrology, dialysis, transplantation*, **27**(2):541–7, February 2012. 153, 177

- [225] C MOERS, J PIRENNE, A PAUL, AND R J PLOEG. **Machine Perfusion or Cold Storage in Deceased-Donor Kidney Transplantation.** *New England Journal of Medicine*, **366**(8):770–771, 2012. 153
- [226] INA JOCHMANS, CYRIL MOERS, JACQUELINE M SMITS, HENRI G D LEUVENINK, JÜRGEN TRECKMANN, ANDREAS PAUL, AXEL RAHMEL, JEAN-PAUL SQUIFFLET, ERNEST VAN HEURN, DIETHARD MONBALIU, RUTGER J PLOEG, AND JACQUES PIRENNE. **Machine perfusion versus cold storage for the preservation of kidneys donated after cardiac death: a multicenter, randomized, controlled trial.** *Annals of surgery*, **252**(5):756–64, November 2010. 153
- [227] T. MELCHIONNA, J. KAREGLIA, C.A. FARRARA, J.H. McVEY, A. DORLINGA, S.H. SACKS, AND R.A.G. SMITH. **Integrating cytotoxic strategy in transplantation: (1) Design of locally-acting coagulation inhibitors for use with anti-complement therapeutics.** *Molecular Immunology*, **47**(13):2198–2294, August 2010. 170
- [228] N BAKIR, W J SLUITER, R J PLOEG, W J VAN SON, AND A M TEGZESS. **Primary renal graft thrombosis.** *Nephrology Dialysis Transplantation*, **11**:140–147, 1996. 177
- [229] A GOK, MUHAMMAD, BRIAN K SHENTON, PAMELA E BUCKLEY, ROBERT PEASTON, CHRIS CORNELL, NAEEM SOOMRO, BRYON C JAQUES, DEREK M MANAS, AND DAVID TALBOT. **How to improve the quality of kidneys from non-heart-beating donors: a randomised controlled trial of thrombolysis in nonheart-beating donors.** *Transplantation*, **76**(12):1714–1719, 2003. 177
- [230] T FATHI, M SAMHAN, A GAWISH, F DONIA, AND M AL-MOUSAWI. **Renal allograft venous thrombosis is salvageable.** *Transplantation proceedings*, **39**(4):1120–1, May 2007. 177
- [231] M K TARZAMNI, H ARGANI, M NURIFAR, AND N NEZAMI. **Vascular complication and Doppler ultrasonographic finding after renal transplantation.** *Transplantation proceedings*, **39**(4):1098–102, May 2007. 177
- [232] A K KELLER, T M JORGENSEN, L H OLSEN, AND L B STOLLE. **Detection of local metabolic changes after progressive and stepwise reduction of renal blood flow in pigs.** *Transplantation proceedings*, **41**(1):44–8, 2009. 177
- [233] S MITTAL AND S C L GOUGH. **Pancreas transplantation: a treatment option for people with diabetes.** *Diabetic medicine : a journal of the British Diabetic Association*, **31**(5):512–21, May 2014. 178, 179
- [234] PHILLIP WEEMS AND MATTHEW COOPER. **Pancreas transplantation in type II diabetes mellitus.** *World journal of transplantation*, **4**(4):216–21, December 2014. 178
- [235] ARIANEB MEHRABI, MOHAMMAD GOLRIZ, FATEMEH ADILI-AGHDAM, MOHAMMADREZA HAFEZI, MARYAM ASHRAFI, CHRISTIAN MORATH, MARTIN ZEIER, THILO HACKERT, AND PETER SCHEMMER. **Expanding the indications of pancreas transplantation alone.** *Pancreas*, **43**(8):1190–3, November 2014. 178
- [236] ALEX T JIANG, NEAL ROWE, ALP SENER, AND PATRICK LUKE. **Simultaneous pancreas-kidney transplantation : The role in the treatment of type 1 diabetes and end-stage renal disease.** *Candian Urological Association Journal*, **8**(2014):135–138, 2014. 179
- [237] K P MCCULLOUGH, D S KEITH, K H MEYER, P G STOCK, K L BRAYMAN, AND A B LEICHTMAN. **Kidney and pancreas transplantation in the United States, 1998-2007: access for patients with diabetes and end-stage renal disease.** *American journal of transplantation*, **9**(4 Pt 2):894–906, April 2009. 179
- [238] PILAR ISLA PERA, JOAQUIN MONCHO VASALLO, ALBERTO TORRAS RABASA, FEDERICO OPPENHEIMER SALINAS, LAUREANO FERNÁNDEZ CRUZ PÉREZ, AND MARÍA JOSÉ RICART BRULLES. **Quality of life in simultaneous pancreas-kidney transplant recipients.** *Clinical transplantation*, **23**(5):600–5, 2009. 179
- [239] TIM SCHULZ, ALEXANDRA PRIES, AMKE CALIEBE, AND MATTHIAS KAPISCHKE. **Long-term survival after simultaneous pancreas-kidney transplantation with primary function of at least one year—a single-center experience.** *Annals of transplantation : quarterly of the Polish Transplantation Society*, **19**:106–11, January 2014. 179
- [240] J P LINDAHL, A HARTMANN, R HORNELAND, H HOLDAAS, A V REISE TER, K MIDTVEDT, T LEIVESTAD, O OYEN, AND T JENSSEN. **Improved patient survival with simultaneous pancreas and kidney transplantation in recipients with diabetic end-stage renal disease.** *Diabetologia*, **56**(6):1364–71, June 2013. 179
- [241] ADAM D BARLOW, SARAH A HOSGOOD, AND MICHAEL L NICHOLSON. **Current state of pancreas preservation and implications for DCD pancreas transplantation.** *Transplantation*, **95**(12):1419–24, June 2013. 179
- [242] M J TAYLOR, S BAICU, B LEMAN, E GREENE, A VAZQUEZ, AND J BRASILE. **Twenty-four hour hypothermic machine perfusion preservation of porcine pancreas facilitates processing for islet isolation.** *Transplantation Proceedings*, **40**(2):480–482, 2008. 179
- [243] ROBERTO TERSIGNI, LUIS H. TOLEDO-PEREYRA, JEFF PINKHAM, AND JOHN S. NAJARIAN. **Pancreaticoduodenal Preservation by Hypothermic Pulsatile Perfusion for Twenty-four Hours.** *Annals of Surgery*, **182**(6):743–748, December 1975. 179
- [244] MASAYUKI KITANO, HIROKI SAKAMOTO, KSHAUNISH DAS, AND TAKAMITSU KOMAKI. **EUS-guided in vivo microdialysis of the pancreas : a novel technique with potential diagnostic and therapeutic application.** *Gastrointestinal Endoscopy*, **71**(1):17–20, 2010. 179
- [245] P-J BLIND, J KRAL, W WANG, I KRALOVA, P ABRAHAMSSON, G JOHANSSON, AND O WINSÖ. **Microdialysis in early detection of temporary pancreatic ischemia in a porcine model.** *European surgical research*, **49**(3-4):113–20, January 2012. 179, 185
- [246] D A HIDALGO, J J DISA, P G CORDEIRO, AND QUN-YING HU. **A review of 716 consecutive free flaps for oncologic surgical defects: refinement in donor-site selection and technique.** *Plastic and reconstructive surgery*, **102**:722–32, 1998. 195
- [247] NEIL F JONES, REZA JARRAHY, J I SONG, MATTHEW R KAUFMAN, AND BERNARD MARKOWITZ. **Postoperative medical complications—not microsurgical complications—negatively influence the morbidity, mortality, and true costs after microsurgical reconstruction for head and neck cancer.** *Plastic and reconstructive surgery*, **119**(7):2053–60, June 2007. 195
- [248] RAMON M ESCLAMADO AND WILLIAM R CARROLL. **The pathogenesis of vascular thrombosis and its impact in microvascular surgery.** *Head & Neck*, **21**(4):355–362, 1999. 195
- [249] T NAKATSUKA, K HARIU, H ASATO, A TAKUSHIMA, S EBIHARA, Y KIMATA, A YAMADA, K UEDA, AND S ICHIOKA. **Analytic review of 2372 free flap transfers for head and neck reconstruction following cancer resection.** *Journal of reconstructive microsurgery*, **19**(6):363–368, August 2003. 195
- [250] MARIA SIEMIONOW AND EMRAH ARSLAN. **Ischemia/reperfusion injury: a review in relation to free tissue transfers.** *Microsurgery*, **24**(6):468–75, January 2004. 195
- [251] W R CARROLL AND R M ESCLAMADO. **Ischemia/reperfusion injury in microvascular surgery.** *Head & Neck*, **22**:700–713, 2000. 195
- [252] C L KERRIGAN, R G ZELT, AND R K DANIEL. **Secondary critical ischemia time of experimental skin flaps.** *Plastic and reconstructive surgery*, **74**(4):522–524, 1984. 195

BIBLIOGRAPHY

- [253] KUANG-TE CHEN, SAMIR MARDINI, DAVID CHWEI-CHIN CHUANG, CHIH-HUNG LIN, MING-HUEI CHENG, YU-TE LIN, WEI-CHAO HUANG, CHUNG-KAN TSAO, AND FU-CHAN WEI. **Timing of presentation of the first signs of vascular compromise dictates the salvage outcome of free flap transfers.** *Plastic and reconstructive surgery*, **120**(1):187–95, July 2007. 196
- [254] JEROEN M SMIT, RAFAEL ACOSTA, CLARK J ZEEBREGTS, ANDERS G LISS, MATTI ANNIKO, AND E D H M HARTMAN. **Early reintervention of compromised free flaps improves success rate.** *Microsurgery*, **27**:612–616, 2007. 196
- [255] I S WHITAKER, V GULATI, G L ROSS, A MENON, AND T K ONG. **Variations in the postoperative management of free tissue transfers to the head and neck in the United Kingdom.** *The British journal of oral & maxillofacial surgery*, **45**(1):16–8, January 2007. 196
- [256] JJ DISA, P G CORDEIRO, AND D A HIDALGO. **Efficacy of conventional monitoring techniques in free tissue transfer: an 11-year experience in 750 consecutive cases.** *Plastic and reconstructive surgery*, **104**(1):97–101, 1999. 196
- [257] KHALID ABDEL-GALIL AND DAVID MITCHELL. **Postoperative monitoring of microsurgical free tissue transfers for head and neck reconstruction: a systematic review of current techniques—part I. Non-invasive techniques.** *The British journal of oral & maxillofacial surgery*, **47**(5):351–5, July 2009. 196
- [258] KHALID ABDEL-GALIL AND DAVID MITCHELL. **Postoperative monitoring of microsurgical free-tissue transfers for head and neck reconstruction: a systematic review of current techniques—part II. Invasive techniques.** *The British journal of oral & maxillofacial surgery*, **47**(6):438–42, September 2009. 196
- [259] JEROEN M SMIT, PAUL M N WERKER, ANDERS G LISS, MORTEZA ENAJAT, GEERTRUIDA H DE BOCK, THORIR AUDOLFSSON, AND RAFAEL ACOSTA. **Introduction of the implantable Doppler system did not lead to an increased salvage rate of compromised flaps: a multivariate analysis.** *Plastic and reconstructive surgery*, **125**(6):1710–7, June 2010. 196
- [260] JEROEN M SMIT, CLARK J ZEEBREGTS, RAFAEL ACOSTA, AND PAUL M N WERKER. **Advancements in free flap monitoring in the last decade: a critical review.** *Plastic and reconstructive surgery*, **125**(1):177–85, January 2010. 196
- [261] JANNE JYRÄNKI, SINIKKA SUOMINEN, JYRKI VUOLA, AND LEIF BÄCK. **Microdialysis in clinical practice: monitoring intraoral free flaps.** *Annals of plastic surgery*, **56**(4):387–93, April 2006. 196
- [262] HENRIK TOFT NIELSEN, NILS GUTBERG, AND HANNE BIRKE-SØRENSEN. **Monitoring of intraoral free flaps with microdialysis.** *The British journal of oral & maxillofacial surgery*, **49**(7):521–6, October 2011. 196
- [263] CONSTANTINOS MOUROUZIS, RAJIV ANAND, JOHN R BOWDEN, AND PETER A BRENNAN. **Microdialysis: Use in the Assessment of a Buried Bone-Only Fibular Free Flap.** *Plastic and Reconstructive Surgery*, **120**(5), 2007. 196
- [264] H BIRKE-SØRENSEN AND N T ANDERSEN. **Metabolic markers obtained by microdialysis can detect secondary intestinal ischemia: an experimental study of ischemia in porcine intestinal segments.** *World Journal of Surgery*, **34**(5):923–932, 2010. 196
- [265] J. RÖJDMARK, P. HEDÉN, AND U. UNGERSTEDT. **Microdialysis - a new technique for free flap surveillance: methodological description.** *European Journal of Plastic Surgery*, **21**(7):344–348, September 1998. 196
- [266] PAULO BONATO. **Wearable Sensors and Systems: From Enabling Technology to Clinical Applications.** *IEEE Engineering in medicine and biology magazine*, **29**(June):25–36, 2010. 219
- [267] DERMOT DIAMOND, SHIRLEY COYLE, SILVIA SCARMAGNANI, AND JER HAYES. **Wireless sensor networks and chemosensing.** *Chemical reviews*, **108**(2):652–79, March 2008. 219
- [268] GIUSY MATZEU, LARISA FLOREA, AND DERMOT DIAMOND. **Advances in wearable chemical sensor design for monitoring biological fluids.** *Sensors and Actuators B: Chemical*, **211**:403–418, January 2015. 219, 220
- [269] VINCENZO F. CURTO, CORMAC FAY, SHIRLEY COYLE, ROBERT BYRNE, CORINNE O'TOOLE, CAROLINE BARRY, SARAH HUGHES, NIALL MOYNA, DERMOT DIAMOND, AND FERNANDO BENITO-LOPEZ. **Real-time sweat pH monitoring based on a wearable chemical barcode micro-fluidic platform incorporating ionic liquids.** *Sensors and Actuators B: Chemical*, **171–172**:1327–1334, August 2012. 219
- [270] WENZHAO JIA, AMAY J BANDODKAR, GABRIELA VALDE, JOSHUA R WINDMILLER, ZHANJUN YANG, JULIAN RAM, GARRETT CHAN, AND JOSEPH WANG. **Electrochemical Tattoo Biosensors for Real-Time Noninvasive Lactate Monitoring in Human Perspiration.** *Analytical chemistry*, **85**:6553–6560, 2013. 219, 220
- [271] SHIGEHITO IGUCHI, HIROYUKI KUDO, TAKAO SAITO, MITSUHIRO OGAWA, HIROKAZU SAITO, KIMIO OTSUKA, AKIO FUNAKUBO, AND KOHJI MITSUBAYASHI. **A flexible and wearable biosensor for tear glucose measurement.** *Biomedical Microdevices*, **9**:603–609, 2007. 219
- [272] SATYAMOORTHY KABILAN, D PH, AND CHRISTOPHER LOWE. **Initial Clinical Testing of a Holographic Non-Invasive Contact Lens Glucose Sensor.** *Diabetes Technology & Therapeutics*, **8**(1):89–93, 2006. 219
- [273] Y. YODA, K.; SHIMAZAKI, K.; UEDA. **Analysis of Glycolysis Relevant Compounds in Saliva by Microbiosensors.** *Annals of the New York Academy of Sciences*, **864**:600–604, 1998. 219
- [274] MANU S. MANNOOR, HU TAO, JEFFERSON D. CLAYTON, AMARTYA SENGUPTA, DAVID L. KAPLAN, RAJESH R. NAIK, NAVEEN VERMA, FIORENZO G. OMENETTO, AND MICHAEL C. MCALPINE. **Graphene-based wireless bacteria detection on tooth enamel,** 2012. 219
- [275] A POSCIA, M MASCINI, D MOSCONE, M LUZZANA, AND G CARAMENTI. **A microdialysis technique for continuous subcutaneous glucose monitoring in diabetic patients (part 1).** *Biosensors & bioelectronics*, **18**:891–898, 2003. 219
- [276] M VARALLI, G MARELLI, A MARAN, S BISTONI, M LUZZANA, AND P CREMONESI. **A microdialysis technique for continuous subcutaneous glucose monitoring in diabetic patients (part 2).** *Biosensors & bioelectronics*, **18**:899–905, 2003. 219
- [277] JOSHUA RAY WINDMILLER AND JOSEPH WANG. **Wearable Electrochemical Sensors and Biosensors: A Review.** *Electroanalysis*, **25**(1):29–46, January 2013. 219
- [278] L V BILLAT. **Use of blood lactate measurements for prediction of exercise performance and for control of training.** *Sports Medicine*, **22**(3):157–175, 1996. 220
- [279] DION KHODAGHOLY, VINCENZO F. CURTO, KEVIN J. FRASER, MOSHE GURFINKEL, ROBERT BYRNE, DERMOT DIAMOND, GEORGE G. MALLIARAS, FERNANDO BENITO-LOPEZ, AND ROISIN M. OWENS. **Organic electrochemical transistor incorporating an ionogel as a solid state electrolyte for lactate sensing.** *Journal of Materials Chemistry*, **22**(10):4440, 2012. 220
- [280] PHILIP J DERBYSHIRE, HUGH BARR, FRANK DAVIS, AND SEAMUS P J HIGSON. **Lactate in human sweat: a critical review of research to the present day.** *The journal of physiological sciences : JPS*, **62**(6):429–40, November 2012. 220

- [281] JAYOUNG KIM, GABRIELA VALDÉS-RAMÍREZ, AMAY J BANDODKAR, WENZHAO JIA, ALEXANDRA G MARTINEZ, JULIAN RAMÍREZ, PATRICK MERCIER, AND JOSEPH WANG. **Non-invasive mouth-guard biosensor for continuous salivary monitoring of metabolites.** *The Analyst*, **139**(7):1632–6, April 2014. 220
- [282] A POSCIA, D MESSERI, D MOSCONE, F RICCI, AND F VALGIMIGLI. **A novel continuous subcutaneous lactate monitoring system.** *Biosensors & bioelectronics*, **20**:2244–2250, 2005. 220
- [283] G VOLPE, D MOSCONE, D COMPAGNONE, AND G PALLESCHI. **In vivo continuous monitoring of L-lactate coupling subcutaneous microdialysis and an electrochemical biocell.** *Sensors and Actuators B: Chemical*, **25**:138–141, 1995. 220
- [284] MENG WANG, GREGORY T ROMAN, KRISTIN SCHULTZ, COLIN JENNINGS, AND ROBERT T KENNEDY. **Improved temporal resolution for in vivo microdialysis by using segmented flow.** *Analytical chemistry*, **80**(14):5607–15, July 2008. 249
- [285] MICHELLE L ROGERS, DELPHINE FEUERSTEIN, CHI LENG LEONG, MASATOSHI TAKAGAKI, XIZE NIU, RUDOLF GRAF, AND MARTYN G BOUTELLE. **Continuous Online Microdialysis Using Microfluidic Sensors: Dynamic Neurometabolic Changes during Spreading Depolarization.** *ACS Chemical Neuroscience*, **4**:799–807, 2013. 249
- [286] M ROGERS, C LEONG, X NIU, A DE MELLO, K H PARKER, AND M G BOUTELLE. **Optimisation of a microfluidic analysis chamber for the placement of microelectrodes.** *Physical chemistry chemical physics : PCCP*, **13**(12):5298–5303, 2011. 250
- [287] JAYDA L ERKAL, ASMIRA SELIMOVIC, BETHANY C GROSS, SARAH Y LOCKWOOD, ERIC L WALTON, STEPHEN MCNAMARA, R SCOTT MARTIN, AND DANA M SPENCE. **3D printed microfluidic devices with integrated versatile and reusable electrodes.** *Lab on a chip*, **14**(12):2023–32, June 2014. 250, 254
- [288] KARI B ANDERSON, SARAH Y LOCKWOOD, R SCOTT MARTIN, AND DANA M SPENCE. **A 3D printed fluidic device that enables integrated features.** *Analytical chemistry*, **85**(12):5622–6, June 2013. 250
- [289] DANIEL THERRIAULT, SCOTT R WHITE, AND JENNIFER A LEWIS. **Chaotic mixing in three-dimensional microvascular networks fabricated by direct-write assembly.** *Nature materials*, **2**(4):265–71, April 2003. 250
- [290] PHILIP J KITSON, MALI H. ROSNES, VICTOR SANS, VINCENZA DRAGONE, AND LEROY CRONIN. **Configurable 3D-Printed millifluidic and microfluidic lab on a chip reactionware devices.** *Lab on a Chip*, **12**:3267, 2012. 250
- [291] MICHAEL E SNOWDEN, PHILIP H KING, JAMES A COVINGTON, JULIE V MACPHERSON, AND PATRICK R UNWIN. **Fabrication of versatile channel flow cells for quantitative electroanalysis using prototyping.** *Analytical chemistry*, **82**(8):3124–31, April 2010. 250
- [292] ANSGAR WALDBAUR, HOLGER RAPP, KERSTIN LÄNGE, AND BASTIAN E. RAPP. **Let there be chiptowards rapid prototyping of microfluidic devices: one-step manufacturing processes.** *Analytical Methods*, **3**:2681, 2011. 250
- [293] PERNILLA ABRAHAMSSON, ANNA-MAJA Å BERG, GÖRAN JOHANSSON, OLA WINSÖ, ANDERS WALDENSTRÖM, AND MICHAEL HANEY. **Detection of myocardial ischaemia using surface microdialysis on the beating heart.** *Clinical Physiology and Functional Imaging*, **31**(3):175–181, 2011. 283
- [294] PERNILLA ABRAHAMSSON, ANNA-MAJA ABERG, OLA WINSO, MICHAEL HANEY, AND PER-JONAS BLIND. **Surface microdialysis sampling : a new approach described in a liver ischaemia model.** *Clinical Physiology and Functional Imaging*, **32**:99–105, 2012. 283

Appendix

Table 1: Copyright permissions

Figure number	Publisher	Publication	Licence number
1.1	Elsevier	Trends in Neurosciences	3592201015916
1.6	Springer	Acta Diabetologica	3592201296637
1.9	American Chemical Society	Analytical Chemistry	Permission to re-use granted for thesis
3.1	Springer	Applied Microbiology and Biotechnology	3592210517215
3.2	Elsevier	Journal of Molecular Biology	3592210649162
4.1	Nature Publishing Group	Nature Reviews Nephrology	3592210375547

